

Studies on Conversion of Indian Biomass to Second Generation Biofuels through Hybridization of Thermochemical and Biochemical Processes

**Thesis Submitted by
Dinabandhu Manna**

Doctor of Philosophy (Engineering)

**Chemical Engineering Department
Faculty Council of Engineering & Technology
Jadavpur University
Kolkata, India**

2024

Dedicated to “Devi Saraswati”

JADAVPUR UNIVERSITY

KOLKATA 700032, INDIA

INDEX No. 132/17/E

1. Title of the thesis: Studies on Conversion of Indian Biomass to Second Generation Biofuels through Hybridization of Thermochemical and Biochemical Processes

2. Name, Designation & Institutions of the Supervisor

Name: Ranjana Chowdhury

Designation: Professor

Department: Chemical Engineering Department

Institute: Jadavpur University, Kolkata-700032

List of Publications

Serial no.	Publication Details	Publication category
1	Manna, D., Chowdhury, R., Hassan, M. K., Vepsäläinen, J., Kuittinen, S., & Pappinen, A. (2024). Catalytic action of hydronium-ion in rice straw pretreatment and enhancement of enzymatic hydrolysis and ethanol production. <i>Next Energy</i> , 3, 100112. https://doi.org/10.1016/j.nxener.2024.100112	Research article
2	Manna, D., Chowdhury, R., Calay, R. K., & Mustafa, M. Y. (2024). Experimental Insights into the Fermentation of Pyro-Syngas to Ethanol in a Semi-Batch and Continuous Stirred Bioreactor with Mathematical Modelling and Optimization. <i>Energies</i> , 17(3), 562. https://doi.org/10.3390/en17030562 .	Research article
3	R. Chowdhury, S. Ghosh, D. Manna, S. Das, S. Dutta, S. Kleinsteuber, H. Strauber, M. K. Hassan, S. Kuittinen, A. Pappinen, Hybridization of sugar-carboxylate-syngas platforms for the production of bio-alcohols from lignocellulosic biomass (LCB)—A state-of-the-art review and recommendations, <i>Energy Conversion and Management</i> 200 (2019) 112111. https://doi.org/10.1016/j.enconman.2019.112111 .	Research article
4	M. K. Hassan, R. Chowdhury, S. Ghosh, D. Manna, A. Pappinen, S. Kuittinen, Energy and environmental impact assessment of Indian rice straw for the production of second-generation bioethanol. <i>Sustainable Energy Technologies and Assessments</i> , 47 (2021) 101546. https://doi.org/10.1016/j.seta.2021.101546 .	Research article
5	Dutta, S., Ghosh, S., Manna, D., & Chowdhury, R. (2021). Energy and environmental performance of a near-zero-effluent rice straw to butanol production plant. <i>Indian Chemical Engineer</i> , 63(2), 139-151. https://doi.org/10.1080/00194506.2020.1831406	Research article
6	Chowdhury, R., Ghosh, S., Debnath, B., & Manna, D. (2018). Indian agro-wastes for 2G biorefineries: strategic decision on conversion processes. <i>Sustainable Energy Technology and Policies: A Transformational Journey, Volume 1</i> , 353-373.	Book chapter

List of Patents: Nil

List of Presentations in National/International Conferences

Serial no.	Details of Presentations
1	Manna, D., Saha, S., Chowdhury R. (2019). Kinetics Torrefaction of Mustard Stalk using a Semi-batch reactor. <i>International Seminar on Sustainable 2-G Biorefinery Platform.</i>
2	Manna, D., Jana, R., Mondal, M., Chowdhury, R. (2023). Kinetics Torrefaction of Jute stick using a Semi-batch reactor. <i>International Conference on Chemical Engineering Innovation & Sustainability (ICEIS 2023)</i>

“Statement of Originality”

I **Dinabandhu Manna** registered on **22/03/2017** do hereby declare that this thesis entitled” **“Studies on Conversion of Indian Biomass to Second Generation Biofuels through Hybridization of Thermochemical and Biochemical Processes”** contains literature survey and original research work done by the undersigned candidate as part of Doctoral studies.

All information in this thesis have been obtained and presented in accordance with existing academic rules and ethical conduct. I declare that, as required by these rules and conduct, I have fully cited and referred all materials and results that are not original to this work.

I also declare that I have checked this thesis as per the “Policy on Anti Plagiarism, Jadavpur University, 2019”, and the level of similarity as checked by iThenticate software is 4%.

Signature of Candidate: *Dinabandhu Manna*

Date: *19/03/2024*

Dr. Ranjana Chowdhury
Professor
Chemical Engineering Department
JADAVPUR UNIVERSITY
Kolkata-700 032

Certified by Supervisor(s):

(Signature with date, seal)

1. *Ranjana Chowdhury 19-03-2024*

Certificate from the Supervisor

This is to certify that the thesis entitled “Studies on Conversion of Indian Biomass to Second Generation Biofuels through Hybridization of Thermochemical and Biochemical Processes” submitted by Dinabandhu Manna, who got his name registered on 22/03/2017 for the award of Ph. D. (Engg.) degree of Jadavpur University is absolutely based upon his own work under the supervision of Prof. Ranjana Chowdhury and that neither his thesis nor any part of the thesis has been submitted for any degree or any other academic award anywhere before.

Dr. Ranjana Chowdhury
Professor
Chemical Engineering Department
JADAVPUR UNIVERSITY
Kolkata-700 032

Ranjana Chowdhury

19-03-2024

Signature of the supervisor and date with office seal

Acknowledgement

It is my privilege to express my sincere thanks and gratitude to Prof. (Dr.) Ranjana Chowdhury, Chemical Engineering Department, Jadavpur University (Kolkata-700032) who has given me this opportunity to work in her research laboratory and constantly gave me invaluable guidance throughout the research work. She also encouraged me in accomplishing the PhD research work and without her support it would not have been possible to complete my PhD thesis.

Also I must express my gratitude to my Lab mates PhD research scholars, for their support and help during my PhD research work which proved to be a constant source of inspiration to me.

I also highly appreciate the prompt help and co-operation extended by the other scholars, faculty members and staff of Department of Chemical Engineering, Jadavpur University (Kolkata) at the various phases of the experimental work.

Contents

Content	Page No.
List of Tables	
List of Figures	
1. Introduction	1-9
1.1 Production of ethanol from biomass through sugar platform	3
1.2 Production of ethanol from biomass through syngas platform	4
1.3 Hydrothermal liquefaction (HTL) of Biomass	4
1.4 Torrefaction of biomass	5
2. Literature review	10-43
2.1 Ferric chloride Pretreatment for the Production of ethanol from Agro-biomass through sugar platform	11
2.2 Production of Ethanol from Biomass through Syngas Platform	19
2.3 Hydrothermal liquefaction (HTL) of biomass	24
2.4 Torrefaction of biomass	36
3.Aims and objectives	44-49
4. Materials and analytical methods	50-58
4.1 Materials	51
4.1.1 Feed material	51
4.1.2 Chemicals	51
4.1.3 Microorganism for ethanol production	51
4.2 Analytical Methods	51
4.2.1 Quantitative Analysis of hydrocarbon polymers (Cellulose-Hemicellulose-Lignin)	51
4.2.2 Proximate analysis	52
4.2.3 Ultimate analysis	52
4.2.4 Thermo-gravimetric analysis (TGA)	52
4.2.5 Fourier Transform Infra-red analysis	52
4.2.6 X-ray diffractive (XRD) analysis	53
4.2.7 Field emission scanning electron microscopy (FESEM) analysis	53

4.2.8 Energy-dispersive X-ray spectroscopy (EDS) analysis	53
4.2.9 Nuclear magnetic resonance spectroscopy (NMR) Analysis	53
4.2.10 Gas chromatography (GC)	54
4.2.11 High performance liquid chromatography (HPLC) analysis	54
4.2.12 Gas chromatography – mass spectrometry (GC-MS) analysis	54
5. Production of Ethanol from Indian Biomass through Sugar Platform	59-128
5.1 Pretreatment Processes	60
5.1.1 Experimental	61
5.1.2 Analytical	62
5.1.3 Reaction kinetics for xylan and glucan degradation	63
5.1.4 Elucidation of Mechanism	64
5.1.5 Experimental Results and Discussion	68
5.1.5.1 Feedstock Characterization	68
5.1.5.2 Comparison of composition of Liquid hydrolysate	69
5.1.5.3 Comparison of degradation kinetics of xylan and glucan during pretreatment	77
5.1.5.4 Comparison of characteristics of untreated and pretreated rice straw	81
5.1.5.5 Effect of ferric chloride concentration on liquid hydrolysate	86
5.1.6 Mathematical modelling for FeCl ₃ pretreatment of rice straw	86
5.1.6 .1 Conversion of xylan into xylose and other products	86
5.1.6.2 Conversion of cellulose into glucose and other products	90
5.1.6.3 Rate Constants	93
5.1.6.4 Comparison of predictions of Model with Experimental Results	94
5.1.6.5 Normalized root mean square error (NRMSE)	97
5.1.7 Degradation of polymer	98
5.1.8 Optimization of the yield of major products and degradation of xylan and glucan	99
5.1.8.1 Optimization of the yield of major products through ferric chloride (0.2M) pretreatment	99
5.1.8.2 Optimization of degradation of xylan and glucan through FeCl ₃ pretreatment	101
5.1.9 Effect of Combined severity on ferric chloride pretreatment	103

5.2 Enzymatic hydrolysis	107
5.2.1 Experimental procedure	107
5.2.2 Comparison of Experimental Results of Enzymatic Hydrolysis	107
5.2.3 Mathematical model for enzymatic hydrolysis	108
5.2.3.1 Comparison of experimental and simulated yield of glucose during enzymatic hydrolysis	109
5.2.4 Optimization of glucose yield of enzymatic hydrolysis and overall glucose yield	110
5.3 Ethanol production	114
5.3.1 Experimental	114
5.3.2 Analytical	114
5.3.3 Comparison of Experimental Results	115
5.4 Overall mass balance	118
5.5 Summary	121
6. Production of Ethanol from Indian Biomass through Syngas Platform	129-165
6.1 Experimental methods	130
6.1.1 Pyrolysis of rice straw	130
6.1.2 Pyro-syngas fermentation	131
6.1.2.1 Microorganism	131
6.1.2.2 Preparation of Modified clostridial medium for growth	131
6.1.2.3 Pre-adaptation of <i>UACJUCHE1</i> to Simulated Pyro-syngas	132
6.1.2.4 Batch Experiments for determination of growth kinetics of <i>UACJUCHE1</i>	133
6.1.2.4.1 Experiments for Growth kinetics on CO	133
6.1.2.4.2 Experiments for Growth kinetics on CO ₂ and H ₂	133
6.1.2.5 Stirred tank Bioreactor for Pyro-syngas Fermentation	134
6.1.2.5.1 Determination of effect of stirring speed and gas velocity on O ₂ Mass transfer coefficient	134
6.1.2.5.2 Strategy of operation of Bioreactor in Semi-batch and Continuous modes	135
6.1.2.5.2.1 Start-up	135
6.1.2.5.2.2 Operation of bioreactor	136

6.2 Theoretical Analysis	138
6.2.1 Kinetics of growth on CO	138
6.2.2 Kinetics of growth on CO ₂ -H ₂ mixture	138
6.3 Mathematical Model	139
6.4 Optimization of Ethanol concentration in Semi-batch and Continuous bioreactors	143
6.4.1 Syngas fermentation in Semi-batch bioreactor	143
6.4.2 Syngas fermentation in continuous bioreactor	144
6.5 Result and discussion	144
6.5.2 Yield of the pyro-products	145
6.5.3 Values of Parameters	146
6.5.3.1 k_La for Different Gases	146
6.5.3.2 Model Parameters	147
6.5.3.3 Significance of Model Parameters and Their Comparison with Similar Studies	149
6.5.4 Performance of the Bioreactor in Semi-Batch and Continuous Modes	150
6.5.4.1 Bioreactor Dynamics in the Semi-Batch Mode	150
6.5.4.2 Bioreactor Dynamics in the Continuous Mode	151
6.5.5 Comparison of Simulated and Experimental	152
6.5.5.1 Semi-Batch Operation	152
6.5.5.2 Continuous Operation	153
6.5.6 Effect of Gas Residence Time (GRT) and Dilution Factor (D) on the Volumetric Productivity of Ethanol	154
6.5.7 Optimization Results for Semi-Batch and Continuous Bioreactors	155
6.5.7.1 Semi-Batch Bioreactor	155
6.5.7.2 Syngas Fermentation in the Continuous Bioreactor	158
6.5.8 Comparison of Semi-Batch and Continuous Operation of a Pyro-Syngas Fermenter	160
6.5.9 Comparison with Similar Studies and Uniqueness	161
6.5.10 Summary	162

7. Hydrothermal liquefaction (HTL) of Indian Biomass (jute stick and rice straw)	166-202
7.1 Experimental Methods for hydrothermal liquefaction	167
7.2 Optimization	169
7.3 Lumped Kinetics of hydrothermal liquefaction	171
7.4 Results and discussion	172
7.4.1 Proximate analysis of jute stick and rice straw	172
7.4.2 Composition of jute stick and rice straw	173
7.4.3 Product Yield obtained from HTL	173
7.4.4 Kinetic parameters	175
7.4.5 Elemental analysis of hydrochar and bio-oil	180
7.4.5.1 Elemental analysis of hydrochar	180
7.4.5.2 Elemental analysis of bio-oil	181
7.4.6 Thermal stability analysis of hydrochar obtained from individual HTL	183
7.4.7 FTIR analysis of hydrochar obtained from individual HTL	184
7.4.8 XRD analysis of hydrochar obtained from individual HTL	185
7.4.9 Surface morphology of hydrochar obtained from individual HTL	185
7.4.10 Bio-oil production from co-HTL of jute stick and rice straw	186
7.4.11 HHV of bio-oil produced from co-HTL	188
7.4.12 GC-MS analysis of Bio-oil obtained from individual and co-HTL	189
7.4.13 Effectiveness of dye (Congo red) removal by JS-Hydrochar	193
7.4.14 Comparison with available literature data	195
7.5 Summary	198
8. Torrefaction of mustard stalk	203-226
8.1 Experimental methods	204
8.2 Lumped kinetics of torrefaction of jute stick	205
8.3 Distributed activation energy model	206
8.4 Thermodynamic Analysis	207
8.5 Results and discussion	207
8.5.1 Composition of mustard stalk	207
8.5.2 Yield of product	208

8.5.3 Kinetic parameters	208
8.5.3.1 Parameters used for lumped kinetics	208
8.5.3.2 Evaluation of kinetic parameters for distributed activation energy model and thermodynamic triplets	211
8.5.4 Proximate analysis of biochar	215
8.5.5 Elemental analysis of biochar and bio-oil	215
8.5.6 Thermal stability analysis of biochar	216
8.5.7 FTIR analysis of biochar	216
8.5.8 XRD analysis of biochar	217
8.5.9 FESEM analysis of biochar	218
8.5.10 GC-MS analysis of bio-oil	218
8.5.11 Life cycle analysis	219
8.5.11.1 LCA Methodology	219
8.5.11.2 Goal & Scope Definition	220
8.5.11.3 Life Cycle Inventory Assessment (LCI)	220
8.5.11.4 Life Cycle Impact Assessment (LCIA)	220
8.5.11.5 LCA Results	221
8.6 Summary	223
9. Conclusions and Future Scope	227-234
Appendix	

List of Tables

Table No.	Table Title	Page No.
2.1	Ferric chloride Pretreatment for the Production of ethanol from Agro-biomass through sugar platform	11-18
2.2	Production of Ethanol from Biomass through Syngas Platform	19-23
2.3	Hydrothermal liquefaction (HTL) of biomass	24-36
2.4	Torrefaction of biomass	36-40
4.1	Association of Materials with Respective objectives	55-56
4.2	Association of Methods with Respective objectives	56-57
5.1	Proximate analysis, elemental analysis, chemical composition and metal composition of rice straw	68
5.2	Maximum products yield obtained from LWP, SAP and FCP	74-75
5.3	The yield of products from acid pretreatment on rice straw (literature and present study).	75-76
5.4	Comparison the composition of feedstock, the process parameters for FeCl_3 pretreatment on lignocellulosic biomass	76
5.5	Comparison the yields of products and degradation of xylan and glucan of present study with literature	77
5.6	Conversion of Xylan and Glucan along with degradation rate constants	80-81
5.7	Temperature span and gradient of %mass loss for RS and PRS following LWP, SAP and FCP corresponding to four distinct regions in TGA.	83
5.8	Reaction rates and Stoichiometric Coefficients of compounds in different reactions	87-88
5.9	Time concentration data for kinetic study	88-89
5.10	Stoichiometric Coefficient matrix for components participating in the reactions in cellulose conversion to glucose and other products	91
5.11	Values of the pre-exponential factors and activation energies for rate constants of xylan and cellulose conversion reactions (FeCl_3 concentration=0.2M)	93
5.12	Values of normalized root mean square error	98

5.13	Solid recovery and composition of pretreated solid (obtained from 0.2M FeCl ₃ pretreatment)	93
5.14	Coded levels of variables for the optimization of yields of xylose, glucose and furfural	99
5.15	Condition for optimum production for glucose, xylose and furfural yield (g/ kg of RS)	100
5.16	Coded levels of independent variables for degradation of carbohydrates	101
5.17	ANOVA Table for optimization xylan degradation.	101
5.18	ANOVA Table for optimization glucan degradation.	102
5.19	Optimum degradation of xylan and glucan	103
5.20	Variables with coded level used for RSM for degradation of xylan and glucan (%)	105
5.21	Coded levels of variables used for the optimization of $Y_{G,EH}$ and $Y_{G,C}$	111
5.22	ANOVA Table for optimization of $Y_{G,EH}$	111
5.23	ANOVA Table for optimization of $Y_{G,EH}$	112
5.24	Optimum glucose yield for enzymatic hydrolysis ($Y_{G,EH}$) and combined glucose yield during pretreatment and enzymatic hydrolysis ($Y_{G,C}$)	113
6.1	Operating parameters used for semi-batch reactor according to RSM	136- 137
6.2	Operating parameters for continuous operation according to RSM	137- 138
6.3	Process kinetics of growth by mixed clostridial strain - UACJUCHE1	140- 141
6.4	Variables with coded level used for semi-batch experimental run	144
6.5	Variables with coded level used for experimental run	144
6.6	Yield of the pyro-products	145- 146
6.7	Comparison the values k_1a for present study with literature	146- 147

6.8	Yield coefficient for different process (Vandecasteele, 2016)	147- 148
6.9	Values of mass transfer coefficients, Henry's constants, and kinetic parameters	148- 149
6.10	ANOVA table for the semi-batch bioreactor	156
6.11	ANOVA table for the continuous bioreactor	159
6.12	Comparison of operating parameters and results of the present study with similar studies	161
7.1	Variables with coded level used for experimental run	169
7.2	Operating parameters for production of bio-oil from co-HTL of JS and RS according to RSM	170
7.3	Proximate analysis of jute stick and rice straw	172
7.4	Values of rate constants involved in the hydrothermal liquefaction of jute stick and rice straw	179
7.5	Activation energies and pre-exponential factors of rate constants for HTL of JS and RS	179- 180
7.6	Ultimate analysis of hydrochar obtained from HTL of jute stick and rice straw	180
7.7	Ultimate analysis of bio-oil obtained from individual HTL of jute stick and rice straw	181
7.8	ANOVA table for Quadratic model	186
7.9	Model predicted and experimental values of the bio-oil yield from co-HTL of JS and RS under optimum condition	188
7.10	Ultimate analysis and HHVs of bio-oils obtained from individual and co-HTL	189
7.11	List of major compounds present in bio-oil obtained from HTL of JS (at 317.2 °C for 28.1 minutes) from GC-MS analysis (R.T. stands for retention time in minute)	190- 191
7.12	List of major compounds present in bio-oil obtained from HTL of RS (at 317.2 °C for 28.1 minutes) from GC-MS analysis	191
7.13	List of major compounds present in bio-oil obtained from co-HTL of JS and RS at optimum condition (at 317.2 °C for 28.1 minutes and 83.1% blending of jute stick in RS-JS mixture) from GC-MS analysis	192

7.14	Comparison the yield of bio-oil of present study with literature for HTL	195
7.15	Comparison the % yield of bio-oil of present study with literature for co-HTL	196
7.16	Comparison the HHV of bio-oil of present study with literature and Petroleum crude oil	197
7.17	Comparison the HHV of hydrochar of present study with literature	197-198
8.1	Values of rate constants involved in the torrefaction of mustard stalk	210
8.2	Activation energies and pre-exponential factors of rate constants for torrefaction and HTL reactions	211
8.3	Thermodynamic Triplets and Pre-exponential Factors for MS Pyrolysis at $\beta=10\text{K/min}$	214
8.4	Proximate analysis of raw-mustard stalk and biochar	215
8.5	Elemental analysis of raw-mustard stalk, biochar and bio-oil	216
8.6	List of major compounds present in bio-oil (produced from torrefaction of mustard stalk at 300°C) from GC-MS analysis.	219
8.7	Midpoint impacts of the torrefaction process at different temperatures	221-222

List of Figures

Figure No.	Figure Title	Page No.
5.1	Reactor used for pretreatment process	61
5.2	Proposed mechanisms for the formation of products obtained from HWP/SAP/FCP pretreatment (a: Xylan hydrolysis; b: Formation of furfural and degraded products from xylose; c: Conversion of glucan in presence of hydronium ions)	65
5.3	Heterogeneous and homogeneous catalytic action of hydronium ions during LWP/SAP/FCP (a: Shrinking core-like propagation of reaction front heterogeneous catalytic action of hydronium ion; b: Homogeneous reactions catalyzed by hydronium ions)	67
5.4	The yield of products obtained from pretreated liquor at different temperatures; (a), (c) and (e): the yield glucose, xylose and furfural obtained from LWP, SAP and FCP respectively; (b), (d) and (f): the yield of 5-HMF, formic acid, acetic acid and levulinic acid obtained from LWP, SAP and FCP	71
5.5	Plots of $\ln \frac{W_{Glucan,0}}{W_{Glucan}}$ against the reaction time using temperature as a parameter ((a): LWP; (c): SAP; (e): FCP) and Plots of $\ln \frac{W_{Xylan,0}}{W_{Xylan}}$ against the reaction time using temperature as a parameter ((b): LWP; (d): SAP; (f): FCP)	78
5.6	TG and DTG curves of RS (a); TG curves of RS and PRS (b)	82
5.7	a: FTIR of untreated and pretreated RS (where T and ν were the transmittance and wavenumber respectively); b: Crystallinity index (CrI) of untreated rice straw and pretreated rice straw; c: FESEM of untreated and pretreated RS (where c1: untreated RS, c2, c3 and c4: pretreated solid obtained from LWP, SAP and FCP at different magnification of image, 400 and 50 μ m); d: EDS results (where d1: untreated RS and d2: pretreated solid obtained from FCP)	85

5.8	Comparison the yield of products at different ferric chloride concentration	86
5.9	Mathematical model for xylan and cellulose conversion into valuable products (a: Conversion of Xylan into xylose and other products; b: Conversion of cellulose into glucose and other products) [* DP1 and DP2: decomposition products and xylose and furfural degradation]	87
5.10	Experimental values and model prediction of xylose (a), furfural (b) and acetic acid (c) concentration obtained from pretreatment of rice straw using 0.2M FeCl ₃ at 150-190°C for 5-15 minutes	95
5.11	Experimental values and model prediction of glucose (a), 5-HMF (b), formic acid (c) and levulinic acid (d) obtained from pretreatment of rice straw using 0.2M FeCl ₃ at 150-190°C for 5-15 minutes	96
5.12	RSM plot for glucose (a), xylose (b) and furfural (c) yield (g/ kg of RS) obtained from pretreatment of rice straw using 0.2M FeCl ₃ at 150-190°C for 5-15 minutes	100
5.13	Effect of pretreatment temperature and time on the response surface of xylan (a) and glucan degradation (b)	102
5.14	CS against pretreatment time and temperature ($CS_{xy}:a;CS_{cellu}:b$)	106
5.15	a: xylan degradation versus CS_{xy} ; b: glucan degradation versus CS_{cellu}	106
5.16	Glucose yield (%) after enzymatic hydrolysis of untreated RS and pretreated solids obtained from LWP, SAP and FCP	108
5.17	Mathematical model for enzymatic hydrolysis	108
5.18	Plot of $\frac{t}{-\ln(1-y_{G,EH})}$ versus t (a); Comparison the yield of glucose during enzymatic hydrolysis from Model with experimental data (b)	109
5.19	Effect of CS_{cellu} and enzyme loading (FPU/ g of dry substrate) on the response surface for glucose yield during enzymatic hydrolysis ($Y_{G,EH}$) (a) and combined glucose yield during pretreatment and enzymatic hydrolysis ($Y_{G,C}$) (b).	113
5.20	Ethanol production after enzymatic hydrolysis of raw-RS and pretreated solids for 72 hours for LWP/ SAP/ FCP (a); Ethanol production after	115

	enzymatic hydrolysis of raw-RS and pretreated solids (obtained at 170 °C, for 10 minutes using 0.2 M FeCl ₃ solution) for 24, 48 and 72 hours (b);	
5.21	Products separation from residual solid and liquid hydrolyzate obtained from the ferric chloride pretreatment of rice straw (Unit operation and Process Blocks: PRETREAT: pretreatment unit, VACUUMF1: vacuum filtration unit 1, REACTOR1: reactor for lignin solubilization, VACUUMF2: vacuum filtration unit 2, WASHING: washing unit, OVEN1: oven for drying cellulose, OVEN2: oven for lignin precipitation, CENTRIFU: centrifuge, VAC-DIST: vacuum distillation unit, MEM1: membrane 1, MEM2: membrane 2, ADSORP: adsorption unit, MEM3: membrane 3, DISTL1: Distillation unit 1, EXT-DSTL: extractive distillation unit)	116-17
5.22	Overall mass balance for LWP of rice straw followed by enzymatic hydrolysis and fermentation	119
5.23	Overall mass balance for SAP of rice straw followed by enzymatic hydrolysis and fermentation	119
5.24	Overall mass balance for FCP(0.1M FeCl ₃) of rice straw followed by enzymatic hydrolysis and fermentation	120
5.25	Overall mass balance 0.2M FeCl ₃ pretreatment of rice straw followed by enzymatic hydrolysis and fermentation	121
6.1	Schematic diagram of pyrolysis of rice straw	131
6.2	Stirred bioreactor for pyro-syngas fermentation (a: schematic diagram; b: reactor set-up)	134
6.3	Schematic diagram of the Wood-Ljungdahl pathway for the production of Ethanol from syngas (Acetyl-CoA: Acetyl coenzyme A; CODH: Carbon monoxide dehydrogenase; FDH: Formate dehydrogenase; Syngas: Synthesis gas)	139-140
6.4	Composition of pyro-syngas produced at different pyrolysis temperatures	145
6.5	Simulated profile for semi-batch reactor ((a): Ethanol; (b): acetic acid; (c): gas conversion %)	151

6.6	Simulated profile for the continuous reactor ((a): ethanol concentration; (b): acetic acid concentration and (c): % gas conversion	152
6.7	Ethanol production in the semi-batch reactor (pyrolysis temperature = 600 °C, $V_G/V_L = 0.5$, and $q_G = 6$ Lpm)	153
6.8	Ethanol production from syngas fermentation in the continuous reactor (model prediction and experimental value). ((a): Variation of experimental and simulated ethanol concentration with $V_G/V_L (=0.6-1)$ at a fixed value of $q_G/q_L = 250$; (b) Variation of experimental and simulated ethanol concentration with $q_G/q_L (=30-250)$ at a fixed value of $V_G/V_L (=0.6)$).	153-154
6.9	Effect of the gas residence time (GRT) and dilution factor (D) on the volumetric productivity of ethanol from syngas fermentation	155
6.10	Comparison between the RSM–predicted and experimental values of ethanol concentration at 30 h of semi-batch operation	156
6.11	Response surface plots for the optimization of ethanol (g/L) production from syngas fermentation ((a–c): interaction between AB, AC and BC respectively)	157
6.12	Comparison between the RSM-predicted and experimental values of ethanol concentration at 300 h of continuous operation	158
6.13	Response surface plots for the optimization of ethanol (g/L) production from syngas fermentation	160
7.1	Schematic diagram of hydrothermal liquefaction of jute stick and rice straw	168
7.2	Reaction network for hydrothermal liquefaction of biomass (jute stick or rice straw)	171
7.3	Composition (cellulose, hemicellulose and lignin) of JS and RS	173
7.4	Product yield (%) at different temperature a: jute stick, b: rice straw) [Holding period: 30 minutes]	174
7.5	Plot of $W_{Biomass_t}$ versus time (a: HTL of JS; d: HTL of RS); Plot of $W_{Bio-oil_t}$ versus time (b: HTL of JS; e: HTL of RS); Plot of W_{Aq-G_t} versus time (c: HTL of JS; f: HTL of RS)	175

7.6	Plot of $\ln\left(\frac{W_{Biomass_0}}{W_{Biomass_t}}\right)$ against holding time, t (a: HTL of JS; b: HTL of RS)	176
7.7	Plot of $W_{Bio-oil,t}$ versus $\left[\frac{W_{Biomass_0}}{k'}[1 - \exp(-k't)]\right]$ at 240°C (a: HTL of JS; d: HTL of RS); Plot of $W_{Bio-oil,t}$ versus $\left[\frac{W_{Biomass_0}}{k'}[1 - \exp(-k't)]\right]$ at 300°C (b: HTL of JS; e: HTL of RS); Plot of $W_{Bio-oil,t}$ versus $\left[\frac{W_{Biomass_0}}{k'}[1 - \exp(-k't)]\right]$ at 360°C (c: HTL of JS; f: HTL of RS)	177
7.8	Plot of $W_{Aq-G,t}$ versus $\left[\frac{W_{Biomass_0}}{k'}[1 - \exp(-k't)]\right]$ at 240°C (a: HTL of JS; d: HTL of RS); Plot of $W_{Aq-G,t}$ versus $\left[\frac{W_{Biomass_0}}{k'}[1 - \exp(-k't)]\right]$ at 300°C (b: HTL of JS; e: HTL of RS); Plot of $W_{Aq-g,t}$ versus $\left[\frac{W_{Biomass_0}}{k'}[1 - \exp(-k't)]\right]$ at 360°C (c: HTL of JS; f: HTL of RS)	178
7.9	Van Krevelen diagram for raw biomass, hydrochar and bio-oil of jute stick (a) and rice straw (b)	182
7.10	TG analysis raw-biomass and hydrochar (a, b: TGA and DTG of raw-JS and raw-RS; c, d: TGA of raw-biomass and hydrochar of JS, RS respectively)	183
7.11	FT-IR analysis raw-biomass and hydrochar (a) (a1: FT-IR of raw-JS and hydrochar of JS; a2: FT-IR of raw-RS and hydrochar of RS respectively); XRD analysis raw-biomass and hydrochar (b) (b1: XRD of raw-JS and hydrochar of JS; b2: XRD of raw-RS and hydrochar of RS respectively)	184- 185
7.12	FESEM analysis raw-JS (a), raw-RS (b), hydrochar of JS (c) and hydrochar of RS (d)	185
7.13	Response surface plots for optimization of bio-oil (%) production from co-HTL of JS and RS (a: interaction between temperature and time; b: interaction between temperature and % blending of jute stick in RS-JS mixture; c: interaction between time and % blending of jute stick in RS-JS mixture; d: actual versus predicted response)	187
7.14	Main class of compounds present in bio-oils	190

7.15	Congo red removal (%) at different reaction time at different pH	193
7.16	Plot of $\frac{t}{q_t}$ versus t (the pH of the solution = 3)	194
8.1	Schematic diagram of experimental setup of torrefaction of mustard stalk	204
8.2	Yield of products at different temperature (for 30 minutes reaction time)	208
8.3	Plot of $\ln\left(\frac{W_0}{W}\right)$ versus time	209
8.4	Plot of W_v versus $\left[\frac{W_0}{k} [1 - \exp(-kt)]\right]$ at 200°C, 300 °C and 400 °C (a, b and c) and Plot of W_c versus $\left[\frac{W_0}{k} [1 - \exp(-kt)]\right]$ at 200°C, 300 °C and 400 °C (d, e and f)	209- 210
8.5	Plot of $\ln k$ versus 1/T (a); Plot of $\ln k_v$ versus 1/T (b) and Plot of $\ln k_c$ versus 1/T (c)	210- 211
8.6	TGA plot of raw-mustard straw at different heating rate (a: 10 °C/min; b: 20 °C/min; c: 30 °C/min; d: 40 °C/min)	212
8.7	Kinetic Plot for determination of kinetic parameters using Tang method and (b) Evolution trend of Activation Energies against for Mustard Stalk (MS) Torrefaction	213
8.8	TGA analysis of raw-MS and biochar (a); FTIR analysis of raw-MS and biochar (b); XRD analysis of raw-MS and biochar (c).	217
8.9	FESEM analysis of raw-MS and biochar (a: raw-mustard stalk, b: biochar)	218
8.10	Main class of compounds present in bio-oil obtained from torrefaction of mustard stalk	218
8.11	System Boundary of LCA of Mustard Stalk Torrefaction.	220
8.12	Comparing Torrefaction at different temperatures Method: ReCiPe 2016 Endpoint (H) V1.04 / World (2010) H/H / Normalization	222

Chapter 1

Introduction

Chapter 1: Introduction

The mitigation of CO₂ emission from energy sector is possible through the switching over from high carbon to low carbon fuels. The use of low-carbon renewable and sustainable biofuels, derived from waste biomass can serve the purpose of reaching the current energy targets along with reduction of CO₂ emissions. Globally, the lignocellulosic waste generated from agricultural sector represents the major waste biomass. India, being rich in agriculture, produces a large quantity of agro-waste, namely, rice husk and straw, jute stick, mustard stalk, mustard press cake, wheat straw, corn stover, sugarcane bagasse, sugarcane tops and leaves rapeseed straw, banana pseudo stem, maize straw, sesame stalks coconut shell, coconut coir and pith, areca nut, etc (Chowdhury et al, 2018). Transformation of biomass to bioenergy is traditionally conducted by employing different thermochemical (gasification, pyrolysis, torrefaction and hydrothermal liquefaction) and biochemical (fermentation and anaerobic digestion) processes or through their integration, e.g., syngas fermentation (Chen et al, 2022; Chowdhury et al, 2019; De Caprariis et al, 2017; Ru et al, 2015). Commercialization of bioethanol production from lignocellulosic biomass is one of the important areas under rigorous research and development to support the national ethanol blend-in targets of India. Under Ethanol Blending Program (EBP20) by 2025, India has to reduce crude import dependence and support “Atmanirbhar Bharat” and “Make in India” initiatives. Lignocellulosic biomass can be converted to ethanol either through sugar or syngas platform. In case of sugar platform biomass is first hydrolysed to simple sugars like hexose (glucose), pentose (xylose, arabinose etc) and the cellulose part of pretreated biomass is enzymatically converted to glucose. Ultimately glucose is fermented to ethanol. The biomass to ethanol conversion through syngas platform is an integration of thermochemical and biochemical pathways. Syngas, generated from biomass through gasification/pyrolysis, is converted to ethanol (Chowdhury et al, 2019; Ru et al, 2015). As India still faces the pollution created by stubble burning, the generation of bioethanol through sugar platform and syngas fermentation from Indian biomass can amply reduce the problem of CO₂ emission. The lignocellulosic biomass can also be converted into valuable products such as char, bio-oil and gaseous products via thermochemical processes like hydrothermal liquefaction, torrefaction, etc (Chen et al, 2022; Pacheco et al, 2023; De Caprariis et al, 2017). While char can be utilized as adsorbent, soil amendment and dye removal, bio-oil and gaseous products can be upgraded to fuel and valuable chemicals (Harisankar et al, 2022; Ru et al, 2015).

Considering the necessity of energy transition to address the issue of CO₂ emission in India and the abundance of agricultural lignocelluloses biomass the thrust areas of the present research are: I) conversion of Indian agro-biomass to ethanol via sugar platform with possible analysis of each step along with kinetic analysis, mathematical modeling and optimization; II) conversion of Indian agro-biomass to ethanol via syngas platform with possible analysis of each step along with kinetic analysis, mathematical modeling and optimization; III) conversion of Indian agro-biomass through HTL and co-HTL and introspective analysis along with kinetic studies and optimization; iv) conversion of Indian agro-biomass through torrefaction with kinetic studies and product characterization

1.1 Production of ethanol from biomass through sugar platform

Pretreatment processes play the key role when lignocellulosic biomass has to be converted to biofuels through sugar platform (Chen et al, 2022; Shen et al, 2022; Fakayode et al, 2021; Choi et al, 2019; Chowdhury et al, 2019). The release of fermentable sugars is the pre-condition for the conversion of lignocellulosic biomass (LCB) to biofuels via heterotrophic microorganisms. The structure of LCB is constituted of carbohydrate polymers like cellulose and hemicellulose, tightly bound to lignin backbone. Therefore, all pretreatment processes focus on the destruction of the chemical bonds of carbohydrates responsible for their bonding to lignin and subsequent depolymerization. As the pretreatment process is actually an auxiliary step for biofuel production it should be simple, less energy consuming and environmentally friendly. From this perspective a few pretreatment processes like mild temperature liquid water pretreatment (LWP), dilute acid pretreatment (DAP) and metal chloride pretreatment (MCP) are followed (Banerjee et al, 2022; Li et al, 2022; Yang et al, 2013; Yu et al, 2010). All of these pretreatment processes are driven by the catalytic action of the hydronium ion. Through all these processes xylose and glucose are released from hemicellulose and cellulose respectively. It has been reported that in addition to xylose and glucose, some valuable intermediate side products, namely, furfural, 5-hydroxymethyl furfural (5-HMF), formic acid, acetic acid, levulinic acid etc are also generated during LWP, DAP and MCP (Yan et al, 2014; Kamireddy et al, 2013). Furfural, 5-HMF and levulinic acid have been used for the production of fuels and other valuable chemicals (Chai et al, 2013; Peng et al, 2010). Being simultaneously an aromatic alcohol, aldehyde and a furan, 5-HMF is an important platform chemical convertible to value-added chemicals (Marcotullio & Jong, 2010). On the other hand, acetic acid and formic acid have many applications of their own. The pretreated solid obtained

after the catalytic pretreatment becomes suitable for enzymatic hydrolysis for further glucose release. Recently, hydronium ion based pretreatment processes, particularly, metal chloride and acid based ones, have been also found effective for the enhancement of biogas generation (Rahmani et al, 2022). Mild temperature liquid water pretreatment (LWP) below the decomposition condition of biomass is also gaining importance because of the greenness of the solvent and less severity of the operating condition. Although the acid pretreatment processes are well studied for many lignocellulosic feedstocks, the data on LWP and MCP are limited. However, unlike LWP and MCP, the liquid effluent of acid pretreatment poses environmental concern (Tang et al, 2021; Chimentão et al, 2104). The enzymatic hydrolysis of pretreated solid is conducted in presence of enzyme (Zhang et al, 2018). The glucose produced from enzymatic hydrolysis, is converted to bio-ethanol via fermentation using microorganism (Drapcho et al, 2008).

1.2 Production of ethanol from biomass through syngas platform

The syngas fermentation is a hybrid process through which syngas, mainly constituted of CO and H₂, is generated from lignocellulosic biomass in the first step, and subsequently the gas is fermented to bioethanol in the second step. In most of the cases syngas from biomass is produced through gasification (Pacheco et al, 2023; Chowdhury et al, 2019). Pyrolysis of biomass generating pyro-char, pyro oil and pyro-syngas is expected to play an important role in the development of hybrid processes combining thermochemical and biochemical processes (Chowdhury et al, 2019). As pyrogas usually contains CO, H₂ and CO₂, it has a prospect to be used in syngas platform of ethanol production. In case of high ash containing biomass, solid waste is generated during gasification. Unlike gasification, the generation of pyro-syngas does not generate any wastes because pyro-char is used as fuel, adsorbent and for soil amendment and pyro-oil can be used as a liquid fuel after up-gradation (Li et al, 2023; Li et al, 2023; Chen et al, 2022; Faraji&Saidi, 2022; Esquivel-Elizondo et al, 2017).

1.3 Hydrothermal liquefaction (HTL) of Biomass

Lignocellulosic biomass (LCB) can be converted into four fractions namely, hydrochar, bio-oil, aqueous and gaseous phase products during hydrothermal liquefaction (HTL) in the temperature range of 200-400 °C (Harisankar et al, 2022; De Caprariis et al, 2017). In HTL pretreatment method, the lignocellulosic feedstocks are easily hydrolyzed to sugar molecules (poly-, oligo and mono-saccharides) which are subsequently converted to cyclic ketones, phenols etc. via

isomerization step. Some alcohols, aldehydes for instance, are also formed particularly during the decomposition of lignin. A part of xylan and glucan in biomass are also converted into small organic compounds, obtained in aqueous phase. The gases namely, carbon mono-oxide (CO), carbon di-oxide (CO₂), hydrogen (H₂), methane (CH₄), nitrogen (N₂) and ethane (C₂H₆) are present in the gaseous fraction (Wang et al, 2023). Solid products are usually formed due to the re-polymerisation of oligosaccharides. The oxygen and water contents of bio-oil, obtained from biomass HTL, are less and the higher heating values (HHV) are, in turn more than those of oil products of conventional pyrolysis (Harisankar et al, 2022; Mathanker et al, 2020). The biomass composition (cellulose, hemicellulose, and lignin) and reaction temperature have a great influence on the yield of the products (Harisankar et al, 2022). Indeed, the HTL pretreatment of LCB for hydrochar, bio-oil and other bio-products is gaining high importance to scale up the biomass conversion technologies. Unlike pyrolysis, HTL can handle wet biomass ensuring the avoidance of pre-drying energy (Mathanker et al, 2020). As non-catalytic HTL does not need addition of chemicals, there is no need of corrosion-resistant materials of construction for hydrolysis reactors (Chandra et al, 2012).

The co-hydrothermal liquefaction of two biomass having different lignocellulosic composition is also a subject of interest of many researchers in the recent years.

1.4 Torrefaction of biomass

Torrefaction has been considered as a promising technology for the production of valuable products like biochar, volatile liquid, and non-condensable gaseous component from biomass at lower temperature range (200 - 400 °C) in absence of air or oxygen (Priya et al, 2023; Jagadale et al, 2023). Other than production of char, bio-oil and gas through structural decomposition, torrefaction also improves flow properties and grindability of biomass (Ru et al, 2015). Torrefaction also enhances the hydrophobicity of biomass and hence reduces the susceptibility to microbial degradation. Under the scenario of the necessity to transport biomass from the sources and subsequent mixing with coal etc. for power generation, torrefaction is considered as one of the promising pretreatment technology (Khan and Chowdhury, 2021; Ru et al, 2015). Compared to pyrolysis, torrefaction is low energy intensive process. All torrefaction products, namely bio-char, bio-oil and gas have prospective usage.

References

- Banerjee, S., Singh, R., Eilts, K., Sacks, E. J., & Singh, V. (2022). Valorization of *Miscanthus x giganteus* for sustainable recovery of anthocyanins and enhanced production of sugars. *Journal of Cleaner Production*, 369, 133508.
- Chai, Y., Bai, M., Chen, A., Yuan, J., Peng, L., Shao, J., Zhou, Z. (2022). Introduction of acid mine drainage in the direct production of 5-hydroxymethylfurfural from raw biomass and expanding the use of biomass conversion residue. *Bioresource Technology*, 364, 128094.
- Chandra, R., Takeuchi, H., & Hasegawa, T. (2012). Hydrothermal pretreatment of rice straw biomass: a potential and promising method for enhanced methane production. *Applied Energy*, 94, 129-140.
- Chen, D., Zhuang, X., Gan, Z., Cen, K., Ba, Y., & Jia, D. (2022). Co-pyrolysis of light bio-oil leached bamboo and heavy bio-oil: Effects of mass ratio, pyrolysis temperature, and residence time on the biochar. *Chemical Engineering Journal*, 437, 135253.
- Chen, X., Liu, S., Zhai, R., Yuan, X., Yu, Y., Shen, G., Jin, M. (2022). Lime pretreatment of pelleted corn stover boosts ethanol titers and yields without water washing or detoxifying pretreated biomass. *Renewable Energy*, 192, 396-404.
- Chimentão, R. J., Lorente, E., Gispert-Guirado, F., Medina, F., & López, F. (2014). Hydrolysis of dilute acid-pretreated cellulose under mild hydrothermal conditions. *Carbohydrate polymers*, 111, 116-124.
- Chowdhury, R., Ghosh, S., Debnath, B., & Manna, D. (2018). Indian agro-wastes for 2G biorefineries: Strategic decision on conversion processes. *Sustainable Energy Technology and Policies: A Transformational Journey, Volume 1*, 353-373.
- Chowdhury, R., Ghosh, S., Manna, D., Das, S., Dutta, S., Kleinstuber, S., Strauber, H., Hassan, M. K., Kuittinen, S., Pappinen, A. (2019). Hybridization of sugar-carboxylate-syngas platforms for the production of bio-alcohols from lignocellulosic biomass (LCB)—A state-of-the-art review and recommendations. *Energy conversion and management*, 200, 112111.

De Caprariis, B., De Filippis, P., Petrullo, A., & Scarsella, M. (2017). Hydrothermal liquefaction of biomass: Influence of temperature and biomass composition on the bio-oil production. *Fuel*, 208, 618-625.

Drapcho, C. M., Nghim, N. P., & Walker, T. (2008). *Biofuels engineering process technology*. McGraw-Hill Education.

Esquivel-Elizondo, S., Delgado, A. G., Rittmann, B. E., & Krajmalnik-Brown, R. (2017). The effects of CO₂ and H₂ on CO metabolism by pure and mixed microbial cultures. *Biotechnology for biofuels*, 10, 1-13.

Fakayode, O. A., Akpabli-Tsigbe, N. D. K., Wahia, H., Tu, S., Ren, M., Zhou, C., & Ma, H. (2021). Integrated bioprocess for bio-ethanol production from watermelon rind biomass: Ultrasound-assisted deep eutectic solvent pretreatment, enzymatic hydrolysis and fermentation. *Renewable Energy*, 180, 258-270.

Harisankar, S., Mohan, R. V., Choudhary, V., & Vinu, R. (2022). Effect of water quality on the yield and quality of the products from hydrothermal liquefaction and carbonization of rice straw. *Bioresource Technology*, 351, 127031.

Jagadale, M., Gangil, S., & Jadhav, M. (2023). Enhancing fuel characteristics of jute sticks (*Corchorus Sp.*) using fixed bed torrefaction process. *Renewable Energy*, 215, 118992.

Kamireddy, S. R., Li, J., Tucker, M., Degenstein, J., & Ji, Y. (2013). Effects and mechanism of metal chloride salts on pretreatment and enzymatic digestibility of corn stover. *Industrial & Engineering Chemistry Research*, 52(5), 1775-1782.

Khan, A. K., & Chowdhury, R. (2021). Parametric sensitivity of municipal solid waste integrated power plant: CO₂ footprint and energy analysis. *Chemical Engineering & Technology*, 44(2), 291-299.

Li, J., Liu, W., Meng, J., Zhao, L., Li, J., & Zheng, M. (2022). Mesothermal pretreatment using FeCl₃ enhances methane production from rice straw. *Renewable Energy*, 188, 670-677.

Li, N., Pan, Y., Yan, Z., Liu, Q., Yan, Y., & Liu, Z. (2023). Cornstalk pyrolysis for syngas in a two-stage electromagnetic induction reactor. *Fuel*, 336, 127124.

- Li, X., Liu, P., Huang, S., Wu, S., Li, Y., Wu, Y., & Lei, T. (2023). Study on the mechanism of syngas production from catalytic pyrolysis of biomass tar by Ni–Fe catalyst in CO₂ atmosphere. *Fuel*, 335, 126705.
- Marcotullio, G., & De Jong, W. (2010). Chloride ions enhance furfural formation from D-xylose in dilute aqueous acidic solutions. *Green chemistry*, 12(10), 1739-1746.
- Mathanker, A., Pudasainee, D., Kumar, A., & Gupta, R. (2020). Hydrothermal liquefaction of lignocellulosic biomass feedstock to produce biofuels: Parametric study and products characterization. *Fuel*, 271, 117534.
- Pacheco, M., Moura, P., & Silva, C. (2023). A systematic review of syngas bioconversion to value-added products from 2012 to 2022. *Energies*, 16(7), 3241.
- Peng, L., Lin, L., Zhang, J., Zhuang, J., Zhang, B., & Gong, Y. (2010). Catalytic conversion of cellulose to levulinic acid by metal chlorides. *Molecules*, 15(8), 5258-5272.
- Priya, A. K., Alagumalai, A., Balaji, D., & Song, H. (2023). Bio-based agricultural products: a sustainable alternative to agrochemicals for promoting a circular economy. *RSC Sustainability*, 1(4), 746-762.
- Rahmani, A. M., Gahlot, P., Moustakas, K., Kazmi, A. A., Ojha, C. S. P., & Tyagi, V. K. (2022). Pretreatment methods to enhance solubilization and anaerobic biodegradability of lignocellulosic biomass (wheat straw): Progress and challenges. *Fuel*, 319, 123726.
- Ru, B., Wang, S., Dai, G., & Zhang, L. (2015). Effect of torrefaction on biomass physicochemical characteristics and the resulting pyrolysis behavior. *Energy & Fuels*, 29(9), 5865-5874.
- Shen, G., Yuan, X., Chen, S., Liu, S., & Jin, M. (2022). High titer cellulosic ethanol production from sugarcane bagasse via DLCA pretreatment and process development without washing/detoxifying pretreated biomass. *Renewable Energy*, 186, 904-913.
- Tang, W., Wu, X., Huang, C., Ling, Z., Lai, C., & Yong, Q. (2021). Revealing the influence of metallic chlorides pretreatment on chemical structures of lignin and enzymatic hydrolysis of waste wheat straw. *Bioresource Technology*, 342, 125983.

Wang, Z. C., Hou, X. K., Wang, Y. B., Collins, E., & Duan, P. G. (2023). Hydrothermal liquefaction of soybean straw: Effect of steam explosion pretreatment and reaction media. *Fuel*, 339, 127418.

Yan, L., Greenwood, A. A., Hossain, A., & Yang, B. (2014). A comprehensive mechanistic kinetic model for dilute acid hydrolysis of switchgrass cellulose to glucose, 5-HMF and levulinic acid. *Rsc Advances*, 4(45), 23492-23504.

Yang, M., Kuittinen, S., Zhang, J., Keinänen, M., & Pappinen, A. (2013). Effect of dilute acid pretreatment on the conversion of barley straw with grains to fermentable sugars. *Bioresource technology*, 146, 444-450.

Yu, G., Yano, S., Inoue, H., Inoue, S., Endo, T., & Sawayama, S. (2010). Pretreatment of rice straw by a hot-compressed water process for enzymatic hydrolysis. *Applied biochemistry and biotechnology*, 160, 539-551.

Zhang, H., Lyu, G., Zhang, A., Li, X., & Xie, J. (2018). Effects of ferric chloride pretreatment and surfactants on the sugar production from sugarcane bagasse. *Bioresource technology*, 265, 93-101.

Chapter 2

Literature review

Chapter 2: Literature review

2.1 Ferric chloride Pretreatment for the Production of ethanol from Agro-biomass through sugar platform

Year of Publication	Biomass treated & Type of hydronium ion- based treatment	Treatment condition	Salient findings	Research limitations	References
2023	Sugarcane postharvest leaves	Concentration of ferric chloride: 0.1M Pretreatment time: 3 hours Pretreatment temperature: 120 °C	<ul style="list-style-type: none"> • The maximum degradation of hemicellulose has been achieved as 85% whereas the delignification was determined as 74%. • The maximum yield of glucose during enzymatic hydrolysis has been found as 85.5%. • The maximum yield of ethanol has been reported as 0.434 g/ g of glucose. 	<ul style="list-style-type: none"> ➤ Hydronium-ion based mechanism has not been explained ➤ Kinetics of the pretreatment methods have not been determined ➤ Mathematical model for the pretreatment method has not been developed. ➤ Relationship between the process severity and the 	Palliprath et al.

				<p>performance of pretreatment method has not been determined.</p> <p>➤ The kinetics of enzymatic hydrolysis of pretreated solid has not been determined.</p> <p>➤ Comparative analysis of ethanol yield from biomass with respect to the variation of pretreatment parameters has not been done.</p>	
2021	Wheat straw	<p>Concentration of ferric chloride:0.02M-0.1M</p> <p>Pretreatment time: 40 minutes</p> <p>Pretreatment temperature: 180 °C</p>	<ul style="list-style-type: none"> The maximum degradation of xylan has been obtained as 97.2% whereas the delignification has been determined as 35.2% for 0.1M FeCl₃. The recovery of glucan has been reported 	<p>➤ Hydronium-ion based mechanism has not been explained</p> <p>➤ Kinetics of the pretreatment methods have not been determined</p>	Tang et al.

			<p>as 50.1% for 0.1M FeCl₃.</p> <ul style="list-style-type: none"> • The maximum xylose, glucose, furfural, 5-hydroxy methyl furfural (5-HMF), formic acid and acetic acid concentration have been measured as 0.4 g/L, 0.9 g/L, 2.6 g/L, 1.1 g/L, 0.8 g/L and 19 g/L respectively. • The maximum yield of glucose during enzymatic hydrolysis has been found as 82.9%. 	<ul style="list-style-type: none"> ➤ Mathematical model for the pretreatment method has not been developed. ➤ Relationship between the process severity and the performance of pretreatment method has not been determined. ➤ The kinetics of enzymatic hydrolysis of pretreated solid has not been determined. ➤ Comparative analysis of ethanol yield from biomass with respect to the variation of pretreatment parameters has not been done. 	
2018	Rapeseed straw	Concentration of ferric	<ul style="list-style-type: none"> • The maximum degradation of 	<ul style="list-style-type: none"> ➤ Hydronium-ion based 	Romero et al.

		chloride: 0.1-0.3M Pretreatment time: 20 minutes Pretreatment temperature: 120-160 °C	<p>hemicellulose and glucan have been reported as 100% and 33.2% respectively for 0.3M FeCl₃ and combined severity (CS) 2.29.</p> <ul style="list-style-type: none"> • At 2.29 CS, the concentrations of glucose and xylose have been determined as 4.93 g/L and 1.09 g/L respectively. • The maximum yield of glucose during enzymatic hydrolysis is 63.08%. 	<p>mechanism has not been explained.</p> <p>➤ Kinetics of the pretreatment methods have not been determined</p> <p>➤ Mathematical model for the pretreatment method has not been developed.</p> <p>➤ Comparative analysis of ethanol yield from biomass with respect to the variation of pretreatment parameters has not been done.</p>	
2018	Sugarcane bagasse	Concentration of ferric chloride: 0.2M Pretreatment time: 20 minutes	<ul style="list-style-type: none"> • The maximum degradation of xylan and glucan have been reported as 99.6% and 34.8% respectively. 	<p>➤ Hydronium-ion based mechanism has not been explained</p> <p>➤ Kinetics of the pretreatment methods have</p>	Zhang et al.

		<p>Pretreatment temperature: 160 °C</p>	<ul style="list-style-type: none"> • The yield (g of product/ 100 g of rapeseed straw) of glucose, xylose, furfural, 5-HMF and acetic acid have been determined as 6.9, 5.2, 6.6, 0.5 and 2.4 respectively. 	<p>not been determined.</p> <ul style="list-style-type: none"> ➤ Mathematical model for the pretreatment method has not been developed. ➤ Relationship between the process severity and the performance of pretreatment method has not been determined. ➤ The kinetics of enzymatic hydrolysis of pretreated solid has not been determined. ➤ Comparative analysis of ethanol yield from biomass with respect to the variation of pretreatment parameters has not been done. 	
--	--	---	--	--	--

2015	Rice straw	<p>Concentration of ferric chloride: 0.1M</p> <p>Pretreatment time: 30 minutes</p> <p>Pretreatment temperature: 170 °C</p>	<ul style="list-style-type: none"> • The maximum degradation of xylan and glucan has been reported as 83.28% and 13.14% respectively. • The maximum concentrations of glucose, xylose, furfural and 5-HMF have been determined as 17.1 g/L, 3.18 g/L, 6.48 g/L and 0.232 g/L respectively. • The highest concentration of glucose obtained from enzymatic hydrolysis of pretreated rice straw has been determined as 11.9 g/L. • 0.143 kg bio-ethanol has been produced from 1 kg of rice straw. 	<ul style="list-style-type: none"> ➤ Hydronium-ion based mechanism has not been explained ➤ Kinetics of the pretreatment methods have not been determined ➤ Mathematical model for the pretreatment method has not been developed. ➤ Relationship between the process severity and the performance of pretreatment method has not been determined. ➤ The kinetics of enzymatic hydrolysis of pretreated solid has not been determined. ➤ Comparative 	Chen et al.
------	------------	--	--	--	-------------

				analysis of ethanol yield from biomass with respect to the variation of pretreatment parameters has not been done.	
2013	Corn stover	<p>Concentration of ferric chloride: 0.075M – 0.125M</p> <p>Pretreatment time: 10 minutes</p> <p>Pretreatment temperature: 150-160 °C</p>	<ul style="list-style-type: none"> The maximum concentration of glucose, furfural, acetic acid and 5-HMF have been determined as 4.65 g/L, 1.96 g/L, 3.30 g/L and 0.52 g/L respectively. 	<ul style="list-style-type: none"> ➤ Hydronium-ion based mechanism has not been explained ➤ Kinetics of the pretreatment methods have not been determined ➤ Mathematical model for the pretreatment method has not been developed. ➤ Relationship between the process severity and the performance of pretreatment method has not been 	Kemireddy et al.

				<p>determined.</p> <ul style="list-style-type: none"> ➤ The kinetics of enzymatic hydrolysis of pretreated solid has not been determined. ➤ Comparative analysis of ethanol yield from biomass with respect to the variation of pretreatment parameters has not been done. 	
--	--	--	--	--	--

Research gap

While the mechanism of action of hydronium ions during ferric chloride pretreatment of biomass has been elucidated in some published literature, there are scopes for the comprehensive representation of a reaction scheme incorporating the role of both homogeneous and heterogeneous reactions during pretreatment (Kamireddy et al, 2013). Ferric chloride pretreatment of different types of biomass have been reported in literature using different experimental parameters, i.e., temperature range and pretreatment time for different pretreatment processes (Kamireddy et al, 2013; Romero et al, 2018). Comparative studies of Ferric chloride pretreatment using same temperature range and pretreatment time for any biomass can only clarify difference in the response pattern towards different pretreatment processes and the justification can be searched through in-depth introspection of product patterns and characteristics as well as reaction kinetics of degradation of carbohydrate polymers.

Although a few studies have been reported on the FeCl_3 pretreatment of rice straw, there is a dearth of systematic data on the effects of pretreatment time, temperature and strength of ferric chloride (Chen et al, 2015). It is understandable that for the implementation of any process in a large scale based on laboratory scale data, it is important to develop the kinetic equations which can be used in process simulation software, like ASPEN Plus. However, no such mathematical model is available. The characterization of pretreated solid is also important for the further use through enzymatic hydrolysis and the thermochemical application of the lignin-rich residual solid after enzymatic hydrolysis. However, such data on FeCl_3 pretreated rice straw are limited (Chen et al, 2015).

2.2 Production of Ethanol from Biomass through Syngas Platform

Year of Publication	Composition of syngas and microorganism used	Mode of operation	Salient findings	Research limitations	References
2022	Pure CO has been used. <i>Clostridium carboxidivorans</i> has been used.	Batch mode and continuous mode	<ul style="list-style-type: none"> • A dynamic CO gas fermentation model was developed. • Ethanol concentration was determined as 0.4 g/L when the reactor was operated in batch mode. • Ethanol concentration was measured as 5.6 g/L when the 	<ul style="list-style-type: none"> ➤ No thermochemical process has been used for the generation of syngas. ➤ Syngas was not generated from lignocellulosic biomass. 	Ruggiero et al.

			reactor was operated in continuous mode.		
2020	The composition of syngas was 25%CO and 75%. <i>Clostridium ljungdahlii</i> has been used.	Continuous mode	<ul style="list-style-type: none"> Ethanol concentration was determined as 1.304 g/L. 	<ul style="list-style-type: none"> ➤ No thermochemical process has been used for the generation of syngas. ➤ Syngas has not generated from lignocellulosic biomass. 	Benalcazar et al.
2019	The composition of syngas was 50% CO, 10% CO ₂ , 20% H ₂ and 15% inert. <i>Clostridium ljungdahlii</i> has been used.	Continuous mode	<ul style="list-style-type: none"> Ethanol concentration was determined as 45.0 g/L. 	<ul style="list-style-type: none"> ➤ No thermochemical process has been used for the generation of syngas. ➤ Syngas has not generated from lignocellulosic biomass. 	de Medeiros et al.
2019	The composition of syngas was 30% CO, 10% CO ₂ , 20% H ₂ and 40% N ₂ .	Continuous mode	<ul style="list-style-type: none"> Ethanol concentration was determined as 5.912 g/L. 	<ul style="list-style-type: none"> ➤ No thermochemical process has been used for the generation of syngas. 	Fernandez-Naveira et al.

	<i>Clostridium carboxidivorans</i> has been used.			<ul style="list-style-type: none"> ➤ Syngas has not generated from lignocellulosic biomass. ➤ Reaction kinetics has not been determined. ➤ No mathematical model is developed. ➤ Optimization of the operation has not been done. 	
2016	<p>The composition of syngas was 32% CO, 8% CO₂, 32% H₂ and 28% N₂.</p> <p><i>Clostridium ljungdahlii</i> has been used.</p>	Batch mode	<ul style="list-style-type: none"> • Ethanol concentration was determined as 0.778 g/L. 	<ul style="list-style-type: none"> ➤ No thermochemical process has been used for the generation of syngas. ➤ Syngas has not been generated from lignocellulosic biomass. ➤ Optimization of the operation has not been done. 	Vandecasteele J.
2014	The composition of syngas was 20% CO, 15% CO ₂ , 20% H ₂ ,	Batch mode	<ul style="list-style-type: none"> • Ethanol concentration was determined as 2.2 g/L. 	<ul style="list-style-type: none"> ➤ No thermochemical process has been used for the 	Singla et al.

	<p>20% CH₄ and 3% N₂.</p> <p>Mixed culture has been used.</p>			<p>generation of syngas.</p> <ul style="list-style-type: none"> ➤ Syngas has not been generated from lignocellulosic biomass. ➤ Reaction kinetics has not been determined. ➤ No mathematical model is developed. ➤ Optimization of the operation has not been done. 	
2014	<p>The composition of syngas was 28% CO, 60% H₂ and 12% N₂.</p> <p><i>Alkalibaculum acchi</i> has been used.</p>	Continuous mode	<ul style="list-style-type: none"> • Ethanol concentration was determined as 6.39 g/L. 	<ul style="list-style-type: none"> ➤ No thermochemical process has been used for the generation of syngas. ➤ Syngas has not been generated from lignocellulosic biomass. ➤ Reaction kinetics has not been determined. 	Liu et al.

				<ul style="list-style-type: none"> ➤ No mathematical model has been developed. ➤ Optimization of the operation has not been done. 	
--	--	--	--	---	--

Research gap

In many cases, simulated gas mixtures are used for the syngas fermentation. Investigations should be made using real syngas generated from thermochemical processes like gasification and pyrolysis. The experimental data should be generated for pyro-syngas fermentation. Although pure cultures are usually used, mixed culture can also be used for syngas fermentation. Very limited studies on the production of bioethanol through syngas fermentation using mixed culture have been reported (Singla et al, 2014). Some of the major challenges associated with syngas fermentation are the limitation of mass transfer of the substrates ($\text{CO} + \text{H}_2$) from the gas phase to the liquid phase and inhibitory effects of CO on the fermentation process. Mathematical modelling is an important tool to analyse the behaviour of syngas fermentation involving an array of parallel and series microbial reactions simultaneously with gas-liquid mass transfer. It is actually a critical task to develop mathematical model because both gas to liquid mass transfer and liquid phase microbial kinetics play important roles in this process. Most of the modelling studies on syngas fermentation are based on literature data of kinetic parameters, derived from experiments using simulated gas mixture. No comparison of the model predictions has been made with the experimental results of really integrated process of gasification/pyrolysis and fermentation. The concentrations of CO and H_2 used in the existing models are much higher than that of typical pyro-syngas.

2.3 Hydrothermal liquefaction (HTL) of biomass (jute stick and rice straw)

Year of Publication	Biomass used	HTL condition	Salient findings	Research limitations	References
2023	Soybean straw	The hydrothermal liquefaction was conducted at 320 °C for 30 minutes.	<ul style="list-style-type: none"> • The maximum yield of bio-oil and hydrochar were obtained 35.30% and 37.72% respectively. • The maximum higher heating value of bio-oil was determined as 38.09 MJ/kg. • The maximum higher heating value of hydrochar was determined as 28.48 MJ/kg. • Ketones and phenol were mainly present in bio-oil. • In the gaseous phase, carbon dioxide (CO₂), carbon mono oxide (CO), hydrogen (H₂), 	<ul style="list-style-type: none"> ➤ Kinetics of the HTL method have not been determined. ➤ Optimization study has not been done with respect to bio-oil yield. ➤ Any assessment has not been done with respect to the application of hydrochar. 	Wang et al.

			nitrogen (N ₂), methane (CH ₄) and ethane (C ₂ H ₆) were detected.		
2023	Sugarcane bagasse	The hydrothermal liquefaction was conducted at 250 °C for 60 minutes using 5% (w of catalyst/ w of sugarcane bagasse) ruthenium on carbon (Ru/C) as catalyst.	<ul style="list-style-type: none"> • The yields of bio-oil, hydrochar, aqueous phase and gaseous products obtained from hydrothermal liquefaction of sugarcane bagasse were 28%, 24%, 44% and 4% respectively. • The maximum higher heating value of bio-oil was determined as 31.6 MJ/kg. • In aqueous phase, levulinic acid, 5-HMF, furfural, lactic acid, levoglucosenone were detected. • In the gaseous phase, carbon dioxide (CO₂), hydrogen (H₂), nitrogen (N₂) and 	<ul style="list-style-type: none"> ➤ Kinetics of the HTL method has not been determined. ➤ Co-HTL has not been conducted. ➤ Optimization study has not been done with respect to bio-oil yield. ➤ No assessment has been done with respect to the application of hydrochar. 	Kopperi et al.

			methane (CH ₄) were detected.		
2022	Rice straw	The hydrothermal liquefaction was conducted at 350 °C for 30 minutes using milli-Q water.	<ul style="list-style-type: none"> • The yield of bio-oil, hydrochar and aqueous phase plus gaseous products obtained from hydrothermal liquefaction of rice straw were 31%, 29% and 40% respectively. • The higher heating value of bio-oil and hydrochar were determined as 24.8 MJ/kg and 15.6 MJ/kg respectively. • In the bio-oil, linear oxygenates, cyclic oxygenates, aromatic oxygenates, phenol and its derivative, aromatic compound, aliphatic compounds were detected. 	<ul style="list-style-type: none"> ➤ Kinetics of the HTL method has not been determined. ➤ Co-HTL has not been conducted. ➤ Optimization study has not been done with respect to bio-oil yield. ➤ Any assessment has not been done with respect to the application of hydrochar. 	Harisankar et al.

2021	Wheat straw and pine wood	The hydrothermal liquefaction was conducted at 400 °C for 10 minutes.	<ul style="list-style-type: none"> • The yield of bio-oil (samples obtained from hydrothermal liquefaction of wheat straw and pine wood) were 22% and 28% respectively. The yield of bio-oil obtained from co-hydrothermal liquefaction of wheat straw and pine wood (blend ratio 1:1 by weight) was 17%. • The yield of hydrochar (samples obtained from hydrothermal liquefaction of wheat straw and pine wood) were 10% and 13% respectively. The yield of hydrochar (obtained from co-hydrothermal liquefaction of wheat straw and pine wood) (blend 	<ul style="list-style-type: none"> ➤ Kinetics of the HTL method hasnot been determined. ➤ Optimization study has notbeen done with respect to bio-oil yield. ➤ Any assessment has not been done with respect to the application of hydrochar. 	Sharma et al.
------	---------------------------	---	--	--	---------------

			<p>ration 1:1 by weight) was 22%.</p> <ul style="list-style-type: none"> • The higher heating value of bio-oil samples obtained from hydrothermal liquefaction of wheat straw and pine wood were 35.50 MJ/kg and 33.66 MJ/kg respectively. The higher heating value of bio-oil obtained from co-hydrothermal liquefaction of wheat straw and pine wood (blend ration 1:1 by weight) was 33.67 MJ/kg. 		
2020	Corn straw, peanut straw, soybean straw and rice straw	The hydrothermal liquefaction was conducted at 320 °C for 60 minutes.	<ul style="list-style-type: none"> • The yield of bio-oil (samples obtained from hydrothermal liquefaction of corn straw, peanut straw, soybean straw and rice straw) were 7.9%, 14.7%, 15.8% and 	<ul style="list-style-type: none"> ➤ Kinetics of the HTL method has not been determined. ➤ Co-HTL has not been conducted. ➤ Optimization study has not been done with 	Tian et al.

			<p>15.1% respectively.</p> <ul style="list-style-type: none"> • The yield of hydrochar (samples obtained from hydrothermal liquefaction of corn straw, peanut straw, soybean straw and rice straw) were 35.5%, 34.4%, 24.5% and 31.2% respectively. • The yield of aqueous products (samples obtained from hydrothermal liquefaction of corn straw, peanut straw, soybean straw and rice straw) were 40.0%, 31.1%, 36.8% and 34.0% respectively. • The higher heating value of bio-oil (samples obtained from hydrothermal liquefaction of corn 	<p>respect to bio-oil yield.</p> <p>➤ No assessment has been done with respect to the application of hydrochar.</p>	
--	--	--	--	---	--

			<p>straw, peanut straw, soybean straw and rice straw) were 33.24 MJ/kg, 33.78 MJ/kg, 32.98 MJ/kg and 33.70 MJ/kg respectively.</p> <ul style="list-style-type: none"> • Aromatics, alkanes, alkenes, ketones, phenolic compounds, alcohols, carboxylic acid and aldehyde were detected in the bio-oil. • In the gaseous phase, carbon dioxide (CO₂), carbon mono oxide (CO), hydrogen (H₂), methane (CH₄), ethane (C₂H₆) and propane (C₃H₈) were found. 		
2020	Corn stover	The hydrothermal liquefaction of corn stover	<ul style="list-style-type: none"> • The maximum yield of 27.15% of heavy-oil was 	➤ Kinetics of the HTL method has not been determined.	Mathanker et al.

		<p>was conducted at 250-375 °C for 15-30 minutes.</p>	<p>obtained at 300 °C for 15 minutes.</p> <ul style="list-style-type: none"> • The maximum yield of 15.60% of aqueous oil was obtained at 250 °C for 15 minutes. • The maximum higher heating value of 24.70 MJ/kg of hydrochar was determined. • The maximum higher heating value of 30.77 MJ/kg of heavy oil was determined. • The maximum higher heating value of 10.95 MJ/kg of light oil phase was determined. • In the bio-oil, linear saturated hydrocarbon, linear unsaturated hydrocarbon, phenol compounds and its derivatives, 	<ul style="list-style-type: none"> ➤ Co-HTL has not been conducted. ➤ Optimization study has not been done with respect to bio-oil yield. ➤ Any assessment has not been done with respect to the application of hydrochar. 	
--	--	---	--	---	--

			<p>aldehyde, fatty acids, fatty acid alkyl esters were detected.</p> <ul style="list-style-type: none"> In gaseous phase, carbon dioxide (CO₂), nitrogen (N₂), methane (CH₄), ethane (C₂H₆), propane (C₃H₈) were detected. 		
2019	Oak wood	The hydrothermal liquefaction was conducted at 260-320 °C for 15 minutes.	<ul style="list-style-type: none"> The maximum yield of bio-oil was reported as 40%. The higher heating value of bio-oil was determined as 32.4 MJ/kg (at 320°C). 	<ul style="list-style-type: none"> ➤ Kinetics of the HTL method has not been determined. ➤ Co-HTL has not been conducted. ➤ Optimization study has not been done with respect to bio-oil yield. ➤ Any assessment has not been done with respect to the application of hydrochar. 	Caprariis et al.
2019	Black pine	The hydrothermal	<ul style="list-style-type: none"> The maximum yield of bio-oil 	<ul style="list-style-type: none"> ➤ Kinetics of the HTL method 	Akalin et al.

	wood and Kukersite oil shale	liquefaction was conducted at 250-350 °C for 30 minutes.	<p>(samples obtained from hydrothermal liquefaction of black pine wood and Kukersite oil shale at 300 °C for 30 minutes) were 11.60% and 4.96% respectively. The maximum yield of bio-oil obtained from co-hydrothermal liquefaction of black pine wood and Kukersite oil shale at 300 °C for 30 minutes (blend ratio 2 (black pine wood):1(Kukersite oil shale) by weight) was 10.24%.</p> <ul style="list-style-type: none"> • The higher heating value of bio-oil (samples obtained from hydrothermal liquefaction of black pine wood and Kukersite oil shale) were 30.80 	<p>has not been determined.</p> <ul style="list-style-type: none"> ➤ Optimization study has not been done with respect to bio-oil yield. ➤ Any assessment has not been done with respect to the application of hydrochar. 	
--	------------------------------	--	---	---	--

			<p>MJ/kg and 36.42 MJ/kg respectively. The maximum higher heating value of bio-oil obtained from co-hydrothermal liquefaction was 30.22 MJ/kg.</p> <ul style="list-style-type: none"> • The higher heating value of hydrochar (samples obtained from hydrothermal liquefaction of black pine wood and Kukersite oil shale) were 18.19 MJ/kg and 5.24 MJ/kg respectively. The maximum higher heating value of bio-oil obtained from co-hydrothermal liquefaction was 16.64 MJ/kg. 		
2017	Natural hay, oak wood	The hydrothermal liquefaction	<ul style="list-style-type: none"> • The yields of hydrochar obtained from hydrothermal 	➤ Kinetics of the HTL method has not been	Caprariis et al.

	and walnut shell	was conducted at 240-320 °C for 30 minutes.	<p>liquefaction of natural hay, oak wood and walnut shell at 240 °C for 30 minutes were 34.0%, 43.5%, and 39.5% respectively.</p> <ul style="list-style-type: none"> • The maximum higher heating value of hydrochar obtained from hydrothermal liquefaction of natural hay, oak wood and walnut shell were 18.7 MJ/kg, 21.3 MJ/kg and 18.9 MJ/kg respectively. • The maximum higher heating value of bio-oil obtained from hydrothermal liquefaction of natural hay, oak wood and walnut shell were 31.5 MJ/kg, 27.5 MJ/kg 	<p>determined.</p> <ul style="list-style-type: none"> ➤ Co-HTL has not been conducted. ➤ Optimization study has not been done with respect to bio-oil yield. ➤ Any assessment has not been done with respect to the application of hydrochar. 	
--	------------------	---	---	--	--

			and 28.5 MJ/kg respectively.		
--	--	--	------------------------------	--	--

Research gap

A few studies have been reported on the hydrothermal liquefaction (HTL) of rice straw (Harisankar et al, 2022; Tian et al, 2020). The effects of time, temperature and quality of water on the yield of bio-oil have also been reported ((Harisankar et al, 2022; Tian et al, 2020). However, there is a dearth of systematic data on the production and characterization of hydrochar obtained from hydrothermal liquefaction of rice straw. More studies are needed on the production and characterization of hydrochar. Although jute sticks are one of the by-products of jute industry in South East Asian countries like India, Bangladesh etc., no attempt has been made to systematically study the HTL conversion of jute sticks.

A few studies have been reported on the co-hydrothermal liquefaction (co-HTL) of two biomasses having different lignocellulosic composition (Sharma et al, 2021; Akalin et al, 2019). The effects of temperature and blend ratio on the yield of bio-oil obtained from co-HTL have been reported (Sharma et al, 2021; Akalin et al, 2019). However, no data are available on the co-HTL of Indian biomass.

2.4 Torrefaction of biomass

Year of Publication	Biomass used	Torrefaction condition	Salient findings	Research limitations	References
2023	Jute sticks	Torrefaction of jute sticks was conducted in a fixed bed reactor at 200 °C, 250 °C, 300 °C and 350 °C for 20	<ul style="list-style-type: none"> At 300 °C for 40 minutes, the yield of bio-char, bio-oil and gaseous product were determined as 	➤ Kinetics of the torrefaction method (Lumped model/ Distributed Activation Energy model) have not been determined.	Jagadale et al.

		minutes, 40 minutes and 60 minutes respectively.	<p>77.38%, 11.15% and 11.47% respectively.</p> <ul style="list-style-type: none"> • The maximum higher heating value of bio-oil was reported as 20.63 MJ/kg. • The range of energy yield was found as 85.5% -99.9%. 	➤ Environmental analysis has not been done.	
2023	Rice straw	Torrefaction of rice straw was conducted at 200°C, 250°C and 300°C for 10, 30 and 50 minutes respectively.	<ul style="list-style-type: none"> • At optimum condition (208.1°C, 50 minutes and rice straw: medium density fireboard = 25: 75), the heater heating value of bio-oil was determined as 22.1 MJ/kg. 	<p>➤ Kinetics of the torrefaction method (Lumped model/ Distributed Activation Energy model) has not been determined.</p> <p>➤ Environmental analysis has not been done.</p>	Manatura et al.
2022	Wheat straw	Torrefaction of wheat straw was conducted in a muffle furnace at 250 °C for 120 minutes in	<ul style="list-style-type: none"> • Thermogravimetric analysis was conducted at four different heating rates i.e. 20 °C/min, 	➤ Environmental analysis has not been done.	Gajera et al.

		absence of oxygen.	<p>30 °C/min, 40 °C/min and 50 °C/min respectively.</p> <ul style="list-style-type: none"> • The kinetic parameters was calculated using Starink model. • The average activation energy of raw-wheat straw was determined as 240 kJ/mol. • The average activation energy of torrefied wheat straw was reported as 238 kJ/mol. 		
2022	Oak wood	Torrefaction of oak wood was conducted in a muffle furnace at 200 °C, 250 °C and 300 °C for 90 minutes in semi-inert condition.	<ul style="list-style-type: none"> • The maximum yield of solid was reported as 93.16%. • The maximum higher heating value of torrefied biomass was 	<p>➤ Kinetics of the torrefaction method (Lumped model/ Distributed Activation Energy model) has not been determined.</p> <p>➤ Environmental analysis has not</p>	Ivanovski et al.

			<p>determined as 22.50 MJ/kg.</p> <ul style="list-style-type: none"> The maximum energy yield was obtained as 95.67%. 	been done.	
2022	Mustard stalk	Thermogravimetric analysis of mustard stalk was conducted in the temperature range of 100 °C-700 °C at three different heating rates 5, 10 and 20 °C/min.	<ul style="list-style-type: none"> The kinetic parameters was calculated using Flynn-Wall-Ozawa (FWO) and Kissinger-Akahira-Sunose (KAS) methods. The activation energy obtained from pyrolysis of mustard stalk were 132.47 MJ/kg and 130.62 MJ/kg for FWO model and KAS model respectively. 	➤ Environmental analysis has not been done.	Patidar et al.
2021	Mustard stalk and straw	Torrefaction of mustard stalk and straw was conducted in a muffle furnace at	<ul style="list-style-type: none"> The maximum yield of solid was reported as 88.0%. 	➤ Kinetics of the torrefaction method (Lumped model/ Distributed Activation Energy	Patidar & Varshishtha

		200 °C, 250 °C and 300 °C for 30, 45 and 60 minutes respectively.	<ul style="list-style-type: none"> • The maximum energy yield of solid was determined as 92.0%. • The maximum fuel ratio was found 0.85. 	<p>model) has not been determined.</p> <p>➤ Environmental analysis has not been done.</p>	
2020	Sugarcane bagasse	Torrefaction of oak wood was conducted in a muffle furnace at 200 °C, 225 °C, 250 °C and 275 °C for 30, 60 minutes respectively.	<ul style="list-style-type: none"> • The maximum yield of solid was reported as 95.54%. • The maximum energy yield of solid was determined as 97.7%. • The maximum higher heating value of char was determined as 21.94 MJ/kg. 	<p>➤ Kinetics of the torrefaction method (Lumped model/ Distributed Activation Energy model) has not been determined.</p> <p>➤ Environmental analysis has not been done.</p>	Manatura K.

Research gap

In recent years, the potential of torrefaction is being explored in the perspective of generation of char and oil through thermochemical conversion of biomass. Torrefaction of different lignocellulosic biomass such as jute stick, wheat straw, sugarcane bagasse, oak wood, etc have been investigated (Jagadale et al, 2022; Gajera et al, 2022; Ivanovski et al, 2022; Manatura K, 2020). Although a few studies have been reported on the torrefaction of the mustard stalk (Patidar et al., 2022; Patidar & Varshishtha, 2021), more investigation is needed on the charectarization of

physical properties of biochar, lumped and distributed activation energy kinetics and life cycle analysis.

References

Akalin, E., Kim, Y. M., Alper, K., Oja, V., Tekin, K., Durukan, I., Karagöz, S. (2019). Co-hydrothermal liquefaction of biomass with Kukersite oil shale. *Energy & Fuels*, 33(8), 7424-7435.

Almeida Benalcázar, E., Noorman, H., Maciel Filho, R., & Posada, J. A. (2020). Modeling ethanol production through gas fermentation: a biothermodynamics and mass transfer-based hybrid model for microbial growth in a large-scale bubble column bioreactor. *Biotechnology for biofuels*, 13(1), 1-19.

Chen, L., Chen, R., & Fu, S. (2015). FeCl₃ pretreatment of three biomass for ethanol production. *ACS Sustainable Chemistry & Engineering*, 3(8), 1794-1800.

de Caprariis, B., Bavasso, I., Bracciale, M. P., Damizia, M., De Filippis, P., & Scarsella, M. (2019). Enhanced bio-crude yield and quality by reductive hydrothermal liquefaction of oak wood biomass: Effect of iron addition. *Journal of analytical and applied pyrolysis*, 139, 123-130.

de Caprariis, B., de Filippis, P., Petrullo, A., & Scarsella, M. (2017). Hydrothermal liquefaction of biomass: Influence of temperature and biomass composition on the bio-oil production. *Fuel*, 208, 618-625.

de Medeiros, E. M., Posada, J. A., Noorman, H., & Filho, R. M. (2019). Dynamic modeling of syngas fermentation in a continuous stirred-tank reactor: Multi-response parameter estimation and process optimization. *Biotechnology and bioengineering*, 116(10), 2473-2487.

Fernández-Naveira, Á., Veiga, M. C., & Kennes, C. (2019). Selective anaerobic fermentation of syngas into either C2-C6 organic acids or ethanol and higher alcohols. *Bioresource technology*, 280, 387-395.

Gajera, B., Tyagi, U., Sarma, A. K., & Jha, M. K. (2022). Impact of torrefaction on thermal behavior of wheat straw and groundnut stalk biomass: kinetic and thermodynamic study. *Fuel Commun* 12: 100073.

- Harisankar, S., Mohan, R. V., Choudhary, V., & Vinu, R. (2022). Effect of water quality on the yield and quality of the products from hydrothermal liquefaction and carbonization of rice straw. *Bioresource Technology*, 351, 127031.
- Ivanovski, M., Goricanec, D., Krope, J., & Urbancl, D. (2022). Torrefaction pretreatment of biomass for sustainable solid biofuel production. *Energy*, 240, 122483.
- Jagadale, M., Gangil, S., & Jadhav, M. (2023). Enhancing fuel characteristics of jute sticks (*Corchorus Sp.*) using fixed bed torrefaction process. *Renewable Energy*, 215, 118992.
- Kamireddy, S. R., Li, J., Tucker, M., Degenstein, J., & Ji, Y. (2013). Effects and mechanism of metal chloride salts on pretreatment and enzymatic digestibility of corn stover. *Industrial & Engineering Chemistry Research*, 52(5), 1775-1782.
- Kopperi, H., & Mohan, S. V. (2023). Catalytic hydrothermal deoxygenation of sugarcane bagasse for energy dense bio-oil and aqueous fraction acidogenesis for biohydrogen production. *Bioresource Technology*, 379, 128954.
- Liu, K., Atiyeh, H. K., Stevenson, B. S., Tanner, R. S., Wilkins, M. R., & Huhnke, R. L. (2014). Continuous syngas fermentation for the production of ethanol, n-propanol and n-butanol. *Bioresource technology*, 151, 69-77.
- Manatura, K. (2020). Inert torrefaction of sugarcane bagasse to improve its fuel properties. *Case Studies in Thermal Engineering*, 19, 100623.
- Manatura, K., Chalermisinsuwan, B., Kaewtrakulchai, N., Chao, Y. C., & Li, Y. H. (2023). Co-torrefaction of rice straw and waste medium density fiberboard: A process optimization study using response surface methodology. *Results in Engineering*, 18, 101139.
- Mathanker, A., Pudasainee, D., Kumar, A., & Gupta, R. (2020). Hydrothermal liquefaction of biomass feedstock to produce biofuels: Parametric study and products characterization. *Fuel*, 271, 117534.
- Palliprath, S., Poolakkalody, N. J., Ramesh, K., Mangalan, S. M., Kabekkodu, S. P., Santiago, R., & Manisseri, C. (2023). Pretreatment of sugarcane postharvest leaves by γ -valerolactone/water/ FeCl_3 system for enhanced glucan and bioethanol production. *Industrial Crops and Products*, 197, 116571.

- Patidar, K., & Vashishtha, M. (2021). Impact of torrefaction conditions on the physicochemical properties of mustard crop residue. *Materials Today: Proceedings*, 44, 4072-4078.
- Patidar, K., Singathia, A., Vashishtha, M., Sangal, V. K., & Upadhyaya, S. (2022). Investigation of kinetic and thermodynamic parameters approaches to non-isothermal pyrolysis of mustard stalk using model-free and master plots methods. *Materials Science for Energy Technologies*, 5, 6-14.
- Romero, I., López-Linares, J. C., Moya, M., & Castro, E. (2018). Optimization of sugar recovery from rapeseed straw pretreated with FeCl₃. *Bioresource technology*, 268, 204-211.
- Ruggiero, G., Lanzillo, F., Raganati, F., Russo, M. E., Salatino, P., & Marzocchella, A. (2022). Bioreactor modelling for syngas fermentation: Kinetic characterization. *Food and Bioproducts Processing*, 134, 1-18.
- Sharma, K., Shah, A. A., Toor, S. S., Seehar, T. H., Pedersen, T. H., & Rosendahl, L. A. (2021). Co-hydrothermal liquefaction of biomass in supercritical water. *Energies*, 14(6), 1708.
- Singla, A., Verma, D., Lal, B., & Sarma, P. M. (2014). Enrichment and optimization of anaerobic bacterial mixed culture for conversion of syngas to ethanol. *Bioresource technology*, 172, 41-49.
- Tang, W., Wu, X., Huang, C., Ling, Z., Lai, C., & Yong, Q. (2021). Revealing the influence of metallic chlorides pretreatment on chemical structures of lignin and enzymatic hydrolysis of waste wheat straw. *Bioresource Technology*, 342, 125983.
- Tian, Y., Wang, F., Djandja, J. O., Zhang, S. L., Xu, Y. P., & Duan, P. G. (2020). Hydrothermal liquefaction of crop straws: Effect of feedstock composition. *Fuel*, 265, 116946.
- Vandecasteele, J. (2016). Experimental and modelling study of pure-culture syngas fermentation for biofuels production. *MSc Universiteit Gent*, 356.
- Wang, Z. C., Hou, X. K., Wang, Y. B., Collins, E., & Duan, P. G. (2023). Hydrothermal liquefaction of soybean straw: Effect of steam explosion pretreatment and reaction media. *Fuel*, 339, 127418.
- Zhang, H., Lyu, G., Zhang, A., Li, X., & Xie, J. (2018). Effects of ferric chloride pretreatment and surfactants on the sugar production from sugarcane bagasse. *Bioresource technology*, 265, 93-101.

Chapter 3

Aims and objectives

Chapter 3: Aims and objectives

The aims and objectives of the overall work has been tabulated in the following section.

Aim 1: Production of Ethanol from Indian Biomass through Sugar Platform

The main objectives and work plan for Aim 1 are as follows:

Objectives	Work Plan
▪ Selection of biomass	• The most abundantly available Indian lignocellulosic agricultural biomass (Rice Straw) is selected.
▪ Pretreatment of biomass	• Experimental studies on methods, like autohydrolysis, dilute acid pretreatment and ferric chloride pretreatment are to be conducted with the variation of operating parameters. • Pretreatment products are to be analysed and the best conditions for each pretreatment process are to be identified through comparison of product quality. • Selection of most effective pretreatment process is to be done through the comparison of quality of hydrolysate and pretreated solid obtained under best suitable condition for each method. • The optimum conditions of time and temperature for the generation of different hydrolytic products are to be determined for the most effective process. • The dependence of degradation of different carbohydrate polymers (cellulose, hemicellulose) on the “severity” of the best

		<p>suitable method is to be determined.</p> <ul style="list-style-type: none"> • A mathematical model for the most effective pretreatment process is to be developed.
<ul style="list-style-type: none"> ▪ Enzymatic hydrolysis of pre-treated biomass 	→	<ul style="list-style-type: none"> • The solid residue obtained under the best conditions of each pretreatment process is to be enzymatically hydrolysed. • Kinetics of enzymatic hydrolysis of cellulose in the solid residue obtained under best operating condition of the most effective pretreatment process are to be determined. • The overall and enzymatic glucose yields are to be optimized with respect to severity of the most effective pretreatment process and enzyme loading.
<ul style="list-style-type: none"> ▪ Ethanol production from enzymatically produced glucose 	→	<ul style="list-style-type: none"> • Glucose produced through enzymatic hydrolysis of solid residue, obtained through all pretreatment processes, under best condition, is to be converted to ethanol using <i>Saccharomyces cerevisiae</i> and the overall yields of ethanol per unit mass of feed solid are to be compared.

Aim 2: Production of Ethanol from Indian Biomass through Syngas Platform

The main objectives and work plan for Aim 2 are as follows:

Objectives		Work Plan
<ul style="list-style-type: none"> ▪ Selection of biomass 	→	<ul style="list-style-type: none"> • The most abundantly available Indian lignocellulosic agricultural biomass (Rice Straw) is selected.
<ul style="list-style-type: none"> ▪ Production of Pyro-syngas 	→	<ul style="list-style-type: none"> • Experimental studies on pyrolysis of rice straw in the temperature range of 400-700°C

	are conducted.
	<ul style="list-style-type: none"> • Yields of products and the pyro-syngas composition are determined.
<ul style="list-style-type: none"> ▪ Selection of microorganism for syngas fermentation and determination of growth kinetics 	<ul style="list-style-type: none"> • Clostridial consortium, <i>UACJUCheI</i> is used for pyro-syngas fermentation and its growth kinetics are determined using batch mode experimental data.
<ul style="list-style-type: none"> ▪ Conversion of pyro-syngas to ethanol 	<ul style="list-style-type: none"> • Experimental runs are conducted in batch and continuous stirred tank bioreactors • Mathematical models for both batch and continuous stirred tank bioreactors are developed • Optimization of both batch and continuous stirred tank bioreactors are done

Aim 3: Hydrothermal liquefaction (HTL) of Indian Biomass (jute stick and rice straw)

The main objectives and work plan for Aim 3 are as follows:

Objectives	Work Plan
<ul style="list-style-type: none"> ▪ Selection of biomass 	<ul style="list-style-type: none"> • Rice straw and jute stick are selected as the feedstock for the hydrothermal liquefaction process
<ul style="list-style-type: none"> ▪ Performance of HTL of Rice straw and jute stick 	<ul style="list-style-type: none"> • Batch experiments are conducted on HTL of rice straw and jute stick to determine the HTL kinetics • Product yields are determined • Bio-oil and hydrochar are characterized • Batch experiments are conducted on co-HTL of rice straw and jute stick and the bio-oil has been characterized

<ul style="list-style-type: none"> ▪ Assessment of sorbent property of hydro-char from jute stick 	→	<ul style="list-style-type: none"> • Optimization has been performed to maximize the bio-oil yield from co-HTL • Batch type adsorption experiments have been conducted to determine the effectiveness of hydro-char from jute stick for dye like Congo-red
--	---	--

Aim 4 Torrefaction of mustard stalk

The main objectives and work plan for Aim 4 are as follows:

Objectives		Work Plan
<ul style="list-style-type: none"> ▪ Selection of biomass 	→	<ul style="list-style-type: none"> • Mustard stalk are selected as the feedstock for the torrefaction process
<ul style="list-style-type: none"> ▪ Performance of Torrefaction of Mustard stalk 	→	<ul style="list-style-type: none"> • Batch experiments in pyrolyser and in TGA are conducted to determine Lumped and Distributed Activation Energy kinetics of Torrefaction of Mustard stalk • Biochar and Bio-oil are characterized
<ul style="list-style-type: none"> ▪ Life Cycle analysis of Torrefaction of Mustard stalk 	→	<ul style="list-style-type: none"> • Life cycle analysis of Torrefaction of Mustard stalk is conducted using SIMAPRO

Novelty of the research study

Based on the research gaps identified from literature review, presented in Chapter 2, the thrust of the research study has been decided and the aims have been identified with the specific objectives to achieve them. In comparison to the existing research data in the fields of ferric chloride pretreatment for ethanol production from agro-wastes through sugar platform; syngas fermentation

for ethanol production; hydrothermal liquefaction of local agro-wastes and torrefaction of lignocellulosic biomass, the following novelties of the present study can be highlighted:

- The mechanism of ferric chloride and other hydronium-ion based pretreatment of agro-wastes, rice straw in particular, is being elucidated from the chemical engineering concept of shrinking core model for the first time.
- A deterministic mathematical model using the kinetics of each reaction, involved in multi-step FeCl_3 -based hydrolysis of hemicellulose and cellulose in Indian rice straw is being developed and validated for the first time.
- The fermentative conversion of pyro-syngas to ethanol, using rice straw as the feedstock, is being studied for the first time. Unlike pure strain, an attempt of using a unique clostridial consortium, isolated from local agricultural field, is being attempted for the first time.
- The hydrothermal liquefaction of jute-stick and co-HTL of biomass pair, namely jute stick and rice straw, with subsequent optimization of performance are being studied for the first time.
- The distributed activation energy model for the torrefaction of mustard stalk using Tang method is being determined for the first time. Other than the technical viability, the addition of database through the life cycle analysis of torrefaction of mustard stalk under this study is expected to facilitate the implementation of the process in industrial scale.

Chapter 4

Materials and analytical methods

Chapter 4: Materials and analytical methods

4.1 Materials

4.1.1 Feed material

The rice straw, jute stick and mustard stalk were collected from West Bengal, India. The rice straw and jute stick samples were first cut into small size and the latter was ground to 1 mm particle size using Ultra-Centrifugal Mill ZM 200 (Retsch GmbH, Germany).

4.1.2 Chemicals

For the investigation of rice straw pretreatment, sulfuric acid and ferric chloride (Sigma-Aldrich) were used. Cellulase purchased from HiMedia, was used for enzymatic hydrolysis of solids. Milli-Q water was used for experimental purposes. 2-(N-morpholino) ethanesulfonic acid (MES), ammonium chloride (NH_4Cl), potassium chloride (KCl), magnesium sulfate heptahydrate ($\text{MgSO}_4 \cdot 7 \text{H}_2\text{O}$), sodium chloride (NaCl), calcium sulfate (CaCl_2) were purchased from Merck, were used to prepare the basal DSMZ 879 medium. HPLC grade ethanol (Sigma Aldrich) and acetic acid (Sigma Aldrich) were used as standard. Acetone and butanol were purchased from Merck and were used for solvent extraction. Yeast, peptone and dextrose (HiMedia) were used to prepare the YPD (Yeast: 3g; Peptone: 10g; Dextrose: 20g and distilled water: 1L) medium.

4.1.3 Microorganism for ethanol production

The *Saccharomyces cerevisiae* (MTCC-173) purchased from MTCC, India and maintained in YPD medium at 28 °C, was used for ethanol production through sugar platform. A mixed clostridial consortium—*UACJUCHeI*, isolated from local paddy fields in West Bengal, was used for ethanol production through syngas platform (Ghosh et al., 2021).

4.2 Analytical Methods

4.2.1 Quantitative Analysis of hydrocarbon polymers (Cellulose-Hemicellulose-Lignin)

The composition of the raw biomasses and pretreated solid samples with respect to Cellulose-Hemicellulose-Lignin were determined through a series of analytical methods following the protocols described in the Technical Report of National Renewable Energy Laboratory (NREL/TP-510-42618) on ‘Determination of Structural Carbohydrates and Lignin in Biomass:

Laboratory Analytical Procedure (LAP) Issue Date: April 2008' (Sluiter et al., 2008). The method, following the NREL protocol, can be described as follows:

Overall, in the first step, 300mg of lignocellulosic sample was soaked with 3mL (4.92g) 72% sulfuric acid by thorough mixing. The mixture was placed in a water-bath maintained at $30 \pm 3^\circ\text{C}$ for 1 h. The reaction mixture was intermittently stirred. After this step, 84 ± 0.04 mL milli-Q water was added to the mixture. Afterwards the reaction mixture was placed in an autoclave at $121 \pm 3^\circ\text{C}$ for 15 minutes and was subsequently cooled to room temperature. This step was followed by filtration under vacuum. The concentration of xylose and glucose in the filtrate was determined using proton nuclear magnetic resonance ($^1\text{H NMR}$) spectroscopy and that of acid soluble lignin (ASL) was determined using UV-VIS spectrophotometer at 320nm. The acid insoluble residual solid, placed in crucible without lid, was exposed to $575 \pm 25^\circ\text{C}$ in a muffle furnace for 24h. The residual solid, left after 24h, was considered as ash. The mass of acid insoluble Klason lignin was determined by subtracting the mass of ash from that of the acid insoluble residual solid, obtained after filtration of the hydrolysis mixture. The experiments were conducted at University of Eastern Finland.

4.2.2 Proximate analysis

The moisture, volatile matter and ash content of raw biomasses and char samples were determined according to ASTM (D-3172-89) protocol. Fixed carbon was measured from equation 1 (Shaaban et al., 2014).

$$\text{Fixed carbon (\%)} = 100 - \text{moisture (\%)} - \text{volatile matter (\%)} - \text{ash (\%)} \quad (4.1)$$

4.2.3 Ultimate analysis

Ultimate analysis of raw biomasses, char and bio-oil samples were performed by using CHNOS analysis using vario MICRO Element Analyser of ElementarAnalysensysteme GmbH.

4.2.4 Thermo-gravimetric analysis (TGA)

TG analyzer (Pyris Diamond TG/DTA, STA 6000, PerkinElmer) was used for the thermogravimetric analysis of biomass and char samples.

4.2.5 Fourier Transform Infra-red analysis

To assess the changes in the chemical bonds of different solid samples, Fourier Transform Infra-red analysis was conducted using an FTIR analyzer (RX-1 FTIR system, Perkin Elmer). The spectra have been generated in the range of 4000 – 400 cm⁻¹.

4.2.6 X-ray diffractive (XRD) analysis

The crystallinity of solid samples were determined by X-ray diffractive (XRD) analysis (Ultima III, Rigaku). The scattering angles (2θ) were varied from 5° to 60° in steps of 0.04° at time intervals of 0.066 s.

The crystallinity index (CrI) was determined using the following equation (Segal et al., 1959).

$$\text{CrI (\%)} = \frac{I_{002} - I_{\text{am}}}{I_{002}} \times 100 \quad (4.2)$$

Where I_{002} is the intensity of the maximum peak at around $2\theta = 22.5^\circ$ and I_{am} is the minimum intensity at about $2\theta = 18^\circ$;

4.2.7 Field emission scanning electron microscopy (FESEM) analysis

The surface morphological analysis of raw biomasses, pretreated solids and char samples were studied by field emission scanning electron microscopy (FESEM) analysis (INSPECT F50). The samples were mounted on a conductive tape. Gold was coated to the samples by using a Quorum (Q150R).

4.2.8 Energy-dispersive X-ray spectroscopy (EDS) analysis

To assess the change in metal distribution due to FeCl₃, the metals in raw rice straw and pretreated solid, obtained from FeCl₃ pretreatment were detected by using energy-dispersive X-ray spectroscopy (EDS) analysis (Bruker).

4.2.9 Nuclear magnetic resonance spectroscopy (NMR) Analysis

The compounds in the hydrolysate, obtained from different pretreatment processes were analyzed using nuclear magnetic resonance spectroscopy (NMR). ¹H NMR data were obtained using a 600 MHz Bruker NMR spectrometer, equipped with a cryoprobe (Bruker Prodigy TCI 600 S3 H&F-C/N D-05 Z) and an automatically cooled Sample Jet sample changer. Use of a 600 MHz spectrometer significantly reduced the signal overlap of studied samples. Standard water-suppressed measurements were applied by using ca. 15 s relaxation delay and 16 scans at 300K.

Before the NMR measurements, 100 μL of the sample liquid was transferred to a 5-mm NMR tube, which was followed by the addition of D_2O (425 μL) containing 3-(trimethylsilyl)-propionic- d_4 acid (1.5 mM). Studied compounds were identified based on two dimensional proton-proton (COSY) and proton-carbon (HMBC, HSQC) NMR experiments or spiking. All measurements were repeated in triplicate

4.2.10 Gas chromatography (GC)

The ethanol concentration and the gas phase concentrations of O_2 , N_2 , CO , CO_2 , CH_4 and H_2 were measured using gas chromatograph (Thermo Fisher Scientific), equipped with Chromeleon software and flame ionization detector (FID) and thermal conductivity detector (TCD). In case of ethanol analysis, Hydrogen, air and nitrogen flow rates were set at 30, 300 and 30 mL/min respectively (Mohammed et al., 2018). The oven and FID detector temperature were 40 and 250 $^\circ\text{C}$ respectively. TR-FAME capillary column was used to perform the experiment (Mohammed et al., 2018). The gas was analyzed with TCD using helium as the carrier gas. The carrier gas flow rate was maintained at 20 mL min^{-1} . The TCD was maintained at 40 $^\circ\text{C}$ for 3 min and was afterwards ramped up to 200 $^\circ\text{C}$.

4.2.11 High performance liquid chromatography (HPLC) analysis

The acetic acid concentration in the liquid sample, obtained from syngas fermentation was analyzed using HPLC. The HPLC (Waters 2489) of Waters, Singapore, equipped with degasser, binary pump, auto-sampler, and UV–Vis detector was used. The analytical column, used in the HPLC, was C18 (250 mm \times 4.6 mm \times 5 μm) of SunFire, Maynooth, Ireland.

4.2.12 Gas chromatography – mass spectrometry (GC-MS) analysis

The components, present in bio-oil from mono- and co-hydrothermal liquefaction of rice straw and jute stick, were detected using GC-MS (Thermo-Scientific) in TG-5MS column (30 m \times 0.25 mm \times 0.25 μm). The maximum oven temperature was set at 230 $^\circ\text{C}$. The injector and MS detector temperatures were set at 200 and 210 $^\circ\text{C}$ respectively. Helium was used as a carrier gas. The mass line range was programmed from 50 to 600 amu.

The following two tables (Table 4.1 and 4.2) show the association of each material and method with respective objectives, described in Chapter 3.

Table 4.1 Association of Materials with Respective objectives

Materials	Respective Objective/s
Rice straw	Pretreatment of biomass under Aim1 Production of pyro-syngas under Aim 2 Performance of HTL of biomass under Aim 3
Jute stick	Performance of HTL of biomass under Aim 3
Mustard stalk	Performance of torrefaction process of biomass under Aim 4
Sulfuric acid	Pretreatment of biomass under Aim1
Ferric chloride	Pretreatment of biomass under Aim1
Cellulase	Enzymatic hydrolysis of pre-treated biomass under Aim 1
Milli-Q water	Pretreatment of biomass under Aim1
2-(N-morpholino) ethanesulfonic acid	Conversion of pyro-syngas to ethanol under Aim 2
Ammonium chloride	Conversion of pyro-syngas to ethanol under Aim 2
Potassium chloride	Conversion of pyro-syngas to ethanol under Aim 2
Magnesium sulfate heptahydrate	Conversion of pyro-syngas to ethanol under Aim 2
Sodium chloride	Conversion of pyro-syngas to ethanol under Aim 2
Calcium sulfate	Conversion of pyro-syngas to ethanol under Aim 2
HPLC grade ethanol	Ethanol production from enzymatically produced glucose under Aim 1 Conversion of pyro-syngas to ethanol under Aim 2
Acetic acid	Conversion of pyro-syngas to ethanol under Aim 2
Acetone	Conversion of pyro-syngas to ethanol under Aim 2 Performance of HTL of Rice straw and jute stick under Aim 3 Performance of Torrefaction of Mustard stalk under Aim 4
Butanol	Ethanol production from enzymatically produced glucose under Aim 1.

Yeast	Ethanol production from enzymatically produced glucose under Aim 1.
Peptone	Ethanol production from enzymatically produced glucose under Aim 1.
Eextrose	Ethanol production from enzymatically produced glucose under Aim 1.
<i>Saccharomyces cerevisiae</i> (MTCC-173)	Ethanol production from enzymatically produced glucose under Aim 1.
Mixed clostridial consortium— <i>UACJUCHE1</i>	Selection of microorganism for syngas fermentation and determination of growth kinetics under Aim 2 Conversion of pyro-syngas to ethanol under Aim 2

Table 4.2 Association of Methods with Respective objectives

Methods	Respective Objective/s
Quantitative Analysis of hydrocarbon polymers (Cellulose-Hemicellulose-Lignin)	Pretreatment of rice straw under Aim 1 Performance of HTL of Rice straw and jute stick under Aim 3 Performance of torrefaction of mustard stalk under Aim 4
Proximate analysis	Pretreatment of rice straw under Aim 1 Performance of HTL of Rice straw and jute stick under Aim 3
Ultimate analysis	Pretreatment of rice straw under Aim 1 Performance of HTL of Rice straw and jute stick under Aim 3 Performance of torrefaction of mustard stalk under Aim 4
Thermo-gravimetric analysis (TGA)	Pretreatment of rice straw under Aim 1 Performance of HTL of Rice straw and jute stick under Aim 3

	Performance of torrefaction of mustard stalk under Aim 4
Fourier Transform Infra-red analysis	Pretreatment of rice straw under Aim 1 Performance of HTL of Rice straw and jute stick under Aim 3 Performance of torrefaction of mustard stalk under Aim 4
X-ray diffractive (XRD) analysis	Pretreatment of rice straw under Aim 1 Performance of HTL of Rice straw and jute stick under Aim 3 Performance of torrefaction of mustard stalk under Aim 4
Field emission scanning electron microscopy (FESEM) analysis	Pretreatment of rice straw under Aim 1 Performance of HTL of Rice straw and jute stick under Aim 3 Performance of torrefaction of mustard stalk under Aim 4
Energy-dispersive X-ray spectroscopy (EDS) analysis	Pretreatment of rice straw under Aim 1
Nuclear magnetic resonance spectroscopy (NMR) Analysis	Pretreatment of rice straw under Aim 1
Gas chromatography (GC)	Ethanol production from enzymatically produced glucose under Aim 1 Production of Pyro-syngas under Aim 2 Conversion of pyro-syngas to ethanol under Aim 2
High performance liquid chromatography (HPLC) analysis	Conversion of pyro-syngas to ethanol under Aim 2
Gas chromatography – mass spectrometry (GC-MS) analysis	Performance of HTL of Rice straw and jute stick under Aim 3 Performance of torrefaction of mustard stalk under Aim 4

References

- Ghosh, S., Pathak, S., Manna, D., & Chowdhury, R. (2021). Acidogenic mixed consortium isolated from soil of agricultural field: Acid production behaviour and growth kinetics under the influence of pretreatment hydrolysate of rice straw (RS). *Indian Chemical Engineer*, 63(2), 206-218.
- Mohammed, A. H., Mohammed, A. K., Kamar, F. H., Abbas, A. A., & Nechifor, G. (2018). Determination of ethanol in fermented broth by headspace gas chromatography using capillary column. *Rev Chim Burcharest-Orig Ed*, 69(11), 2969-2972.
- Segal, L. G. J. M. A., Creely, J. J., Martin Jr, A. E., & Conrad, C. M. (1959). An empirical method for estimating the degree of crystallinity of native cellulose using the X-ray diffractometer. *Textile research journal*, 29(10), 786-794.
- Shaaban, A., Se, S. M., Dimin, M. F., Juoi, J. M., Husin, M. H. M., & Mitan, N. M. M. (2014). Influence of heating temperature and holding time on biochars derived from rubber wood sawdust via slow pyrolysis. *Journal of Analytical and Applied Pyrolysis*, 107, 31-39.
- Sluiter, A., Hames, B., Ruiz, R., Scarlata, C., Sluiter, J., Templeton, D., & Crocker, D. L. A. P. (2008). Determination of structural carbohydrates and lignin in biomass. *Laboratory analytical procedure*, 1617(1), 1-16.

Chapter 5

Production of Ethanol from Indian Biomass through Sugar Platform

Chapter 5: Production of Ethanol from Indian Biomass through Sugar Platform

The most abundant lignocellulosic biomass in the world, rice straw is a post-harvesting residue during rice processing. In India, about 44 million ha of land is used for the cultivation of rice. The quantity of rice straw, produced annually in India, is as high as 141120 kiloton and is the highest among all agro-wastes (Chowdhury et al, 2018; Hassan et al, 2021). To make the land ready for the next crop cycle, rice straws are often burnt causing environmental pollution. Considering the large availability, sustainable supply, suitable elemental composition, carbon content lying in the range of 36.02% - 38.80%, rice straw is a prospective post-harvest agro-waste to appear as a promising feedstock for producing 2G bioethanol (Chowdhury et al, 2018; Hassan et al, 2021). Although many studies on acid pretreatment of rice straw is available in the literature, reports on studies using other pretreatment methods using less polluting chemical reagents like metal chlorides etc are limited. However, for the implementation of ethanol plants on rice straw in commercial scale, thorough studies on the use of these alternative reagents are to be done along with determination of rate kinetics of reactions involved in the pretreatment processes. This can only enable the design of suitable reactors in large scale. As discussed in Chapter 3 the ethanol production from Indian Biomass through sugar platform has been focused following the objectives incorporated under aim 1

5.1 Pretreatment Processes

Objectives

- Experimental studies on methods like autohydrolysis, dilute acid pretreatment and ferric chloride pretreatment with the variation of operating parameters.
- Analysis of pretreatment products and identification of the best conditions for each pretreatment process through comparison of product quality.
- Selection of most effective pretreatment process under study through the comparison of quality of hydrolysate and pretreated solid obtained under best suitable condition for each method.
- Elucidation of hydronium-ion catalyzed mechanism during the pretreatment processes under study
- Optimization of time and temperature for the generation of different hydrolytic products through

the most effective process under study

- Determination of the dependence of degradation of different carbohydrate polymers (cellulose, hemicellulose) on the “severity” of the best suitable method
- A mathematical model for the most effective pretreatment process is to be developed.

5.1.1 Experimental

A cylindrical stainless steel reactor of 60 mm inner diameter and 150 mm height was used for the investigation of pretreatment of rice straw in batch mode. The reactor was equipped with temperature controller and pressure gauge. The reactor used for pretreatment process is shown in Fig 5.1.

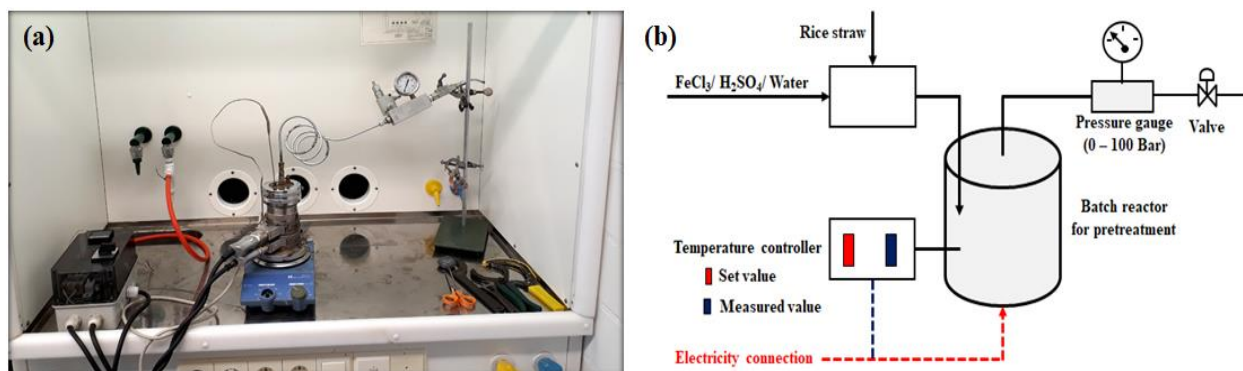


Fig. 5.1 Reactor used for pretreatment process (a); Schematic diagram of the pretreatment process (b)

In the present study, 10 g rice straw was subjected to 100 mL of 0.1 M ferric chloride solution or 0.1 M sulfuric acid or water under isothermal condition at the temperature of 140, 150, 160, 170 and 180°C for 10 minutes respectively. Subsequently the pressure was released and the treated slurry was collected at 25 °C after natural cooling. The liquid and the solid phases of the cold pretreated slurry were separated by passing through a vacuum filter. The pretreated liquor and the residual solid were stored at 4 °C for further analyses. The products in liquid hydrolyzate (glucose, xylose, furfural, 5-HMF, formic acid, acetic acid and levulinic acid) were determined by NMR analysis. The composition (glucan, xylan and lignin) of pretreated solid was analyzed according to NREL protocol. Experiments were also conducted with FeCl₃ concentration of 0.15M and 0.2M. All experiments were conducted in triplicate. The strength of FeCl₃ corresponding to the maximum degradation of hemicellulose and cellulose over 10 minutes at all temperature (140-180°C) was

determined through comparison of experimental data. The rate kinetics of the reactions involved in the hydrolysis pathways of both hemicellulose and cellulose, as proposed in the mathematical model, were determined by conducting systematic batch experiments. For kinetic studies the hydrolysis was run for 3, 6, 9, 12 and 15 minutes separately in the reactor following the protocol, described above. The most effective strength of FeCl_3 with respect to degradation of cellulose and hemicellulose over 10 minutes was maintained. The time concentration data of all components, obtained after each pretreatment time at 150°C , 170°C and 190°C were used to determine the rate kinetics. Separate experiments were conducted using pretreatment time of 5 and 15 minutes. For the validation of mathematical model incorporating the kinetic data, determined under the present study, the experimental data obtained at 5, 10 and 15 minutes have been compared with the simulated ones.

5.1.2 Analytical

The moisture, volatile matter and ash content, fixed carbon of raw RS were determined according to ASTM (D-3172-89) protocol. Ultimate analysis of raw RS was performed by using CHNOS analysis. The thermos-gravimetric analysis (TGA) was carried out in the $50 - 900^\circ\text{C}$ temperature range in a TG analyzer. The experiment was conducted at 20 K min^{-1} heating rate. Untreated RS and pretreated solids obtained from LWP, SAP and FCP at 180°C were subjected to TGA following the same protocol. To assess the changes in the chemical bonds of rice straw during different pretreatment processes, Fourier Transform Infra-red analysis of feed rice straw and pretreated solid residue was conducted using an FTIR analyzer. Raw RS and residual solids obtained from LWP, SAP and FCP at 180°C were subjected to FTIR analysis. The spectra have been generated in the range of $4000 - 400\text{ cm}^{-1}$. The crystallinity of raw RS and pretreated solid were determined by X-ray diffractive (XRD) analysis (Ultima III, Rigaku). The scattering angles (2θ) were varied from 5° to 60° in steps of 0.04° at time intervals of 0.066 s. The surface morphological analysis of untreated and pretreated (LWP, SAP and FCP at 180°C) rice straw were studied by field emission scanning electron microscopy (FESEM) analysis (INSPECT F50). To assess the change in metal distribution due to FeCl_3 , the metals in raw-RS and pretreated solid, obtained from FCP were detected by using energy-dispersive X-ray spectroscopy (EDS). The compounds (xylose, glucose, furfural, etc) in the hydrolyzate, obtained from LWP, SAP and FCP were analyzed using nuclear magnetic resonance spectroscopy (NMR) to determine sugars,

platform chemicals and organic acids. ^1H NMR data were obtained using a 600 MHz Bruker NMR spectrometer, equipped with a cryoprobe. All analytical methods have been described in detail in Chapter 4.

The yield of glucose, 5-HMF, formic acid and levulinic acid (Y_G , Y_{HMF} , Y_{FA} and Y_{LA}) were calculated from the equation 5.1. Similarly, the yield of xylose, furfural and acetic acid (Y_X , Y_F and Y_{AA}) were determined from the equation 5.2.

$$Y_{G/\text{HMF}/\text{FA}/\text{LA}} = \frac{\text{Mass of Glucose/5-HMF/Levulinic acid/Formic acid produced (g)}}{1 \text{ kg of rice straw}} \quad (5.1)$$

$$Y_{X/F/\text{AA}} = \frac{\text{Mass of xylose/Furfural/Acetic acid produced (g)}}{1 \text{ kg of rice straw}} \quad (5.2)$$

Glucan degradation and xylan degradation were determined from the equation 5.3 and 5.4 respectively.

$$\text{Degradation of glucan (\%)} = \left(\frac{\text{Glucan in RS fed} - \text{glucan remaining in the pretreated RS}}{\text{glucan in rice straw fed}} \right) \times 100 \quad (5.3)$$

$$\text{Degradation of Xylan (\%)} = \left(\frac{\text{Xylan in RS fed} - \text{Xylan remaining in the pretreated RS}}{\text{Xylan in rice straw fed}} \right) \times 100 \quad (5.4)$$

$$\text{Solid recovery (\%)} = \frac{\text{Weight of recovered solid residue}}{\text{weight of rice straw fed to the reactor}} \times 100 \quad (5.5)$$

5.1.3 Reaction kinetics for xylan and glucan degradation

As clearly indicated in previous literature, the rate of degradation of carbohydrate polymers can usually be represented as a first order function of concentration of carbohydrate polymer (Krzelj et al, 2020; Kapu et al, 2016). The 1st order rate kinetics for the xylan and glucan degradation through liquid water pretreatment(LWP), sulfuric acid pretreatment(SAP) and ferric chloride pretreatment (FCP) have been represented generally by the following rate equations:

$$-\frac{dW_{\text{Glucan}}}{dt} = k_{\text{Glucan}} W_{\text{Glucan}} \quad (5.6)$$

$$-\frac{dW_{\text{Xylan}}}{dt} = k_{\text{Xylan}} W_{\text{Xylan}} \quad (5.7)$$

Equation 5.6 on integration reduces to the following:

$$\text{Or, } - \int_{W_{Glucan,0}}^{W_{Glucan}} \frac{dW_{Glucan}}{W_{Glucan}} = k_{Glucan} \int_0^t dt \quad (5.6.1)$$

$$\text{Or, } \ln \frac{W_{Glucan,0}}{W_{Glucan}} = k_{Glucan} t \quad (5.6.2)$$

$$\text{Or, } k_{Glucan} = \frac{\ln \frac{W_{Glucan,0}}{W_{Glucan}}}{t} \quad (5.6.3)$$

Where, $W_{Glucan,0}$ and W_{Glucan} represent the weight of glucan at $t=0$ and at any time, t . (Basis: 10g initial RS sample being hydrolysed).

Equation 5.7 on integration reduces to the following:

$$\text{Or, } - \int_{W_{Xylan,0}}^{W_{Xylan}} \frac{dW_{Xylan}}{W_{Xylan}} = k_{Xylan} \int_0^t dt \quad (5.7.1)$$

$$\text{Or, } \ln \frac{W_{Xylan,0}}{W_{Xylan}} = k_{Xylan} t \quad (5.7.2)$$

$$\text{Or, } k_{Xylan} = \frac{\ln \frac{W_{Xylan,0}}{W_{Xylan}}}{t} \quad (5.7.3)$$

Where, $W_{Xylan,0}$ and W_{Xylan} represent the weight of xylan at $t=0$ and at any time, t . (Basis: 10g initial RS sample being hydrolysed).

The values of rate constants have been determined based on the experimental values of xylan and glucan contents of the original and rice straw. Using the principle of integral method of analysis,

$\ln \frac{W_{Xylan,0}}{W_{Xylan}}$ and $\ln \frac{W_{Glucan,0}}{W_{Glucan}}$ have been plotted against the reaction time to test the validity of 1st order reaction kinetics (Levenspiel, 1998).

5.1.4 Elucidation of Mechanism

The analysis of liquid hydrolysis products of LWP, SAP and FCP reveals that fermentable sugars (glucose, xylose), platform chemicals (furfural, 5-hydroxymethyl furfural (5-HMF) and levulinic acid) and organic acid (formic acid and acetic acid) are the major products. From the present analysis and the literature it is clear that all three processes, LWP, SAP and FCP, are catalyzed by hydronium ion. (Wen, 1968; Heidari et al, 2021; Bandura & Lvov, 2006). The hydronium ion

catalyzes both in 1) heterogeneous and 2) homogeneous modes. During heterogeneous catalysis, H_3O^+ acts on the solid rice straw and mostly breaks the linkage of hemicelluloses with lignin and depolymerizes most of the hemicellulose and a part of amorphous cellulose (Canales & Guàrdia, 2022). The monomers of hemicelluloses, namely xylose and that of cellulose, namely glucose are transferred to the aqueous phase from the solid matrix (Yu et al, 2010; Yang et al, 2013). In the aqueous phase xylose and glucose are respectively converted to furfural and 5-HMF under the catalytic action of H_3O^+ . In the aqueous phase, 5-HMF is again converted to levulinic acid and formic acid (Kamireddy et al, 2013; Chai et al, 2022). The reactions involving hydronium ions, as available in the literature, have been provided in Figures 5.2.

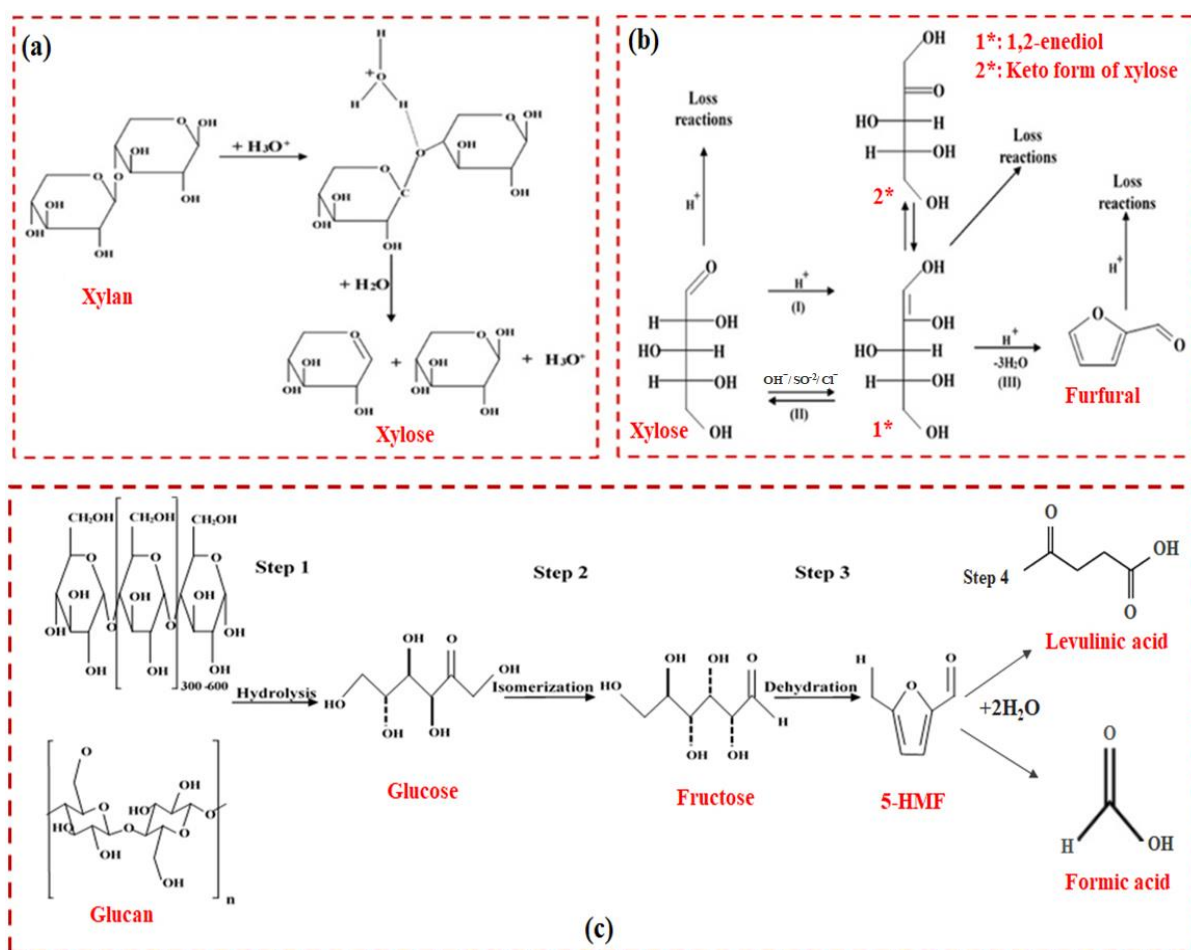


Fig. 5.2. Proposed mechanisms for the formation of products obtained from HWP/SAP/FCP pretreatment (a: Xylan hydrolysis; b: Formation of furfural and degraded products from xylose; c: Conversion of glucan in presence of hydronium ions)

In agreement with literature, a shrinking core behavior, as applicable in case of heterogeneous non-catalytic solid-fluid chemical reaction, can be postulated for the heterogeneous catalysis of hydronium ion (Bandura & Lvov, 2006; Guàrdia, 2022). In this case the catalyst is originally in aqueous phase and the reactants (hemicelluloses, cellulose etc.) are in solid phase. Whatever may be the type of pretreatment (LWP/SAP/FCP), the following steps appear to be common for this mechanism (shown in the Figure 5.3a):

- i. The solid particles are submerged in either hot water or hot dilute acid or hot ferric chloride solution and a stagnant liquid film is developed around each solid sphere.
- ii. The hydronium ions reach the solid surface through the liquid film.
- iii. First the reaction starts at the surface and the reaction front propagates towards the centre as hydronium ion diffuses through the reacted layer to the unreacted core.
- iv. As time progresses the radius of the unreacted core decreases although the overall size remains almost unaltered. The reacted layers are expected to be porous as reactants (Hemicellulose and amorphous cellulose) are removed.
- v. The products diffuse through the reacted layer to the aqueous phase and participate in homogeneous catalytic reactions in presence of hydronium ions. As hydronium ion acts as the catalyst, it remains unchanged and is again transferred to the aqueous medium.

The propagation of the reaction front in the postulated mechanism and the homogeneous catalytic reactions are shown in Fig. 5.3b.

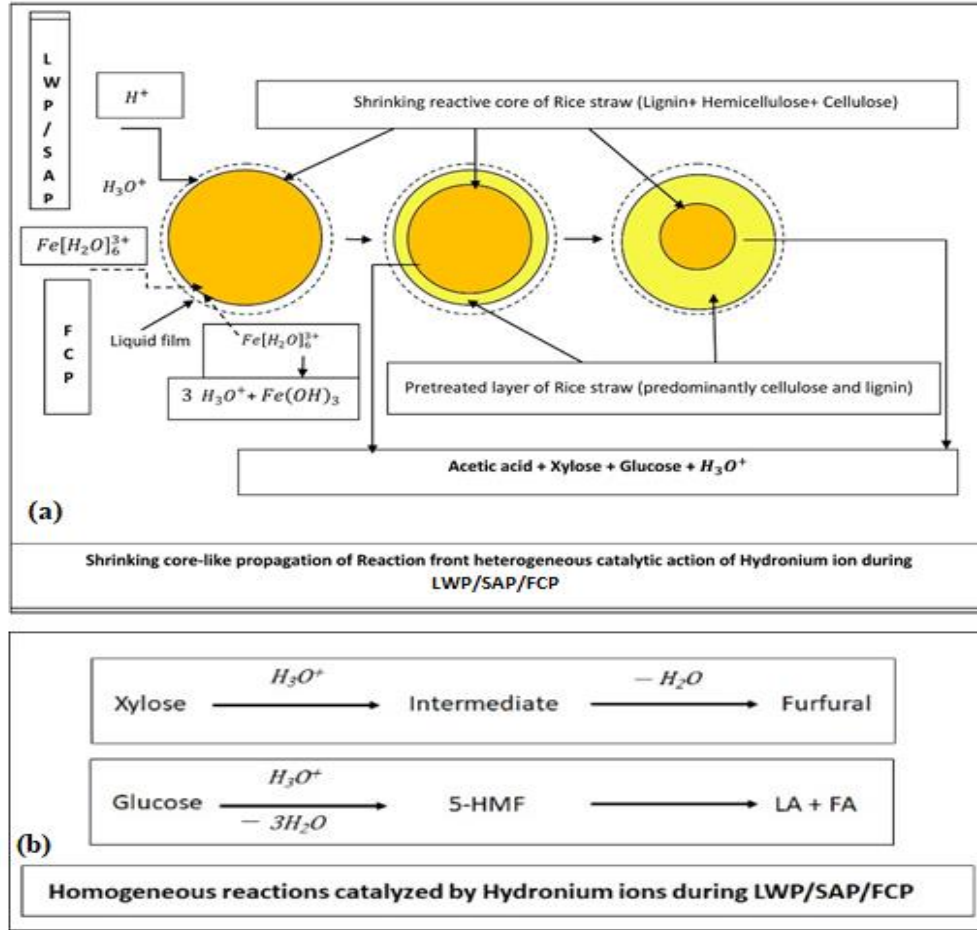


Fig. 5.3. Heterogeneous and homogeneous catalytic action of hydronium ions during LWP/SAP/FCP (a: Shrinking core-like propagation of reaction front heterogeneous catalytic action of hydronium ion; b: Homogeneous reactions catalyzed by hydronium ions)

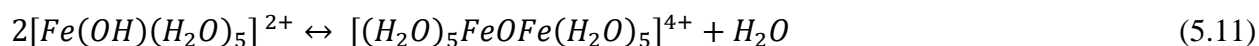
Self-ionization of water occurs through the reaction, $2H_2O \leftrightarrow H_3O^+ + OH^-$ with the ionization constant, $K_W = [H_3O^+][OH^-]$ (Bandura & Lvov, 2006). At each temperature, the concentration of H_3O^+ and $[OH^-]$ ions are equal ($= \sqrt{K_W}$).

In case of sulfuric acid, the dissociation follows the following steps (Bandura & Lvov, 2006):



As reported in a recent literature, the acid diffuses through the cell wall during pre-hydrolysis followed by hydrolysis of carbohydrate polymers (Zhibo et al, 2018). The hydrolysis products also diffuse back to the liquid (aqueous) medium.

On dissolution, FeCl_3 acts as a Lewis acid and water molecules are attracted by sharing electron pairs towards the ferric cation (Fe^{3+}). As reported in the literature a complex cation $\text{Fe}[\text{H}_2\text{O}]_6^{3+}$ of radius 0.268nm is formed by the bonding of six water molecules through monodentate ligands (Zhibo et al, 2018). H_3O^+ is formed through the following reactions:



5.1.5 Experimental Results and Discussion

5.1.5.1 Feedstock Characterization

The proximate analysis (moisture, fixed carbon, volatile matter and ash), elemental analysis (carbon, hydrogen, nitrogen and sulfur), chemical composition (glucan, xylan, Klason lignin and acid soluble lignin) and metal composition (silicon, potassium, calcium and iron) of rice straw have been reported in Table 5.1 respectively.

Table 5.1 Proximate analysis, elemental analysis, chemical composition and metal composition of rice straw

Proximate analysis % (w)	Elemental analysis % (w)	Chemical composition % (w)	Metal composition % (w)
Moisture: 5.7 ± 0.11	Carbon: 37.3	Glucan: 38.8 ± 0.57	Silicon: 5.73
FC*: 3.4 ± 0.33	Hydrogen: 5.2	Xylan: 17.6 ± 0.12	Potassium: 6.34
VM*: 71.9 ± 2.7	Nitrogen: 0.22	KL*: 15.3 ± 0.15	Calcium: 0.04
Ash: 10.9 ± 0.42	Sulfur: 0.27	ASL*: 2.5 ± 0.02	Iron: 0.01

(FC*, VM*, KL* and ASL refer as fixed carbon, volatile matter, Klason lignin and acid soluble lignin respectively)

The most abundant biopolymer on earth is β – 1,4 *glucan*. Most of the plant cellulose is β – 1,4 *glucan* (Bulmer et al., 2021). Therefore, in the present study, cellulose has been considered

as glucan (β – 1,4 *glucan*). In many reported articles on lignocellulosic biomass pretreatment, cellulose and glucan have been used as synonyms (Wu et al., 2023; Han et al., 2020; Agbor et al, 2011). Hemicellulose is composed majorly of xylan and insignificant quantities of arabinan, mannan and galactan (Ye and Zhong, 2022). Hence, in the present study, xylan has been considered as hemicellulose. There are many other literature evidences where hemicellulose has been considered as xylan (Scapini et al, 2021; Otieno and Ahring, 2012; Carvalheiro et al, 2008).

5.1.5.2 Comparison of composition of Liquid hydrolysate

In Fig. 5.4, the yield (g of product / kg of RS) of fermentable sugars (glucose, xylose), platform chemicals (furfural, 5-hydroxymethyl furfural (5-HMF) and levulinic acid) and organic acid (formic acid and acetic acid) in the hydrolysate, obtained after 10 minutes of LWP, SAP and FCP have been compared over the temperature range of 140 – 180°C. In Fig. 5.4a, 5.4c and 5.4e the yield of xylose, glucose and furfural in the hydrolysate, obtained respectively through LWP, SAP and FCP have been plotted respectively against temperature. Similarly, in Fig. 5.4b, 5.4d and 5.4f the yield of 5-HMF, formic acid, acetic acid and levulinic acid in the hydrolysate, obtained respectively through LWP, SAP (=0.1M) and FCP (=0.1M) have been plotted. Yields have been determined using equations 5.1 and 5.2.

Scrutiny of production data of xylose, glucose and furfural

From the analysis of Fig. 5.4a, it has been clearly observed that the glucose and xylose yields from LWP have an increasing trend with temperature right from 140 – 180°C during LWP. While the yield of xylose has increased from 1.1 g/kg RS to 3.8 g/kg RS, that of glucose has increased from 0.5 g/kg RS to 3.1 g/kg RS as the temperature is increased from 140°C to 180°C. The structures of lignocellulosic biomass is constituted of interconnected network of carbohydrate polymers, cellulose, hemicellulose and lignin. According to literature, the microfibrils of cellulose are embedded on hemicellulose network through lignin aggregates (Smith, 2019). This can be considered as the “skeletal structure” of lignocellulosic biomass. As reported in case of wheat straw, it is expected that the skeletal structure is weakened at high temperature (Rahmani et al, 2022). Thus, the whole conversion of hemicelluloses during LWP, can be represented by the following scheme: (I) Formation of surface radicals, acting as pre-hydrolysis step; (II) Dissociation of hemicellulose from the structure through decarboxylation and release of acetic acid ; (III) hydrolysis of hemicellulose to xylose, furfural, formic acid etc by the synergistic action of acetic

acid and catalysis of hydronium ion, H_3O^+ , released through the ionization of H_2O . In parallel, the amorphous portion of cellulose is decomposed to glucose in presence of H_3O^+ generated by the ionization of water. Further, there is a possibility of dehydration of xylose and glucose respectively to furfural and 5-HMF through the homogeneous catalysis of hydronium ion. Thus it is expected that the whole process is influenced by the rate of release of hydronium ions. The value of ionization constant of water, K_W , as described in Section 3.3, increases with temperature (Bandura&Lvov, 2006). As reported in Bandura and Lvov, the values of $(-\log(K_W))$ are 4.25, (i.e., $K_W = 10^{-4.25}$), 3.64, (i.e., $K_W = 10^{-3.64}$) and 3.31 (i.e., $K_W = 10^{-3.31}$) at 100°C, 150°C and 200°C respectively. Therefore, the concentration of H_3O^+ ion also increases with temperature under the present range of study (140-180°C). As shown in Figure 5.3, the released hydronium diffuse through the rice straw and depolymerisation of both xylan and glucan has occurred. Further, xylose is converted to furfural with the aid of hydronium ions. This can clearly explain the increasing trend of concentration of xylose, glucose and furfural during LWP. At 140°C, no furfural is formed during LWP. The increasing trend in the yield of furfural has been observed from 150°C. The yield of furfural has increased from 0.13 g/kg RS to 0.72 g/kg RS when temperature is increased from 150°C to 180°C. As evident from the representation of reaction network in Figure 5.3, furfural is generated through homogeneous dehydration of released xylose through catalysis of H_3O^+ . As the release of hydronium ion is increased with the rise of temperature, furfural is produced only at high temperature range during LWP. It is an established fact that the severity of autohydrolysis increases with temperature due to the increase in the release of H_3O^+ in the subcritical condition and it passes through a maximum at 300°C (Sarkar et al, 2021; Kumar et al, 2010).

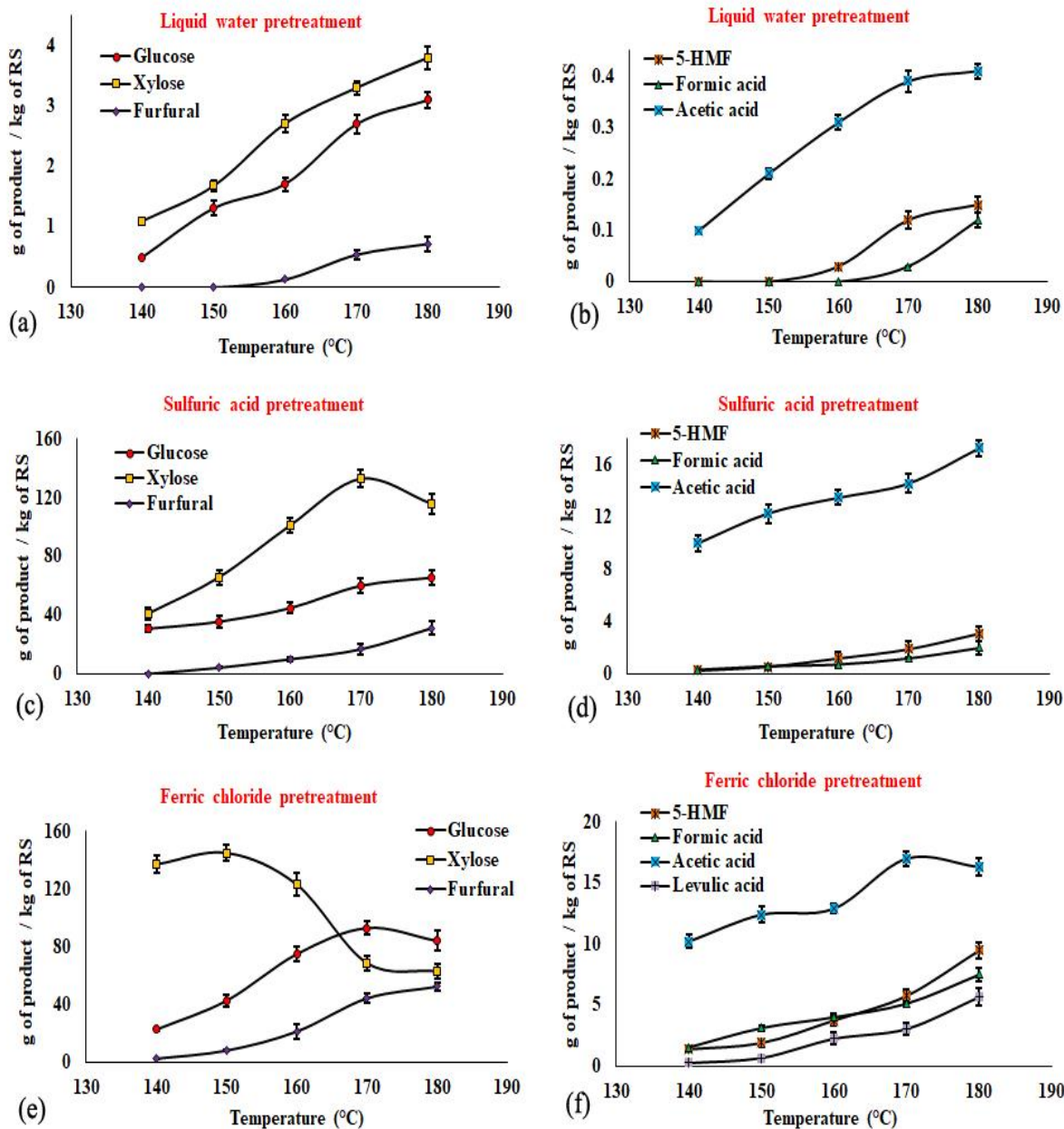


Fig. 5.4. The yield of products obtained from pretreated liquor at different temperatures; (a), (c) and (e): the yield glucose, xylose and furfural obtained from LWP, SAP and FCP respectively; (b), (d) and (f): the yield of 5-HMF, formic acid, acetic acid and levulinic acid obtained from LWP, SAP and FCP

In case of SAP, it has been observed from the Fig. 5.4c that glucose yield follows an increasing pattern with temperature over the range of 140-180°C during SAP. Xylose yield increases from

140°C to 170°C after which it has decreased at 180°C. While xylose yield has increased from 41.2 g/kg RS at 140°C to the maximum of 115.9 g/kg RS at 170°C, glucose yield in the hydrolysate varies from 30.9 g/kg RS to 65.7 g/kg RS as the temperature is increased from 140°C to 180°C. Unlike the result of LWP, the Fig. 5.4c also shows that the furfural yield of 0.19 g/kg RS has been detected even at 140°C for SAP and follows an increasing trend with the increase of temperature up to 180°C. At 180°C, the furfural yield reaches the value of 31.3 g/kg RS through SAP. As sulfuric acid is a strong acid, its dissociation, represented by Equations 5.8 and 5.9, is instantaneous and the concentration of H_3O^+ ions in the 0.1M H_2SO_4 solution is 0.2M. Therefore, it is expected that the rate of hydrolysis of both hemicellulose and cellulose is much faster in case of SAP, compared to LWP. That is why the highest values of xylose and glucose concentration, obtained in case of SAP are 35.9 fold and 21.0 fold higher than those obtained through LWP. However, as in case of LWP, the drastic weakening of overall structure of the feedstock is expected at high temperature. Therefore, as the temperature increases besides the enhancement of hydrolysis rate, the resistance to internal diffusion of H_3O^+ is expected to be lowered and the overall rates of release of products increase. The ever increasing trend of furfural yield and decreasing pattern of xylose yield beyond 170°C clearly indicate that beyond a certain temperature, the rate of dehydration of xylose to furfural is higher than the rate of xylose formation from xylan depolymerization. Although both LWP and SAP are expected to follow the same mechanism driven by hydronium ion, the concentration of hydronium ions is much higher than that of LWP leading to much more depolymerisation of the carbohydrate polymers, xylan and glucan releasing xylose and glucose. From the analysis of Fig. 5.4e it is clear that in case of FCP, yield-temperature pattern for xylose is different from those observed for LWP and SAP. Although for LWP and SAP, increasing trend is observed up to 180°C and 170°C respectively, xylose yield passes through a maximum at 150°C beyond which it decreases in case of FCP. Xylose yield increases from 137 g/kg RS at 140 °C to 145 g/kg RS at 150 °C after which it has sharply decreased to 63.1 g/kg RS at 180 °C. The yield of furfural exhibits an increasing trend with temperature throughout the entire temperature range. Furfural yield increases from 2.7 g/kg RS at 140°C to 52.5 g/kg RS at 180°C. The difference in behavior of RS towards SAP and FCP is due to the influence of Bronsted acid behavior of ferric chloride solution as represented by Equations 5.10 and 5.11.

The H^+ , and hence H_3O^+ formed from complex cation, diffuses across the surface of rice straw and catalyzes heterogeneous reaction. As in case of LWP and SAP, acetic acid is formed and

hemicellulose is solubilized. With the help of the complex cation, protonation of ether bond in hemicellulose occurs via hydronium (H_3O^+) ion (Sun et al, 2021). The hydrolysis products diffuse to the medium. The decreasing trend of xylose right from 150°C indicates higher rate of dehydration of xylose to furfural than that of production rate of xylose at temperature higher than 150°C. Glucose yield shows an increasing trend with temperature up to 170°C, followed by a decreasing trend till 180°C. As the temperature is increased, glucose yield first increases from 22.9 g/kg RS at 140°C 93.1 g/kg RS at 170°C and then decreases further to 85.2 g/kg RS at 180°C. This indicates that at higher temperature the conversion rate of glucose to 5-HMF, as described under the reaction network (Figure 5.3), exceeds the rate of its formation from glucan.

When the highest values of xylose yield in the hydrolysate obtained through LWP (3.8 g/kg RS), SAP (132.9 g/kg RS) and FCP (145.1 g/kg RS) are compared it can be inferred that there are 35.97 fold (or 3397%) and 38.18 fold (or 3718%) increase for SAP and FCP with reference to LWP. Similarly, for the highest values of glucose yield, there is 21.0 fold (or 2000%) and 30.03 fold (or 2903%) increase for SAP and FCP with reference to LWP. When the highest yield of furfural obtained after LWP (0.72 g/kg RS), SAP (31.3 g/kg RS) and FCP (52.5 g/kg RS) are compared it is clear that 13.75 times (or 4247%) and 72.91 times (7191%) increase is achieved through SAP and FCP respectively, compared to LWP. As reported in the literature the capability of Fe^{3+} to attract six water molecules, as shown in Figure 5.3, facilitates the availability of hydronium ions resulting in drastic depolymerization of carbohydrate polymers, particularly, xylan (Marcotullio & Jong, 2010). For the same reason, the decomposition of cellulose is also accelerated to a greater extent for FCP compared to LWP and SAP in the same temperature zone. Moreover, chloride ion present in ferric chloride has been reported to catalyze the enolization of pentose xylose (Marcotullio & Jong, 2010). That is the reason why the generation of furfural during FWP of RS has occurred at a much higher rate compared to LWP and SAP.

Scrutiny of production data of Acetic acid, 5-HMF, Levulinic acid and Formic acid

From Fig. 5.4b, representing the yield-temperature pattern for LWP, it appears that the yield of acetic acid has an increasing trend with the increase of pretreatment temperature from 140°C to 180°C. Fig. 5.4b also indicates that although 5- HMF appears at 150°C, there is an increase in the yield up to 180°C. No formation of LA has been observed during LWP. From the inspection of Fig. 5.4b, it is also observed that formic acid first appears at 160°C and there is an increase in the

yield up to 180°C. Hydronium ion driven hydrolysis of rice straw, represented in Figure 5.3 can explain the product trajectory. Acetic acid is released when xylan –lignin linkage gets broken. 5-HMF forms from the homogeneous catalysis of dehydration of glucose released from depolymerisation of cellulose. As the hydronium ion concentration is low at temperature 150°C, 5-HMF is not produced. From Fig. 5.4d, used from SAP, it appears that the yields of both acetic acid, 5-HMF and formic acid exhibit slightly increasing trends with the increase of pretreatment temperature from 140°C to 180°C. This signifies that in case of SAP, the sufficient presence of hydronium ion results in the formation of 5-HMF from a temperature as low as 140°C. From the inspection of Fig. 5.4d Levulinic acid is not detected even in case of SAP. However, in some reported works levulinic acid could be obtained by SAP of biomass either by elongating pretreatment time, increase of acid strength, decrease in liquid: solid ratio and by the increase in acid strength or by using two-step acid pretreatment (Elumalai et al, 2016; Lee et al, 2023; Liu et al, 2020). In a recent study 114 g levulinic acid /kg sugar cane bagasse has been obtained at 170°C, which is within the present experimental range (Shen et al, 2023). In that study the acid concentration was 1.5% (i.e., 0.153M), pretreatment time was 2h and the liquid to solid ratio was maintained at 6:1 (Shen et al, 2023). Therefore while the acid concentration and pretreatment time are much higher (0.15M>0.1M; 120min>>10min) compared to those of the present study, the liquid to solid ratio is much lower (6:1>10:1) (Shen et al, 2023). In case of FCP, as depicted by Fig. 5.4f, the yield of acetic acid, 5-HMF and levulinic acid show increasing trend as the temperature is increased from 140°C to 170°C. Although acetic acid exhibits a slightly decreasing trend beyond 170°C, the increasing trend is maintained by 5-HMF and levulinic acid up to 180°C. From FCP, the yields of all these products are much higher. The maximum yield of products (glucose, xylose, furfural, 5-HMF, formic acid, acetic acid and levulinic acid) obtained from different pretreatment methods (LWP, SAP and FCP), have been reported in the Table 5.2.

Table 5.2 Maximum product yields obtained from LWP, SAP and FCP

Pretreatment	Maximum products yield (g of product / kg of RS)						
Type	Glucose	Xylose	Furfural	5-HMF	FA*	AA*	LA*
LWP	3.1 ± 0.01	3.8 ± 0.012	0.72 ± 0.015	0.15 ± 0.011	0.12 ± 0.009	0.41 ± 0.01	Nd*
SAP	65.7	115.9	31.3	3.1	2.0	17.3	Nd*

	± 3.1	± 5.6	± 1.4	± 0.16	± 0.1	± 0.59	
FCP	93.1	145.0	52.5	9.4	7.4	17.0	5.67
	± 5.8	± 6.0	± 2.7	± 0.081	± 0.49	± 0.69	± 0.27

(FA*, AA*, LA* and Nd* referred as formic acid, acetic acid, levulinic acid and not detected respectively).

The enhanced production of all hydrolysis products via FCP can be explained by the influence of Fe³⁺ ions attracting six water molecules, facilitating the release of hydronium ion at all temperature under study. The influence of chloride ions also facilitates the enolization reaction during the dehydration of xylose to furfural.

The yields of products obtained from LWP have been found to be comparable with literature (Syafrika & Matsumura, 2018). However, in another reported higher value of glucose yield, namely, 7-11 g/kg has been reported (Syafrika & Matsumura, 2018). In their analysis, they also reported that for the same operating conditions, the glucose yield is higher from pure cellulose, present in a simulated mixture of cellulose, hemi-cellulose and lignin in the same ration as in RS. Therefore it is established that the structural bonding of the carbohydrates play a vital role during hydrothermal pretreatment.

The yield of products achieved from SAP have been compared with the literature data on nitric acid and sulfuric acid pretreatment of rice straw, as shown in Table 5.3 (Hsu et al., 2010).

Table 5.3 The yield of products from acid pretreatment on rice straw (literature and present study)

Yield (g of product/kg of RS)	Temperature (°C)	H ₂ SO ₄ Pretreatment Literature	H ₂ SO ₄ Pretreatment Present study
Glucose	140	-	30.9
	160	43.0	45.8
	180	63.1	65.7
Xylose	140	-	41.2
	160	136.0	101.2
	180	115.0	115.9

Furfural	140	-	0.19
	160	15.0	10.1
	180	27.0	31.3
5-HMF	140	-	0.26
	160	1.0	1.2
	180	3.0	3.1
Acetic acid	140	-	10.1
	160	13.0	13.5
	180	17.0	17.3

[H₂SO₄ pretreatment literature (Hsu et al., 2010)]

It has been observed that the yield of products obtained from SAP in present study is slightly higher than the yield of the products reported in literature (sulfuric acid pretreatment on rice straw).

The results of the present study are compared with the literature data for ferric chloride pretreatment of rice straw and other lignocellulosic feedstocks such as wheat straw, rapeseed straw and sugarcane bagasse (Chen et al, 2021; Tang et al, 2018; Romero et al, 2015; Zhang et al, 2018). The comparison of the process parameters and composition of feedstock are reported in Table 5.4.

Table 5.4 Comparison the composition of feedstock, the process parameters for FeCl₃ pretreatment on lignocellulosic biomass

Feedstock	Conditions of pretreatment				Composition of feed (w/w)			Reference
	Conc. mol/L	L:S* (v/w)	Temp (°C)	Time (min)	Glucan (%)	Xylan (%)	Lignin (%)	
Rice straw	0.1	10:1	170	30	31.3	31.3	15.5	Chen et al.
Wheat straw	0.1	10:1	180	40	28.7	17.4	20.0	Tang et al.
RSS*	0.1	8.3:1	160	20	31.6	13.2	17.8	Romeroet al.
SCB*	0.1	10:1	160	10	40.5	22.3	25.5	Zhang et al.
Rice straw	0.1	10:1	180	10	38.8	17.6	16.8	Present study

(L:S* referred as Liquid : Solid; RSS* and SCB* referred as rapeseed straw and sugarcane bagasse respectively)

The yields of different products in the hydrolysate, determined using equations 5.1 and 5.2 and % degradation of glucan and xylan, determined using equations 5.3 and 5.4, are compared with literature data, as provided in Table 5.5.

Table 5.5 Comparison the yields of products and degradation of xylan and glucan of present study with literature

Study	Yield of Products (g of product / kg of RS)							Degradation (%)	
	Glu*	Xyl*	Fur*	HMF*	FA*	AA*	LA*	Glucan	Xylan
Chen et al.	67.0	113.0	51.1	7.5	-	-	-	3.9	83.3
Tang et al.	9.0	5.0	26.0	3.0	8.0	19.0	0	19.0	97.2
Romeroet al.	36.2	96.12	-	-	-	-	-	17.0	78.2
Zhang et al.	35.0	52.0	37.0	2.0	-	26.0	-	16.4	100
Present study	85.2	63.1	52.5	9.4	7.4	16.3	5.6	31.4	96.8

(Glu*, Xyl*, Fur*, HMF*, FA*, AA* and LA* referred as glucose, xylose, furfural, 5-hydroxymethyl furfural, formic acid, acetic acid and levulinic acid respectively)

The yields of products namely, xylose, glucose, furfural, 5-HMF, formic acid, acetic acid and levulinic acid (obtained at 180 °C) for present study are comparable with literature data. In the present study, the yield of glucose and furfural are higher than the data reported in literature. Xylose yield at 180 °C for present study is lower than literature data. In the present study, at 150 °C, the yield of xylose is the highest. With increase in temperature, a major part of xylose is converted to furfural and as a result the yield of xylose becomes lower. However, the performance of ferric chloride in the pretreatment of Indian rice straw parameters seems to be the most effective among the three processes.

5.1.5.3 Comparison of degradation kinetics of xylan and glucan during pretreatment

$\ln \frac{W_{Xylan,0}}{W_{Xylan}}$ and $\ln \frac{W_{Glucan,0}}{W_{Glucan}}$ have been plotted against the reaction time (shown in the Figure 5.5) using temperature (140 °C -180°C) as a parameter for LWP, SAP and FCP. For all processes (LWP, SAP and FCP), straight lines have been obtained at each temperature (for different reaction time 4, 6, 8 and 10 minutes).

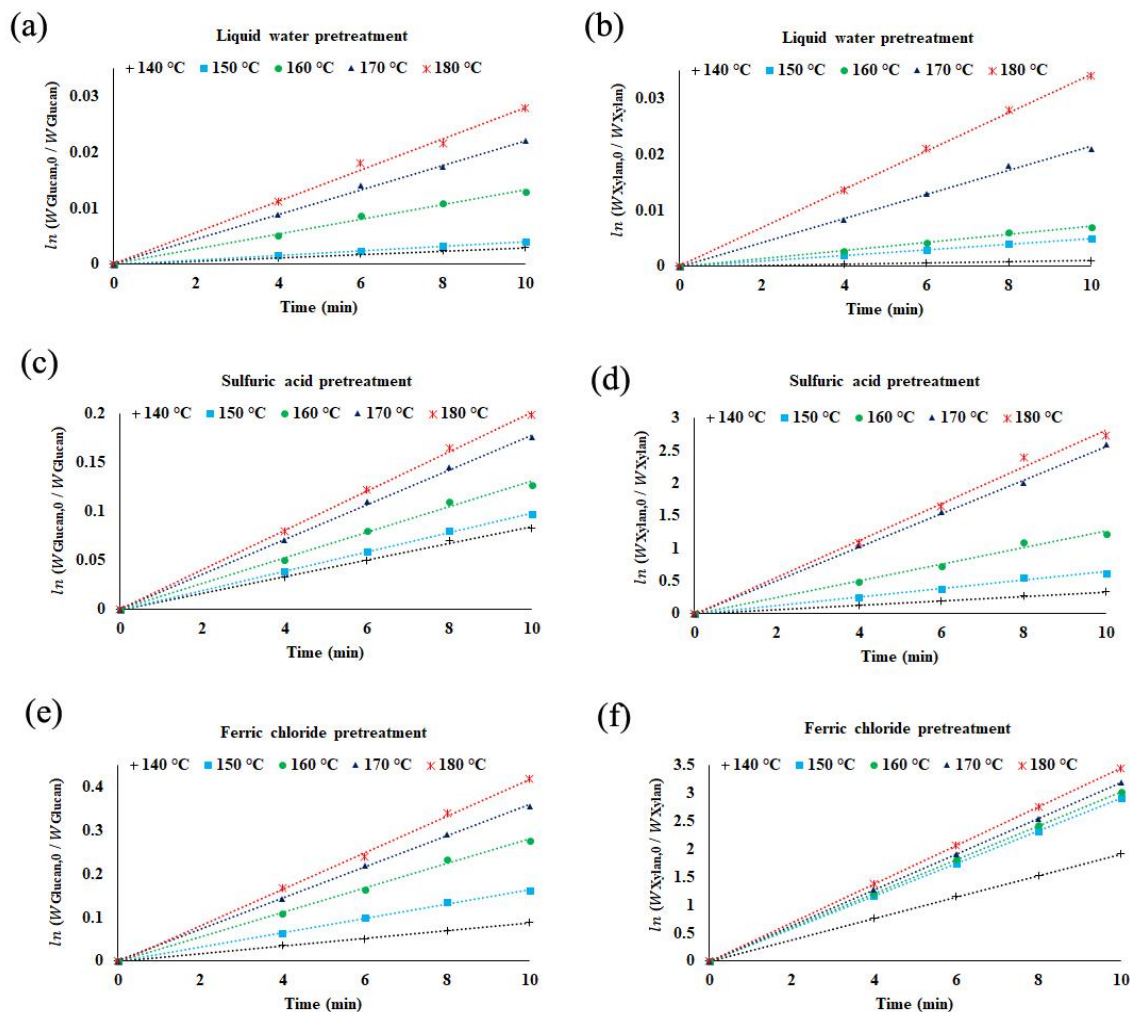


Fig. 5.5. Plots of $\ln \frac{W_{Glucan,0}}{W_{Glucan}}$ against the reaction time using temperature as a parameter ((a): LWP; (c): SAP; (e): FCP) and Plots of $\ln \frac{W_{Xylan,0}}{W_{Xylan}}$ against the reaction time using temperature as a parameter ((b): LWP; (d): SAP; (f): FCP)

Thus it is proved that the degradation of both xylan and glucan follows first order rate kinetics with respect to their respective concentrations. The rate constants have been determined from the slope of the linear plots and are provided in Table 5.6. From the analysis of the Table 5.6 it is clear that the rate constants increase with temperature. As per reported literature, the rate constants are functions of both temperature and concentration of hydronium ions (Krzelj et al, 2020).

All the rate constants have Arrhenius-type temperature dependence. However, different types of functionality of rate constant on the hydronium ions are reported. Thus, $k = k_0 e^{-\frac{E}{RT}} f(C_{H_3O^+})$. An usual representation of the functionality of rate constants on temperature and acid, in turn, hydronium ion, concentration is $k = k_0 A^n e^{-\frac{E}{RT}}$, where, A is the acid concentration, k_0 is pre-exponential factor, E activation energy and R universal rate constant (Krzelj et al, 2020; Kapu et al, 2016). As reported by Springer and Harris, there can be a change of H_3O^+ concentration with time due to the interaction with biomass leading to cation exchange following the reaction $BCOO^-M^+ + H^+ \rightarrow BCOO^-H^+ + M^+$, where, B is biomass and M^+ is the cation on it (Springer and Harris, 1985). As this increases the pH value by decreasing the quantity of H^+ or H_3O^+ ions in the solution, this is also called neutralisation effect. According to Springer and Harris, at a given temperature a correlation $\ln k = a * \ln H^+ + b$ was obtained for acid treatment of Aspen wood (Springer and Harris, 1985). According to Kapu et al, for autohydrolysis $f(C_{H_3O^+}) = a + bt$, t is hydrolysis time (Kapu et al, 2016). This signifies the dependence of k with time. This can be due to the time dependent release of H^+ or H_3O^+ ions during hydrolysis in presence of only water (Kapu et al, 2016). Under the present investigation, the concentration of acid (H_2SO_4) or metal chloride ($FeCl_3$) has been kept constant i.e. 0.1 M. At each temperature, the function $f(C_{H_3O^+})$ is thus constant. The time dependence of rate constant during LWP is also not considered. Therefore, the rate constant at each temperature incorporates a factor dependent on concentration of hydronium ion. Under the present study, the hydronium ion concentration during hydrolysis has not been determined. The temperature variation of rate constants, determined under the study, incorporates the effects of temperature on the ionization of water, acid and ferric chloride as well as the hydrolysis reactions. The comparison of rate contents of degradation of xylan and glucan clearly indicates that at all temperature the highest value is obtained for FCP. The high values of rate constant ensure that the same extent of hydrolysis at a particular temperature can be achieved at much smaller time. The comparison of the rate constant thus reveals the dependence of the hydrolysis kinetics of xylan and glucan of rice straw on the concentration of hydronium ion, polymer concentration and temperature. This knowledge can further be utilized for reactor design in the industrial scale. The glucan, xylan and lignin content in untreated rice straw are 38.84%, 17.59% and 16.85% respectively. The degradation (%) of glucan and xylan along with the composition (glucan, xylan and lignin mass fractions) have been reported in the Table 5.6. The

solid recovery (%), degradation of glucan and xylan (%) have been determined. It is observed that the percentage of solid recovery has decreased with increase in temperature. At 180 °C, the solid recovery (%) for LWP, SAP and FCP are 98.18, 89.53 and 69.69 respectively. The degradation of xylan and glucan have also shown an increasing trend with temperature.

Table 5.6 Conversion of Xylan and Glucan along with degradation rate constants

Pretreatment		Solid Residue (%)		Composition (w/w)			Degradation		Rate Constant	
Type	Temp (°C)			Glucan (%)	Xylan (%)	Lignin (%)	Glucan (%)	Xylan (%)	k _{Glucan} (min ⁻¹)	k _{Xylan} (min ⁻¹)
LWP	140	99.71 ± 0.03		38.81 ± 0.07	17.57 ± 0.01	16.89 ± 0.02	0.36	0.40	0.0003	0.0001
SAP	140	90.71 ± 0.04		39.35 ± 0.10	13.72 ± 0.01	18.52 ± 0.04	8.11	29.21	0.0083	0.0335
FCP	140	77.15 ± 0.32		45.98 ± 0.21	3.31 ± 0.03	21.65 ± 0.08	8.67	85.41	0.0089	0.1918
LWP	150	99.65 ± 0.04		38.79 ± 0.08	17.51 ± 0.01	16.88 ± 0.01	0.47	0.81	0.0004	0.0005
SAP	150	87.3 ± 0.10		40.27 ± 0.27	10.69 ± 0.02	19.17 ± 0.02	8.10	46.91	0.0098	0.0622
FCP	150	73.55 ± 0.51		45.91 ± 0.09	1.29 ± 0.29	22.42 ± 0.13	15.95	95.61	0.0161	0.2909
LWP	160	99.14 ± 0.05		38.63 ± 0.08	17.47 ± 0.03	16.97 ± 0.05	1.39	1.53	0.0013	0.0007
SAP	160	81.3 ± 0.54		42.01 ± 0.09	6.28 ± 0.05	20.55 ± 0.07	4.05	70.94	0.0127	0.1226
FCP	160	71.90 ± 1.09		40.92 ± 1.13	1.17 ± 0.07	22.43 ± 0.05	25.25	95.22	0.0276	0.3029
LWP	170	98.76 ± 0.09		38.44 ± 0.10	17.22 ± 0.03	17.07 ± 0.08	2.25	3.31	0.0022	0.0021

SAP	170	76.0	±	42.78	1.51	21.96	16.27	93.46	0.0176	0.2718
		0.78		± 0.03	± 0.12	± 0.12				
FCP	170	69.81	±	38.92	1.03	21.20	30.04	95.91	0.0356	0.3186
		1.31		± 0.79	± 0.19	± 0.21				
LWP	180	98.18	±	38.41	17.01	17.05	2.91	5.05	0.0028	0.0034
		0.12		± 0.01	± 0.01	± 0.02				
SAP	180	75.07	±	42.91	1.54	22.31	18.22	93.51	0.0199	0.2724
		0.89		± 0.17	± 0.03	± 0.11				
FCP	180	69.69	±	38.23	0.79	21.03	31.40	96.87	0.0420	0.3453
		1.29		± 1.01	± 0.46	± 0.33				

The maximum degradation of glucan and xylan occurred at 180 °C. The maximum xylan degradation from LWP, SAP and FCP are determined as 5.05 %, 93.51 % and 96.87 % respectively. Whereas, the maximum glucan degradation from LWP, SAP and FCP have been reported as 2.91 %, 18.22 % and 31.40 % respectively. Thus the solid composition again establishes the trend observed in case of products appearing in the hydrolysate.

5.1.5.4 Comparison of characteristics of untreated and pretreated rice straw

TGA and DTG of untreated and pretreated rice straw

Fig. 5.6 represents the thermos-gravimetric (TG) plots, showing the change in mass with temperature in the range of 50°C to 900 °C RS and pretreated RS. From the Fig. 5.6a, showing the TGA and DTG plots for RS, it appears that the % mass (with respect to initial sample mass) - Temperature profile can be divided into four distinct regions, I: 50 –110°C; II: 110-220°C; III: 220-370°C; IV: 370– 900 °C. In region I, there is 4% decrease in the mass, signifying the loss of moisture. In Region II there is no change in % mass and hence no thermal decomposition of rice straw below 220 °C. In regions III and IV, loss in mass has been observed, however the temperature gradient of mass loss in these two regions are different. In Region II (220-370°C), temperature gradient of % mass loss is 0.3384%/°C as the % mass has decreased from 96% to 45%. Whereas in Region IV (370– 900 °C), % mass loss is 0.0547%/°C as the % mass has decreased from 45% to 16%. Thus the gradient in region IV is much lower than that obtained in Region III.

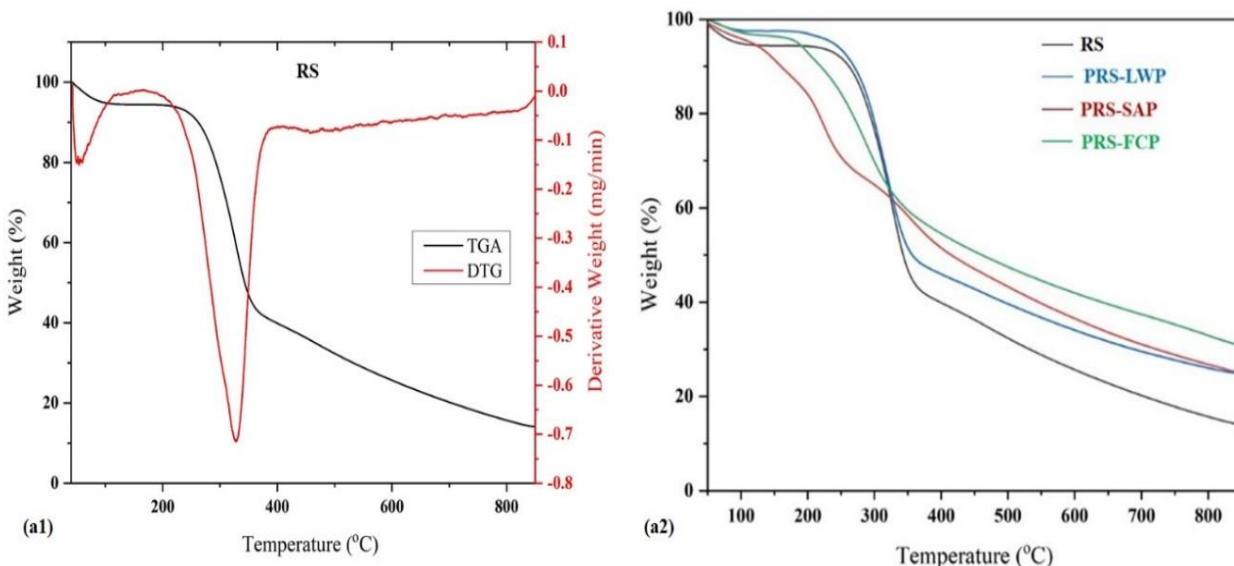


Fig. 5.6 TG and DTG curves of RS (a); TG curves of RS and PRS (b)

As reported in the literature, hemicellulose, cellulose and lignin decompose at the temperature range of 220 – 315 °C, 300 – 400 °C and 150 – 900 °C respectively (Waters et al, 2017). Therefore, it can be envisaged that region III signifies the thermal decomposition of hemicellulose and cellulose. Region IV stands for the thermal decomposition of lignin. Although the rates of decomposition of cellulose and hemicellulose increase sharply with temperature that of lignin changes slowly with lesser sensitivity towards temperature.

As it is not the intention of the present work to combine the effect of thermal decomposition and pretreatment, the temperature is chosen to be 180 °C where the effect of hydronium-ion based catalytic pretreatment can be exclusively studied.

In Fig. 5.6b, the % mass (with respect to initial sample mass) -Temperature profiles of untreated rice straw and pretreated rice straw obtained through LWP, SAP (=0.1M) and FCP (=0.1M) have been plotted. Similar to the TG profile of untreated rice straw four regions are observed for treated samples, except that obtained for FCP. In case of FCP, three regions are obtained. The temperature span and the temperature gradient of %mass are different for the pretreated RS (PRS) obtained through LWP, SAP and FCP. These are shown in Table 5.7.

Table 5.7 Temperature span and gradient of %mass loss for RS and PRS following LWP, SAP and FCP corresponding to four distinct regions in TGA.

Region	Temperature Span (°C)				Temperature gradient of % mass loss (°C ⁻¹)			
	RS	PRS-LWP	PRS-SAP	PRS-FCP	RS	PRS-LWP	PRS-SAP	PRS-FCP
I	50-110	50-200	50-110	50-200	0.0705	0.0133	0.05	0.04
II	110-220	200-300	110-200	200-300	0	0.17	0.1333	0.19
III	220-370	300-400	200-300	300-900	0.3384	0.33	0.2	0.0733
IV	370-900	400-900	300-900	Nil	0.0547	0.038	0.06	Nil

The difference in the TG profiles clearly reflects the effect of de-polymerization and removal of carbohydrate polymers, namely, hemicellulose and amorphous part of cellulose during different pretreatment process.

FTIR analysis of untreated and pretreated RS

From the Fig. 5.7a, it is clearly noted that the absorption peaks are obtained at 3333 cm⁻¹, 2919 cm⁻¹, 1625 and 1034 cm⁻¹. From the literature, it is known that the absorption peak at 3333 cm⁻¹ signifies O – H stretching produced by the vibration of hydroxyl group linked in lignin and cellulose (Costa Lopes et al, 2013). The peak at 2919 cm⁻¹ signifies the C – H stretching from CH₂ -group. The absorption peak at 1625 and 1034 cm⁻¹ indicate C = C and C – O stretching respectively. At each position there is a decrease in the peak area for pretreated sample, in the order of PRS- FCP < PRS- SAP < PRS-LWP < RS. In case of ferric chloride treatment on rice straw, the peaks from 3500 – 2500 cm⁻¹ have almost disappeared. The FTIR spectra actually re-establish the effectiveness of de-polymerization and removal of carbohydrate polymers during different pretreatment process.

XRD analysis of untreated and pretreated RS

From the Fig. 5.7b, it has been observed that while the value of CrI (%) for RS is 37.08%, those of PRS-LWP; PRS- SAP and PRS- FCP are 41.94%, 43.53% and 47.86% respectively. The increment of CrI (%) through the pretreatment processes is due to the removal of hemicellulose

and amorphous cellulose, as already established through the products identified in the aqueous hydrolysate.

FESEM analysis of untreated and pretreated RS

The inspection of the Fig. 5.7c1 reveals that untreated RS has smooth, flat and fibrillary surface. As observed from Fig. 5.7c2-c4, the external surface has developed cracks, pores and disruptions through pretreatment in the order FCP>SAP>LWP. As postulated by shrinking core model, the reaction front starts from the surface and progresses towards the centre and hence it is expected that the structural breakdown appears on the surface of the pretreated solid due to each pretreatment.

EDS analysis of untreated RS and pretreated solid

EDS analysis of PRS-FCP has been conducted to check how much containment of iron in the RS occurs after pretreatment through FCP. Fig. 5.7d ascertains that some Fe metal is retained after FCP- When compared with the EDS of untreated RS, it appears that besides the confirmation of the presence of iron in PRS-FCP, the content of metals like Si, Ca and Mg increases. The content of K however decreases. The increase in the content of Si, Ca and Mg is due to the decrease in the total solid content.

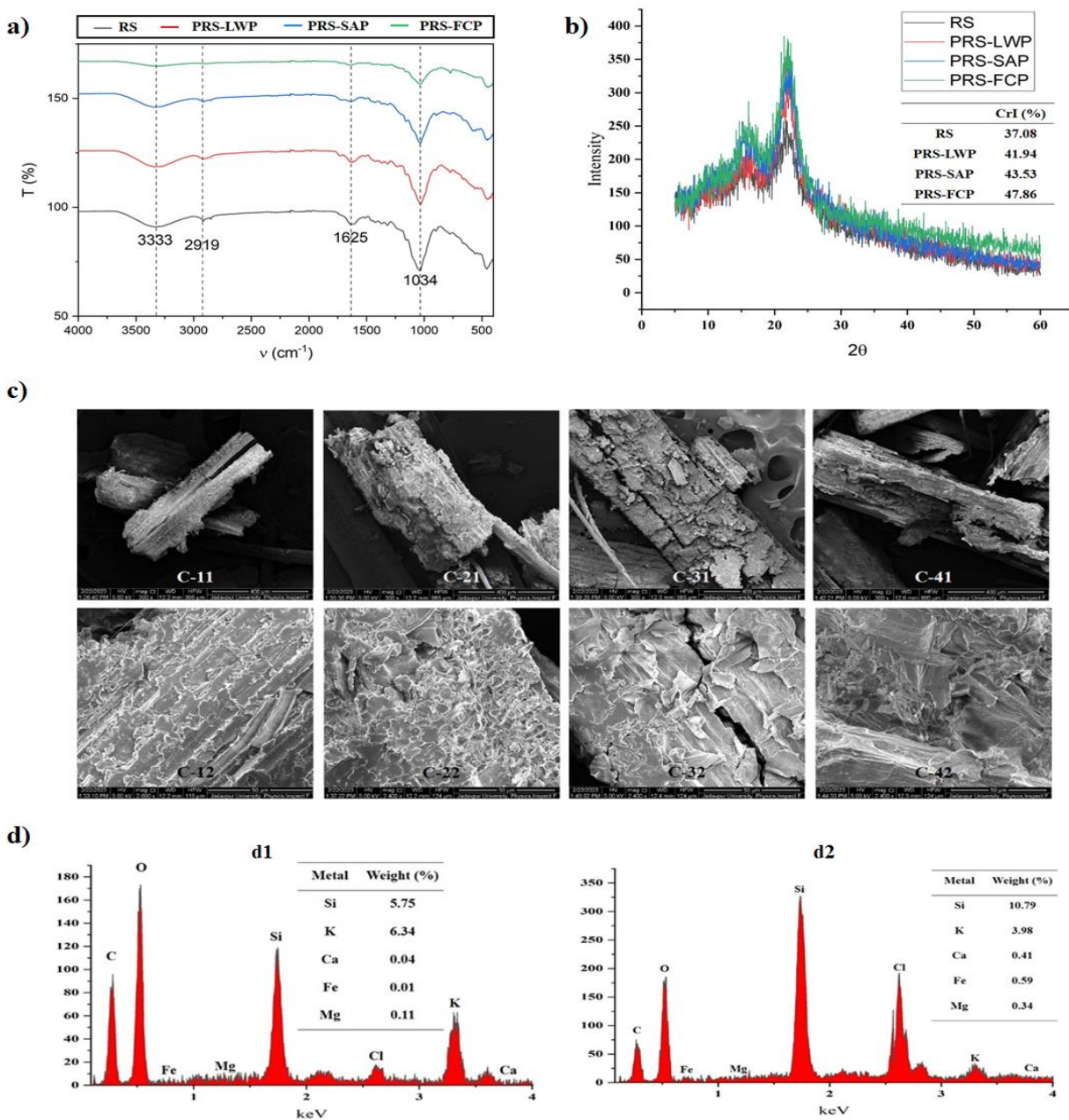


Fig. 5.7. a: FTIR of untreated and pretreated RS (where T and ν were the transmittance and wavenumber respectively); **b:** Crystallinity index (CrI) of untreated rice straw and pretreated rice straw; **c:** FESEM of untreated and pretreated RS (where c1: untreated RS, c2, c3 and c4: pretreated solid obtained from LWP, SAP and FCP at different magnification of image, 400 and 50 μ m); **d:** EDS results (where d1: untreated RS and d2: pretreated solid obtained from FCP)

5.1.5.5 Effect of ferric chloride concentration on liquid hydrolysate

For all products of hydrolysis of both xylan and glucan (except xylose), higher values of concentration are obtained using 0.2M FeCl₃ compared to those using 0.1 and 0.15 M strength (shown in the Fig. 5.8). This is due to the increase of rate of hydronium ion-assisted depolymerization of xylan and glucan with ferric chloride concentration. The highest yield (sum of all products in liquid hydrolysate) has been achieved at 170°C using 0.2M FeCl₃ solution and determined as 267.6 ± 10.41 (g of product / kg of rice straw).

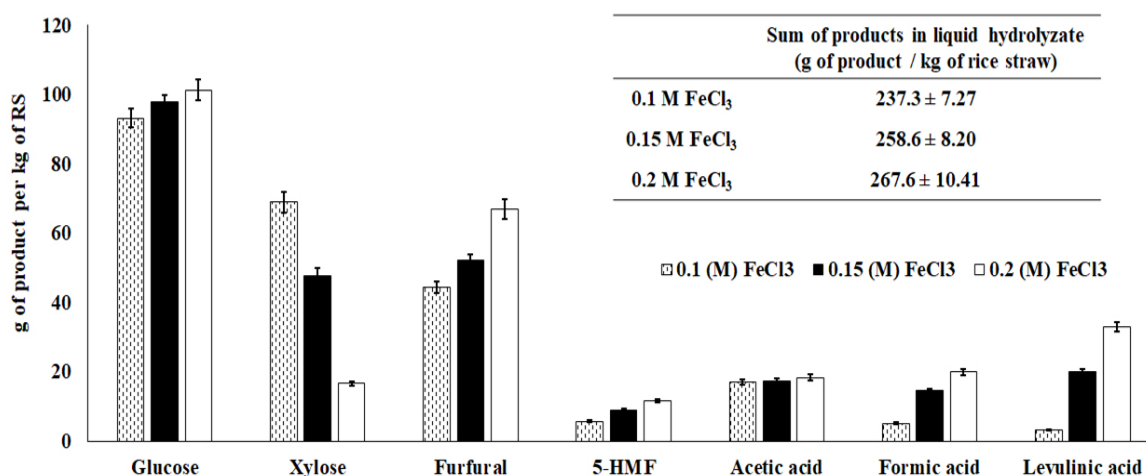


Fig. 5.8 Comparison the yield of products at different ferric chloride concentration

5.1.6 Mathematical modelling for FeCl₃ pretreatment of rice straw

A mathematical model has been developed for the conversion of xylan (into xylose and valuable products) and cellulose (into glucose and valuable products) respectively. 0.2 M ferric chloride solution has been used for experimental purpose.

5.1.6.1 Conversion of xylan into xylose and other products

In the proposed model, reaction scheme has been used for the conversion of xylan series and parallel reactions. According to this scheme, xylan in rice straw is first converted to soluble xylan. The soluble xylan is subsequently converted to xylose and furfural following different reactions. Xylose is also converted to furfural. Portions of xylose and furfural are also converted to degradation products similar to the reaction mechanism of acid hydrolysis (Morinelly et al, 2009; Lee et al, 1998; Dussan et al, 2015). The reaction scheme has been presented in Figure 5.9.a.

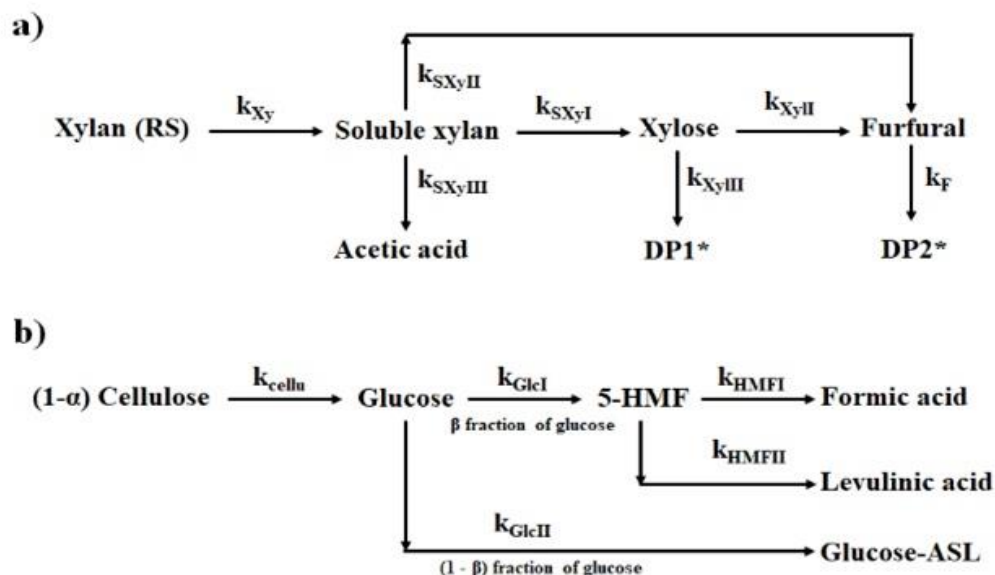
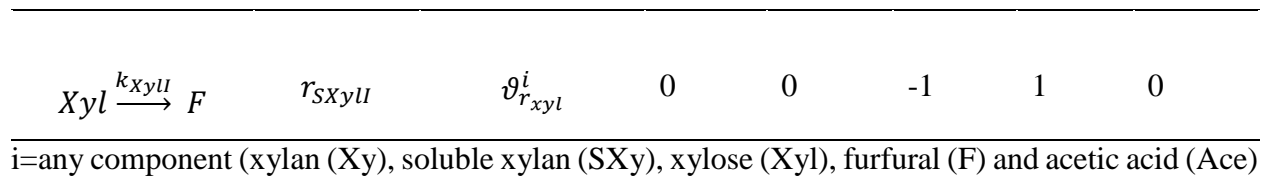


Fig. 5.9. Mathematical model for xylan and cellulose conversion into valuable products (a: Conversion of Xylan into xylose and other products; b: Conversion of cellulose into glucose and other products) [* DP1 and DP2: decomposition products and xylose and furfural degradation]

Except the reactions generating decomposition products, the reaction rate and stoichiometric coefficients of different compounds in the corresponding reactions are represented, along with their values, in Table 5.8.

Table 5.8 Reaction rates and Stoichiometric Coefficients of compounds in different reactions

Reaction	Reaction rate	Generalized Stoichiometric Coefficient	Values of Component-wise Stoichiometric Coefficient				
			Xy	SXy	Xyl	F	Ace
$Xy \xrightarrow{k_{Xy}} SXy$	r_{xy}	$\vartheta_{r_{xy}}^i$	-1	1	0	0	0
$SXy \xrightarrow{k_{SXyI}} Xyl$	r_{SXyI}	$\vartheta_{r_{SXyI}}^i$	0	-1	1	0	0
$SXy \xrightarrow{k_{SXyII}} F$	r_{SXyII}	$\vartheta_{r_{SXyII}}^i$	0	-1	0	1	0
$SXy \xrightarrow{k_{SXyIII}} Ace$	r_{SXyIII}	$\vartheta_{r_{SXyIII}}^i$	0	-1	0	0	1



The mass balance equations for different components during xylan conversion are as follows:

$$\frac{dC_{Xy}}{dt} = \vartheta_{r_{xy}}^{Xy} r_{xy} + \vartheta_{r_{SXyl}}^{Xy} r_{SXyl} + \vartheta_{r_{SXylII}}^{Xy} r_{SXylII} + \vartheta_{r_{SXylIII}}^{Xy} r_{SXylIII} + \vartheta_{r_{xyl}}^{Xy} r_{Xyl} \quad (5.12)$$

$$\frac{dC_{SXy}}{dt} = \vartheta_{r_{xy}}^{SXy} r_{xy} + \vartheta_{r_{SXyl}}^{SXy} r_{SXyl} + \vartheta_{r_{SXylII}}^{SXy} r_{SXylII} + \vartheta_{r_{SXylIII}}^{SXy} r_{SXylIII} + \vartheta_{r_{xyl}}^{SXy} r_{Xyl} \quad (5.13)$$

$$\frac{dC_{Xyl}}{dt} = \vartheta_{r_{xy}}^{Xyl} r_{xy} + \vartheta_{r_{SXyl}}^{Xyl} r_{SXyl} + \vartheta_{r_{SXylII}}^{Xyl} r_{SXylII} + \vartheta_{r_{SXylIII}}^{Xyl} r_{SXylIII} + \vartheta_{r_{xyl}}^{Xyl} r_{Xyl} \quad (5.14)$$

$$\frac{dC_F}{dt} = \vartheta_{r_{xy}}^F r_{xy} + \vartheta_{r_{SXyl}}^F r_{SXyl} + \vartheta_{r_{SXylII}}^F r_{SXylII} + \vartheta_{r_{SXylIII}}^F r_{SXylIII} + \vartheta_{r_{xyl}}^F r_{Xyl} \quad (5.15)$$

$$\frac{dC_{Ace}}{dt} = \vartheta_{r_{xy}}^{Ace} r_{xy} + \vartheta_{r_{SXyl}}^{Ace} r_{SXyl} + \vartheta_{r_{SXylII}}^{Ace} r_{SXylII} + \vartheta_{r_{SXylIII}}^{Ace} r_{SXylIII} + \vartheta_{r_{xyl}}^{Ace} r_{Xyl} \quad (5.16)$$

Time-concentration data, used for the determination of rate constants of reactions involved in the hydrolysis pathways of xylan and glucan, as respectively represented in Figures 5.9a and 5.9b, have been represented in Table 5.9 as follows:

Table 5.9 Time concentration data for kinetic study

Concentration of the product	Temperature (°C)	Reaction time (min)					
		0	3	6	9	12	15
Xylose (g/L)	150	0	3.17	6.21	7.42	8.01	7.94
	170	0	5.22	4.88	2.64	2.11	1.94
	190	0	0.91	0.44	0.37	0.19	0.11
Furfural (g/L)	150	0	0.74	1.22	1.59	1.76	2.15
	170	0	3.75	4.32	4.92	4.81	4.79
	190	0	6.46	7.59	7.14	6.46	6.19
Acetic acid (g/L)	150	0	0.38	0.78	1.10	1.30	1.43
	170	0	1.18	1.62	1.70	1.71	1.71
	190	0	1.23	1.47	1.48	1.47	1.47
Glucose	150	0	1.58	3.04	5.49	6.01	6.89

(g/L)	170	0	4.17	6.18	7.92	7.83	7.71
	190	0	5.49	7.70	6.99	6.43	5.70
5-HMF (g/L)	150	0	0.19	0.26	0.63	0.71	0.86
	170	0	0.29	0.61	0.95	0.87	0.83
	190	0	0.43	0.64	0.61	0.54	0.49
Formic acid (g/L)	150	0	0.01	0.02	0.21	0.33	0.51
	170	0	0.03	0.16	1.24	1.46	1.58
	190	0	0.08	1.21	2.40	3.17	3.41
Levulinic acid (g/L)	150	0	0.01	0.03	0.97	1.42	1.37
	170	0	0.04	0.87	2.37	2.68	2.59
	190	0	1.12	2.70	4.61	6.99	7.81

From the time-trajectories of xylan (Xy), soluble xylan (SXY), xylose (Xyl), furfural (F) and acetic acid (Ace), represented in Figure 5.10, the values of $\frac{dC_{Xy}}{dt}$, $\frac{dC_{SXY}}{dt}$, $\frac{dC_{Xyl}}{dt}$, $\frac{dC_F}{dt}$ and $\frac{dC_{Ace}}{dt}$ at different time have been determined by evaluating the slope of tangents to the corresponding trajectories at that instant. Using those values of concentration derivatives, the set of equations (Eq. 5.12-5.16) have been solved for the values of rates of reactions (r_{xy} , r_{SXYI} , r_{SXYII} , r_{SXYIII} and r_{SXYl}) at different pretreatment time (5, 10, 15 min) using linsolve of MATLAB. As the values of concentration of all the components (xylan, soluble xylan, xylose, furfural and acetic acid) are known at those time, the rate constants for the first order reactions have been determined at each temperature (150-190°C). According to the recommended form of linsolve, $\mathbf{AX}=\mathbf{B}$, the matrices \mathbf{A} , \mathbf{B} and \mathbf{X} for the equations 5.12 to 5.16 are as follows:

$$\mathbf{B} = \begin{bmatrix} \frac{dC_{Xy}}{dt} \\ \frac{dC_{SXY}}{dt} \\ \frac{dC_{Xyl}}{dt} \\ \frac{dC_F}{dt} \\ \frac{dC_{Ace}}{dt} \end{bmatrix}; \mathbf{X} = \begin{bmatrix} r_{xy} \\ r_{SXYI} \\ r_{SXYII} \\ r_{SXYIII} \\ r_{SXYl} \end{bmatrix}; \mathbf{A} = \begin{bmatrix} \vartheta_{r_{xy}}^{Xy} \vartheta_{r_{SXYI}}^{Xy} \vartheta_{r_{SXYII}}^{Xy} \vartheta_{r_{SXYIII}}^{Xy} \vartheta_{r_{SXYl}}^{Xy} \\ \vartheta_{r_{xy}}^{SXY} \vartheta_{r_{SXYI}}^{SXY} \vartheta_{r_{SXYII}}^{SXY} \vartheta_{r_{SXYIII}}^{SXY} \vartheta_{r_{SXYl}}^{SXY} \\ \vartheta_{r_{xy}}^{Xyl} \vartheta_{r_{SXYI}}^{Xyl} \vartheta_{r_{SXYII}}^{Xyl} \vartheta_{r_{SXYIII}}^{Xyl} \vartheta_{r_{SXYl}}^{Xyl} \\ \vartheta_{r_{xy}}^F \vartheta_{r_{SXYI}}^F \vartheta_{r_{SXYII}}^F \vartheta_{r_{SXYIII}}^F \vartheta_{r_{SXYl}}^F \\ \vartheta_{r_{xy}}^{Ace} \vartheta_{r_{SXYI}}^{Ace} \vartheta_{r_{SXYII}}^{Ace} \vartheta_{r_{SXYIII}}^{Ace} \vartheta_{r_{SXYl}}^{Ace} \end{bmatrix};$$

The elements of **B**, i.e., the time derivatives of concentrations of different components have been determined from the slope of the tangent on the concentration-time profile of different components. By making the inputs for **B** and **A**, **X** is evaluated using linsolve. The rate constants have been evaluated by plotting the rates against the concentration of relevant components.

Considering all reactions, except those for the generation of decomposition products, involved in the xylan hydrolysis pathway presented in Figure 9a, the differential mass balance equations for different components can be written as follows:

$$\frac{dC_{Xy}}{dt} = -k_{Xy}C_{Xy} \quad (5.17)$$

$$\frac{dC_{Sxy}}{dt} = k_{Xy}C_{Xy} - k_{SxyI}C_{Sxy} - k_{SxyII}C_{Sxy} - k_{SxyIII}C_{Sxy} \quad (5.18)$$

$$\frac{dC_{Xyl}}{dt} = k_{SxyI}C_{Sxy} - k_{Xyl}C_{Xyl} \quad (5.19)$$

$$\frac{dC_F}{dt} = k_{Xyl}C_{Xyl} + k_{SxyII}C_{Sxy} \quad (5.20)$$

$$\frac{dC_{Ace}}{dt} = k_{SxyIII}C_{Sxy} \quad (5.21)$$

The initial conditions are as follows:

$$\text{At } t=0 \left[C_{Xy} = C_{Xy0}; C_{Sxy} = C_{Xyl} = C_F = 0 \right] \quad (5.22)$$

5.1.6.2 Conversion of cellulose into glucose and other products

Cellulose of rice straw is constituted of two fractions – crystalline and amorphous (Xiang et al., 2003). According to the proposed model, the value of mass fraction of crystalline part of cellulose, α , is determined to be 0.3708. According to the proposed scheme, due to the action of metal chloride, only the amorphous fraction ($1 - \alpha = 0.6292$) of cellulose is converted to glucose. It is proposed that a fraction (β) of glucose, produced through hydrolysis of amorphous cellulose is converted to 5-HMF, and the residual fraction, $(1 - \beta)$, combines with acid soluble lignin (ASL) to form Glucose-ASL complex (Qing et al., 2018; Tan-Soetedjo et al., 2017; Xiang et al., 2003). The value of β has been used as an adjustable parameter and is evaluated to be 0.99. Ultimately, 5-HMF is converted to levulinic acid and formic acid (Tian et al., 2021). The scheme is represented in Figure 5.9.b.

The reaction rate and stoichiometric coefficients of different compounds in the corresponding reactions during glucan conversion through FCP are represented, along with their values, in Table 5.10.

Table 5.10 Stoichiometric Coefficient matrix for components participating in the reactions in cellulose conversion to glucose and other products

Reaction	Generalized Stoichiometric Coefficient	Values of Stoichiometric Coefficient	Component-wise				
			Cell	Glc	HMF	LA	FA
$(1 - \alpha)Cell \xrightarrow{k_{Cell}} Glc$	r_{Cell}	$\vartheta_{r_{Cell}}^i$	-(1- α)	1	0	0	0
$\beta Glc \xrightarrow{k_{GlcI}} 5-HMF$	r_{GlcI}	$\vartheta_{r_{GlcI}}^i$	0	-\beta	1	0	0
$(1 - \beta)Glc \xrightarrow{k_{GlcII}} Glc-ASL$	r_{GlcII}	$\vartheta_{r_{GlcII}}^{Cell}$	0	-(1-\beta)	0	0	0
$5-HMF \xrightarrow{k_{HMF I}} FA$	$r_{HMF I}$	$\vartheta_{r_{HMF I}}^i$	0	0	-1	0	1
$5-HMF \xrightarrow{k_{HMF II}} LA$	$r_{HMF II}$	$\vartheta_{r_{HMF II}}^i$	0	0	-1	1	0

i=any component (Cellulose (Cell), glucose (Glc), 5-HMF, formic acid (FA) and levulinic acid (LA))

The mass balance equations for different components during glucan conversion are as follows:

$$\frac{dC_{Cell}}{dt} = \vartheta_{r_{Cell}}^{Cell} r_{Cell} + \vartheta_{r_{GlcI}}^{Cell} r_{GlcI} + \vartheta_{r_{GlcII}}^{Cell} r_{GlcII} + \vartheta_{r_{HMF I}}^{Cell} r_{HMF I} + \vartheta_{r_{HMF II}}^{Cell} r_{HMF II} \quad (5.23)$$

$$\frac{dC_{Glc}}{dt} = \vartheta_{r_{Cell}}^{Glc} r_{Cell} + \vartheta_{r_{GlcI}}^{Glc} r_{GlcI} + \vartheta_{r_{GlcII}}^{Glc} r_{GlcII} + \vartheta_{r_{HMF I}}^{Glc} r_{HMF I} + \vartheta_{r_{HMF II}}^{Glc} r_{HMF II} \quad (5.24)$$

$$\frac{dC_{HMF}}{dt} = \vartheta_{r_{Cell}}^{HMF} r_{Cell} + \vartheta_{r_{GlcI}}^{HMF} r_{GlcI} + \vartheta_{r_{GlcII}}^{HMF} r_{GlcII} + \vartheta_{r_{HMF I}}^{HMF} r_{HMF I} + \vartheta_{r_{HMF II}}^{HMF} r_{HMF II} \quad (5.25)$$

$$\frac{dC_{FA}}{dt} = \vartheta_{r_{Cell}}^{FA} r_{Cell} + \vartheta_{r_{GlcI}}^{FA} r_{GlcI} + \vartheta_{r_{GlcII}}^{FA} r_{GlcII} + \vartheta_{r_{HMF I}}^{FA} r_{HMF I} + \vartheta_{r_{HMF II}}^{FA} r_{HMF II} \quad (5.26)$$

$$\frac{dC_{LA}}{dt} = \vartheta_{r_{Cell}}^{LA} r_{Cell} + \vartheta_{r_{GlcI}}^{LA} r_{GlcI} + \vartheta_{r_{GlcII}}^{LA} r_{GlcII} + \vartheta_{r_{HMF I}}^{LA} r_{HMF I} + \vartheta_{r_{HMF II}}^{LA} r_{HMF II} \quad (5.27)$$

From the time-trajectories of cellulose (Cell), glucose (Glc), 5-hydroxymethyl furfural (5-HMF), formic acid (FA) and levulinic acid (LA), represented in Figure 5.11, the values of

$\frac{dC_{Cell}}{dt}$, $\frac{dC_{Glc}}{dt}$, $\frac{dC_{HMF}}{dt}$, $\frac{dC_{FA}}{dt}$ and $\frac{dC_{LA}}{dt}$ at different time have been determined by evaluating the slope of tangents to the corresponding trajectories at that instant. The set of equations (Eq. 5.23-5.27) have been solved for the values of rate of reactions (r_{cell} , r_{GlcI} , r_{GlcII} , $r_{HMF I}$ and $r_{HMF II}$) at different pretreatment time (5, 10, 15 min) using linsolve of MATLAB. As the values of concentration of all the components (cellulose, glucose, 5-HMF, formic acid and levulinic acid) are known, the rate constants for the first order reactions have been determined at each temperature (150-190°C). According to the recommended form of linsolve, **CY=D**, the matrices **C**, **D** and **Y** for the equations 5.23 to 5.27 are as follows:

$$D = \begin{bmatrix} \frac{dC_{Cell}}{dt} \\ \frac{dC_{Glc}}{dt} \\ \frac{dC_{HMF}}{dt} \\ \frac{dC_{FA}}{dt} \\ \frac{dC_{LA}}{dt} \end{bmatrix}; Y = \begin{bmatrix} r_{Cell} \\ r_{GlcI} \\ r_{GlcII} \\ r_{HMF I} \\ r_{HMF II} \end{bmatrix}; C = \begin{bmatrix} \vartheta_{r_{Cell}^{Cell}} & \vartheta_{r_{GlcI}^{Cell}} & \vartheta_{r_{GlcII}^{Cell}} & \vartheta_{r_{HMF I}^{Cell}} & \vartheta_{r_{HMF II}^{Cell}} \\ \vartheta_{r_{Cell}^{Glc}} & \vartheta_{r_{GlcI}^{Glc}} & \vartheta_{r_{GlcII}^{Glc}} & \vartheta_{r_{HMF I}^{Glc}} & \vartheta_{r_{HMF II}^{Glc}} \\ \vartheta_{r_{Cell}^{HMF}} & \vartheta_{r_{GlcI}^{HMF}} & \vartheta_{r_{GlcII}^{HMF}} & \vartheta_{r_{HMF I}^{HMF}} & \vartheta_{r_{HMF II}^{HMF}} \\ \vartheta_{r_{Cell}^{FA}} & \vartheta_{r_{GlcI}^{FA}} & \vartheta_{r_{GlcII}^{FA}} & \vartheta_{r_{HMF I}^{FA}} & \vartheta_{r_{HMF II}^{FA}} \\ \vartheta_{r_{Cell}^{LA}} & \vartheta_{r_{GlcI}^{LA}} & \vartheta_{r_{GlcII}^{LA}} & \vartheta_{r_{HMF I}^{LA}} & \vartheta_{r_{HMF II}^{LA}} \end{bmatrix}$$

The elements of D, i.e., the time derivatives of concentrations of different components have been determined from the slope of the tangent on the concentration-time profile of different components. By making the inputs for **D** and **C**, **Y** is evaluated using linsolve. The rate constants have been evaluated by plotting the rates against the concentration of relevant components.

The differential mass balance equations for different components (for cellulose degradation) can be written as follows:

$$\frac{dC_{Cell}}{dt} = -(1 - \alpha)k_{cell}C_{Cell} \quad (5.28)$$

$$\frac{dC_{Glc}}{dt} = k_{cell}C_{Cell} - k_{GlcI}C_{Glc} \quad (5.29)$$

$$\frac{dC_{HMF}}{dt} = k_{GlcI}\beta C_{Glc} - k_{HMF I}C_{HMF} - k_{HMF II}C_{HMF} \quad (5.30)$$

$$\frac{dC_{FA}}{dt} = k_{HMF I}C_{HMF} \quad (5.31)$$

$$\frac{dC_{LA}}{dt} = k_{HMF2}C_{HMF} \quad (5.32)$$

The initial conditions are as follows:

$$\text{At } t=0 [C_{Cellu} = C_{Cellu0}; C_{Glc} = C_{HMF} = C_{LA} = C_{FA} = 0] \quad (5.33)$$

Arrhenius equation has been used to represent the functionality of all rate constants on temperature.

$$k_i = k_{oi} \exp\left(\frac{-E_i}{RT}\right) \quad (5.34)$$

k_i = rate constant of i^{th} reaction; k_{oi} = pre – exponential factor of i^{th} reaction ;

E_i = Activation energy of i^{th} reaction

The values of activation energies and pre-exponential factors have been determined through regression analysis using natural logarithm of each rate constant, $\ln(k_i)$ against the inverse of temperature in kelvin, $\frac{1}{T}$.

The series of differential equations, Eq. 5.17-5.21 and Eq. 5.28-5.32, along with respective initial conditions, i.e., equations 5.22 and 5.33, have been solved simultaneously using ode45 solver of MATLAB software.

5.1.6.3 Rate Constants

The values of pre-exponential factors and activation energies have been provided in Table 5.11.

Table 5.11 Values of the pre-exponential factors and activation energies for rate constants of xylan and cellulose conversion reactions (FeCl₃ concentration=0.2M)

Rate constants	Pre-exponential factor (min ⁻¹)	Activation energy (kJ/mol)	Rate constants	Pre-exponential factor (min ⁻¹)	Activation energy (kJ/mol)
k _{Xy}	3.3039×10 ¹¹	99.56	k _{Cell}	9.5420×10 ⁴	51.31
k _{SXyI}	1.7961×10 ⁴	37.75	k _{GlcI}	3.4424×10 ⁴	45.99
k _{XyII}	6.3310×10 ¹⁰	106.00	k _{GlcII}	4.7791×10 ⁴	65.12
k _{SXyII}	5.5707×10 ¹³	120.00	k _{HMF I}	5.2538×10 ⁷	67.25
k _{SXyIII}	5.3198×10 ⁶	65.10	k _{HMF II}	2.1279×10 ⁶	57.04

5.1.6.4 Comparison of predictions of Model with Experimental Results

The simulated and experimental time histories of concentration of xylose, furfural and acetic acid have been plotted in Figure 5.10 (a, b and c). Similarly, simulated and experimental dynamics of concentration of glucose, 5-HMF, formic acid and levulinic acid have been plotted in Figure 5.11 (a, b, c and d). The component-wise comparative trends are described below:

Xylose

From the analysis of Figure 5.10a, it is observed that the release of xylose initially increases with time up to 5 minutes and then decreases with the increase in time for 170°C and 190°C. This can be due to the fact that initially the rate of xylose formation is higher than the rate of xylose degradation to furfural. One of the major reasons is the decrease in the reactant, i.e., xylan. After 5 minutes, the rate of degradation of xylose is higher than the rate of formation of xylose. But in case of 150°C, the concentration of xylose increases monotonically with time. It is also evident from Figure 5.10a that the experimental trend agrees well with those predicted by Model.

Furfural

From the analysis of Figure 5.10.b, it is clear that the concentration of furfural increases monotonically with the increase in time up to 10 minutes for 170°C. This signifies that the availability of hydronium ion is greater as the time proceeds. As a result, the conversion of xylose to furfural is facilitated to an extent greater than that of depolymerization of hemicellulose to xylose. After 10 minutes the formation of furfural decreases. This behavior of furfural trend can be explained from the scheme. Initially the rate of formation of furfural from xylose is higher than the rate of conversion of furfural to degraded product. After 10 minutes the rate of degradation of furfural is higher than the rate of formation of furfural. In case of 150°C, the concentration of furfural increases monotonically with time. In case of 190°C, the release of furfural initially increases with time up to 5 minutes and then decreases with the increase in time. The predicted trend of Model is in agreement with the experimental one.

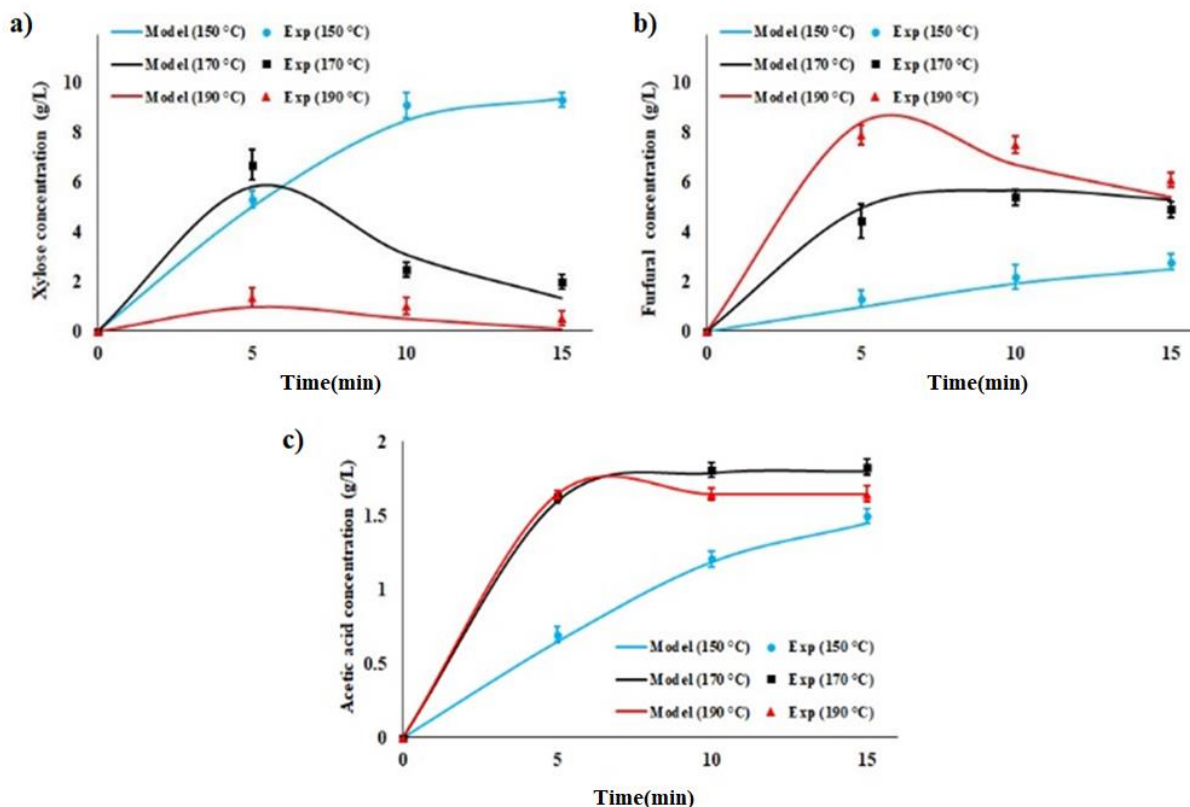


Fig. 5.10 Experimental values and model prediction of xylose (a), furfural (b) and acetic acid (c) concentration obtained from pretreatment of rice straw using 0.2M FeCl₃ at 150-190°C for 5-15 minutes

Acetic acid

From Figure 5.10c, it appears that there is an increasing trend of acetic acid with time up to 5 minutes. After 5 minutes, the yield of acetic acid is almost saturated with respect to time for 170°C and 190°C. This is because of the fact that the acetic acid is released during the solubilization of hemicellulose, the rate of which is very fast during FeCl₃ assisted pretreatment. The predicted value of Model is almost same which are very close to experimental values at each time.

Glucose

From the analysis of Figure 5.11a, it is evident that the release of glucose increases with time up to 10 minutes and after that decreases with the increase in time for 170°C. This can be due to the fact that initially the rate of formation of glucose from amorphous cellulose is higher than the rate of degradation of glucose to 5-hydroxymethylfurfural and glucose-acid soluble lignin complex.

After 10 minutes the degradation of glucose is higher than the formation of glucose. In case of 190°C, the release of glucose initially increases with time up to 5 minutes and then decreases with the increase in time. In case of 150°C, the concentration of glucose increases monotonically with time. It is clear from the figure that the predicted trend is in good agreement with the experimental one.

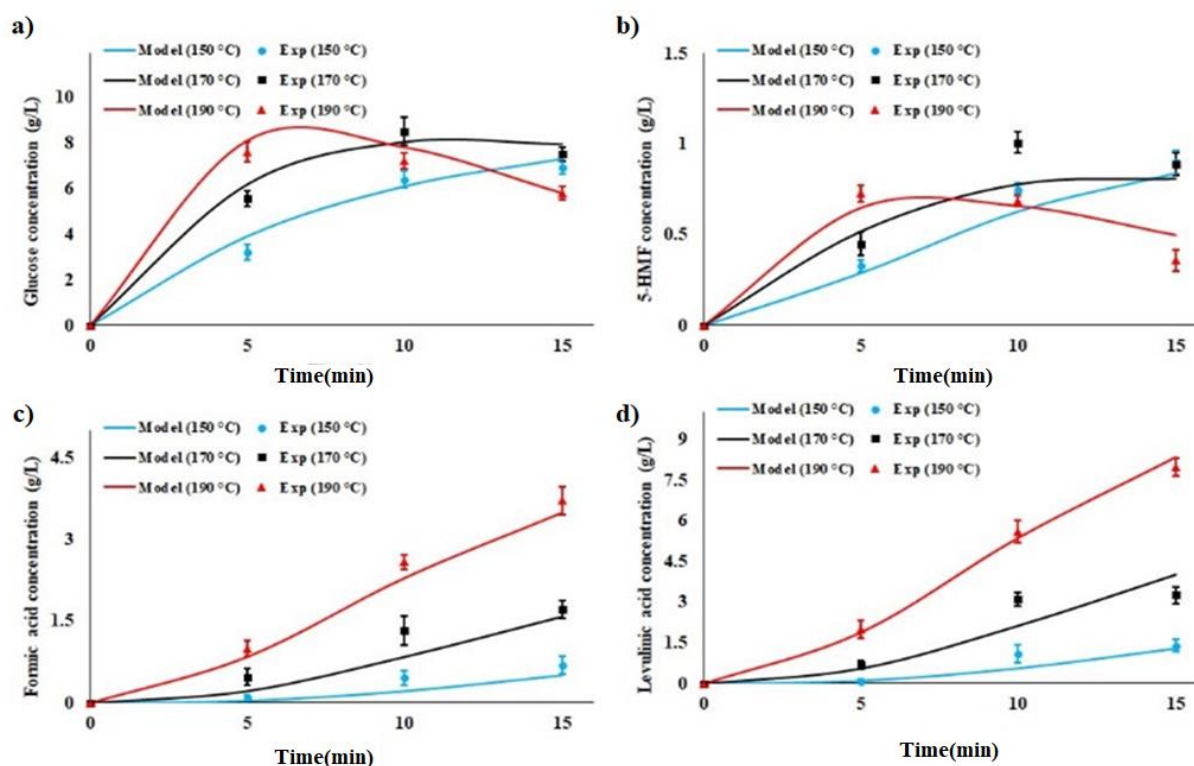


Fig. 5.11 Experimental values and model prediction of glucose (a), 5-HMF (b), formic acid (c) and levulinic acid (d) obtained from pretreatment of rice straw using 0.2M FeCl₃ at 150-190°C for 5-15 minutes

HMF

It is clear from the analysis of Figure 5.11b that the concentration of 5-hydroxymethylfurfural increases with the increase in time up to 10 minutes for 170°C. After 10 minutes the release of 5-HMF decreases. Initially, the rate of formation of 5-HMF from glucose is higher than the rate of degradation of 5-HMF to formic acid and levulinic acid. After 10 minutes the rate of degradation of 5-HMF is higher than the rate of formation of 5-HMF. In case of 190°C, the release of 5-HMF initially increases with time up to 5 minutes and then decreases with the increase in time. In case

of 150°C, the concentration of 5-HMF increases monotonically with time. It is observed that the simulated data are in good agreement with the experimental data.

Formic Acid

From the analysis of Figure 5.11c, it is evident that the rate of formation of formic acid increases with time for all temperature. There are differences between the simulated and experimental values of formic acid concentration at 10 minutes. This may be due to the participation of formic acid as a catalyst for the conversion of xylose to furfural etc, which are not considered in the models.

Levulinic acid

From the analysis of Figure 5.11d, it is evident that the rate of formation of formic acid increases with time for all temperature.

The discrepancy in the prediction of yields of formic acid and levulinic acid indicates the possibility of involvement of some other reactions in the overall pathway of cellulose conversion. Hence, there are scopes of modification of the pathway in future.

5.1.6.5 Normalized root mean square error (NRMSE)

For the assessment of the validity of the model, statistical parameter, namely normalized root mean square error (NRMSE) has been calculated using the following equation (Soler et al, 2007):

$$\text{Normalized RMSE} = \sqrt{\frac{\sum_{i=1}^n (P_i - O_i)^2}{n}} \times \frac{100}{M} = \frac{\text{RMSE}}{M} \times 100 \quad (5.35)$$

Where M is the mean of the observed variable (Soler et al, 2007); P_i , O_i and n are predicted values, observed experimental values, number of runs respectively (Soler et al, 2007).

The values of NRMSE for the predictability of the concentration of different hydrolysis products are provided in Table 12.

It is clear from the Table 12 that the values of NRMSE for model are less than 10 in most of the cases except for formic and levulinic acids. The NRMSE values for degradation of xylan and glucan are also less than 10. Hence, the deterministic mathematical model is valid.

Table 5.12 Values of normalized root mean square error

	Glucose	Xylose	Furfural	5-HMF	AA*	FA*	LA*
NRMSE	9.76	9.69	6.97	7.33	3.11	>10	>10

(AA*, FA* and LA* refer to acetic acid, formic acid and levulinic acid respectively)

5.1.7 Degradation of polymer

Pretreated solid obtained using different temperature, time and FeCl₃ concentration have been reported in Table 13. The degradation of glucan and xylan (%) and solid recovery (%), have been determined from equations 5.3-5.5.

Table 5.13 Solid recovery and composition of pretreated solid (obtained from 0.2M FeCl₃ pretreatment)

Parameter		Solid recovery	Composition (w/w)			Degradation	
Time (min)	T (°C)		Glucan (%)	Xylan (%)	Lignin (%)	Glucan (%)	Xylan (%)
5	150	69.03 ± 1.40	51.33 ± 0.70	13.86 ± 0.09	22.13 ± 0.22	8.67	45.63
5	170	67.82 ± 1.59	48.01 ± 0.99	10.01 ± 0.11	22.78 ± 0.41	16.08	61.42
5	190	66.31 ± 1.02	46.57 ± 0.23	5.22 ± 0.03	23.17 ± 0.21	20.41	80.33
10	150	67.21 ± 1.31	36.20 ± 0.79	2.57 ± 0.19	23.18 ± 0.21	37.29	90.18
10	170	64.85 ± 1.29	34.31 ± 0.27	0.41 ± 0.02	23.99 ± 0.23	42.65	98.49
10	190	62.54 ± 1.07	32.01 ± 0.27	0.21 ± 0.02	24.06 ± 0.23	48.40	99.25
15	150	64.18 ± 1.31	35.17 ± 0.79	0.33 ± 0.19	23.21 ± 0.21	41.82	98.75
15	170	61.57 ± 1.29	32.97 ± 0.27	0.14 ± 0.02	24.01 ± 0.23	47.68	99.51
15	190	59.80 ± 1.07	32.03 ± 0.27	0.01 ± 0.02	24.17 ± 0.23	50.63	99.96

It is observed that the percentage of solid recovery has decreased with increase in pretreatment temperature and time. Whereas, the percentage of glucan and xylan degradation have increased with increase in temperature and time. The maximum degradation of glucan and xylan have been obtained as 50.63% and 99.96% at 190 °C for 15 minutes using 0.2 M FeCl₃ respectively.

5.1.8 Optimization of the yield of major products and degradation of xylan and glucan

5.1.8.1 Optimization of the yield of major products through ferric chloride (0.2M) pretreatment

The response surface methodology (RSM) has been used to optimize the individual yield of major products (xylose, glucose and furfural) through the FeCl_3 (0.2M) pretreatment with respect to the combined effects of pretreatment time and temperature. The 2-factor Central Composite statistical design has been used. The coded levels of variables used for the optimization of yields (g/ kg of RS) of xylose, glucose and furfural have been reported in the Table 5.14.

Table 5.14 Coded levels of variables for the optimization of yields of xylose, glucose and furfural

Input variables	Unit	Coded variable level			Model Response
		-1	0	1	
Pretreatment temperature (A)	°C	150	170	190	(i) Xylose yield (g/ kg of RS)
Pretreatment time (B)	min	5	10	15	(ii) Glucose yield (g/ kg of RS) (iii) Furfural yield (g/ kg of RS)

The RSM plot for the yield of glucose, xylose and furfural have been shown in the Fig. 5.12a, 5.12 and 5.12c respectively. The optimum yield of glucose, xylose and furfural have been reported in the Table 5.15.

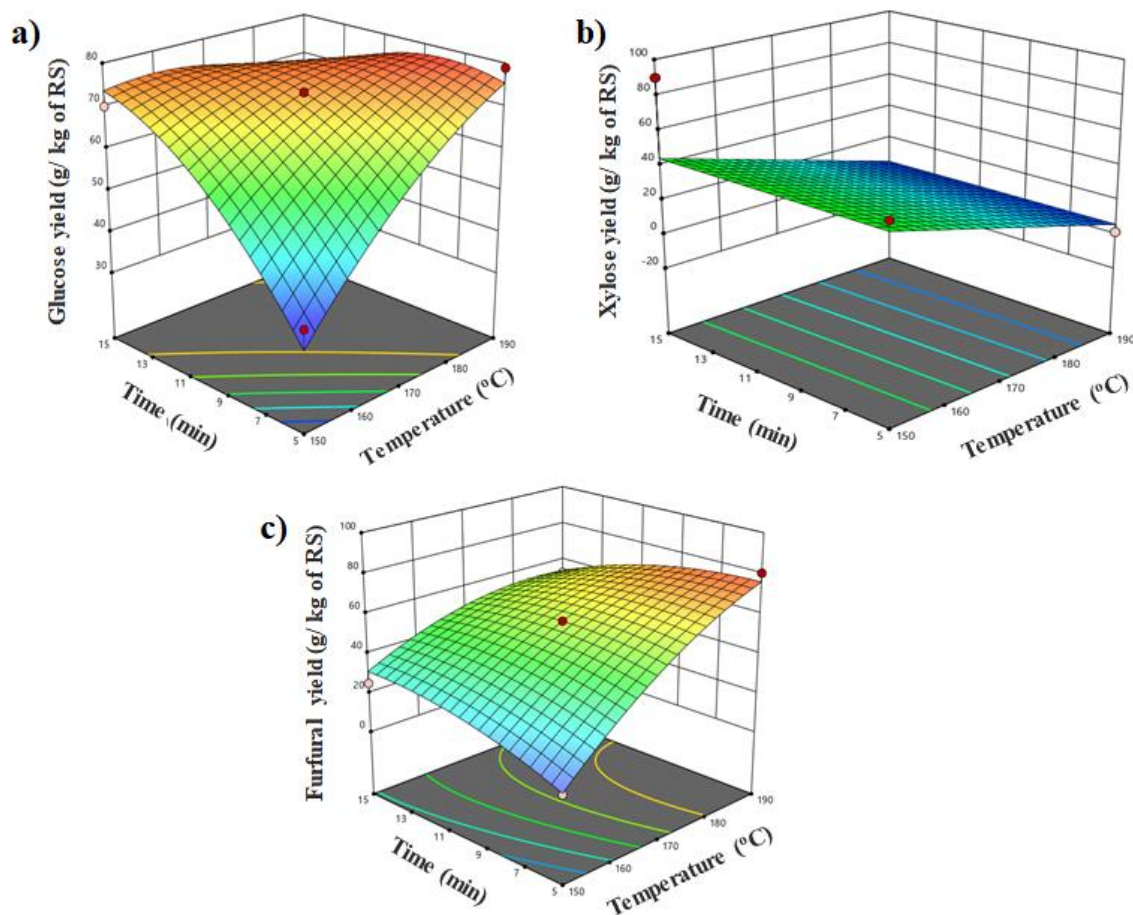


Fig. 12 RSM plot for glucose (a), xylose (b) and furfural (c) yield (g/ kg of RS) obtained from pretreatment of rice straw using 0.2M FeCl₃ at 150-190°C for 5-15 minutes

Table 5.15 Condition for optimum production for glucose, xylose and furfural yield (g/ kg of RS)

	Temperature (°C)	Time (min)	Optimum Yield (g/ kg of RS)
Glucose	166.673	9.499	70.82
Xylose	152.242	5.841	43.34
Furfural	183.591	7.807	70.21

5.1.8.2 Optimization of degradation of xylan and glucan through $FeCl_3$ pretreatment

A 2-factor Central Composite statistical design in response surface methodology (RSM) has been used to understand the effects of pretreatment temperature and time on the degradation of xylan and glucan (%). Design-Expert Software (version 11) has been used for this purpose. The Table 5.16 represents the coded levels of independent variables for degradation of carbohydrates.

Table 5.16 Coded levels of independent variables for degradation of carbohydrates

Input variables	Unit	Coded variable level			Model Response
		-1	0	1	
Pretreatment temperature (A)	°C	150	170	190	(i) Xylan degradation (%)
Pretreatment time (B)	min	5	10	15	(ii) Glucan degradation (%)

The Table 5.17 represents ANOVA table for xylan degradation. The adjusted and predicted R^2 values for the model are good.

Table 5.17 ANOVA Table for optimization xylan degradation

Source	Sum of Squares	df	Mean Square	F-value	p-value	
Model	4472.93	5	894.59	75.49	< 0.0001	significant
A-Temperature	2651.91	1	2651.91	223.79	< 0.0001	
B-Time	321.10	1	321.10	27.10	0.0012	
AB	187.69	1	187.69	15.84	0.0053	
A ²	1305.67	1	1305.67	110.18	< 0.0001	
B ²	52.61	1	52.61	4.44	0.0731	
Residual	82.95	7	11.85			
Lack of Fit	82.95	3	27.65			
Pure Error	0.0000	4	0.0000			
Cor Total	4555.88	12				

(R^2 : 0.9818; adjusted R^2 : 0.9688; Predicted R^2 : 0.9259)

The Table 5.18 represents ANOVA Table for glucan degradation. The adjusted and predicted R^2 values for the model are good.

Table 5.18 ANOVA Table for optimization glucan degradation

Source	Sum of Squares	df	Mean Square	F-value	p-value	
Model	3050.65	5	610.13	586.83	< 0.0001	significant
A-Temperature	2232.44	1	2232.44	2147.21	< 0.0001	
B-Time	293.32	1	293.32	282.12	< 0.0001	
AB	110.25	1	110.25	106.04	< 0.0001	
A ²	374.53	1	374.53	360.23	< 0.0001	
B ²	77.49	1	77.49	74.53	< 0.0001	
Residual	7.28	7	1.04			
Lack of Fit	7.28	3	2.43			
Pure Error	0.0000	4	0.0000			
Cor Total	3057.93	12				

(R^2 : 0.9976; adjusted R^2 : 0.9959; Predicted R^2 : 0.9831)

From the Fig. 5.13a, it is observed that, as expected, the pretreatment temperature and time have a positive impact on the degradation of xylan. From the Fig. 5.13b, it is observed that the pretreatment temperature and time have a positive impact on the degradation of glucan.

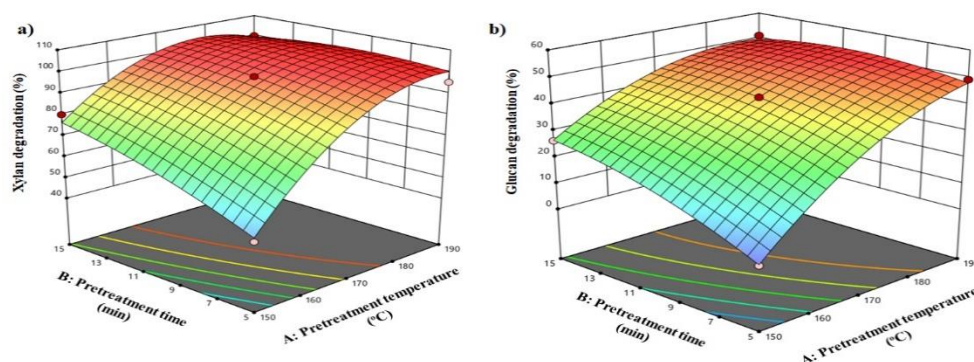


Fig. 5.13 Effect of pretreatment temperature and time on the response surface of xylan (a) and glucan degradation (b)

The optimum degradation of xylan and glucan have been reported in the Table 5.19.

Table 5.19 Optimum degradation of xylan and glucan

	Temperature (°C)	Time (min)	% Optimum degradation
Xylan	165.277	11.477	97.344
Glucan	172.848	9.823	43.817

5.1.9 Effect of Combined severity on ferric chloride pretreatment

Combining the effects of time and temperature of thermal cycle of pretreatment and the pH of the FeCl₃ solution, the combined severity (CS) for hydrolysis of any component (hemicellulose, cellulose etc.), i, has been defined as follows (Ruiz et al, 2021; Abouelela et al, 2023):

$$CS_i = \log R_{0i} - pH \quad (5.36)$$

Where, R_{0i} represents the severity factor of pretreatment reaction of any component, i .

$$\log R_{0i} = \log[R_{0iHEATING} + R_{0iOPERATING} + R_{0iCOOLING}] \quad (5.37)$$

$$\log R_{0i} = \log\left[\int_{t_0}^{t_1} \exp\left(\frac{T(t)-T_{Ref}}{\omega_i}\right) dt + (t_2 - t_1)\exp\left(\frac{T_{hy}-T_{Ref}}{\omega_i}\right) + \int_{t_2}^{t_f} \exp\left(\frac{T'(t)-T_{Ref}}{\omega_i}\right) dt\right]$$

Where,

$$\int_{t_0}^{t_1} \exp\left(\frac{T(t)-T_{Ref}}{\omega_i}\right) dt = R_{0i,heating} ;$$

$$(t_2 - t_1)\exp\left(\frac{T_{hy}-T_{Ref}}{\omega_i}\right) = R_{0i,iso} ;$$

$$\int_{t_2}^{t_f} \exp\left(\frac{T'(t)-T_{Ref}}{\omega_i}\right) dt = R_{0i,cooling} ;$$

Where, t_0 : initial time; T_{Ref} : reference temperature; T_{hy} : hydrolysis temperature; $T(t)$: time-temperature profile on the heating cycles; $T'(t)$: time-temperature profile on the cooling cycles; $\omega_i = \frac{RT_R^2}{E_{Ai}}$ and t refers as time in minutes (Ruiz et al, 2021). The reference temperature has been considered to be 100°C. E_{Ai} is the activation energy of hydrolysis reaction of any component (hemicellulose, cellulose etc.). The values of $R_{0i,iso}$ is dependent on time and temperature of

isothermal hydrolysis. As the activation energies of hydrolysis of cellulose and hemicellulose are different, the values of ω and R_0 are also different. The definitions of R_0 and ω , the hydrolysis kinetics of hemicellulose and cellulose can be written as,

$$-\frac{1}{C_{Xy}} \frac{dC_{Xy}}{dt} = k_{Xy} \quad (5.38)$$

As there is no hydrolysis during the heating up and cooling down period,

$$-\frac{1}{C_{Xy}} \frac{dC_{Xy}}{dt} = k_{Xy0} \exp\left(-\frac{E_{Xy}}{RT}\right) \quad (5.39)$$

$$\text{Or, } -\ln\left(\frac{1}{C_{Xy}} \frac{dC_{Xy}}{dt}\right) = \ln k_{Xy0} - \frac{E_{Xy}}{RT} \quad (5.40)$$

Through Taylor series expansion, neglecting higher terms, around reference temperature T_R ,

$$-\ln\left(\frac{1}{C_{Xy}} \frac{dC_{Xy}}{dt}\right) = \ln k_{Xy0} - \frac{E_{Xy}}{RT_R} + \frac{E_{Xy}}{RT_R^2 T_R} (T - T_R) \quad (5.41)$$

$$\text{or, } \frac{1}{C_{Xy}} \frac{dC_{Xy}}{dt} = k_{Xy0} \exp\left(-\frac{E_{Xy}}{RT_R}\right) \exp\left(\frac{E_{Xy}}{RT_R^2} (T - T_R)\right) = k_{XyR} \exp\left(\frac{(T - T_R)}{\omega_{Xy}}\right) \quad (5.42)$$

$$\frac{RT_R^2}{E_{Xy}} = \omega_{Xy}; k_{Xy0} \exp\left(-\frac{E_{Xy}}{RT_R}\right) = k_{XyR} \quad (5.43)$$

$$\text{Or, } \int_{C_{Xy0}}^{C_{Xy}} \frac{dC_{Xy}}{C_{Xy}} = \int_0^t k_{XyR} \exp\left(\frac{(T - T_R)}{\omega_{Xy}}\right) dt = k_{XyR} t \exp\left(\frac{(T - T_R)}{\omega_{Xy}}\right) = k_{XyR} R_{0Xy,iso} \quad (5.44)$$

Where,

$$R_{0Xy,iso} = t \exp\left(\frac{(T - T_R)}{\omega_{Xy}}\right) \quad (5.45)$$

= severity factor for xylose degradation under isothermal condition (Ruiz et al, 2021)

Similarly, for hydrolysis of cellulose,

$$\int_{C_{Cellu0}}^{C_{Cellu}} \frac{dC_{Cellu}}{C_{Cellu}} = \int_0^t k_{CellR} \exp\left(\frac{(T - T_R)}{\omega_{Cellu}}\right) dt = k_{CellR} t \exp\left(\frac{(T - T_R)}{\omega_{Cellu}}\right) = k_{CellR} R_{0Cellu,iso} \quad (5.46)$$

Where,

$$R_{0Cellu,iso} = t \exp\left(\frac{(T - T_R)}{\omega_{Cellu}}\right) \quad (5.47)$$

= severity factor for Cellulose degradation under isothermal condition (Ruiz et al, 2021)

Under the present study, FeCl₃ concentration has been chosen to be 0.2M and hence the pH (=1.38) was same for all experiments. The choice of concentration was made based on literature data and the best hydrolytic performance. Using Equation 5.36, the combined severity factors for xylose and cellulose are as follows:

$$CS_{xy} = \log R_{0xy} - pH \quad (5.48)$$

$$CS_{cellu} = \log R_{0cellu} - pH \quad (5.49)$$

The values of R_{0xy} and R_{0cellu} have been calculated using equations 5.45 and 5.47.

The combined parameters, CS_{xy} and CS_{cellu} have also been correlated with time and temperature of isothermal hydrolysis using a 2-parameter Central Composite response surface design.

Table 5.20 Variables with coded level used for RSM for degradation of xylan and glucan (%)

Input variables	Unit	Coded variable level			Model Response	
		-1	0	1		
Pretreatment temperature (A)	°C	150	170	190	(i)	CS_{xy}
Pretreatment time (B)	min	5	10	15	(ii)	CS_{cellu}

The combined severity has been correlated to pretreatment time and temperature using RSM. The second order equations obtained are as follows:

$$CS_{xy} = 2.81286 - 0.0478042A + 0.212355B + 0.00015AB + 0.000203251A^2 - 0.00775B^2 \quad (5.50)$$

$$CS_{cellu} = 4.69605 - 0.065561A + 0.188213B + (0.9251 \times 10^{-7})AB + 0.00022185A^2 - 0.00665B^2 \quad (5.51)$$

The corresponding plot of CS against pretreatment time and temperature is shown in Figure 5.14.

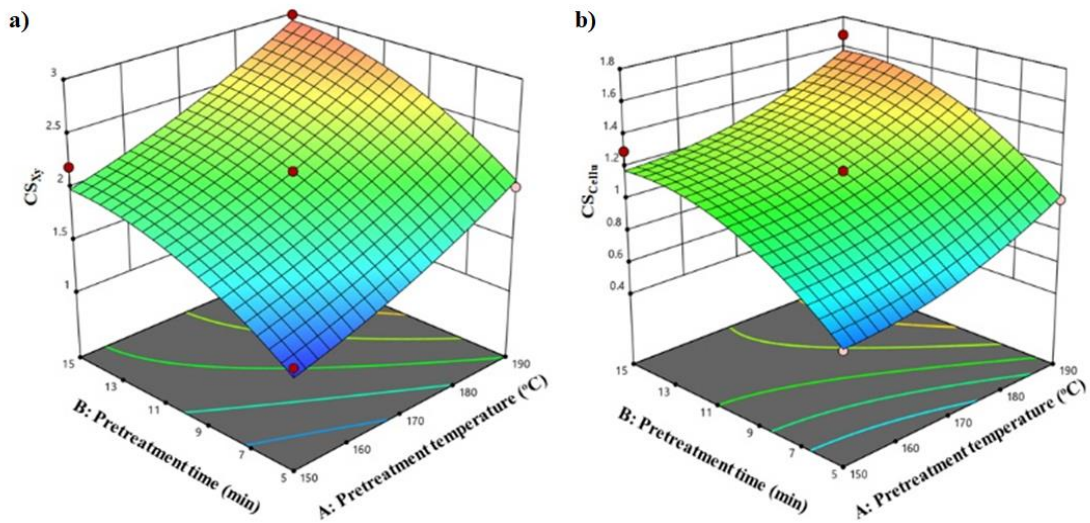


Fig. 5.14 CS against pretreatment time and temperature (CS_{Xy} :a; CS_{Cellu} :b)

The value of CS_{Xy} varies from 1.28 to 2.99. Whereas, the value of CS_{Cellu} varies from 0.62 to 1.68.

The fit of the combined severity factor with xylan and glucan degradation is presented in the Figure 5.15.

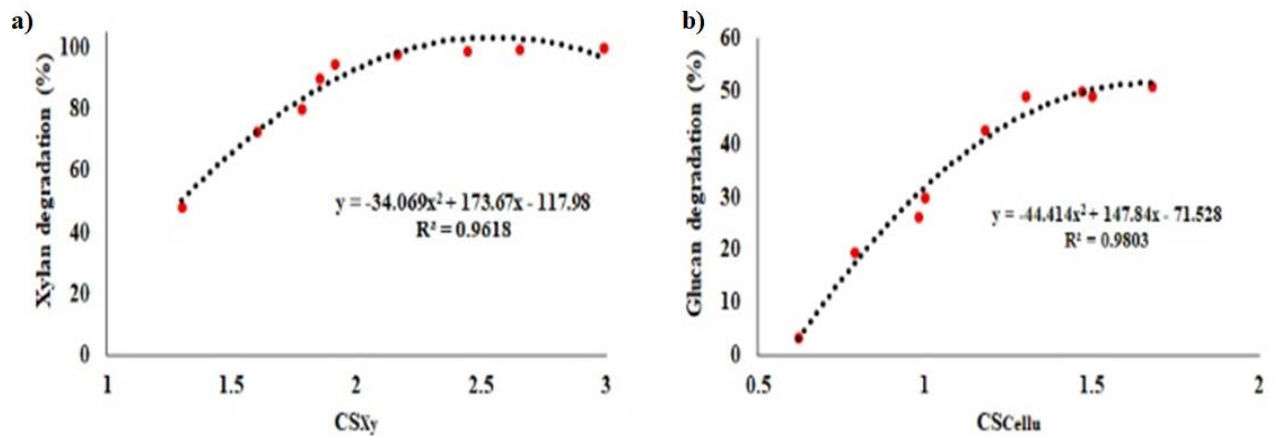


Fig. 5.15 a: xylan degradation versus CS_{Xy} ; b: glucan degradation versus CS_{Cellu}

From the analysis Fig. 5.15, there is a non-linear (second order polynomial) relationship between degradation of xylan/glucan and combined severity factor. The co-relation of xylan degradation & CS_{Xy} and glucan degradation & CS_{Cellu} are written in the equation 5.52 and 5.53 respectively.

$$Xylan\ degradation\ (\%) = -34.069CS_{xy}^2 + 173.67CS_{xy} - 117.98 \quad (5.52)$$

$$Glucan\ degradation\ (\%) = -44.41CS_{cellu}^2 + 147.84CS_{cellu} - 71.528 \quad (5.53)$$

5.2 Enzymatic hydrolysis

5.2.1 Experimental procedure

Enzymatic hydrolysis of raw-RS and pretreated solid from LWP, SAP and FCP was conducted in a glass test tube at 50°C for 24, 48 and 72 hours with shaking at a speed of 150 rpm. 4 mL sodium acetate buffer (0.05 M, pH 5.8) and 0.2 g solid (raw-RS and pretreated solid from LWP, SAP and FCP) were taken. The enzyme, i.e., cellulase loading was 20 FPU/g dry substrate. After enzymatic hydrolysis, the product was centrifuged at 10000 rpm for 5 minutes. The supernatants were collected to determine the released glucose using NMR. All experiments of enzymatic hydrolysis were conducted in triplicate.

The relative glucose yield was calculated from the equation 5.54 (Zhang et al., 2018).

$$\text{Glucose yield, } Y_{G,EH}(\%) = \frac{\text{Glucose produced during enzymatic hydrolysis}}{\text{Glucan in pretreated solid} \times 1.11} \times 100 \quad (5.54)$$

Where, 1.11 = conversion factor of glucan to its equivalent glucose ((Zhang et al., 2018)

The molar yield (%) of glucose, $y_{G,EH}$, is defined as follows:

$$y_{G,EH}(\%) = \frac{\text{Moles of Glucose produced during enzymatic hydrolysis}}{\text{Moles of Glucan in pretreated solid}} \times 100 \quad (5.55)$$

5.2.2 Comparison of Experimental Results of Enzymatic Hydrolysis

The glucose yields have been calculated from equation 5.8. It has been observed that the yields of glucose have an increasing trend with time, shown in the Fig. 5.16. The glucose yields after 72 hours of enzymatic hydrolysis of untreated RS and pretreated solids (obtained from LWP, SAP and FCP) are determined as 27.9%, 32.3%, 45.4% and 78.9% respectively. The results signified that the $FeCl_3$ pretreatment (concentration = 0.1M) on rice straw is very efficient for glucose yield during enzymatic hydrolysis.

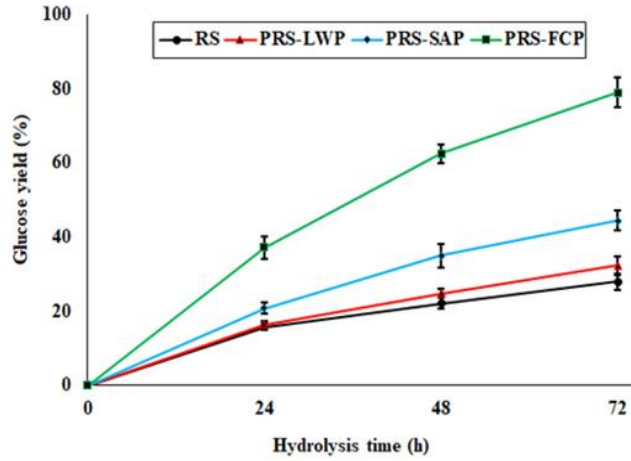


Fig. 5.16 Glucose yield (%) after enzymatic hydrolysis of untreated RS and pretreated solids obtained from LWP, SAP and FCP

5.2.3 Mathematical model for enzymatic hydrolysis

A mathematical model for enzymatic hydrolysis has been developed based the reaction scheme shown in the Figure 5.17.

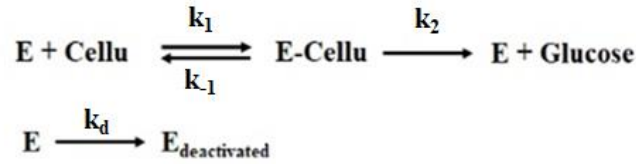


Fig. 5.17 Mathematical model for enzymatic hydrolysis

Kinetic parameters, γ and k_0 have been introduced. The first order deactivation rate constant of the enzyme is k_d . According to the model, γ is correlated to k_d as $\frac{2\gamma}{1+\gamma t} = k_d$ and another parameter, $k_0 = \frac{k_2 C_{E0}}{K_M}$ (Yang and Fang, 2015). Figure 5.17, k_2 is the rate constant for the irreversible reaction involved in the formation of the product, glucose from the cellulose-cellulase complex and K_M is Michaelis-Menten constant. According to Briggs –Haldane quasi-steady state concept for the enzyme-substrate complex, $K_M = \frac{k_2 + k_{-1}}{k_1}$ and according to rapid equilibrium concept of the reversible complexation of enzyme and substrate, $K_M = \frac{k_{-1}}{k_1}$.

On the basis of mole balance, the rate of change of molar yield of glucose can be written as,

$$\frac{dy_{G,EH}}{dt} = k_0 \frac{1}{(1+\gamma t)^2} (1 - y_{G,EH}) \quad (5.56)$$

$$\frac{dy_{Cellu,EH}}{dt} = -k_0 \frac{1}{(1+\gamma t)^2} (1 - y_{G,EH}) \quad (5.57)$$

$$\frac{t}{-\ln(1-y_{G,EH})} = \frac{\gamma}{k_0} t + \frac{1}{k_0} \quad (5.58)$$

The equation of prediction glucose yield is given below

$$y_{G,EH}^{Predicted} = 1 - \exp\left(-\frac{k_0 t}{1+\gamma t}\right) \quad (5.59)$$

$y_{G,EH}$ is the molar glucose yield.

5.2.3 Comparison of experimental and simulated yield of glucose during enzymatic hydrolysis

The parameters, γ and k_0 have been calculated from the slope ($\frac{\gamma}{k_0}$) and intercept ($\frac{1}{k_0}$) of $\frac{t}{-\ln(1-y_{G,EH})}$ versus t plot, shown in the Fig. 5.18a. The parameters, γ and k_0 are 0.0297 h^{-1} and 0.0738 h^{-1} . Figure 5.18 represents the simulated and experimental profile of glucose yield. From the close analysis of the figure, it can be inferred that the model can predict the experimental trend.

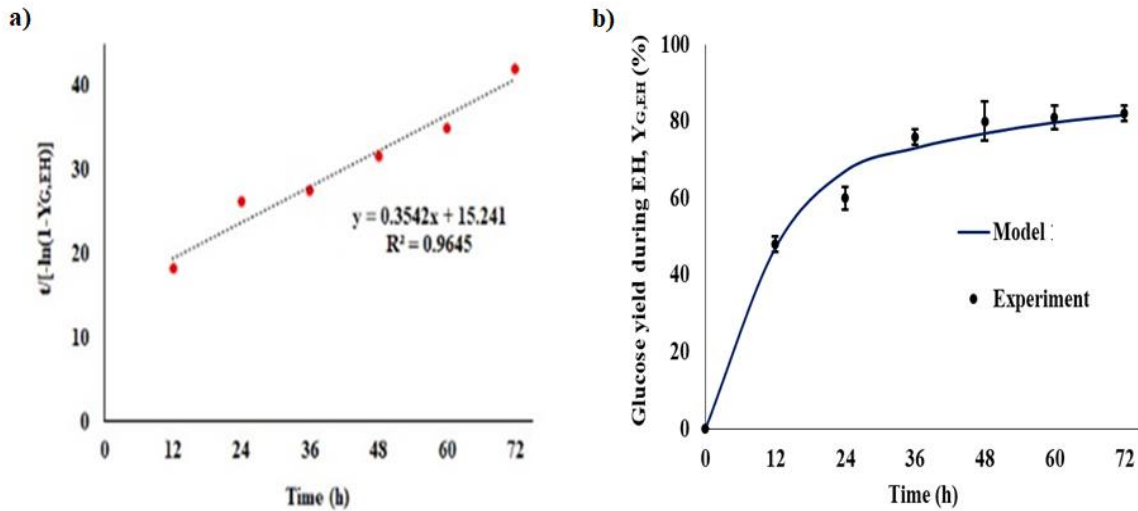


Fig. 5.18 Plot of $\frac{t}{-\ln(1-y_{G,EH})}$ versus t (a); Comparison the yield of glucose during enzymatic hydrolysis from Model with experimental data (b)

5.2.4 Optimization of glucose yield of enzymatic hydrolysis and overall glucose yield

The response surface methodology (RSM) has been used to optimize the of glucose yield through enzymatic hydrolysis of pretreated rice straw and overall glucose yield combining the quantities of glucose obtained directly through pretreatment and that produced through enzymatic hydrolysis. The combined severity (CS) of pretreatment and the enzyme loading are expected to influence both the yields. The combined severity, representing a combined index of pretreatment time, temperature and the strength of FeCl_3 solution, is expected to affect the composition of the hydrolysate as well the pretreated solid. The composition of the pretreated solid is expected to affect the behavior during enzymatic hydrolysis. The loading of enzyme, i.e. the enzyme to pretreated solid ratio is expected to affect the hydrolysis process. The combined yield of glucose is calculated based on the summation of quantities of glucose appearing in the pretreatment hydrolysate and that obtained through enzymatic hydrolysis of pretreated RS. Therefore, glucose yield through enzymatic hydrolysis ($Y_{G,EH}$) and combined glucose yield during pretreatment and enzymatic hydrolysis ($Y_{G,C}$) are optimized with respect to combined severity (CS) of pretreatment and the enzyme loading (FPU/ g of dry substrate using response surface methodology (RSM)). The 2-factor Central Composite statistical design has been used. Design-Expert Software (version 11) has been used for this purpose. During optimization, second order functionalities of $Y_{G,EH}$ and $Y_{G,C}$ with respect to combined severity (CS_{cellu}) of pretreatment and the enzyme loading have also been obtained. The values of $Y_{G,EH}$ have been calculated from Eq. 5.8. The combined glucose yield (%), $Y_{G,C}$ incorporating the glucose released from both pretreatment and enzymatic hydrolysis has been calculated as follows:

$$\begin{aligned} \text{Combined Glucose yield, } Y_{G,C}(\%) = \\ \frac{\text{Glucose produced during enzymatic hydrolysis and pretreatment}}{\text{Glucan in RS fed to the pretreatment process}} \times 100 \end{aligned} \quad (5.60)$$

The Table 5.21 represents the coded levels of independent variables used for the optimization of $Y_{G,EH}$ and $Y_{G,C}$ respectively.

Table 5.21 Coded levels of variables used for the optimization of $Y_{G,EH}$ and $Y_{G,C}$

Input variables	Coded variable level			Model Response
	-1	0	1	
A: Combined severity (CS_{cellu})	0.62	1.15	1.68	(i), $Y_{G,EH}(\%)$
B: enzyme loading (FPU/ g of dry substrate)	10	20	30	(ii) $Y_{G,C}(\%)$

The minimum value (0.62) and maximum value (1.68) of CS_{cellu} are obtained for 150°C for 5 minutes and 190°C for 15 minutes. The value of CS_{cellu} at 170°C for 10 minutes is 1.18 which is almost close to the mid-point of CS_{cellu} , i.e., 1.15, used in RSM. Thereafter, the data obtained at 170°C for 10 minutes are used.

The ANOVA tables for optimization of $Y_{G,EH}$ and $Y_{G,C}$ have been reported in the Table 5.22 and 5.23 respectively. It has observed that the R^2 , adjusted R^2 , predicted R^2 values are acceptable.

Table 5.22 ANOVA Table for optimization of $Y_{G,EH}$

Source	Sum of Squares	df	Mean Square	F-value	p-value	
Model	36.54	5	7.31	44.94	< 0.0001	significant
A-CS	13.04	1	13.04	80.23	< 0.0001	
B-Enzyme loading	11.68	1	11.68	71.86	< 0.0001	
AB	3.39	1	3.39	20.82	0.0026	
A ²	0.0095	1	0.0095	0.0582	0.8163	
B ²	8.20	1	8.20	50.43	0.0002	
Residual	1.14	7	0.1626			
Lack of Fit	1.14	3	0.3794			
Pure Error	0.0000	4	0.0000			
Cor Total	37.68	12				

(R^2 : 0.9763; adjusted R^2 : 0.9642; Predicted R^2 : 0.9471)

Table 5.23 ANOVA Table for optimization of $Y_{G,EH}$

Source	Sum of Squares	df	Mean Square	F-value	p-value	
Model	670.27	5	134.05	30.51	0.0001	significant
A-CS	411.54	1	411.54	93.68	< 0.0001	
B-EH	66.94	1	66.94	15.24	0.0059	
AB	20.25	1	20.25	4.61	0.0689	
A ²	139.15	1	139.15	31.67	0.0008	
B ²	51.56	1	51.56	11.74	0.0110	
Residual	30.75	7	4.39			
Lack of Fit	30.75	3	10.25			
Pure Error	0.0000	4	0.0000			
Cor Total	701.02	12				

(R²: 0.9652; adjusted R²: 0.9431; Predicted R²: 0.9132)

The equation obtained from ANOVA quadratic model for $Y_{G,EH}(\%)$ and $Y_{G,C}(\%)$, have been provided in the Eq. 5.61 and 5.62.

$$Y_{G,EH}(\%) = 81.6772 - 6.1829A + 0.355477B + 0.173585AB + 0.131274A^2 - 0.0108562B^2 \quad (5.61)$$

$$Y_{G,C}(\%) = 40.66 + 31.5786A + 1.86648B - 0.424528AB - 15.922A^2 - 0.027225B^2 \quad (5.62)$$

The impact of CS_{cellu} and enzyme loading on $Y_{G,EH}$ and $Y_{G,C}$ have been shown in the Fig. 19a and 19b respectively.

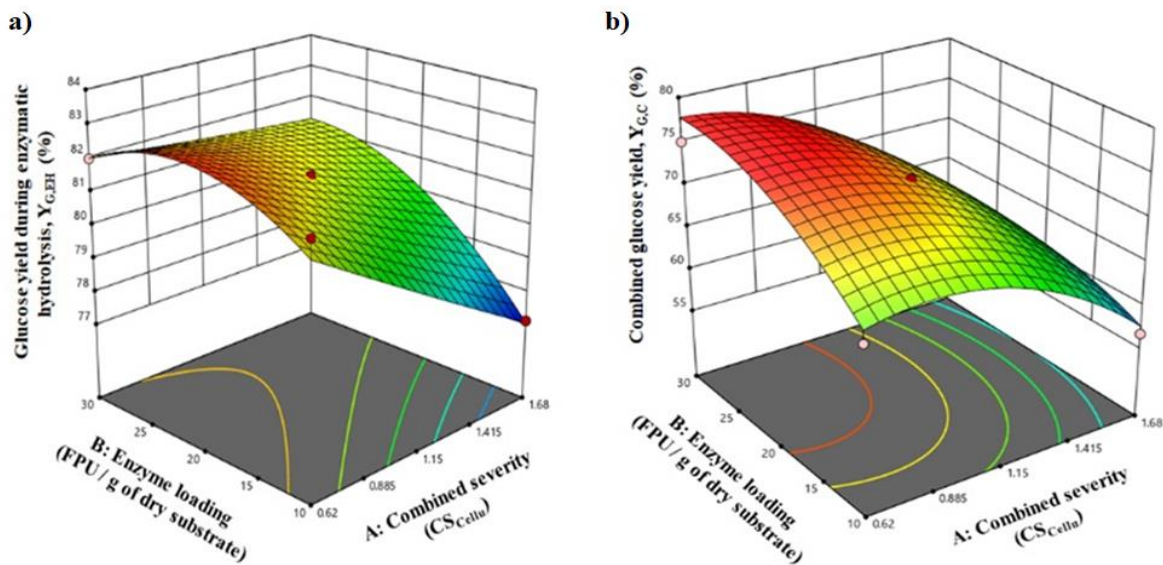


Fig.5.19 Effect of CS_{Cellu} and enzyme loading (FPU/ g of dry substrate) on the response surface for glucose yield during enzymatic hydrolysis ($Y_{G,EH}$) (a) and combined glucose yield during pretreatment and enzymatic hydrolysis ($Y_{G,C}$) (b)

The optimum glucose yield for enzymatic hydrolysis ($Y_{G,EH}$) and combined glucose yield during pretreatment and enzymatic hydrolysis ($Y_{G,C}$) have been reported in the Table 24.

Table 24 Optimum glucose yield for enzymatic hydrolysis ($Y_{G,EH}$) and combined glucose yield during pretreatment and enzymatic hydrolysis ($Y_{G,C}$)

	Combined severity (CS_{Cellu})	Enzyme loading (FPU/ g of dry substrate)	Optimum yield (%)
$Y_{G,EH}$	0.983	18.474	81.387
$Y_{G,C}$	1.032	21.528	74.673

5.3 Ethanol production

5.3.1 Experimental

Enzymatic hydrolysate (1.8 mL) of pretreated rice straw and untreated rice straw was inoculated with 0.2 mL of 24h old stock culture of *Saccharomyces cerevisiae*(MTCC-173) and was allowed for ethanol fermentation under anaerobic condition at 30 °C, under stirring (150 rpm). All experiments were conducted in triplicate. The *Saccharomyces cerevisiae*(MTCC-173) was purchased from MTCC, India. The bacterial culture was maintained in YPD medium (3 g yeast extract, 10 g peptone, 20 g dextrose and 1 L distilled water) at 28 °C.

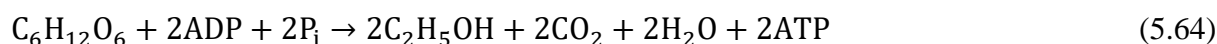
5.3.2 Analytical

The ethanol concentration of fermentation sample was determined in gas chromatography analyzer (TRACE 1110, Thermo Fisher Scientific). The fermentation broth was centrifuged for 5 minutes at 10000 rpm. 1 mL of supernatant and 1.5 mL of 1-butanol (Merck) were mixed in a glass tube closed with rubber cap. As ethanol is highly soluble in butanol, two layers – bottom layer containing the aqueous phase were separated and top layer containing butanol-ethanol mixture. The top layer was analyzed for ethanol concentration using GC with the aid of a standard curve constructed using known concentration of ethanol in aqueous phase. The GC was equipped with Chromeleon software and flame ionization detector (FID). Hydrogen, air and nitrogen flow rate were set as 30, 300 and 30 mL/min respectively. The oven and FID detector temperature were 40 and 250 °C respectively. TR-FAME capillary column was used to perform the experiment.

The % relative yield of ethanol (on the basis of theoretical yield) $Y_{\text{Ethanol}}(\%)$ was determined from equation 5.66.

$$Y_{\text{Ethanol}}(\%) = \frac{\text{Ethanol produced } \left(\frac{\text{g}}{\text{L}}\right)}{\text{Theoretically achievable concentration of Ethanol } \left(\frac{\text{g}}{\text{L}}\right)} \times 100 \quad (5.63)$$

Again, the stoichiometric equation for conversion of glucose to ethanol is as follows (Drapcho & Nghim, 2008)



Therefore, from 1g glucose, theoretically achievable ethanol is as follows:

$$\frac{2 \times \text{Molecular weight of Ethanol} \left(\frac{46\text{g}}{\text{mol}} \right)}{\text{Molecular weight of glucose} \left(\frac{180\text{g}}{\text{mol}} \right)} \times 1\text{g Glucose} = 0.511\text{g Ethanol} \quad (5.65)$$

Therefore, equation (5.53) can also be written as follows:

$$Y_{\text{Ethanol}}(\%) = \frac{\text{Ethanol produced} \left(\frac{\text{g}}{\text{L}} \right)}{\text{Initial glucose concentration} \left(\frac{\text{g}}{\text{L}} \right) \times 0.511} \times 100 \quad (5.66)$$

5.3.3 Comparison of Experimental Results

The ethanol productions from fermentable sugar namely, glucose released during enzymatic hydrolysis of untreated RS and pretreated solids (obtained from LWP, SAP (0.1M) and FCP(0.1M)) are determined as 2.01, 2.49, 3.41 and 5.01 g/L respectively, shown in the Fig. 5.20a. Ethanol conversion yield (for FCP, calculated from equation 12) is 83.79 %.

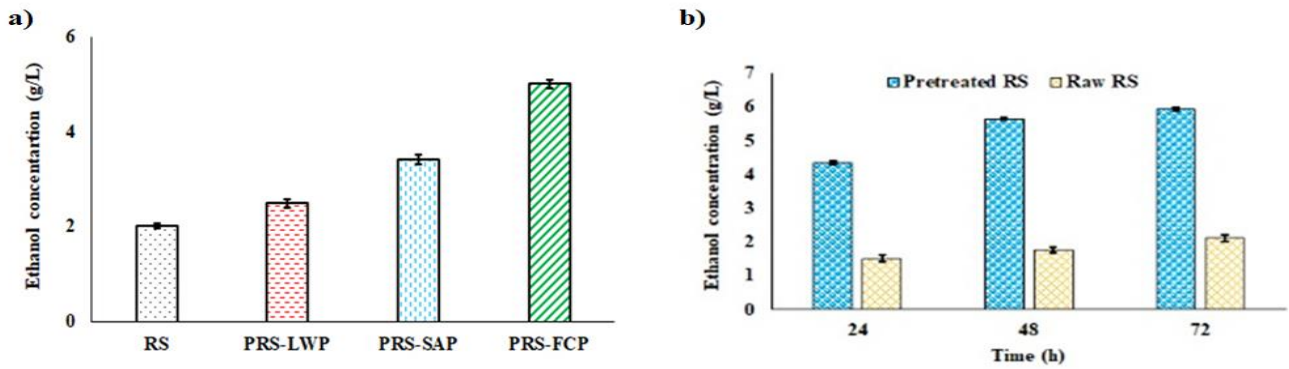


Fig. 5.20 Ethanol production after enzymatic hydrolysis of raw-RS and pretreated solids for 72 hours for LWP/ SAP/ FCP (a); Ethanol production after enzymatic hydrolysis of raw-RS and pretreated solids (obtained at 170 °C, for 10 minutes using 0.2 M FeCl₃ solution) for 24, 48 and 72 hours (b)

The ethanol productions (for batch time 72 hours) from fermentable sugar namely, glucose released during enzymatic hydrolysis of untreated RS and pretreated solid (obtained from pretreatment of rice straw at 170 °C, for 10 minutes using 0.2 M FeCl₃ solution) are determined as 2.01 and 6.09 g/L for respectively.

Under the present study, the residual solid samples obtained from pretreatment, have been subjected to enzymatic hydrolysis for the production of glucose. Glucose, released during enzymatic hydrolysis, has been used for ethanol fermentation. As the hydrolysate is not being used

for ethanol production, there is no chance of interference from furfural. For the utilization of glucose from hydrolysate, separation processes for the recovery of each product have to be adopted. A typical separation scheme can be represented as follows:

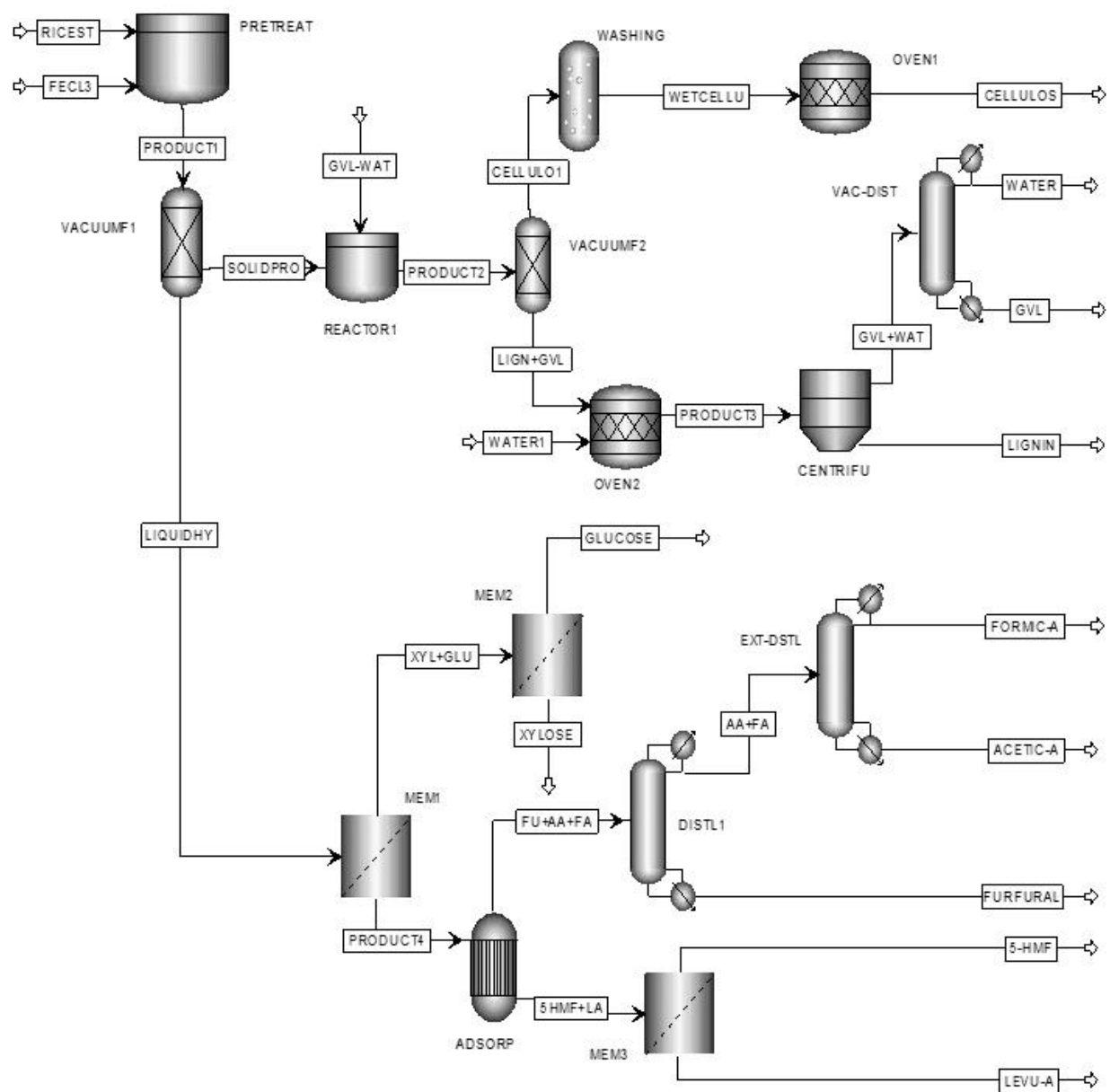


Fig. 5.21 Products separation from residual solid and liquid hydrolyzate obtained from the ferric chloride pretreatment of rice straw (Unit operation and Process Blocks: PRETREAT: pretreatment unit, VACUUMF1: vacuum filtration unit 1, REACTOR1: reactor for lignin solubilization, VACUUMF2: vacuum filtration unit 2, WASHING: washing unit, OVEN1:

oven for drying cellulose, OVEN2: oven for lignin precipitation, CENTRIFU: centrifuge, VAC-DIST: vacuum distillation unit, MEM1: membrane 1, MEM2: membrane 2, ADSORP: adsorption unit, MEM3: membrane 3, DISTL1: Distillation unit 1, EXT-DSTL: extractive distillation unit)

Streams: PRODUCT1: products obtained from pretreatment, SOLIDPRO: pretreated solid, GVL-WATER: GVL-water solution, PRODUCT2: products obtained from REACTOR1, CELLULO1: cellulose obtained from filtration unit, WETCELLU: wet cellulose, CELLULOS: high purity cellulose, LIGN+ GVL: lignin-GVL mixture, PRODUCT3: products obtained from OVEN2, GVL+WAT: GVL-water mixture as supernatant, LIQUIDHY: liquid hydrolyzate, XYL+GLU: xylose and glucose, PRODUCT 4: permeate from membrane 1, FU+AA+FA: furfural, acetic acid and formic acid, 5-HMF+LA: 5-hydroxymethylfurfural and levulinic acid, FORMIC-A: Formic acid, ACETIC-A: acetic acid, LEVU-A: levulinic acid. In the pretreatment unit (PRETREAT), rice straw can be treated with ferric chloride at 170°C for 10 minutes. The pretreated solid (SOLIDPRO) and liquid hydrolyzate (LIQUIDHY) can be separated in a vacuum filter (VACUUMF1). The pretreated solid containing cellulose and lignin can be mixed with GVL and water in a unit (REACTOR1) at 80°C for 30 minutes (L:S = 4:1) and lignin is solubilized in GV. Thereafter, another vacuum filter (VACUUMF2) can be used where cellulose and lignin-GVL mixture are separated.

In this process, high purity cellulose can be washed with water in a unit (WASHING block) and subsequent dried in OVEN1 at 105°C. The separation of lignin and GVL can take place with the addition of water and overnight exposure to a temperature of 40°C in OVEN 2. Afterwards, through centrifugation in the CENTRIFU block, solid lignin can be recovered and GVL-rich supernatant can be obtained for further purification (Alonso et al, 2017). GVL and water can be separated using a distillation unit [VAC-DIST] (Li et al, 2018). The hydrolysate containing glucose, xylose, 5-HMF, levulinic acid, furfural, acetic acid and formic acid can pass through a membrane unit (MEM1) using TS40 to separate the mixture of glucose and xylose as retentate (Zdarta et al, 2020). Xylose can be separated from glucose in a membrane unit (MEM2) using Desal-5 DK, -DL and NF270 membranes in stack (Sjoman et al, 2007).The permeate can pass through an adsorber (ADSORP) containing XAD761 to absorb 5-HMF and levulinic acid (Hu et al, 2021). A membrane unit (MEM3) using anion exchange membrane- Neosepta ACS and cation

exchange membrane- Neosepta CIMS can be used to separate 5-HMF and levulinic acid (Kim et al, 2013). The exit stream of the adsorber (ADSORP) containing FU+AA+FA can be fed to a distillation column (DISTL1) where furfural (boiling point 162°C) can be separated from the mixture of acetic acid and formic acid having boiling points of 118°C and 100.8°C respectively (Purrunen, 1978). Formic acid and acetic acid can be separated in an extractive distillation unit (EXT-DSTL) using nitrobenzene as a solvent (Berg, 1997). From the reaction schemes, it is clear that by changing the extend of reactions, different arrays of biomolecules can be produced. The pervaporation technique using hydrophobic membrane, e.g., polydimethylsiloxane (PDMS) can also be used to separate furfural (Qin et al, 2014). Reports are available on the extraction of 5-HMF by using either methyl isobutyl ketone or tetrahydrofuran. Use of GVL along with the solvents during the FeCl₃ pretreatment can further enhance the recovery of HMF (Menegazzo et al, 2018). Several studies revealed that levulinic acid can be recovered from the liquid effluent of FeCl₃ assisted pretreatment of biomass using methyl tetrahydrofuran efficiently (Wang et al, 2018). Therefore, FeCl₃ can play a vital role to implement the concept of biorefinery using abundantly available Indian agro-waste, namely, rice straw. The process will simultaneously produce fermentable sugars, treated solid suitable for enzymatic hydrolysis and extractable platform chemicals. As reported in recent literature, recovery of furfural during FeCl₃ pretreatment is possible by using γ -valerolactone assisted lignin separation through pH control, followed by extraction using ethyl acetate and finally separation through distillation (Ding et al, 2021). Further studies are, therefore, required for the implementation of the scheme and is not included in the present study.

5.4 Overall mass balance

The overall mass balance for LWP/ SAP (0.1M)/ FCP (0.1M) of rice straw followed by enzymatic hydrolysis and fermentation has been shown in the Fig. 5.22, 5.23 and 5.24 respectively.

Pretreatment of rice straw takes place in the PRETREAT block. ENZYHYDR and FERMENTA signify the enzymatic hydrolysis unit and fermentation unit respectively. The productions of ethanol (kg ethanol / kg of rice straw) through LWP, SAP (0.1M) and FCP (0.1M) pretreatment of rice straw followed by enzymatic hydrolysis and fermentation have been determined as 0.0444, 0.0609 and 0.0899 respectively.

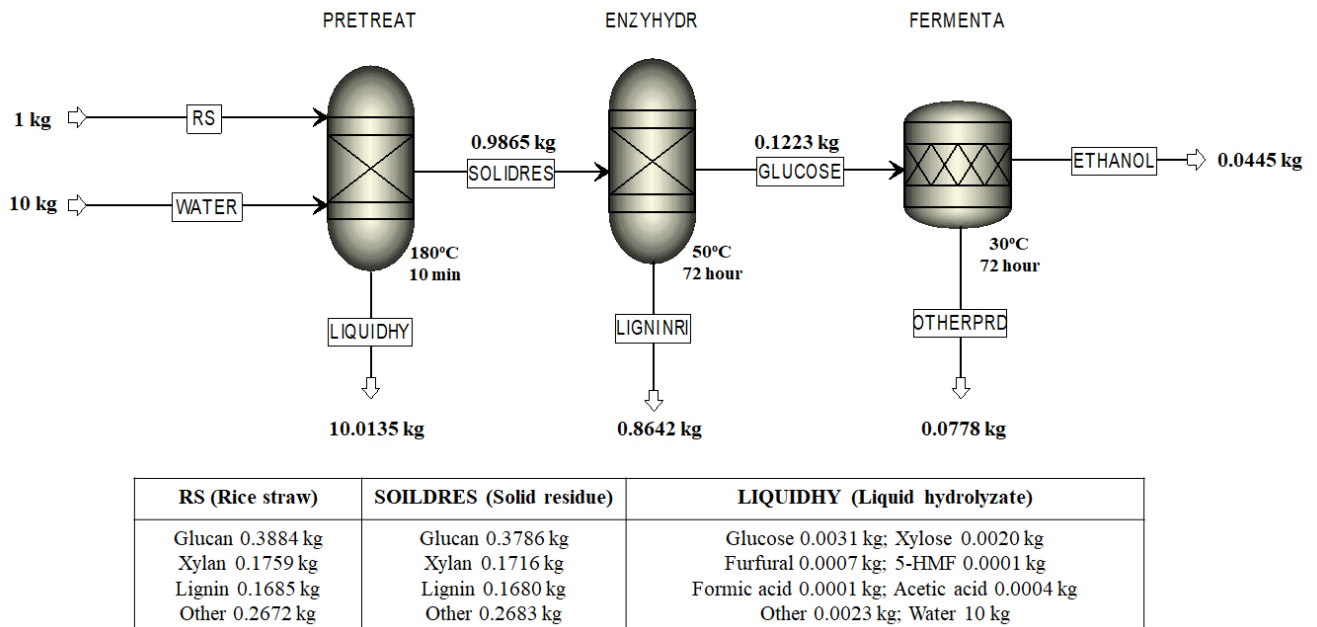


Fig. 5.22 Overall mass balance for LWP of rice straw followed by enzymatic hydrolysis and fermentation

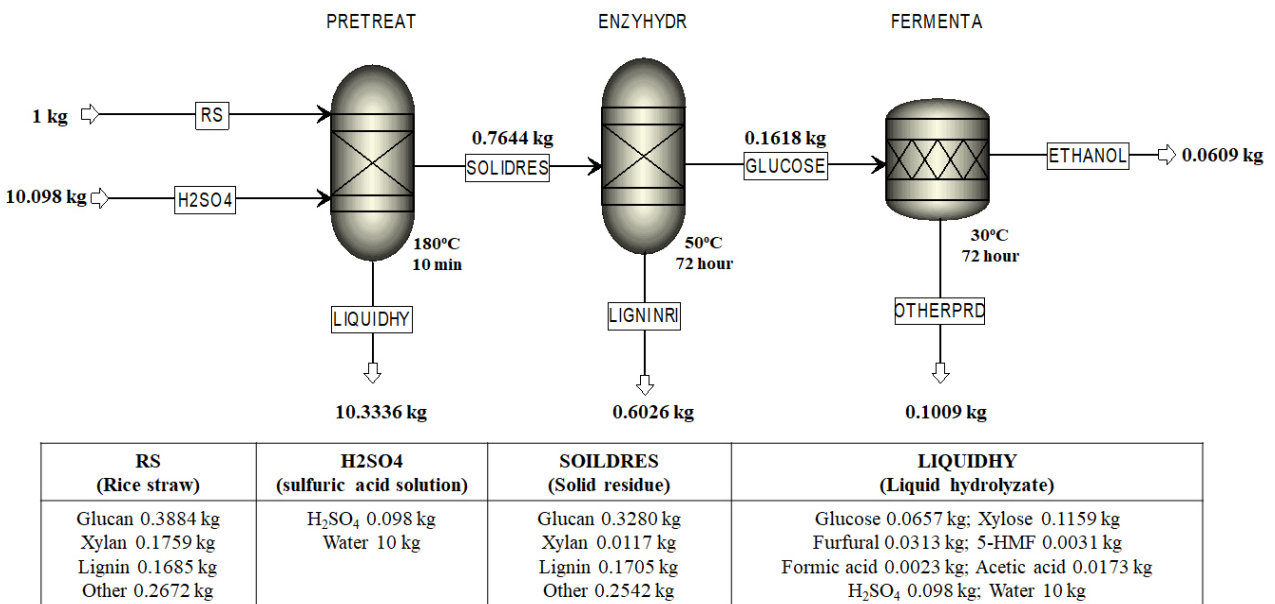


Fig. 5.23 Overall mass balance for SAP of rice straw followed by enzymatic hydrolysis and fermentation

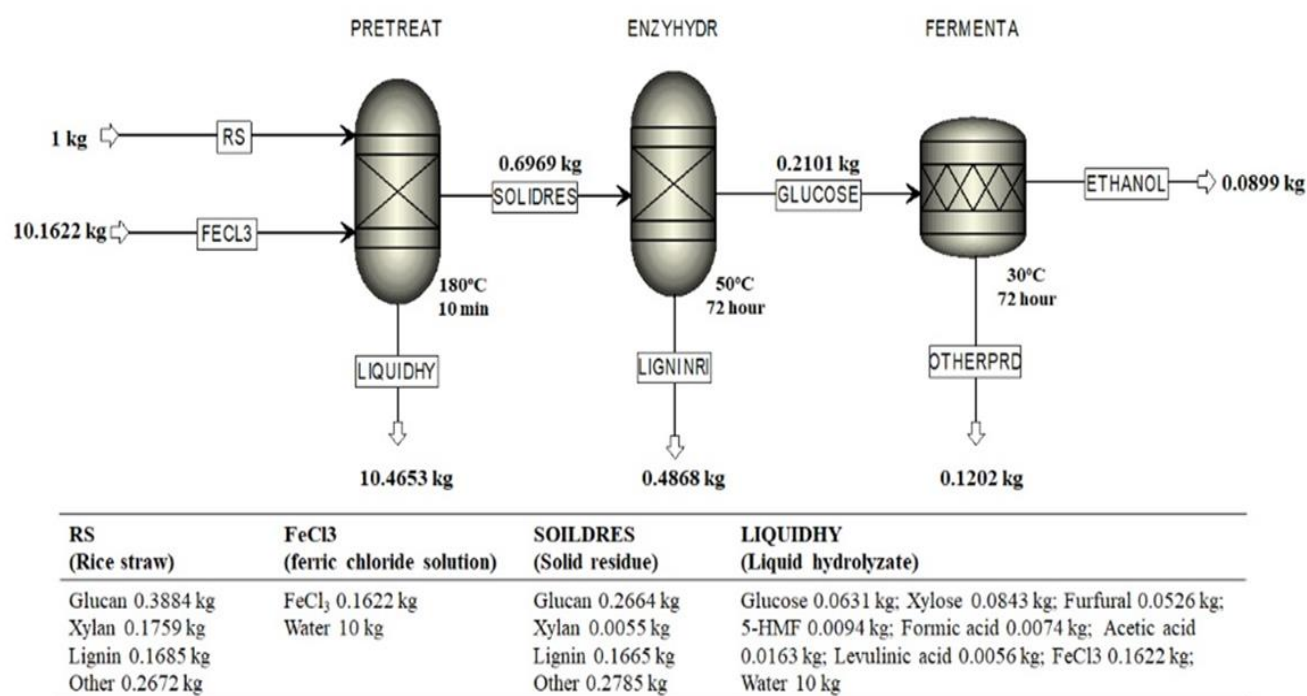


Fig. 5.24 Overall mass balance for FCP (0.1M FeCl₃) of rice straw followed by enzymatic hydrolysis and fermentation

The overall mass balance 0.2M FeCl₃ pretreatment of rice straw followed by enzymatic hydrolysis and fermentation has been shown in the Fig. 5.25. In this process, 0.0851 kg ethanol has been produced from 1 kg of rice straw.

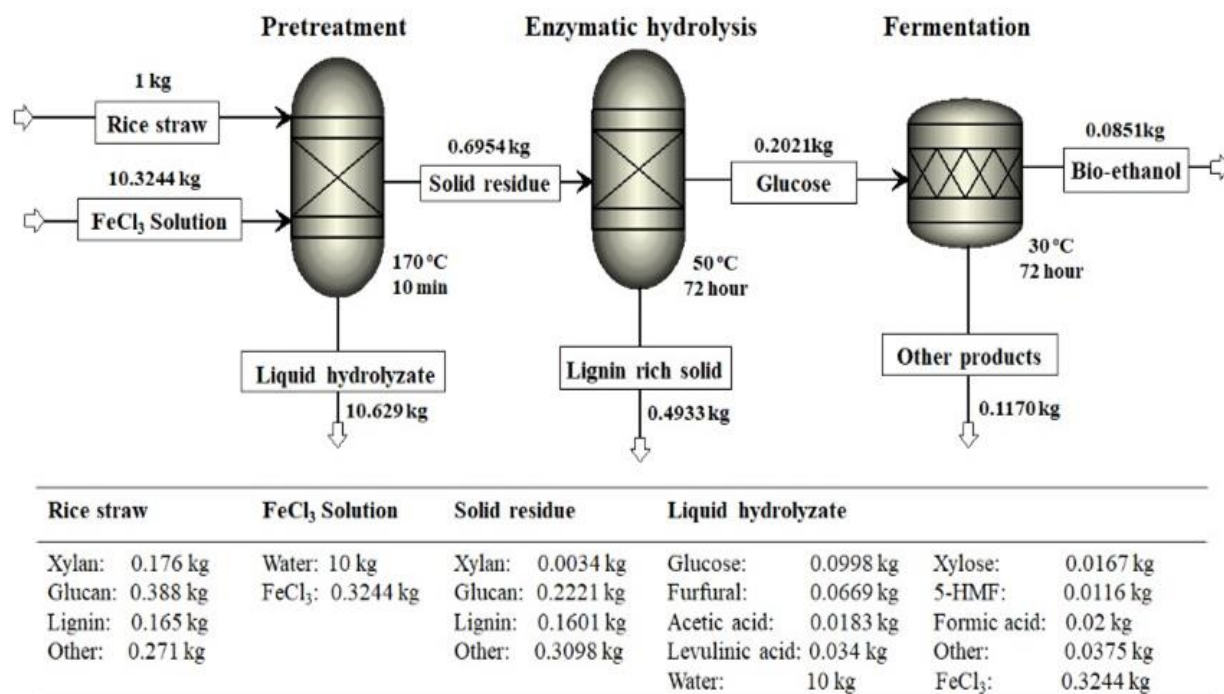


Fig. 5.25 Overall mass balance 0.2M FeCl₃ pretreatment of rice straw followed by enzymatic hydrolysis and fermentation

5.5 Summary

The mechanism of hydronium-ion based pretreatment, namely, LWP, SAP and FCP of hemicellulose and cellulose of rice straw has been explained through shrinking core model using chemical engineering concept for the first time. The degradation rate constants of hemicellulose and cellulose of rice straw have been compared for the first time. The analysis of hydrolysate and the pretreated solid clearly indicate the most efficient action of FCP in comparison to acid pretreatment in the present range of temperature (140-180°C). From this study it is clear that the yields of all hydrolysis products, namely, xylose, glucose, acetic acid, furfural, 5-HMF, levulinic acid and formic acid are higher in case of FCP compared to LWP and SAP. As the amount of furfural and 5-HMF, produced in case of FCP is high, they can be utilized as fuel additives and the use of the hydrolysate part for ethanol production is not recommended due to their inhibitory effects. As furfural, 5-HMF and levulinic acid contents increase monotonically with the increase in temperature during FCP, one can strategize to focus on these products in the hydrolysate and

production of glucose from the pretreated straw only. It is clear from the study that FCP can play a vital role to implement the concept of biorefinery using abundantly available Indian agro-waste, namely, rice straw for the production of ethanol, furfural, 5-HMF and levulinic acid as the main products. From the best of our knowledge, a deterministic mathematical model for conversion of xylan and cellulose into xylose and glucose (and valuable products) for ferric chloride pretreatment of Indian rice straw has also been developed and validated for the first time. Deterministic mathematical models for enzymatic hydrolysis has also been developed. The effect of combined severity and enzyme loading on the yield of glucose have been investigated.

References

- Agbor, V. B., Cicek, N., Sparling, R., Berlin, A., & Levin, D. B. (2011). Biomass pretreatment: fundamentals toward application. *Biotechnology advances*, 29(6), 675-685.
- Alonso, D. M., Hakim, S. H., Zhou, S., Won, W., Hosseinaei, O., Tao, J., & Dumesic, J. A. (2017). Increasing the revenue from lignocellulosic biomass: Maximizing feedstock utilization. *Science advances*, 3(5), e1603301.
- Bandura, A. V., & Lvov, S. N. (2006). The ionization constant of water over wide ranges of temperature and density. *Journal of physical and chemical reference data*, 35(1), 15-30.
- Berg, L. (1997). *U.S. Patent No. 5,599,979*. Washington, DC: U.S. Patent and Trademark Office.
- Bulmer, G. S., De Andrade, P., Field, R. A., & van Munster, J. M. (2021). Recent advances in enzymatic synthesis of β -glucan and cellulose. *Carbohydrate Research*, 508, 108411.
- Canales, M., & Guàrdia, E. (2022). Computer simulation study of ion-water and water-water hydrogen bonds in sulfuric acid solutions at low temperatures. *Journal of Molecular Liquids*, 347, 118351.
- Carvalho, F., Duarte, L. C., & Gírio, F. (2008). Hemicellulose biorefineries: a review on biomass pretreatments. *Journal of scientific & industrial research*, 849-864.
- Chen, L., Chen, R., & Fu, S. (2015). FeCl₃ pretreatment of three lignocellulosic biomass for ethanol production. *ACS Sustainable Chemistry & Engineering*, 3(8), 1794-1800.

- Chowdhury, R., Ghosh, S., Debnath, B., & Manna, D. (2018). Indian agro-wastes for 2G biorefineries: Strategic decision on conversion processes. *Sustainable Energy Technology and Policies: A Transformational Journey, Volume 1*, 353-373.
- da Costa Lopes, A. M., João, K. G., Rubik, D. F., Bogel-Lukasik, E., Duarte, L. C., Andreaus, J., & Bogel-Lukasik, R. (2013). Pre-treatment of lignocellulosic biomass using ionic liquids: wheat straw fractionation. *Bioresource technology*, 142, 198-208.
- Ding, D., Hu, J., Hui, L., Liu, Z., & Shao, L. (2021). Valorization of *Miscanthus* × *giganteus* by γ -Valerolactone/H₂O/FeCl₃ system toward efficient conversion of cellulose and hemicelluloses. *Carbohydrate Polymers*, 270, 118388.
- Drapcho, C. M., Nhuan, N. P., & Walker, T. H. (2008). *Biofuels engineering process technology* (pp. 160-180). New York: McGraw-Hill.
- Dussan, K., Girisuta, B., Lopes, M., Leahy, J. J., & Hayes, M. H. (2015). Conversion of hemicellulose sugars catalyzed by formic acid: kinetics of the dehydration of D-xylose, L-arabinose, and D-glucose. *ChemSusChem*, 8(8), 1411-1428.
- Elumalai, S., Agarwal, B., & Sangwan, R. S. (2016). Thermo-chemical pretreatment of rice straw for further processing for levulinic acid production. *Bioresource Technology*, 218, 232-246.
- Han, Y., Bai, Y., Zhang, J., Liu, D., & Zhao, X. (2020). A comparison of different oxidative pretreatments on polysaccharide hydrolyzability and cell wall structure for interpreting the greatly improved enzymatic digestibility of sugarcane bagasse by delignification. *Bioresources and Bioprocessing*, 7, 1-16.
- Hassan, M. K., Chowdhury, R., Ghosh, S., Manna, D., Pappinen, A., & Kuittinen, S. (2021). Energy and environmental impact assessment of Indian rice straw for the production of second-generation bioethanol. *Sustainable Energy Technologies and Assessments*, 47, 101546.
- Heidari, A., Niknahad, N., Iljana, M., & Fabritius, T. (2021). A review on the kinetics of iron ore reduction by hydrogen. *Materials*, 14(24), 7540.
- Hsu, T. C., Guo, G. L., Chen, W. H., & Hwang, W. S. (2010). Effect of dilute acid pretreatment of rice straw on structural properties and enzymatic hydrolysis. *Bioresource technology*, 101(13), 4907-4913.

- Hu, L., Zheng, J., Li, Q., Tao, S., Zheng, X., Zhang, X., & Lin, X. (2021). Adsorption of 5-hydroxymethylfurfural, levulinic acid, formic acid, and glucose using polymeric resins modified with different functional groups. *ACS omega*, 6(26), 16955-16968.
- Jeong, H., Jang, S. K., Hong, C. Y., Kim, S. H., Lee, S. Y., Lee, S. M., ... & Choi, I. G. (2017). Levulinic acid production by two-step acid-catalyzed treatment of *Quercusmongolica* using dilute sulfuric acid. *Bioresource technology*, 225, 183-190.
- Ji, X., Shen, Z., Wang, C., Yao, S., Xiong, L., Zhang, H., & Chen, X. (2023). Amino-functionalized hyper-cross-linked resins for levulinic acid adsorption from sugarcane bagasse hydrolysate. *Journal of Chemical Technology & Biotechnology*, 98(12), 2958-2970.
- Kamireddy, S. R., Li, J., Tucker, M., Degenstein, J., & Ji, Y. (2013). Effects and mechanism of metal chloride salts on pretreatment and enzymatic digestibility of corn stover. *Industrial & Engineering Chemistry Research*, 52(5), 1775-1782.
- Kapu, N. S., Yuan, Z., Chang, X. F., Beatson, R., Martinez, D. M., & Trajano, H. L. (2016). Insight into the evolution of the proton concentration during autohydrolysis and dilute-acid hydrolysis of hemicellulose. *Biotechnology for Biofuels*, 9, 1-10.
- Kim, I., Lee, B., Park, J. Y., Choi, S. A., & Han, J. I. (2014). Effect of nitric acid on pretreatment and fermentation for enhancing ethanol production of rice straw. *Carbohydrate polymers*, 99, 563-567.
- Kim, J. H., Na, J. G., Yang, J. W., & Chang, Y. K. (2013). Separation of galactose, 5-hydroxymethylfurfural and levulinic acid in acid hydrolysate of agarose by nanofiltration and electro dialysis. *Bioresource technology*, 140, 64-72.
- Krzelj, V., Ferreira Liberal, J., Papaioannou, M., van der Schaaf, J., & Neirad'Angelo, M. F. (2020). Kinetic model of xylose dehydration for a wide range of sulfuric acid concentrations. *Industrial & Engineering Chemistry Research*, 59(26), 11991-12003.
- Kumar, S., Gupta, R., Lee, Y. Y., & Gupta, R. B. (2010). Cellulose pretreatment in subcritical water: Effect of temperature on molecular structure and enzymatic reactivity. *Bioresource technology*, 101(4), 1337-1347.

- Lê, H. Q., Pokki, J. P., Borrega, M., Uusi-Kyyny, P., Alopaeus, V., & Sixta, H. (2018). Chemical recovery of γ -valerolactone/water biorefinery. *Industrial & Engineering Chemistry Research*, 57(44), 15147-15158.
- Lee, J. P., Lee, J., & Min, K. (2023). Development of bioprocess for corncob-derived levulinic acid production. *Bioresource Technology*, 371, 128628.
- Lee, Y. Y., Iyer, P., Xiang, Q., & Hayes, J. (2004). *Kinetic and Modeling Investigation to Provide Design Guidelines for the NREL Dilute-Acid Process Aimed at Total Hydrolysis/Fractionation of Lignocellulosic Biomass: July 1998* (No. NREL/SR-510-36392). National Renewable Energy Lab.(NREL), Golden, CO (United States).
- Levenspiel, O. (1998). *Chemical reaction engineering*. John Wiley & sons.
- Liu, C., Lu, X., Yu, Z., Xiong, J., Bai, H., & Zhang, R. (2020). Production of levulinic acid from cellulose and cellulosic biomass in different catalytic systems. *Catalysts*, 10(9), 1006.
- Martín, C., Dixit, P., Momayez, F., & Jönsson, L. J. (2022). Hydrothermal pretreatment of lignocellulosic feedstocks to facilitate biochemical conversion. *Frontiers in Bioengineering and Biotechnology*, 10, 846592.
- Menegazzo, F., Ghedini, E., & Signoretto, M. (2018). 5-Hydroxymethylfurfural (HMF) production from real biomasses. *Molecules*, 23(9), 2201.
- Morinelly, J. E., Jensen, J. R., Browne, M., Co, T. B., & Shonnard, D. R. (2009). Kinetic characterization of xylose monomer and oligomer concentrations during dilute acid pretreatment of lignocellulosic biomass from forests and switchgrass. *Industrial & engineering chemistry research*, 48(22), 9877-9884.
- Otieno, D. O., & Ahring, B. K. (2012). The potential for oligosaccharide production from the hemicellulose fraction of biomasses through pretreatment processes: xylooligosaccharides (XOS), arabinooligosaccharides (AOS), and mannoooligosaccharides (MOS). *Carbohydrate Research*, 360, 84-92.
- Puurunen, J. (1978). *U.S. Patent No. 4,088,660*. Washington, DC: U.S. Patent and Trademark Office.

- Qin, F., Li, S., Qin, P., Karim, M. N., & Tan, T. (2014). A PDMS membrane with high pervaporation performance for the separation of furfural and its potential in industrial application. *Green Chemistry*, 16(3), 1262-1273.
- Romero, I., López-Linares, J. C., Moya, M., & Castro, E. (2018). Optimization of sugar recovery from rapeseed straw pretreated with FeCl₃. *Bioresource technology*, 268, 204-211.
- Romero, I., Ruiz, E., & Castro, E. (2016). Pretreatment with metal salts. In *Biomass Fractionation Technologies for a Lignocellulosic Feedstock Based Biorefinery* (pp. 209-227).
- Sarker, T. R., Pattnaik, F., Nanda, S., Dalai, A. K., Meda, V., & Naik, S. (2021). Hydrothermal pretreatment technologies for lignocellulosic biomass: A review of steam explosion and subcritical water hydrolysis. *Chemosphere*, 284, 131372.
- Scapini, T., Dos Santos, M. S., Bonatto, C., Wancura, J. H., Mulinari, J., Camargo, A. F., & Treichel, H. (2021). Hydrothermal pretreatment of lignocellulosic biomass for hemicellulose recovery. *Bioresource Technology*, 342, 126033.
- Sitaraman, H., Danes, N., Lischeske, J. J., Stickel, J. J., & Sprague, M. A. (2019). Coupled CFD and chemical-kinetics simulations of cellulosic-biomass enzymatic hydrolysis: Mathematical-model development and validation. *Chemical Engineering Science*, 206, 348-360.
- Sjöman, E., Mänttari, M., Nyström, M., Koivikko, H., & Heikkilä, H. (2007). Separation of xylose from glucose by nanofiltration from concentrated monosaccharide solutions. *Journal of Membrane Science*, 292(1-2), 106-115.
- Smith, M. D. (2019). An abbreviated historical and structural introduction to lignocellulose. In *Understanding lignocellulose: Synergistic computational and analytic methods* (pp. 1-15).
- Soler, C. M. T., Sentelhas, P. C., & Hoogenboom, G. (2007). Application of the CSM-CERES-Maize model for planting date evaluation and yield forecasting for maize grown off-season in a subtropical environment. *European Journal of Agronomy*, 27(2-4), 165-177.
- Springer, E. L., & Harris, J. F. (1985). Procedures for determining the neutralizing capacity of wood during hydrolysis with mineral acid solutions. *Industrial & engineering chemistry product research and development*, 24(3), 485-489.

- Sun, D., Lv, Z. W., Rao, J., Tian, R., Sun, S. N., & Peng, F. (2022). Effects of hydrothermal pretreatment on the dissolution and structural evolution of hemicelluloses and lignin: A review. *Carbohydrate Polymers*, 281, 119050.
- Syaftika, N., & Matsumura, Y. (2018). Comparative study of hydrothermal pretreatment for rice straw and its corresponding mixture of cellulose, xylan, and lignin. *Bioresource Technology*, 255, 1-6.
- Wang, C., Zhang, Q., Chen, Y., Zhang, X., & Xu, F. (2018). Highly efficient conversion of xylose residues to levulinic acid over FeCl_3 catalyst in green salt solutions. *ACS Sustainable Chemistry & Engineering*, 6(3), 3154-3161.
- Waters, C. L., Janupala, R. R., Mallinson, R. G., & Lobban, L. L. (2017). Staged thermal fractionation for segregation of lignin and cellulose pyrolysis products: An experimental study of residence time and temperature effects. *Journal of analytical and applied pyrolysis*, 126, 380-389.
- Wen, C. Y. (1968). Noncatalytic heterogeneous solid-fluid reaction models. *Industrial & Engineering Chemistry*, 60(9), 34-54.
- Wu, Y., Ji, H., & Ji, X. (2023). Biomass pretreatment using biomass-derived organic solvents facilitates the extraction of lignin and enzymatic hydrolysis of glucan. *Cellulose*, 30(5), 2859-2872.
- Xiang, Q., Lee, Y. Y., & Torget, R. W. (2004). Kinetics of glucose decomposition during dilute-acid hydrolysis of lignocellulosic biomass. In *Proceedings of the Twenty-Fifth Symposium on Biotechnology for Fuels and Chemicals Held May 4–7, 2003, in Breckenridge, CO* (pp. 1127-1138). Humana Press.
- Yang, C. Y., & Fang, T. J. (2015). Kinetics of enzymatic hydrolysis of rice straw by the pretreatment with a bio-based basic ionic liquid under ultrasound. *Process Biochemistry*, 50(4), 623-629.
- Ye, Z. H., & Zhong, R. (2022). Outstanding questions on xylan biosynthesis. *Plant Science*, 325, 111476.

- Zdarta, J., Thygesen, A., Holm, M. S., Meyer, A. S., & Pinelo, M. (2020). Direct separation of acetate and furfural from xylose by nanofiltration of birch pretreated liquor: Effect of process conditions and separation mechanism. *Separation and Purification Technology*, 239, 116546.
- Zhang, H., Lyu, G., Zhang, A., Li, X., & Xie, J. (2018). Effects of ferric chloride pretreatment and surfactants on the sugar production from sugarcane bagasse. *Bioresource technology*, 265, 93-101.
- Zhibo, S., Liyi, L., Yong, H., & Jie, B. (2018). Influence on ferric chloride aqueous solution caused by external electrostatic field: a molecular dynamics simulation study. *RSC advances*, 8(68), 38706-38714.

Chapter 6

Production of Ethanol from Indian Biomass through Syngas Platform

Chapter 6: Production of Ethanol from Indian Biomass through Syngas Platform

Syngas fermentation can play an important role to implement the concept of biorefinery as it can serve as a platform to convert high-lignin biomass to biofuels. The syngas fermentation is a hybrid process through which syngas, mainly constituted of CO and H₂, is generated from lignocellulosic biomass in the first step, and subsequently the gas is fermented to bioethanol in the second step. There is also scarcity of data on syngas fermentation of Indian rice straw. Studies have been conducted according to the objectives under aim 2, as described in Chapter 3. The objectives are as follows:

- Experimental studies on pyrolysis of rice straw in the temperature range of 400-700°C
- Determination of yields of products and the pyro-syngas composition
- Determination of growth kinetics of Clostridial consortium, *UACJUCHEI*, used for pyro-syngas fermentation using batch mode experimental data.
- Experimental studies on pyro-syngas fermentation in semi-batch and continuous stirred tank bioreactors
- Development of mathematical models for both semi-batch and continuous stirred tank bioreactors, used for pyro-syngas fermentation
- Optimization of both semi-batch and continuous stirred tank bioreactors, used for pyro-syngas fermentation

6.1 Experimental methods

6.1.1 Pyrolysis of rice straw

The pyrolysis of rice straw was carried out in a semi-batch reactor (35 mm diameter and 210 mm long) under isothermal condition at the temperature of 400, 450, 500, 550, 600, 650 and 700 °C in an inert atmosphere maintained by nitrogen. The reactor equipped with furnace, temperature controller (PID controller) and digital weight box. Rice straw was pyrolysed at a rate of 10g/hand nitrogen flow rate was maintained at 2.5g/h, i.e., .The nitrogen flow rate was maintained at value so that sufficient time is available for the reaction of higher molecular weight volatile compounds to form gaseous compounds. For the recovery of pyro-oil, the volatile product from the pyrolyser

was passed through a condenser using circulation of water at 20 °C. The non-condensable part of volatile product constitutes pyro-syngas. The solid product, pyro-char, was collected after atmospheric cooling of the pyrolyser. The schematic diagram of the pyrolyser is represented in the Fig. 6.1. The yields of each product have been calculated and the pyro-gas was analyzed using gas chromatograph (GC).

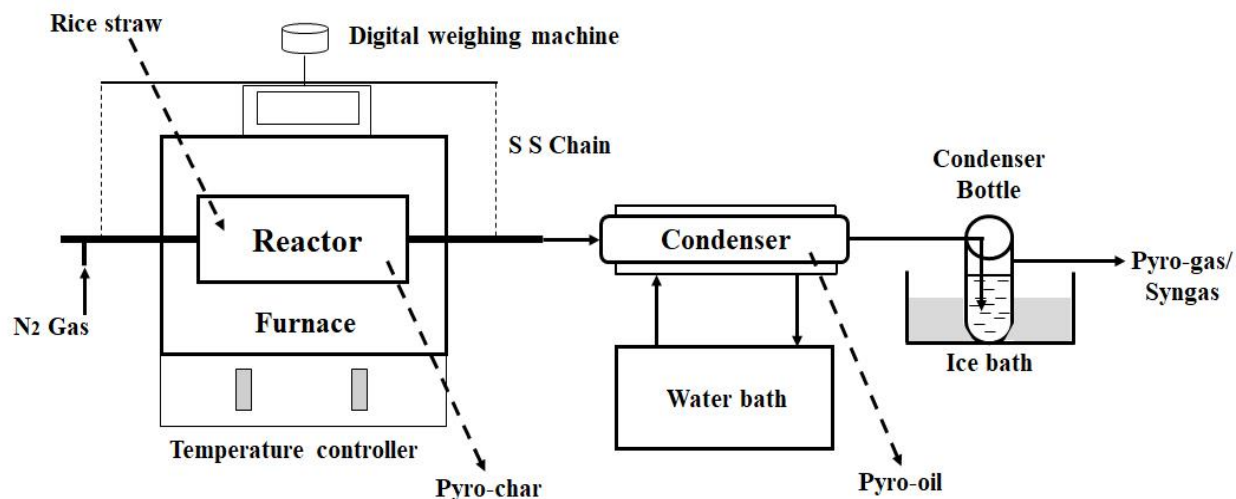


Fig. 6.1 Schematic diagram of pyrolysis of rice straw

The yield of the pyro-products namely, pyro-char, pyro-oil, and pyro-gas have been determined using the following equations:

$$\% \text{ Yield of pyro - char} = \frac{\text{mass of pyro-char obtained from pyrolysis}}{\text{mass of biomass fed to the reactor}} \times 100 \quad (6.1)$$

$$\% \text{ Yield of pyro - oil} = \frac{\text{mass of pyro-oil obtained from pyrolysis}}{\text{mass of biomass fed to the reactor}} \times 100 \quad (6.2)$$

$$\% \text{ Yield of pyro - gas} = 100 - \text{Yields of (pyro - char + pyro - oil)} \quad (6.3)$$

6.1.2 Pyro-syngas fermentation

6.1.2.1 Microorganism

A mixed clostridial strain - *UACJUCHE1*, isolated from local paddy field of West Bengal was used as inoculum (Ghose et al, 2021).

6.1.2.2 Preparation of Modified clostridial medium for growth

Modified clostridial medium was prepared according to ATCC (American Type Culture Collection) 1754 medium. Similar to the protocol, followed by Vandecasteele, fructose, yeast extract and sodium bi carbonate were excluded from the medium and a pH buffer, namely 2-(N-morpholino)ethanesulfonic acid (MES) was used (Vandecasteele, 2016). The basal DSMZ 879 medium containing 1 g NH₄Cl, 0.1 g KCl, 0.2 g MgSO₄ · 7 H₂O, 0.8 g NaCl, 0.1 g CaCl₂ · 2 H₂O, 100 mM MES, 10 ml reducing agent, 1 ml trace elements and 1 ml Wolfe's vitamin solution per liter was used. 1 mg of resazurin (10 mg/L), an indicator of anaerobic conditions, was also added to 1L basal medium). The pH of the medium was adjusted to 6 using 0.1N NaOH. The basal medium, thus prepared was transferred to sterile vessels (rubber sealed bottles/ Erlenmeyer flasks/bioreactor) already degassed with nitrogen. The medium was further autoclaved and cooled to 37°C. Gas (CO or simulated CO₂-H₂ mixture or simulated pyro-syngas, i.e., CO-CO₂-H₂-CH₄-N₂ mixture or pyro-syngas generated in the pyrolyser) transfer was done to prepare modified clostridial medium as per requirement of the experimental runs. Only CO or CO₂ or CO and CO₂, supplied either through pure gas (CO or CO₂-H₂ mixture or simulated CO-CO₂-H₂-CH₄-N₂ mixture) or from pyro-syngas, used according to experimental protocol, were the carbon source. Gas was transferred through flushing of head space for 125mL bottles and 250mL conical flasks used for pre-adaptation as well as stock culture and batch reactions for the determination of growth kinetics respectively. For the bioreactor, the gas was transferred through sparging.

6.1.2.3 Pre-adaptation of *UACJUCHEI* to Simulated Pyro-syngas

From the analysis of the pyrolysis gas obtained in the temperature range of 400-700°C, it has been observed that molar concentration (%) of CO, H₂, CO₂ and CH₄ increases from 17.07%, 13.32%, 9.11% and 7.19% to 23.08%, 17.23%, 10.59% and 8.82%. In the present study the pyro-syngas, generated from the pyrolyser, was ultimately fermented in a 3L bioreactor operated under semi-batch and continuous modes. Therefore, the *UACJUCHEI* consortium was exposed to simulated pyro-syngas mixture containing CO, H₂, CO₂, CH₄ and N₂ (25:20:15:10:35) for pre-adaptation. The basal sterile medium, as described, of 25mL volume was transferred to 10 sterile and sealed glass serum bottles of 125mL each. The medium in each bottle was inoculated with 4% (v/v) *UACJUCHEI* culture and was subsequently flushed with the simulated pyro-syngas (CO:H₂:CO₂:CH₄:N₂::25:20:15:10:35) mixture to maintain a pressure of 100kPa in the head space. All bottles were incubated at 37°C in an anaerobic chamber and orbital shaking of 150rpm was

maintained. Anaerobic condition was maintained by the flow of pure nitrogen. After adaptation, weekly transfer of 4% (v/v) inoculum to new serum bottles was followed to retain the activity of the consortium.

6.1.2.4 Batch Experiments for determination of growth kinetics of UACJUCHE1

Separate sets of batch experiments were conducted for the determination of growth kinetics of *UACJUCHE1* on CO and on CO₂ and H₂.

6.1.2.4.1 Experiments for Growth kinetics on CO

The basal sterile medium, as described, of 50mL volume was transferred to 250mL sterile and sealed Erlenmeyer flask for each experiment. Batch experiments were conducted to know the effect of gas phase concentration of CO on the growth dynamics of *UACJUCHE1*. Considering the concentration of CO in pyro-syngas, the inlet molar concentration of CO was varied in the range of 15-25%. For each inlet concentration of CO, the growth dynamics were studied for 24h. To get the data at 2h interval 12 Erlenmeyer flasks were used for each inlet molar concentration of CO of 15%, 17.5%, 20%, 22.5% and 25%. In each flask gas was transferred through flushing. All flasks were inoculated with 4% (v/v) stock culture before the introduction of gas. For each experiment, the initial pH was maintained at 6. Incubation was done under anaerobic condition at 37°C and orbital shaking speed of 150rpm was maintained. All experiments were conducted in triplicate. For any experiment, meant for each inlet CO concentration, the Erlenmeyer flasks, demarcated for the particular sampling period was taken out of the incubator and the biomass concentration was determined by the assessment of optical density at 600nm using spectrophotometer.

6.1.2.4.2 Experiments for Growth kinetics on CO₂ and H₂

The experimental protocol followed in case of the determination of growth kinetics on CO₂ and H₂ is similar to that used for the growth kinetics on CO. Considering the concentration of CO₂ and H₂ in pyro-syngas, the inlet molar concentration of CO₂ and H₂ were kept in the ranges of 8-12% and 15-20% respectively. Nine sets of batch experiments were conducted using the inlet gas composition of CO₂:H₂ : :8:15; CO₂:H₂ : :8:17.5; CO₂:H₂ : :8:20; CO₂:H₂ : :10:15; CO₂:H₂ : :10:17.5; CO₂:H₂ : :10:20; CO₂:H₂ : :12:15; CO₂:H₂ : :12:17.5 and CO₂:H₂ : :12:20. For each inlet composition of CO₂-H₂ mixture, the growth dynamics were studied for 24h under anaerobic

condition. To get the data at 2h interval 12 Erlenmeyer flasks were used. In each flask gas was transferred through flushing. All experimental parameters like temperature, pH, stirring speed etc. were kept same as those maintained in case of growth on CO. The biomass concentration was determined by the assessment of optical density at 600nm using spectrophotometer.

6.1.2.5 Stirred tank Bioreactor for Pyro-syngas Fermentation

Experiments were conducted in a 3L glass bioreactor of 135mm diameter and 235mm height equipped with two 50mm Rushton gas dispersion impellers, each with six flat blades mounted vertically around a central horizontal disc and gas sparger. The impellers were spaced at a distance of 60mm. The lower impeller is situated 30mm above the bottom. The bioreactor was provided with inlet and outlet lines for both gas and liquid streams. The main gas sparger, connected with the gas outlet was located in between the lower impeller and the bottom of the bioreactor. A bioreactor, already existing in the laboratory, has been used in the present study. The values of volumetric flow rate of liquid have been kept in a way so that the values dilution rate (inverse of residence time) are always less than the specific growth rate, μ , and do not lead to wash-out condition leading to loss of microbial cells in the bioreactor (Fogler, 2010).

The bioreactor is shown in Figure 6.2.

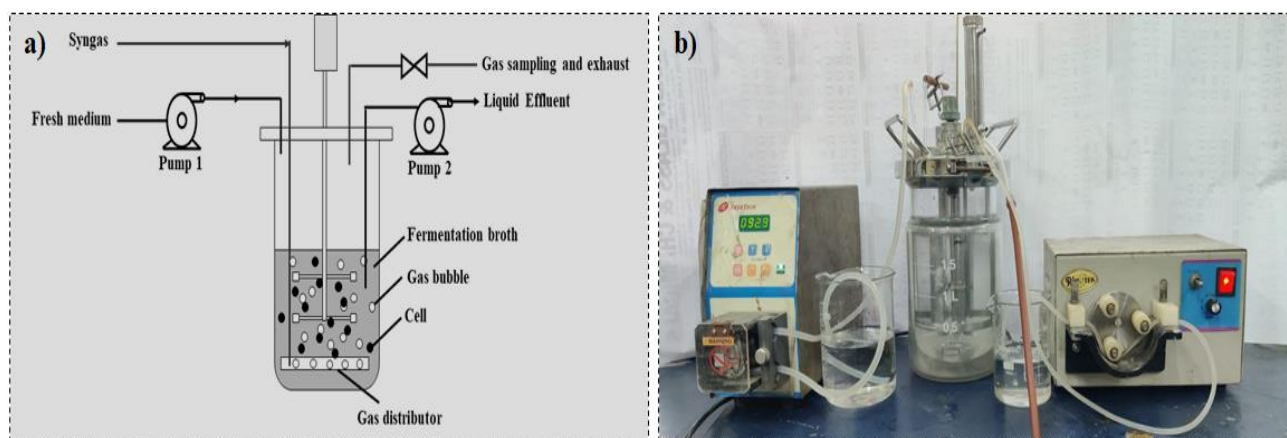


Fig. 6.2 Stirred bioreactor for pyro-syngas fermentation (a: schematic diagram; b: reactor set-up)

6.1.2.5.1 Determination of effect of stirring speed and gas velocity on O_2 Mass transfer coefficient

Experiments were conducted in the 3L glass bioreactor at 37°C. The bioreactor was filled with 2.5L basal sterile medium. Experiments were conducted to determine mass transfer coefficient of O₂. Before flowing oxygen, the vessel was flushed with pure N₂. The oxygen flow rate was varied from 0.6-10 LPM and the stirring speed was varied from 150–900 rpm. All the experiments were conducted in triplicate. The correlation of $k_L a$ on gas phase superficial velocity, u_{sg} determined by dividing the volumetric flow rate of gas by cross sectional area of vessel, and power consumption of gassed system per unit volume, P_G/V_L , as recommended by Gill et al, was validated from the experimental data. The correlation is as follows (Gill et al, 2008):

$$k_L a_{O_2} = 0.224 \left(\frac{P_G}{V_L} \right)^{0.35} (u_{sg})^{0.52} \quad (6.4)$$

The correlation between power consumption of gassed (P_G) and ungassed (P_{UG}) system is as follows:

$$\frac{P_G}{P_{UG}} = 0.497 \left(\frac{Q}{N d_i^3} \right)^{-0.38} \left(\frac{N^2 d_i^3 \rho}{\sigma} \right)^{-0.18} \quad (6.5)$$

$$P_{UG} = N_P \rho N^3 d_i^5 \quad (6.6)$$

N_P = Power number; N = stirring speed (rpm); ρ = density of solution; σ = surfacer tension

The value of power number has been considered to be 10 (Gill et al, 2008; Wang et al, 2019).

The value of $k_L a$ for any component, j can be determined by knowing the value of $k_L a$ of oxygen as follows (Chen et al, 2015):

$$k_L a_j = k_{La, O_2} \sqrt{\frac{D_{Lj}}{D_{LO_2}}} \quad (6.7)$$

Accordingly, the $k_L a$ values for CO, CO₂ and H₂ have been determined.

6.1.2.5.2 Strategy of operation of Bioreactor in Semi-batch and Continuous modes

6.1.2.5.2.1 Start-up

For both continuous and semi-batch operations, 2.5L basal sterile medium was first saturated with pyro-syngas obtained at 700°C by running the bioreactor vessel at a stirring speed of 900rpm and

inlet gas flow rate of 0.6L/h for 12h. The medium saturated with the pyro-syngas was transferred to a storage tank and was fed to the bioreactor at the start-up.

6.1.2.5.2.2 Operation of bioreactor

In case of semi-batch operation continuous flow of gas was maintained at different values. No input and output of liquid phase was used. For continuous mode of operation both gas and liquid were fed and discharged at the respective same rates. While the semi-batch operation was continued for 30hours, the operation time for continuous mode was 300h. The concentration of ethanol was optimized through response surface methodology (RSM) using Design Expert software. The experiments were conducted according to design of experiments. The operating parameters used for semi-batch and continuous operations are represented in Table 6.1 and 6.2 respectively. For semi-batch operation, pyrolysis temperature, gas to liquid volume ratio (V_G/V_L) and volumetric flow rate of gas were used as parameters. The variation of pyrolysis temperature is actually reflected in the composition of inlet gas. For continuous operation pyro-syngas obtained at 700°C was fed continuously using gas to liquid volume ratio (V_G/V_L) and the ratio of gas to liquid volumetric flow rates (q_G/q_L) as parameters. The sterile basal medium without any dissolved gas was fed during continuous operation. As a result of variation of these parameters, the dilution ratio, $D (= q_L/V_L)$ and gas residence time, $GRT (= V_L/q_G)$ were varied from 0.0106-0.0133h⁻¹ and 0.3-3.125h respectively. For both modes of operations, concentrations of ethanol, and gas phase concentrations of CO, CO₂ and H₂ were measured using Gas Chromatograph and acetic acid concentration was analyzed using HPLC. High performance liquid chromatography (HPLC) was performed to analysis the liquid sample, obtained from syngas fermentation.

Table 6.1 Operating parameters used for semi-batch reactor according to RSM

SL No.	T (°C)	V_G/V_L	q_G (L/h)	CO:CO ₂ :H ₂ :CH ₄ :N ₂	V_G (L)	V_L (L)
1	550	0.6	5.3	22.8:10.5:17.1:8.7:21.7	1.125	1.875
2	550	0.6	5.3	22.8:10.5:17.1:8.7:21.7	1.125	1.875
3	400	0.6	10	17.0:9.1:13.3:7.1:27.0	1.125	1.875
4	700	1	5.3	23.1:10.6:17.2:8.8:21.5	1.5	1.5

5	400	1	5.3	17.0:9.1:13.3:7.1:27.0	1.5	1.5
6	550	0.2	10	22.8:10.5:17.1:8.7:21.7	0.5	2.5
7	700	0.2	5.3	23.1:10.6:17.2:8.8:21.5	0.5	2.5
8	400	0.2	5.3	17.0:9.1:13.3:7.1:27.0	0.5	2.5
9	550	1	10	22.8:10.5:17.1:8.7:21.7	1.5	1.5
10	700	0.6	0.6	23.1:10.6:17.2:8.8:21.5	1.125	1.875
11	700	0.6	10	23.1:10.6:17.2:8.8:21.5	1.125	1.875
12	550	0.2	0.6	22.8:10.5:17.1:8.7:21.7	0.5	2.5
13	550	1	0.6	22.8:10.5:17.1:8.7:21.7	1.5	1.5
14	550	0.6	5.3	22.8:10.5:17.1:8.7:21.7	1.125	1.875
15	550	0.6	5.3	22.8:10.5:17.1:8.7:21.7	1.125	1.875
16	550	0.6	5.3	22.8:10.5:17.1:8.7:21.7	1.125	1.875
17	400	0.6	0.6	17.0:9.1:13.3:7.1:27.0	1.125	1.875

Table 6.2 Operating parameters for continuous operation according to RSM

SL No.	V_G/V_L	q_G/q_L	V_G (L)	V_L (L)	q_G (L/h)	q_L (L/h)
1	1	500	1.5	1.5	10	0.02
2	1	30	1.5	1.5	0.6	0.02
3	0.6	265	1.125	1.875	5.3	0.02
4	0.6	265	1.125	1.875	5.3	0.02
5	0.6	265	1.125	1.875	5.3	0.02
6	0.2	30	0.5	2.5	0.6	0.02
7	0.6	265	1.125	1.875	5.3	0.02

8	0.2	500	0.5	2.5	10	0.02
9	0.6	265	1.125	1.875	5.3	0.02
10	0.6	597.3	1.125	1.875	11.94	0.02
11	0.03	265	0.1	2.9	5.3	0.02
12	0.6	0	1.125	1.875	0	0.02
13	1.16	265	1.62	1.38	5.3	0.02

6.2 Theoretical Analysis

6.2.1 Kinetics of growth on CO

As evident from the literature, Haldane type growth kinetics is usually followed by clostridial strains grown on CO as the carbon source (Abubackar et al, 2011). Therefore, Haldane type growth model incorporating substrate inhibition along with inhibition of undissociated acetic acid, formed as product, has been attempted for the growth on CO. This is as follows:

$$\mu_1 = \mu_1^{max} \frac{C_{CO}}{K_{CO} + C_{CO} + \frac{C_{CO}^2}{K_{I,CO}}} \frac{K_{I,UA}}{K_{I,UA} + C_{UA}} \quad (6.8)$$

Where, μ = specific growth rate = $\frac{1}{C_X} \frac{dC_X}{dt}$ and C_X is biomass concentration

μ_1 is specific growth rate on CO; μ_1^{max} is maximum specific growth rate on CO; C_{CO} is concentration of CO; K_{CO} is the saturation constant for CO and $K_{I,CO}$ is the inhibition constant for growth on CO; $K_{I,UA}$ is the inhibition constant of undissociated acetic acid; C_{UA} is the concentration of undissociated acetic acid.

$$C_{UA} = C_{AA} \left(1 - \frac{10^{(pH-pKa)}}{(10^{(pH-pKa)} + 1)} \right) \quad (6.9)$$

pH= 6.7; For acetic acid, pKa=4.77 at 37°C; C_{AA} is acetic acid concentration.

Under this study μ_1^{max} has been adjusted to fit the experimental growth data, obtained using different mole fraction of pure CO in gas phase in the Erlenmeyer flasks. The other constants obtained by Vandecasteele for *C. Ljungdahlii* have been used (Vandecasteele, 2016).

6.2.2 Kinetics of growth on CO₂-H₂ mixture

The multiplicative growth kinetic model followed by *C. Ljungdahlii*, as reported by Vandecasteele has been attempted (Vandecasteele, 2016). The form of the kinetic equation is as follows:

$$\mu_2 = \mu_2^{max} \frac{C_{CO_2}}{K_{CO_2} + C_{CO_2}} \frac{C_{H_2}}{K_{H_2} + C_{H_2}} \frac{K_{I,CO}^{hy}}{K_{I,CO}^{hy} + C_{CO}} \frac{K_{I,UA}}{K_{I,UA} + C_{UA}} \quad (6.10)$$

Under this study μ_2^{max} has been adjusted to fit the experimental growth data, obtained using pure CO₂-H₂ mixture in the Erlenmeyer flasks. The other constants obtained by Vandecasteele (2016) for *C. Ljungdahlii* have been used (Vandecasteele, 2016).

6.3 Mathematical Model

The reactions for the generation of ethanol from pyro-syngas are chosen according to Vandecasteele as they used the effects of mixture of CO, CO₂ and H₂ on syngas fermentation. As they used *C. Ljungdahlii* and not any mixed culture like *UACJUCHE1*, the some growth kinetic data determined under the present study have been used. Similar to *C. Ljungdahlii* the molecular formula for *UACJUCHE1* has been assumed to be $CH_{1.81}O_{0.58}N_{0.24}$. Wood-Ljungdahl pathway for the production of Ethanol from syngas has been represented in Figure 6.3.

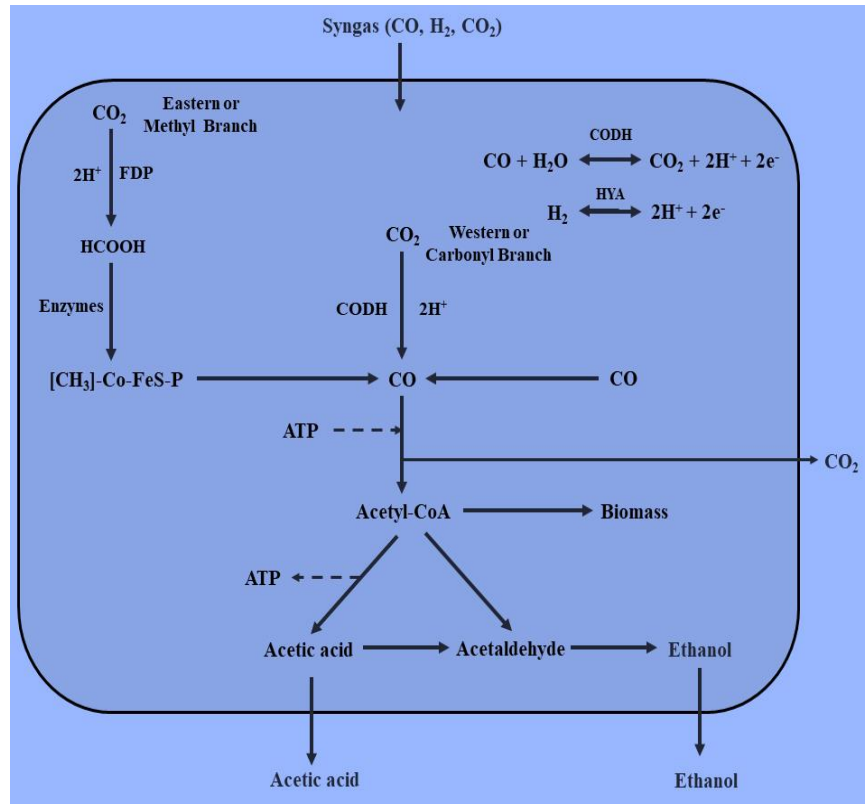
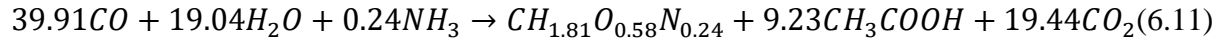


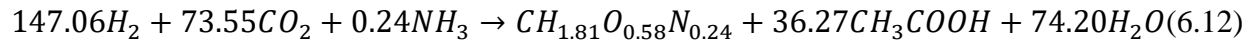
Fig. 6.3 Schematic diagram of the Wood-Ljungdahl pathway for the production of Ethanol from syngas (Acetyl-CoA: Acetyl coenzyme A; CODH: Carbon monoxide dehydrogenase; FDH: Formate dehydrogenase; Syngas: Synthesis gas)

The reactions under consideration of the model are as follows:

Biomass growth on carbon monoxide



Biomass growth on carbon dioxide and hydrogen

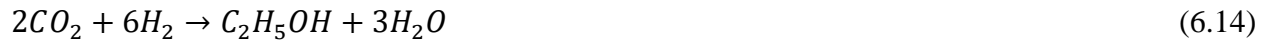


Ethanol production from carbon monoxide

In this path, the production of ethanol is considered to take place through direct conversion of acetyl-CoA into ethanol and is non-growth associated.



Ethanol production from carbon dioxide and hydrogen



Conversion of acetate into ethanol in presence of CO

To reduce acetate to ethanol, the water-gas shift reaction can be used, in which CO acts as the electron donor through the conversion of CO into CO₂ delivering the necessary reducing power.



Conversion of acetic acid into ethanol in presence of H₂

Acetate can also be reduced by using hydrogen as the electron donor during the conversion of molecular hydrogen to two protons and two electrons using the enzyme hydrogenase.



The biomass growth kinetics and the ethanol production kinetics are represented in Table 6.3.

Table 6.3 Process kinetics of growth by mixed clostridial strain - *UACJUCHE1*

Process	Specific growth or product generation rate (μ)
i) Biomass growth on CO	$\mu_1 = \mu_1^{max} \frac{C_{CO}}{K_{CO} + C_{CO} + \frac{C_{CO}^2}{K_{I,CO}}} \frac{K_{I,UA}}{K_{I,UA} + C_{UA}}$
ii) Biomass growth on CO ₂ and H ₂	$\mu_2 = \mu_2^{max} \frac{C_{CO_2}}{K_{CO_2} + C_{CO_2}} \frac{C_{H_2}}{K_{H_2} + C_{H_2}} \frac{K_{I,CO}^{hy}}{K_{I,CO}^{hy} + C_{CO}} \frac{K_{I,UA}}{K_{I,UA} + C_{UA}}$
iii) Ethanol production from CO	$q_{E1} = q_{E1}^{max} \frac{C_{CO}}{K_{CO} + C_{CO} + \frac{C_{CO}^2}{K_{I,CO}}} \frac{C_{UA}}{K_{UA} + C_{UA}}$
iv) Ethanol production from CO ₂ and H ₂	$q_{E2} = q_{E2}^{max} \frac{C_{CO_2}}{K_{CO_2} + C_{CO_2}} \frac{C_{H_2}}{K_{H_2} + C_{H_2}} \frac{K_{I,CO}^{hy}}{K_{I,CO}^{hy} + C_{CO}} \frac{C_{UA}}{K_{UA} + C_{UA}}$
v) Conversion of acetate into ethanol using CO as electron donor	$q_{E3} = q_{E3}^{max} \frac{C_{CO}}{K_{CO} + C_{CO} + \frac{C_{CO}^2}{K_{I,CO}}} \frac{C_{UA}}{K_{UA}^{AA} + C_{UA}}$
vi) Conversion of acetate into ethanol using H ₂ as electron donor	$q_{E4} = q_{E4}^{max} \frac{C_{H_2}}{K_{H_2} + C_{H_2}} \frac{C_{UA}}{K_{UA}^{AA} + C_{UA}} \frac{K_{I,CO}^{hy}}{K_{I,CO}^{hy} + C_{CO}}$

$q_E = \text{specific production rate of ethanol} = \frac{1}{C_X} \frac{dC_E}{dt}$ and C_E is ethanol concentration.

The molar yield coefficients of different participating reactants and products with respect to biomass have been calculated from their stoichiometric coefficients. Similarly molar yield coefficients of different participating reactants and products with respect to ethanol have been calculated from their stoichiometric coefficients.

Yield coefficient of any component, i with respect to biomass, $Y_{i/X}$ and with respect to ethanol, $Y_{i/E}$ can be defined as follows:

$$Y_{i/X} = \frac{\left| \frac{dC_i}{dt} \right|}{\frac{dC_X}{dt}} \quad (6.17)$$

$$Y_{i/E} = \frac{\left| \frac{dC_i}{dt} \right|}{\frac{dC_E}{dt}} \quad (6.18)$$

Mole Balance Equations

Semi-batch Reactor

Gas Phase

The mole balance equations for CO, CO₂ and H₂ in gas phase are as follows:

$$\frac{dp_{CO}}{dt} = \frac{q_G}{V_G} (p_{CO_{in}} - p_{CO}) - (k_L a)_{CO} \frac{V_L}{V_G} RT (p_{CO} H_{CO} - C_{CO_L}) \quad (6.19)$$

Where, p stands for partial pressure, R is universal gas law constant and T is temperature in Kelvin

$$\frac{dp_{H_2}}{dt} = \frac{q_G}{V_G} (p_{H_2_{in}} - p_{H_2}) - (k_L a)_{H_2} \frac{V_L}{V_G} RT (p_{H_2} H_{H_2} - C_{H_2_L}) \quad (6.20)$$

$$\frac{dp_{CO_2}}{dt} = \frac{q_G}{V_G} (p_{CO_2_{in}} - p_{CO_2}) - (k_L a)_{CO_2} \frac{V_L}{V_G} RT (p_{CO_2} H_{CO_2} - C_{CO_2_L}) \quad (6.21)$$

Liquid Phase

$$\frac{dC_{CO_L}}{dt} = (k_L a)_{CO} (p_{CO} H_{CO} - C_{CO_L}) + r_{CO} \quad (6.22)$$

$$\frac{dC_{H_2_L}}{dt} = (k_L a)_{H_2} (p_{H_2} H_{H_2} - C_{H_2_L}) + r_{H_2} \quad (6.23)$$

$$\frac{dC_{CO_2_L}}{dt} = (k_L a)_{CO_2} (p_{CO_2} H_{CO_2} - C_{CO_2_L}) + r_{CO_2} \quad (6.24)$$

$$\frac{dC_X}{dt} = r_X \quad (6.25)$$

$$\frac{dAA}{dt} = r_{AA} \quad (6.26)$$

$$\frac{dC_E}{dt} = r_E \quad (6.27)$$

Where,

$$r_{CO} = -(\mu_1 Y_{CO/X} + q_{E1} Y_{CO/E} + q_{E3} Y_{CO/E}^{AA-CO}) C_X \quad (6.28)$$

$$r_{H_2} = -(\mu_2 Y_{H_2/X} + q_{E2} Y_{H_2/E} + q_{E4} Y_{H_2/E}^{AA-H_2}) C_X \quad (6.29)$$

$$r_{CO_2} = (\mu_1 Y_{CO_2/X} + q_{E1} Y_{CO_2/E} + q_{E3} Y_{CO_2/E}^{AA-CO}) - (\mu_2 Y_{CO_2/X} + q_{E2} Y_{CO_2/E}) C_X \quad (6.30)$$

$$r_X = (\mu_1 + \mu_2) C_X \quad (6.31)$$

$$r_{AA} = \left((\mu_1 Y_{AA/X} + \mu_2 Y_{AA/X}) - (q_{E3} Y_{AA/E}^{AA-CO} + q_{E4} Y_{AA/E}^{AA-H_2}) \right) C_X \quad (6.32)$$

$$r_E = (q_{E1} + q_{E2} + q_{E3} + q_{E4}) C_X \quad (6.33)$$

Continuous Reactor

The dynamic mole balance equations (6.19-6.21) of components in gas phase are the same for the semi-batch and the continuous reactors. As there are both input and output for the liquid stream in the continuous reactor, the liquid phase dynamic mole balance equations take the following forms:

$$\frac{dC_{CO_L}}{dt} = (k_L a)_{CO} (p_{CO} H_{CO} - C_{CO_L}) + r_{CO} - \frac{q_L}{V_L} C_{CO_L} \quad (6.34)$$

$$\frac{dC_{H_2L}}{dt} = (k_L a)_{H_2} (p_{H_2} H_{H_2} - C_{H_2L}) + r_{H_2} - \frac{q_L}{V_L} C_{H_2L} \quad (6.35)$$

$$\frac{dC_{CO_2L}}{dt} = (k_L a)_{CO_2} (p_{CO_2} H_{CO_2} - C_{CO_2L}) + r_{CO_2} - \frac{q_L}{V_L} C_{CO_2L} \quad (6.36)$$

$$\frac{dC_X}{dt} = r_X - \frac{q_L}{V_L} C_X \quad (6.37)$$

$$\frac{dAA}{dt} = r_{AA} - \frac{q_L}{V_L} C_{AA} \quad (6.38)$$

$$\frac{dC_E}{dt} = r_E - \frac{q_L}{V_L} C_E \quad (6.39)$$

C_{AA} and C_E stand for acetic acid and ethanol concentration respectively.

All the equations have been numerically solved using the initial concentrations, given in Equation 6.40. The values of $p_{CO_{in}}$, $p_{H_2_{in}}$ and $p_{CO_2_{in}}$ have been set according to the concentration of inlet pyro-syngas. Initial values of liquid phase concentration of CO, H₂ and CO₂ have been set to the saturation values because as per the strategy the sterile basal medium is saturated with the pyro-syngas during the start-up of both semi-batch and continuous bioreactors. Initial condition is presented in equation 6.40 as follows:

$$\text{At } t=0, \left[\begin{array}{l} p_{CO} = 0 \\ p_{H_2} = 0 \\ p_{CO_2} = 0 \\ C_{CO_L} = C_{CO_L}^* \\ C_{H_2L} = C_{H_2L}^* \\ C_{CO_2L} = C_{CO_2L}^* \\ C_X = 0.05 \text{ mol/L} \\ C_{AA} = 0 \\ C_E = 0 \end{array} \right] \quad (6.40)$$

6.4 Optimization of Ethanol concentration in Semi-batch and Continuous bioreactors

6.4.1 Syngas fermentation in Semi-batch bioreactor

For the bioreactors operated under semi-batch mode, a three-level, 3-factor Box-Behnken statistical design of response surface methodology (RSM) has been used to fit the trend of dependence of the response variable, namely, ethanol concentration, obtained at the time of saturation, depicted by the simulated trend, represented in Figure 6.5. Three variables namely temperature of pyrolysis (A), the ratio V_G/V_L (B) and q_G (C) have been considered as the parameters. The variables (A, B and C) with coded level (-1, 0 and 1) are shown in the Table 6.4.

Table 6.4 variables with coded level used for semi-batch experimental run

Input variables	Unit	Coded variable level			Model Response
		-1	0	1	
Temperature (A)	°C	400	550	700	Ethanol concentration (g/L) after 30h operation
V_G/V_L (B)	-	0.2	0.6	1	
q_G (C)	L/h	0.6	6.3	10	

6.4.2 Syngas fermentation in continuous bioreactor

As indicated in the experimental description, the bioreactor was operated in continuous mode using the inlet gas generated in the pyrolyser at 700°C. For the bioreactor operated under continuous mode, a 2-factor Box-Behnken statistical design in response surface methodology (RSM) has been used to fit the trend of dependence of the response variable, namely, ethanol concentration, obtained after 300h, on different relevant operating variables by second-order models. Two variables, namely, V_G/V_L (A) and q_G/q_L (B) have been considered as the parameters. The ranges of variables (A and B) with coded level (-1, 0 and 1) are shown in the Table 6.5.

Table 6.5 variables with coded level used for experimental run

Input variables	Unit	Coded variable level			Model Response
		-1	0	1	
V_G/V_L (A)	-	0.2	0.6	1	Ethanol concentration (g/L) after 300h operation
q_G/q_L (B)	-	30	265	500	

6.5 Result and discussion

6.5.1 Composition and volumetric flow rates of pyro-syngas

In Figure 6.4 the mole fractions of different constituent gases, namely, CO, H₂, CO₂ and CH₄ in pyro-syngas have been plotted against temperature.

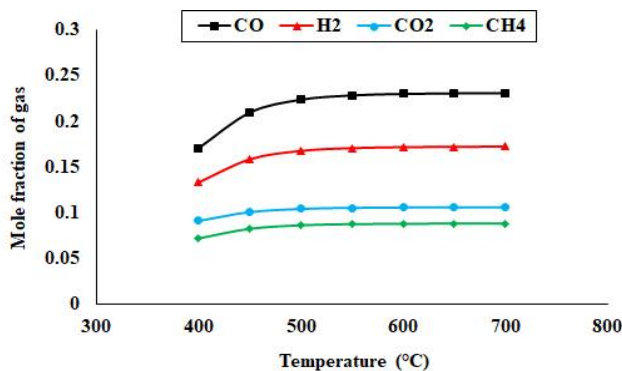


Fig. 6.4 Composition of pyro-syngas produced at different pyrolysis temperatures

It is evident that the mole fraction of each gaseous component increases with temperature up to 550°C after which a saturation trend is observed. Molar concentration (%) of CO, H₂, CO₂ and CH₄ increases from 17.07%, 13.32%, 9.11% and 7.19% to 23.08%, 17.23%, 10.59% and 8.82% respectively as the pyrolysis temperature is increased from 400°C to 700°C. As the temperature increases from 400°C to 700°C, gas flow rate increases from 30.3L/h to 51.41L/h.

6.5.2 Yield of the pyro-products

From the analysis of the Table 6.6, it appears that with the rise in temperature the yields of char and oil decreases and increases respectively. The yield of pyro-oil, however passes through a maximum at 500°C after which it decreases. The trends can be explained by the fact that with the increase in temperature the extent of thermal degradation of rice straw increases releasing lower molecular weight compounds, as compared to those obtained at lower temperature range.

Table 6.6 Yield of the pyro-products

Temperature	Yield of pyro-products		
°C	Pyro-char	Pyro-oil	Pyro-syngas
400	41.39 ± 1.97	27.01 ± 1.12	31.60 ± 1.01
450	37.98 ± 1.32	27.33 ± 1.01	34.69 ± 1.29
500	34.91 ± 1.89	28.02 ± 1.39	37.07 ± 1.33
550	30.09 ± 1.08	27.07 ± 1.02	42.84 ± 1.40
600	28.51 ± 0.52	26.37 ± 0.72	46.12 ± 2.11

650	26.34 ± 0.32	23.98 ± 0.15	50.68 ± 2.39
700	23.32 ± 0.33	22.09 ± 0.17	54.59 ± 2.42

6.5.3 Values of Parameters

6.5.3.1 k_La for Different Gases

The sterile basal medium was first saturated with pyro-syngas obtained at 700 °C by maintaining a stirring speed of 900 rpm and an inlet gas flow rate of 0.6 L/h for 12 h. The values of k_La , for CO, CO₂, and H₂, as determined experimentally and using Equations (6.4) and (6.7), are 144.9 h⁻¹, 166.9 h⁻¹, and 123.6 h⁻¹, respectively. During semi-batch and continuous operations, the stirring speed was maintained at 150 rpm and the volumetric flow rate of syngas was varied from 0.6–10 L/h. There is a wide variation of values of k_La because of their dependence on both the superficial velocity of gas and hence the volumetric flow rate. With the increase of gas flow rate there is an increase in the K_La values. According to Equations (6.4) and (6.7), the values of k_La for CO, CO₂, and H₂ have varied from 23.5 -100.7 h⁻¹, 27 -116.7 h⁻¹, and 20 - 87.4 h⁻¹, respectively, as the gas flow rate is varied from 0.6 to 10 L/h. In the following table, the present values of mass transfer coefficients have been compared with the literature data:

Table 6.7 Comparison the values k_La for present study with literature

k_La	Value (h ⁻¹)	Reference
$(k_La)_{CO}$	180.0	Puiman et al, 2023
$(k_La)_{CO}$	374.4	Almeida Benalcázar et al, 2020
$(k_La)_{CO}$	19.3	Ruggiero et al, 2022
$(k_La)_{CO}$	23.5–100.7	Present study
$(k_La)_{CO_2}$	27	Vandecasteele, 2016
$(k_La)_{CO_2}$	352.2	Almeida Benalcázar et al, 2020
$(k_La)_{CO_2}$	27–116.7	Present study
$(k_La)_{H_2}$	266.4	Puiman et al, 2023
$(k_La)_{H_2}$	590.4	Almeida Benalcázar et al, 2020

$(k_l a)_{H_2}$	20–87.4	Present study
-----------------	---------	---------------

According to reported studies, the values of $k_l a$ for CO, CO₂, and H₂ have varied from 19.3–374.4 h⁻¹, 27–352.2 h⁻¹, and 266.4–590.4 h⁻¹, respectively (Vandecasteele, 2016; Almeida Benalcázar et al, 2020; Puiman et al, 2023; Ruggiero et al, 2022). Thus, it can be inferred that the mass transfer rate in the present case is similar to those in the reported literature. Although the mass transfer coefficients of hydrogen are a bit lower than the literature value, those of CO and CO₂, the main carbon sources, are within the range. In case of stirred system, although the mass transfer coefficient can be increase by increasing the stirring rate, it should be done cautiously as there is a chance of microbial cells at high stirring rates. There are scopes of further studies to determine the limiting values of stirring rate to maximize the mass transfer coefficients without any detrimental effects on microbial cells due to shear (Bulut et al, 1999).

6.5.3.2 Model Parameters

The values of molar yield coefficients are provided in Table 6.8. Different model parameters, namely mass transfer coefficients, Henry's constants, and kinetic parameters are provided in Table 6.9.

Table 6.8 Yield coefficient for different process (Vandecasteele, 2016)

Process	Yield Coefficients (mol/mol)
(i) Biomass growth on CO	$Y_{\frac{CO}{X}} = 39.91, Y_{\frac{AA}{X}} 9.23, Y_{\frac{CO_2}{X}} = 19.44$
(ii) Biomass growth on CO ₂ and H ₂	$Y_{\frac{H_2}{X}} = 147.06, Y_{\frac{AA}{X}} 36.27, Y_{\frac{CO_2}{X}} = 73.55$
(iii) Ethanol production from CO	$Y_{\frac{CO}{E}}^{CO} = 6, Y_{\frac{CO_2}{E}}^{CO} = 4$
(iv) Ethanol production from CO ₂ and H ₂	$Y_{\frac{CO_2}{E}}^{CO_2} = 2, Y_{\frac{H_2}{E}}^{CO_2} = 6$
(v) Conversion of acetate into ethanol using CO as electron donor	$Y_{\frac{AA}{E}}^{AA-CO} = 1, Y_{\frac{CO}{E}}^{AA-CO} = 2, Y_{\frac{CO_2}{E}}^{AA-CO} = 2,$

(vi) Conversion of acetate into ethanol

$$Y_{\frac{H_2}{E}}^{AA-H_2} = 2, Y_{\frac{AA}{E}}^{AA-H_2} = 1$$

using H_2 as electron donor

Table 6.9 Values of mass transfer coefficients, Henry's constants, and kinetic parameters

Symbol	Significance		Unit	Source
$(K_L a)_{CO}$	Product of mass transfer coefficient (mh^{-1}) and specific surface area (m^2/m^3) of CO in the bioreactor	23.5–100.7	h^{-1}	Determined
$(K_L a)_{CO_2}$	Product of mass transfer coefficient (mh^{-1}) and specific surface area (m^2/m^3) of CO_2 in the bioreactor	27–116.7	h^{-1}	Determined
$(K_L a)_{H_2}$	Product of mass transfer coefficient (mh^{-1}) and specific surface area (m^2/m^3) of H_2 in the bioreactor	20–87.4	h^{-1}	Determined
H_{CO}	Henry's law constant of CO	0.0008	mol/L/atm	(Green & Perry, 2008)
H_{H_2}	Henry's law constant of CO_2	0.00066	mol/L/atm	(Green & Perry, 2008)
H_{CO_2}	Henry's law constant of H_2	0.025	mol/L/atm	(Green & Perry, 2008)
μ_1^{max}	Maximum specific growth rate on CO	0.192	h^{-1}	Determined
μ_2^{max}	Maximum specific growth rate on CO_2 and H_2	0.045	h^{-1}	Determined
q_1^{max}	Maximum specific production rate of ethanol from CO	0.20	h^{-1}	(Vandecasteele, 2016)
q_2^{max}	Maximum specific production rate of ethanol from CO_2 and H_2	0.0001	h^{-1}	(Vandecasteele, 2016)

q_3^{max}	Maximum specific production rate of ethanol through conversion of acetate using CO as electron donor	0.20	h^{-1}	(Vandecasteele, 2016)
q_4^{max}	Maximum specific production rate of ethanol through conversion of acetate using H ₂ as electron donor	0.20	h^{-1}	(Vandecasteele, 2016)
K_{CO}	Saturation constant for CO for growth	0.000078	mol/L	(Vandecasteele, 2016)
K_{H_2}	Saturation constant for H ₂ for growth	0.00022	mol/L	(Vandecasteele, 2016)
K_{CO_2}	Saturation constant for CO ₂ for growth	0.00022	mol/L	(Vandecasteele, 2016)
K_{UA}	Saturation constant of acetic acid for ethanol production from CO/CO ₂ and H ₂	0.0005	mol/L	(Vandecasteele, 2016)
K_{UA}^{Ac}	Saturation constant of acetic acid for ethanol production from acetate	0.0005	mol/L	(Vandecasteele, 2016)
$K_{i,CO}$	Inhibition constant of CO for growth on CO	0.002	mol/L	(Vandecasteele, 2016)
$K_{i,CO}^{Hy}$	Inhibition constant of CO for growth on CO ₂ and H ₂	7×10^{-9}	mol/L	(Vandecasteele, 2016)
$K_{i,UA}$	Inhibition constant of acetic acid for growth on CO/CO ₂ and H ₂	0.0104	mol/L	(Vandecasteele, 2016)

6.5.3.3 Significance of Model Parameters and Their Comparison with Similar Studies

The model parameters related to mass transfer are the values of $K_L a$ and Henry's constants for CO, CO₂, and H₂. Henry's constant, correlating the gas and liquid phase concentration of a component under equilibrium, varies with temperature for all gases and hence is the same for all

studies. In the present case, the growth of the clostridial consortium on CO as well as CO₂ and H₂ has been considered. The maximum specific growth rate on CO has been determined to be 0.192 h⁻¹, while for different clostridial strains, the value lies in the range of 0.22–0.37 h⁻¹ (Ruggiero et al, 2022). The value of the maximum specific growth rate on H₂ has been determined to be 0.045 h⁻¹. In the literature, the maximum specific growth rate on H₂ has been reported to be 0.031–0.045 h⁻¹ (Vandecasteele, 2016; Ruggiero et al, 2022). Therefore, the growth rate for the presently used consortium is comparable to other established pure clostridial strains. The values of the saturation constant, signifying the substrate concentration corresponding to half of the maximum specific growth rate, have also been determined for CO, H₂, and CO₂ and the values are 0.000078 mol/L, 0.00022 mol/L, and 0.00022 mol/L. This signifies that the specific growth rate reaches the maximum at a lower value of CO concentration compared to H₂ and CO₂. The reported values of the saturation constants for CO and H₂ are 0.000045–0.00039 mol/L and 0.00022–0.00071 mol/L, respectively. This again proves that the saturation constants of the consortium are in the same range as with the recognized strains. The inhibition constants of CO on the growth on CO itself and on hydrogen are 0.002 mol/L and 7×10^{-9} mol/L, respectively. As the inhibition constant signifies the concentration level of the component rendering a strong inhibitory effect, it is clear that the growth on hydrogen is heavily inhibited by the presence of CO compared to CO-based growth. Perhaps the growth on H₂ and CO₂ can only occur after CO is fully utilized. Similar observations have been reported by other researchers (Vandecasteele, 2016; Ruggiero et al, 2022). The yield coefficients, $Y_{\frac{X}{CO}}$, $Y_{\frac{X}{H_2}}$, and $Y_{\frac{CO}{E}}$ of the present study are 0.67 g/mol, 0.18 g/mol, and 6 mol/mol, respectively whereas the reported ranges are 0.24–2.6 g/mol, 0.20–0.37 g/mol, and 2–10.5 mol/mol, respectively (Vandecasteele, 2016; Almeida Benalcázar et al, 2020; Mohammadi et al, 2014; Puiman et al, 2023; de Medeiros et al, 2019; Ruggiero et al, 2022; Fox et al, 1996; Rajagopalan et al, 2002; Ranzi et al, 2008). Therefore, the model parameters are very much comparable with the literature data.

6.5.4 Performance of the Bioreactor in Semi-Batch and Continuous Modes

6.5.4.1 Bioreactor Dynamics in the Semi-Batch Mode

Using the mathematical model for semi-batch operation, the transient behavior of ethanol concentration and acetic acid up to 30 h of operation at q_G of 6.3 L/h has been presented in Fig. 6.5a and Fig. 6.5b respectively using V_G/V_L , in the range of 0.2–1, as a parameter. It is observed

that the concentration of ethanol almost gets saturated at 30 h of operating time. With the increase of V_G/V_L , there is a decrease in the concentration of both ethanol and acetic acid. This can be explained by the fact that with the increase in the volume of head space, less mass transfer to the liquid phase occurs, causing a decrease in the reaction rate and hence the concentration of both products. The transient behavior of the conversion of different gaseous component, namely CO, H₂, and CO₂ has been presented in Figure 6.5 c. The conversion of any gaseous component, i , has been calculated by $\frac{p_{i,i} - p_{i,out}}{p_{i,in}}$. From the Figure 6.5, it can be observed that after 12 h of operation the gas phase conversion reached equilibrium. All the trends are very similar to those obtained by other researchers (de Medeiros et al, 2019; Ruggiero et al, 2022).

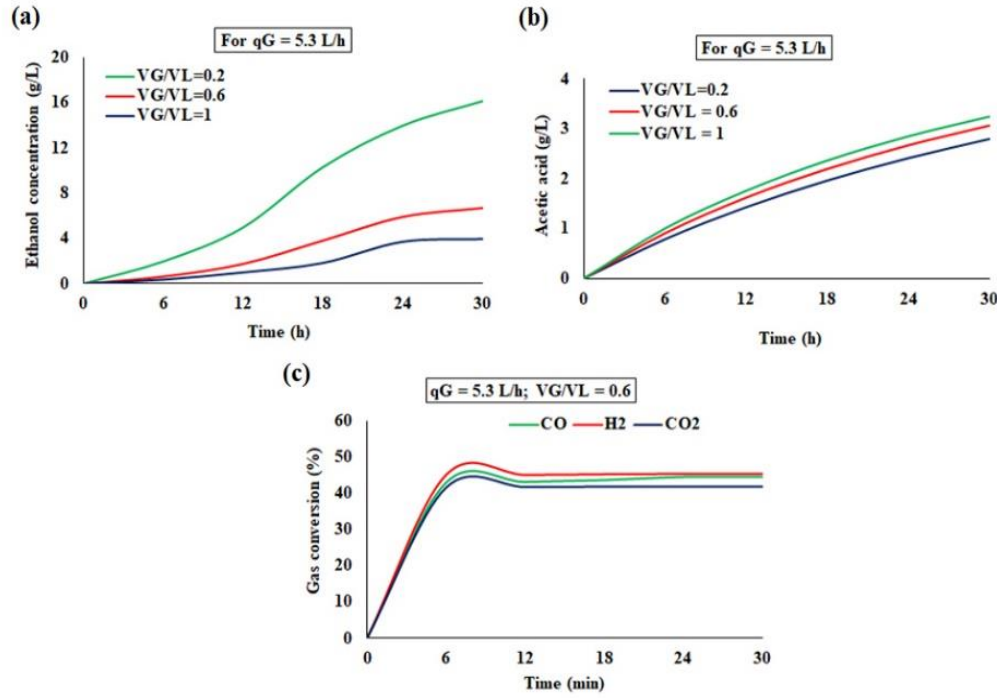


Fig. 6.5 Simulated profile for semi-batch reactor ((a): Ethanol; (b): acetic acid; (c): gas conversion %)

6.5.4.2 Bioreactor Dynamics in the Continuous Mode

Simulated Profile for the Continuous Reactor

Using the mathematical model for continuous operation, the dynamics of ethanol concentration and acetic acid up to 300 h of operation at q_G/q_L of 250 have been presented in Fig. 6.6 using

V_G/V_L in the range of 0.6–1 as a parameter. It has been observed that both ethanol and acetic acid concentrations reach saturation after 180h of operation although the reactor was run for 300h. For continuous reactor, the time has been chosen keeping similarity with the values used by other researchers (Vandecasteele, 2016; Diender, 2019). Similar to the trend of Semi-batch operation, the concentrations of both products decrease with the increase of V_G/V_L . The transient behavior of conversion of different gaseous component, namely, CO, H₂ and CO₂ has been represented in Fig. 6.6. From the figure it can be observed that after 120 h of operation the gas phase conversion reaches equilibrium. All the trends are very similar to those obtained by other researchers (de Medeiros et al, 2019; Ruggiero et al, 2022).

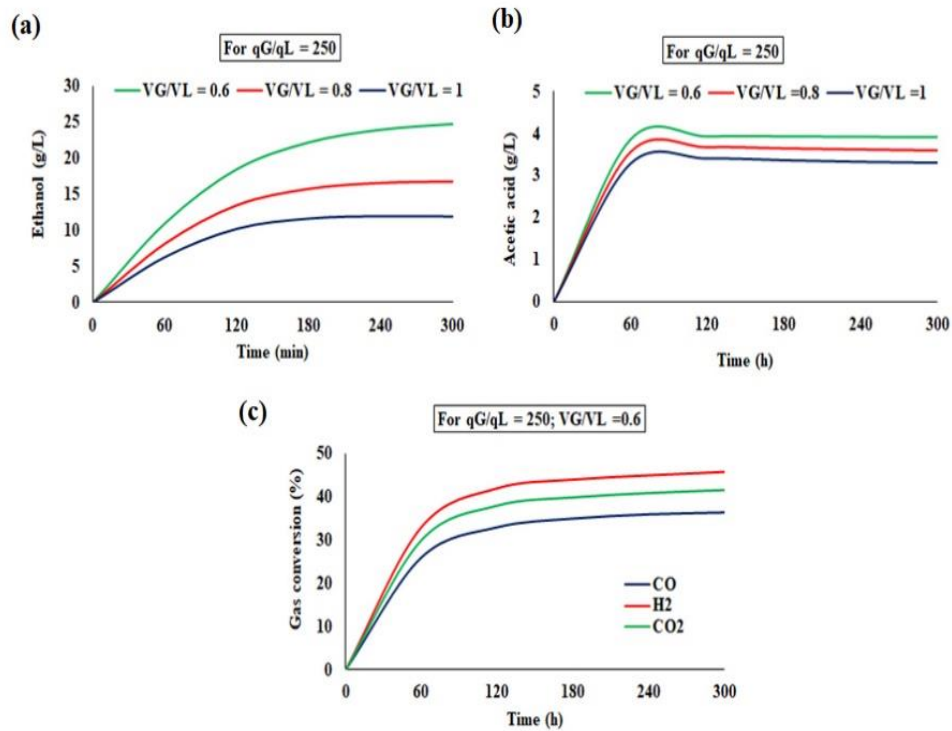


Fig. 6.6 Simulated profile for the continuous reactor ((a): ethanol concentration; (b): acetic acid concentration and (c): % gas conversion

6.5.5 Comparison of Simulated and Experimental Data

6.5.5.1 Semi-Batch Operation

In Fig. 6.7, the experimental and simulated values of ethanol concentration in the semi-batch reactor were plotted against operation time (=6 h, 12 h, 18 h, 24 h and 30 h) in a bar-plot. The

experimental results were obtained at a pyrolysis temperature of 600 °C, V_G/V_L of 0.5, and q_G of 6 Lpm. From the analysis of the figure, it appears that the agreement between the model prediction and the experimental results is very good.

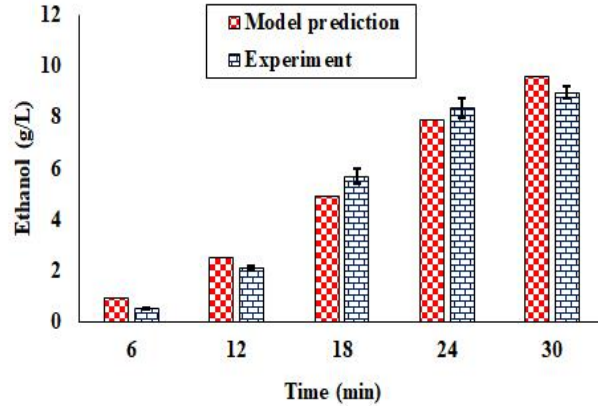


Fig. 6.7 Comparison of simulated and experimental time trajectory of ethanol concentration in the semi-batch reactor (pyrolysis temperature = 600 °C, $V_G/V_L = 0.5$, and $q_G = 6$ Lpm)

6.5.5.2 Continuous Operation

The experimental and simulated values of ethanol concentration at 300 h of continuous operation have been plotted against V_G/V_L in the range of 0.6–1 at a fixed value of q_G/q_L of 250 in Figure 6.8a. Similarly, the experimental and simulated values of ethanol concentration at 300 h have been plotted against q_G/q_L in the range of 30–250 at a fixed value of V_G/V_L of 0.6 in Figure 6.8b. It is observed that while the ethanol concentration decreases with the increase in V_G/V_L , it shows an increasing trend with the increase in q_G/q_L .

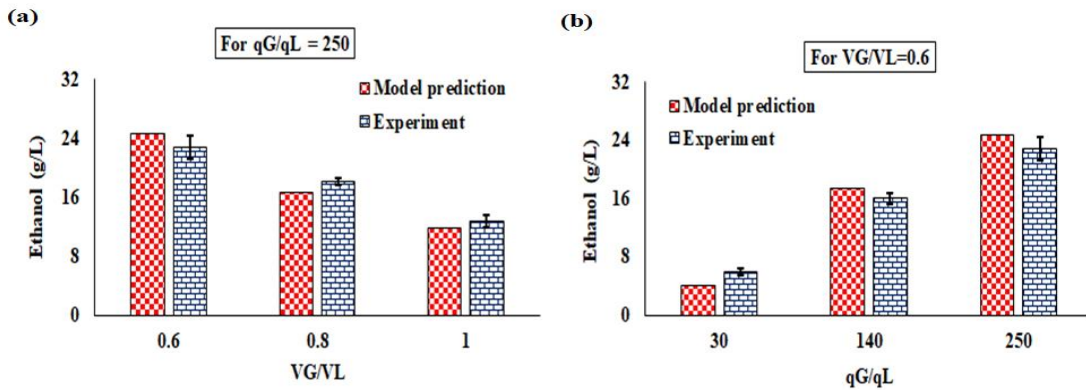


Fig. 6.8 Comparison of simulated and experimental trends of ethanol concentration in the continuous reactor with a) V_G/V_L : 0.6–1; (b) q_G/q_L : 30–250 (pyrolysis temperature = 600 °C; $V_G/V_L = 0.5$; $q_G = 6$ Lpm)

A decrease and increase in the mass transfer to liquid phase with the increase in gas volume fraction, i.e., head space, and the gas velocity, respectively, and the increase in reaction time with the decrease in liquid volume, i.e., the decrease in dilution rate, can explain this behavior.

For both semi-batch and continuous operations, the mathematical models appear to predict realistic results.

6.5.6 Effect of Gas Residence Time (GRT) and Dilution Factor (D) on the Volumetric Productivity of Ethanol

For the experimental ranges of the parameters for the continuous mode of operation, the ethanol production behavior over 300 h has been assessed as a function of the gas residence time (GRT) and dilution rate, D, in Fig. 6.9. The values of dilution rate have been calculated by dividing the volumetric flow rate of liquid by the liquid volume, i.e., $\frac{q_L}{V_L}$, and the values of gas residence time have been calculated by dividing the liquid volume by the volumetric flow rate of gas, i.e., $\frac{V_L}{q_G}$. In this figure, the volumetric productivity of ethanol, calculated by the multiplication of D and the ethanol concentration at 300 h, i.e., $D * C_{Ethanol \text{ at } 300 \text{ h}}$, has been plotted simultaneously against D and GRT through a 3D plot using the meshgrid function in MATLAB software version R2016a.

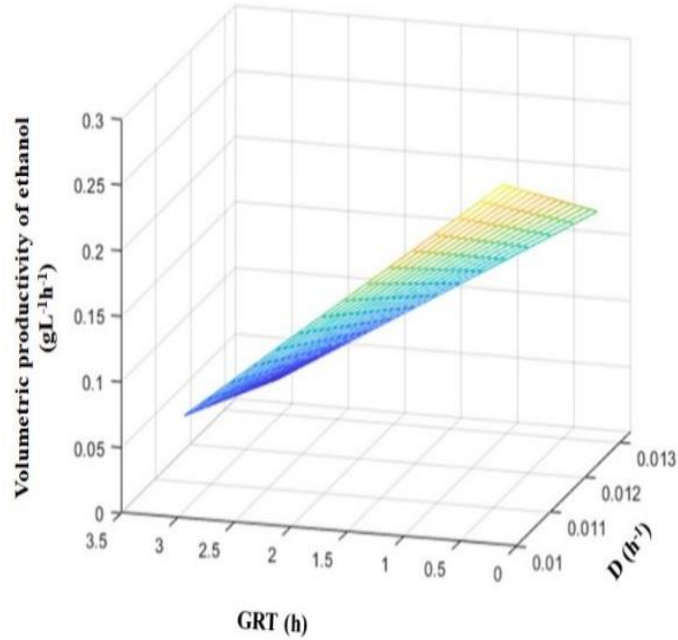


Fig. 6.9 Effect of the gas residence time (GRT) and dilution factor (D) on the volumetric productivity of ethanol from syngas fermentation

From Fig. 6.9, it is evident that the increase of GRT has a positive impact on the volumetric productivity of ethanol from syngas fermentation. The increment of D, however, has a negative impact on the volumetric productivity of ethanol.

6.5.7 Optimization Results for Semi-Batch and Continuous Bioreactors

6.5.7.1 Semi-Batch Bioreactor

The second order regression equation, obtained to represent the relationships among the response variable, ethanol concentration obtained after 30 h, and the operating variables, namely the temperature of pyrolysis (A), the ratio V_G/V_L (B), and q_G (C) is as follows:

$$\text{Ethanol concentration (g/L)} = 1.06651 + 0.00345496A + 3.2557B - 0.0558511C - 0.0119167AB + 0.00393617AC - 1.55984BC \quad (6.41)$$

The analysis of variance (ANOVA), presented in Table 6.10, shows that the model can represent the trend of dependence of ethanol concentration on the selected operating variables.

Table 6.10 ANOVA table for the semi-batch bioreactor

Source	Sum of Squares	df	Mean Square	F-value	p-value	
Model	534.72	6	89.12	34.53	< 0.0001	significant
A-Temperature	53.05	1	53.05	20.55	0.0011	
B- V_G/V_L	171.22	1	171.22	66.34	< 0.0001	
C- q_G	243.21	1	243.21	94.23	< 0.0001	
AB	2.04	1	2.04	0.7923	0.3943	
AC	30.80	1	30.80	11.93	0.0062	
BC	34.40	1	34.40	13.33	0.0045	
Residual	26.81	10	2.58			
Lack of Fit	26.81	6	4.30			
Pure Error	0.0000	4	0.0000			
Cor Total	560.53	16				

(Std. Dev. 1.61; Mean 7.21; C.V. (%) 22.30; R^2 0.9540; Adjusted R^2 0.9263).

The comparison between the predicted and actual values of the response variables, is represented in Figure 6.10.

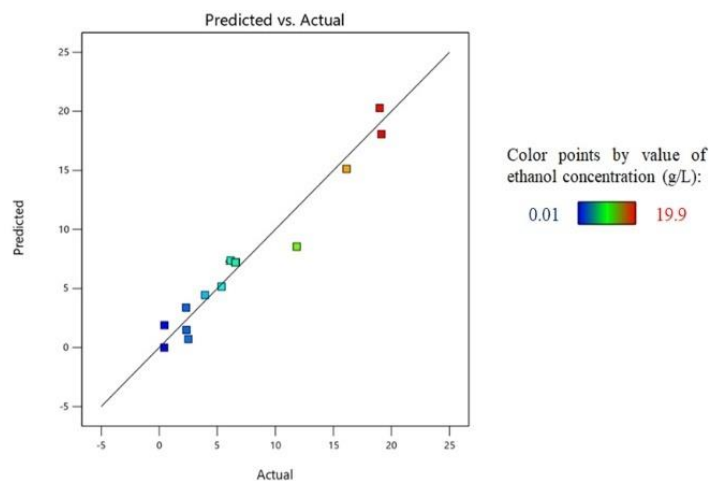


Fig. 6.10 Comparison between the RSM–predicted and experimental values of ethanol concentration at 30 h of semi-batch operation

From the ANOVA table, it appears that the factors, B ($=V_G/V_L$) and C (q_G) significantly affect the ethanol concentration obtained after 30 h of operation of the semi-batch reactor. Both factors bear

linear relationships with the response. The pyrolysis temperature, however, does not have significant effect. This can be due to close variation of gas composition in the present range of pyrolysis temperatures. Three response surface 3D plots, representing the combined effect of interaction between A-B, A-C, and B-C on the response variable, are shown in Figure 6.11.

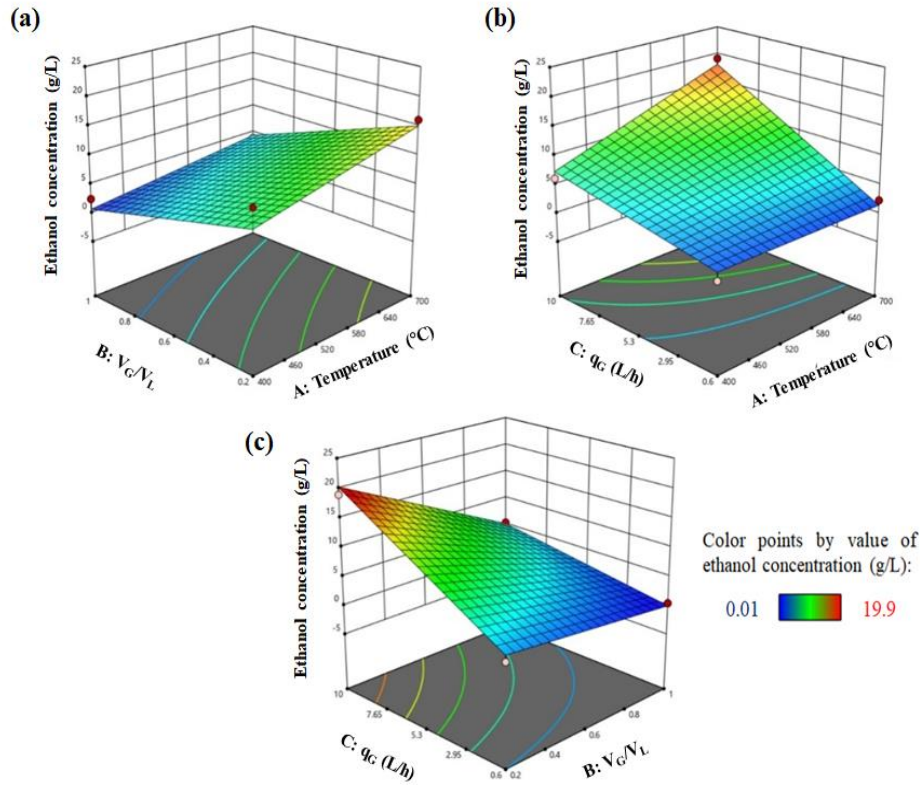


Figure 6.11 Response surface plots for the optimization of ethanol (g/L) production from syngas fermentation ((a–c): interaction between AB, AC and BC respectively)

From Figure 6.11, it is evident that the increase of variable A and C had a positive impact on the production of ethanol. This is because of the fact that with the increase of the pyrolysis temperature, T ($=A$) the concentration of all carbon substrates (CO and CO_2), and the electron donors (H_2 and CO) in the inlet gas increase, favoring the formation of ethanol. With the increase of the gas flow rate, q_G ($=C$), the mass transfer rate was enhanced and hence the growth rates and ethanol generation rates, governed by the liquid phase concentration of CO , CO_2 , and H_2 increased. As a consequence, the ethanol concentration increased with the increase of C. The increment of variable B ($=V_G/V_L$) had a negative impact on ethanol production. This can be explained by the fact that with the increase of V_G with respect to liquid volume, the effective mass transfer to liquid

phase was lowered, causing an overall decreasing trend in ethanol concentration. The optimum level of the independent variables, pyrolysis temperature, V_G/V_L , and q_G giving the maximum ethanol concentration ($=13.122$ g/L) after 30 h of semi-batch operation are 648°C , 0.46 , and 6.7 L/h, respectively.

6.5.7.2 Syngas Fermentation in the Continuous Bioreactor

The second order regression equation, obtained to represent the relationships among the response, i.e., ethanol concentration, obtained after 300 h and the operating variables, namely, V_G/V_L (A), and q_G/q_L (B) is as follows:

$$\text{Ethanol concentration } \left(\frac{\text{g}}{\text{L}}\right) = 10.9595 + 11.9048A + 0.0868944B + 0.0101862AB - 26.5316A^2 - 0.000115026B^2 \quad (6.42)$$

From the comparison between the predicted and actual values of the response variables, represented in Figure 6.12, and from the analysis of variance (ANOVA) presented in Table 6.11, it appears that the model can represent the trend of dependence of ethanol concentration, obtained under 300 h of operation on the selected operating variables, A and B, very well.

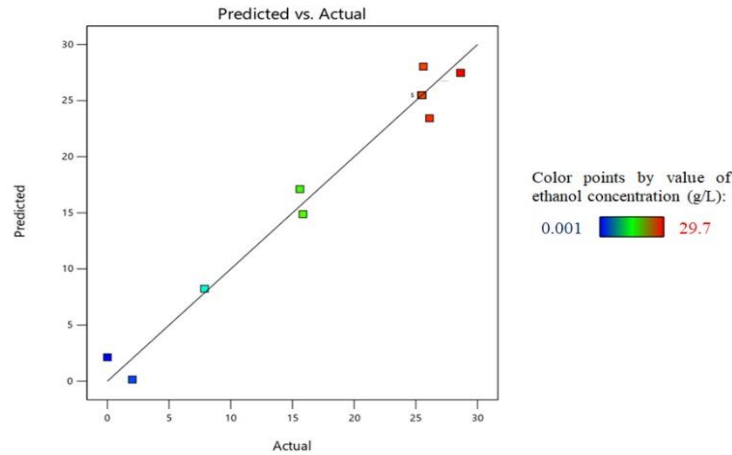


Fig. 6.12 Comparison between the RSM-predicted and experimental values of ethanol concentration at 300 h of continuous operation.

Table 6.11 ANOVA table for the continuous bioreactor

Source	Sum of Squares	df	Mean Square	F-value	p-value	
Model	1142.09	5	228.42	63.15	< 0.0001	significant
A- V_G/V_L	329.07	1	329.07	90.97	< 0.0001	
B- q_G/q_L	453.60	1	453.60	126.40	< 0.0001	
AB	3.67	1	3.67	1.01	0.3475	
A ²	116.09	1	116.09	32.09	0.0008	
B ²	280.71	1	280.71	77.61	< 0.0001	
Residual	26.32	7	3.62			
Lack of Fit	26.32	3	8.44			
Pure Error	0.0000	4	0.0000			
Cor Total	1167.41	12				

(Std. Dev. 1.90; Mean 19.06; C.V. (%) 9.98; R^2 0.9783; Adjusted R^2 0.9628).

From the ANOVA table, it appears that both factors, A ($=V_G/V_L$) and B (q_G/q_L), significantly affected the ethanol concentration obtained after 300 h of operation of the continuous reactor. While V_G/V_L linearly affected the response variable, the change of q_G/q_L shows a combined effect of second order and linear relationship. As the variation of q_G/q_L simultaneously affects the gas residence time for the reaction and extent of mass transfer, the influence of this factor is large. A response surface 3D plot showing the influence of both V_G/V_L and q_G/q_L is represented in Figure 6.13.

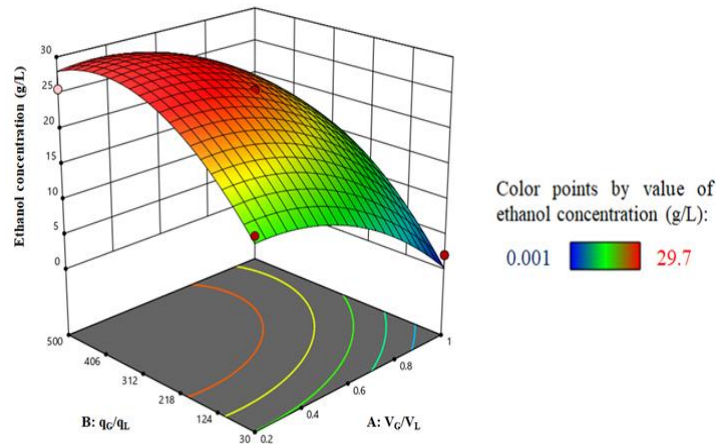


Figure 6.13 Response surface plots for the optimization of ethanol (g/L) production from syngas fermentation

From Figure 6.13, it is evident that the increase of variable B had a positive impact on the production of ethanol from syngas fermentation. However, an increment of variable A had a negative impact on ethanol production. The optimum level of the independent variables, V_G/V_L and q_G/q_L , giving the maximum ethanol concentration (≈ 29.450 g/L) after 300 h of continuous operation are 0.28 and 336.148, respectively.

6.5.8 Comparison of Semi-Batch and Continuous Operation of a Pyro-Syngas Fermenter

As the semi-batch operation is always in an unsteady state, it is not suitable for large-scale fermentation. On the contrary, continuous operation is always preferred for large

-scale operation. Over 30 h, 171 mL of liquid broth containing 13.12 g/L ethanol can be produced under the optimum conditions of a semi-batch fermenter. For the continuous reactor, 0.02 L/h liquid broth with an ethanol concentration of 29.45 g/L can be produced for 300 h. The average optimum production rate of ethanol is 0.074.7 g/h, calculated by dividing the product of reactor volume (≈ 0.171 L) and ethanol concentration (≈ 13.12 g/L) by operating time (≈ 30 h) obtained in semi-batch operation. In the case of continuous operation of the bioreactor, 0.589 g/h, calculated by multiplying the liquid outlet rate with ethanol concentration, can be obtained through continuous operation of the same reactor using same volumetric flow rate of gas of 6.7 L/h. However, overall, the running cost of the semi-batch bioreactor is much lower than the continuous one due to the savings in the inlet and outlet pumping rate of liquid.

6.5.9 Comparison with Similar Studies and Uniqueness

The operating parameters and the results of the present study are compared with similar studies in Table 6.12.

Table 6.12 Comparison of operating parameters and results of the present study with similar studies

Feed Gas Composition	Mode of Operation	Microorganism Used	Maximum Ethanol Concentration (g/L)	Reference
CO:CO ₂ :H ₂ :N ₂ 32:8:32:28	Batch	<i>Clostridium ljungdahlii</i>	0.778	Vandecasteele, 2016
H ₂ :CO 75:25	Continuous	<i>Clostridium ljungdahlii</i>	1.304	Almeida Benalcázar et al, 2020
CO:CO ₂ :H ₂ :inert 55:10:20:15	Continuous	<i>Clostridium ljungdahlii</i>	46.0	de Medeiros et al, 2019
100% CO	Batch	<i>Clostridium carboxidivorans</i>	0.4	Ruggiero et al, 2022
100% CO	Continuous	<i>Clostridium carboxidivorans</i>	6.6	Ruggiero et al, 2022
CO:CO ₂ :H ₂ :CH ₄ : N ₂ 17.0:9.1:13.3:7.1:27.0; 22.8:10.5:17.1:8.7:21.7; 23.1:10.6:17.2:8.8:21.5	Semi-batch	Clostridial consortium, <i>UACJUCHE1</i>	13.1	Present study
CO:CO ₂ :H ₂ :CH ₄ : N ₂ 23.1:10.6:17.2:8.8:21.5	Continuous	Clostridial consortium, <i>UACJUCHE1</i>	29.4	Present study

Most of the modelling studies on syngas fermentation are based on literature data of kinetic parameters, derived from experiments using simulated gas mixture. From Table 6.12, it is clear that the feed gas mixtures in those studies are mainly constituted of CO, H₂, and CO₂. The concentrations of CO and H₂ in the gas used in those studies usually range from 32–55% and 20–

32%, respectively. In the model developed by Ruggiero et al., pure CO was used (Ruggiero et al, 2022). No comparison of the model predictions was made with the experimental results of a truly integrated process of gasification and fermentation. The concentrations of CO and H₂ used in the existing models are much higher than those of typical pyro-syngas. The unique feature of the present models for both semi-batch and continuous operation lies in the fact that the real pyro-gas composition was used as the input instead of any arbitrarily chosen composition. It is also clear from the table that although the concentrations of CO and H₂ of pyro-syngas, used in the present study, are much lower than those used in other similar studies, the achieved ethanol concentration is comparable with the reported ones. Although most of the studies reported the use of pure clostridial strains, the *UACJUCheI*, used in the present study is the first clostridial consortium, isolated from Indian soil, which has proved to be capable of pyro-syngas fermentation.

6.6 Summary

A deterministic mathematical models along with experimental data on the bioconversion of pyro-syngas to ethanol and acetic acid in a gas-sparged stirred tank reactor, operated in Semi-batch and continuous modes, have been reported for the first time. The locally isolated clostridial consortium *UACJUCheI* has been proved to be capable of utilizing CO, CO₂ and H₂ present in the pyro-syngas. The mathematical models have been validated through the comparison of the predictions with the experimental results. The optimization of the performance of the semi-batch and continuous modes of operation has been done using response surface methodology. Since pyrolysis has been used as the precursor process for syngas fermentation, other valuable products like pyro-oil and pyro-char are also generated and the criterion of zero-waste generation for the circular economy concept is fulfilled.

Reference

Abubackar, H. N., Veiga, M. C., & Kennes, C. (2011). Biological conversion of carbon monoxide: rich syngas or waste gases to bioethanol. *Biofuels, Bioproducts and Biorefining*, 5(1), 93-114.

Almeida Benalcázar, E., Noorman, H., MacielFilho, R., & Posada, J. A. (2020). Modeling ethanol production through gas fermentation: a biothermodynamics and mass transfer-based hybrid model for microbial growth in a large-scale bubble column bioreactor. *Biotechnology for biofuels*, 13(1), 1-19.

Bulut, S., Waites, W. M., & Mitchell, J. R. (1999). Effects of combined shear and thermal forces on destruction of *Microbacterium lacticum*. *Applied and environmental microbiology*, 65(10), 4464-4469.

Chen J, Gomez JA, Höffner K, et al (2015) Metabolic modeling of synthesis gas fermentation in bubble column reactors. *Biotechnol Biofuels* 8:1–12.

Chen, J., Gomez, J. A., Höffner, K., Barton, P. I., & Henson, M. A. (2015). Metabolic modeling of synthesis gas fermentation in bubble column reactors. *Biotechnology for biofuels*, 8(1), 1-12.

Chowdhury, R. and Sarkar, A., 2012. Reaction kinetics and product distribution of slow pyrolysis of Indian textile wastes. *International Journal of Chemical Reactor Engineering*, 10(1).

de Medeiros, E. M., Posada, J. A., Noorman, H., & Filho, R. M. (2019). Dynamic modeling of syngas fermentation in a continuous stirred-tank reactor: Multi-response parameter estimation and process optimization. *Biotechnology and bioengineering*, 116(10), 2473-2487.

Diender, M. (2019). *Exploration of microbial systems as biocatalysts for conversion of synthesis gas to bio-based chemicals* (Doctoral dissertation, Wageningen University and Research). <https://research.wur.nl/en/publications/exploration-of-microbial-systems-as-biocatalysts-for-conversion-o>

Fogler, H. S. (2010). *Essentials of chemical reaction engineering*. Pearson education.

Fox, J.D., Kerby, R.L., Roberts, G.P. & Ludden, P.W., 1996. Characterization of the CO-induced, CO-tolerant hydrogenase from *Rhodospirillum rubrum* and the gene encoding the large subunit of the enzyme. *Journal of Bacteriology*, 178(6), pp.1515-1524.

Ghosh, S., Pathak, S., Manna, D., & Chowdhury, R. (2021). Acidogenic mixed consortium isolated from soil of agricultural field: acid production behaviour and growth kinetics under the influence of pretreatment hydrolysate of rice straw (RS). *Indian Chemical Engineer*, 63(2), 206-218.

Gill, N. K., Appleton, M., Baganz, F., & Lye, G. J. (2008). Quantification of power consumption and oxygen transfer characteristics of a stirred miniature bioreactor for predictive fermentation scale-up. *Biotechnology and bioengineering*, 100(6), 1144-1155.

Green, D. W., & Perry, R. H. (2008). *Perry's chemical engineers' handbook*. McGraw-Hill Education.

- Kennes, D., Abubackar, H. N., Diaz, M., Veiga, M. C., & Kennes, C. (2016). Bioethanol production from biomass: carbohydrate vs syngas fermentation. *Journal of Chemical Technology & Biotechnology*, 91(2), 304-317.
- Mohammadi, M., Mohamed, A. R., Najafpour, G. D., Younesi, H., & Uzir, M. H. (2014). Kinetic studies on fermentative production of biofuel from synthesis gas using *Clostridium Ljungdahlii*. *The Scientific World Journal*, 2014.
- Mohammadi, M., Mohamed, A.R., Najafpour, G., Younesi, H. and Uzir, M.H., 2016. *Clostridium Ljungdahlii* for production of biofuel from synthesis gas. *Energy Sources, Part A: recovery, utilization, and environmental Effects*, 38(3), pp.427-434.
- Pati, S., De, S. and Chowdhury, R., 2023. Integrated techno-economic, investment risk and life cycle analysis of Indian lignocellulosic biomass valorisation via co-gasification and syngas fermentation. *Journal of Cleaner Production*, 423, p.138744.
- Pati, S., De, S., Chowdhury, R., 2023. Exploring the hybrid route of bio-ethanol production via biomass co-gasification and syngas fermentation from wheat straw and sugarcane bagasse: model development and multi-objective optimization. *Journal of Cleaner Production*, 395, p.136441.
- Phillips, J.R., Clausen, E.C. and Gaddy, J.L., 1994. Synthesis gas as substrate for the biological production of fuels and chemicals. *Applied biochemistry and biotechnology*, 45, pp.145-157.
- Puiman, L., Almeida Benalcázar, E., Picioreanu, C., Noorman, H. J., & Haringa, C. (2023). Downscaling Industrial-Scale Syngas Fermentation to Simulate Frequent and Irregular Dissolved Gas Concentration Shocks. *Bioengineering*, 10(5), 518.
- Rajagopalan, S., Datar, R.P. and Lewis, R.S., 2002. Formation of ethanol from carbon monoxide via a new microbial catalyst. *Biomass and bioenergy*, 23(6), pp.487-493.
- Ranzi, E., Cuoci, A., Faravelli, T., Frassoldati, A., Migliavacca, G., Pierucci, S., & Sommariva, S. (2008). Chemical kinetics of biomass pyrolysis. *Energy & Fuels*, 22(6), 4292-4300.
- Ruggiero, G., Lanzillo, F., Raganati, F., Russo, M. E., Salatino, P., & Marzocchella, A. (2022). Bioreactor modelling for syngas fermentation: Kinetic characterization. *Food and Bioproducts Processing*, 134, 1-18.

Sarkar, A. and Chowdhury, R., 2016. Co-pyrolysis of paper waste and mustard press cake in a semi-batch pyrolyzer—optimization and bio-oil characterization. *International Journal of Green Energy*, 13(4), pp.373-382.

Siebler, F., Lapin, A., & Takors, R. (2020). Synergistically applying 1-D modeling and CFD for designing industrial scale bubble column syngas bioreactors. *Engineering in Life Sciences*, 20(7), 239-251.

Sluiter, A., Hames, B., Ruiz, R., Scarlata, C., Sluiter, J., Templeton, D., & Crocker, D. L. A. P. (2008). Determination of structural carbohydrates and lignin in biomass. *Laboratory analytical procedure*, 1617(1), 1-16.

Vandecasteele, J. (2016). Experimental and modelling study of pure-culture syngas fermentation for biofuels production. *MSc Universiteit Gent*, 356. <https://lib.ugent.be/catalog/rug01:002275054>

Wang, T., Wang, Q., Soklun, H., Qu, G., Xia, T., Guo, X., Lia, H., & Zhu, L. (2019). A green strategy for simultaneous Cu (II)-EDTA decomplexation and Cu precipitation from water by bicarbonate-activated hydrogen peroxide/chemical precipitation. *Chemical Engineering Journal*, 370, 1298-1309.

Chapter 7

Hydrothermal liquefaction (HTL) of Indian Biomass (jute stick and rice straw)

Chapter 7: Hydrothermal liquefaction (HTL) of Indian Biomass (jute stick and rice straw)

Hydrothermal liquefaction has been considered as a promising technology for the production of hydrochar, bio-oil and aqueous hydrolysate rich in valuable chemicals. Lignocellulosic biomass (LCB) can be converted into four fractions namely, hydrochar, bio-oil, aqueous and gaseous phase products during hydrothermal liquefaction (HTL) in the temperature range of 200-400°C. The present study was performed to investigate the effect of temperature and biomass composition on the yield and quality of the bio-products, obtained from two biomass namely, jute stick (JS) and rice straw (RS) having different lignocellulosic composition. Studies have been conducted according to the objectives under aim 3, as described in Chapter 3. The objectives are as follows:

- Determination of the HTL kinetics of rice straw and jute stick through Batch experiments
- Determination of product yields
- Characterization of bio-oil and hydrochar
- Conduction of batch experiments on co-HTL of rice straw and jute stick and characterization of bio-oil
- Optimization of rice straw -jute stick ratio, time and temperature to maximize the bio-oil yield from co-HTL
- Determination of effectiveness of hydro-char from jute stick for adsorption of dye like Congo-red through Batch type adsorption experiments

7.1 Experimental Methods for hydrothermal liquefaction

A cylindrical stainless-steel reactor of 45 mm inner diameter and 80 mm height was used for the investigation of the hydrothermal liquefaction of jute stick and rice straw in batch mode. The schematic diagram of the HTL of JS and RS pretreatment process under this study is represented in Figure 7.1.

Under the present investigation, 5 g biomass was subjected to 50 mL of water (milli-Q) in the cylindrical reactor. For incubation, the reactor was kept for 30 minutes at 25 °C. Thereafter, the reactor was placed in a programmable muffle furnace (Nabertherm GmbH, Germany), installed at University of Eastern Finland. The experiment was carried out at three different temperatures of

240, 300 and 360 °C. The heating rate was 10 °C/min until the reaction temperature was reached. The reaction temperature remained constant for 30 minutes (holding time). For the experiments meant for the determination of rate kinetics, different holding time (10, 15, 20, 25 and 30 minutes) was used at three different temperatures, i.e., 240, 300 and 360 °C. At the end of the holding period, the reactor was cooled to 25 °C for each experimental run. Residual solids and aqueous phase were separated by filtration. Bio-oil was extracted from the solid residue by using acetone as the solvent. Subsequently, the acetone was extracted and evaporated by using a rotary evaporator. After washing the acetone, the solid residue was dried at 70°C for 1 hour and the dried mass was considered as the hydrochar. The co-HTL of mixture of rice straw and jute stick was conducted following the same experimental protocol. Optimum values of time, temperature and % blending of jute stick in RS-JS mixture was determined to maximize the yield of bio-oil. The set of values of input parameters was determined through design of experiments of Box-Behnken type response surface methodology, as described under section 7.2. All experiments of HTL of JS and RS were conducted in triplicate.

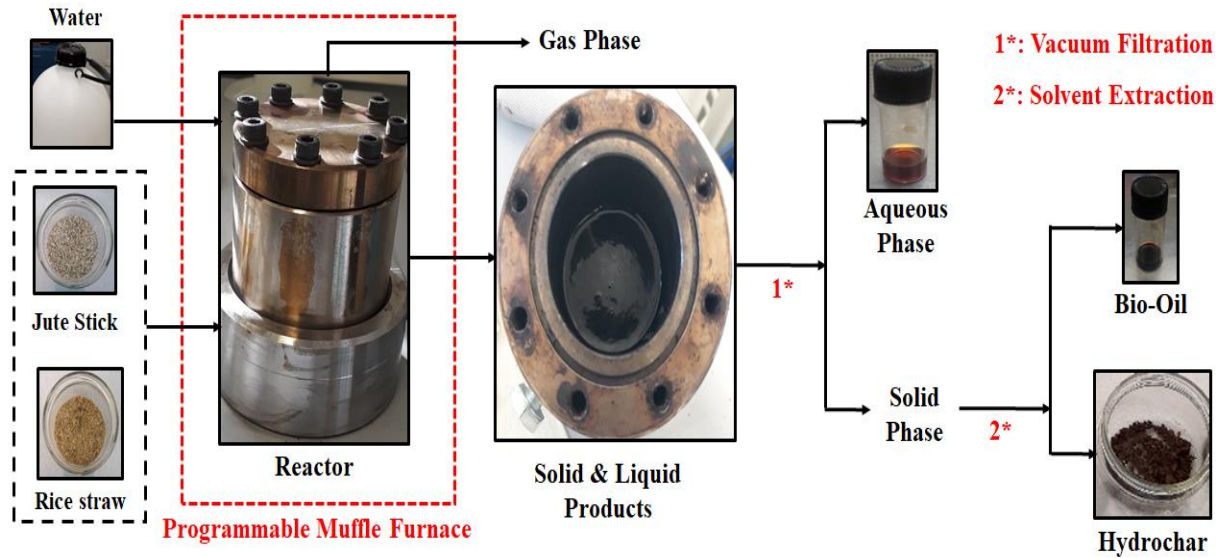


Fig. 7.1 Schematic diagram of hydrothermal liquefaction of jute stick and rice straw

The yields of hydrochar and bio-oil have been calculated using the following equations:

$$\% \text{ Yield of hydrochar} = \frac{\text{mass of hydrochar}}{\text{mass of biomass}} \times 100 \quad (7.1)$$

$$\% \text{ Yield of bio - oil} = \frac{\text{mass of bio-oil}}{\text{mass of biomass}} \times 100 \quad (7.2)$$

However, the combined yields of aqueous and gaseous phases of the samples have been determined by the following standard equation described by Harisankar et al. (Harisankar et al, 2022).

$$\% \text{Yield of (aqueous + gas) phase} = 100 - \text{Yields of (hydrochar + bio - oil)} \quad (7.3)$$

7.2 Optimization

A three-level, 3-factor Box-Behnken statistical design in response surface methodology (RSM) has been used to fit a second-order model to correlate the response variable, yield of bio-oil with the most important operating factors, temperature (A), time (B) and % blending of jute stick in RS-JS mixture (C). The % blending of jute stick in RS-JS mixture is defined by $\frac{\text{mass of jute stick}}{\text{mass of jute stick} + \text{mass of rice straw}} \times 100$. The variables, A, B and C with coded level (-1, 0 and 1) are shown in the Table 7.1. The three level of % blending of jute stick in RS-JS mixture in the present study have been considered as 10 (0.5 g JS and 4.5 g RS), 50 (2.5 g JS and 2.5 g RS) and 90 (4.5 g JS and 0.5 g RS) respectively.

Table 7.1 Variables with coded level used for experimental run

Input variables	Unit	Coded variable level			Model Response
		-1	0	1	
Temperature (A)	°C	240	300	360	Yield of Bio-oil (%)
Time (B)	min	10	20	30	
% blending of jute stick in RS-JS mixture (C)	-	10	50	90	

The generalized form of second-order polynomial equation is mentioned as follows (Vashishtha et al, 2021):

$$Y = a_0 + \sum_{i=1}^n a_i x_i + \sum_{i=1}^{n-1} \sum_{j=i+1}^n a_{ij} x_i x_j + \sum_{i=1}^n a_{ii} x_i^2 \quad (7.4)$$

Where Y is the predicted % yield of bio-oil, a_0 , a_i , a_{ij} and a_{ii} are the constant coefficient, linear coefficient, interaction coefficient and quadratic coefficient respectively and x_i represents the coded variables (A, B and C). The regression analysis and analysis of variance (ANOVA) have

been performed with Design-Expert Software (version 11). The model has been used to predict the optimum operating condition for the production of bio-oil from co-hydrothermal liquefaction of jute stick and rice straw. In the present study, Box-Behnken statistical design is based on 17 experimental runs, detailed in Table 7.2.

Table 7.2 Operating parameters for production of bio-oil from co-HTL of JS and RS according to RSM

Run	Factor 1 A: Temp. (°C)	Factor 2 B: Time (min)	Factor 3 C: % blending of jute stick in RS-JS mixture
1	240	20	90
2	300	20	50
3	360	20	10
4	300	20	50
5	300	10	90
6	360	10	50
7	360	30	50
8	300	30	10
9	360	20	90
10	300	10	10
11	240	10	50
12	240	20	10
13	240	30	50
14	300	20	50
15	300	30	90
16	300	20	50
17	300	20	50

7.3 Lumped Kinetics of hydrothermal liquefaction

Lumped kinetics of hydrothermal liquefaction of jute stick and rice straw have been determined using the experimental data. The reaction pathway represented by Fig. 7.2 has been considered for HTL of Indian biomass (jute stick or rice straw) (Kumar et al, 2022). All reactions are assumed to be of first order.

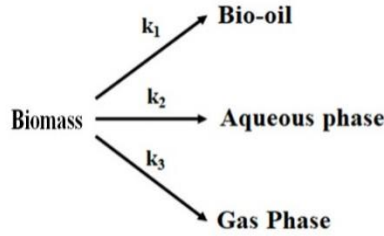


Fig. 7.2 Reaction network for hydrothermal liquefaction of biomass (jute stick or rice straw)

The differential mass balance equations are as follows:

$$-\frac{dW_{Biomass}}{dt} = (k_1 + k_2 + k_3) W_{Biomass} = k' W_{Biomass} \quad (7.5)$$

Where $k_1 + k_2 + k_3 = k'$

$$\frac{dW_{Bio-oil}}{dt} = k_1 W_{Biomass} \quad (7.6)$$

$$\frac{dW_{Aqueous}}{dt} = k_2 W_{Biomass} \quad (7.7)$$

$$\frac{dW_{Gas}}{dt} = k_3 W_{Biomass} \quad (7.8)$$

The overall rate constant of HTL, k' has been calculated from Eq. 7.5.

$$\ln\left(\frac{W_{Biomass_0}}{W_{Biomass_t}}\right) = k' t \quad (7.9)$$

Where $W_{Biomass_t}$ and $W_{Biomass_0}$ are the weight of solid residue at time t and initial weight of biomass (jute stick or rice straw) respectively. Using the experimental data on the residual solid mass after different holding time at different temperature, the validity of first order rate kinetics has been verified from the nature of the plots of $\ln\left(\frac{W_{Biomass_0}}{W_{Biomass_t}}\right)$ against holding time, t , and the values of k' have been determined from the slope if the plots are linear in nature. The plot has been

shown in Figure 7.6a and Figure 7.6b for JS and RS respectively. Although there are possibilities of occurrence of some interactions between the products, like conversion of bio-oil to aqueous and gaseous products through series reactions etc., no such secondary reactions are considered in this model. The values of rate constants (k_1 , k_2 and k_3) at different temperatures can be determined using regression analysis of following equations (7.10), (7.11) and (7.12) respectively. As at time $t=0$, $(W_{Bio-oil})_0 = (W_{Aqueous})_0 = (W_{Gas})_0 = 0$,

$$(W_{Bio-oil})_t = \left(\frac{k_1}{k'}\right) W_{Biomass_0} [1 - \exp(-k't)] \quad (7.10)$$

$$(W_{Aqueous})_t = \left(\frac{k_2}{k'}\right) W_{Biomass_0} [1 - \exp(-k't)] \quad (7.11)$$

$$(W_{Gas})_t = \left(\frac{k_3}{k'}\right) W_{Biomass_0} [1 - \exp(-k't)] \quad (7.12)$$

According to the present experimental investigation, the combined aqueous and gaseous phase products have been determined.

$$(W_{Aq-G})_t = \left(\frac{k_{Aq-G}}{k'}\right) W_{Biomass_0} [1 - \exp(-k't)] \quad (7.13)$$

Where, k_{Aq-G} is the combined rate constant of generation of aqueous and gaseous phase products. The applicability of first order rate kinetics has been checked from the nature of plots of $(W_{Bio-oil})_t$ and $(W_{Aq-G})_t$ against $\left(\frac{W_{Biomass_0}}{k'} [1 - \exp(-k't)]\right)$ and the values of k_1 and k_{Aq-G} have been determined from the slopes of the plots, if they are linear.

7.4 Results and discussion

7.4.1 Proximate analysis of jute stick and rice straw

The proximate analysis (moisture, fixed carbon, volatile matter, and ash) of jute stick and rice straw have been reported in Table 7.3.

Table 7.3 Proximate analysis of jute stick and rice straw

Proximate analysis % (w)	Moisture	Fixed carbon	Volatile matter	Ash
Jute stick	7.81 ± 0.30	12.72 ± 0.56	77.89 ± 3.11	3.58 ± 0.11
Rice straw	5.69 ± 0.12	11.42 ± 0.48	71.91 ± 2.04	10.99 ± 0.29

7.4.2 Composition of jute stick and rice straw

The composition (w/w) of JS were determined as 31.67 % cellulose (glucan considering as cellulose), 15.99 % hemicellulose (xylan 13.91 %, arabinan 2.01 % and mannan 0.07 %) and 32.77 % lignin (Klason lignin 31.17 % and acid soluble lignin 1.60 %) respectively. Whereas in rice straw, 38.24% cellulose (glucan considering as cellulose), 21.17 % hemicellulose (xylan 17.61 %, arabinan 3.27 and mannan 0.29 %) and 17.85 % lignin (Klason lignin 14.37 % and acid soluble lignin 2.48 %) have been measured. The comparison of cellulose, hemicellulose and lignin present in jute stick and rice straw are shown Fig. 7.3.

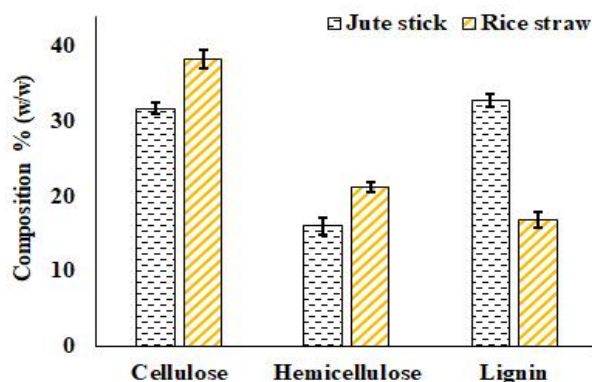


Fig. 7.3 Composition (cellulose, hemicellulose and lignin) of JS and RS

Cello:Hemi ratio (weight fraction of cellulose: weight fraction of hemicellulose) for biomass ($W_{\text{Cello/Hemi}}$) is defined as follows:

$$W_{\frac{\text{Cello}}{\text{Hemi}}} = \frac{\text{Weight (\%)} \text{ of cellulose in raw biomass}}{\text{Weight (\%)} \text{ of hemicellulose in raw biomass}} \quad (7.14)$$

The ratio, $W_{\text{Cello/Hemi}}$ (cellulose: hemicelluloses (w/w)) for JS and RS are determined (using Eq. 7.14) as 1.98 and 1.81 respectively.

7.4.3 Product Yield obtained from HTL

In Fig. 7.4, the yield of hydrochar, bio-oil and combined gaseous and aqueous products have been plotted against HTL temperature for JS and RS for holding period of 30 minutes. It is evident that with increase in temperature, the yield of hydrochar decreases for both feedstocks. The rise in temperature appears to increase the dissociation of chemical bonds and subsequently to increase the depolymerization. As such the yield of hydrochar decreases from 43.97% - 22.15 % for JS and

48.36% to 25.17% for RS when the temperature is increased from 240 to 360 °C. A rapid decrease in the yield of hydrochar has also been observed at the temperature range of 240 – 300 °C. At each temperature, the yield of hydrochar from JS is lower, in comparison to that from RS. This may be due to the higher value of the ratio of Cello: Hemi, $W_{\frac{Cello}{Hemi}}$, in JS compared to that of RS.

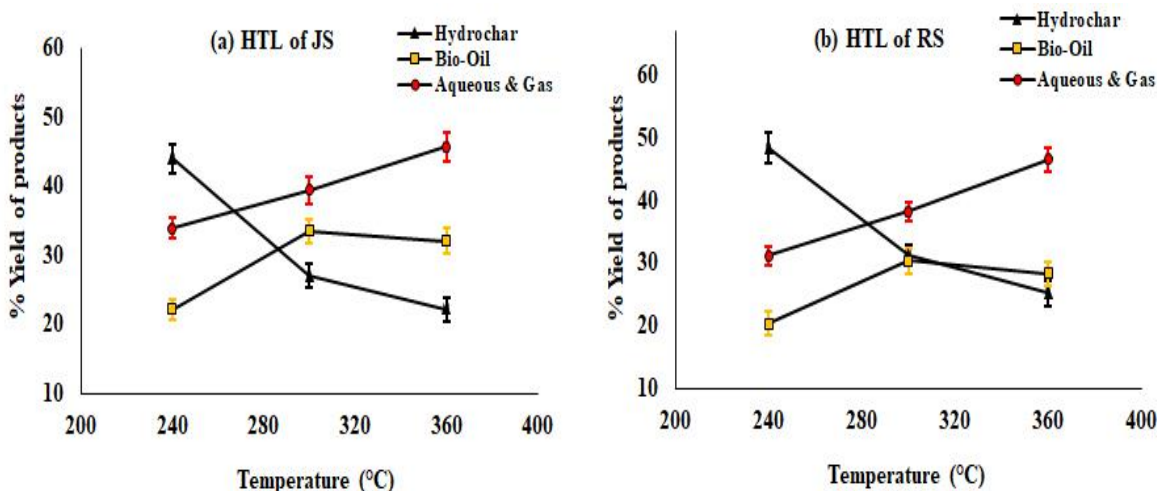


Fig. 7.4 Product yield (%) at different temperature a: jute stick, b: rice straw) [Holding period: 30 minutes]

The yield of bio-oil increases from 22.15% - 33.81% for jute sticks and 20.39% to 30.34% for rice straw when the temperature is increased from 240 to 300 °C. When, the temperature is increased from 300 to 360 °C, the yield of bio-oil decreases from 33.81% - 32.09% for jute sticks and 30.34% to 28.31% for rice straw. The maximum bio-oil yield is obtained at 300°C. This trend for the yield of bio-oil is also in agreement with the available reported data on HTL of LCBs (Akalin et al, 2019). Beyond 300°C, the yield of bio-oil decreases due secondary degradation of bio-oil to gaseous products (Akalin et al, 2019).

The yield of bio-oil for RS has been observed somewhat lower than that of JS at each temperature. This can be explained by the higher lignin content and larger value of Cello: Hemi, $W_{\frac{Cello}{Hemi}}$, of JS with respect to RS (Wang et al, 2023; Tian et al, 2023). Similar impacts of lignin content and Cello: Hemi ratio on bio-oil yield during the HTL of several LBs have also been reported in other studies (Wang et al, 2023; Tian et al, 2023). For both JS and RS feedstocks, the combined yield of aqueous and gaseous products has been observed to increase with the rise in temperature. This

trend is also in agreement with the available reported data on HTL of LCBs (De Caprariis et al, 2017).

7.4.4 Kinetic parameters

The kinetic parameters of hydrothermal liquefaction of JS and rice straw RS have been determined using the experimental data obtained after different holding time (5, 10, 15, 20, 25 and 30 minutes) at each reaction temperature (240, 300 and 360°C). Time-trajectories of mass of solid residue, $W_{Biomass,t}$, bio-oil, $W_{Bio-oil,t}$, and combined aqueous and gaseous products, $W_{Aq-G,t}$ have been shown respectively for jute stick and rice straw in Figures 7.5 a and 7.5 d; Figures 7.5 b and 7.5 e; Figures 7.5 c and 7.5 f respectively.

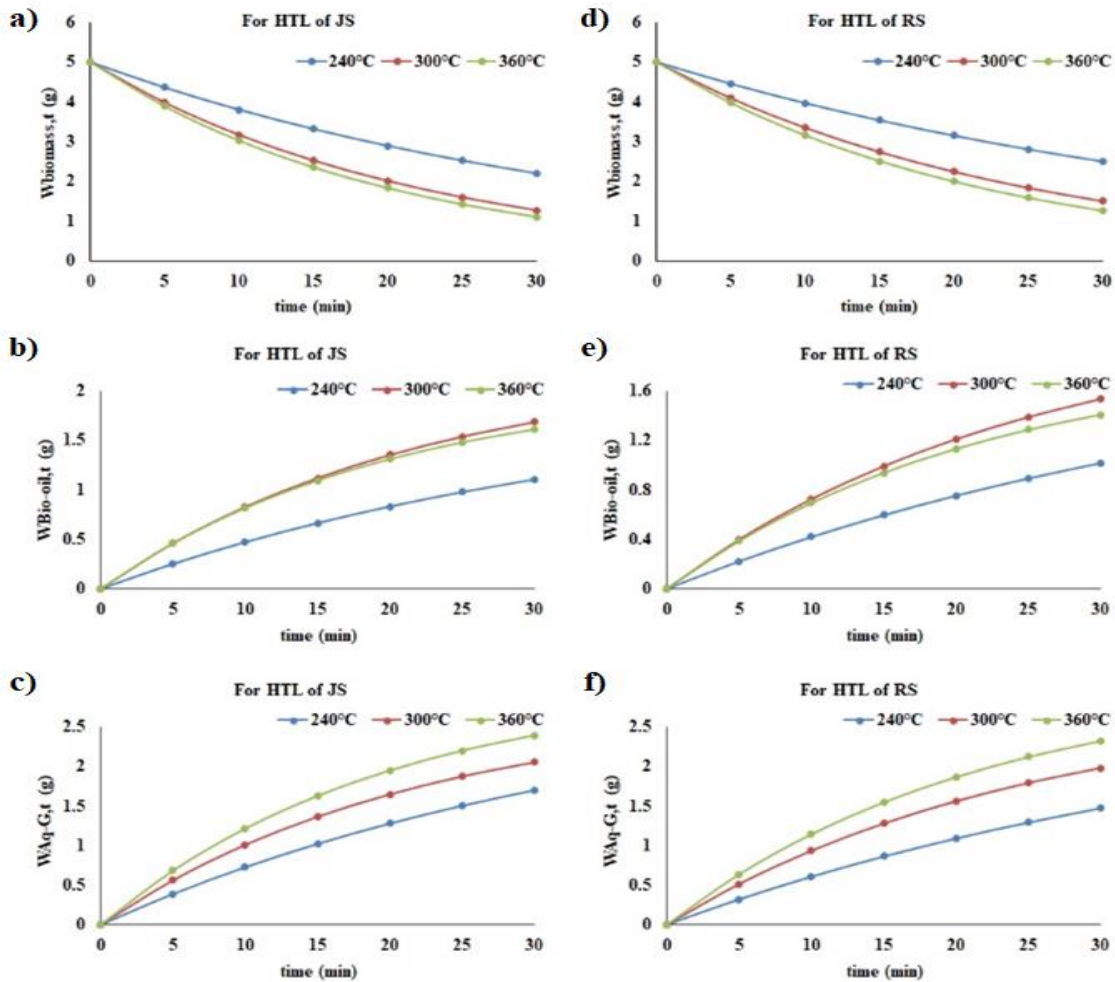


Fig. 7.5 Plot of $W_{Biomass,t}$ versus time (a: HTL of JS; d: HTL of RS); Plot of $W_{Bio-oil,t}$ versus time (b: HTL of JS; e: HTL of RS); Plot of $W_{Aq-G,t}$ versus time (c: HTL of JS; f: HTL of RS)

From the analysis of the figure it is evident that as per expectation, the trajectory of biomass has a declining trend and those of bio-oil and combined aqueous and gaseous products follow increasing trends.

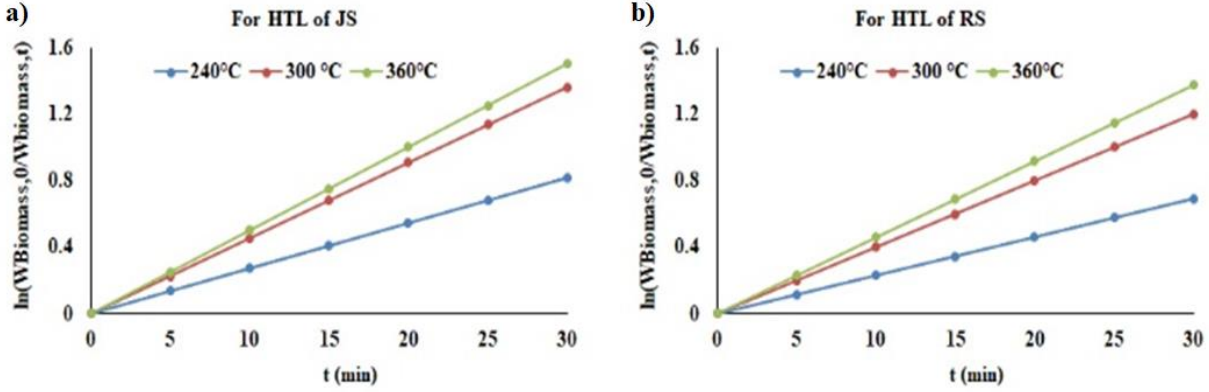


Fig 7.6 Plot of $\ln\left(\frac{W_{Biomass_0}}{W_{Biomass_t}}\right)$ against holding time, t (a: HTL of JS; b: HTL of RS)

In Figures 7.6a and 7.6b, the values of $\ln\left(\frac{W_{Biomass_0}}{W_{Biomass_t}}\right)$, obtained at different temperature (240°C, 300°C and 360°C) have been plotted against time of HTL for rice straw and jute stick respectively. The linear nature of the plots prove the validity of the first order rate kinetics. The rate constants have been determined from the slopes of the plots at different temperatures.

The plots of $W_{Bio-oil,t}$ versus $\left[\frac{W_{Biomass_0}}{k'}[1 - \exp(-k't)]\right]$ for JS at 240°C, 300°C and 360°C are shown in Figures 7.7 a, 7.7 b and 7.7 c respectively. Similarly, the plots of $W_{Bio-oil,t}$ versus $\left[\frac{W_{Biomass_0}}{k'}[1 - \exp(-k't)]\right]$ for RS at 240°C, 300°C and 360°C are shown in Figures 7.7 d, 7.7 e and 7.7 f respectively. The plots of $W_{Aq-G,t}$ versus $\left[\frac{W_{Biomass_0}}{k'}[1 - \exp(-k't)]\right]$ for JS at 240°C, 300°C and 360°C are shown in Figures 7.8 a, 7.8 b and 7.8 c respectively. Similarly, the plots of $W_{Aq-G,t}$ versus $\left[\frac{W_{Biomass_0}}{k'}[1 - \exp(-k't)]\right]$ for RS at 240°C, 300°C and 360°C are shown in Figures 7.8 a, 7.8 b and 7.8 c respectively. The linearity of all plots, represented in Figures 7.7a-f and Figures 7.8 a-f proves the validity of first order rate kinetics for all the relevant reactions. Thus the values of rate constants, k_1 and k_{Aq-G} are determined.

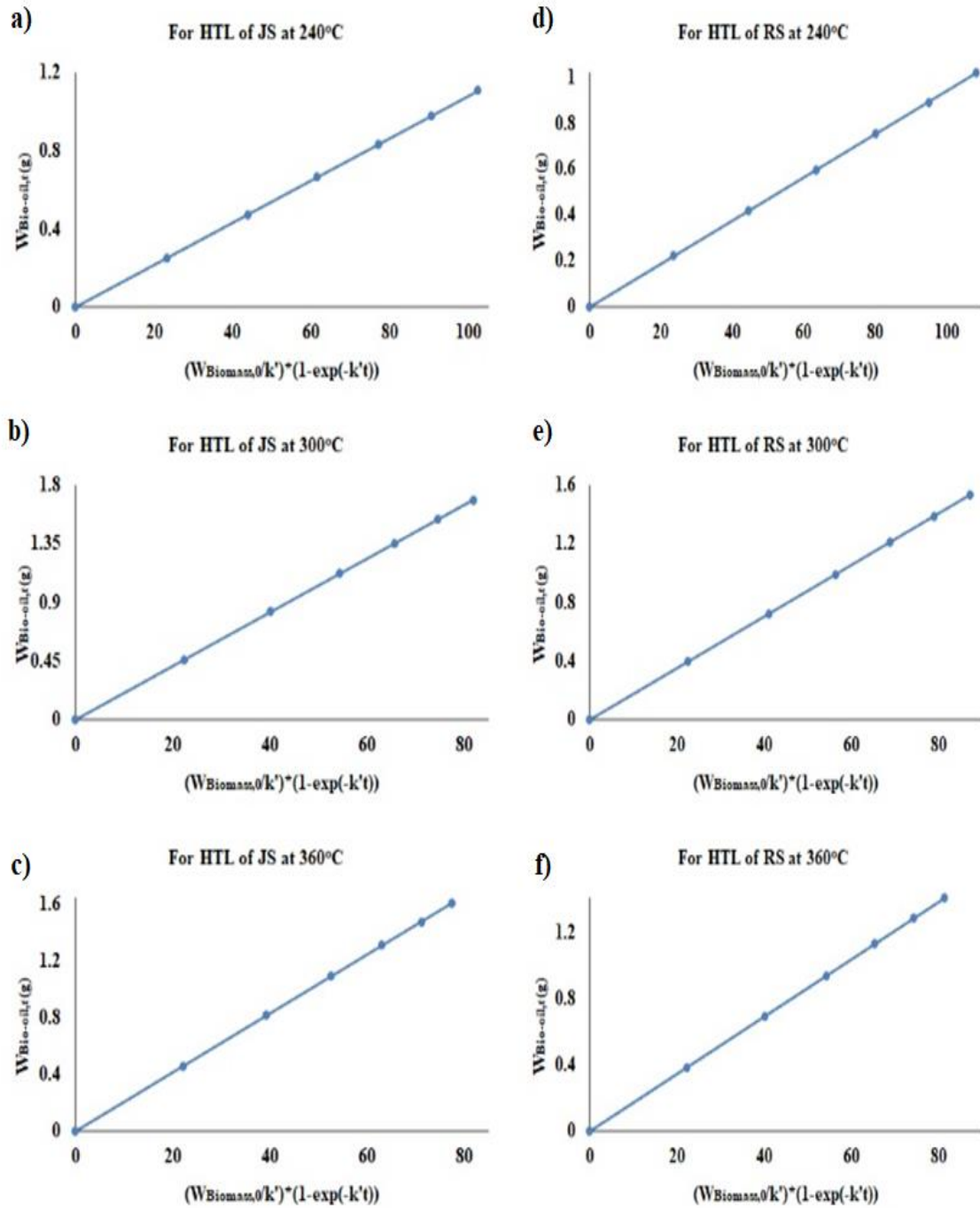


Fig. 7.7 Plot of $W_{Bio-oil,t}$ versus $\left[\frac{W_{Biomass,0}}{k'} [1 - \exp(-k't)]\right]$ at 240°C (a: HTL of JS; d: HTL of RS); Plot of $W_{Bio-oil,t}$ versus $\left[\frac{W_{Biomass,0}}{k'} [1 - \exp(-k't)]\right]$ at 300°C (b: HTL of JS; e: HTL of RS); Plot of $W_{Bio-oil,t}$ versus $\left[\frac{W_{Biomass,0}}{k'} [1 - \exp(-k't)]\right]$ at 360°C (c: HTL of JS; f: HTL of RS)

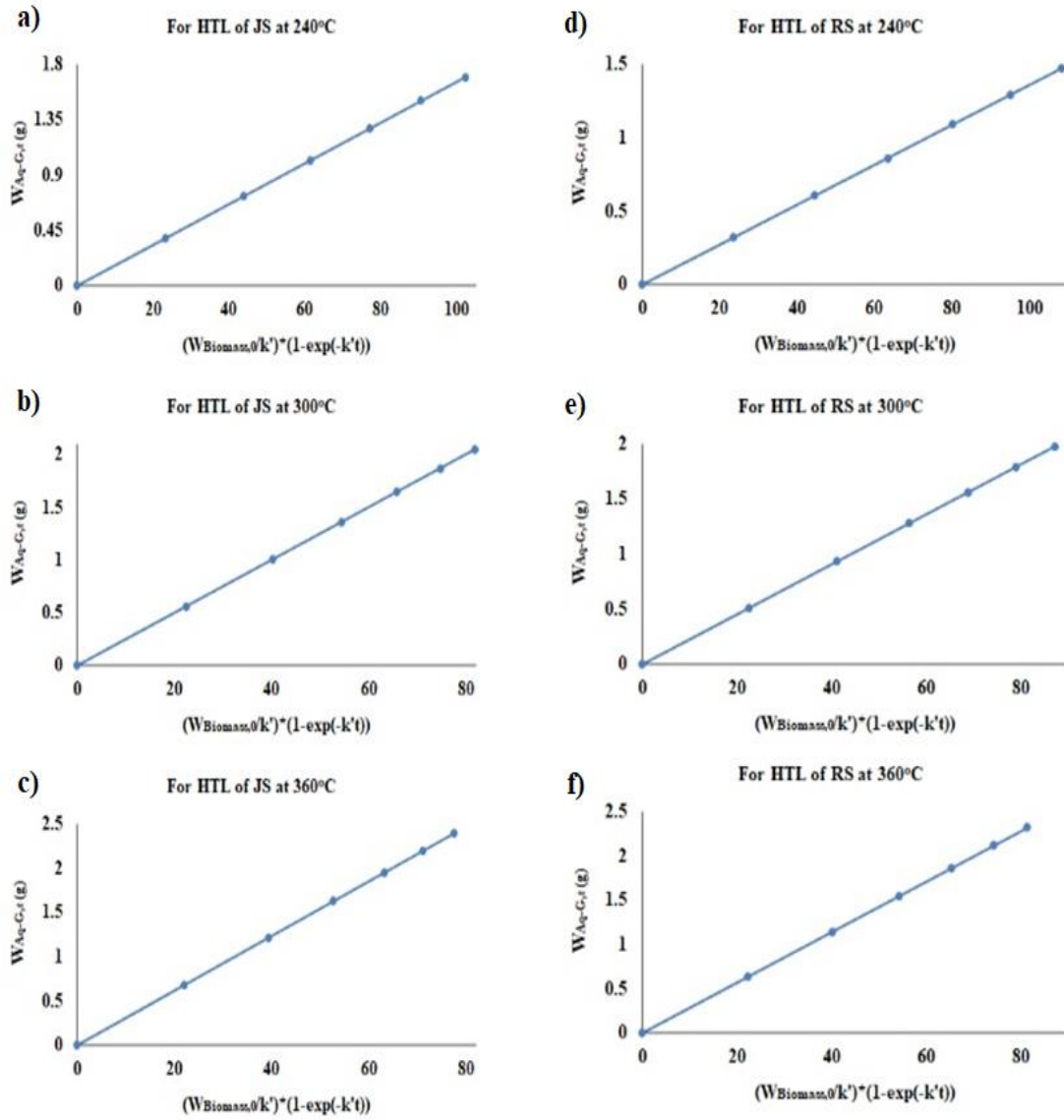


Fig. 7.8 Plot of $W_{Aq-G,t}$ versus $\left[\frac{W_{Biomass,0}}{k'} [1 - \exp(-k't)]\right]$ at 240°C (a: HTL of JS; d: HTL of RS); Plot of $W_{Aq-G,t}$ versus $\left[\frac{W_{Biomass,0}}{k'} [1 - \exp(-k't)]\right]$ at 300°C (b: HTL of JS; e: HTL of RS); Plot of $W_{Aq-G,t}$ versus $\left[\frac{W_{Biomass,0}}{k'} [1 - \exp(-k't)]\right]$ at 360°C (c: HTL of JS; f: HTL of RS)

All the rate constants involved in the HTL of JS and RS at different temperatures have been provided in the Table 7.4.

Table 7.4 Values of rate constants involved in the hydrothermal liquefaction of jute stick and rice straw

For	Rate constant	At 240 °C	At 300 °C	At 360 °C
HTL of JS	k' (min ⁻¹)	0.0273	0.0455	0.0502
	k_1 (min ⁻¹)	0.0108	0.0206	0.0208
	k_{Aq-G} (min ⁻¹)	0.0166	0.0251	0.0309
HTL of RS	k' (min ⁻¹)	0.0231	0.0401	0.0459
	k_1 (min ⁻¹)	0.0094	0.0176	0.0173
	k_{Aq-G} (min ⁻¹)	0.0136	0.0227	0.0285

Arrhenius equation has been used to represent the functionality of rate constants on temperature as follows:

$$k_i = k_{oi} \exp\left(\frac{-E_i}{RT}\right) \quad (7.15)$$

$$\text{Or, } \ln k_i = \ln k_{oi} - \frac{E_i}{RT}$$

k_i = rate constant of i^{th} reaction; k_{oi} = pre – exponential factor of i^{th} reaction ;

E_i = Activation energy of i^{th} reaction;

The values of activation energies and pre-exponential factors of all rate constants for HTL of JS and RS have been determined by plotting $\ln(k_i)$ against the inverse of temperature in kelvin ($1/T$). They are provided in the Table 7.5.

Table 7.5 Activation energies and pre-exponential factors of rate constants for HTL of JS and RS

For	Rate constant (min ⁻¹)	Activation energy (kJ/mol)	Pre-exponential factors (min ⁻¹)	R ² value
HTL of JS	k'	13.97	0.7619	0.9569
	k_1	15.18	0.4137	0.8917

	k_{Aq-G}	14.08	0.4611	0.9836
HTL of RS	k'	15.71	0.9689	0.9621
	k_1	14.17	0.2846	0.8893
	k_{Aq-G}	16.80	0.7216	0.9904

7.4.5 Elemental analysis of hydrochar and bio-oil

7.4.5.1 Elemental analysis of hydrochar

The elemental analyses (carbon, hydrogen, nitrogen, and oxygen) and higher heating value (HHV) of RS and JS and those of their hydrochar, obtained through individual HTL at 240 °C, 300 °C and 360 °C, have been reported in Table 7.6. From the analysis, it is evident that the HHV of JS (14.31 MJ/kg) is higher than that of RS (9.50 MJ/kg). While the HHV of JS hydrochar varies from 19.01 MJ/kg to 20.72 MJ/kg, the HHV of RS hydrochar varies from 18.22 MJ/kg to 20.61 MJ/kg as the HTL temperature is increased from 240 °C to 360°C.

Table 7.6 Ultimate analysis of hydrochar obtained from HTL of jute stick and rice straw

Sample	Type	Temp (°C)	C (%w)	H (%w)	N (%w)	O (%w)	H/C	O/C	HHV (MJ/kg)
Jute stick	Raw	-	44.79	5.71	0.29	49.21	1.51	0.824	14.31
Rice straw	Raw	-	37.28	5.13	0.22	57.37	1.63	1.15	9.50
Jute stick	Char	240	58.63	4.08	1.6	35.69	0.828	0.456	19.01
Rice straw	Char	240	57.32	4.01	1.56	37.11	0.832	0.485	18.22
Jute stick	Char	300	59.37	4.29	2.11	34.23	0.860	0.432	19.82
Rice straw	Char	300	58.32	4.27	1.98	35.43	0.871	0.455	19.23
Jute stick	Char	360	61.01	4.25	2.8	31.94	0.829	0.392	20.72
Rice straw	Char	360	60.93	4.24	2.49	32.34	0.828	0.398	20.61
Peat	-	-	54.50	5.10	1.65	33.09	1.120	0.455	21.33
Lignite	-	-	62.50	4.38	0.94	17.20	0.840	0.206	24.45

7.4.5.2 Elemental analysis of bio-oil

The elemental analysis and HHV of bio-oil obtained from HTL of JS and RS at different temperatures, have been reported in Table 7.7. The atomic ratios H/C and O/C of bio-oil, as obtained at different HTL temperatures, are less than that of both the raw feedstocks (JS and RS). It has been observed that the trend of hydrochar, oxygen content of bio-oil of both JS and RS decreases with HTL temperature. However, HHV of bio-oils shows an increasing trend with temperature. The HHVs of bio-oil obtained from JS have greater values than those obtained from at each HTL temperature level. Under the present investigation, the bio-oil obtained from JS at 360 °C appears to have the maximum HHV as 29.44 MJ/kg.

Table 7.7 Ultimate analysis of bio-oil obtained from individual HTL of jute stick and rice straw

Sample	Type	Temp (°C)	C (%w)	H (%w)	N (%w)	O (%w)	H/C	O/C	HHV (MJ/kg)
Jute stick	Oil	240	61.89	7.63	0.98	30.5	1.275	0.369	24.70
Rice straw	Oil	240	60.12	7.11	0.7	33.07	1.209	0.412	22.90
Jute stick	Oil	300	67.31	7.91	1.05	25.73	1.240	0.291	27.43
Rice straw	Oil	300	63.18	7.32	0.73	29.77	1.190	0.353	24.81
Jute stick	Oil	360	69.34	7.19	1.06	22.41	1.234	0.242	29.44
Rice straw	Oil	360	67.01	7.67	0.97	25.35	1.184	0.283	27.39
Petroleum crude			85-87	14-15	0.1	0.2-2	1.4-1.5	0.01- 0.02	42-45

Among all atomic components (C, H, N, O and S) present in a fuel, only C and H contribute towards the heating value. Particularly, the oxygen content influences the heating value negatively. Hence following the convention of Van Krevelen diagram, used for the assessment of quality of fuel, H/C values of hydro char and bio-oil have been plotted against the corresponding O/C values for JS and RS respectively (shown in the Fig. 7.9 a and b).

The H/C versus O/C plot of peat and lignite has been used as the reference. Both H/C and O/C ratios of hydrochar of RS and JS, obtained at all HTL temperatures under this present study, are

much less than the raw feedstocks. The O/C values of hydrochar of both feedstocks are in between those of peat and lignite. For the hydrochar of both feedstocks, the value of H/C increases with temperature up to 300 °C beyond which a decreasing trend has been observed. The O/C ratio shows a decreasing trend with temperature in case of hydrochar for both feedstocks.

The H/C and O/C ratios of bio-oil of JS and RS, obtained at all HTL temperatures under the present investigation are much less than the original raw feedstocks. The H/C and O/C values of bio-oil decreases with increase in temperature. The H/C values of bio-oil obtained from JS and RS vary from 1.275 to 1.234 and 1.209 to 1.184 respectively, while the O/C values of bio-oil obtained from JS and RS fall in the range of 0.369 to 0.242 and 0.412 to 0.283 respectively. The amount of HHV of bio-oil obtained from both feedstocks are less than petroleum crude.

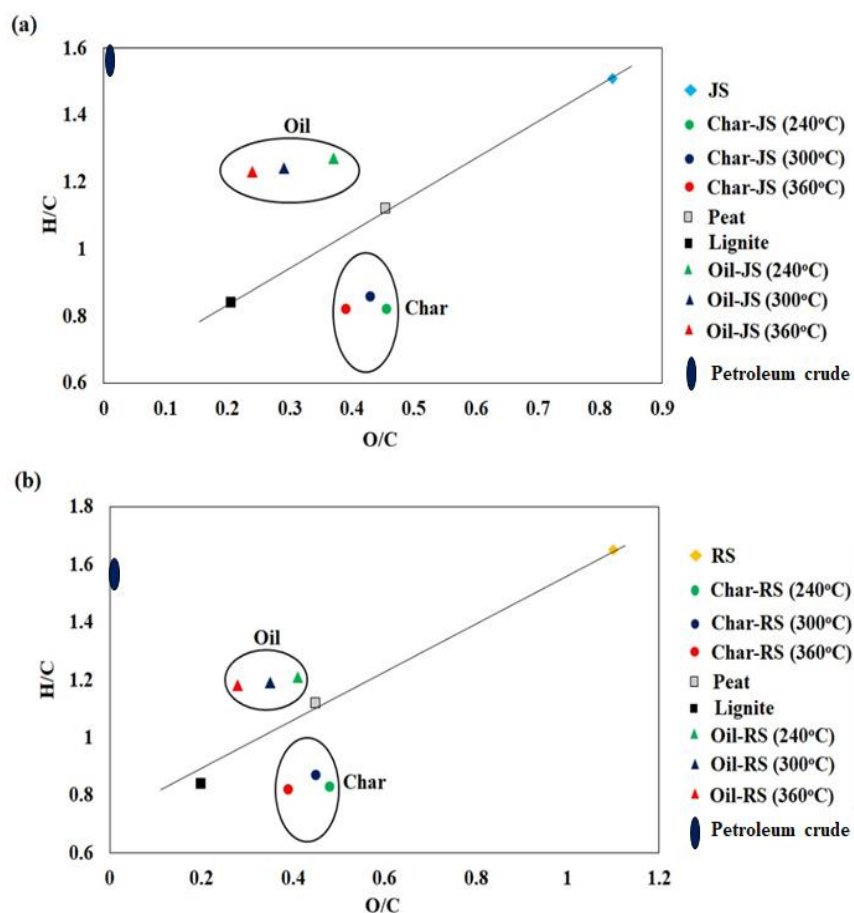


Fig. 7.9 Van Krevelen diagram for raw biomass, hydrochar and bio-oil of jute stick (a) and rice straw (b)

7.4.6 Thermal stability analysis of hydrochar obtained from individual HTL

In Fig. 7.10a, the thermogravimetric (TG) and derivative thermogravimetric (DTG) curves of jute sticks have been shown. The weight loss of raw-JS in Stage I (50 – 297 °C), Stage II (298 – 369 °C), Stage III (370– 690 °C) and stage IV (691– 900 °C) have been determined as 2.83%, 51.38%, 34.34% and 0% respectively. In this present study, the peak of the DTG curve of JS occurs at a temperature of 407 °C. The weight loss of hydrochar (obtained from HTL of JS at 300 °C) in Stage I (50 – 297 °C), Stage II (298 – 369 °C) and Stage III (370– 900 °C) have been measured as 2.27 %, 8.17 % and 73.72 % respectively (Fig.7.10b).

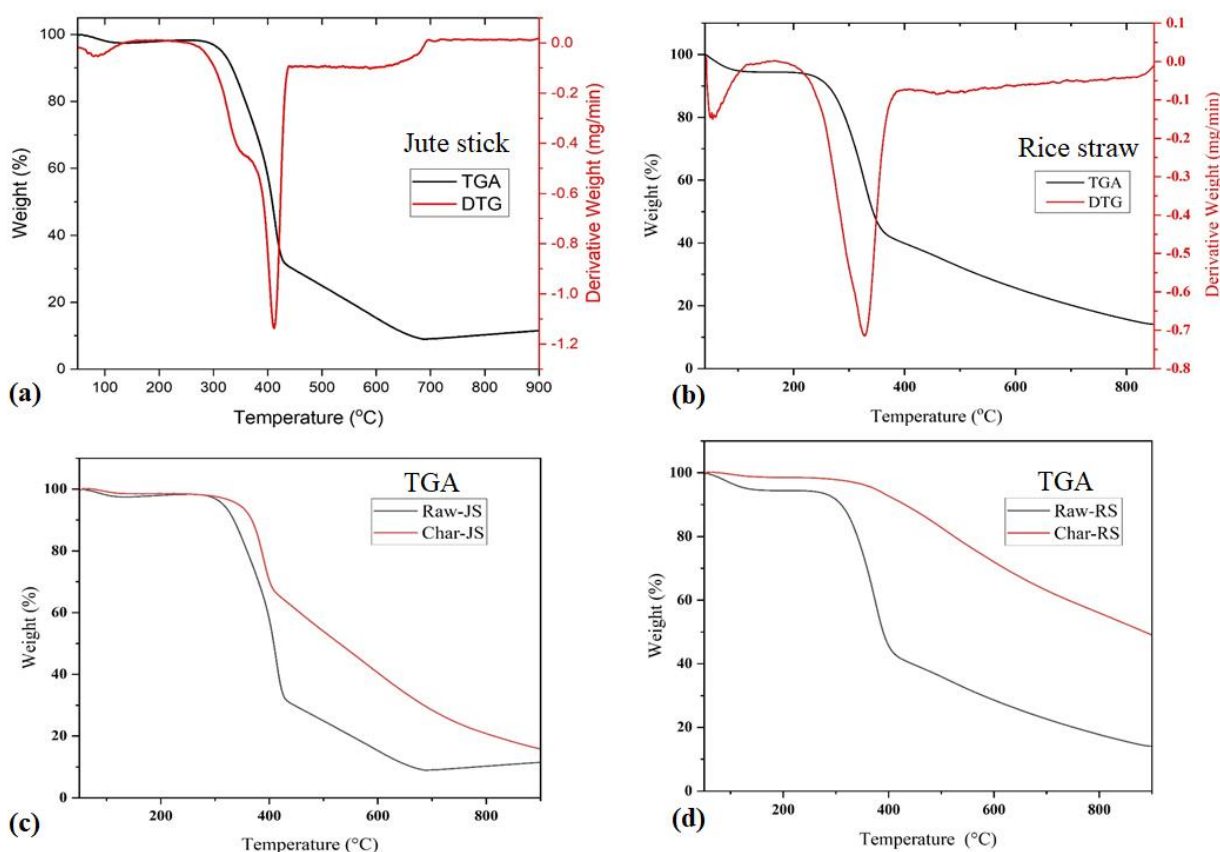


Fig. 7.10 TG analysis raw-biomass and hydrochar (a, b: TGA and DTG of raw-JS and raw-RS; c, d: TGA of raw-biomass and hydrochar of JS, RS respectively)

The TG and DTG curves of rice straw have been shown in Figure 7.10c. In the present investigation, the percentage weight loss of raw-RS in Stage I (50 – 277 °C), Stage II (278 – 371 °C) and Stage III (372– 900 °C) have been determined as 7.48, 31.21 and 47.90 respectively. The

peak of the DTG curve of raw-RS occurs at a temperature of 329 °C. The weight loss of hydrochar (obtained from HTL of RS at 300 °C) in Stage I (50 – 277 °C), Stage II (278 – 371 °C) and Stage III (372– 900 °C) are 1.79 %, 2.99 % and 47.16 % respectively (Fig. 7.10d). The decomposition of hemicellulose, cellulose and lignin generally occur at the temperature range of 220 – 315 °C, 300 – 400 °C and 150 – 900 °C respectively (Waters et al, 2017).

7.4.7 FTIR analysis of hydrochar obtained from individual HTL

In Fig. 7.11a1 and 7.11a2, the FTIR analysis of raw-JS, raw-RS and hydrochar (obtained from HTL of JS, RS at 300 °C) have been shown respectively. As 400-4000 cm^{-1} are the most used region for all organic compounds, peaks within this zone have been analyzed. The adsorption peaks at 3329, 2879 and 1031 cm^{-1} indicate O – H, C – H and C – O stretching respectively. Whereas the adsorption peaks 3333, 2919 and 1034 cm^{-1} show O – H, C – H and C – O stretching respectively. In both cases, the areas under the stretch of hydrochar are less than that of the original raw samples.

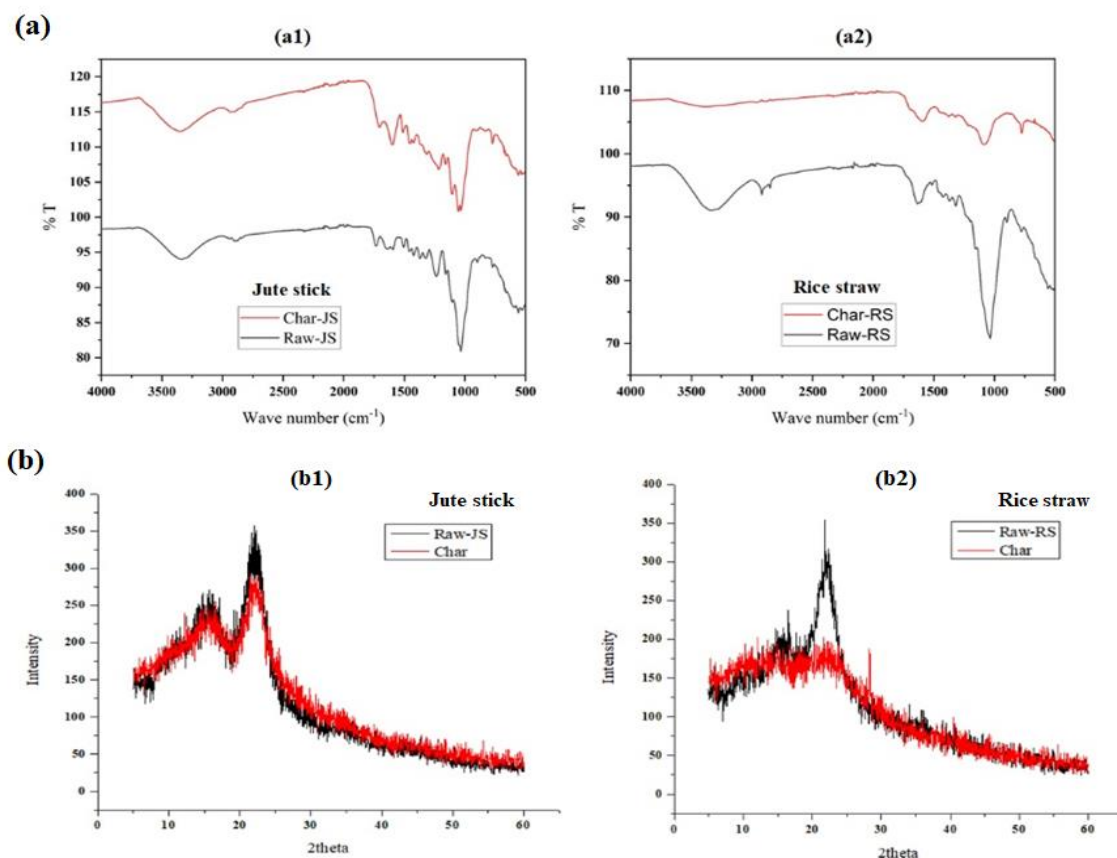


Fig. 7.11 FT-IR analysis raw-biomass and hydrochar (a) (a1: FT-IR of raw-JS and hydrochar of JS; a2: FT-IR of raw-RS and hydrochar of RS respectively); XRD analysis raw-biomass and hydrochar (b) (b1: XRD of raw-JS and hydrochar of JS; b2: XRD of raw-RS and hydrochar of RS respectively)

7.4.8 XRD analysis of hydrochar obtained from individual HTL

The XRD analysis of raw JS, RS and hydrochar of JS and RS (obtained at 300°C) have been shown in the Fig. 7.11b1 and 7.11b2 respectively. The characteristic peaks have been observed at 18.5° and 22.5°C. The sharpness of the peaks for hydrochar in both case are reduced significantly compared to raw jute stick and rice straw. This phenomena signifies that the crystalline structure of cellulose is disrupted.

7.4.9 Surface morphology of hydrochar obtained from individual HTL

The FESEM analysis of raw-JS, raw-RS and hydrochar (obtained from HTL of JS and RS at 300°C) are shown in Fig. 7.12. The surface of raw biomasses is smooth whereas thermal cracks have been observed while they are transformed into hydrochar. The possible reason for the generation of the thermal cracks is the cell disruption of cellulose and hemicellulose.

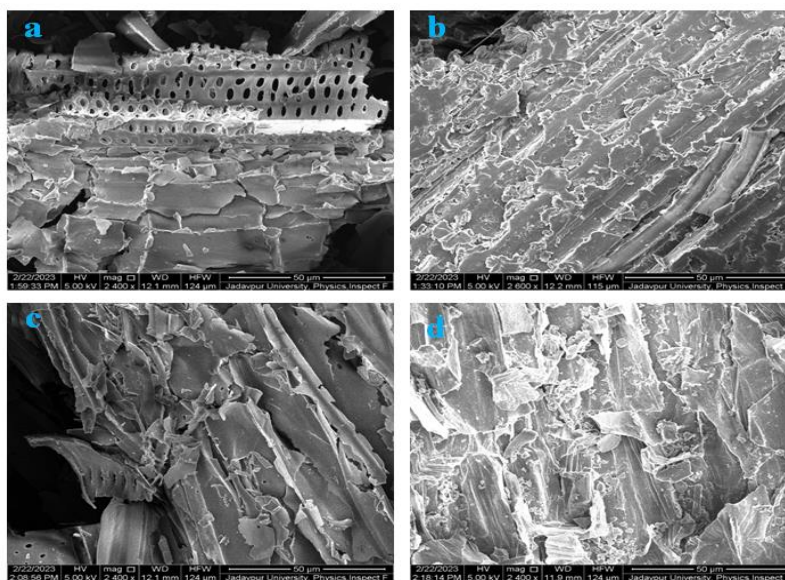


Fig. 7.12 FESEM analysis raw-JS (a), raw-RS (b), hydrochar of JS (c) and hydrochar of RS (d)

7.4.10 Bio-oil production from co-HTL of jute stick and rice straw

Using Box-Behnken statistical design, 17 experiments, described in Table 7.2, have been conducted in triplicate basis to determine the yield of bio-oil from co-hydrothermal liquefaction of mixture of jute stick and rice straw. The correlation of the yield of bio-oil with three variables namely, temperature (A), time (B) and % blending of jute stick in RS-JS mixture (C) has been obtained as follows:

$$\text{Bio-oil (\%)} = -165.433 + 1.03102A + 1.59437B + 0.109125C + 0.000291667AB - 0.000285417AC + 0.0013625BC - 0.00159861A^2 - 0.02525B^2 + 0.000109375C^2 \quad (7.16)$$

The analysis of the adequacy and fitness of quadratic model generated from ANOVA is presented in Table 7.8.

Table 7.8 ANOVA table for Quadratic model

Source	Sum of Squares	df	Mean Square	F-value	p-value	
Model	789.44	9	87.72	173.69	< 0.0001	significant
A	242.00	1	242.00	479.21	< 0.0001	
B	468.95	1	468.95	928.61	< 0.0001	
C	25.81	1	25.81	51.11	0.0002	
AB	1.89	1	1.89	3.74	0.0942	
AC	0.3080	1	0.3080	0.6100	0.4604	
BC	1.19	1	1.19	2.35	0.1689	
A ²	33.96	1	33.96	67.25	< 0.0001	
B ²	9.25	1	9.25	18.32	0.0037	
C ²	7.29	1	7.29	12.46	0.0096	
Residual	3.53	7	0.5050			
Lack of Fit	3.53	3	1.18			
Pure Error	0.0000	4	0.0000			
Cor Total	792.97	16				

(A: temperature; B: time; C: % blending of jute stick in RS-JS mixture)

The R^2 , adjusted R^2 and predicted R^2 of the present model are 0.99, 0.98 and 0.94 respectively. From the analysis of the ANOVA table, it appears that the parameters, A (temperature), B (time) and A^2 (square of temperature) are the significant parameters. According to this analysis, % blending of jute stick in RS-JS mixture is not a significant parameter. Similar observation has been reported by previous researchers (Akalin et al, 2019).

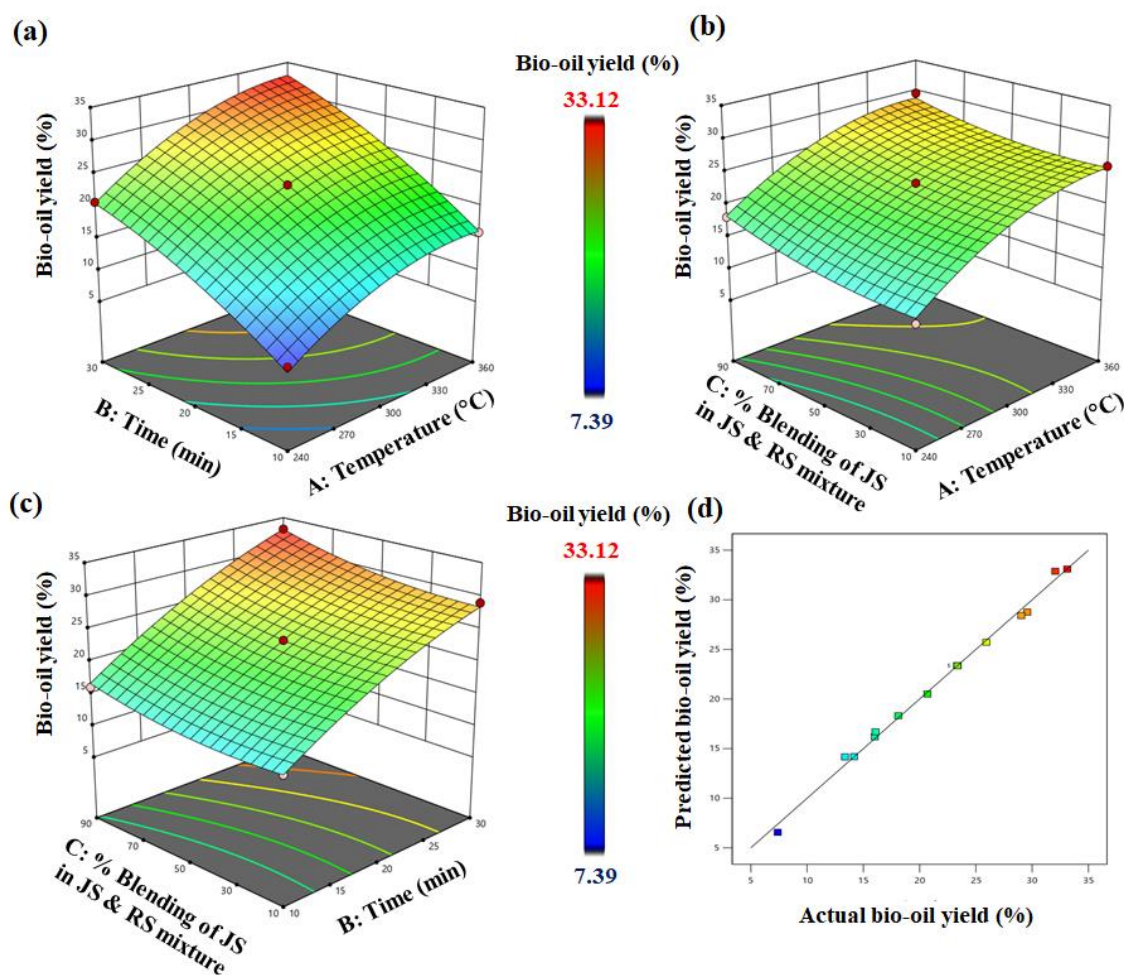


Fig. 7.13 Response surface plots for optimization of bio-oil (%) production from co-HTL of JS and RS (a: interaction between temperature and time; b: interaction between temperature and % blending of jute stick in RS-JS mixture; c: interaction between time and % blending of jute stick in RS-JS mixture; d: actual versus predicted response)

Three response surface 3D plots, representing the interaction between A-B, A-C and B-C, are shown in the Fig. 7.13 (a, b and c) respectively. From Figure 7.13a and 7.13b it is evident that

increment of temperature has a mixed impact (both positive and negative) for the formation of bio-oil. The initial increment of temperature has enhanced the bio-oil yield but after a certain point, the production of bio-oil has started to decrease. From the Fig. 7.13c, it is observed that the increase of time and % blending of jute stick in RS-JS mixture have a positive impact on the production of bio-oil from co-HTL of JS and RS. From the Fig. 7.13d, it is evident that the predicted and experimental values are in good agreement.

The optimum condition for the maximum yield of bio-oil from co-HTL of JS and RS has been reported in the Table 7.9.

Table 7.9 Model predicted and experimental values of the bio-oil yield from co-HTL of JS and RS under optimum condition

Run	A	B	C	% Yield of Bio-oil
Model Predicted	317.2	28.1	83.1	32.76
Experimental	317.2	28.1	83.1	32.85± 0.84

(A: Temperature (°C); B: Time (min) and C: % blending of jute stick in RS-JS mixture)

From Table 7.9, it is observed that the experimental result are in good agreement with the model predictions. It further establishes the fitness of the model. For the purpose of comparison, individual HTL of JS and RS has been conducted at the optimum condition of co-HTL. At the optimal condition of co-HTL (temperature: 317.2°C and holding time: 28.1 minutes) the yields of bio-oil of 34.14% and 30.73% have been obtained from JS and RS respectively. Therefore, the yield of bio-oil from co-HTL lies in between that of JS and RS.

7.4.11 HHV of bio-oil produced from co-HTL

At the optimal condition of co-HTL (temperature: 317.2°C and holding time: 28.1 minutes; % blending of jute stick in RS-JS mixture: 83.1%), the ultimate analysis of bio-oils obtained from individual and co-HTL have been conducted. The HHVs have also been determined. The values have been reported in the Table 7.10.

Table 7.10 Ultimate analysis and HHVs of bio-oils obtained from individual and co-HTL

Bio-oil sample	C (% w)	H (% w)	N (% w)	O (% w)	H/C	O/C	HHV (kJ/kg)
HTL-JS	68.01	7.01	1.05	23.93	1.24	0.26	28.74
HTL-RS	64.18	7.53	0.79	28.50	1.22	0.33	25.94
Co-HTL	67.79	7.97	1.04	24.20	1.23	0.26	28.56

From the analysis of the Table 7.10, it is observed that the HHV of bio-oil obtained from co-HTL of JS and RS (28.56 kJ/kg) is much greater than that of individual HTL of RS (25.94 kJ/kg) and is slightly less than individual HTL of JS (28.74 kJ/kg). It is also observed that HHV of bio-oil obtained from co-HTL (28.56 kJ/kg) is also greater than peat (21.33 kJ/kg) and lignite (24.45 kJ/kg) (the values of HHV of peat and lignite have been provided in the Table 7.6).

7.4.12 GC-MS analysis of Bio-oil obtained from individual and co-HTL

The main class of compounds present in bio-oils (obtained from HTL of JS, RS (at 317.2 °C for 28.1 minutes) and co-HTL of JS & RS (at 317.2 °C for 28.1 minutes and blending of jute stick in RS-JS mixture 83.1%)) have been shown in the Fig. 7.14. The distribution of class of compounds in the bio-oil, obtained from RS and JS is different. This is due to the fact that the lignocellulosic composition of JS and RS is different. As the RS is much richer in cellulose content, the abundance of aliphatic and cyclic compounds is higher. It has already been reported in the available literature that cellulose, being a homo-polymer of glucose, usually decomposes to ketones, aldehydes, furans, acids, esters, fatty acid alkyl esters, alcohols, and ether (Zhu et al, 2015). Compared to bio-oil obtained through individual HTL of RS, that of JS is much richer in aromatics and phenolic compounds which are usually generated from the decomposition of lignin. This can be justified by higher content of lignin in JS with respect to RS. From the analysis of the Figure 7.14, it appears that % area of GC-MS spectrum of bio-oil produced from co-HTL of JS and RS is dominated by phenolic compounds (45.59%) followed by aromatic (24.28%), cyclic (11.79%) and aliphatic (0.04%) compounds. More introspection is required to explain the distribution of compounds in the bio-oil from co-HTL.

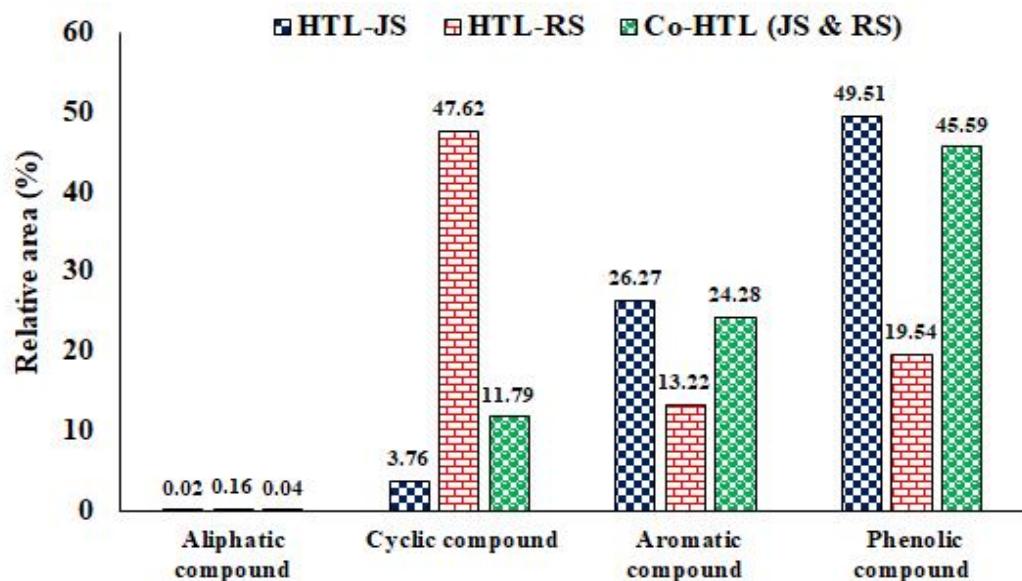


Fig. 7.14 Main class of compounds present in bio-oils

The GC-MS analysis of bio-oils have been provided in the Table 7.11, 7.12 and 7.13 respectively.

Table 7.11 List of major compounds present in bio-oil obtained from HTL of JS (at 317.2 °C for 28.1 minutes) from GC-MS analysis (R.T. stands for retention time in minute)

R.T.	Major compounds	Area (%)
2.1	2-Pentanone, 4-hydroxy-4-methyl-	3.83
2.5	Acetic acid	0.02
2.7	Furfural	2.42
3.3	2-Cyclopenten-1-one, 3-methyl-	1.62
3.5	2-Furancarboxaldehyde, 5-methyl-	4.21
3.9	2-Acetyl-5-methylfuran	1.19
5.5	2-Cyclopenten-1-one, 2-hydroxy, 3-methyl	2.14
5.7	Phenol, 2-methoxy-	9.01
7.3	Phenol, 2-methoxy-4-methyl-	4.33
7.6	Phenol	3.57
7.1	Phenol, 4-ethyl-2-methoxy-	7.87
7.2	Phenol, 2-methyl-	1.49
7.3	Phenol, 2-methoxy-4-propyl-	2.36

8.8	Phenol, 2-methoxy-4-(1-propenyl)-	5.01
9.8	2-Furancarboxaldehyde, 5-(hydroxy methyl)	3.42
10.1	Vanillin	12.8
10.3	Phenol, 2-methoxy-4-propyl-	4.07
10.5	Ethanone, 1-(4-hydroxy-3-methoxy-phenyl)	4.68
10.6	Benzeneacetic acid, 4-hydroxy-3-methoxy, methyl ester	7.49
	Total	79.53

Table 7.12 List of major compounds present in bio-oil obtained from HTL of RS (at 317.2 °C for 28.1 minutes) from GC-MS analysis

R.T.	Major compounds	Area (%)
2.1	2-Pentanone, 4-hydroxy-4-methyl-	1.93
2.5	Acetic acid	0.16
2.7	Furfural	3.97
3.5	2-Furancarboxaldehyde, 5-methyl-	4.01
3.9	2-Acetyl-5-methylfuran	2.02
4.8	2-cyclopenten-1-one, 2-methyl-	17.03
5.7	Phenol, 2-methoxy-	3.97
7.3	Phenol, 2-methoxy-4-methyl-	3.89
7.6	Phenol	3.01
7.1	Phenol, 4-ethyl-2-methoxy-	2.97
7.2	Phenol, 2-methyl-	0.59
7.3	Phenol, 2-methoxy-4-propyl-	1.04
8.4	2-cyclopenten-1-one, 2,3-dimethyl-	15.98
8.8	Phenol, 2-methoxy-4-(1-propenyl)-	3.01
9.7	2-cyclopenten-1-one, 2,3,4-trimethyl-	15.61
9.8	2-Furancarboxaldehyde, 5-(hydroxy methyl)	1.29
10.3	Phenol, 2-methoxy-4-propyl-	1.06
	Total	80.54

Table 7.13 List of major compounds present in bio-oil obtained from co-HTL of JS and RS at optimum condition (at 317.2 °C for 28.1 minutes and 83.1% blending of jute stick in RS-JS mixture) from GC-MS analysis

R.T.	Major compounds	Area (%)
2.1	2-Pentanone, 4-hydroxy-4-methyl-	3.49
2.5	Acetic acid	0.04
2.7	Furfural	2.83
3.3	2-Cyclopenten-1-one, 3-methyl-	3.79
3.5	2-Furancarboxaldehyde, 5-methyl-	4.31
3.9	2-Acetyl-5-methylfuran	1.31
4.8	2-cyclopenten-1-one, 2-methyl-	3.09
5.5	2-Cyclopenten-1-one, 2-hydroxy, 3-methyl	2.08
5.7	Phenol, 2-methoxy-	8.90
7.3	Phenol, 2-methoxy-4-methyl-	4.13
7.6	Phenol	3.45
7.1	Phenol, 4-ethyl-2-methoxy-	7.01
7.2	Phenol, 2-methyl-	1.33
7.3	Phenol, 2-methoxy-4-propyl-	2.19
8.8	Phenol, 2-methoxy-4-(1-propenyl)-	4.99
9.8	2-Furancarboxaldehyde, 5-(hydroxy methyl)	3.31
10.1	Vanillin	11.03
10.3	Phenol, 2-methoxy-4-propyl-	3.56
10.5	Ethanone, 1-(4-hydroxy-3-methoxy-phenyl)	4.97
10.6	Benzeneacetic acid, 4-hydroxy-3-methoxy, methyl ester	7.89
	Total	81.70

7.4.13 Effectiveness of dye (Congo red) removal by JS-Hydrochar

Color removal tests of Congo red dye (Hi-media, India), was conducted in batch mode. 50 mL of 50 mg/L aqueous dye solution and 50 mg hydrochar, obtained from HTL of JS at 360°C, were stirred in 100 mL beaker at 500 rpm in a magnetic stirrer at 30 °C. The pH and reaction time were varied from 3-11 and 30- 90 minutes respectively. Following the protocol of previous researchers, 0.1M HNO₃ and 0.1M KOH solution were used to adjust the pH of the dye solution (Rubangakene et al., 2023). After each batch time, the sample was taken and centrifuged at 6000 rpm for 10 minutes. The absorbance of the solution was determined at 498 nm. The known concentration of dye solution was calibrated against absorbance.

$$\text{Congo red removal (\%)} = \frac{C_i - C_f}{C_i} \times 100 \quad (7.17)$$

Where, C_i and C_f are the initial and final concentration of the Congo red.

From the Figure 7.15, it is evident that the Congo red removal (%) increases when reaction time has increased from 30 to 90 minutes. Whereas, the Congo red removal (%) decreases when the pH of the aqueous solution is increased from 3 to 11. The maximum Congo red removal has been determined as 87% at pH = 3 and stirring time of 90 minutes. From the results it is established that hydrochar, obtained from hydrothermal liquefaction of jute stick, could be efficiently used for Congo red dye removal.

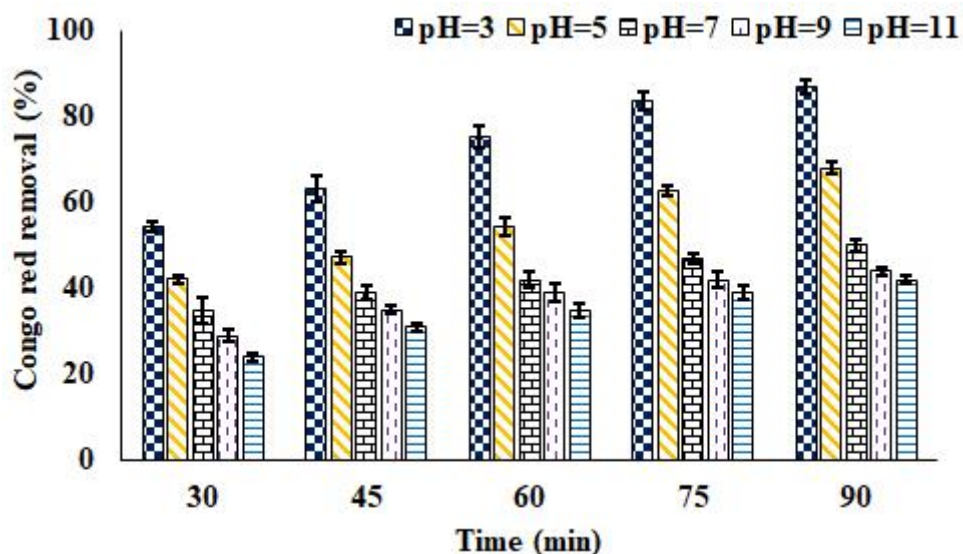


Fig. 7.15 Congo red removal (%) at different reaction time at different pH

The pseudo-second-order rate equation for adsorption kinetics, represented in Equation 7.18, has been attempted:

$$\frac{dq_t}{dt} = k_2(q_e - q_t)^2 \quad (7.18)$$

where t is time (in minutes), k_2 is the pseudo-second-order rate constant ($\text{g mg}^{-1} \text{min}^{-1}$), q_t is the amount of adsorbate adsorbed per unit mass of adsorbent at time t (mg g^{-1}) and q_e is the amount of adsorbate adsorbed at equilibrium (mg g^{-1}).

The concentration of adsorbate (dye) in the solid phase can be determined as follows:

$$q_t = \frac{(C_0 - C_t)V}{m} \quad (7.19)$$

Where, C_0 and C_t are the dye concentration in the aqueous phase at the beginning and at equilibrium (mg/L), V is the solution volume (L) of aqueous solution and m is the mass of adsorbent used (g).

Integration of 7.18 with the initial condition, $q = 0$ at $t = 0$, leads to the following:

$$\frac{t}{q_t} = \frac{1}{k_2 q_e^2} + \frac{t}{q_e} \quad (7.20)$$

From the experimental data, at $\text{pH}=3$, $\frac{t}{q_t}$ has been plotted against t in Figure 7.16.

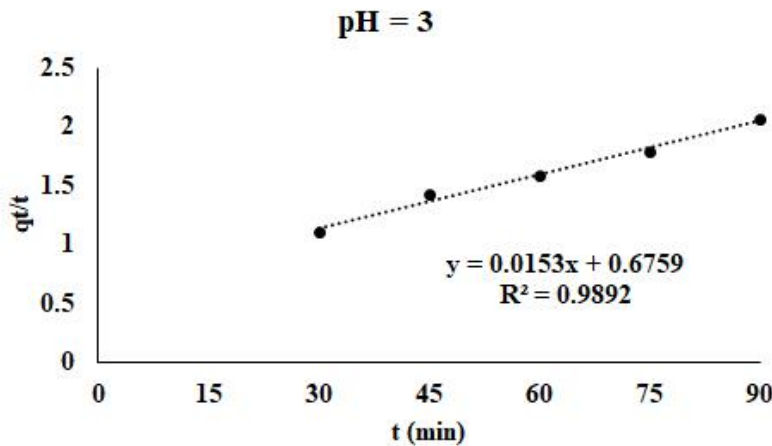


Fig. 7.16 Plot of $\frac{t}{q_t}$ versus t (the pH of the solution = 3)

The linearity of the plot validates the applicability of pseudo second order kinetics for adsorption of Congo red dye using hydrochar. This has also been observed for other studies using biochar (Bullen et al, 2021). The rate constant, k_2 and q_e have been determined by plotting $\frac{t}{q_t}$ against t . The

values of q_e and k_2 are 65.35 mg/g and 0.00034 mg g⁻¹ min⁻¹ respectively. The plot at pH 3 is shown in Figure 7.16.

More in-depth studies, like determination of isotherms etc. are required for the ultimate application of hydrochar as an adsorbent.

7.4.14 Comparison with available literature data

The findings of the present study (HTL of JS and RS) have been compared with the literature data for hydrothermal liquefaction of different lignocellulosic biomass such as soybean straw (SS), corn straw (CS), peanut straw (PS), barley straw (BS) and rice straw (RS). The comparison of the bio-oil yield obtained from hydrothermal liquefaction of different biomasses are reported in Table 7.14.

Table 7.14 Comparison the yield of bio-oil of present study with literature for HTL

Bio-mass	HTL Conditions	Composition of feedstock			Yield	Study
		Cellulose % (w)	Hemicellulose % (w)	Lignin % (w)	Bio-oil (%)	
SS	350°C, 60 min	27.25	20.28	29.57	21.6	I
CS	320°C, 60 min	30.81	25.50	16.76	7.9	II
PS	320°C, 60 min	36.56	20.27	18.36	14.7	III
BS	300°C, 15 min	46.00	23.00	15.00	34.5	IV
RS	350°C, 30 min	37.70	17.80	26.0	32.6	V
RS	317°C, 28 min	38.24	21.17	16.85	30.7	Present
JS	317°C, 28 min	31.67	15.99	32.77	34.1	Present

At 317.2 °C for 28.1 minutes, the yield of bio-oils obtained from individual HTL of JS and RS under present study, are measured as 34.14% and 30.73% respectively. The yield of products obtained from our study are comparable with literature data, as provided in Table 7.14 (Study-I (Wang et al, 2023; Study-II (Tian et al, 2020); Study-III (Tian et al, 2020); Study-IV (Zhu et al, 2015); and Study V (Harisankar et al,2022)).

The findings of the present investigation on co-HTL of JS and RS have been compared with the literature data for co-HTL on different pairs of feedstocks such as wheat straw (WS) and

eucalyptus (EU), EU and pinewood (PW), PW and WS, black pine wood (BPW) and Kukersite oil shell (KOS) (Sharma et al, 2024; Akalin et al, 2019) in Table 7.15. The comparison reveals that the yield of bio-oil obtained from present study is comparable with the data of co-HTL of BPW-KOS mixture and is higher than all others, available in the literature data, as provided in the table (Study-VI (Sharma et al, 2024); Study-VII (Sharma et al, 2024); Study-VIII (Sharma et al, 2024) and Study-IX (Akalin et al, 2019)).

Table 7.15 Comparison the % yield of bio-oil of present study with literature for co-HTL

HTL Conditions	Blending	Yield of bio-oil (%)	Study
400°C, 15 min	WS: EU = 50 : 50	17.6	VI
400°C, 15 min	EU: PW = 50 : 50	17.2	VII
400°C, 15 min	PW:WS = 50 : 50	22.1	VIII
300°C, 30 min	BPW: KOS = 66.7 : 33.3	31.8	IX
317 °C, 28 min	JS : RS = 83.1 : 16.9	32.8	Present study

(WS contains 37.9% cellulose, 26.8% hemicellulose and 18.3% lignin; EU contains 43.2% cellulose, 22.5% hemicellulose and 25.0% lignin; PW contains 43.6% cellulose, 24.9% hemicellulose and 25.6% lignin; BPW contains 48.51% α cellulose and 28.2% lignin; The composition of JS and RS have been provided in the Table 7.14)

Bio-oil can be considered as a renewable feedstock for the production of fuels and chemicals. The oxygen content of bio-oil (25% w/w) is high with respect to that of diesel which contains negligible quantity of oxygen (Azizian & Khosravi, 2019; McCarthy et al, 2011). As oxygen does not contribute towards heating value, its presence in any fuel is actually detrimental for its energy applications. Therefore, direct use of bio-oil as a substitute of fuel oil is not possible without de-oxygenation. The blending of bio-oil with petroleum crude is a better option and is useful for the production of different fuel cuts through further refining processes (Krutof & Hawboldt, 2016). The HHVs of bio-oil of rice straw and jute stick have been compared with literature data in Table 7.16. In the same table, the HHVs of bio-oil have been compared with that of petroleum crude.

Table 7.16 Comparison the HHV of bio-oil of present study with literature and Petroleum crude oil

Feedstock	Process parameters	HHV of bio-oil (MJ/kg)	Reference
Rice straw	350°C; 30 min	24.80	Harisankar et al, 2022
Corn stover	300°C; 60 min	30.77	Matankar et al, 2020
Soybean straw	320°C; 60 min	32.98	Tian et al, 2020
Barley straw	300°C; 15 min	27.40	Zhu et al, 2015
Petroleum crude oil	-	42 - 45	Ben et al, 2019
Rice straw	240-360°C, 30 min	22.9-27.3	Present study
Jute stick	240-360°C, 30 min	24.7-29.4	Present study

From the analysis of the Table 7.16 it is evident that the HHVs of bio-oil from rice straw and JS are in the same range compared to the reported literature data on ligno-cellulosic biomass (Matankar et al, 2020; Tian et al, 2020; Zhu et al, 2015 and Harisankar et al, 2022). The HHVs of bio-oil from both biomass (RS and JS) are much less than that of petroleum crude. This is due to the disparity in the oxygen content of petroleum crude which contains 2% oxygen — a value much lower than that of bio-oil (25%). From the literature data, it is evident that while the range of HHVs of bio-oil from different lignocellulosic biomass lies between 24.80 – 32.98 MJ/kg, the range of HHV of petroleum crude is 42.0 – 45.0 MJ/kg (Matankar et al, 2020; Tian et al, 2020; Zhu et al, 2015 and Harisankar et al, 2022). The HHVs of bio-oils obtained from individual HTL of JS and RS under present study vary from 24.7 MJ/kg to 29.4 MJ/kg and 22.9 MJ/kg to 27.3 MJ/kg as the HTL temperature is varied from 240°C to 300°C.

The HHVs of hydro-char, produced from HTL of JS and RS have been compared with the literature data for different lignocellulosic biomass, peat and lignite in Table 7.17.

Table 7.17 Comparison the HHV of hydrochar of present study with literature

Feedstock	Process parameters	HHV of hydrochar (MJ/kg)	Reference
Rice straw	350°C; 30 min	15.60	Harisankar et al, 2022

Corn stover	300°C; 30 min	21.97	Matankar et al, 2020
Barley straw	300°C; 15 min	27.40	Zhu et al, 2015
Peat	-	21.33	
Lignite	-	24.45	
Jute stick	240-360°C, 30 min	19.01 - 20.72	Present study
Rice straw	240-360°C, 30 min	18.22 - 20.61	Present study

The HHVs of hydrochar from RS and JS under the present study are comparable with literature data on hydrochar those from other lignocellulosic wastes. Although the HHV of hydrochar of RS is slightly less than peat and lignite, that of JS hydrochar is comparable. Thus, the hydrochar of both feedstocks, particularly JS, can act as a substitute of peat and lignite.

7.5 Summary

Through the present systematic study, a data base has been generated for the hydrothermal liquefaction of jute stick and jute stick -rice straw mixture in the temperature range of 240°C-360°C. for the first time. It has been established that the HHV of hydrochar of JS is higher than that of RS and lies in between the HHVs of peat and lignite. The HHVs of bio-oil from both JS and RS are less than petroleum crude. The bio-oil yield for co-HTL of JS and RS has been optimized with respect to time and temperature of HTL as well as JS:RS mass ratio in their mixture. It is observed that at optimum condition the HHV of bio-oil obtained from co-HTL of JS and RS is much higher than that obtained through individual HTL of RS and is slightly less than individual HTL of JS. It is expected that the results of HTL of JS and RS will open up a new arena in their application in bioenergy sector of India.

References

- Akalin, E., Kim, Y. M., Alper, K., Oja, V., Tekin, K., Durukan, I., & Karagöz, S. (2019). Co-hydrothermal liquefaction of lignocellulosic biomass with Kukersite oil shale. *Energy & Fuels*, 33(8), 7424-7435.
- Akbarian, A., Andooz, A., Kowsari, E., Ramakrishna, S., Asgari, S., & Cheshmeh, Z. A. (2022). Challenges and opportunities of lignocellulosic biomass gasification in the path of circular bioeconomy. *Bioresource Technology*, 362, 127774.
- Asadullah, M., Rahman, M. A., Ali, M. M., Motin, M. A., Sultan, M. B., Alam, M. R., & Rahman, M. S. (2008). Jute stick pyrolysis for bio-oil production in fluidized bed reactor. *Bioresource technology*, 99(1), 44-50.
- Azizian, S., & Khosravi, M. (2019). Advanced oil spill decontamination techniques. In *Interface Science and Technology* (Vol. 30, pp. 283-332). Elsevier.
- Ben, H., Wu, F., Wu, Z., Han, G., Jiang, W., & Ragauskas, A. J. (2019). A comprehensive characterization of pyrolysis oil from softwood barks. *Polymers*, 11(9), 1387.
- Bullen, J. C., Saleesongsom, S., Gallagher, K., & Weiss, D. J. (2021). A revised pseudo-second-order kinetic model for adsorption, sensitive to changes in adsorbate and adsorbent concentrations. *Langmuir*, 37(10), 3189-3201.
- Chandra, R., Takeuchi, H., & Hasegawa, T. (2012). Hydrothermal pretreatment of rice straw biomass: a potential and promising method for enhanced methane production. *Applied Energy*, 94, 129-140.
- Chowdhury, R., Ghosh, S., Debnath, B., & Manna, D. (2018). Indian agro-wastes for 2G biorefineries: Strategic decision on conversion processes. *Sustainable Energy Technology and Policies: A Transformational Journey, Volume 1*, 353-373.
- Chowdhury, R., Ghosh, S., Manna, D., Das, S., Dutta, S., Kleinsteuber, S., Strauber, Hassan, M. K., Kuittinen, S., & Pappinen, A. (2019). Hybridization of sugar-carboxylate-syngas platforms for the production of bio-alcohols from lignocellulosic biomass (LCB)—A state-of-the-art review and recommendations. *Energy conversion and management*, 200, 112111.

- De Caprariis, B., De Filippis, P., Petrullo, A., & Scarsella, M. (2017). Hydrothermal liquefaction of biomass: Influence of temperature and biomass composition on the bio-oil production. *Fuel*, 208, 618-625.
- Harisankar, S., Mohan, R. V., Choudhary, V., & Vinu, R. (2022). Effect of water quality on the yield and quality of the products from hydrothermal liquefaction and carbonization of rice straw. *Bioresource Technology*, 351, 127031.
- Hassan, M. K., Chowdhury, R., Ghosh, S., Manna, D., Pappinen, A., & Kuittinen, S. (2021). Energy and environmental impact assessment of Indian rice straw for the production of second-generation bioethanol. *Sustainable Energy Technologies and Assessments*, 47, 101546.
- Kopperi, H., & Mohan, S. V. (2023). Catalytic hydrothermal deoxygenation of sugarcane bagasse for energy dense bio-oil and aqueous fraction acidogenesis for biohydrogen production. *Bioresource Technology*, 379, 128954.
- Krutof, A., & Hawboldt, K. (2016). Blends of pyrolysis oil, petroleum, and other bio-based fuels: a review. *Renewable and Sustainable Energy Reviews*, 59, 406-419.
- Kuittinen, S., Hietaharju, J., Bhattarai, I., Hassan, M. K., Kupiainen, L., Kangas, J., J. Tanskanen & Pappinen, A. (2022). Technoeconomic analysis and environmental sustainability estimation of bioalcohol production from barley straw. *Biocatalysis and Agricultural Biotechnology*, 43, 102427.
- Kumar, R. (2022). A review on the modelling of hydrothermal liquefaction of biomass and waste feedstocks. *Energy Nexus*, 5, 100042.
- Leng, S., Leng, L., Chen, L., Chen, J., Chen, J., & Zhou, W. (2020). The effect of aqueous phase recirculation on hydrothermal liquefaction/carbonization of biomass: A review. *Bioresource technology*, 318, 124081.
- Mathanker, A., Pudasainee, D., Kumar, A., & Gupta, R. (2020). Hydrothermal liquefaction of lignocellulosic biomass feedstock to produce biofuels: Parametric study and products characterization. *Fuel*, 271, 117534.

McCarthy, P., Rasul, M. G., & Moazzem, S. (2011). Analysis and comparison of performance and emissions of an internal combustion engine fuelled with petroleum diesel and different bio-diesels. *Fuel*, 90(6), 2147-2157.

Rubangakene, N. O., Elwardany, A., Fujii, M., Sekiguchi, H., Elkady, M., & Shokry, H. (2023). Biosorption of Congo Red dye from aqueous solutions using pristine biochar and ZnO biochar from green pea peels. *Chemical Engineering Research and Design*, 189, 636-651.

Shaaban, A., Se, S. M., Dimin, M. F., Juoi, J. M., Husin, M. H. M., & Mitan, N. M. M. (2014). Influence of heating temperature and holding time on biochars derived from rubber wood sawdust via slow pyrolysis. *Journal of Analytical and Applied Pyrolysis*, 107, 31-39.

Sharma, K., Shah, A. A., Toor, S. S., Seehar, T. H., Pedersen, T. H., & Rosendahl, L. A. (2021). Co-hydrothermal liquefaction of lignocellulosic biomass in supercritical water. *Energies*, 14(6), 1708.

Sluiter, A., Hames, B., Ruiz, R., Scarlata, C., Sluiter, J., Templeton, D., & Crocker, D. L. A. P. (2008). Determination of structural carbohydrates and lignin in biomass. *Laboratory analytical procedure*, 1617(1), 1-16.

Tian, Y., Wang, F., Djandja, J. O., Zhang, S. L., Xu, Y. P., & Duan, P. G. (2020). Hydrothermal liquefaction of crop straws: Effect of feedstock composition. *Fuel*, 265, 116946.

Usman, M., Chen, H., Chen, K., Ren, S., Clark, J. H., Fan, J., & Zhang, S. (2019). Characterization and utilization of aqueous products from hydrothermal conversion of biomass for bio-oil and hydro-char production: a review. *Green chemistry*, 21(7), 1553-1572.

Vaishnavi, M., Kumar, K. S., & Gopinath, K. P. (2023). Comparative studies on catalytic hydrothermal liquefaction of mixed household waste into bio crude. *Biomass Conversion and Biorefinery*, 13(15), 14253-14265.

Vashishtha, M., & Patidar, K. (2021). Property enhancement of mustard stalk biomass by Torrefaction: characterization and optimization of process parameters using response surface methodology. *Materials Science for Energy Technologies*, 4, 432-441.

Wang, Z. C., Hou, X. K., Wang, Y. B., Collins, E., & Duan, P. G. (2023). Hydrothermal liquefaction of soybean straw: Effect of steam explosion pretreatment and reaction media. *Fuel*, 339, 127418.

Waters, C. L., Janupala, R. R., Mallinson, R. G., & Lobban, L. L. (2017). Staged thermal fractionation for segregation of lignin and cellulose pyrolysis products: An experimental study of residence time and temperature effects. *Journal of analytical and applied pyrolysis*, 126, 380-389.

Yin, S., & Tan, Z. (2012). Hydrothermal liquefaction of cellulose to bio-oil under acidic, neutral and alkaline conditions. *Applied Energy*, 92, 234-239.

Zhu, Z., Rosendahl, L., Toor, S. S., Yu, D., & Chen, G. (2015). Hydrothermal liquefaction of barley straw to bio-crude oil: Effects of reaction temperature and aqueous phase recirculation. *Applied Energy*, 137, 183-192.

Chapter 8

Torrefaction of mustard stalk

Chapter 8: Torrefaction of mustard stalk

As discussed in Chapter 3 the torrefaction of mustard stalk has been focused following the objectives incorporated under aim 4. These are as follows:

- Determination of lumped and Distributed Activation Energy kinetics of torrefaction of mustard stalk through semi-batch experiments in pyrolyser and in TGA respectively
- Biochar and Bio-oil are characterized
- Life cycle analysis of torrefaction of mustard stalk is conducted using SIMAPRO

Mustard stalk is also a post-harvesting residue. The mustard stalk is one of the Indian agro-wastes which can be used for energy generation. The production of mustard stalk in India 12841 kiloton (Chowdhury et al, 2018). As it is completely dry in nature, this feedstock is considered for torrefaction.

8.1 Experimental methods

The semi-batch torrefaction process for mustard stalk was conducted in a 35 mm diameter and 210 mm long reactor, already existing in the laboratory. The existing reactor was indigenously designed by the supervisor along with previous research scholars of the laboratory and was manufactured by S. C. Dey & Co, Kolkata. The schematic diagram of the experimental setup of torrefaction of mustard stalk is illustrated in the Fig. 8.1.

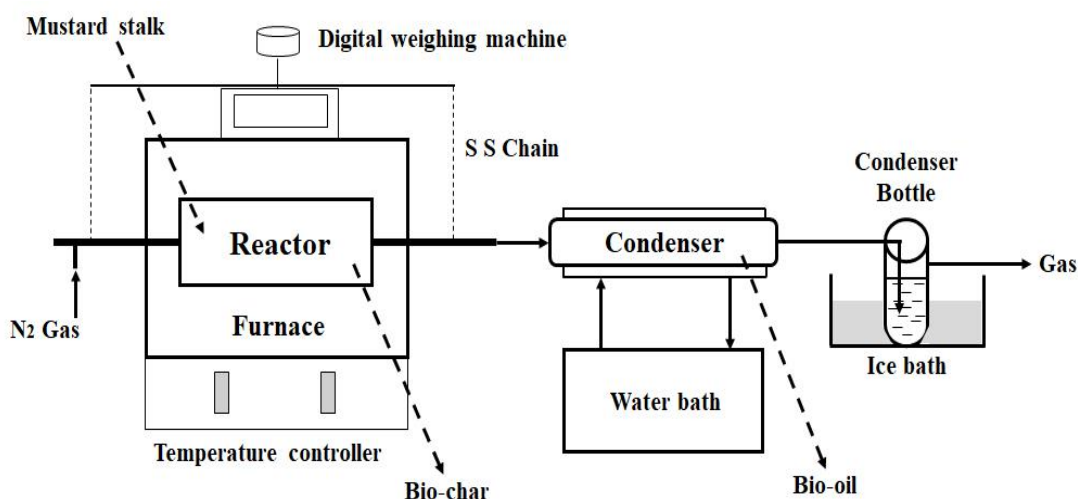


Fig.8.1 Schematic diagram of experimental setup of torrefaction of mustard stalk

The torrefaction was carried out under isothermal conditions in the temperature range of 200°C – 400°C, in an inert atmosphere maintained by the continuous flow of nitrogen for a duration of 30 minutes. The experimental setup included a reactor equipped with a furnace, a precise temperature controller utilizing a PID controller, and a digital weight box. The experiment was conducted with 10 g mustard stalk (on dry basis). The volatile products exited from the pyrolyser passed through a condenser through which cooling water at 20°C was circulated. Upon completion of the experiments, the reactor was allowed to naturally cool to room temperature (30°C). The solid product, i.e., biochar, resulting from torrefaction, was recovered from the reactor. The condensable volatiles from the condenser were collected as liquid product and the non-condensable volatiles were collected as gaseous product of torrefaction.

The yields of biochar, bio-oil, and gaseous products have been determined using the following equations:

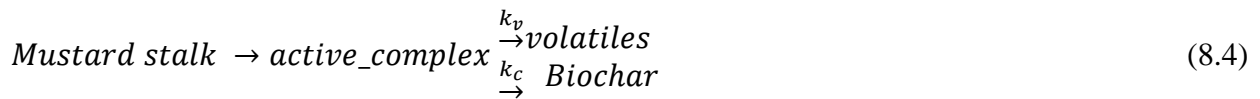
$$\% \text{ Yield of biochar} = \frac{\text{mass of biochar obtained from torrefaction}}{\text{mass of biomass fed to the reactor}} \times 100 \quad (8.1)$$

$$\% \text{ Yield of bio – oil} = \frac{\text{mass of bio–oil obtained from torrefaction}}{\text{mass of biomass fed to the reactor}} \times 100 \quad (8.2)$$

$$\% \text{ Yield of gaseous product} = 100 - \text{Yields of (biochar + bio – oil)} \quad (8.3)$$

8.2 Lumped kinetics of torrefaction of jute stick

The reaction pathway, considering parallel degradation reactions forming solid product (char) and volatiles (oil and gas) has been represented by Equation (8.4) as follows



Therefore, the differential mass balance equations are as follows:

$$\frac{dW}{dt} = -(k_c + k_v)W = -kW \quad (8.5)$$

$$\frac{dW_c}{dt} = k_c W = k_c W_0 \exp(-kt) \quad (8.6)$$

$$\frac{dW_v}{dt} = k_v W = k_v W_0 \exp(-kt) \quad (8.7)$$

Where $k = k_c + k_v$

The values of rate constants k , k_v , k_c and k at different temperatures have been determined using regression analysis of following equations (8.8), (8.9) and (8.10) respectively,

$$W(t) = W_0 \exp(-kt) \quad (8.8)$$

$$\left(\frac{W_v(t)}{W_0}\right) = \left(\frac{k_v}{k}\right)[1 - \exp(-kt)] \quad (8.9)$$

$$\left(\frac{W_c(t)}{W_0}\right) = \left(\frac{k_c}{k}\right)[1 - \exp(-kt)] \quad (8.10)$$

Using the experimental data on the residual solid mass after different holding time at different temperature values of k have been determined by plotting $\ln\left(\frac{W_0}{W}\right)$ against reaction time, t . The plot has been shown in Figure 8.3. The values of k_v and k_c have been determined from the slopes by plotting W_v and W_c against $\left[\frac{W_0}{k}[1 - \exp(-kt)]\right]$. The plots have been shown in Figure 8.4.

8.3 Distributed activation energy model

The TG results can be demonstrated as a function of conversion (α)

$$\alpha = \frac{m_i - m_t}{m_i - m_f} \quad (8.11)$$

where m_i and m_f are the initial and final mass of sample respectively, whereas m_t represents the instantaneous solid mass. The conversion rate ($d\alpha/dt$) of solids can be illustrated as

$$\frac{d\alpha}{dt} = \beta \frac{d\alpha}{dT} = k(T) \times f(\alpha) \quad (8.12)$$

where β is the heating rate (dT/dt , °C/min); $k(T)$ refers to the reaction rate constant; $f(\alpha)$ is the kinetic model function. According to Arrhenius equation $k(T)$ can be expressed as –

$$k(T) = A e^{-\frac{E_a}{RT}} \quad (8.13)$$

where A is known as the pre-exponential factor (min^{-1}) and E_a is the apparent activation energy (kJ mol^{-1}). R is the universal gas constant ($8.314 \text{ J (mol} \cdot \text{K)}^{-1}$) and T is the absolute temperature (K). At constant heating rate, combining Equations (8.12) and (8.13) yields

$$\frac{d\alpha}{dT} = \frac{A}{\beta} e^{-\frac{E_a}{RT}} f(\alpha) \quad (8.14)$$

$$g(\alpha) = \int_0^\alpha \frac{d\alpha}{f(\alpha)} = \frac{A}{\beta} \int_{T_0}^T e^{-\frac{E_a}{RT}} dT = \frac{AE_a}{\beta R} \int_x^\alpha \frac{e^{-x}}{x^2} dx = \frac{AE_a}{\beta R} p(x) \quad (8.15)$$

$$\text{Where, } p(x) = \int_x^\alpha \frac{e^{-x}}{x^2} dx \quad (8.16)$$

An estimation of the Arrhenius temperature integral was reported by Tang et al. (2003) as follows

$$p(x) = \frac{e^{-x}}{x} \left(\frac{1}{1.001989x + 1.873912} \right) \quad (8.17)$$

The relation between heating rate and inverse temperature takes the following form

$$\ln \left(\frac{\beta}{T^{1.894661}} \right) = -1.00145033 \left(\frac{E_a}{RT} \right) + C \quad (8.18)$$

Where C is a constant and equals to

$$\ln \left(\frac{AE_a}{Rg(\alpha)} \right) + 3.63504095 - 1.894661 \ln(E_a) \quad (8.19)$$

The E_a values has been determined through the slope of $-1.000145033E_a/R$ over straight lines of $\ln \left(\frac{\beta}{T^{1.894661}} \right)$ versus $\frac{1}{T}$ over a series of α . Frequency factor has been evaluated by inserting E_a values in equation 8.19.

8.4 Thermodynamic Analysis

The thermodynamic analysis was conducted utilizing data derived from TGA-DTG analysis and kinetic parameters determined following the method developed by Tang. The analytical methodology employed in this study aligns with the equations specified in the works of Liu et al. (2021) and Ali et al. (2021). The enthalpy change (ΔH), Gibbs free energy change (ΔG), and entropy change (ΔS) have been calculated by using the equations below:

$$\Delta H = E_a - RT_\alpha \quad (8.20)$$

$$\Delta G = E_a + RT_m \ln \left(\frac{k_B T_m}{hA} \right) \quad (8.21)$$

$$\Delta S = \frac{\Delta H - \Delta G}{T_m} \quad (8.22)$$

where E_a is the activation energy; T_α is the temperature at a particular α ; T_m is the highest temperature at which extreme mass loss occurs; k_B is the Boltzmann constant (1.381×10^{-23} J/K); and h is the Planck constant (6.626×10^{-34} J s).

8.5 Results and discussion

8.5.1 Composition of mustard stalk

The cellulose (%), hemicellulose (%) and lignin (%) present in mustard stalk have been determined as 37.19 ± 0.72 , 28.31 ± 0.63 and 15.56 ± 0.21 respectively.

8.5.2 Yield of product

In Fig. 8.2, the yield of biochar, bio-oil and gaseous product have been plotted against torrefaction temperature of mustard stalk. The yield of biochar decreases from 67.91% - 34.33 % when the temperature is increased from 200 to 400°C. The maximum bio-oil yield is 21.32% at 300°C. The yield of gas increases from 20.31% - 44.75 % when the temperature is increased from 200 to 400°C.

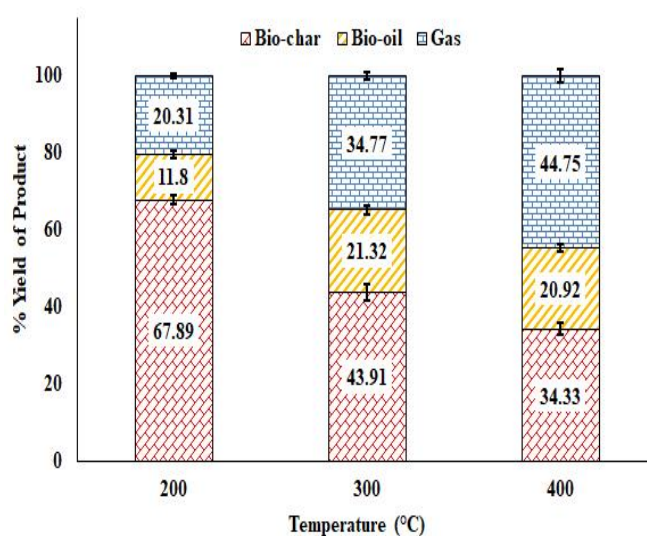


Fig. 8.2 Yield of products at different temperature (for 30 minutes reaction time)

It is observed that with increase in temperature, the yield of biochar decreases. The yield of bio-oil increases when the temperature is increased from 200 to 300°C and beyond 300°C, the yield of bio-oil decreases. Beyond 300°C, a part of bio-oil is converted to gaseous fraction and as a result the yield of oil decreases. The yield of gaseous product increase with rise in temperature.

8.5.3 Kinetic parameters

8.5.3.1 Parameters used for lumped kinetics

The kinetic parameters of torrefaction of mustard stalk have been determined using the experimental data obtained after different holding time (5, 10, 15, 20, 25 and 30 minutes) at each reaction temperature (200, 300 and 400°C).

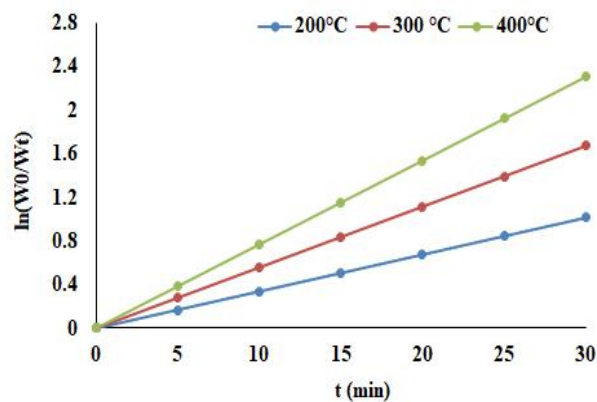


Fig. 8.3 Plot of $\ln\left(\frac{W_0}{W}\right)$ versus time

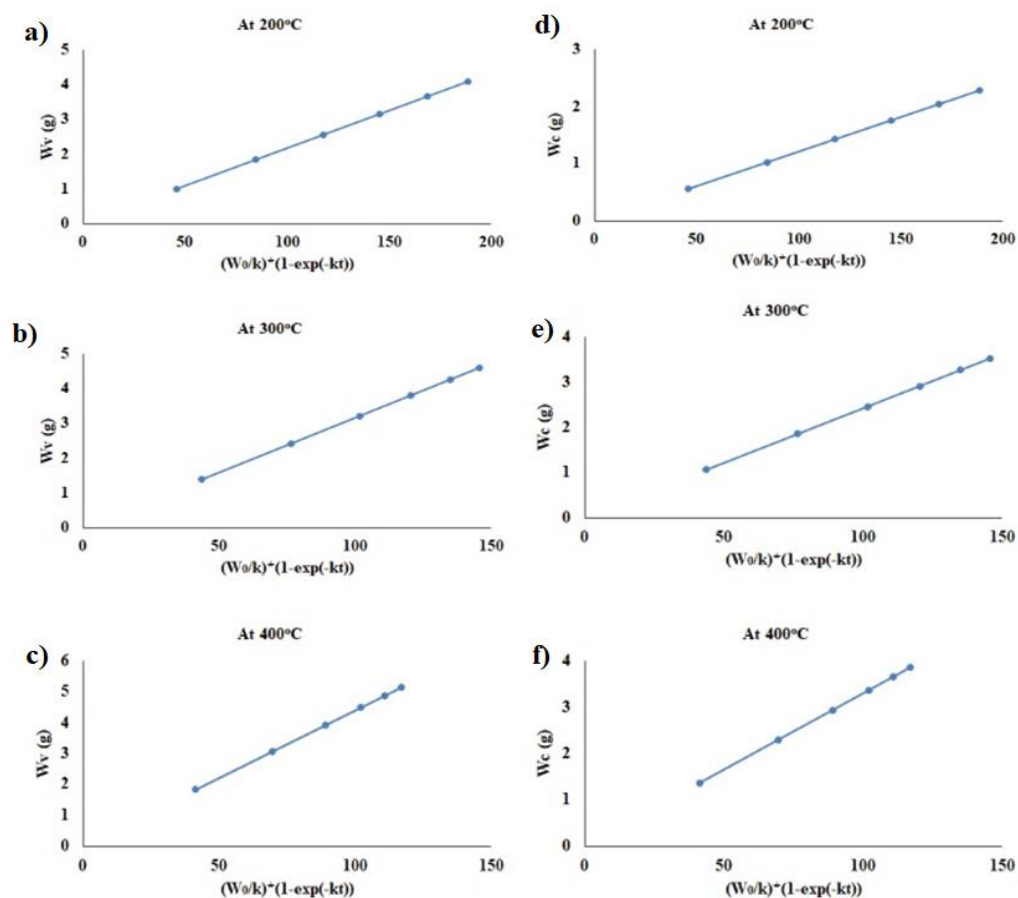


Fig. 8.4 Plot of W_v versus $[\frac{W_0}{k}[1 - \exp(-kt)]]$ at 200°C, 300 °C and 400 °C (a, b and c) and Plot of W_c versus $[\frac{W_0}{k}[1 - \exp(-kt)]]$ at 200°C, 300 °C and 400 °C (d, e and f)

All the rate constants involved in the torrefaction of mustard stalk at different temperatures have been determined and reported in the Table 8.1.

Table 8.1 Values of rate constants involved in the torrefaction of mustard stalk

Rate constant	At 200 °C	At 300 °C	At 400 °C
$k(\text{min}^{-1})$	0.0338	0.0558	0.0769
$k_v (\text{min}^{-1})$	0.0217	0.0316	0.0439
$k_c (\text{min}^{-1})$	0.0121	0.0242	0.0330

Arrhenius equation has been used to determine activation energy and frequency factor, as follows:

$$k_i = k_{oi} \exp\left(\frac{-E_i}{RT}\right) \quad (8.23)$$

k_i = rate constant of i^{th} reaction; k_{oi} = pre – exponential factor of i^{th} reaction ;

E_i = Activation energy of i^{th} reaction;

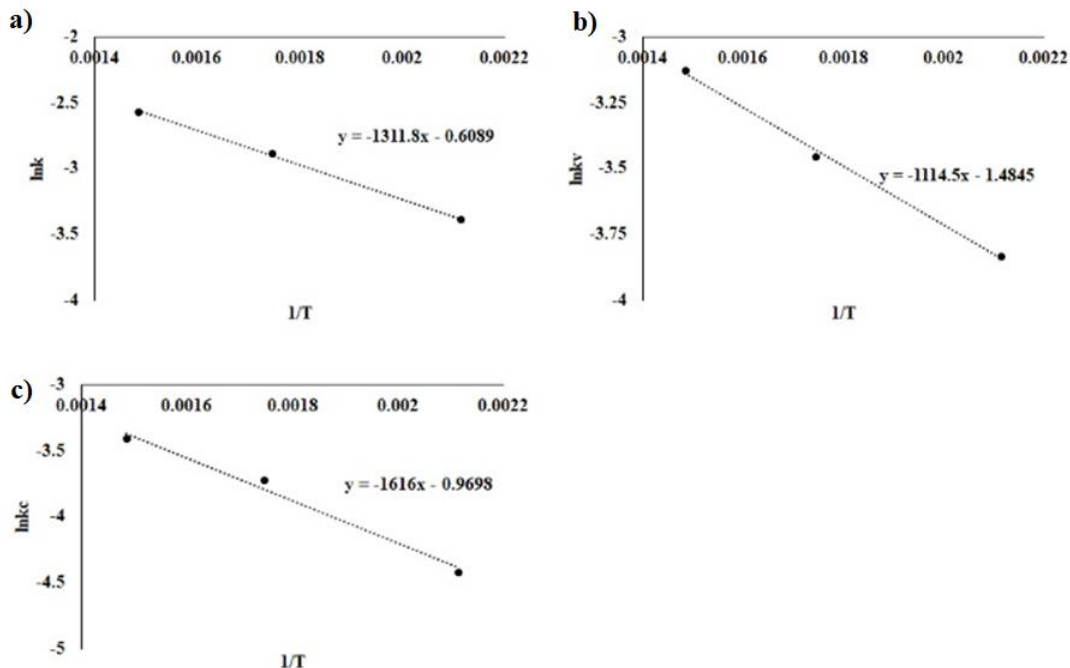


Fig. 8.5 Plot of $\ln k$ versus $1/T$ (a); Plot of $\ln k_v$ versus $1/T$ (b) and Plot of $\ln k_c$ versus $1/T$ (c)

The values of activation energies and pre-exponential factors have been determined by plotting $\ln(k_i)$ against the inverse of temperature in kelvin ($1/T$) (shown in the Fig 8.5). The values of activation energies and pre-exponential factors of all rate constants of torrefaction of mustard stalk have been represented in the Table 8.2.

Table 8.2 Activation energies and pre-exponential factors of rate constants for torrefaction and HTL reactions

Rate constant (min^{-1})	Activation energy (kJ/mol)	Pre-exponential factors (min^{-1})	R^2 value
k	10.91	0.5439	0.9973
k_v	9.26	0.2266	0.9942
k_c	13.43	0.3791	0.9865

8.5.3.2 Evaluation of kinetic parameters for distributed activation energy model and thermodynamic triplets

TGA plots of raw-mustard stalk at different heating rate have been shown in Figure 8.6. Figure 8.7a illustrates the linear fitting results obtained for the torrefaction of MS. Parallel straight lines have been obtained with satisfactory regression coefficients i.e., 0.92–0.99. The overall high R^2 value for $\alpha > 0.05$ signifies the activation energies obtained via the analysis are reliable. The profile of the family of curves vividly displays the evolution of the thermal degradation process with an increase in the heating rate. Notably, in Fig. 8.7a that the gap between the lines is more pronounced in the range $\alpha = 0.1$ to 0.3 , indicating a slow conversion rate MS torrefaction. This suggests that at lower temperatures, the energy levels are insufficient to initiate the breakage of molecular bonds. As the temperature gradually rises, it becomes adequate to break the molecular bonds, resulting in the emergence of parallel straight lines beyond the conversion of 0.25 .

Parallel straight lines has been obtained in the 0.3 to 0.7 conversion range. This parallel alignment of lines implies that the activation energies for these reactions are closely distributed, indicating a

relatively uniform reaction mechanism in this range. However, as α surpasses 0.7, the parallel alignment of straight lines begins to diverge. This divergence suggests the possibility of different torrefaction reactions occurring compared to those in the intermediate range (i.e., $\alpha = 0.3$ – 0.7).

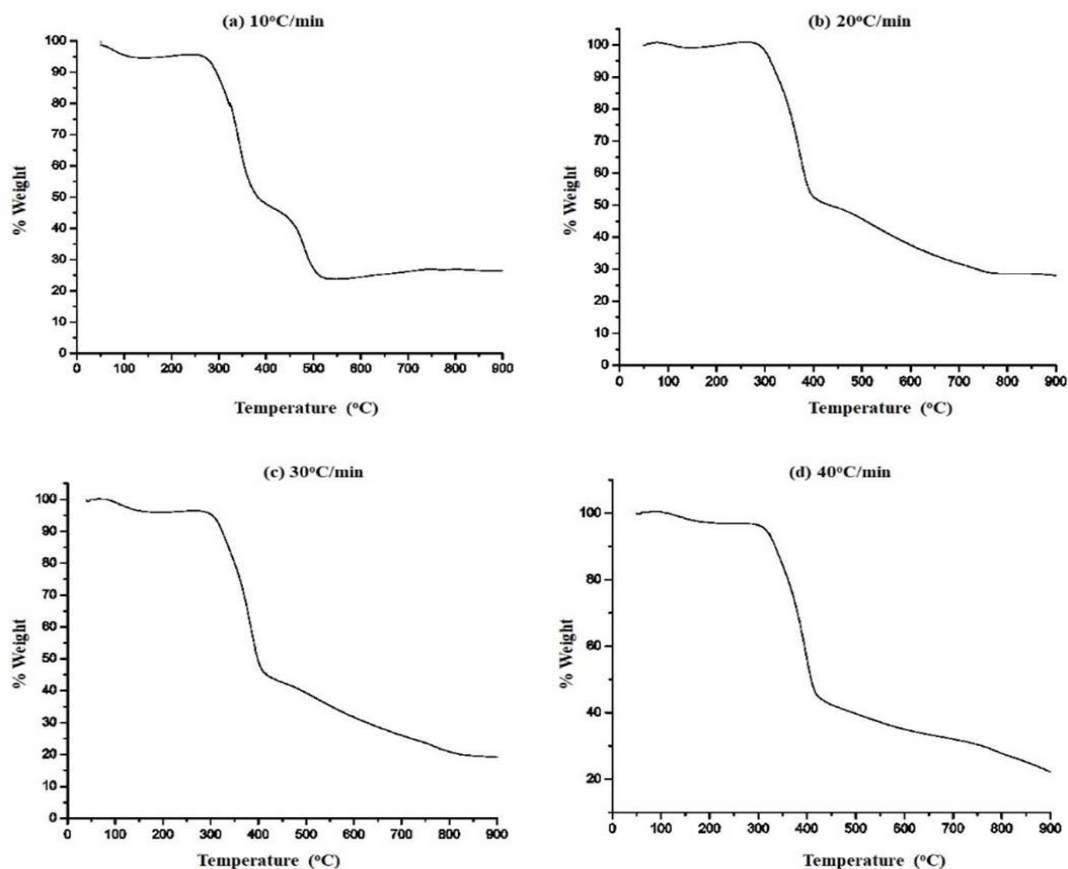


Fig. 8.6 TGA plot of raw-mustard stalk at different heating rate (a: 10 °C/min; b: 20 °C/min; c: 30 °C/min; d: 40 °C/min)

Fig.8.7b display the development of E_a with the conversion for MS torrefaction. In the initial conversion zone ($\alpha = 0.1 - 0.25$), the activation energy values remain relatively constant, hovering around 122 to 123 kJ/mol. After that, a prominent increase in the E_a value is observed signifying a change in the torrefaction dynamics. At $\alpha = 0.3$, the E_a value increases to 130.23 kJ/mol, only to follow an exponentially decreasing profile till $\alpha = 0.6$ (109.31 kJ/mol). The peak at $\alpha = 0.3$ is indicative of the destruction of hemicellulose. The subsequent decline in E_a values in the range of 0.3 to 0.6 can be attributed to the decomposition of cellulose (Werner et al. 2014). With the advancement in the torrefaction process lignin decomposition becomes more pronounced, as the E_a values exhibit an exponential increase, reaching 166.18 kJ/mol at $\alpha = 0.85$. It is important to

note that for $\alpha > 0.85$, the E_a values become less reliable, as this phase corresponds to a stage of passive pyrolysis (Gajera et al. 2022). The values activation energies are in a similar range with a similar research on mustard stalk where KAS and FWO methods were used with a lesser reported value of $R^2 = 0.88-0.94$ (Nawaz and Kumar, 2021).

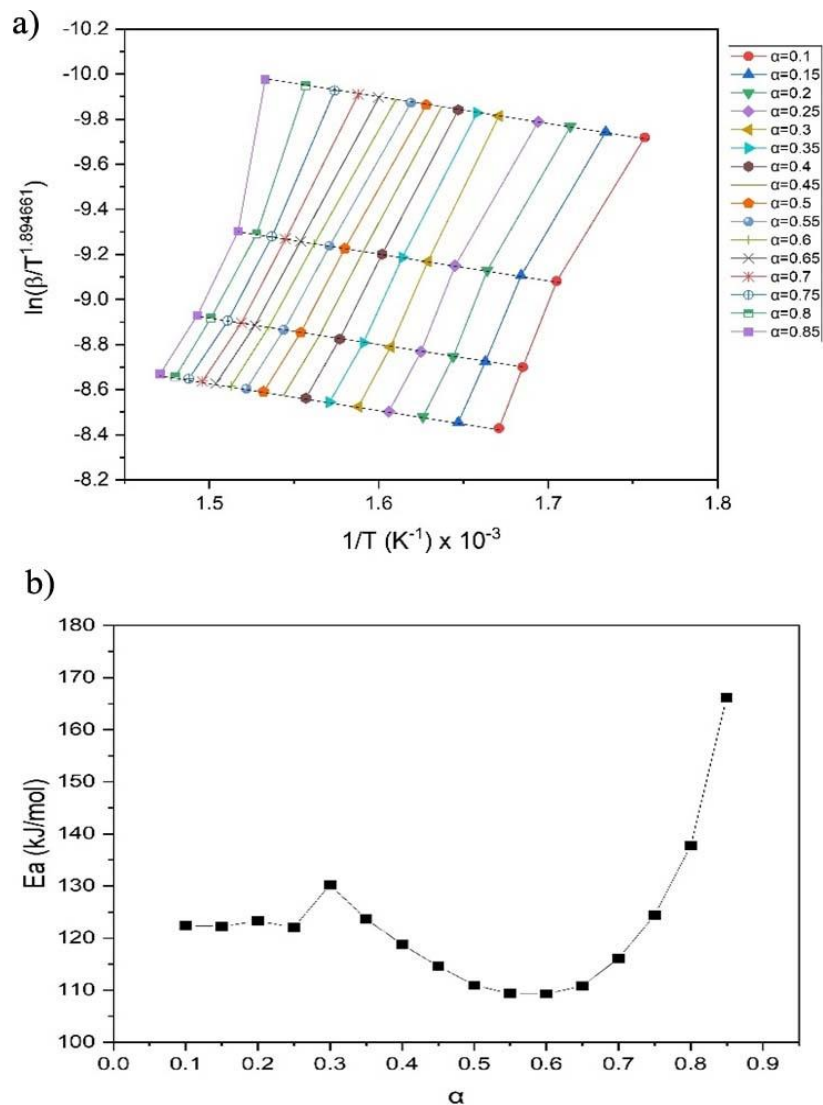


Fig. 8.7 (a): Kinetic Plot for determination of kinetic parameters using Tang method and (b) Evolution trend of Activation Energies against for Mustard Stalk (MS) Torrefaction

The pre-exponential factor or the frequency factor and thermodynamic triplets at four heating rates have been estimated as per equation 18-20. The results at $\beta = 10$ K/min are shown in Tables 8.3.

Table 8.3 Thermodynamic Triplets and Pre-exponential Factors for MS Pyrolysis at $\beta=10\text{K/min}$

α	T α (K)	A (s ⁻¹)	ΔH (kJ/mol)	ΔG (kJ/mol)	ΔS (J/mol)
0.05	560.61	1.15×10^8	127.55	191.7	-104.18
0.1	569.44	1.76×10^7	117.69	191.53	-119.92
0.15	577	1.83×10^7	117.44	191.15	-119.71
0.2	584.09	2.26×10^7	118.43	191.11	-118.03
0.25	590.46	1.68×10^7	117.2	191.44	-120.59
0.3	598.73	8.05×10^7	125.26	191.56	-107.68
0.35	603.21	2.03×10^7	118.68	192.08	-119.22
0.4	607.21	4.24×10^6	113.71	195.15	-132.27
0.45	610.98	3.13×10^6	109.53	192.55	-134.84
0.5	614.46	1.50×10^6	105.83	192.65	-141.02
0.55	617.84	1.11×10^6	104.25	192.65	-143.57
0.6	621.23	1.27×10^6	104.15	191.87	-142.47
0.65	625.15	1.48×10^6	105.6	192.57	-141.24
0.7	629.84	4.16×10^6	110.89	192.62	-132.74
0.75	635.46	2.03×10^7	119.12	192.8	-119.65
0.8	642.61	2.45×10^8	132.37	193.35	-99.04
0.85	652.57	4.69×10^{10}	160.76	194.91	-55.47

The frequency factor (A) represents a fundamental kinetic parameter, the significance of which is directly linked to the intricacy and reactivity of the feedstock under consideration. The values of A have been found in the range of 10^6 to 10^{10} s^{-1} within the conversion range of 0.05–0.85. For the first-order reaction, the values of A can vary from 10^4 to 10^{18} s^{-1} . Hence, the order of torrefaction of mustard stalk could be analytically classified as a first-order (Maia et al. 2016).

At constant pressure, the change in enthalpy (ΔH) is a thermodynamic state function that indicates the heat received or released (Ali et al. in 2021). In the early conversion zone ($\alpha < 0.35$) high energy is required for torrefaction of mustard stalk to dissociate the bonds with enthalpy values around

127.55 kJ/mol and the lowest being 117.2 kJ/mol. During this period, this high energy demand can be attributed to removal of remaining moisture and dissociation of potential barriers of complex bonds present in mustard stalk. Whereas for $0.35 < \alpha < 0.7$; less energy is required for torrefaction of mustard stalk as the enthalpy values declines to 104.15 kJ/mol. For $\alpha > 0.7$; enthalpy value increases as the process starts approaching the pyrolysis zone, reaching ~ 161 kJ/mol.

Gibbs free energy (ΔG) plays a pivotal role in determining the overall change in energy required for the reactants to transition into an activated complex. A higher value of ΔG indicates a less favourable reaction (Mian et al. in 2019). The ΔG values are in the range of 191 – 195 kJ/mol. This range of values signifies external heat source is required for torrefaction of mustard stalk.

8.5.4 Proximate analysis of biochar

The proximate analysis of raw-mustard stalk (MS) and biochar (obtained at 300°C) have been reported in the Table 8.4. The fuel ratio (FR) of raw-mustard stalk and biochar are 0.21 and 0.29 respectively.

Table 8.4 Proximate analysis of raw-mustard stalk and biochar

Type	VM (% w)	FC (% w)	Ash (% w)	FR
Raw MS	77.98	16.32	5.79	0.21
Biochar	73.52	22.05	4.43	0.29

(VM: Volatile matter; FC: Fixed carbon)

Where fuel ratio (FR) has been defined as

$$FR = \frac{\text{Fixed carbon}}{\text{Volatile matter}} \quad (8.24)$$

8.5.5 Elemental analysis of biochar and bio-oil

The elemental analysis (carbon, hydrogen, nitrogen, and oxygen), higher heating value (HHV), energy densification ratio (EDR) and energy yield (EY) of biochar and bio-oil obtained through torrefaction of mustard stalk (MS) at 300°C, have been reported in Table 8.5.

Table 8.5 Elemental analysis of raw-mustard stalk, biochar and bio-oil

Type	C (% w)	H (% w)	N (% w)	O (% w)	HHV (MJ/kg)	EDR	EY (%)
Raw MS	44.52	5.59	0.79	49.10	14.25	-	-
Biochar	51.12	4.68	1.84	42.36	16.37	1.14	50.05
Bio-oil	54.32	5.89	1.06	38.73	19.85	1.39	29.63

$$\text{Where, Energy densification ratio (EDR)} = \frac{\text{Higher heating value of char}}{\text{Higher heating value of biomass}} \quad (8.25)$$

$$\text{Energy yield (EY)(\%)} = \text{The yield of product (\%)} \times \text{EDR} \quad (8.26)$$

The HHV of raw MS, biochar and bio-oil have been measured as 14.25 MJ/kg, 16.37 MJ/kg and 19.85 MJ/kg respectively. The values of energy yield (EY) of biochar and bio-oil are 50.05% and 29.63% respectively.

8.5.6 Thermal stability analysis of biochar

The thermogravimetric curves of mustard stalk and biochar (obtained at 300°C) have been shown in Fig 8.8a. The weight loss of raw-MS in Stage I (50 – 290 °C), Stage II (291 – 370 °C), Stage III (371– 689 °C) and stage IV (690– 900 °C) have been measured as 0.2%, 45.9%, 23.9% and 1.8% respectively. The weight loss of biochar in Stage I (50 – 290 °C), Stage II (291 – 370 °C) and Stage III (371– 900 °C) have been determined as 4.8%, 2.8% and 38.7% respectively. It has been reported in a recent literature, the decomposition of hemicellulose, cellulose and lignin occur at the temperature range of 220 – 315 °C, 300 – 400 °C and 150 – 900 °C respectively (Water et al, 2017).

8.5.7 FTIR analysis of biochar

The FTIR analysis of raw mustard stalk, biochar (obtained at 300°C) have been shown in the Fig. 8.8b. The peaks within 4000-400 cm⁻¹ region have been analysed. The absorption peaks at 3330, 2879 and 1030 cm⁻¹ indicate O – H, C – H and C – O stretching respectively. The areas under the stretch of biochar are less than the raw mustard stalk. The lowering of O-H, C-H and C-O peaks

signify increase of hydrophobicity and decrease in ether and carboxylic bonds, present in hemicelluloses.

8.5.8 XRD analysis of biochar

The XRD analysis of raw biomass, biochar (obtained at 300 °C) have been shown in the Fig. 8.8c. The characteristic peaks have been observed at 18.5° and 22.5°C. The peaks for biochar are almost flat. This phenomenon signifies that the crystalline structure of cellulose is disrupted.

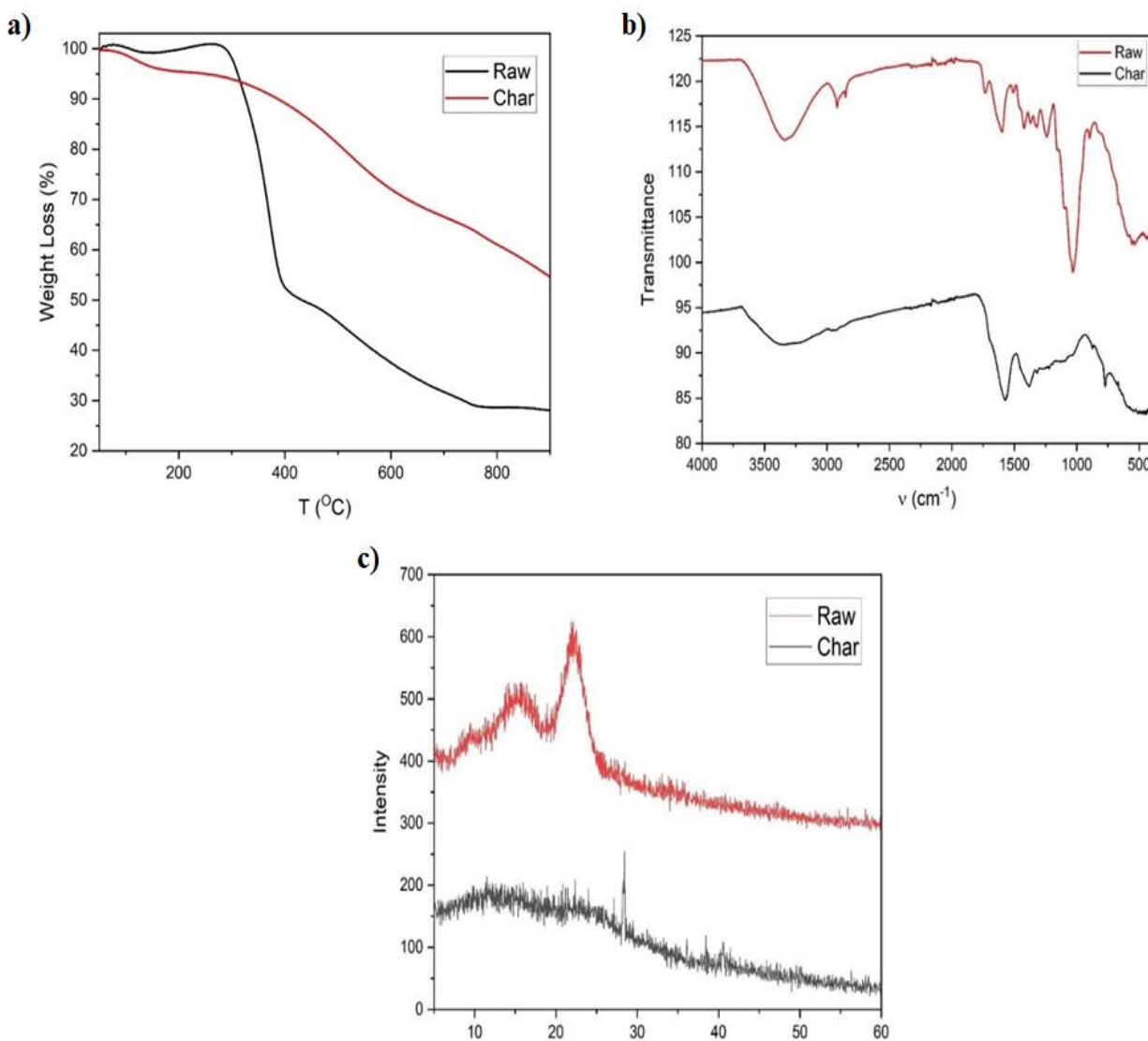


Fig. 8.8 TGA analysis of raw-MS and biochar (a); FTIR analysis of raw-MS and biochar (b); XRD analysis of raw-MS and biochar (c)

8.5.9 FESEM analysis of biochar

In the Fig. 8.9, the FESEM of mustard stalk and biochar (obtained at 300 °C) have been shown. The surface of untreated mustard stalk is smooth. The thermal cracks have been generated when mustard stalk is subjected to torrefaction. The thermal cracks appear due to the cell disruption of cellulose and hemicellulose.

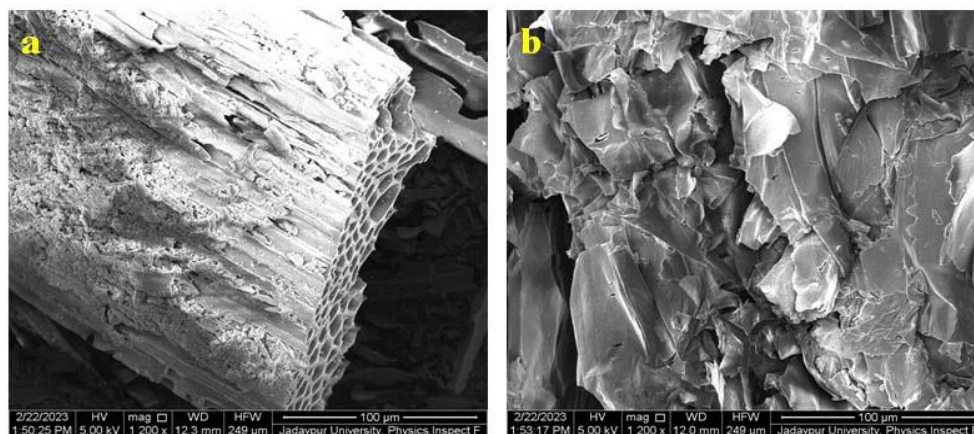


Fig. 8.9 FESEM analysis of raw-MS and biochar (a: raw-mustard stalk, b: biochar)

8.5.10 GC-MS analysis of bio-oil

Main class of compounds present in bio-oil obtained from torrefaction of mustard stalk at 300 °C, are shown in the Fig. 8.10. Aliphatic and cyclic compounds are being produced from the decomposition of hemicellulose and cellulose present in mustard stalk. Whereas, the aromatic and phenolic compounds formed during decomposition of lignin. The % area occupied by aliphatic, cyclic, aromatic and phenolic compounds, have been determined as 25.70, 12.82, 12.91 and 20.41.

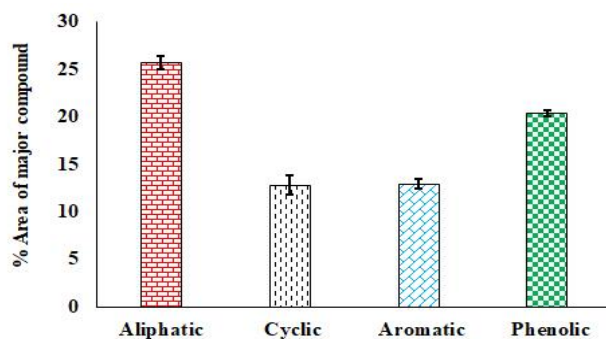


Fig. 8.10 Main class of compounds present in bio-oil obtained from torrefaction of mustard stalk

The GC-MS results of bio-oil has been provided in the Table 8.6.

Table 8.6 List of major compounds present in bio-oil (produced from torrefaction of mustard stalk at 300°C) from GC-MS analysis

R.T.	Major compounds	Area (%)
2.5	Acetic acid	25.7
2.7	Furfural	0.01
3.3	2-Cyclopenten-1-one, 3-methyl-	6.31
3.5	2-Furancarboxaldehyde, 5-methyl-	6.72
3.9	2-Acetyl-5-methylfuran	4.59
5.5	2-Cyclopenten-1-one, 2-hydroxy, 3-methyl	6.51
5.7	Phenol, 2-methoxy-	1.39
6.3	Phenol, 2-methoxy-4-methyl-	0.98
6.6	Phenol	3.75
7.1	Phenol, 4-ethyl-2-methoxy-	1.32
7.2	Phenol, 2-methyl-	0.60
7.3	Phenol, 2-methoxy-4-propyl-	1.14
8.8	Phenol, 2-methoxy-4-(1-propenyl)-	0.61
9.6	Guaiacol	2.80
10.1	Vanillin	1.96
10.3	Phenol, 2-methoxy-4-propyl-	1.24
10.5	Ethanone, 1-(4-hydroxy-3-methoxy-phenyl)	5.98
	Total	71.64

8.5.11 Life cycle analysis

8.5.11.1 LCA Methodology

The ISO 14040 series, clearly disseminates the four steps of life cycle assessment (LCA) – goal and scope definition, life cycle inventory (LCI), life cycle impact assessment (LCIA), and interpretation, which are based on the environmental life cycle assessment approach (ISO14044, 2006). This study follows the generic guidelines of LCA as described by the ISO 14040 standards.

8.5.11.2 Goal & Scope Definition

The environmental impact of the mustard stalk torrefaction process has been assessed using LCA in SimaPro V 9.1 software. The temperature sensitivity of the impacts are also within the scope of this study. The functional unit considered here was 1 kg of torrefied mustard stalk. A cradle-to-gate approach was considered while preparing the inventory and a substitutional approach has been taken to deal with the multi-functionality of the process. The system boundary of the processes considered in the LCA are provided in Fig.8.11.

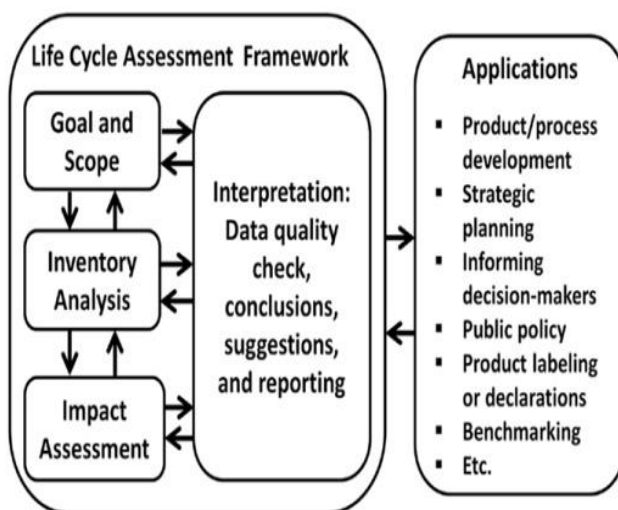


Fig.8.11 System Boundary of LCA of Mustard Stalk Torrefaction

8.5.11.3 Life Cycle Inventory Analysis (LCI)

The inventory data of this process has been collected from the current experimental setup. A transportation of the mustard stalk from the collection point to the torrefaction facility has been assumed to be 30 km. Land requirement for the torrefaction process has been collected from Adam et al. (2015) after proper interpolation according to the plant capacity of the present study. Electricity for the process has been taken to be supplied from the Indian country mix of the eastern zone. This data has been taken from the eco-invent data bank, already available in the SimaPro software. The inventory of the process has been provided in the supplementary section.

8.5.11.4 Life Cycle Impact Assessment (LCIA)

Life Cycle Impact Assessment (LCIA) aims to assess the potential environmental impacts by utilizing data derived from the LCI phase. The evaluation process was conducted using the

ReCiPe2016 Midpoint (H) and Endpoint (H) version 1.04 through Simapro software version 9.1. ReCiPe 2016 Midpoint method represents the most current indicator approach available in LCA analysis (Huijbregts et al. 2016). This method encompasses an extensive array of 18 midpoint impact categories, encompassing factors such as human carcinogenic toxicity, non-carcinogenic toxicity, particulate matter formation, ionizing radiation, ozone formation affecting human health, among others. These midpoint impact categories are later consolidated into three endpoint categories, reflecting the specific damages they cause—human health, ecosystem, and resources. This comprehensive classification offers a holistic view of the environmental implications linked with the evaluated systems and processes within the LCA framework.

8.5.11.5 LCA Results

The overall impact of the torrefaction process assessed following the ReCiPe 2016 Midpoint (H) method for different temperatures has been listed in Table 8.7.

Table 8.7 Midpoint impacts of the torrefaction process at different temperatures

Impact category	Unit	Torrefaction Temperature		
		200°C	300°C	400°C
Global warming	kg CO ₂ eq	1.543	3.494	5.237
Stratospheric ozone depletion	kg CFC11 eq	4.134E-7	9.366 E-7	1.403 E-6
Ionizing radiation	kBq Co-60 eq	0.004	0.009	0.013
Ozone formation, Human health	kg NO _x eq	0.004	0.008	0.012
Fine particulate matter formation	kg PM _{2.5} eq	0.004	0.009	0.014
Ozone formation, Terrestrial ecosystems	kg NO _x eq	0.004	0.008	0.012
Terrestrial acidification	kg SO ₂ eq	0.005	0.012	0.017
Freshwater eutrophication	kg P eq	0.001	0.002	0.003
Marine eutrophication	kg N eq	4.619 E-5	1.047 E-4	1.571 E-4
Terrestrial ecotoxicity	kg 1,4-DCB	1.221	2.625	3.878
Freshwater ecotoxicity	kg 1,4-DCB	0.031	0.069	0.104
Marine ecotoxicity	kg 1,4-DCB	0.042	0.094	0.141
Human carcinogenic toxicity	kg 1,4-DCB	0.064	0.146	0.219

Human non-carcinogenic toxicity	kg 1,4-DCB	1.395	3.153	4.725
Land use	m ² a crop eq	0.392	0.889	1.333
Mineral resource scarcity	kg Cu eq	0.001	0.001	0.002
Fossil resource scarcity	kg oil eq	0.415	0.939	1.407
Water consumption	m ³	0.005	0.010	0.016

The results show an increasing trend of the environmental impacts as temperature is increased. The GHG potential of the process is calculated to vary between 1.543-5.237 kg CO₂equivalent. The results are at par to the results presented by Christoforou and Fokaides, (2016). Lower values of GHG emission has been found to be reported in the work of Zhang et al. (2022). Main contributor to the GHG emission in the present study is the transportation of the mustard stalk from collection point to the torrefaction facility. Fig. 8.12 shows the normalized endpoint impacts of the torrefaction process at different temperatures. The normalized endpoint impacts are considerably low in each of the categories. However, the impact on human health is higher than on resources and ecosystem.

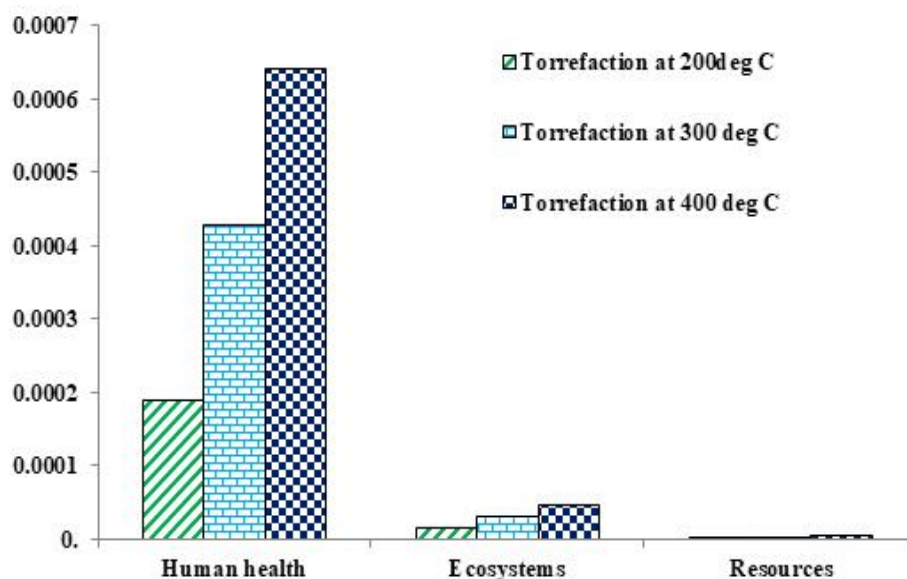


Fig. 8.12 Comparing Torrefaction at different temperatures Method: ReCiPe 2016 Endpoint (H) V1.04 / World (2010) H/H / Normalization

8.6 Summary

An extensive study of torrefaction of mustard stalk has been performed in the present study. Yields of char and bio-oil have been determined in the temperature range of 200-400 °C. The highest oil yield has been determined to be 21.32% at 300°C beyond which a decreasing trend is observed with the rise in temperature and it drops to 20.92% at 400°C mainly due to secondary cracking. Parameters used for lumped kinetic and distributed activation energy model of torrefaction of mustard stalk have been determined. The structural characterization of bio-char confirms porous morphology indicating its potential applications as an adsorbent. The higher heating values of bio-char and bio-oil, obtained at 300°C are 16.37 MJ/kg and 19.85 MJ/kg citing the energy potential of the products. The values of energy yield (EY) of biochar and bio-oil are 50.05% and 29.63% respectively. The environmental impact of the mustard stalk torrefaction process has also been assessed using life cycle analysis. It is expected that the results of torrefaction of mustard stalk will open up a new arena for the application of this agro-waste and similar feed-stocks in the bioenergy sector of India.

References

- Ali, I., Tariq, R., Naqvi, S. R., Khoja, A. H., Mehran, M. T., Naqvi, M., & Gao, N. (2021). Kinetic and thermodynamic analyses of dried oily sludge pyrolysis. *Journal of the Energy Institute*, 95, 30-40.
- Chowdhury, R., Ghosh, S., Debnath, B., & Manna, D. (2018). Indian agro-wastes for 2G biorefineries: Strategic decision on conversion processes. *Sustainable Energy Technology and Policies: A Transformational Journey, Volume 1*, 353-373.
- Chowdhury, R., Ghosh, S., Debnath, B., & Manna, D. (2018). Indian agro-wastes for 2G biorefineries: Strategic decision on conversion processes. *Sustainable Energy Technology and Policies: A Transformational Journey, Volume 1*, 353-373.
- Chowdhury, R., Ghosh, S., Manna, D., Das, S., Dutta, S., Kleinstuber, S., Strauber, Hassan, M. K., Kuittinen, S., & Pappinen, A. (2019). Hybridization of sugar-carboxylate-syngas platforms for

the production of bio-alcohols from lignocellulosic biomass (LCB)—A state-of-the-art review and recommendations. *Energy conversion and management*, 200, 112111.

Dinçer, H., Yüksel, S., & Çağlayan, Ç. (2023). Generating Appropriate Policies to Minimize Environmental Pollution in Developing Countries. In *Economic, Environmental and Health Consequences of Conservation Capital: A Global Perspective* (pp. 15-28). Singapore: Springer Nature Singapore.

Gajera, B., Tyagi, U., Sarma, A. K., & Jha, M. K. (2022). Impact of torrefaction on thermal behavior of wheat straw and groundnut stalk biomass: Kinetic and thermodynamic study. *Fuel Communications*, 12, 100073.

Ghorbannezhad, P., Soleymani, N., & Abbasi, M. (2023). Co-pyrolysis of municipal and horticultural wastes for enhanced biochar and bio-oil production: a response surface methodology approach. *Fuel*, 350, 128795.

Hassan, M. K., Chowdhury, R., Ghosh, S., Manna, D., Pappinen, A., & Kuittinen, S. (2021). Energy and environmental impact assessment of Indian rice straw for the production of second-generation bioethanol. *Sustainable Energy Technologies and Assessments*, 47, 101546.

Inthalaeng, N., Gao, Y., Remón, J., Dugmore, T. I., Ozel, M. Z., Sulaeman, A., & Matharu, A. S. (2023). Ginger waste as a potential feedstock for a zero-waste ginger biorefinery: a review. *RSC Sustainability*, 1(2), 213-223.

Jagadale, M., Gangil, S., & Jadhav, M. (2023). Enhancing fuel characteristics of jute sticks (*Corchorus Sp.*) using fixed bed torrefaction process. *Renewable Energy*, 215, 118992.

Khan, A. K., & Chowdhury, R. (2021). Parametric sensitivity of municipal solid waste integrated power plant: CO₂ footprint and energy analysis. *Chemical Engineering & Technology*, 44(2), 291-299.

Liu, J., Jiang, Q., Wang, H., Li, J., & Zhang, W. (2021). Catalytic effect and mechanism of in-situ metals on pyrolysis of FR4 printed circuit boards: insights from kinetics and products. *Chemosphere*, 280, 130804.

Maia, A. A. D., & de Moraes, L. C. (2016). Kinetic parameters of red pepper waste as biomass to solid biofuel. *Bioresource technology*, 204, 157-163.

- Mian, I., Li, X., Jian, Y., Dacres, O. D., Zhong, M., Liu, J., & Rahman, N. (2019). Kinetic study of biomass pellet pyrolysis by using distributed activation energy model and Coats Redfern methods and their comparison. *Bioresource technology*, 294, 122099.
- Nawaz, A., & Kumar, P. (2021). Pyrolysis of mustard stalk: evaluation of optimum process parameters, kinetic and thermodynamic study. *Bioresource Technology*, 340, 125722.
- Nawaz, A., & Kumar, P. (2021). Pyrolysis of mustard stalk: evaluation of optimum process parameters, kinetic and thermodynamic study. *Bioresource Technology*, 340, 125722.
- Priya, A. K., Alagumalai, A., Balaji, D., & Song, H. (2023). Bio-based agricultural products: a sustainable alternative to agrochemicals for promoting a circular economy. *RSC Sustainability*, 1(4), 746-762.
- Ru, B., Wang, S., Dai, G., & Zhang, L. (2015). Effect of torrefaction on biomass physicochemical characteristics and the resulting pyrolysis behavior. *Energy & Fuels*, 29(9), 5865-5874.
- Saleh, T. A. (2022). Nanomaterials and hybrid nanocomposites for CO₂ capture and utilization: environmental and energy sustainability. *RSC advances*, 12(37), 23869-23888.
- Shaaban, A., Se, S. M., Dimin, M. F., Juoi, J. M., Husin, M. H. M., & Mitan, N. M. M. (2014). Influence of heating temperature and holding time on biochars derived from rubber wood sawdust via slow pyrolysis. *Journal of Analytical and Applied Pyrolysis*, 107, 31-39.
- Sluiter, A., Hames, B., Ruiz, R., Scarlata, C., Sluiter, J., Templeton, D., & Crocker, D. L. A. P. (2008). Determination of structural carbohydrates and lignin in biomass. *Laboratory analytical procedure*, 1617(1), 1-16.
- Waters, C. L., Janupala, R. R., Mallinson, R. G., & Lobban, L. L. (2017). Staged thermal fractionation for segregation of lignin and cellulose pyrolysis products: An experimental study of residence time and temperature effects. *Journal of analytical and applied pyrolysis*, 126, 380-389.
- Werner, K., Pommer, L., & Broström, M. (2014). Thermal decomposition of hemicelluloses. *Journal of Analytical and Applied Pyrolysis*, 110, 130-137.

Xiaorui, L., Jiamin, Y., & Longji, Y. (2023). Predicting the high heating value and nitrogen content of torrefied biomass using a support vector machine optimized by a sparrow search algorithm. *RSC advances*, 13(2), 802-807.

Chapter 9

Conclusions and Future Scope

Chapter 9: Conclusions and Future Scope

As outlined in Chapter-1 the research studies have been conducted on I) conversion of rice straw to ethanol via sugar platform with possible analysis of each step along with kinetic analysis, mathematical modeling and optimization; II) conversion of rice straw to ethanol via syngas platform with possible analysis of each step along with kinetic analysis, mathematical modeling and optimization; III) conversion of rice straw and jute stick through HTL and co-HTL with kinetic studies and optimization; IV) conversion of mustard stalk through with kinetic studies and product characterization. The salient findings of the present research are as follows:

9.1 Ethanol product from rice straw through sugar platform

- The analysis of hydrolysate and the pretreated solid clearly indicate the most efficient action of FCP in comparison to acid pretreatment in the present range of temperature.
- The maximum yield (g of product/ kg of rice straw) of glucose, xylose, furfural, 5-HMF, formic acid, acetic acid and levulinic acid have been determined as 93.1, 145.0, 52.5, 9.4, 7.4, 17.0 and 5.67 from 0.1 M ferric chloride treatment of rice straw at 180°C for 10 minutes respectively.
- The degradation rate constants of xylan and glucose for rice straw for LWP, SAP and FCP have been compared for the first time.
- From this study it is clear that the yields of all hydrolysis products, namely, xylose, glucose, acetic acid, furfural, 5-HMF, levulinic acid and formic acid are enhanced during FCP. As the amount of furfural and 5-HMF, produced in case of FCP, is high they can be utilized as fuel additives and the use of the hydrolysate part for ethanol production is not recommended due to their inhibitory effects.
- As furfural, 5-HMF and levulinic acid contents increase monotonically with the increase in temperature during FCP, one can strategize to focus on these products in the hydrolysate and production of glucose from the pretreated straw only. Although the degradation rates of xylan and glucan are slow in case of LWP, effectiveness of water points towards its utilization as a green solvent for mild pretreatment in this temperature zone and beyond by allowing more reaction time.
- From the research outcome it is clear that the treatment time and hence the energy expenditure can be saved to a great extent by using FCP instead of conventionally followed

SAP. Although the pretreatment time requirement and hence the energy expenditure is much higher, LWP is also attractive from the environmental perspective.

- The glucose yields after 72 hours of enzymatic hydrolysis of untreated RS and pretreated solids (obtained from LWP, SAP and FCP) are determined as 27.9%, 32.3%, 45.4% and 78.9% respectively.
- A deterministic mathematical model for conversion of xylan and cellulose into xylose and glucose (and valuable products) for ferric chloride pretreatment of Indian rice straw has also been developed and validated for the first time.
- A deterministic mathematical model for enzymatic hydrolysis has also been developed.
- The effect of combined severity and enzyme loading on the yield of glucose have been investigated.
- The yields of ethanol (kg ethanol / kg of rice straw) through LWP, SAP and FCP (0.1M FeCl₃) pretreatment of rice straw have been measured as 0.0444, 0.0609 and 0.0899 respectively. 0.0851 kg ethanol has been produced from 1 kg of rice straw when 0.2M FeCl₃ solution has been used for pretreatment.
- It is clear from the study that FCP can play a vital role to implement the concept of biorefinery using abundantly available Indian agro-waste, namely, rice straw for the production of ethanol, furfural, 5-HMF and levulinic acid as the main products.
- The outcomes of this study would be quite worthwhile and can be used in scaling up of hydronium ion-driven pretreatment of LCB for the production of bio-fuels and bio-chemicals.

9.2 Ethanol product from rice straw through syngas platform

The salient findings of ethanol production from rice straw through syngas platform are as follows:

- Deterministic mathematical models along with experimental data on the bioconversion of pyro-syngas to ethanol and acetic acid in a gas-sparged stirred tank reactor, operated in semi-batch and continuous modes, have been reported for the first time.
- The locally isolated clostridial consortium *UACJUCheI* was proved to be capable of utilizing CO, CO₂, and H₂ present in the pyro-syngas.
- The mathematical models have been validated through the comparison of the predictions with the experimental results.

- The optimization of the performance of the semi-batch and continuous modes of operation was achieved using response surface methodology.
- The optimum level of the independent variables, pyrolysis temperature, V_G/V_L , and q_G giving the maximum ethanol concentration (=13.122 g/L) after 30 h of semi-batch operation are 648 °C, 0.46, and 6.7 L/h, respectively.
- The optimum level of the independent variables, V_G/V_L and q_G/q_L , giving the maximum ethanol concentration (=29.450g/L) after 300 h of continuous operation are 0.28 and 336.148, respectively.
- Since pyrolysis is used as the precursor process for syngas fermentation, other valuable products like pyro-oil and pyro-char are also generated, and the criterion of zero-waste generation for the circular economy concept is fulfilled.
- It is expected that the mathematical model developed in the present study can be used for the scale-up purposes needed for commercialization.
- The outcome of this research study can also be useful for the utilization of other lignocellulosic agro-wastes of Indian and other origins.

9.3 Hydrothermal liquefaction of jute stick and rice straw

The salient findings of hydrothermal liquefaction of jute stick and rice straw are as follows:

- The first attempt has been made to study the hydrothermal liquefaction of jute stick.
- The yield of hydrochar decreases from 43.97% to 22.15 % for hydrothermal liquefaction of jute stick and 48.36% to 25.17% for hydrothermal liquefaction of rice straw when the temperature is increased from 240 to 360°C.
- The yield of bio-oil increases from 22.15% - 33.81% for jute sticks and 20.39% to 30.34% for rice straw when the temperature is increased from 240 to 300°C. When, the temperature is increased from 300 to 360 °C, the yield of bio-oil decreases from 33.81% - 32.09% for jute sticks and 30.34% to 28.31% for rice straw. The maximum bio-oil yield obtained at 300°C.
- The kinetic parameters of hydrothermal liquefaction (HTL) of jute stick (JS) and rice straw (RS) have been determined.

- The convention of Van Krevelen diagram, used for the assessment of quality of fuel, H/C values of hydrochar and bio-oil have been plotted against the corresponding O/C values for JS and RS respectively
- The higher heating value of bio-oil samples obtained from hydrothermal liquefaction of jute stick and rice straw have been determined as 28.74 kJ/kg and 25.94 kJ/kg respectively.
- The optimum bio-oil yield obtained from co-hydrothermal liquefaction of jute stick and rice straw has been measured as 32.8% at 317.2 °C for 28.1 minutes with 83.1% blend ratio.
- The higher heating value of bio-oil obtained from co-hydrothermal liquefaction of jute stick and rice straw has been measured as 28.56 kJ/kg.
- The higher heating value of bio-oil samples obtained from HTL of JS, RS and co-HTL of JS & RS are greater than peat (21.33 kJ/kg) and lignite (24.45 kJ/kg).
- The area of GC-MS spectrum of bio-oil produced from co-HTL of JS and RS is dominated by phenolic compounds (45.59%) followed by aromatic (24.28%), cyclic (11.79%) and aliphatic (0.04%) compounds.
- It is observed that hydrochar, obtained from hydrothermal liquefaction of jute stick, could be efficiently used for Congo red dye removal.
- It is expected that the results of individual and co-HTL of JS and RS will open up a new arena in their application in bioenergy sector of India.

9.4 Torrefaction of mustard stalk

The salient findings of torrefaction of mustard stalk are as follows:

- The yield of biochar decreases from 67.91% - 34.33 % when the temperature is increased from 200 to 400°C. The maximum bio-oil yield is 21.32% at 300°C. The yield of gas increases from 20.31% - 44.75 % when the temperature is increased from 200 to 400°C.
- Parameters for lumped kinetic and distributed activation energy model of torrefaction of mustard stalk have been determined.
- The fuel ratio (FR) of raw-mustard stalk and biochar are 0.21 and 0.29 respectively.
- The HHV of raw MS, biochar and bio-oil have been measured as 14.25 MJ/kg, 16.37 MJ/kg and 19.85 MJ/kg respectively. The values of energy yield (EY) of biochar and bio-oil are 50.05% and 29.63% respectively.

- The % area occupied by aliphatic, cyclic, aromatic and phenolic compounds, have been determined as 25.70, 12.82, 12.91 and 20.41.
- The area of GC-MS spectrum of bio-oil produced from torrefaction of mustard stalk is dominated by aliphatic compounds (25.70%) followed by phenolic (20.41), aromatic (12.91%) and cyclic (12.82%) compounds.
- The environmental impact of the torrefaction of mustard stalk has also been assessed using life cycle analysis in SimaPro software.
- It is expected that the results of torrefaction of mustard stalk will be of use for the development of in bioenergy sector of India.

Among seventeen sustainable development goals (SDGs) of United Nations, the SDG7 stands for “affordable clean energy” and the de-carbonization of energy sector is one of the main plans to achieve the goal (2030-agenda-sustainable-development). The main thrust of the present research is towards the achievement of SDG7. The generation of bioenergy from biomass is one of the possible pathways of de-carbonization of energy resources. As agro-wastes are abundantly available in India, the investigation on the performance of those as fuel source is under focus of the study. The bioenergy generated from agro-wastes are expected to be either CO₂ neutral or sometimes CO₂ negative because of their generation as plant parts via photosynthetic route. Therefore, there is a reduction in CO₂ emission by the use of fuels generated from the agro-wastes. Thus, the research outcomes are also expected to be useful for the achievement of SDG13 which stands for “Climate Action”. For decentralized energy generation, the bioenergy production facilities are to be set up near agricultural field, located in rural areas (2030-agenda-sustainable-development). This ensures the generation of revenue and employment prospects in rural areas. Therefore, the research outcomes are expected to strengthen the pathway of achievement of SDG 17 meant for “reduced inequalities” by reducing the economic gap between rural and urban population and that between developing and developed countries under “clean development management” (CDM) strategy (2030-agenda-sustainable-development). It is obvious that in the achievement of SDGs, all countries have to concentrate on their own natural resources, environmental condition and overall topographic characteristics. Therefore for the bioenergy generation in India, agro-wastes like rice straw, mustard stalk, jute sticks etc. are chosen for their natural abundance. However, the studies are made in such a way that the outcomes like mathematical models, effect of mode of operation of reactors etc. can be generally applied for

other similar feedstocks irrespective of the geographic location of their natural abundance. Therefore, from the perspective of application towards the global achievement of SDGs 7 and 13 the present research outcomes have both national and international significance.

Future scope

The experiments (for sugar platform, syngas platform, hydrothermal liquefaction and torrefaction) have been conducted in a wide range of values of different relevant parameters. Although the results of all the studies establish the prospect of utilization of Indian agricultural wastes for the production of fuels and chemicals, there are scopes for widening the range of parameters for the ultimate application of the processes. As there is diversity in the characteristics biomass more data should be generated to decide on a common strategy for utilization of agro-waste for bioenergy in general. Process modelling using ASPEN Plus V10 etc. can further open up an arena for the prediction of performance of large scale reactors based on the presently determined kinetic data and the mathematical models, developed under the study (Pati et al, 2023). In addition to the predictions of process models, economic and life cycle analyses are also important to assess the viability of the thermochemical and hybrids of thermochemical and biochemical processes on large and commercial scales.

Overall, further research studies should be conducted to generate more insights in the following areas:

- To explore the possibility of using diverse Indian lignocellulosic biomasses, experiments should be conducted with other feedstocks having different lignocellulosic composition.
- In case of pretreatment of agro-wastes using metal chloride like FeCl_3 , a strategic decision can be made about the reaction period and temperature using the model predictions. However, the scope for more research studies are open for the complete elucidation of reaction mechanism and complete extraction of platform chemicals using such novel sustainable solvents.
- For large scale implementation, process modelling can be carried out using standard software like ASPEN Plus.
- Extensive life cycle analysis must be conducted for the proper implementation of research outcomes.

- In-depth studies on the integration strategies of different processes should be undergone for the holistic development of the Indian Bioenergy sector.

References

Pati, S., De, S. and Chowdhury, R., 2023. Integrated techno-economic, investment risk and life cycle analysis of Indian lignocellulosic biomass valorisation via co-gasification and syngas fermentation. *Journal of Cleaner Production*, 423, p.138744.

<https://www.cepal.org/en/topics/2030-agenda-sustainable-development/sustainable-development-goals-sdgs>

Appendix

MATLAB codes have been provided below:

a) Code for glucan conversion at 170°C using 0.2M FeCl₃ (Sugar platform)

`% function file`

`function dydt = glucanconversion(t, y)`

`a=0.1230;`

`a1=0.1550;`

`b=0.1616;`

`c=2.6316;`

`d=0.0197;`

`e=0.3314;`

`dydt = zeros(7,1);`

`dydt(1) = -a*y(1);`

`dydt(2) = a*y(1)-a1*y(2);`

`dydt(3) = a1*y(2)-b*y(3)-d*y(3);`

`dydt(4) = (b*y(3)*126/180)-c*y(4)-e*y(4);`

`dydt(5)= c*y(4)*(116.1/126);`

`dydt(6)= dydt(5)*(46/116);`

`dydt(7)= d*y(3);`

`end`

`% Script file`

`tspan = [0: 5: 15];`

`Y0 = [38.8 0 0 0 0 0 0];`

`[T, Y] = ode45(@(t, Y) glucanconversion(t, Y), tspan, Y0);`

`[T Y]`

`plot(T,Y)`

b) Code for xylan conversion at 170°C using 0.2M FeCl₃ (Sugar platform)

% function file

function dydt = xylanconversion(t, y)

a=0.6017;

b1=0.8298;

b=0.5340;

c=0.0200;

d=0.2237;

e=0.2464;

f=0.0502;

g=0.0721;

dydt = zeros(7,1);

dydt(1) = -a*y(1);

dydt(2) = a*y(1)-b1*y(2);

dydt(3) = b*y(2)-c*y(3)-e*y(3);

dydt(4) = c*y(3)+d*y(2)-f*y(4);

dydt(5)=e*y(3);

dydt(6)=f*y(4);

dydt(7)=g*y(2);

end

end

% Script file

tspan = [0: 5: 15];

Y0 = [38.8 0 0 0 0 0 0];

[T, Y] = ode45(@(t, Y) xylanconversion(t, Y), tspan, Y0);

[T Y]

plot(T,Y)

c) Code for syngas fermentation in semi-batch reactor (Syngas platform)

% function file

function dydt = semibatch(t, y)

R=0.082;

T=310;

a1=144.9;

a2=166.9;

a3=123.6;

H1=0.0008;

H2=0.00066;

H3=0.025;

vg=1.5;

vl=1.5;

qg=5.3;

pcoi=0.2307;

phi=0.1723;

pcdoi=0.1059;

b1=(qg/vg);

b2=(vl/vg)*(R*T);

c1=(vl/vg);

m1=0.195;

m2=0.042;

m3=0.2;

m4=0.0;

m5=0.2;

m6=0.2;

k1=0.000078;

k2=0.00022;

k3=0.00022;

ki1=0.002;

ki2=0.002;

```

ki3=0.0104;
ki4=0.0005;
dydt = zeros(9,1);
dydt(1) = (b1*(pcoi-y(1)))-((a1*b2)*((y(1)*H1)-y(4)));
dydt(2) = (b1*(phi-y(2)))-((a2*b2)*((y(2)*H2)-y(5)));
dydt(3) = (b1*(pcdoi-y(3)))-((a3*b2)*((y(3)*H3)-y(6)));
dydt(4) = (a1*c1)*((y(1)*H1)-y(4))-
(((39.91*(m1*y(4)*y(7))/(k1+y(4)+(y(4)^2)/ki1))*(ki3/(ki3+y(9)))));
dydt(5) = (a2*c1)*((y(2)*H2)-y(5))-
((((m2*y(5)*y(7))/(k2+y(5))*((y(7))/(k2+y(6)))*(ki2/(ki2+y(4))))*147.06)*ki3/(ki3+y(9)));
dydt(6) = (a3*c1)*((y(3)*H3)-y(6))-
((((m2*y(5)*y(7))/(k2+y(5))*((y(7))/(k2+y(6)))*(ki2/(ki2+y(4))))*73.55)*ki3/(ki3+y(9)));
dydt(7)=
(((m1*y(4)*y(7))/(k1+y(4)+(y(4)^2)/ki1)+((m2*y(5)*y(7))/(k2+y(5))*((m3*y(6)*y(7))/(k3+y(6)))*(ki2/(ki2+y(4))))*(ki3/(ki3+y(9))));
dydt(8)=
(((m3*y(4)*y(7))/(k1+y(4)+(y(4)^2)/ki1)+((y(5)/(k2+y(5))*((m4*y(6)*y(7))/(k3+y(6)))*(ki2/(ki2+y(4))))+(m5*y(4)*y(7))/(k1+y(4)+(y(4)^2)/ki1))+(((m6*y(5)*y(7))/(k2+y(5)))*(ki2/(ki2+y(4))))*(y(9)/(ki4+y(9))));
dydt(9)=
((((m1*y(4)*y(7))/(k1+y(4)+(y(4)^2)/ki1))*9.23)+(36.27*(((m2*y(5)*y(7))/(k2+y(5)))*(y(6)/(k3+y(6)))*(ki2/(ki2+y(4))))*(ki3/(ki3+y(9)))-
(((m5*y(4)*y(7))/(k1+y(4)+(y(4)^2)/ki1))+(((m6*y(5)*y(7))/(k2+y(5)))*(ki2/(ki2+y(4))))*(y(9)/(ki4+y(9))));
end
% Script file
tspan = [0: 10: 30];
Y0 = [0.2199 0.1599 0.1089 0.0002 0.0001 0.0027 0.05 0 0];
[T, Y] = ode45(@ (t, Y) semibatch(t, Y), tspan, Y0);
[T Y]
plot(T,Y)

```

d) Code for syngas fermentation in continuous reactor (Syngas platform)

% function file

function dydt = continuous(t, y)

R=0.082;

T=310;

a1=144.9;

a2=166.9;

a3=123.6;

H1=0.0008;

H2=0.00066;

H3=0.025;

vg=0.1;

vl=2.9;

qg=5.3;

pcoi=0.2307;

phi=0.1723;

pcdoi=0.1059;

b1=(qg/vg);

b2=(vl/vg)*(R*T);

c1=(vl/vg);

m1=0.195;

m2=0.042;

m3=0.2;

m4=0.0;

m5=0.2;

m6=0.2;

k1=0.000078;

k2=0.00022;

```

k3=0.00022;
ki1=0.002;
ki2=0.002;
ki3=0.0104;
ki4=0.0005;
dydt = zeros(9,1);
dydt(1) = (b1*(pcoi-y(1)))-((a1*b2)*((y(1)*H1)-y(4)));
dydt(2) = (b1*(phi-y(2)))-((a2*b2)*((y(2)*H2)-y(5)));
dydt(3) = (b1*(pcdoi-y(3)))-((a3*b2)*((y(3)*H3)-y(6)));
dydt(4) = (a1*c1)*((y(1)*H1)-y(4))-
(((39.91*(m1*y(4)*y(7))/(k1+y(4)+(y(4)^2)/ki1))*(ki3/(ki3+y(9))))-((0.02/vl)*y(4)));
dydt(5) = (a2*c1)*((y(2)*H2)-y(5))-
((((m2*y(5)*y(7))/(k2+y(5))*((y(7))/(k2+y(6)))*(ki2/(ki2+y(4))))*147.06)*ki3/(ki3+y(9)))-
((0.02/vl)*y(5));
dydt(6) = (a3*c1)*((y(3)*H3)-y(6))-
((((m2*y(5)*y(7))/(k2+y(5))*((y(7))/(k2+y(6)))*(ki2/(ki2+y(4))))*73.55)*ki3/(ki3+y(9)))-
((0.02/vl)*y(6));
dydt(7)=
(((m1*y(4)*y(7))/(k1+y(4)+(y(4)^2)/ki1)+((m2*y(5)*y(7))/(k2+y(5))*((m3*y(6)*y(7))/(k3+y(
6)))*(ki2/(ki2+y(4))))*(ki3/(ki3+y(9)))-((0.02/vl)*y(7)));
dydt(8)=
(((m3*y(4)*y(7))/(k1+y(4)+(y(4)^2)/ki1)+((y(5)/(k2+y(5))*((m4*y(6)*y(7))/(k3+y(6)))*(ki2/(
ki2+y(4))))+(m5*y(4)*y(7))/(k1+y(4)+(y(4)^2)/ki1)+(((m6*y(5)*y(7))/(k2+y(5)))*(ki2/(ki2+
y(4))))*(y(9)/(ki4+y(9)))-((0.02/vl)*y(8)));
dydt(9)=
((((m1*y(4)*y(7))/(k1+y(4)+(y(4)^2)/ki1))*9.23)+(36.27*(((m2*y(5)*y(7))/(k2+y(5)))*(y(6)/(
k3+y(6)))*(ki2/(ki2+y(4))))*(ki3/(ki3+y(9)))-
((((m5*y(4)*y(7))/(k1+y(4)+(y(4)^2)/ki1)+(((m6*y(5)*y(7))/(k2+y(5)))*(ki2/(ki2+y(4))))*(y
(9)/(ki4+y(9)))-((0.02/vl)*y(9)));
end

```

```
%Script file
```

```
tspan = [0: 100: 300];
```

```
Y0 = [0.2199 0.1599 0.1089 0.0002 0.0001 0.0027 0.05 0 0];
```

```
[T, Y] = ode45(@(t, Y) continuous(t, Y), tspan, Y0);
```

```
[T Y]
```

```
plot(T,Y)
```



Research article

Catalytic action of hydronium-ion in rice straw pretreatment and enhancement of enzymatic hydrolysis and ethanol production



Dinabandhu Manna^a, Ranjana Chowdhury^{a,*}, Md. Kamrul Hassan^b, Jouko Vepsäläinen^c, Suvi Kuittinen^b, Ari Pappinen^b

^a Chemical Engineering Department, Jadavpur University, Kolkata, West Bengal 700032, India

^b School of Forest Sciences, University of Eastern Finland, P.O. Box 111, Joensuu FI80101, Finland

^c School of Pharmacy, University of Eastern Finland, P.O. Box 1627, Kuopio FI70211, Finland

ARTICLE INFO

Keywords:

Rice straw

Pretreatment

Hydronium-ion

Fermentable sugars

Bio-ethanol

ABSTRACT

The present investigation will focus on the catalytic effect of hydronium ion during liquid-water/ dilute sulfuric acid/ferric chloride pretreatment (LWP/ SAP/ FCP) on the hydrolysate and pretreated rice straw. The overall pretreatment process has been represented as a sequential catalytic reactions. The temperature range of pretreatment is varied in the range of 140–180 °C and the concentration of dilute sulfuric acid and ferric chloride is 0.1 M. The first order rate constants of xylan and glucan degradation have been determined for LWP/ SAP/ FCP. The maximum xylan and glucan conversion of 96.8% w/wand 31.4%w/w respectively are achieved for FCP at 180 °C. Xylose, glucose, furfural, 5-hydroxymethyl furfural, acetic acid and formic acid appear as the main products for all pretreatments. Only in case of FCP levulinic acid also appears as a hydrolysis product. The thermal characteristics, functional groups, crystallinity, surface morphology of untreated and pretreated rice straw have been evaluated. Among all pretreatment processes under study, the highest values of glucose yield of 78.96% (w/w) using enzymatic hydrolysis and 83.79% of theoretical yield of ethanol using *Saccharomyces cerevisiae* have been achieved for ferric chloride pretreatment.

1. Introduction

Pretreatment processes play the key role when lignocellulosic biomass has to be converted to biofuels through sugar platform [1–5]. The release of fermentable sugars is the pre-condition for the conversion of lignocellulosic biomass (LCB) to biofuels via heterotrophic micro-organisms. The structure of LCB is constituted of carbohydrate polymers like cellulose and hemicellulose, tightly bound to lignin backbone. Therefore, all pretreatment processes focus on the destruction of the chemical bonds of carbohydrates responsible for their bonding to lignin and subsequent de-polymerization. As the pretreatment process is actually an auxiliary step for biofuel production it should be simple, less energy consuming and environmentally friendly. From this perspective a few pretreatment processes like mild temperature liquid water pretreatment (LWP), dilute sulfuric acid pretreatment (SAP) and ferric chloride pretreatment (FCP) are followed [6–9]. All of these three pretreatment processes are driven by the catalytic action of the hydronium ion. Through all these processes xylose and glucose are released from hemicellulose and cellulose respectively. It has been reported that in addition to xylose and glucose, some valuable

intermediate side products, namely, furfural, 5-hydroxymethyl furfural (5-HMF), formic acid, acetic acid, levulinic acid etc are also generated during LWP, SAP and FCP in the temperature range of 140 – 180 °C [10,11]. Furfural, 5-HMF and levulinic acid have been used for the production of fuels and other valuable chemicals [12,13]. Being simultaneously an aromatic alcohol, aldehyde and a furan, 5-HMF is an important platform chemical convertible to value-added chemicals [14]. On the other hand, acetic acid and formic acid have many applications of their own. The pretreated solid obtained after the catalytic pretreatment becomes suitable for enzymatic hydrolysis for further glucose release. Recently, hydronium ion based pretreatment processes, particularly, FeCl₃ and acid based ones, have been also found effective for the enhancement of biogas generation [15]. Mild temperature liquid water pretreatment (LWP) below the decomposition condition of biomass is also gaining importance because of the greenness of the solvent and less severity of the operating condition. Although the acid pretreatment processes are well studied for many lignocellulosic feed stocks, the data on LWP and FC are limited. However, unlike LWP and FC, the liquid effluent of acid pretreatment poses environmental concern [16,17].

* Corresponding author.

E-mail address: ranjana.chowdhury@jadavpuruniversity.in (R. Chowdhury).

While the mechanism of action of H_3O^+ ions during LWP/ SAP/ FCP of biomass has been elucidated in some published literature, there are scopes for the comprehensive representation of a reaction scheme incorporating the role of both homogeneous and heterogeneous reactions during pretreatment [11,18,19]. Many studies on LWP/ SAP/ FCP of same biomass have been reported in literature using different experimental parameters, i.e., temperature range and pretreatment time for different pretreatment processes [11,19,20]. Comparative studies of LWP/ SAP/ FCP using same temperature range and pretreatment time for any biomass can only clarify difference in the response pattern towards different pretreatment processes and the justification can be searched through in-depth introspection of product patterns and characteristics as well as reaction kinetics of degradation of carbohydrate polymers. The present article intends to address the above research needs by studying LWP/ SAP/ FCP of rice straw in the same temperature range and pretreatment time. Rice straw (RS) has been selected because it is the most abundantly available Indian lignocellulosic agricultural waste which can be utilized for bioenergy generation [21,22]. The article will focus on the complete depiction of the trajectory of reaction front for the heterogeneous catalysis along with subsequent homogeneous reactions occurring during the pretreatment process and the comparative elucidation of response of RS towards LWP, SAP and FCP with respect to A) composition of hydrolysate; B) composition, structure and thermochemical properties of pretreated solid rice straw and C) reaction kinetics of degradation of xylan and glucan and D) hydrolytic capability and ethanol productivity of pretreated rice straw.

2. Materials and methods

2.1. Materials

2.1.1. Chemicals

In the present study, sulfuric acid and ferric chloride (Sigma-Aldrich) were used. Cellulase purchased from HiMedia, was used for enzymatic hydrolysis of solids. Milli-Q water was used for experimental purposes.

2.1.2. Feed material

The rice straw was collected from West Bengal, India. The rice straw samples were first cut into small size and the latter was ground to 1 mm particle size using Ultra-Centrifugal Mill ZM 200 (Retsch GmbH, Germany).

2.1.3. Microorganism for ethanol fermentation

The *Saccharomyces cerevisiae* (MTCC-173) was purchased from MTCC, India and was maintained in YPD medium (3 g yeast extract, 10 g peptone, 20 g dextrose and 1 L distilled water) at 28 °C.

2.2. Methods

2.2.1. Analytical methods

2.2.1.1. Quantitative analysis of hydrocarbon polymers (cellulose-hemicellulose-lignin). The composition of the untreated and pretreated rice straw with respect to Cellulose-Hemicellulose-Lignin was determined through a series of analytical methods following the protocols described in the Technical Report of National Renewable Energy Laboratory (NREL/TP-510-42618) on 'Determination of Structural Carbohydrates and Lignin in Biomass: Laboratory Analytical Procedure (LAP) Issue Date: April 2008' [23].

2.2.1.2. Proximate analysis. The moisture, volatile matter and ash content of raw RS were determined according to ASTM (D-3172-89) protocol. Fixed carbon was measured from Eq. (1) [24].

$$\text{Fixed carbon(\%)} = 100 - \text{moisture(\%)} - \text{volatile matter(\%)} - \text{ash(\%)} \quad (1)$$

2.2.1.3. Ultimate analysis. Ultimate analysis of raw RS was performed by using CHNOS analysis using vario MICRO Element Analyser of ElementarAnalysensysteme GmbH.

2.2.1.4. Thermo-gravimetric analysis (TGA). The thermos-gravimetric analysis (TGA) was carried out in the 50 – 900 °C temperature range in a TG analyzer (Pyris Diamond TG/DTA, STA 6000, PerkinElmer). The experiment was conducted at 20 K min⁻¹ heating rate. Untreated RS and pretreated solids obtained from LWP, SAP and FCP at 180 °C were subjected to TGA following the same protocol.

2.2.1.5. FTIR analysis. To assess the changes in the chemical bonds of rice straw during different pretreatment processes, Fourier Transform Infrared analysis of feed rice straw and pretreated solid residue was conducted using an FTIR analyzer (RX-1 FTIR system, Perkin Elmer). Raw RS and residual solids obtained from LWP, SAP and FCP at 180 °C were subjected to FTIR analysis. The spectra have been generated in the range of 4000 – 400 cm⁻¹.

2.2.1.6. XRD analysis. The crystallinity of raw RS and pretreated solid were determined by X-ray diffractive (XRD) analysis (Ultima III, Rigaku). The scattering angles (2θ) were varied from 5° to 60° in steps of 0.04° at time intervals of 0.066 s.

The crystallinity index (CrI) was determined using the following equation [25].

$$\text{CrI(\%)} = \frac{I_{002} - I_{am}}{I_{002}} \times 100 \quad (2)$$

Where I_{002} is the intensity of the maximum peak at around $2\theta = 22.5^\circ$ and I_{am} is the minimum intensity at about $2\theta = 18^\circ$;

2.2.1.7. FESEM analysis. The surface morphological analysis of untreated and pretreated (LWP, SAP and FCP at 180 °C) rice straw were studied by field emission scanning electron microscopy (FESEM) analysis (INSPECT F50). The samples were mounted on a conductive tape. Gold was coated to the samples by using a Quorum (Q150R).

2.2.1.8. EDS analysis. To assess the change in metal distribution due to $FeCl_3$, the metals in raw-RS and pretreated solid, obtained from FCP were detected by using energy-dispersive X-ray spectroscopy (EDS) analysis (Bruker). The solid residue obtained after other pretreatment processes were not analyzed with respect to metal distribution because no metal ions were present in those pretreatment agents.

2.2.1.9. NMR analysis. The compounds (xylose, glucose, furfural, etc) in the hydrolyzate, obtained from LWP, SAP and FCP were analyzed using nuclear magnetic resonance spectroscopy (NMR) to determine sugars, platform chemicals and organic acids. ¹H NMR data were obtained using a 600 MHz Bruker NMR spectrometer, equipped with a cryoprobe (Bruker Prodigy TCI 600 S3H&F-C/N D-05 Z).

2.2.1.10. GC analysis for ethanol concentration. The ethanol concentration of fermentation sample was measured in gas chromatography analyzer (Thermo Fisher Scientific). The fermentation broth was centrifuged for 5 minutes at 10,000 rpm. 1 mL of supernatant and 1.5 mL of 1-butanol (Merck) were mixed in a glass tube closed with rubber cap [26]. As ethanol is highly soluble in butanol, two layers – top layer containing butanol-ethanol mixture and bottom layer containing the aqueous phase were separated. The top layer was analyzed for ethanol concentration using GC with the aid of a standard curve constructed using known concentration of ethanol in aqueous phase. The GC was equipped with Chromeleon software and

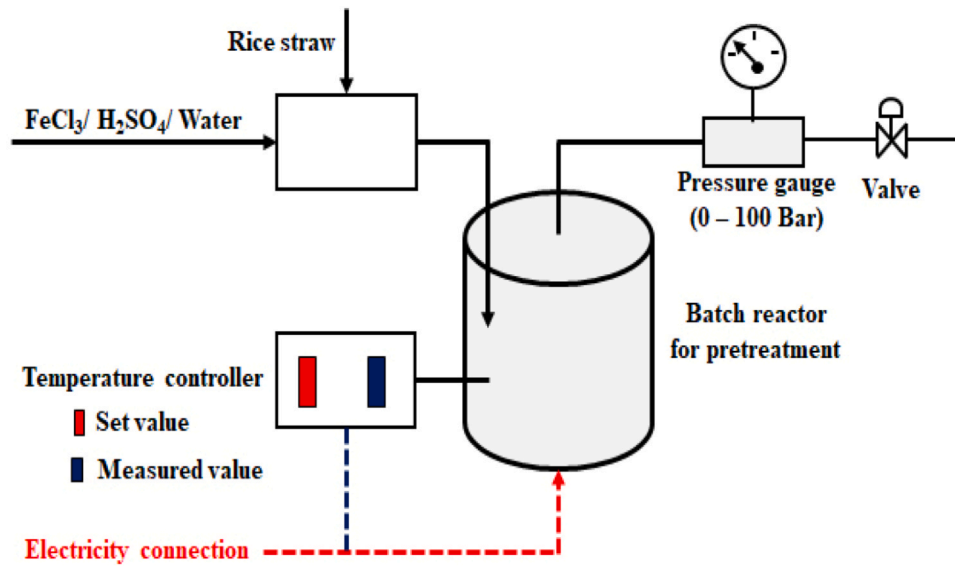


Fig. 1. Schematic diagram of the pretreatment process.

flame ionization detector (FID). Hydrogen, air and nitrogen flow rate were set as 30, 300 and 30 mL/min respectively. The oven and FID detector temperature were 40 and 250 °C respectively. TR-FAME capillary column was used to perform the experiment [26].

2.2.2. Experimental methods

2.2.2.1. Pretreatment method. A cylindrical stainless steel reactor of 60 mm inner diameter and 150 mm height was used for the investigation of pretreatment of rice straw in batch mode. The reactor was equipped with temperature controller and pressure gauge. The schematic diagram was shown in Fig. 1.

In the present study, 10 g rice straw was subjected to 100 mL of 0.1 M ferric chloride solution or 0.1 M sulfuric acid or water under isothermal condition at the temperature of 140, 150, 160, 170 and 180 °C for 10 minutes respectively. Subsequently the pressure was released and the treated slurry was collected at 25 °C after natural cooling. The liquid and the solid phases of the cold pretreated slurry were separated by passing through a vacuum filter. The pretreated liquor and the residual solid were stored at 4 °C for further analyses. The products in liquid hydrolyzate (glucose, xylose, furfural, 5-HMF, formic acid, acetic acid and levulinic acid) were determined by NMR analysis. The composition (glucan, xylan and lignin) of pretreated solid was analyzed according to NREL protocol. All experiments were conducted in triplicate. The yield of glucose, 5-HMF, formic acid and levulinic acid (Y_G , Y_{HMF} , Y_{FA} and Y_{LA}) were calculated from the Eq. (3). Similarly, the yield of xylose, furfural and acetic acid (Y_X , Y_F and Y_{AA}) were determined from the Eq. (4).

$$Y_{G/HMF/FA/LA} = \frac{\text{Mass of Glucose/5-HMF/Levulinic acid/Formic acid produced (g)}}{1 \text{ kg of rice straw}} \quad (3)$$

$$Y_{X/F/AA} = \frac{\text{Mass of xylose/Furfural/Acetic acid produced (g)}}{1 \text{ kg of rice straw}} \quad (4)$$

Glucan degradation and xylan degradation were determined from the Eqs. (5) and (6) respectively,

$$\text{Solid recovery (\%)} = \frac{\text{Weight of recovered solid residue}}{\text{weight of rice straw fed to the reactor}} \times 100 \quad (5)$$

Degradation of glucan (%)

$$= \left(\frac{\text{Glucan in RS fed} - \text{glucan remaining in the pretreated RS}}{\text{glucan in rice straw fed}} \right) \times 100 \quad (6)$$

Degradation of Xylan (%)

$$= \left(\frac{\text{Xylan in RS fed} - \text{Xylan remaining in the pretreated RS}}{\text{Xylan in rice straw fed}} \right) \times 100 \quad (7)$$

Reaction kinetics for xylan and glucan degradation.

As clearly indicated in previous literature, the rate of degradation of carbohydrate polymers can usually be represented as a first order function of concentration of carbohydrate polymer [27,28]. The 1st order rate kinetics for the xylan and glucan degradation through LWP, SAP and FCP, have been represented generally by the following rate equations are used:

$$-\frac{dW_{\text{Glucan}}}{dt} = k_{\text{Glucan}} W_{\text{Glucan}} \quad (8)$$

$$-\frac{dW_{\text{Xylan}}}{dt} = k_{\text{Xylan}} W_{\text{Xylan}} \quad (9)$$

Eq. (8) on integration reduces to the following:

$$\text{Or, } -\int_{W_{\text{Glucan} \cdot 0}}^{W_{\text{Glucan}}} \frac{dW_{\text{Glucan}}}{W_{\text{Glucan}}} = k_{\text{Glucan}} \int_0^t dt \quad (8.1)$$

$$\text{Or, } \ln \frac{W_{\text{Glucan} \cdot 0}}{W_{\text{Glucan}}} = k_{\text{Glucan}} t \quad (8.2)$$

$$\text{Or, } k_{\text{Glucan}} = \frac{\ln \frac{W_{\text{Glucan} \cdot 0}}{W_{\text{Glucan}}}}{t} \quad (8.3)$$

Where, $W_{\text{Glucan} \cdot 0}$ and W_{Glucan} represent the weight of glucan at $t=0$ and at any time, t . (Basis: 10 g initial RS sample being hydrolyzed).

Eq. (9) on integration reduces to the following:

$$\text{Or, } -\int_{W_{\text{Xylan} \cdot 0}}^{W_{\text{Xylan}}} \frac{dW_{\text{Xylan}}}{W_{\text{Xylan}}} = k_{\text{Xylan}} \int_0^t dt \quad (9.1)$$

$$\text{Or, } \ln \frac{W_{\text{Xylan} \cdot 0}}{W_{\text{Xylan}}} = k_{\text{Xylan}} t \quad (9.2)$$

Table 1

Proximate analysis, elemental analysis, chemical composition and metal composition of rice straw.

Proximate analysis % (w)	Elemental analysis % (w)	Chemical composition % (w)	Metal composition % (w)
Moisture: 5.7 ± 0.11 FC*: 11.4 ± 0.33 VM*: 71.9 ± 2.7 Ash: 10.9 ± 0.42	Carbon: 37.3 Hydrogen: 5.2 Nitrogen: 0.22 Sulfur: 0.27	Glucan: 38.8 ± 0.57 Xylan: 17.6 ± 0.12 KL*: 14.3 ± 0.15 ASL*: 2.5 ± 0.02	Silicon: 5.73 Potassium: 6.34 Calcium: 0.04 Iron: 0.01

(FC*, VM*, KL* and ASL refer as fixed carbon, volatile matter, Klason lignin and acid soluble lignin respectively).

$$\text{Or, } k_{Xylan} = \frac{\ln \frac{W_{Xylan,0}}{W_{Xylan}}}{t} \quad (9.3)$$

Where, $W_{Xylan,0}$ and W_{Xylan} represent the weight of xylan at $t=0$ and at any time, t . (Basis: 10 g initial RS sample being hydrolyzed).

The values of rate constants have been determined based on the experimental values of xylan and glucan contents of the original and rice straw. Using the principle of integral method of analysis, $\ln \frac{W_{Xylan,0}}{W_{Xylan}}$ and $\ln \frac{W_{Glucan,0}}{W_{Glucan}}$ have been plotted against the reaction time to test the validity of 1st order reaction kinetics [29].

2.2.2.2. Enzymatic hydrolysis. Enzymatic hydrolysis of raw-RS and pretreated solid from LWP, SAP and FCP was conducted in a glass test tube at 50°C for 24, 48 and 72 hours with shaking at a speed of 150 rpm. 4 mL sodium acetate buffer (0.05 M, pH 4.8) and 0.2 g solid (raw-RS and pretreated solid from LWP, SAP and FCP) were taken. The enzyme, i.e., cellulase loading was 20 FPU/g dry substrate. After enzymatic hydrolysis, the product was centrifuged at 10,000 rpm for 5 minutes. The supernatants were collected to determine the released glucose. All experiments of enzymatic hydrolysis were conducted in triplicate. The glucose yield was calculated from the Eq. (10) [30].

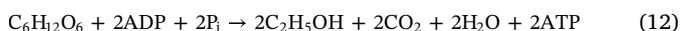
$$\text{Glucose yield(\%)} = \frac{\text{Glucose produced during enzymatic hydrolysis}}{\text{Glucan in pretreated solid} \times 1.11} \times 100 \quad (10)$$

Where, 1.11 = conversion factor of glucan to its equivalent glucose [29].

2.2.2.3. Ethanol fermentation. 1.8 mL of enzymatic hydrolysate was inoculated with 0.2 mL of 24 h old stock culture of *Saccharomyces cerevisiae* (MTCC-173) and was allowed for ethanol fermentation under anaerobic condition at 30 °C, under stirring (150 rpm). All experiments were conducted in triplicate. The% yield of ethanol (on the basis of theoretical yield) $Y_{\text{Ethanol}}(\%)$ was determined from Eq. (14).

$$Y_{\text{Ethanol}}(\%) = \frac{\text{Ethanol produced} \left(\frac{\text{g}}{\text{L}} \right)}{\text{Theoretically achievable concentration of Ethanol} \left(\frac{\text{g}}{\text{L}} \right)} \times 100 \quad (11)$$

Again, the stoichiometric equation for conversion of glucose to ethanol is as follows [31]



Therefore, from 1 g glucose, theoretically achievable ethanol is as follows:

$$\frac{2 \times \text{Molecular weight of Ethanol} \left(\frac{46\text{g}}{\text{mol}} \right)}{\text{Molecular weight of glucose} \left(\frac{180\text{g}}{\text{mol}} \right)} \times 1\text{g Glucose} = 0.511\text{g Ethanol} \quad (13)$$

Therefore, Eq. (13) can also be written as follows:

$$Y_{\text{Ethanol}}(\%) = \frac{\text{Ethanol produced} \left(\frac{\text{g}}{\text{L}} \right)}{\text{Initial glucose concentration} \left(\frac{\text{g}}{\text{L}} \right) \times 0.511} \times 100 \quad (14)$$

3. Results and discussion

3.1. Feedstock characterization

The proximate analysis (moisture, fixed carbon, volatile matter and ash), elemental analysis (carbon, hydrogen, nitrogen and sulfur), chemical composition (glucan, xylan, Klason lignin and acid soluble lignin) and metal composition (silicon, potassium, calcium and iron) of rice straw have been reported in Table 1 respectively.

3.2. Representation of sequential heterogeneous and homogeneous catalysis

From the analysis of the hydrolysate, obtained from LWP, SAP and FCP in the present temperature range, it can be observed that fermentable sugars (glucose, xylose), platform chemicals (furfural, 5-hydroxymethyl furfural (5-HMF) and levulinic acid) and organic acid (formic acid and acetic acid) are the major products of all hydrolysis processes. From the observation of the product array in the hydrolysate and from the data base of reported literature a common hydronium-ion catalyzed mechanism is revealed for all three pretreatment processes [32–35]. It is confirmed that all three processes, LWP, SAP and FCP, are catalyzed by hydronium ion in 1) heterogeneous and 2) homogeneous modes. In case of heterogeneous catalysis, H_3O^+ acts on the solid rice straw and mostly breaks the linkage of hemicelluloses with lignin and depolymerizes most of the hemicellulose and a part of amorphous cellulose [7–10,36,37]. The monomers of hemicelluloses, namely xylose and that of cellulose, namely glucose are transferred to the aqueous phase from the solid matrix [8–11]. In the aqueous phase xylose and glucose are respectively converted to furfural and 5-HMF under the catalytic action of H_3O^+ . In the aqueous phase, 5-HMF is again converted to levulinic acid and formic acid [10–14]. The reactions involving hydronium ions, as available in the literature, have been provided in Fig. 2.

In agreement with literature, a shrinking core behavior, as applicable in case of heterogeneous non-catalytic solid-fluid chemical reaction, can be postulated for the heterogeneous catalysis of hydronium ion [29,32–34]. In this case the catalyst is originally in aqueous phase and the reactants (hemicelluloses, cellulose etc.) are in solid phase. Whatever may be the type of pretreatment (LWP/SAP/FCP), the following steps appear to be common for this mechanism (shown in the Fig. 3a):

- The solid particles are bathed in either hot water or hot dilute acid or hot ferric chloride solution and a stagnant liquid film is developed around each solid sphere.
- The hydronium ions reach the solid surface through the liquid film.
- First the reaction starts at the surface and the reaction front propagates towards the center as hydronium ion diffuses through the reacted layer to the unreacted core.
- As time progresses the radius of the unreacted core decreases although the overall size remains almost unaltered. The reacted layers are expected to be porous as reactants (Hemicellulose and amorphous cellulose) are removed.
- The products diffuse through the reacted layer to the aqueous phase and participate in homogeneous catalytic reactions in presence of

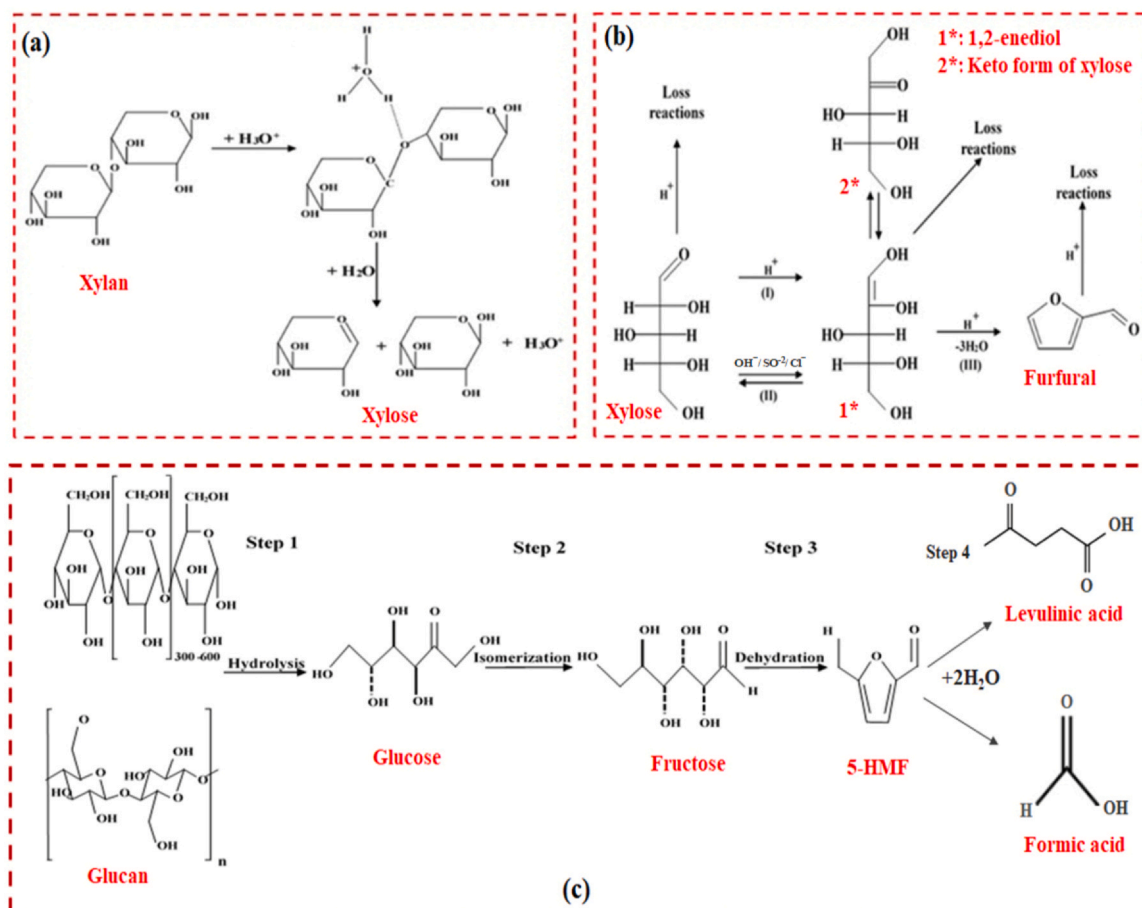


Fig. 2. Proposed mechanisms for the formation of products obtained from LWP/SAP/FCP pretreatment (a: Xylan hydrolysis; b: Formation of furfural and degraded products from xylose; c: Conversion of glucan in presence of hydronium ions).

hydronium ions. As hydronium ion acts as the catalyst, it remains unchanged and is again transferred to the aqueous medium.

The propagation of the reaction front in the postulated mechanism and the homogeneous catalytic reactions are shown in Fig. 3b.

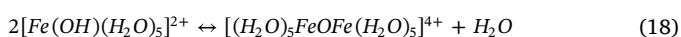
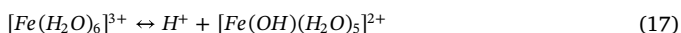
Self-ionization of water occurs through the reaction, $2H_2O \leftrightarrow H_3O^+ + OH^-$ with the ionization constant, $K_w = [H_3O^+][OH^-]$ [34]. At each temperature, the concentration of H_3O^+ and OH^- ions are equal ($= \sqrt{K_w}$).

In case of sulfuric acid, the dissociation follows the following steps [34]:



As reported in a recent literature, the acid diffuses through the cell wall during pre-hydrolysis followed by hydrolysis of carbohydrate polymers [38]. The hydrolysis products also diffuse back to the liquid (aqueous) medium.

On dissolution, $FeCl_3$ acts as a Lewis acid and water molecules are attracted by sharing electron pairs towards the ferric cation (Fe^{3+}). As reported in the literature a complex cation $Fe[H_2O]_6^{3+}$ of radius 0.268 nm is formed by the bonding of six water molecules through monodentate ligands [38]. H_3O^+ is formed through the following reaction:



3.3. Comparison of composition of liquid hydrolysate

In Fig. 4, the yield (g of product / kg of RS) of fermentable sugars (glucose, xylose), platform chemicals (furfural, 5-hydroxymethyl furfural (5-HMF) and levulinic acid) and organic acid (formic acid and acetic acid) in the hydrolysate, obtained after 10 minutes of LWP, SAP and FCP have been compared over the temperature range of 140 – 180 °C. In Fig. 4a, c and e the yield of xylose, glucose and furfural in the hydrolysate, obtained respectively through LWP, SAP and FCP have been plotted respectively against temperature. Similarly, in Fig. 4b, d and f the yield of 5-HMF, formic acid, acetic acid and levulinic acid in the hydrolysate, obtained respectively through LWP, SAP and FCP have been plotted.

3.3.1. Scrutiny of production data of xylose, glucose and furfural

From the analysis of Fig. 4a, it has been clearly observed that the glucose and xylose yields from LWP have an increasing trend with temperature right from 140 – 180 °C during LWP. While the yield of xylose has increased from 1.1 g/kg RS to 3.8 g/kg RS, that of glucose has increased from 0.5 g/kg RS to 3.1 g/kg RS as the temperature is increased from 140 °C to 180 °C. The structures of lignocellulosic biomass is constituted of interconnected network of carbohydrate polymers, cellulose, hemicellulose and lignin. According to literature, the microfibers of cellulose are embedded on hemicellulose network through lignin aggregates [39]. This can be considered as the “skeletal structure” of lignocellulosic biomass. As reported in case of wheat straw, it is expected that the skeletal structure is weakened at high temperature [15]. Thus, the whole conversion of hemicelluloses during LWP, can be represented by the following scheme: (I) Formation of

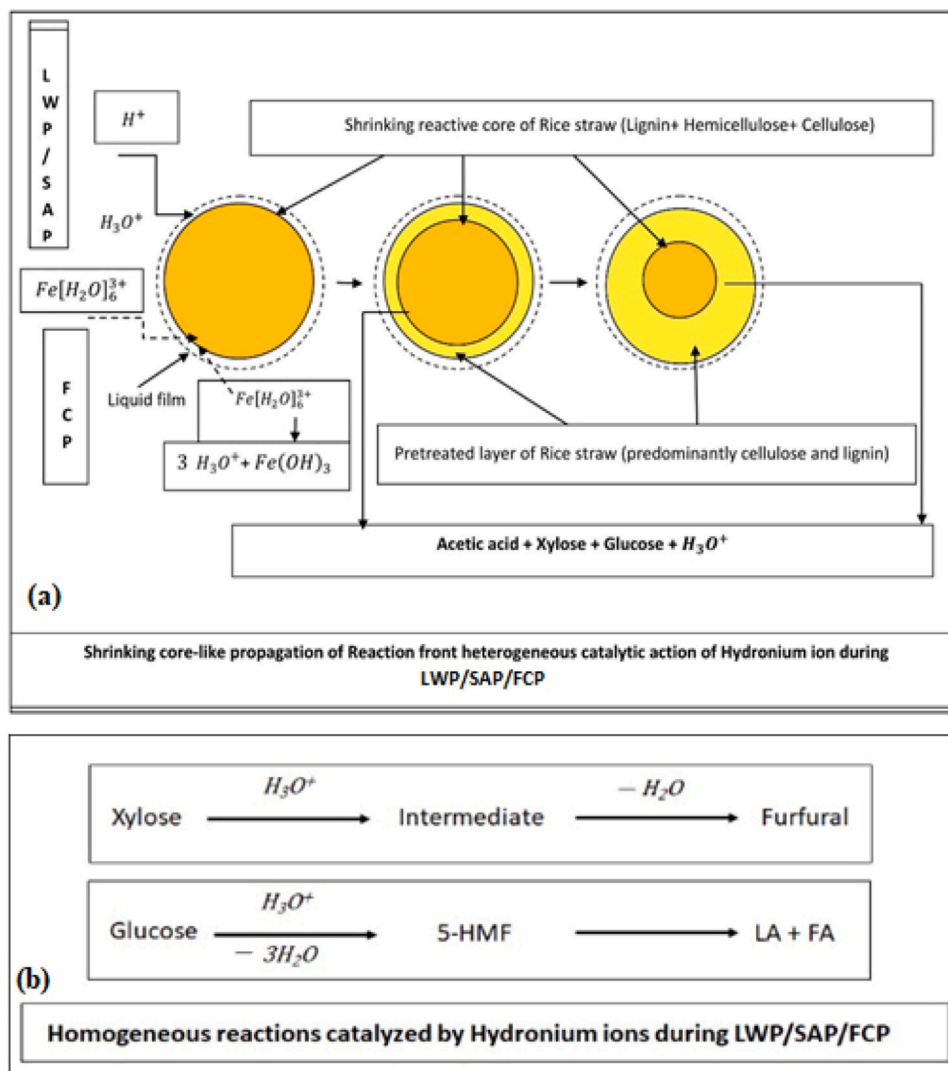


Fig. 3. Heterogeneous and homogeneous catalytic action of hydronium ions during LWP/SAP/FCP (a: Shrinking core-like propagation of reaction front heterogeneous catalytic action of hydronium ion; b: Homogeneous reactions catalyzed by hydronium ions).

surface radicals, acting as pre-hydrolysis step; (II) Dissociation of hemicellulose from the structure through decarboxylation and release of acetic acid; (III) hydrolysis of hemicellulose to xylose, furfural, formic acid etc by the synergistic action of acetic acid and catalysis of hydronium ion, H_3O^+ , released through the ionization of H_2O . In parallel, the amorphous portion of cellulose is decomposed to glucose in presence of H_3O^+ generated by the ionization of water. Further, there is a possibility of dehydration of xylose and glucose respectively to furfural and 5-HMF through the homogeneous catalysis of hydronium ion. Thus it is expected that the whole process is influenced by the rate of release of hydronium ions. The value of ionization constant of water, K_w , as described in Section 3.3, increases with temperature [34]. As reported in Bandura and Lvov, the values of $(-\log(K_w))$ are 12.25, (i. e. $K_w = 10^{-12.25}$), 11.64, (i. e. $K_w = 10^{-11.64}$) and 11.31 (i. e. $K_w = 10^{-11.31}$) at 100 °C, 150 °C and 200 °C respectively. Therefore, the concentration of H_3O^+ ion also increases with temperature under the present range of study (140–180 °C). As shown in Fig. 3, the released hydronium diffuse through the rice straw and depolymerization of both xylan and glucan has occurred. Further, xylose is converted to furfural with the aid of hydronium ions. This can clearly explain the increasing trend of concentration of xylose, glucose and furfural during LWP. At 140 °C, no furfural is formed during LWP. The increasing trend in the yield of furfural has been observed from 150 °C. The yield of furfural has increased from 0.13 g/kg RS to 0.72 g/kg RS when

temperature is increased from 150 °C to 180 °C. As evident from the representation of reaction network in Fig. 3, furfural is generated through homogeneous dehydration of released xylose through catalysis of H_3O^+ . As the release of hydronium ion is increased with the rise of temperature, furfural is produced only at high temperature range during LWP. It is an established fact that the severity of autohydrolysis increases with temperature due to the increase in the release of H_3O^+ in the subcritical condition and it passes through a maximum at 300 °C [27,28,37,40].

In case of SAP, it has been observed from the Fig. 4c that glucose yield follows an increasing pattern with temperature over the range of 140–180 °C during SAP. Xylose yield increases from 140 °C to 170 °C after which it has decreased at 180 °C. While xylose yield has increased from 41.2 g/kg RS at 140 °C to the maximum of 115.9 g/kg RS at 170 °C, glucose yield in the hydrolysate varies from 30.9 g/kg RS to 65.7 g/kg RS as the temperature is increased from 140 °C to 180 °C. Unlike the result of LWP, the Fig. 4c also shows that the furfural yield of 0.19 g/kg RS has been detected even at 140 °C for SAP and follows an increasing trend with the increase of temperature up to 180 °C. At 180 °C, the furfural yield reaches the value of 31.3 g/kg RS through SAP. As sulfuric acid is a strong acid, its dissociation, represented by Eqs. (13) and (14), is instantaneous and the concentration of H_3O^+ ions in the 0.1 M H_2SO_4 solution is 0.2 M. Therefore, it is expected that the rate of hydrolysis of both hemicellulose and cellulose is much faster in

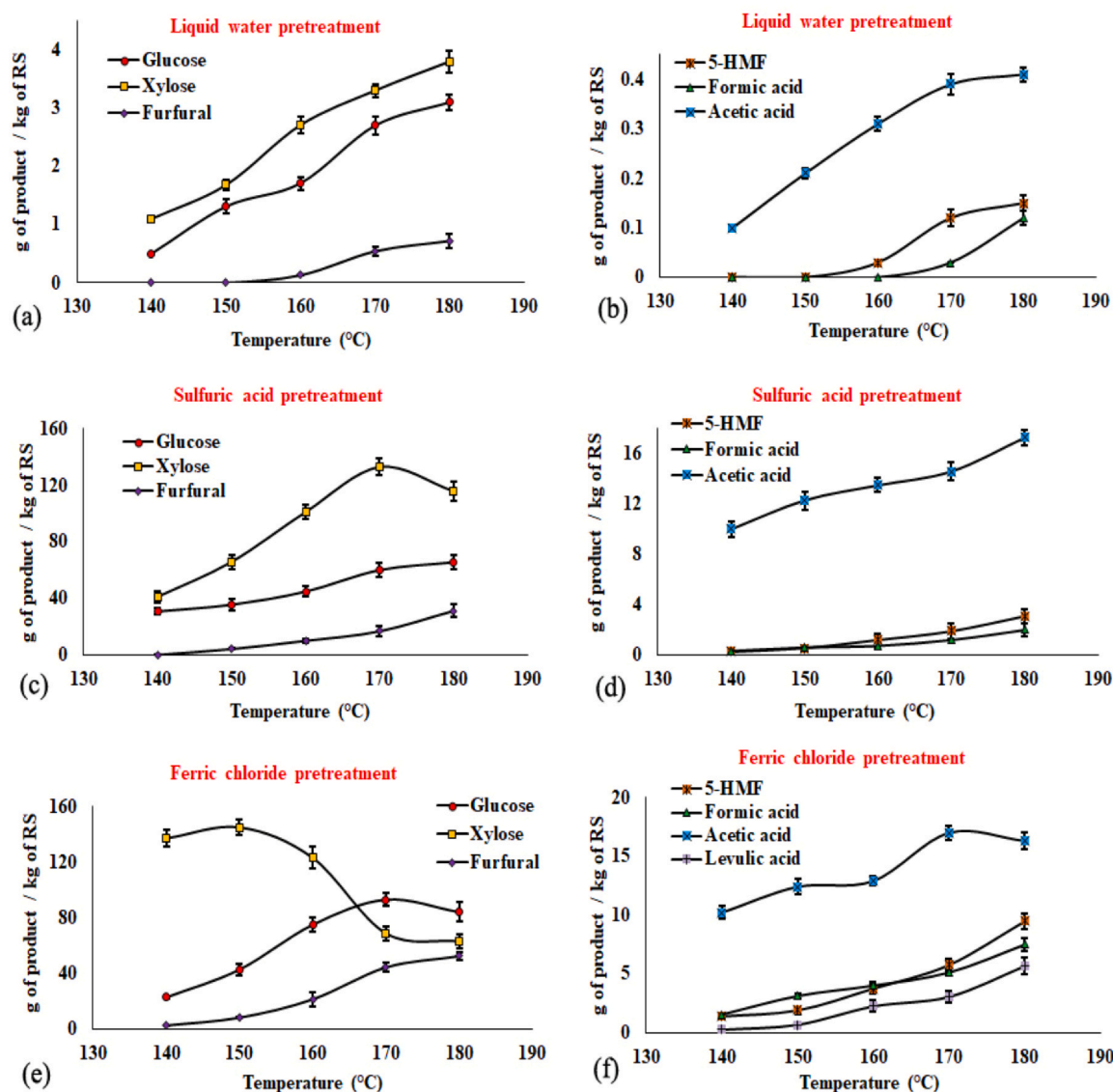


Fig. 4. The yield of products obtained from pretreated liquor at different temperatures; (a), (c) and (e): the yield glucose, xylose and furfural obtained from LWP, SAP and FCP respectively; (b), (d) and (f): the yield of 5-HMF, formic acid, acetic acid and levulinic acid obtained from LWP, SAP and FCP respectively.

case of SAP, compared to LWP. That is why the highest values of xylose and glucose concentration, obtained in case of SAP are 34.9 fold and 21.0 fold higher than those obtained through LWP. However, as in case of LWP, the drastic weakening of overall structure of the feedstock is expected at high temperature. Therefore, as the temperature increases besides the enhancement of hydrolysis rate, the resistance to internal diffusion of H_3O^+ is expected to be lowered and the overall rates of release of products increase. The ever increasing trend of furfural yield and decreasing pattern of xylose yield beyond 170 °C clearly indicate that beyond a certain temperature, the rate of dehydration of xylose to furfural, as represented in Fig. 3, is higher than the rate of xylose formation from xylan depolymerization (Fig. 3). Although both LWP and SAP are expected to follow the same mechanism driven by hydronium ion, the concentration of hydronium ions is much higher than that of LWP leading to much more depolymerization of the carbohydrate polymers, xylan and glucan releasing xylose and glucose. From the analysis of Fig. 4e it is clear that in case of FCP, yield-temperature pattern for xylose is different from those observed for LWP and SAP. Although for LWP and SAP, increasing trend is observed up to 180 °C and 170 °C respectively, xylose yield passes through a maximum at 150 °C beyond which it decreases in case of FCP. Xylose yield increases

from 137 g/kg RS at 140 °C to 145 g/kg RS at 150 °C after which it has sharply decreased to 63.1 g/kg RS at 180 °C. The yield of furfural exhibits an increasing trend with temperature throughout the entire temperature range. Furfural yield increases from 2.7 g/kg RS at 140 °C to 52.5 g/kg RS at 180 °C. The difference in behavior of RS towards SAP and FCP is due to the influence of Bronsted acid behavior of ferric chloride solution as represented by Equations 17 and 18.

As represented in Fig. 3, the H^+ , and hence H_3O^+ formed from complex cation, diffuses across the surface of rice straw and catalyzes heterogeneous reaction. As in case of LWP and SAP, acetic acid is formed and hemicellulose is solubilized. With the help of the complex cation, protonation of ether bond in hemicellulose occurs via hydronium (H_3O^+) ion [41]. The hydrolysis products diffuse to the medium. The decreasing trend of xylose right from 150 °C indicates higher rate of dehydration of xylose to furfural than that of production rate of xylose at temperature higher than 150 °C. Glucose yield shows an increasing trend with temperature up to 170 °C, followed by a decreasing trend till 180 °C. As the temperature is increased, glucose yield first increases from 22.9 g/kg RS at 140 °C to 93.1 g/kg RS at 170 °C and then decreases further to 84.2 g/kg RS at 180 °C. This indicates that at higher temperature the conversion rate of glucose to 5-HMF, as described under

Table 2

Maximum products yield obtained from LWP, SAP and FCP.

Pretreatment	Maximum products yield (g of product/kg of RS)						
Type	Glucose	Xylose	Furfural	5-HMF	FA*	AA*	LA*
LWP	3.1 ± 0.01	3.8 ± 0.012	0.72 ± 0.015	0.15 ± 0.011	0.12 ± 0.009	0.41 ± 0.01	Nd*
SAP	65.7 ± 3.1	115.9 ± 5.6	31.3 ± 1.4	3.1 ± 0.16	2.0 ± 0.1	17.3 ± 0.59	Nd*
FCP	93.1 ± 4.8	145.0 ± 6.0	52.5 ± 2.7	9.4 ± 0.081	7.4 ± 0.49	17.0 ± 0.69	5.67 ± 0.27

(FA*, AA*, LA* and Nd* referred as formic acid, acetic acid, levulinic acid and not detected respectively).

the reaction network (Fig. 3), exceeds the rate of its formation from glucan.

When the highest values of xylose yield in the hydrolysate obtained through LWP (3.8 g/kg RS), SAP (132.9 g/kg RS) and FCP (145.1 g/kg RS) are compared it can be inferred that there are 34.97 fold (or 3397%) and 38.18 fold (or 3718%) increase for SAP and FCP with reference to LWP. Similarly, for the highest values of glucose yield, there is 21.0 fold (or 2000%) and 30.03 fold (or 2903%) increase for SAP and FCP with reference to LWP. When the highest yield of furfural obtained after LWP (0.72 g/kg RS), SAP (31.3 g/kg RS) and FCP (52.5 g/kg RS) are compared it is clear that 13.75 times (or 4247%) and 72.91 times (7191%) increase is achieved through SAP and FCP respectively, compared to LWP. As reported in the literature the capability of Fe³⁺ to attract six water molecules, as shown in Fig. 3, facilitates the availability of hydronium ions resulting in drastic depolymerization of carbohydrate polymers, particularly, xylan [14]. For the same reason, the decomposition of cellulose is also accelerated to a greater extent for FCP compared to LWP and SAP in the same temperature zone. Moreover, chloride ion present in ferric chloride has been reported to catalyze the enolization of pentose xylose [14]. That is the reason why the generation of furfural during FWP of RS has occurred at a much higher rate compared to LWP and SAP.

3.3.2. Scrutiny of production data of acetic acid, 5-HMF, levulinic acid and formic acid

From Fig. 4b, representing the yield-temperature pattern for LWP, it appears that the yield of acetic acid has an increasing trend with the increase of pretreatment temperature from 140 °C to 180 °C. Fig. 4b also indicates that although 5-HMF appears at 150 °C, there is an increase in the yield up to 180 °C. No formation of LA has been observed during LWP. From the inspection of Fig. 4b, it is also observed that formic acid first appears at 160 °C and there is an increase in the yield up to 180 °C. Hydronium ion driven hydrolysis of rice straw, represented in Fig. 3 can explain the product trajectory. Acetic acid is released when xylan–lignin linkage gets broken. 5-HMF forms from the homogeneous catalysis of dehydration of glucose released from depolymerisation of cellulose. As the hydronium ion concentration is low at temperature 150 °C, 5-HMF is not produced. From Fig. 4d, used from SAP, it appears that the yields of both acetic acid, 5-HMF and formic acid exhibit slightly increasing trends with the increase of pretreatment temperature from 140 °C to 180 °C. This signifies that in case of SAP, the sufficient presence of hydronium ion results in the formation of 5-HMF from a temperature as low as 140 °C. From the inspection of Fig. 4d Levulinic acid is not detected even in case of SAP. However, in some reported works levulinic acid could be obtained by SAP of biomass either by elongating pretreatment time, increase of acid strength, decrease in liquid: solid ratio and by the increase in acid strength or by using two-step acid pretreatment [42–45]. In a recent study 114 g levulinic acid /kg sugar cane bagasse has been obtained at 170 °C, which is within the present experimental range [46]. In that study the acid concentration was 1.5% (i.e., 0.153 M), pretreatment time was 2 h and the liquid to solid ratio was maintained at 6:1 [46]. Therefore while the acid concentration and pretreatment time are much higher (0.15 M > 0.1 M; 120 min > 10 min) compared to those of the present study, the liquid to solid ratio is much lower (6:1 > 10:1) [46]. In case of FCP, as

depicted by Fig. 4f, the yield of acetic acid, 5-HMF and levulinic acid show increasing trend as the temperature is increased from 140 °C to 170 °C. Although acetic acid exhibits a slightly decreasing trend beyond 170 °C, the increasing trend is maintained by 5-HMF and levulinic acid up to 180 °C. From FCP, the yields of all these products are much higher. The maximum yield of products (glucose, xylose, furfural, 5-HMF, formic acid, acetic acid and levulinic acid) obtained from different pretreatment methods (LWP, SAP and FCP), have been reported in the Table 2.

The enhanced production of all hydrolysis products via FCP can be explained by the influence of Fe³⁺ ions attracting six water molecules, facilitating the release of hydronium ion at all temperature under study. The influence of chloride ions also facilitates the enolization reaction during the dehydration of xylose to furfural.

The yield of products obtained from LWP have been found to be comparable with literature [8]. However, in another reported higher value of glucose yield, namely, 7–11 g/kg has been reported [47]. In their analysis, they also reported that for the same operating conditions, the glucose yield is higher from pure cellulose, present in a simulated mixture of cellulose, hemicellulose and lignin in the same ratio as in RS. Therefore it is established that the structural bonding of the carbohydrates play a vital role during hydrothermal pretreatment. The yield of products achieved from SAP have been compared with the literature data on nitric acid and sulfuric acid pretreatment of rice straw, as shown in Table S1 provided in the supplementary material [48,49]. It has been observed that the yield of products obtained from SAP in present study is slightly higher than the yield of the products reported in literature (sulfuric acid pretreatment on rice straw). The yield of products obtained from nitric acid pretreatment is higher than sulfuric acid pretreatment (except xylose and furfural). The results of the present study are compared with the literature data for ferric chloride pretreatment of rice straw and other lignocellulosic feedstocks such as wheat straw, rapeseed straw and sugarcane bagasse [17,31,50,51]. The comparison of the process parameters and composition of feedstock are reported in Table S2. The yields of different products obtained from pretreated liquor, degradation of glucan and xylan are compared with literature data, provided in supplementary material (Table S3). The yield of products namely, xylose, glucose, furfural, 5-HMF, formic acid, acetic acid and levulinic acid (obtained at 180 °C) for present study are comparable with literature data. In the present study, the yield of glucose and furfural are higher than the data reported in literature. Xylose yield at 180 °C for present study is lower than literature data. In the present study, at 150 °C, the yield of xylose is the highest. With increase in temperature, a major part of xylose is converted to furfural and as a result the yield of xylose becomes lower. However, the performance of ferric chloride in the pretreatment of Indian rice straw, using present process parameters, seems very effective.

3.4. TGA and DTG of untreated and pretreated rice straw

Fig. 5, represents the thermogravimetric (TG) plots, showing the change in mass with temperature in the range of 50 °C to 900 °C. From the Fig. 5a, it appears that the % mass (with respect to initial sample mass) -Temperature profile can be divided into four distinct regions, I: 50–110 °C; II: 110–220 °C; III: 220–370 °C; IV: 370–900 °C. In region I, there is 4% decrease in the mass, signifying the loss of moisture. In Region II there is no change in % mass and hence no thermal

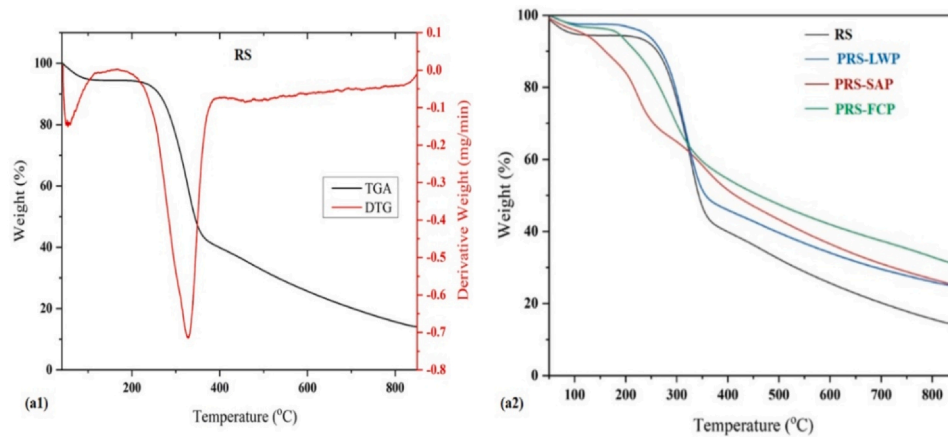


Fig. 5. TG and DTG curves of RS (a); TG curves of RS and PRS (b).

decomposition of rice straw below 220 °C. In regions III and IV, loss in mass has been observed, however the temperature gradient of mass loss in these two regions are different. In Region II (220–370°C), temperature gradient of % mass loss is 0.3384%/°C as the % mass has decreased from 96% to 45%. Whereas in Region IV (370– 900 °C), % mass loss is 0.0547%/°C as the % mass has decreased from 45% to 16%. Thus the gradient in region IV is much lower than that obtained in Region III.

As reported in the literature, hemicellulose, cellulose and lignin decompose at the temperature range of 220 – 315 °C, 300 – 400 °C and 150 – 900 °C respectively [52]. Therefore, it can be envisaged that region III signifies the thermal decomposition of hemicellulose and cellulose. Region IV stands for the thermal decomposition of lignin. Although the rate of decomposition of cellulose and hemicellulose increases sharply with temperature that of lignin changes slowly with lesser sensitivity towards temperature.

As it is not the intention of the present work to combine the effect of thermal decomposition and pretreatment, the temperature is chosen to be 180 °C where the effect of hydronium-ion based catalytic pretreatment can be exclusively studied.

In Fig. 5b, the % mass (with respect to initial sample mass) -Temperature profiles of untreated rice straw and pretreated rice straw obtained through LWP, SAP and FCP have been plotted. Similar to the TG profile of untreated rice straw four regions are observed for treated samples, except that obtained for FCP. In case of FCP, three regions are obtained. The temperature span and the temperature gradient of %mass are different for the pretreated RS (PRS) obtained through LWP, SAP and FCP. These are shown in Table 3.

The difference in the TG profiles clearly reflects the effect of de-polymerization and removal of carbohydrate polymers, namely, hemicellulose and amorphous part of cellulose during different pretreatment process.

3.5. Pretreated solid analysis

3.5.1. Composition analysis and reaction kinetics

3.5.1.1. Composition of untreated, pretreated RS. The glucan, xylan and lignin content in untreated rice straw are 38.84%, 17.59% and 16.85%

respectively. The degradation (%) of glucan and xylan along with the composition (glucan, xylan and lignin mass fractions) have been reported in the Table 4.

3.5.1.2. Rate equations and rate constants of degradation reaction kinetics. As discussed in Section 2.2.2.1, $\ln \frac{W_{Xylan-0}}{W_{Xylan}}$ and $\ln \frac{W_{Glucan-0}}{W_{Glucan}}$ have been plotted against the reaction time (shown in the Fig. 6) using temperature (140 °C – 180°C) as a parameter for LWP, SAP and FCP.

For all processes (LWP, SAP and FCP), straight lines have been obtained at each temperature (for different reaction time 4, 6, 8 and 10 minutes). Thus it is proved that the degradation of both xylan and glucan follows first order rate kinetics with respect to their respective concentrations. The rate constants have been determined from the slope of the linear plots and are provided in Table 4. From the analysis of the Table 4 it is clear that the rate constants increase with temperature. As per reported literature, the rate constants are functions of both temperature and concentration of hydronium ions [27]. All the rate constants have Arrhenius-type temperature dependence. However, different types of functionality of rate constant on the hydronium ions are reported. Thus, $k = k_0 e^{-\frac{E}{RT}} f(C_{H_3O^+})$. An usual representation of the functionality of rate constants on temperature and acid, in turn, hydronium ion, concentration is $k = k_0 A^n e^{-\frac{E}{RT}}$, where, A is the acid concentration, k_0 is pre-exponential factor, E activation energy and R universal rate constant [27,28]. As reported by Springer and Harris, there can be a change of H_3O^+ concentration with time due to the interaction with biomass leading to cation exchange following the reaction $BCOO^-M^+ + H^+ \rightarrow BCOO^-H^+ + M^+$, where, B is biomass and M^+ is the cation on it [53]. As this increases the pH value by decreasing the quantity of H^+ or H_3O^+ ions in the solution, this is also called neutralization effect. According to Springer and Harris, at a given temperature a correlation $\ln k = a \ln H^+ + b$ was obtained for acid treatment of Aspen wood [53]. According to Kapu et al., for autohydrolysis $f(C_{H_3O^+}) = a + bt$, t is hydrolysis time [28]. This signifies the dependence of k with time. This can be due to the time dependent release of H^+ or H_3O^+ ions during hydrolysis in presence of only water [28]. Under the present investigation, the

Table 3

Temperature span and gradient of %mass loss for RS and PRS following LWP, SAP and FCP corresponding to four distinct regions in TGA.

Region	Temperature Span (oC)				Temperature gradient of % mass loss (oC-1)			
	RS	PRS-LWP	PRS- SAP	PRS- FCP	RS	PRS-LWP	PRS- SAP	PRS- FCP
I	50–110	50–200	50–110	50–200	0.0705	0.0133	0.05	0.04
II	110–220	200–300	110–200	200–300	0	0.17	0.1333	0.19
III	220–370	300–400	200–300	300–900	0.3384	0.33	0.2	0.0733
IV	370–900	400–900	300–900	Nil	0.0547	0.038	0.06	Nil

Table 4
Conversion of Xylan and Glucan along with degradation rate constants.

Pretreatment		Solid	Composition (w/w)			Degradation		Rate Constant	
Type	Temp (°C)		Glucan(%)	Xylan(%)	Lignin(%)	Glucan (%)	Xylan (%)	k _{Glucan} (min ⁻¹)	k _{Xylan} (min ⁻¹)
LWP	140	99.71 ± 0.03	38.81 ± 0.07	17.57 ± 0.01	16.89 ± 0.02	0.36	0.40	0.0003	0.0001
SAP	140	90.71 ± 0.04	39.35 ± 0.10	13.72 ± 0.01	18.52 ± 0.04	8.11	29.21	0.0083	0.0335
FCP	140	77.15 ± 0.32	45.98 ± 0.21	3.31 ± 0.03	21.65 ± 0.08	8.67	85.41	0.0089	0.1918
LWP	150	99.65 ± 0.04	38.79 ± 0.08	17.51 ± 0.01	16.88 ± 0.01	0.47	0.81	0.0004	0.0005
SAP	150	87.3 ± 0.10	40.27 ± 0.27	10.69 ± 0.02	19.17 ± 0.02	8.10	46.91	0.0098	0.0622
FCP	150	73.55 ± 0.51	44.91 ± 0.09	1.29 ± 0.29	22.42 ± 0.13	14.95	94.61	0.0161	0.2909
LWP	160	99.14 ± 0.05	38.63 ± 0.08	17.47 ± 0.03	16.97 ± 0.05	1.39	1.53	0.0013	0.0007
SAP	160	81.3 ± 0.54	42.01 ± 0.09	6.28 ± 0.05	20.55 ± 0.07	12.05	70.94	0.0127	0.1226
FCP	160	71.90 ± 1.09	40.92 ± 1.13	1.17 ± 0.07	22.43 ± 0.05	24.25	95.22	0.0276	0.3029
LWP	170	98.76 ± 0.09	38.44 ± 0.10	17.22 ± 0.03	17.07 ± 0.08	2.25	3.31	0.0022	0.0021
SAP	170	76.0 ± 0.78	42.78 ± 0.03	1.51 ± 0.12	21.96 ± 0.12	16.27	93.46	0.0176	0.2718
FCP	170	69.81 ± 1.31	38.92 ± 0.79	1.03 ± 0.19	21.20 ± 0.21	30.04	95.91	0.0356	0.3186
LWP	180	98.18 ± 0.12	38.41 ± 0.01	17.01 ± 0.01	17.05 ± 0.02	2.91	5.05	0.0028	0.0034
SAP	180	74.07 ± 0.89	42.91 ± 0.17	1.54 ± 0.03	22.31 ± 0.11	18.22	93.51	0.0199	0.2724
FCP	180	69.69 ± 1.29	38.23 ± 1.01	0.79 ± 0.46	21.03 ± 0.33	31.40	96.87	0.0420	0.3453

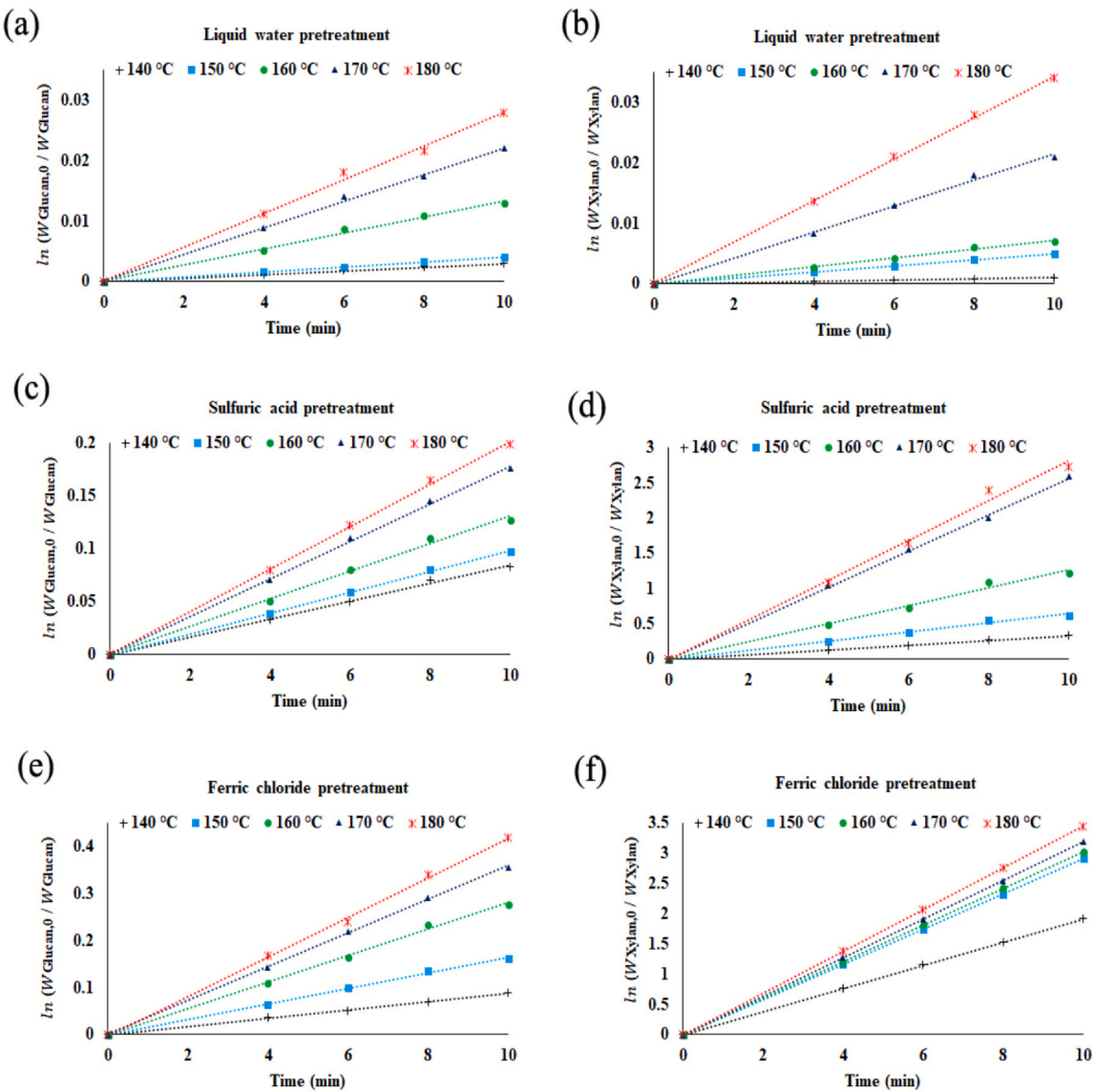


Fig. 6. Plots of $\ln \frac{W_{Glucan,0}}{W_{Glucan}}$ against the reaction time using temperature as a parameter ((a): LWP; (c): SAP; (e): FCP) and Plots of $\ln \frac{W_{Xylan,0}}{W_{Xylan}}$ against the reaction time using temperature as a parameter ((b): LWP; (d): SAP; (f): FCP).

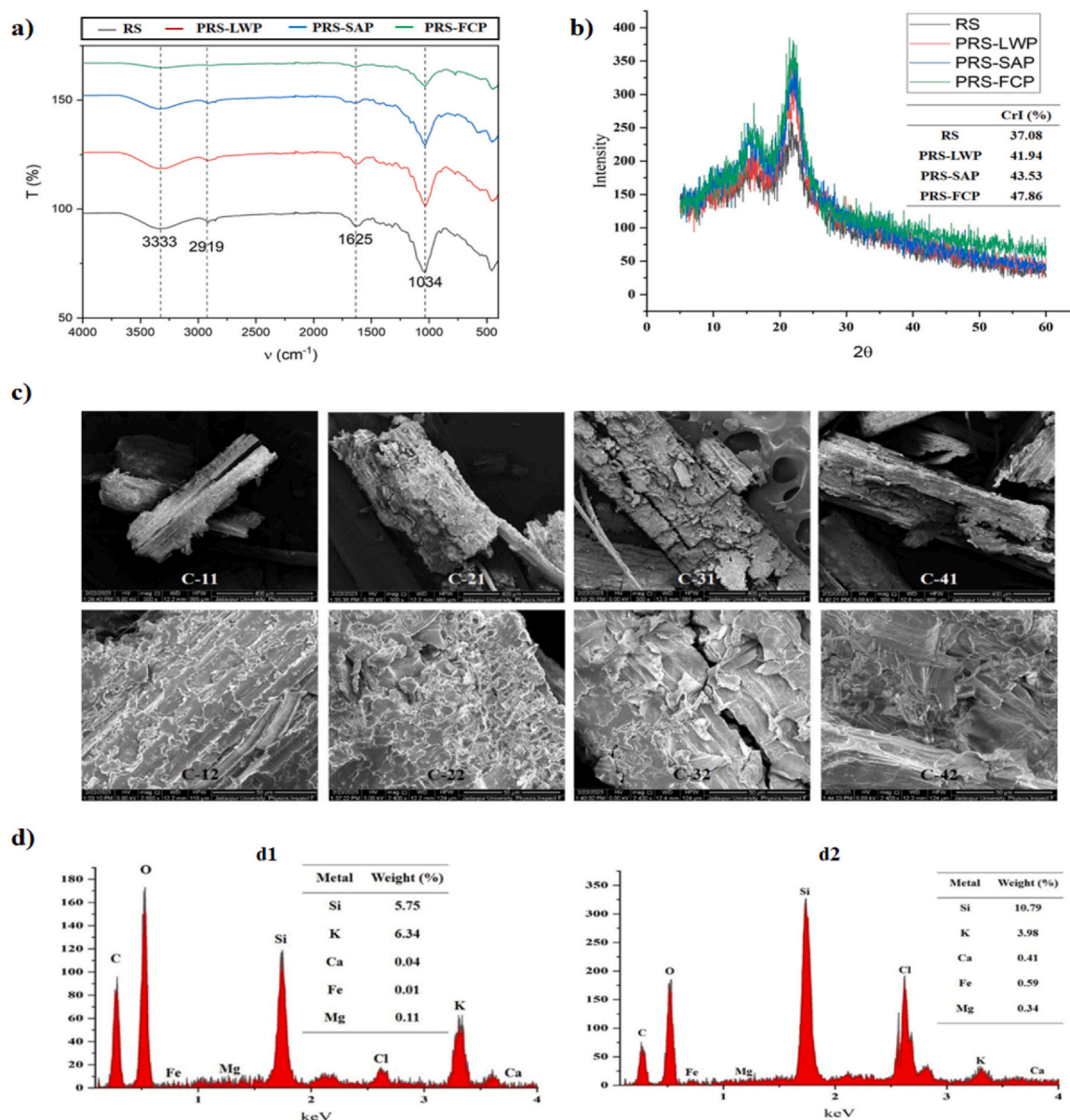


Fig. 7. a: FTIR of untreated and pretreated RS (where T and ν were the transmittance and wavenumber respectively); b: Crystallinity index (CrI) of untreated rice straw and pretreated rice straw; c: FESEM of untreated and pretreated RS (where c1: untreated RS, c2, c3 and c4: pretreated solid obtained from LWP, SAP and FCP at different magnification of image, 400 and 50 μm); d: EDS results (where d1: untreated RS and d2: pretreated solid obtained from FCP).

concentration of acid (H_2SO_4) or metal chloride (FeCl_3) has been kept constant i.e. 0.1 M. At each temperature, the function $f(C_{\text{H}_3\text{O}^+})$ is thus constant. The time dependence of rate constant during LWP is also not considered. Therefore, the rate constant at each temperature incorporates a factor dependent on concentration of hydronium ion. Under the present study, the hydronium ion concentration during hydrolysis has not been determined. The temperature variation of rate constants, determined under the study, incorporates the effects of temperature on the ionization of water, acid and ferric chloride as well as the hydrolysis reactions. The comparison of rate contents of degradation of xylan and glucan clearly indicates that at all temperature the highest value is obtained for FCP. The high values of rate constant ensure that the same extent of hydrolysis at a particular temperature can be achieved at much smaller time. The comparison of the rate constant thus reveals the dependence of the hydrolysis kinetics of xylan and glucan of rice straw on the concentration of hydronium ion, polymer concentration and temperature. This knowledge can further be utilized for reactor design in the industrial scale.

The solid recovery (%), degradation of glucan and xylan (%) have been determined from Eqs. (5), (6) and (7) respectively. It is observed that the percentage of solid recovery has decreased with increase in temperature. At 180 $^{\circ}\text{C}$, the solid recovery (%) for LWP, SAP and FCP are 98.18, 89.53 and 69.69 respectively. The degradation of xylan and glucan have also an increasing trend with temperature. The maximum degradation of glucan and xylan occurred at 180 $^{\circ}\text{C}$. The maximum xylan degradation from LWP, SAP and FCP are determined as 5.05%, 93.51% and 96.87% respectively. Whereas, the maximum glucan degradation from LWP, SAP and FCP have been reported as 2.91%, 18.22% and 31.40% respectively. Thus the solid composition again establishes the trend observed in case of products appearing in the hydrolysate.

3.5.2. FTIR analysis of untreated and pretreated RS

From the Fig. 7a, it is clearly noted that the absorption peaks are obtained at 3333 cm^{-1} , 2919 cm^{-1} , 1625 and 1034 cm^{-1} . From the literature, it is known that the absorption peak at 3333 cm^{-1} signifies O

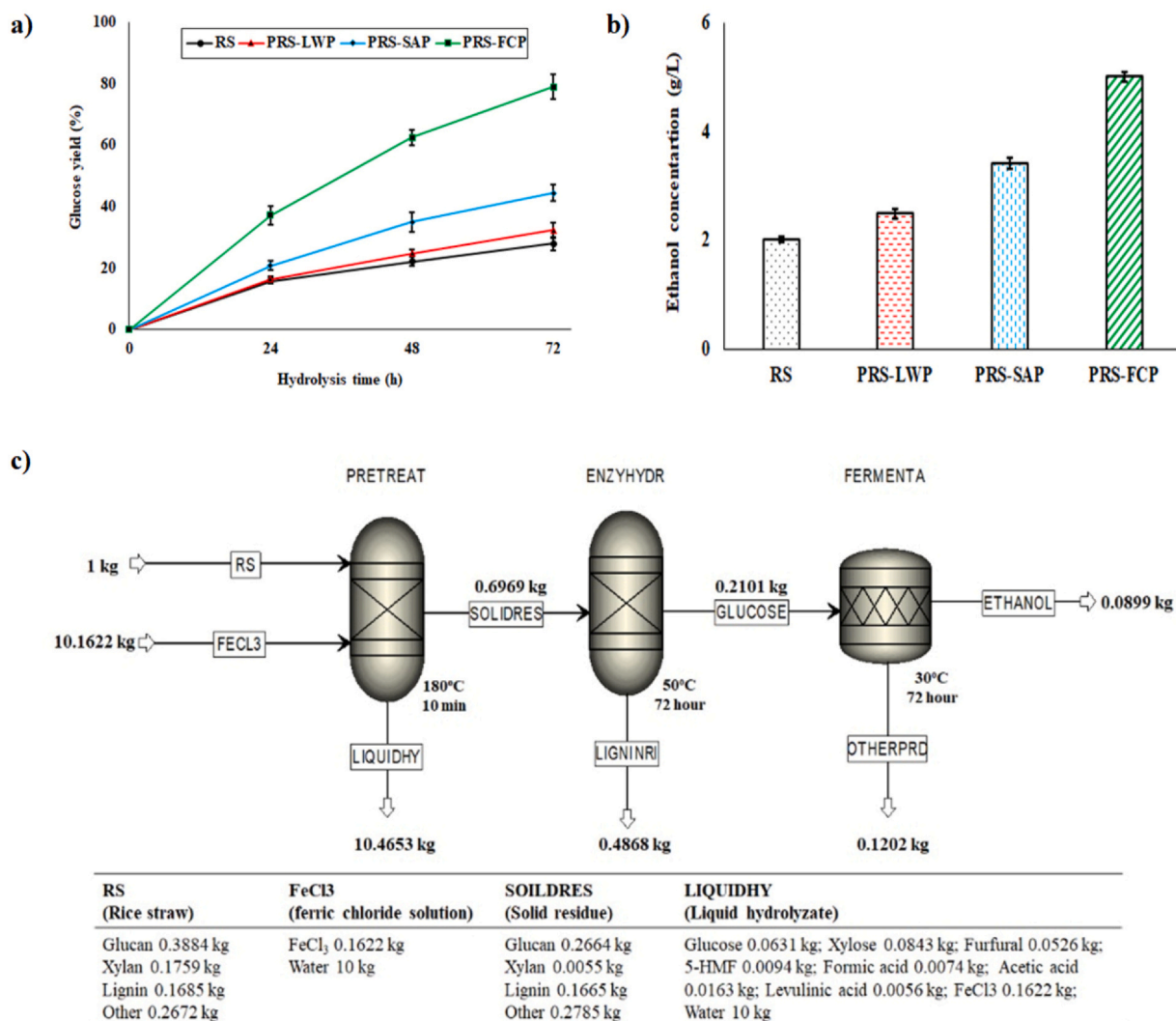


Fig. 8. a: Glucose yield (%) after enzymatic hydrolysis of untreated RS and pretreated solids obtained from LWP, SAP and FCP; b: Ethanol production after enzymatic hydrolysis of raw-RS and pretreated solids for 72 hours; c: Mass balance flow sheet for FeCl₃ pretreatment of rice straw followed by enzymatic hydrolysis and fermentation.

– H stretching produced by the vibration of hydroxyl group linked in lignin and cellulose [54]. The peak at 2919 cm^{-1} signifies the C – H stretching from CH₂ -group. The absorption peak at 1625 and 1034 cm^{-1} indicate C = C and C – O stretching respectively. At each position there is a decrease in the peak area for pretreated sample, in the order of PRS- FCP < PRS- SAP < PRS-LWP < RS. In case of ferric chloride treatment on rice straw, the peaks from $3500 - 2500\text{ cm}^{-1}$ have almost disappeared. The FTIR spectra actually re-establish the effectiveness of de-polymerization and removal of carbohydrate polymers during different pretreatment process.

3.5.3. XRD analysis of untreated and pretreated RS

From the Fig. 7b, it has been observed that while the value of CrI (%) for RS is 37.08%, those of PRS-LWP; PRS- SAP and PRS- FCP are 41.94%, 43.53% and 47.86% respectively. The increment of CrI (%) through the pretreatment processes is due to the removal of hemicellulose and amorphous cellulose, as already established through the products identified in the aqueous hydrolysate.

3.5.4. FESEM analysis of untreated and pretreated RS

The inspection of the Fig. 7c1 reveals that untreated RS has smooth, flat and fibrillary surface. As observed from Fig. 7c2-c4, the external surface has developed cracks, pores and disruptions through pretreatment in the order FCP > SAP > LWP. As postulated by shrinking core

model, the reaction front starts from the surface and progresses towards the center and hence it is expected that the structural breakdown appears on the surface of the pretreated solid due to each pretreatment.

3.5.5. EDS analysis of untreated RS and pretreated solid

EDS analysis of PRS-FCP has been conducted to check how much containment of iron in the RS occurs after pretreatment through FCP. Fig. 7d ascertains that some Fe metal is retained after FCP- When compared with the EDS of untreated RS, it appears that besides the confirmation of the presence of iron in PRS-FCP, the content of metals like Si, Ca and Mg increases. The content of K however decreases. The increase in the content of Si, Ca and Mg is due to the decrease in the total solid content.

3.6. Enzymatic hydrolysis

In the present investigation, enzymatic hydrolysis of untreated RS and pretreated solids have been performed. The glucose yields have been calculated from Eq. (8). It has been observed that the yields of glucose have an increasing trend with time, shown in the Fig. 8a. The glucose yields after 72 hours of enzymatic hydrolysis of untreated RS and pretreated solids (obtained from LWP, SAP and FCP) are determined as 27.9%, 32.3%, 44.4% and 78.9% respectively. The results signified that the FeCl₃ pretreatment on rice straw is very efficient for glucose yield during enzymatic hydrolysis. Although there are

evidences that iron sometimes inhibits the enzymatic action of cellulase, instead of any decrease there is an increase in glucose yield. This can be due to the fact that the positive effect of significant increase in pore size, presented in FESEM (Fig. 7c) has outweighed any inhibitory effect, if any, of iron on cellulase [48]. Moreover there is a possibility of reduction of non-specific binding of lignin to the active sites during FCP, as reported in some literature [55].

3.7. Ethanol fermentation

The ethanol productions from fermentable sugar namely, glucose released during enzymatic hydrolysis of untreated RS and pretreated solids (obtained from LWP, SAP and FCP) are determined as 2.01, 2.49, 3.41 and 5.01 g/L respectively, shown in the Fig. 8b. Ethanol conversion yield (for FCP, calculated from Eq. (12)) is 83.79%.

3.8. Overall mass balance

The overall mass balance for FeCl_3 pretreatment of rice straw followed by enzymatic hydrolysis and fermentation has been shown in the Fig. 8c. The overall mass balance for liquid water and sulfuric acid pretreatment of rice straw for bio-ethanol production have been provided in the supplementary material (Figs. S1 and S2).

Pretreatment of rice straw takes place in the PRETREAT block. ENZYHYDR and FERMENTA signify the enzymatic hydrolysis unit and fermentation unit respectively. The productions of ethanol (kg ethanol / kg of rice straw) through LWP, SAP and FCP pretreatment of rice straw followed by enzymatic hydrolysis and fermentation have been determined as 0.0444, 0.0609 and 0.0899 respectively.

4. Conclusion

The analysis of hydrolysate and the pretreated solid clearly indicate the most efficient action of FCP in comparison to acid pretreatment in the present range of temperature. The degradation rate constants of xylan and glucose for rice straw for LWP, SAP and FCP have been compared for the first time. From this study it is clear that the yields of all hydrolysis products, namely, xylose, glucose, acetic acid, furfural, 5-HMF, levulinic acid and formic acid are enhanced during FCP. As the amount of furfural and 5-HMF, produced in case of FCP, is high they can be utilized as fuel additives and the use of the hydrolysate part for ethanol production is not recommended due to their inhibitory effects. As furfural, 5-HMF and levulinic acid contents increase monotonically with the increase in temperature during FCP, one can strategize to focus on these products in the hydrolysate and production of glucose from the pretreated straw only. Although the degradation rates of xylan and glucan are slow in case of LWP, effectiveness of water points towards its utilization as a green solvent for mild pretreatment in this temperature zone and beyond by allowing more reaction time. The yields of ethanol (kg ethanol / kg of rice straw) through LWP, SAP and FCP pretreatment of rice straw have been measured as 0.0444, 0.0609 and 0.0899 respectively. From the research outcome it is clear that the treatment time and hence the energy expenditure can be saved to a great extent by using FCP instead of conventionally followed SAP. Although the pretreatment time requirement and hence the energy expenditure is much higher, LWP is also attractive from the environmental perspective. It is clear from the study that FCP can play a vital role to implement the concept of biorefinery using abundantly available Indian agro-waste, namely, rice straw for the production of ethanol, furfural, 5-HMF and levulinic acid as the main products. The outcomes of this study would be quite worthwhile and can be used in scaling up of hydronium ion-driven pretreatment of LCB for the production of bio-fuels and bio-chemicals.

Declaration of Competing Interest

The authors declare that they have no known competing financial interests or personal relationships that could have appeared to influence the work reported in this paper.

Acknowledgments

The corresponding author sincerely acknowledges DST, India for the financial support necessary for this research study under INNO-INDIGO research project CONVER-B (Sanction Ref. DST/IMRCD/INNO-INDIGO/CONVER-B/2017(G) DATED January 29, 2018). The first author acknowledges DST, India, Finnish National Agency for Education, and CONVER-B (AKA Grant no. 311972) for providing Research Fellowship as well as covering the expenses related to the visit to University of Eastern Finland and to carry out the experimental work for this research. The authors are indebted to the learned reviewers for their valuable suggestions for the improvement of the manuscript.

Appendix A. Supporting information

Supplementary data associated with this article can be found in the online version at doi:10.1016/j.nxener.2024.100112.

References

- [1] G. Shen, X. Yuan, S. Chen, S. Liu, M. Jin, High titer cellulosic ethanol production from sugarcane bagasse via DLCA pretreatment and process development without washing/detoxifying pretreated biomass, *Renew. Energy* 186 (2022) 904–913, <https://doi.org/10.1016/j.renene.2022.01.062>.
- [2] O.A. Fakayode, N.D.K. Akpabli-Tsigbe, H. Wahia, S. Tu, M. Ren, C. Zhou, H. Ma, Integrated bioprocess for bio-ethanol production from watermelon rind biomass: ultrasound-assisted deep eutectic solvent pretreatment, enzymatic hydrolysis and fermentation, *Renew. Energy* 180 (2021) 258–270, <https://doi.org/10.1016/j.renene.2021.08.057>.
- [3] X. Chen, S. Liu, R. Zhai, X. Yuan, Y. Yu, G. Shen, Z. Wang, J. Yu, M. Jin, Lime pretreatment of pelleted corn stover boosts ethanol titers and yields without water washing or detoxifying pretreated biomass, *Renew. Energy* 192 (2022) 396–404, <https://doi.org/10.1016/j.renene.2022.04.095>.
- [4] J.H. Choi, S.K. Jang, J.H. Kim, S.Y. Park, J.C. Kim, H. Jeong, H.Y. Kim, I.G. Choi, Simultaneous production of glucose, furfural, and ethanol organosolv lignin for total utilization of high recalcitrant biomass by organosolv pretreatment, *Renew. Energy* 130 (2019) 952–960, <https://doi.org/10.1016/j.renene.2018.05.052>.
- [5] R. Chowdhury, S. Ghosh, D. Manna, S. Das, S. Dutta, S. Kleinstaub, H. Strauber, M.K. Hassan, S. Kuittinen, A. Pappinen, Hybridization of sugar-carboxylate-syngas platforms for the production of bio-alcohols from lignocellulosic biomass (LCB)—a state-of-the-art review and recommendations, *Energy Convers. Manag.* 200 (2019) 112111, <https://doi.org/10.1016/j.enconman.2019.112111>.
- [6] J. Li, W. Liu, J. Meng, L. Zhao, J. Li, M. Zheng, Mesothermal pretreatment using FeCl_3 enhances methane production from rice straw, *Renew. Energy* 188 (2022) 670–677, <https://doi.org/10.1016/j.renene.2022.02.028>.
- [7] S. Banerjee, R. Singh, K. Eilts, E.J. Sacks, V. Singh, Valorization of Miscanthus x giganteus for sustainable recovery of anthocyanins and enhanced production of sugars, *J. Clean. Prod.* 369 (2022) 133508, <https://doi.org/10.1016/j.jclepro.2022.133508>.
- [8] G. Yu, S. Yano, H. Inoue, S. Inoue, T. Endo, S. Sawayama, Pretreatment of rice straw by a hot-compressed water process for enzymatic hydrolysis, *Appl. Biochem. Biotechnol.* 160 (2010) 539–551, <https://doi.org/10.1007/s12010-008-8420-z>.
- [9] M. Yang, S. Kuittinen, J. Zhang, M. Keinänen, A. Pappinen, Effect of dilute acid pretreatment on the conversion of barley straw with grains to fermentable sugars, *Bioresour. Technol.* 146 (2013) 444–450, <https://doi.org/10.1016/j.biortech.2013.07.107>.
- [10] L. Yan, A.A. Greenwood, A. Hossain, B. Yang, A comprehensive mechanistic kinetic model for dilute acid hydrolysis of switchgrass cellulose to glucose, 5-HMF and levulinic acid, *RSC Adv.* 4 (45) (2014) 23492–23504, <https://doi.org/10.1039/C4RA01631A>.
- [11] S.R. Kamireddy, J. Li, M. Tucker, J. Degenstein, Y. Ji, Effects and mechanism of metal chloride salts on pretreatment and enzymatic digestibility of corn stover, *Ind. Eng. Chem. Res.* 52 (5) (2013) 1775–1782, <https://doi.org/10.1021/ie3019609>.
- [12] Y. Chai, M. Bai, A. Chen, J. Yuan, L. Peng, J. Shao, J. Zhang, P. Qin, C. Peng, Z. Zhou, Introduction of acid mine drainage in the direct production of 5-hydroxymethylfurfural from raw biomass and expanding the use of biomass conversion residue, *Bioresour. Technol.* 364 (2022) 128094, <https://doi.org/10.1016/j.biortech.2022.128094>.
- [13] L. Peng, L. Lin, J. Zhang, J. Zhuang, B. Zhang, Y. Gong, Catalytic conversion of cellulose to levulinic acid by metal chlorides, *Molecules* 15 (8) (2010) 5258–5272, <https://doi.org/10.3390/molecules15085258>.
- [14] G. Marcotullio, W. De Jong, Chloride ions enhance furfural formation from D-xylose in dilute aqueous acidic solutions, *Green Chem.* 12 (10) (2010) 1739–1746.

- [15] A.M. Rahmani, P. Gahlot, K. Moustakas, A.A. Kazmi, C.S.P. Ojha, V.K. Tyagi, Pretreatment methods to enhance solubilization and anaerobic biodegradability of lignocellulosic biomass (wheat straw): progress and challenges, *Fuel* 319 (2022) 123726, <https://doi.org/10.1016/j.fuel.2022.123726>.
- [16] R.J. Chimentão, E. Lorente, F. Gispert-Guirado, F. Medina, F. López, Hydrolysis of dilute acid-pretreated cellulose under mild hydrothermal conditions, *Carbohydr. Polym.* 111 (2014) 116–124, <https://doi.org/10.1016/j.carbpol.2014.04.001>.
- [17] W. Tang, X. Wu, C. Huang, Z. Ling, C. Lai, Q. Yong, Revealing the influence of metallic chlorides pretreatment on chemical structures of lignin and enzymatic hydrolysis of waste wheat straw, *Bioresour. Technol.* 342 (2021) 125983, <https://doi.org/10.1016/j.biortech.2021.125983>.
- [18] A. Mittal, S.G. Chatterjee, G.M. Scott, E.T. Amidon, Modeling Xylan Solubilization during Autohydrolysis of Sugar Maple Wood Meal: Reaction Kinetics, 2009. <https://doi.org/10.1515/HF.2009.054>.
- [19] A. Mittal, S.G. Chatterjee, G.M. Scott, E.T. Amidon, Modeling xylan solubilization during autohydrolysis of sugar maple and aspen wood chips: reaction kinetics and mass transfer, *Chem. Eng. Sci.* 64 (13) (2009) 3031–3041, <https://doi.org/10.1016/j.ces.2009.03.011>.
- [20] S. Palliprath, N.J. Poolakkalody, K. Ramesh, S.M. Mangalan, S.P. Kabekkodu, R. Santiago, C. Manisseri, Pretreatment of sugarcane postharvest leaves by γ -valerolactone/water/ FeCl_3 system for enhanced glucan and bioethanol production, *Ind. Crop. Prod.* 197 (2023) 116571, <https://doi.org/10.1016/j.indcrop.2023.116571>.
- [21] M.K. Hassan, R. Chowdhury, S. Ghosh, D. Manna, A. Pappinen, S. Kuittinen, Energy and environmental impact assessment of Indian rice straw for the production of second-generation bioethanol, *Sustain. Energy Technol. Assess.* 47 (2021) 101546, <https://doi.org/10.1016/j.seta.2021.101546>.
- [22] M. Kaur, D.P. Malik, G.S. Malhi, V. Sardana, N.S. Bolan, R. Lal, K.H. Siddique, Rice residue management in the Indo-Gangetic Plains for climate and food security. A review, *Agron. Sustain. Dev.* 42 (5) (2022) 92.
- [23] A. Sluiter, B. Hames, R. Ruiz, C. Scarlata, J. Sluiter, D. Templeton, D. Crocker, Determination of structural carbohydrates and lignin in biomass, *Lab. Anal. Proced.* 1617 (1) (2008) 1–16.
- [24] A. Shaaban, S.M. Se, M.F. Dimin, J.M. Juoi, M.H.M. Husin, N.M.M. Mitran, Influence of heating temperature and holding time on biochars derived from rubber wood sawdust via slow pyrolysis, *J. Anal. Appl. Pyrolysis* 107 (2014) 31–39, <https://doi.org/10.1016/j.jaap.2014.01.021>.
- [25] L.G.J.M.A. Segal, J.J. Creely, A.E. Jr. Martin, C.M. Conrad, An empirical method for estimating the degree of crystallinity of native cellulose using the X-ray diffractometer, *Text. Res. J.* 29 (10) (1959) 786–794, <https://doi.org/10.1177/004051755902901003>.
- [26] A.H. Mohammed, A.K. Mohammed, F.H. Kamar, A.A. Abbas, G. Nechifor, Determination of ethanol in fermented broth by headspace gas chromatography using capillary column, *Rev. Chim. Burcharest Orig. Ed.* 69 (11) (2018) 2969–2972.
- [27] V. Krželj, J. Ferreira Liberal, M. Papaioannou, J. van der Schaaf, M. Neira d'Angelo, Kinetic model of xylose dehydration for a wide range of sulfuric acid concentrations (M. F.), *Ind. Eng. Chem. Res.* 59 (26) (2020) 11991–12003, <https://doi.org/10.1021/acs.iecr.0c01197>.
- [28] N.S. Kapu, Z. Yuan, X.F. Chang, R. Beatson, D.M. Martinez, H.L. Trajano, Insight into the evolution of the proton concentration during autohydrolysis and dilute-acid hydrolysis of hemicellulose, *Biotechnol. Biofuels* 9 (1) (2016) 1–10, <https://doi.org/10.1186/s13068-016-0619-6>.
- [29] O. Levenspiel, *Chemical Reaction Engineering*, John Wiley & Sons, 1998.
- [30] H. Zhang, G. Lyu, A. Zhang, X. Li, J. Xie, Effects of ferric chloride pretreatment and surfactants on the sugar production from sugarcane bagasse, *Bioresour. Technol.* 265 (2018) 93–101, <https://doi.org/10.1016/j.biortech.2018.05.111>.
- [31] C.M. Drapcho, N.P. Nghim, T. Walker, *Biofuels Engineering Process Technology*, McGraw-Hill Education, 2008.
- [32] C.Y. Wen, Noncatalytic heterogeneous solid-fluid reaction models, *Ind. Eng. Chem.* 60 (9) (1968) 34–54.
- [33] A. Heidari, N. Niknahad, M. Iljana, T. Fabritius, A review on the kinetics of iron ore reduction by hydrogen, *Materials* 14 (24) (2021) 7540, <https://doi.org/10.3390/ma14247540>.
- [34] A.V. Bandura, S.N. Lvov, The ionization constant of water over wide ranges of temperature and density, *J. Phys. Chem. Ref. Data* 35 (1) (2006) 15–30, <https://doi.org/10.1063/1.1928231>.
- [35] M. Canales, E. Guàrdia, Computer simulation study of ion-water and water-water hydrogen bonds in sulfuric acid solutions at low temperatures, *J. Mol. Liq.* 347 (2022) 118351, <https://doi.org/10.1016/j.molliq.2021.118351>.
- [36] C. Martín, P. Dixit, F. Momayez, L.J. Jönsson, Hydrothermal pretreatment of lignocellulosic feedstocks to facilitate biochemical conversion, *Front. Bioeng. Biotechnol.* 10 (2022) 846592, <https://doi.org/10.3389/fbioe.2022.846592>.
- [37] T.R. Sarker, F. Pattnaik, S. Nanda, A.K. Dalai, V. Meda, S. Naik, Hydrothermal pretreatment technologies for lignocellulosic biomass: a review of steam explosion and subcritical water hydrolysis, *Chemosphere* 284 (2021) 131372, <https://doi.org/10.1016/j.chemosphere.2021.131372>.
- [38] S. Zhibo, L. Liyi, H. Yong, B. Jie, Influence on ferric chloride aqueous solution caused by external electrostatic field: a molecular dynamics simulation study, *RSC Adv.* 8 (68) (2018) 38706–38714, <https://doi.org/10.1039/C8RA08349E>.
- [39] M.D. Smith, An abbreviated historical and structural introduction to lignocellulose, *Understanding lignocellulose: Synergistic computational and analytic methods*, American Chemical Society, 2019, pp. 1–15. <https://doi.org/10.1021/bk-2019-1338.ch001>.
- [40] S. Kumar, R. Gupta, Y.Y. Lee, R.B. Gupta, Cellulose pretreatment in subcritical water: effect of temperature on molecular structure and enzymatic reactivity, *Bioresour. Technol.* 101 (4) (2010) 1337–1347, <https://doi.org/10.1016/j.biortech.2009.09.035>.
- [41] D. Sun, Z.W. Lv, J. Rao, R. Tian, S.N. Sun, F. Peng, Effects of hydrothermal pretreatment on the dissolution and structural evolution of hemicelluloses and lignin: a review, *Carbohydr. Polym.* 281 (2022) 119050, <https://doi.org/10.1016/j.carbpol.2021.119050>.
- [42] H. Jeong, S.K. Jang, C.Y. Hong, S.H. Kim, S.Y. Lee, S.M. Lee, J.W. Choi, I.G. Choi, Levulinic acid production by two-step acid-catalyzed treatment of Quercusmongolica using dilute sulfuric acid, *Bioresour. Technol.* 225 (2017) 183–190, <https://doi.org/10.1016/j.biortech.2016.11.063>.
- [43] S. Elumalai, B. Agarwal, R.S. Sangwan, Thermo-chemical pretreatment of rice straw for further processing for levulinic acid production, *Bioresour. Technol.* 218 (2016) 232–246, <https://doi.org/10.1016/j.biortech.2016.06.037>.
- [44] J.P. Lee, J. Lee, K. Min, Development of bioprocess for corn-cob-derived levulinic acid production, *Bioresour. Technol.* 371 (2023) 128628, <https://doi.org/10.1016/j.biortech.2023.128628>.
- [45] C. Liu, X. Lu, Z. Yu, J. Xiong, H. Bai, R. Zhang, Production of levulinic acid from cellulose and cellulosic biomass in different catalytic systems, *Catalysts* 10 (9) (2020) 1006, <https://doi.org/10.3390/catal10091006>.
- [46] X. Ji, Z. Shen, C. Wang, S. Yao, L. Xiong, H. Zhang, H. Zhou, X. Chen, X. Chen, Amino-functionalized hyper-cross-linked resins for levulinic acid adsorption from sugarcane bagasse hydrolysate, *J. Chem. Technol. Biotechnol.* 98 (12) (2023) 2958–2970, <https://doi.org/10.1002/jctb.7502>.
- [47] N. Syaifika, Y. Matsumura, Comparative study of hydrothermal pretreatment for rice straw and its corresponding mixture of cellulose, xylan, and lignin, *Bioresour. Technol.* 255 (2018) 1–6, <https://doi.org/10.1016/j.biortech.2018.01.085>.
- [48] I. Kim, B. Lee, J.Y. Park, S.A. Choi, J.I. Han, Effect of nitric acid on pretreatment and fermentation for enhancing ethanol production of rice straw, *Carbohydr. Polym.* 99 (2014) 563–567, <https://doi.org/10.1016/j.carbpol.2013.08.092>.
- [49] T.C. Hsu, G.L. Guo, W.H. Chen, W.S. Hwang, Effect of dilute acid pretreatment of rice straw on structural properties and enzymatic hydrolysis, *Bioresour. Technol.* 101 (13) (2010) 4907–4913, <https://doi.org/10.1016/j.biortech.2009.10.009>.
- [50] L. Chen, R. Chen, S. Fu, FeCl_3 pretreatment of three lignocellulosic biomass for ethanol production, *ACS Sustain. Chem. Eng.* 3 (8) (2015) 1794–1800, <https://doi.org/10.1021/acssuschemeng.5b00377>.
- [51] I. Romero, J.C. López-Linares, M. Moya, E. Castro, Optimization of sugar recovery from rapeseed straw pretreated with FeCl_3 , *Bioresour. Technol.* 268 (2018) 204–211, <https://doi.org/10.1016/j.biortech.2018.07.112>.
- [52] C.L. Waters, R.R. Janupala, R.G. Mallinson, L.L. Lobban, Staged thermal fractionation for segregation of lignin and cellulose pyrolysis products: an experimental study of residence time and temperature effects, *J. Anal. Appl. Pyrolysis* 126 (2017) 380–389, <https://doi.org/10.1016/j.jaap.2017.05.008>.
- [53] E.L. Springer, J.F. Harris, Procedures for determining the neutralizing capacity of wood during hydrolysis with mineral acid solutions, *Ind. Eng. Chem. Prod. Res. Dev.* 24 (3) (1985) 485–489.
- [54] A.M. da Costa Lopes, K.G. João, D.F. Rubik, E. Bogel-Lukasik, L.C. Duarte, J. Andreas, R. Bogel-Lukasik, Pre-treatment of lignocellulosic biomass using ionic liquids: wheat straw fractionation, *Bioresour. Technol.* 142 (2013) 198–208, <https://doi.org/10.1016/j.biortech.2013.05.032>.
- [55] I. Romero, E. Ruiz, E. Castro, Pretreatment with metal salts, *Biomass Fractionation Technologies for a Lignocellulosic Feedstock Based Biorefinery*, (2016), pp. 209–227.

Article

Experimental Insights into the Fermentation of Pyro-Syngas to Ethanol in a Semi-Batch and Continuous Stirred Bioreactor with Mathematical Modelling and Optimization

Dinabandhu Manna ¹, Ranjana Chowdhury ^{1,†}, Rajnish K. Calay ² and Mohamad Y. Mustafa ^{2,*} 

¹ Chemical Engineering Department, Jadavpur University, Kolkata 700032, India; dinabandhu.juchem@gmail.com (D.M.); ranjana.chowdhury@jadavpuruniversity.in (R.C.)

² Department of Building, Energy and Material Technology, UiT the Arctic University of Norway, Narvik Campus, 8514 Narvik, Norway; rajnish.k.calay@uit.no

* Correspondence: mohamad.y.mustafa@uit.no; Tel.: +47-917-29-801

† Research supervisor.

Abstract: Syngas fermentation can play an important role in implementing the concept of biorefinery as it can serve as a platform to convert high-lignin biomass to biofuels. For the utilization of this process in commercial scale, the generation of an experimental database supported by a deterministic mathematical model and optimization is necessary. In this study, a locally isolated clostridial consortium, *UACJUCHE1*, was used to convert pyro-syngas to ethanol and acetic acid. Mathematical models were developed and validated for a 3 L stirred and gas-sparged bioreactor operated in both semi-batch and continuous modes. The volumetric productivity of ethanol was correlated with the dilution rate and the gas residence time. The performance of the bioreactor, run in both semi-batch and continuous modes, was optimized using response surface methodology. For the semi-batch operation, a maximum ethanol concentration of 13.122 g/L after 30 h operation was achieved at optimum values of pyrolysis temperature, ratio of gas to liquid volume (V_G/V_L), and volumetric gas flow rate of 648 °C, 0.46, and 6.7 L/h respectively. For continuous operation, a maximum ethanol concentration of 29.450 g/L after 300 h is obtained at optimum values of V_G/V_L and ratio of gas to liquid volumetric flow rate of 0.28 and 335.148, respectively.

Keywords: pyro-syngas; semi-batch and continuous stirred bioreactor; mixed clostridial consortium; mathematical modelling; optimization



Citation: Manna, D.; Chowdhury, R.; Calay, R.K.; Mustafa, M.Y. Experimental Insights into the Fermentation of Pyro-Syngas to Ethanol in a Semi-Batch and Continuous Stirred Bioreactor with Mathematical Modelling and Optimization. *Energies* **2024**, *17*, 562. <https://doi.org/10.3390/en17030562>

Academic Editors: João Fernando Pereira Gomes and Toufik Boushaki

Received: 10 December 2023

Revised: 15 January 2024

Accepted: 21 January 2024

Published: 24 January 2024



Copyright: © 2024 by the authors. Licensee MDPI, Basel, Switzerland. This article is an open access article distributed under the terms and conditions of the Creative Commons Attribution (CC BY) license (<https://creativecommons.org/licenses/by/4.0/>).

1. Introduction

The switching over from high-carbon to low-carbon fuels aids in the mitigation of CO₂ emissions. To reach the current energy targets, the utilization of low-carbon renewable and sustainable biofuels derived from waste biomass can also serve the purpose of reducing CO₂ emissions. In all countries, agro-waste represents the major waste biomass. Being an agricultural country, India produces a large quantity of agro-waste dominated by rice residues, like rice straw, rice husk, etc. [1]. According to recent literature, 165.8 Mt of rice straw is produced annually in India [2]. Although India still faces the pollution created by stubble burning, the generation of bioethanol from rice straw can amply reduce the problem of CO₂ emissions. In an earlier publication by the present group, it was estimated that under the 2030–2031 benchmark, 11,165 million L of bioethanol can be produced with a potential of 6928 GWh energy with a reduction of 14,375 kt CO₂ emissions. In that analysis, the generation of bioethanol through a sugar platform via the generation of fermentable sugars (glucose, xylose, arabinose, etc.) from rice straw through medium temperature hydrolytic pretreatment using dilute sulfuric acid was considered [3]. Rice straw has a lignin content as high as 17% and due to recalcitrance of lignin, the generation

of bioethanol through a syngas platform seems more suitable for the utilization of all C-polymers including cellulose, hemicelluloses, and lignin in it [1,4].

Syngas fermentation is a hybrid process through which syngas, mainly constituting CO and H₂, is generated from lignocellulosic biomass in the first step, and subsequently the gas is fermented to bioethanol in the second step. In most cases, syngas from biomass is produced through gasification [4,5]. As disclosed in the previous publication of the present group, pyrolysis of biomass generating pyro-char, pyro-oil, and pyro-gas is expected to play an important role in the development of hybrid processes combining thermochemical and biochemical processes [4]. As pyro-gas usually contains CO, H₂, and CO₂, it has the prospect of being used in a syngas platform of ethanol production. No such attempt has, however, been reported in the literature. In the case of high ash containing biomass like rice straw, solid waste is generated during gasification. Unlike gasification, the generation of pyro-gas does not generate any waste because pyro-char is used as fuel, as an adsorbent, and for soil amendment, and pyro-oil can be used as a liquid fuel after upgradation. Although usually pyro-oil is considered as the target product, recent research studies have also been reported with the focus on pyro-syngas generation [6–10].

In gasification, the biomass reacts with a sub-stoichiometric amount of oxygen, required for complete combustion. During syngas fermentation, while CO and CO₂ act as carbon sources, CO and H₂ act as electron donors [11]. Since most of the microorganisms suffer from toxicity of CO, only those capable of utilizing CO as a carbon source are suitable. *Acetobacterium woodii* and the clostridial strains, namely, *C. ljungdahlii*, *C. acetium*, *C. carboxidivorans*, *C. ragsdalei*, *C. autoethanogenum*, *C. thermoaceticum*, etc. are usually employed. Although Diender et al. reported that mixed clostridial culture can produce ethanol, only a few studies are available in this regard [12]. The clostridial microorganisms are strictly anaerobic and hence oxygen is detrimental for their growth. Therefore, it is expected that pyro-gas can be a better substitute for syngas because the former never contains any oxygen unlike the latter which sometimes contains unconverted gasifying reactant, i.e., oxygen. Experimental data should be generated for pyro-syngas fermentation. In many cases, simulated gas mixtures are used for syngas fermentation. Investigations should be made using real syngas generated from thermochemical processes like gasification and pyrolysis. Although pure cultures are usually used, mixed culture can also be used for syngas fermentation. Very limited studies on the production of bioethanol through syngas fermentation using mixed culture were reported [11]. Some of the major challenges associated with syngas fermentation are the limitation of mass transfer of the substrates (CO + H₂) from the gas phase to the liquid phase and inhibitory effects of CO on the fermentation process. Mathematical modelling is an important tool to analyze the behavior of syngas fermentation involving an array of parallel and series microbial reactions simultaneously with gas-liquid mass transfer. It is actually a critical task to develop a mathematical model, because both gas-to-liquid mass transfer and liquid-phase microbial kinetics play important roles in this process. Different models were reported for syngas fermentation. In a successful attempt, Siebler et al. synergistically combined a one-dimensional model with a computational fluid dynamics (CFD) model for syngas fermentation in a bubble reactor [13]. Chen et al. developed a mathematical model for a bubble reactor using *C. ljungdahlii* through metabolic modelling in which they considered growth on CO and H₂ [14]. As per Vandecasteele, models were proposed for syngas fermentation by *C. ljungdahlii* using a mixture of CO, H₂, and CO₂ [15]. Most of the possible metabolic reactions were considered with their stoichiometric representations. They considered growth kinetics on CO following the Haldane equation, along with inhibition by acetic acid; growth on CO₂ and H₂ with the inhibition by CO and acetic acid; conversion of CO into ethanol incorporating inhibition by acetic acid; production of ethanol from CO₂ and H₂ including inhibition by CO and acetic acid; and direct conversion of acetic acid to ethanol through two reactions, one with the participation of CO and another with the participation of H₂ [15]. Almeida Benalcázar et al. proposed a hybrid model consisting of a bio-thermodynamic black box model and fermenter hydrodynamics. They tested the model for a bubble bioreactor using (a) pure CO

and (b) a mixture of CO₂ and H₂ [16]. Mohammadi et al. developed models for *L. jundahlia* using growth kinetics on a CO and H₂ mixture [17]. Very recently, Puiman et al. developed a scale-down model using a Euler–Lagrange simulation to assess the fluctuations of gaseous components, CO, H₂, etc. during the industrial-scale operation of syngas fermentation [18]. Elisa M. de Medeiros et al. developed a dynamic model using growth kinetics on CO and H₂ and also dealt with optimization of the operation of a continuous stirred tank bioreactor [19]. A comprehensive model of a gas-fed stirred tank reactor was reported by Ruggiero et al. for the utilization of pure CO. They developed the model for *Carboxidivorans* and simulated gas was used as the substrate. Other than the production of ethanol from CO, they also considered direct production of ethanol from acetic acid. The inhibitory effects of both acetic acid and ethanol were considered [20].

The present article focuses on the biochemical conversion of pyro-syngas to ethanol using a mixed clostridial consortium, *UACJUCHE1*, and a mathematical model was developed. To the best of our knowledge, both experimental studies and model development on pyro-syngas fermentation to produce ethanol were conducted for the first time. The article includes (1) an experimental study on the pyrolysis of Indian rice straw in the range of 400–700 °C along with the determination of the product yield and pyro-syngas composition; (2) the performance of a 3 L stirred tank gas-fed bioreactor in semi-batch and continuous modes of operation with mathematical modelling; and (4) the optimization of performance of the semi-batch and continuous bioreactors.

2. Materials and Methods

2.1. Chemical Composition of Rice Straw

The rice straw was collected from West Bengal, India. The rice straw samples (φ 4.5 mm × 140 mm) were shredded to a shorter size (Φ 4.5 mm × 10 mm). The moisture content of rice straw was 5.39%. The analysis of the lignocellulosic composition was carried out through National Renewable Energy Laboratory (NREL) protocol [21]. The composition is reported in Table 1 on a dry basis.

Table 1. Chemical composition of rice straw.

Component	Cellulose	Hemicellulose	Lignin
% (w/w)	38.31 ± 1.67	21.09 ± 0.92	±0.59

2.2. Pyrolysis of Rice Straw

The pyrolysis of rice straw was carried out in a semi-batch reactor (35 mm diameter and 210 mm long) under isothermal conditions at the temperatures of 400, 450, 500, 550, 600, 650, and 700 °C in an inert atmosphere maintained by nitrogen [22,23]. The reactor was equipped with a furnace, a temperature controller (PID controller), and a digital weight box. The rice straw was pyrolyzed at a rate of 10 g/h. To provide sufficient reaction time to convert the higher molecular weight volatile compounds to gaseous compounds, the nitrogen flow rate was maintained at a value of 2.5 g/h. For the recovery of pyro-oil, the volatile product from the pyrolyzer was passed through a condenser using circulation of water at 20 °C. The non-condensable part of the volatile product constituted pyro-syngas. The solid product, pyro-char, was collected after atmospheric cooling of the pyrolyzer. A schematic diagram of the pyrolyzer is represented in Figure 1. The pyro-gas was analyzed using a GC. The GC (Thermo Scientific, Nashik, India TRACE1110) was equipped with Chromeleon 7 software and a thermal conductivity detector (TCD). The hydrogen, air, and nitrogen flow rates were set as 30, 300, and 30 mL/min, respectively. The oven and TCD detector temperatures were 40 and 250 °C, respectively. A TR-FAME (60 m × 0.22 mm × 0.25 µm) column was used.

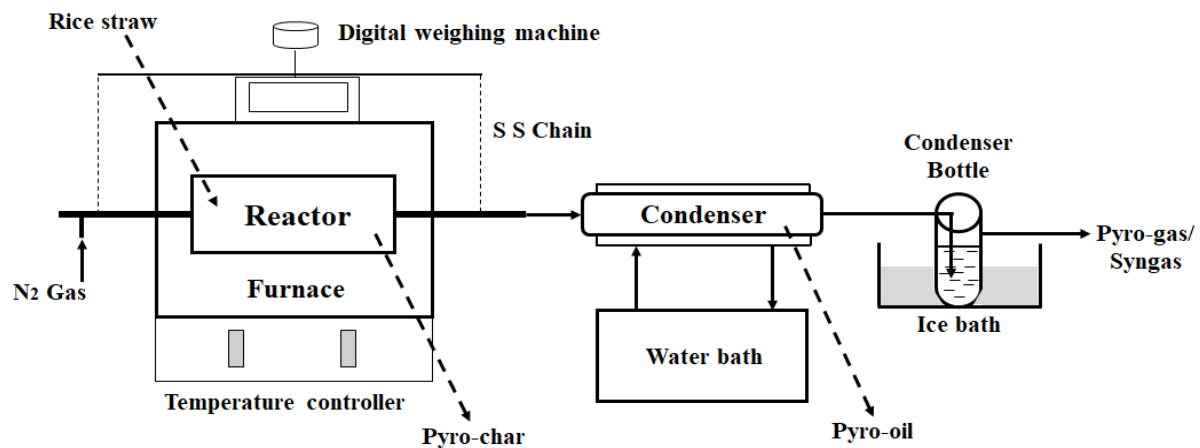


Figure 1. Schematic diagram of the pyrolysis of rice straw.

The yield of the pyro-products namely, pyro-char, pyro-oil, and pyro-gas were determined using the following equations:

$$\% \text{ Yield of pyro - char} = \frac{\text{mass of pyro - char obtained from pyrolysis}}{\text{mass of biomass fed to the reactor}} \times 100 \quad (1)$$

$$\% \text{ Yield of pyro - oil} = \frac{\text{mass of pyro - oil obtained from pyrolysis}}{\text{mass of biomass fed to the reactor}} \times 100 \quad (2)$$

$$\% \text{ Yield of pyro - gas} = 100 - \text{Yields of (pyro - char + pyro - oil)} \quad (3)$$

2.3. Pyro-Syngas Fermentation

2.3.1. Microorganism

A mixed clostridial consortium—UACJUChe1, isolated from local paddy fields in West Bengal, was used as inoculum [24].

2.3.2. Preparation of Modified Clostridial Medium for Growth

The modified clostridial medium was prepared according to ATCC (American Type Culture Collection) 1754 medium. Similar to the protocol followed by Vandecasteele, fructose, yeast extract, and sodium bicarbonate were excluded from the medium and a pH buffer, namely 2-(N-morpholino) ethanesulfonic acid (MES), was used [15]. The basal DSMZ 879 medium containing 1 g NH_4Cl , 0.1 g KCl , 0.2 g $\text{MgSO}_4 \cdot 7 \text{H}_2\text{O}$, 0.8 g NaCl , 0.1 g $\text{CaCl}_2 \cdot 2 \text{H}_2\text{O}$, 100 mM MES, 10 mL reducing agent, 1 mL trace elements, and 1 mL Wolfe's vitamin solution per liter was used. A total of 1 mg of resazurin (10 mg/L), an indicator of anaerobic conditions, was also added to 1 L basal medium. The pH of the medium was adjusted to 6 using 0.1 N NaOH. The basal medium thus prepared was transferred to sterile vessels (rubber sealed bottles/Erlenmeyer flasks/bioreactor) already degassed with nitrogen. The medium was further autoclaved and cooled to 37 °C. Gas (CO or simulated $\text{CO}_2\text{-H}_2$ mixture or simulated pyro-syngas, i.e., $\text{CO-CO}_2\text{-H}_2\text{-CH}_4\text{-N}_2$ mixture or pyro-syngas generated in the pyrolizer) transfer was undertaken to prepare modified clostridial medium as per the requirement of the experimental runs. Only CO or CO_2 or CO and CO_2 , supplied either through pure gas (CO or $\text{CO}_2\text{-H}_2$ mixture or simulated $\text{CO-CO}_2\text{-H}_2\text{-CH}_4\text{-N}_2$ mixture) or from pyro-syngas, used according to experimental protocol, were the carbon source. Gas was transferred through flushing of the head space for 125 mL bottles and 250 mL conical flasks used for pre-adaptation as well as stock culture and batch reactions for the determination of growth kinetics, respectively. For the bioreactor, the gas was transferred through sparging.

2.3.3. Pre-Adaptation of *UACJUCHE1* to Simulated Pyro-Syngas and Maintenance of Stock Culture

According to the results of the analysis of the pyrolysis gas obtained in the temperature range of 400–700 °C, as provided in Section 4, it was observed that molar concentration (%) of CO, H₂, CO₂, and CH₄ increases from 17.07%, 13.32%, 9.11%, and 7.19% to 23.08%, 17.23%, 10.59%, and 8.82%. In the present study the pyro-syngas, generated from the pyrolyzer, was ultimately fermented in a 3 L bioreactor operated in semi-batch and continuous modes. Therefore, the *UACJUCHE1* consortium was exposed to a simulated pyro-syngas mixture containing CO, H₂, CO₂, CH₄, and N₂ (25:20:15:10:35) for pre-adaptation. The basal sterile medium, as described, of 25 mL volume was transferred to 10 sterile and sealed glass serum bottles of 125 mL each. The medium in each bottle was inoculated with 4% (v/v) *UACJUCHE1* culture and was subsequently flushed with the simulated pyro-syngas (CO:H₂:CO₂:CH₄:N₂::25:20:15:10:35) mixture to maintain a pressure of 100 kPa in the head space. All bottles were incubated at 37 °C in an anaerobic chamber and orbital shaking of 150 rpm was maintained. Anaerobic conditions were maintained by the flow of pure nitrogen. After adaptation, a weekly transfer of 4% (v/v) inoculum to new serum bottles was followed to retain the activity of the consortium.

2.3.4. Batch Experiments for Determination of Growth Kinetics of *UACJUCHE1*

Separate sets of batch experiments were conducted for the determination of growth kinetics of *UACJUCHE1* on CO and on CO₂ and H₂.

Experiments for Growth Kinetics on CO

The basal sterile medium, as described, of 50 mL volume was transferred to a 250 mL sterile and sealed Erlenmeyer flask for each experiment. Batch experiments were conducted to know the effect of gas phase concentration of CO on the growth dynamics of *UACJUCHE1*. Considering the concentration of CO in pyro-syngas, the inlet molar concentration of CO was varied in the range of 15–25%. For each inlet concentration of CO, the growth dynamics were studied for 24 h. To obtain the data at 2 h intervals, 12 Erlenmeyer flasks were used for each inlet molar concentration of CO of 15%, 17.5%, 20%, 22.5%, and 25%. In each flask, gas was transferred through flushing. All flasks were inoculated with 4% (v/v) stock culture before the introduction of gas. For each experiment, the initial pH was maintained at 6. Incubation was performed under anaerobic conditions at 37 °C and an orbital shaking speed of 150 rpm was maintained. All experiments were conducted in triplicate. For any experiment meant for each inlet CO concentration, the Erlenmeyer flasks, demarcated for the particular sampling period, were taken out of the incubator and the biomass concentration was determined by the assessment of optical density at 600 nm using a spectrophotometer.

Experiments for Growth Kinetics on CO₂ and H₂

The experimental protocol followed, in case of the determination of growth kinetics on CO₂ and H₂, was similar to that used for the growth kinetics on CO. Considering the concentration of CO₂ and H₂ in pyro-syngas, the inlet molar concentration of CO₂ and H₂ were kept in the ranges of 8–12% and 15–20%, respectively. Nine sets of batch experiments were conducted using the inlet gas composition of CO₂:H₂::8:15; CO₂:H₂::8:17.5; CO₂:H₂::8:20; CO₂:H₂::10:15; CO₂:H₂::10:17.5; CO₂:H₂::10:20; CO₂:H₂::12:15; CO₂:H₂::12:17.5; and CO₂:H₂::12:20. For each inlet composition of CO₂–H₂ mixture, the growth dynamics were studied for 24 h under anaerobic conditions. To obtain the data at 2 h intervals, 12 Erlenmeyer flasks were used. In each flask, gas was transferred through flushing. All experimental parameters like temperature, pH, stirring speed, etc. were kept the same as those maintained in case of growth on CO. The biomass concentration was determined by the assessment of optical density at 600 nm using a spectrophotometer.

2.3.5. Stirred Tank Bioreactor for Pyro-Syngas Fermentation

Experiments were conducted in a 3 L glass bioreactor of 135 mm diameter and 235 mm height, equipped with two 50 mm Rushton gas dispersion impellers, each with six flat blades mounted vertically around a central horizontal disc and gas sparger. The impellers were spaced at a distance of 60 mm. The lower impeller was situated 30 mm above the bottom. The bioreactor was provided with inlet and outlet lines for both gas and liquid streams. The main gas sparger, connected with the gas outlet, was located in between the lower impeller and the bottom of the bioreactor. The bioreactor is schematically represented in Figure 2.

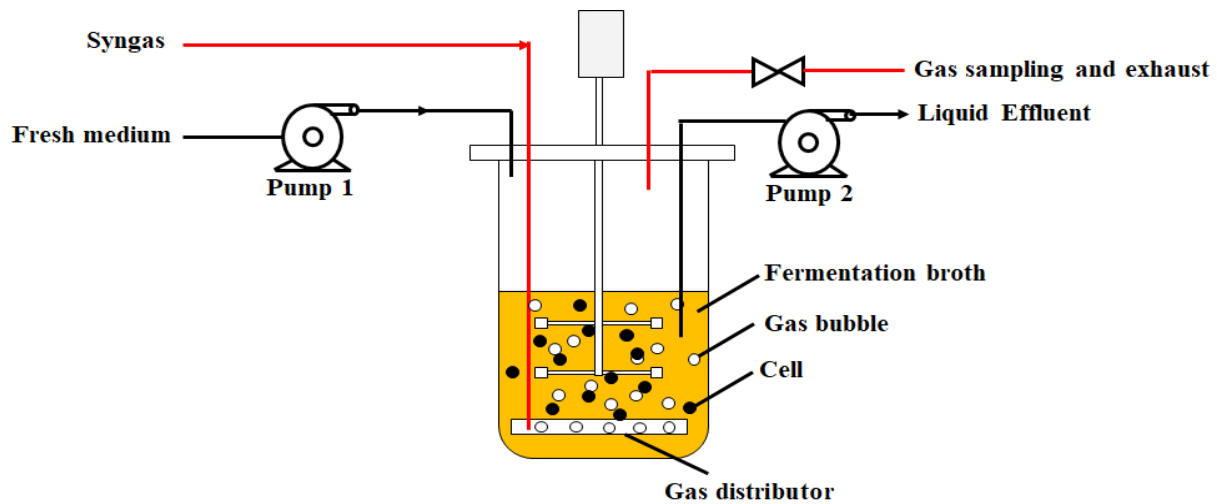


Figure 2. Schematic representation of the stirred bioreactor.

Determination of Effect of Stirring Speed and Gas Velocity on O_2 Mass Transfer Coefficient

Experiments were conducted in the 3 L glass bioreactor at 37 °C. The bioreactor was filled with 2.5 L basal sterile medium, as described in Section 2.3.3. Experiments were conducted to determine the mass transfer coefficient of O_2 . Before flowing oxygen, the vessel was flushed with pure N_2 . The oxygen flow rate was varied from 0.6–10 LPM, and the stirring speed was varied from 150–900 rpm. All the experiments were conducted in triplicate. The correlation of K_La on gas phase superficial velocity, u_{sg} , determined by dividing the volumetric flow rate of gas by the cross-sectional area of the vessel, and the power consumption of the gassed system per unit volume, P_G/V_L , as recommended by Gill et al., were validated from the experimental data. The correlation is as follows [25]:

$$k_{la,O_2} = 0.224 \left(\frac{P_G}{V_L} \right)^{0.35} (u_{sg})^{0.52} \quad (4)$$

The correlation between the power consumption of gassed (P_G) and ungassed (P_{UG}) systems is as follows:

$$\frac{P_G}{P_{UG}} = 0.497 \left(\frac{Q}{Nd_i^3} \right)^{-0.38} \left(\frac{N^2 d_i^3 \rho}{\sigma} \right)^{-0.18} \quad (5)$$

$$P_{UG} = N_p \rho N^3 d_i^5 \quad (6)$$

N_p = Power number; N = stirring speed (rpm); ρ = density of solution; σ = surface tension. The value of the power number was considered to be 10 [25,26].

The value of k_{la} for any component, j , can be determined by knowing the value of k_{la} of oxygen as follows [14]:

$$k_{la,j} = k_{la,O_2} \sqrt{\frac{D_{l,j}}{D_{lO_2}}} \quad (7)$$

Accordingly, the k_{la} values for CO, CO₂, and H₂ were determined.

Strategy of Operation of the Bioreactor in Semi-Batch and Continuous Modes

Start-up

For both continuous and semi-batch operations, 2.5 L of basal sterile medium was first saturated with pyro-syngas obtained at 700 °C by running the bioreactor vessel at a stirring speed of 900 rpm and an inlet gas flow rate of 0.6 L/h for 12 h. The medium, saturated with the pyro-syngas, was transferred to a storage tank and was fed to the bioreactor up to a desired liquid volume, as set by the experimental strategy, at the start-up.

Operation of the bioreactor

In the case of semi-batch operation, a continuous flow of gas was maintained at different volumetric flow rates. No input and output of the liquid phase was used. For the continuous mode of operation, both gas and liquid were fed and discharged at the respective same rates. While the semi-batch operation was continued for 30 h, the operation time for the continuous mode was 300 h. The concentration of ethanol was optimized through response surface methodology (RSM) using Design-Expert software (version 13). The experiments were conducted according to the design of the experiments. The operating parameters used for semi-batch and continuous operations are represented in Tables 2 and 3. For semi-batch operation, the pyrolysis temperature, gas to liquid volume ratio (V_G/V_L), and volumetric flow rate of gas were used as parameters. The variation of the pyrolysis temperature is actually reflected in the composition of inlet gas. For the continuous operation, the pyro-syngas obtained at 700 °C was fed continuously using a gas to liquid volume ratio (V_G/V_L) and the ratio of gas to liquid volumetric flow rates (q_G/q_L) as parameters. According to the values of V_G/V_L , the bioreactor was filled with the required volume of sterile basal medium, already saturated with pyro-syngas, as described in Section 2.3.4, and was subsequently inoculated with 4% (v/v) stock culture. Considering the shear sensitivity of microorganisms, the stirring speed was maintained at 150 rpm. The sterile basal medium without any dissolved gas was fed during continuous operation. As a result of variation of these parameters, the dilution ratio, $D (=q_L/V_L)$ and gas residence time, $GRT (=V_L/q_G)$ were varied from 0.0106–0.0133 h^{−1} and 0.3–3.125 h, respectively. For both modes of operation, the concentrations of ethanol, and gas phase concentrations of CO, CO₂, and H₂ were measured using GC, and the acetic acid concentration was analyzed using HPLC. HPLC was performed to analyze the liquid sample, obtained from syngas fermentation. The HPLC (Waters 2489) of Waters, Singapore, consists of degasser, binary pump, auto-sampler, and UV-Vis detector. The analytical column was C18 (250 mm × 4.6 mm × 5 μm) of SunFire, Maynooth, Ireland.

Table 2. Operating parameters used for the semi-batch reactor according to RSM.

SL No.	T (°C)	V_G/V_L	q_G (L/h)	CO:CO ₂ :H ₂ :CH ₄ :N ₂	V_G (L)	V_L (L)
1	550	0.6	5.3	22.8:10.5:17.1:8.7:21.7	1.125	1.875
2	550	0.6	5.3	22.8:10.5:17.1:8.7:21.7	1.125	1.875
3	400	0.6	10	17.0:9.1:13.3:7.1:27.0	1.125	1.875
4	700	1	5.3	23.1:10.6:17.2:8.8:21.5	1.5	1.5
5	400	1	5.3	17.0:9.1:13.3:7.1:27.0	1.5	1.5
6	550	0.2	10	22.8:10.5:17.1:8.7:21.7	0.5	2.5
7	700	0.2	5.3	23.1:10.6:17.2:8.8:21.5	0.5	2.5
8	400	0.2	5.3	17.0:9.1:13.3:7.1:27.0	0.5	2.5

Table 2. Cont.

SL No.	T (°C)	V _G /V _L	q _G (L/h)	CO:CO ₂ :H ₂ :CH ₄ :N ₂	V _G (L)	V _L (L)
9	550	1	10	22.8:10.5:17.1:8.7:21.7	1.5	1.5
10	700	0.6	0.6	23.1:10.6:17.2:8.8:21.5	1.125	1.875
11	700	0.6	10	23.1:10.6:17.2:8.8:21.5	1.125	1.875
12	550	0.2	0.6	22.8:10.5:17.1:8.7:21.7	0.5	2.5
13	550	1	0.6	22.8:10.5:17.1:8.7:21.7	1.5	1.5
14	550	0.6	5.3	22.8:10.5:17.1:8.7:21.7	1.125	1.875
15	550	0.6	5.3	22.8:10.5:17.1:8.7:21.7	1.125	1.875
16	550	0.6	5.3	22.8:10.5:17.1:8.7:21.7	1.125	1.875
17	400	0.6	0.6	17.0:9.1:13.3:7.1:27.0	1.125	1.875

Table 3. Operating parameters for continuous operation according to RSM.

SL No.	VG/VL	qG/qL	V _G (L)	V _L (L)	q _G (L/h)	q _L (L/h)
1	1	500	1.5	1.5	10	0.02
2	1	30	1.5	1.5	0.6	0.02
3	0.6	265	1.125	1.875	5.3	0.02
4	0.6	265	1.125	1.875	5.3	0.02
5	0.6	265	1.125	1.875	5.3	0.02
6	0.2	30	0.5	2.5	0.6	0.02
7	0.6	265	1.125	1.875	5.3	0.02
8	0.2	500	0.5	2.5	10	0.02
9	0.6	265	1.125	1.875	5.3	0.02
10	0.6	597.3	1.125	1.875	11.94	0.02
11	0.03	265	0.1	2.9	5.3	0.02
12	0.6	0	1.125	1.875	0	0.02
13	1.16	265	1.62	1.38	5.3	0.02

3. Theoretical Analysis

3.1. Growth Kinetics

3.1.1. Kinetics of Growth on CO

As is evident from the literature, Haldane-type growth kinetics are usually followed by clostridial strains grown on CO as the carbon source [27]. Therefore, a Haldane-type growth model incorporating substrate inhibition along with inhibition of undissociated acetic acid, formed as a product, was attempted for the growth on CO. This is as follows:

$$\mu_1 = \mu_1^{max} \frac{C_{CO}}{K_{CO} + C_{CO} + \frac{C_{CO}^2}{K_{I,CO}}} \frac{K_{I,UA}}{K_{I,UA} + C_{UA}} \quad (8)$$

where, μ = specific growth rate = $\frac{1}{C_X} \frac{dC_X}{dt}$ and C_X is biomass concentration.

μ_1 is specific growth rate on CO; μ_1^{max} is the maximum specific growth rate on CO; C_{CO} is the concentration of CO; K_{CO} is the saturation constant for CO, and $K_{I,CO}$ is the inhibition constant for growth on CO; $K_{I,UA}$ is the inhibition constant of undissociated acetic acid; and C_{UA} is the concentration of undissociated acetic acid.

$$C_{UA} = C_{AA} \left(1 - \frac{10^{(pH-pK_a)}}{(10^{(pH-pK_a)} + 1)} \right) \quad (9)$$

pH = 6.7; for acetic acid, pK_a = 4.77 at 37 °C; C_{AA} is the acetic acid concentration.

In this study μ_1^{max} was adjusted to fit the experimental growth data, obtained using different mole fraction of pure CO in the gas phase in the Erlenmeyer flasks, as described in the section titled “Experiments for Growth Kinetics on CO”. The other constants obtained by Vandecasteele for *C. ljungdahlii* were used [15].

3.1.2. Kinetics of Growth on CO₂–H₂ Mixture

The multiplicative growth kinetic model followed by *C. ljungdahlii*, as reported by Vandecasteele, was attempted [15]. The form of the kinetic equation is as follows:

$$\mu_2 = \mu_2^{max} \frac{C_{CO_2}}{K_{CO_2} + C_{CO_2}} \frac{C_{H_2}}{K_{H_2} + C_{H_2}} \frac{K_{I, CO}^{hy}}{K_{I, CO}^{hy} + C_{CO}} \frac{K_{I, UA}}{K_{I, UA} + C_{UA}} \quad (10)$$

In this study μ_2^{max} was adjusted to fit the experimental growth data, obtained using pure CO₂–H₂ mixture in the Erlenmeyer flasks, as described in the section titled “Experiments for Growth Kinetics on CO₂ and H₂”. The other constants obtained by Vandecasteele (2016) for *C. ljungdahlii* were used [15].

3.2. Mathematical Model

The reactions for the generation of ethanol from pyro-syngas were chosen according to Vandecasteele as they used the effects of the mixture of CO, CO₂, and H₂ on syngas fermentation. As they used *C. ljungdahlii* and not a mixed culture like *UACJUCHE1*, some kinetic growth data were separately determined in the present study. Similar to *C. ljungdahlii*, the molecular formula for *UACJUCHE1* was assumed to be CH_{1.81}O_{0.58}N_{0.24}. The Wood–Ljungdahl pathway for the production of ethanol from syngas is represented in Figure 3.

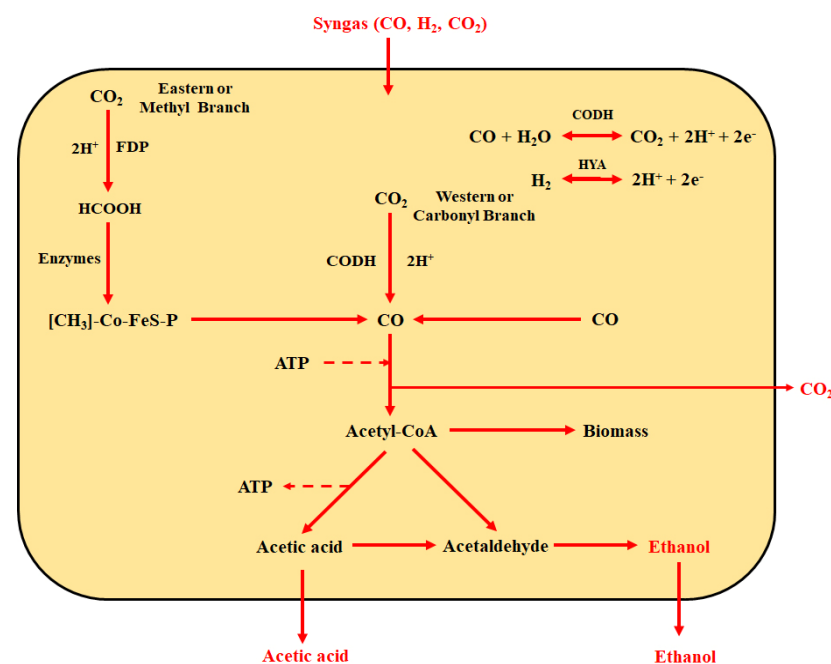
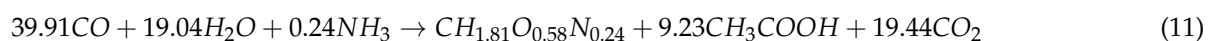


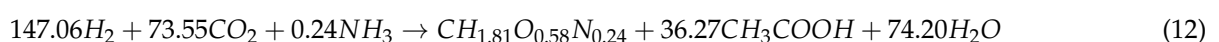
Figure 3. Schematic diagram of the Wood–Ljungdahl pathway for the production of ethanol from syngas (Acetyl-CoA: Acetyl coenzyme A; CODH: Carbon monoxide dehydrogenase; FDH: Formate dehydrogenase; Syngas: Synthesis gas).

The reactions under consideration of the model are as follows:

Biomass growth on carbon monoxide



Biomass growth on carbon dioxide and hydrogen

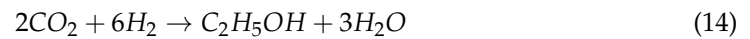


Ethanol production from carbon monoxide

In this path, the production of ethanol is considered to take place through direct conversion of acetyl-CoA into ethanol and is non-growth associated.

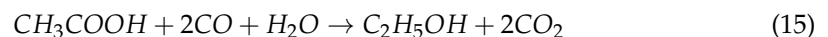


Ethanol production from carbon dioxide and hydrogen



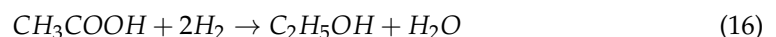
Conversion of acetate into ethanol in the presence of CO

To reduce acetate to ethanol, the water–gas shift reaction can be used, in which CO acts as the electron donor through the conversion of CO into CO₂ delivering the necessary reducing power.



Conversion of acetic acid into ethanol in the presence of H₂

Acetate can also be reduced by using hydrogen as the electron donor during the conversion of molecular hydrogen to two protons and two electrons using the enzyme hydrogenase.



The biomass growth kinetics and ethanol production kinetics are represented in Table 4.

Table 4. Kinetics of growth and kinetics of mixed clostridial consortium—UACJUCHe1.

Process	Specific Growth or Product Generation Rate (μ)
(i) Biomass growth on CO	$\mu_1 = \mu_1^{\max} \frac{C_{\text{CO}}}{K_{\text{CO}} + C_{\text{CO}} + \frac{C_{\text{CO}}^2}{K_{\text{I,CO}}}} \frac{K_{\text{I,UA}}}{K_{\text{I,UA}} + C_{\text{UA}}}$
(ii) Biomass growth on CO ₂ and H ₂	$\mu_2 = \mu_2^{\max} \frac{C_{\text{CO}_2}}{K_{\text{CO}_2} + C_{\text{CO}_2}} \frac{C_{\text{H}_2}}{K_{\text{H}_2} + C_{\text{H}_2}} \frac{K_{\text{I,CO}}^{\text{hy}}}{K_{\text{I,CO}}^{\text{hy}} + C_{\text{CO}}} \frac{K_{\text{I,UA}}}{K_{\text{I,UA}} + C_{\text{UA}}}$
(iii) Ethanol production from CO	$q_{\text{E1}} = q_{\text{E1}}^{\max} \frac{C_{\text{CO}}}{K_{\text{CO}} + C_{\text{CO}} + \frac{C_{\text{CO}}^2}{K_{\text{I,CO}}}} \frac{C_{\text{UA}}}{K_{\text{UA}} + C_{\text{UA}}}$
(iv) Ethanol production from CO ₂ and H ₂	$q_{\text{E2}} = q_{\text{E2}}^{\max} \frac{C_{\text{CO}_2}}{K_{\text{CO}_2} + C_{\text{CO}_2}} \frac{C_{\text{H}_2}}{K_{\text{H}_2} + C_{\text{H}_2}} \frac{K_{\text{I,CO}}^{\text{hy}}}{K_{\text{I,CO}}^{\text{hy}} + C_{\text{CO}}} \frac{C_{\text{UA}}}{K_{\text{UA}} + C_{\text{UA}}}$
(v) Conversion of acetate into ethanol using CO as electron donor	$q_{\text{E3}} = q_{\text{E3}}^{\max} \frac{C_{\text{CO}}}{K_{\text{CO}} + C_{\text{CO}} + \frac{C_{\text{CO}}^2}{K_{\text{I,CO}}}} \frac{C_{\text{UA}}}{K_{\text{UA}} + C_{\text{UA}}}$
(vi) Conversion of acetate into ethanol using H ₂ as electron donor	$q_{\text{E4}} = q_{\text{E4}}^{\max} \frac{C_{\text{H}_2}}{K_{\text{H}_2} + C_{\text{H}_2}} \frac{C_{\text{UA}}}{K_{\text{UA}} + C_{\text{UA}}} \frac{K_{\text{I,CO}}^{\text{hy}}}{K_{\text{I,CO}}^{\text{hy}} + C_{\text{CO}}}$

Specific production rate of ethanol = $\frac{1}{C_X} \frac{dC_E}{dt}$ and C_E is ethanol concentration.

The molar yield coefficients of different participating reactants and products with respect to biomass were calculated from their stoichiometric coefficients represented in Equations (11) and (12). Similarly, molar yield coefficients of different participating reactants and products with respect to ethanol were calculated from their stoichiometric coefficients represented in Equations (13)–(16).

The yield coefficient of any component, i with respect to biomass, $Y_{i/X}$ and with respect to ethanol, $Y_{i/E}$ can be defined as follows:

$$Y_{i/X} = \frac{\left| \frac{dC_i}{dt} \right|}{\frac{dC_X}{dt}} \quad (17)$$

$$Y_{i/E} = \frac{\left| \frac{dC_i}{dt} \right|}{\frac{dC_E}{dt}} \quad (18)$$

Mole Balance Equations Semi-batch Reactor Gas Phase

The mole balance equations for CO, CO₂, and H₂ in the gas phase are as follows:

$$\frac{dp_{CO}}{dt} = \frac{q_G}{V_G}(p_{COin} - p_{CO}) - (k_L a)_{CO} \frac{V_L}{V_G} RT(p_{CO}H_{CO} - C_{COL}) \quad (19)$$

where, p stands for partial pressure, R is universal gas law constant, and T is temperature in Kelvin:

$$\frac{dp_{H2}}{dt} = \frac{q_G}{V_G}(p_{H2in} - p_{H2}) - (k_L a)_{H2} \frac{V_L}{V_G} RT(p_{H2}H_{H2} - C_{H2L}) \quad (20)$$

$$\frac{dp_{CO2}}{dt} = \frac{q_G}{V_G}(p_{CO2in} - p_{CO2}) - (k_L a)_{CO2} \frac{V_L}{V_G} RT(p_{CO2}H_{CO2} - C_{CO2L}) \quad (21)$$

Liquid Phase

$$\frac{dC_{COL}}{dt} = (k_L a)_{CO}(p_{CO}H_{CO} - C_{COL}) + r_{CO} \quad (22)$$

$$\frac{dC_{H2L}}{dt} = (k_L a)_{H2}(p_{H2}H_{H2} - C_{H2L}) + r_{H2} \quad (23)$$

$$\frac{dC_{CO2L}}{dt} = (k_L a)_{CO2}(p_{CO2}H_{CO2} - C_{CO2L}) + r_{CO2} \quad (24)$$

$$\frac{dC_X}{dt} = r_X \quad (25)$$

$$\frac{dA_A}{dt} = r_{AA} \quad (26)$$

$$\frac{dC_E}{dt} = r_E \quad (27)$$

where,

$$r_{CO} = -(\mu_1 Y_{CO/X} + q_{E1} Y_{CO/E} + q_{E3} Y_{CO/E}^{AA-CO}) C_X \quad (28)$$

$$r_{H2} = -(\mu_2 Y_{H2/X} + q_{E2} Y_{H2/E} + q_{E4} Y_{H2/E}^{AA-H2}) C_X \quad (29)$$

$$r_{CO2} = (\mu_1 Y_{CO2/X} + q_{E1} Y_{CO2/E} + q_{E3} Y_{CO2/E}^{AA-CO}) - (\mu_2 Y_{CO2/X} + q_{E2} Y_{CO2/E}) C_X \quad (30)$$

$$r_X = (\mu_1 + \mu_2) C_X \quad (31)$$

$$r_{AA} = \left((\mu_1 Y_{AA/X} + \mu_2 Y_{AA/X}) - (q_{E3} Y_{AA/E}^{AA-CO} + q_{E4} Y_{AA/E}^{AA-H2}) \right) C_X \quad (32)$$

$$r_E = (q_{E1} + q_{E2} + q_{E3} + q_{E4}) C_X \quad (33)$$

Continuous Reactor

The dynamic mole balance Equations (19)–(21) of components in the gas phase are the same for the semi-batch and the continuous reactors. As there are both input and output for the liquid stream in the continuous reactor, the liquid phase dynamic mole balance equations take the following forms:

$$\frac{dC_{COL}}{dt} = (k_L a)_{CO}(p_{CO}H_{CO} - C_{COL}) + r_{CO} - \frac{q_L}{V_L} C_{COL} \quad (34)$$

$$\frac{dC_{H2L}}{dt} = (k_L a)_{H2}(p_{H2}H_{H2} - C_{H2L}) + r_{H2} - \frac{q_L}{V_L} C_{H2L} \quad (35)$$

$$\frac{dC_{CO_2L}}{dt} = (k_L a)_{CO_2}(p_{CO_2}H_{CO_2} - C_{CO_2L}) + r_{CO_2} - \frac{q_L}{V_L}C_{CO_2L} \quad (36)$$

$$\frac{dC_X}{dt} = r_X - \frac{q_L}{V_L}C_X \quad (37)$$

$$\frac{dA_A}{dt} = r_{AA} - \frac{q_L}{V_L}C_{AA} \quad (38)$$

$$\frac{dC_E}{dt} = r_E - \frac{q_L}{V_L}C_E \quad (39)$$

C_{AA} and C_E stand for acetic acid and ethanol concentration, respectively.

The values of $p_{CO_{in}}$, $p_{H_2_{in}}$, and $p_{CO_2_{in}}$ were set according to the concentration of inlet pyro-syngas. The initial values of liquid phase concentration of CO, H₂ and CO₂ were set to the saturation values because as per the experimental strategy, the sterile basal medium was saturated with the pyro-syngas at the start-up of both semi-batch and continuous bioreactors. The initial condition is presented in Equation (40) as follows:

$$\text{At } t = 0, \begin{bmatrix} p_{CO} = 0 \\ p_{H_2} = 0 \\ p_{CO_2} = 0 \\ C_{CO_L} = C_{CO_L}^* \\ C_{H_2L} = C_{H_2L}^* \\ C_{CO_2L} = C_{CO_2L}^* \\ C_X = 0.05 \text{ mol/L} \\ C_{AA} = 0 \\ C_E = 0 \end{bmatrix} \quad (40)$$

All the equations were numerically solved using the initial condition, given in Equation (40) using ode45 of MATLAB software version R2016a.

3.3. Optimization of Ethanol Concentration in Semi-Batch and Continuous Bioreactors

3.3.1. Semi-Batch Bioreactor

For the bioreactors operated in the semi-batch mode, a three-level, three-factor Box–Behnken statistical design of response surface methodology (RSM) was used to fit the trend of dependence of the response variable, namely, ethanol concentration, obtained after 30 h, on different relevant operating variables by second-order models. Design Expert software (version 13) was used for this purpose. Three variables, namely the temperature of pyrolysis (A), the ratio V_G/V_L (B), and q_G (C) were considered as the parameters. According to the method, 17 experiments were conducted at the set points recommended by the Design of Experiment, represented in Table 2. The variables (A, B, and C) with coded levels (−1, 0, and 1) are shown in Table 5.

Table 5. Variables with coded levels used for the semi-batch experimental run.

Input Variables	Unit	Coded Variable Level			Model Response
		−1	0	1	
Temperature (A)	°C	400	550	700	Ethanol concentration (g/L) after 30 h operation
V_G/V_L (B)		0.2	0.6	1	
q_G (C)	L/h	0.6	5.3	10	

The pyrolysis temperature was chosen as a parameter because it influences the input gas composition. The ratio of the overhead volume and the liquid volume, V_G/V_L , was considered as a parameter because it influences the driving force, i.e., the difference between the interfacial concentration of nutrient gases (CO, H₂, and CO₂) at the gas–liquid interface under equilibrium and the bulk liquid concentration [20]. Ruggiero et al. also used a similar

parameter, $V_L/(V_G + V_L)$, i.e., the filling ratio, as a parameter [20]. The volumetric flow rate, q_G , was used as a parameter because it indirectly influences the mass transfer coefficient, k_{Ga} , by altering the gas phase superficial velocity, u_{sg} , as represented in Equation (4). Refs. [19,20] also used this parameter in their model.

3.3.2. Continuous Bioreactor

As indicated in the experimental description, the bioreactor was operated in continuous mode using the inlet gas generated in the pyrolyzer at 700 °C. For the bioreactor operated in the continuous mode, a two-factor Box–Behnken statistical design in response to surface methodology (RSM) was used to fit the trend of dependence of the response variable, namely ethanol concentration, obtained after 300 h, on different relevant operating variables by second-order models. Design Expert software (version 13) was used for this purpose. Two variables, namely, V_G/V_L (A) and q_G/q_L (B), were considered as the parameters. Accordingly, 13 experiments were conducted at the set points recommended by the Design of Experiment, represented in Table 3. The ranges of variables (A and B) with coded levels (−1, 0, and 1) are shown in Table 6. These parameters were used because they actually influence the gas phase residence time, GRT, important for mass transfer and the liquid phase residence time and hence the dilution rate (D) which is important for both mass transfer and the fermentation reaction [19]. Elisa M. de Medeiros et al. used GRT and D as the parameters of optimization in their study [19]. We separately analyzed the effects of GRT and D on the volumetric productivity of ethanol during continuous operation.

Table 6. Variables with coded levels used for the experimental run.

Input Variables	Unit	Coded Variable Level			Model Response
		−1	0	1	
V_G/V_L (A)	-	0.2	0.6	1	Ethanol concentration (g/L) after 300 h operation
q_G/q_L (B)	-	30	265	500	

4. Results and Discussion

4.1. Composition and Volumetric Flow Rates of Pyro-Syngas

In Figure 4, the mole fractions of different constituent gases, namely CO, H₂, CO₂, and CH₄ in pyro-syngas were plotted against temperature.

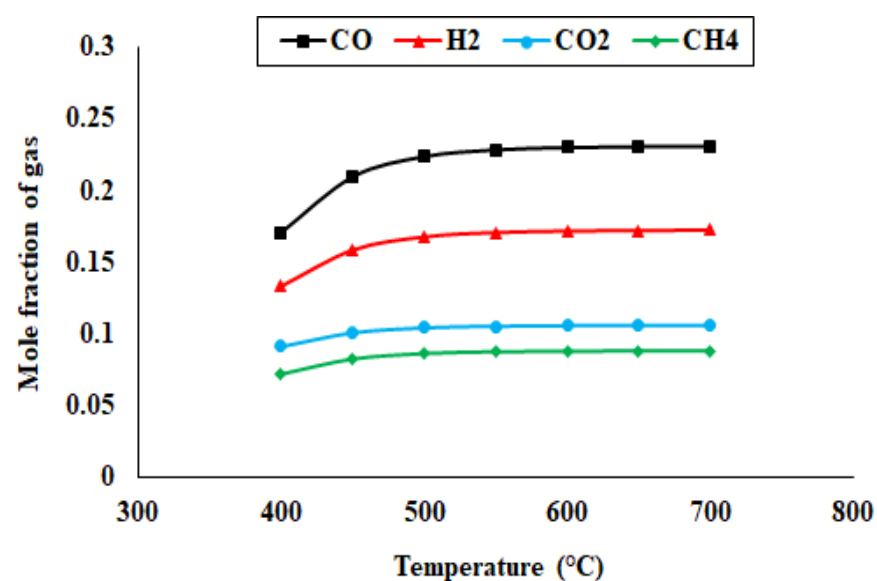


Figure 4. Composition of pyro-syngas produced at different pyrolysis temperatures.

It is evident that the mole fraction of each gaseous component increased with the temperature up to 550 °C, after which a saturation trend was observed. Molar concentration (%) of CO, H₂, CO₂, and CH₄ increased from 17.07%, 13.32%, 9.11%, and 7.19% to 23.08%, 17.23%, 10.59%, and 8.82%, respectively, as the pyrolysis temperature was increased from 400 °C to 700 °C. As the temperature increased from 400 °C to 700 °C, the gas flow rate increased from 30.3 L/h to 51.41 L/h.

From the analysis of Table 7, it appears that the yields of char and oil decreased and increased respectively with the rise in temperature. The yield of pyro-oil, however, passed through a maximum at 500 °C after which it decreased. These trends can be explained by the fact that with the increase in temperature, the extent of thermal degradation of rice straw increases, releasing lower molecular weight compounds as compared to those obtained at a lower temperature range.

Table 7. Yield of the pyro-products.

Temperature °C	Yield of Pyro-Products Pyro-Char	Pyro-Oil	Pyro-Syngas
400	41.39 ± 1.97	27.01 ± 1.12	31.60 ± 1.01
450	37.98 ± 1.32	27.33 ± 1.01	34.69 ± 1.29
500	34.91 ± 1.89	28.02 ± 1.39	37.07 ± 1.33
550	30.09 ± 1.08	27.07 ± 1.02	42.84 ± 1.40
600	28.51 ± 0.52	25.37 ± 0.72	46.12 ± 2.11
650	25.34 ± 0.32	23.98 ± 0.15	50.68 ± 2.39
700	23.32 ± 0.33	22.09 ± 0.17	54.59 ± 2.42

4.2. Values of Parameters

4.2.1. K_La for Different Gases

As described in Section 2.3.3, the sterile basal medium was first saturated with pyro-syngas obtained at 700 °C by maintaining a stirring speed of 900 rpm and an inlet gas flow rate of 0.6 L/h for 12 h. The values of K_La , for CO, CO₂, and H₂, as determined experimentally and using Equations (4) and (7), are 144.9 h^{−1}, 166.9 h^{−1}, and 123.6 h^{−1}, respectively. During semi-batch and continuous operations, the stirring speed was maintained at 150 rpm and the volumetric flow rate of syngas was varied from 0.6–10 L/h. There is a wide variation of values of K_La because of their dependence on both the superficial velocity of gas and hence the volumetric flow rate. With the increase of gas flow rate there was an increase in the K_La values. According to Equations (4) and (7), the values of K_La for CO, CO₂, and H₂ varied from 23.5 to 100.7 h^{−1}, 27 to 116.7 h^{−1}, and 20 to 87.4 h^{−1}, respectively, as the gas flow rate was varied from 0.6 to 10 L/h.

4.2.2. Model Parameters

The values of molar yield coefficients are provided in Table 8, and different model parameter and constants are provided in Tables 8 and 9, respectively.

Table 8. Yield coefficient for different process [15].

Process	Yield Coefficients (mol/mol)
(i) Biomass growth on CO	$Y_{\frac{CO}{X}} = 39.91$, $Y_{\frac{AA}{X}} = 9.23$, $Y_{\frac{CO_2}{X}} = 19.44$
(ii) Biomass growth on CO ₂ and H ₂	$Y_{\frac{H_2}{X}} = 147.06$, $Y_{\frac{AA}{X}} = 36.27$, $Y_{\frac{CO_2}{X}} = 73.55$
(iii) Ethanol production from CO	$Y_{\frac{CO}{E}} = 6$, $Y_{\frac{CO_2}{E}} = 4$
(iv) Ethanol production from CO ₂ and H ₂	$Y_{\frac{CO_2}{E}} = 2$, $Y_{\frac{H_2}{E}} = 6$
(v) Conversion of acetate into ethanol using CO as electron donor	$Y_{\frac{AA}{E}}^{AA-CO} = 1$, $Y_{\frac{CO}{E}}^{AA-CO} = 2$, $Y_{\frac{CO_2}{E}}^{AA-CO} = 2$,
(vi) Conversion of acetate into ethanol using H ₂ as electron donor	$Y_{\frac{H_2}{E}}^{AA-H_2} = 2$, $Y_{\frac{AA}{E}}^{AA-H_2} = 1$

Table 9. Values of mass transfer coefficients, Henry's constants, and kinetic parameters.

Symbol	Significance		Unit	Source
$(K_La)_{CO}$	Product of mass transfer coefficient (mh^{-1}) and specific surface area (m^2/m^3) of CO in the bioreactor	23.5–100.7	h^{-1}	Determined
$(K_La)_{CO_2}$	Product of mass transfer coefficient (mh^{-1}) and specific surface area (m^2/m^3) of CO ₂ in the bioreactor	27–116.7	h^{-1}	Determined
$(K_La)_{H_2}$	Product of mass transfer coefficient (mh^{-1}) and specific surface area (m^2/m^3) of H ₂ in the bioreactor	20–87.4	h^{-1}	Determined
H_{CO}	Henry's law constant of CO	0.0008	mol/L/atm	[28]
H_{H_2}	Henry's law constant of CO ₂	0.00066	mol/L/atm	[28]
H_{CO_2}	Henry's law constant of H ₂	0.025	mol/L/atm	[28]
μ_1^{max}	Maximum specific growth rate on CO	0.192	h^{-1}	Determined
μ_2^{max}	Maximum specific growth rate on CO ₂ and H ₂	0.045	h^{-1}	Determined
q_1^{max}	Maximum specific production rate of ethanol from CO	0.20	h^{-1}	[15]
q_2^{max}	Maximum specific production rate of ethanol from CO ₂ and H ₂	0.0001	h^{-1}	[15]
q_3^{max}	Maximum specific production rate of ethanol through conversion of acetate using CO as electron donor	0.20	h^{-1}	[15]
q_4^{max}	Maximum specific production rate of ethanol through conversion of acetate using H ₂ as electron donor	0.20	h^{-1}	[15]
K_{CO}	Saturation constant for CO for growth	0.000078	mol/L	[15]
K_{H_2}	Saturation constant for H ₂ for growth	0.00022	mol/L	[15]
K_{CO_2}	Saturation constant for CO ₂ for growth	0.00022	mol/L	[15]
K_{UA}	Saturation constant of acetic acid for ethanol production from CO/CO ₂ and H ₂	0.0005	mol/L	[15]
K_{UA}^{Ac}	Saturation constant of acetic acid for ethanol production from acetate	0.0005	mol/L	[15]
K_{iCO}	Inhibition constant of CO for growth on CO	0.002	mol/L	[15]
K_{iCO}^{Hy}	Inhibition constant of CO for growth on CO ₂ and H ₂	7×10^{-9}	mol/L	[15]
K_{iUA}	Inhibition constant of acetic acid for growth on CO/CO ₂ and H ₂	0.0104	mol/L	[15]

Different model parameters, namely mass transfer coefficients, Henry's constants, and kinetic parameters are provided in Table 9.

4.2.3. Significance of Model Parameters and Their Comparison with Similar Studies

The model parameters related to mass transfer are the values of K_La and Henry's constants for CO, CO₂, and H₂. Henry's constant, correlating the gas and liquid phase concentration of a component under equilibrium, varies with temperature for all gases and hence is the same for all studies. The values of K_La for CO, CO₂, and H₂ have varied from 23.5–100.7 h^{-1} , 27–116.7 h^{-1} , and 20–87.4 h^{-1} , whereas in reported studies their values have varied from 4.69–22.7 h^{-1} , 2.54–26.2 h^{-1} , and 6.67–19.4 h^{-1} , respectively [15–20]. The value of K_La for CO has also been reported to be 198 h^{-1} in one study [20]. Thus, it is inferred that the mass transfer rate in the present case is similar to those in the reported literature. In the present case, the growth of the clostridial consortium on CO as well as CO₂ and H₂ has been considered. The maximum specific growth rate on CO was determined to be 0.192 h^{-1} , while for different clostridial strains, the value lay in the range of 0.22–0.37 h^{-1} [20]. The value of the maximum specific growth rate on H₂ was determined to be 0.045 h^{-1} . In the literature, the maximum specific growth rate on H₂ was reported to be 0.031–0.045 h^{-1} [15,20]. Thus, the growth rate for the presently used consortium is comparable to other established pure clostridial strains. The values of the saturation constant, signifying the substrate concentration corresponding to half of the maximum specific growth rate, have also been determined for CO, H₂, and CO₂ and the values are 0.000078 mol/L, 0.00022 mol/L, and 0.00022 mol/L. This signifies that the specific growth rate reaches the maximum at a lower value of CO concentration compared to H₂ and CO₂. The reported values of the saturation constants for CO and H₂ are 0.000045–0.00039 mol/L and 0.00022–0.00071 mol/L, respectively. This again proves that the saturation constants of the consortium are in the same range as with the recognized

strains. The inhibition constants of CO on the growth on CO itself and on hydrogen are 0.002 mol/L and 7×10^{-9} mol/L, respectively. As the inhibition constant signifies the concentration level of the component rendering a strong inhibitory effect, it is clear that the growth on hydrogen is heavily inhibited by the presence of CO compared to CO-based growth. Perhaps the growth on H_2 and CO_2 can only occur after CO is fully utilized. Similar observations have been reported by other researchers [15]. The yield coefficients, Y_{CO}^X , $Y_{H_2}^X$, and $Y_{CO_2}^E$ of the present study are 0.67 g/mol, 0.18 g/mol, and 6 mol/mol, respectively whereas the reported ranges are 0.24–2.6 g/mol, 0.20–0.37 g/mol, and 2–10.5 mol/mol, respectively [15–20,29–32]. Therefore, the model parameters are very much comparable with the literature data.

4.3. Performance of the Bioreactor in Semi-Batch and Continuous Modes

4.3.1. Bioreactor Dynamics in the Semi-Batch Mode

Using the mathematical model for semi-batch operation, the transient behavior of ethanol concentration and acetic acid up to 30 h of operation at q_G of 5.3 L/h was presented using V_G/V_L in the range of 0.2–1 as a parameter. It was observed that for ethanol and acetic acid concentration, the increasing trend persisted even at 30 h. With the increase of V_G/V_L , there was a decrease in the concentration of both ethanol and acetic acid. This can be explained by the fact that with the increase in the volume of head space, less mass transfer to the liquid phase occurs, causing a decrease in the reaction rate and hence the concentration of both products. The transient behavior of the conversion of different gaseous component, namely CO, H_2 , and CO_2 , was represented in Figure 5. The conversion of any component, i , was calculated by $\frac{p_{i,in} - p_{i,out}}{p_{i,in}}$. From the figure it can be observed that after 12 h of operation the gas phase conversion reached equilibrium. All the trends are very similar to those obtained by other researchers [19,20].

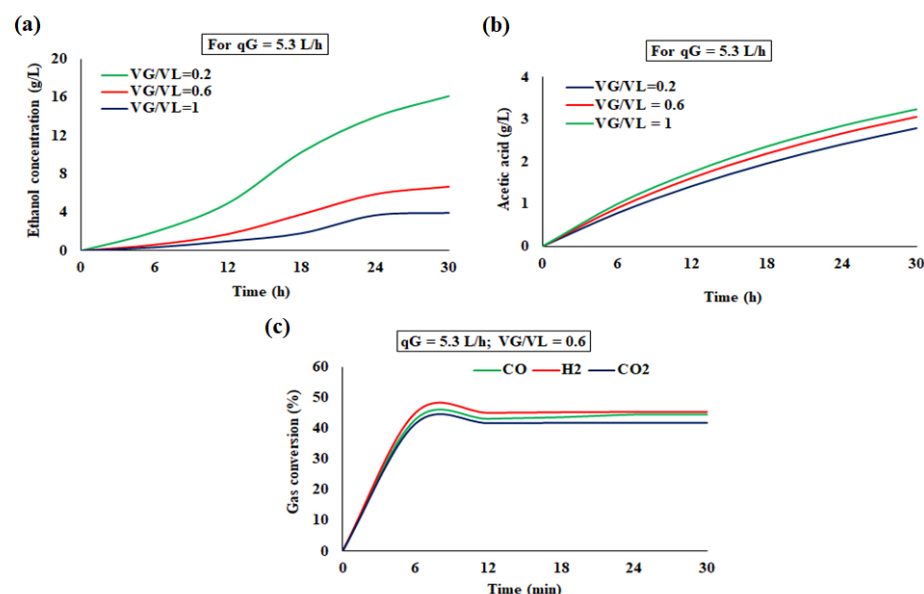


Figure 5. Simulated profile for semi-batch reactor ((a): Ethanol; (b): acetic acid; (c): gas conversion %).

4.3.2. Bioreactor Dynamics in the Continuous Mode

Simulated Profile for the Continuous Reactor

Using the mathematical model for continuous operation, the transient behavior of ethanol concentration and acetic acid up to 300 h of operation at q_G/q_L of 250 were presented using V_G/V_L in the range of 0.6–1 as a parameter. It was observed that both ethanol and acetic acid concentration reaches saturation after 180 h of running. Similar to the trend of Semi-batch operation, the concentration of both products decreases with the increase of V_G/V_L . The transient behavior of conversion of different gaseous component,

namely, CO, H₂ and CO₂ was represented in Figure 6. From the figure it can be observed that after 120 h of operation the gas phase conversion reaches equilibrium. All the trends are very similar to those obtained by other researchers [19,20].

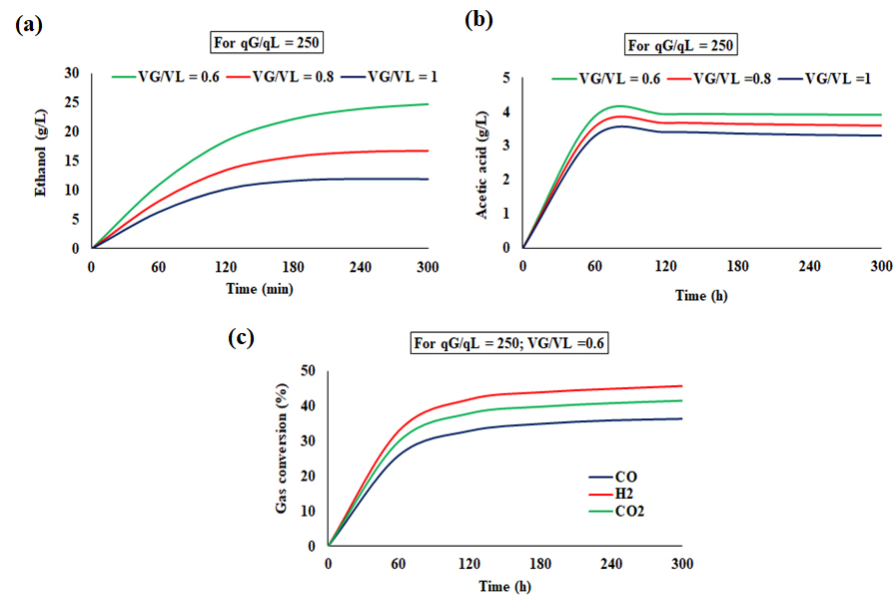


Figure 6. Simulated profile for the continuous reactor ((a): ethanol concentration; (b): acetic acid concentration and (c): % gas conversion).

4.4. Comparison of Simulated and Experimental Results

4.4.1. Semi-Batch Operation

In Figure 7, the experimental and simulated values of ethanol concentration in the semi-batch reactor were plotted against operation time (=6 h, 12 h, 18 h, 24 h and 30 h) in a bar-plot. The results were obtained at a pyrolysis temperature of 600 °C, V_G/V_L of 0.5, and q_G of 6 Lpm. From the analysis of the figure, it appears that the agreement between the model prediction and the experimental results is very good.

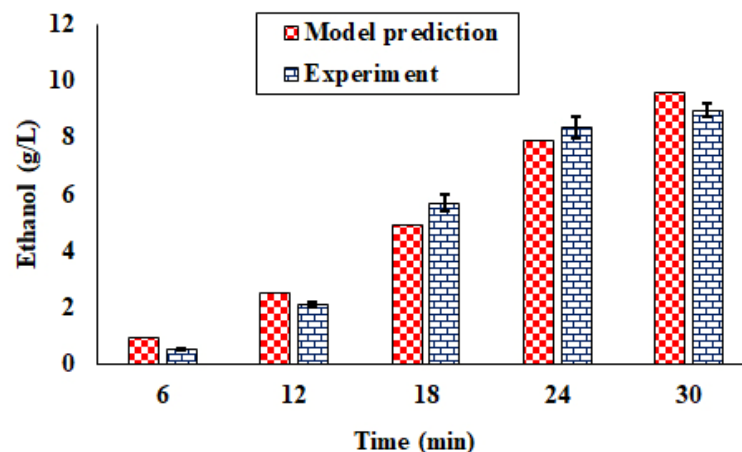


Figure 7. Ethanol production in the semi-batch reactor (pyrolysis temperature = 600 °C, V_G/V_L = 0.5, and q_G = 6 Lpm).

4.4.2. Continuous Operation

The experimental and simulated values of ethanol concentration at 300 h of continuous operation were plotted against V_G/V_L in the range of 0.6–1 at a fixed value of q_G/q_L of 250 in Figure 8a. Similarly, the experimental and simulated values of ethanol concentration at 300 h were plotted against q_G/q_L in the range of 30–250 at a fixed value of V_G/V_L of

0.6 in Figure 8b. While the ethanol concentration decreased with the increase in V_G/V_L , it showed an increasing trend with the increase in q_G/q_L . A decrease and increase in the mass transfer to liquid phase with the increase in gas volume fraction, i.e., head space, and the gas velocity, respectively, and the increase in reaction time with the decrease in liquid volume, i.e., the decrease in dilution rate, can explain this behavior.

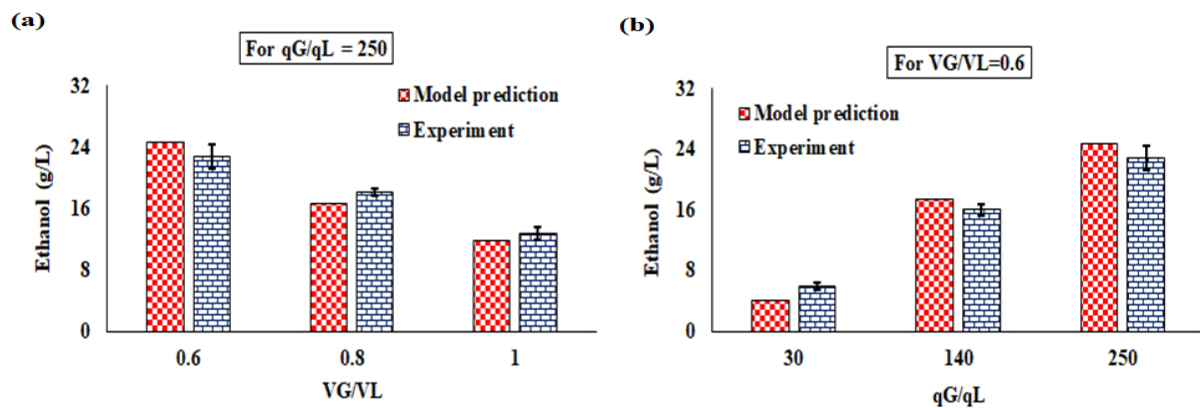


Figure 8. Ethanol production from syngas fermentation in the continuous reactor (model prediction and experimental value). ((a): Variation of experimental and simulated ethanol concentration with V_G/V_L ($=0.6$ – 1) at a fixed value of $q_G/q_L = 250$; (b) Variation of experimental and simulated ethanol concentration with q_G/q_L ($=30$ – 250) at a fixed value of V_G/V_L ($=0.6$)).

The experimental and simulated values of ethanol concentration at 300 h of continuous operation were plotted against V_G/V_L in the range of 0.6–1 at a fixed value of q_G/q_L of 250 in Figure 8a. Similarly, the experimental and simulated values of ethanol concentration at 300 h were plotted against q_G/q_L in the range of 30–250 at a fixed value of V_G/V_L of 0.6 in Figure 8b.

For both semi-batch and continuous operations, the mathematical models appear to predict realistic results.

4.5. Effect of Gas Residence Time (GRT) and Dilution Factor (D) on the Volumetric Productivity of Ethanol

For the experimental ranges of the parameters, preset according to Table 3 for the continuous mode of operation, the ethanol production behavior over 300 h was assessed as a function of the gas residence time (GRT) and dilution rate, D , in Figure 9. The dilution rate was calculated by dividing the volumetric flow rate of liquid by the liquid volume, i.e., $\frac{q_L}{V_L}$, and the gas residence time was calculated by dividing the liquid volume by the volumetric flow rate of gas, i.e., $\frac{V_L}{q_G}$. In this figure, the volumetric productivity of ethanol, calculated by the multiplication of D and the ethanol concentration at 300 h, i.e., $D * C_{Ethanol \text{ at } 300 \text{ h}}$, was plotted simultaneously against D and GRT through a 3D plot using the meshgrid function in MATLAB software version R2016a.

From Figure 9, it is evident that the increase of GRT has a positive impact on the volumetric productivity of ethanol from syngas fermentation. The increment of D , however, has a negative impact on the volumetric productivity of ethanol.

4.6. Optimization Results for Semi-Batch and Continuous Bioreactors

4.6.1. Semi-Batch Bioreactor

The second order regression equation, obtained to represent the relationships among the response variable, ethanol concentration obtained after 30 h, and the operating variables, namely the temperature of pyrolysis (A), the ratio V_G/V_L (B), and q_G (C) is as follows:

$$\text{Ethanol concentration} = 1.06651 + 0.00345496 \times A + 3.2557 \times B - 0.0558511 \times C - 0.0119167 \times A \times B + 0.00393617 \times A \times C - 1.55984 \times B \times C \quad (41)$$

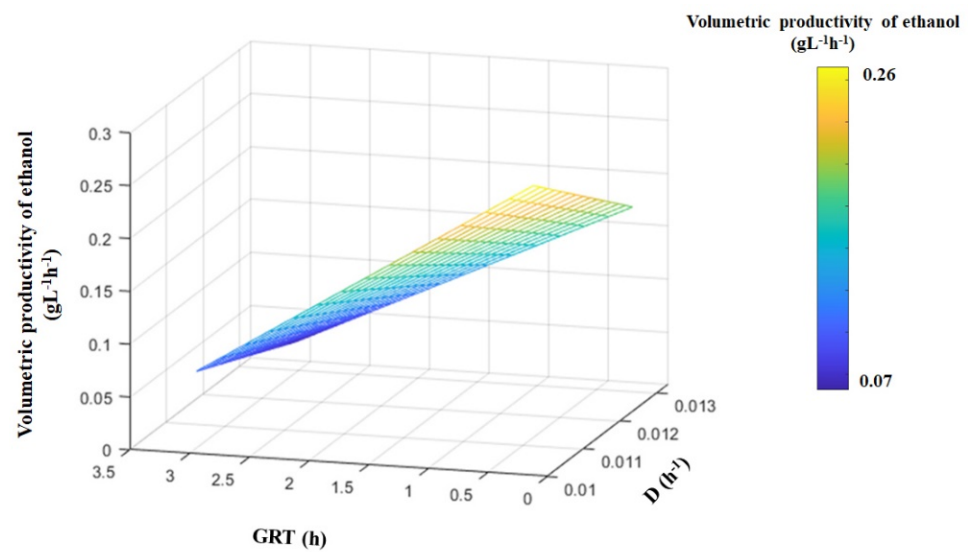


Figure 9. Effect of the gas residence time (GRT) and dilution factor (D) on the volumetric productivity of ethanol from syngas fermentation.

The comparison between the predicted and actual values of the response variables, represented in Figure 10, and the analysis of variance (ANOVA), presented in Table 10, shows that the model can represent the trend of dependence of ethanol concentration of the selected operating variables.

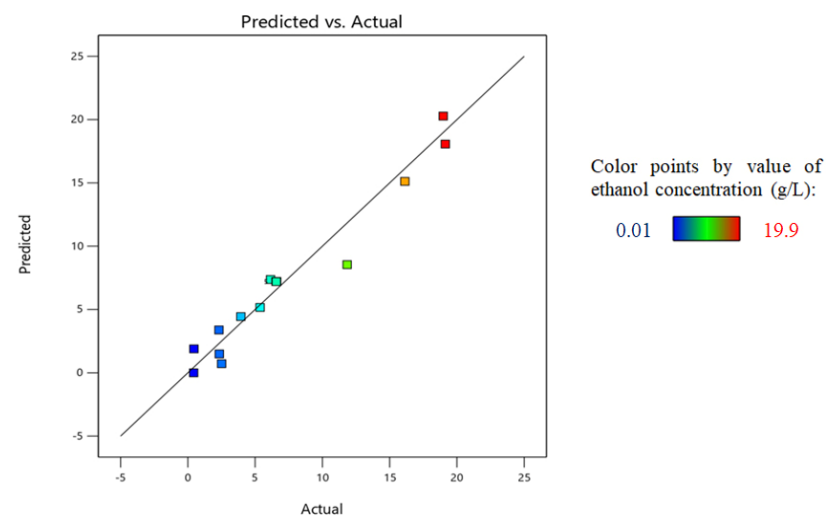


Figure 10. Comparison between the RSM-predicted and experimental values of ethanol concentration at 30 h of semi-batch operation.

Table 10. ANOVA table for the semi-batch bioreactor.

Source	Sum of Squares	df	Mean Square	F-Value	p-Value	
Model	534.72	6	89.12	34.53	<0.0001	significant
A-Temperature	53.05	1	53.05	20.55	0.0011	
B- V_G/V_L	171.22	1	171.22	66.34	<0.0001	
C- q_G	243.21	1	243.21	94.23	<0.0001	
AB	2.04	1	2.04	0.7923	0.3943	
AC	30.80	1	30.80	11.93	0.0062	
BC	34.40	1	34.40	13.33	0.0045	
Residual	25.81	10	2.58			

Table 10. Cont.

Source	Sum of Squares	df	Mean Square	F-Value	p-Value	
Model	534.72	6	89.12	34.53	<0.0001	significant
Lack of Fit	25.81	6	4.30			
Pure Error	0.0000	4	0.0000			
Cor Total	560.53	16				

(Std. Dev. 1.61; Mean 7.21; C.V. (%) 22.30; R^2 0.9540; Adjusted R^2 0.9263).

From the ANOVA table, it appears that the factors, B ($=V_G/V_L$) and C (q_G) significantly affect the ethanol concentration obtained after 30 h of operation of the semi-batch reactor. Both factors bear linear relationships with the response. The pyrolysis temperature, however, does not have significant effect. This can be due to close variation of gas composition in the present range of pyrolysis temperatures. Three response surface 3D plots, representing the combined effect of interaction between A-B, A-C, and B-C on the response variable, are shown in Figure 11.

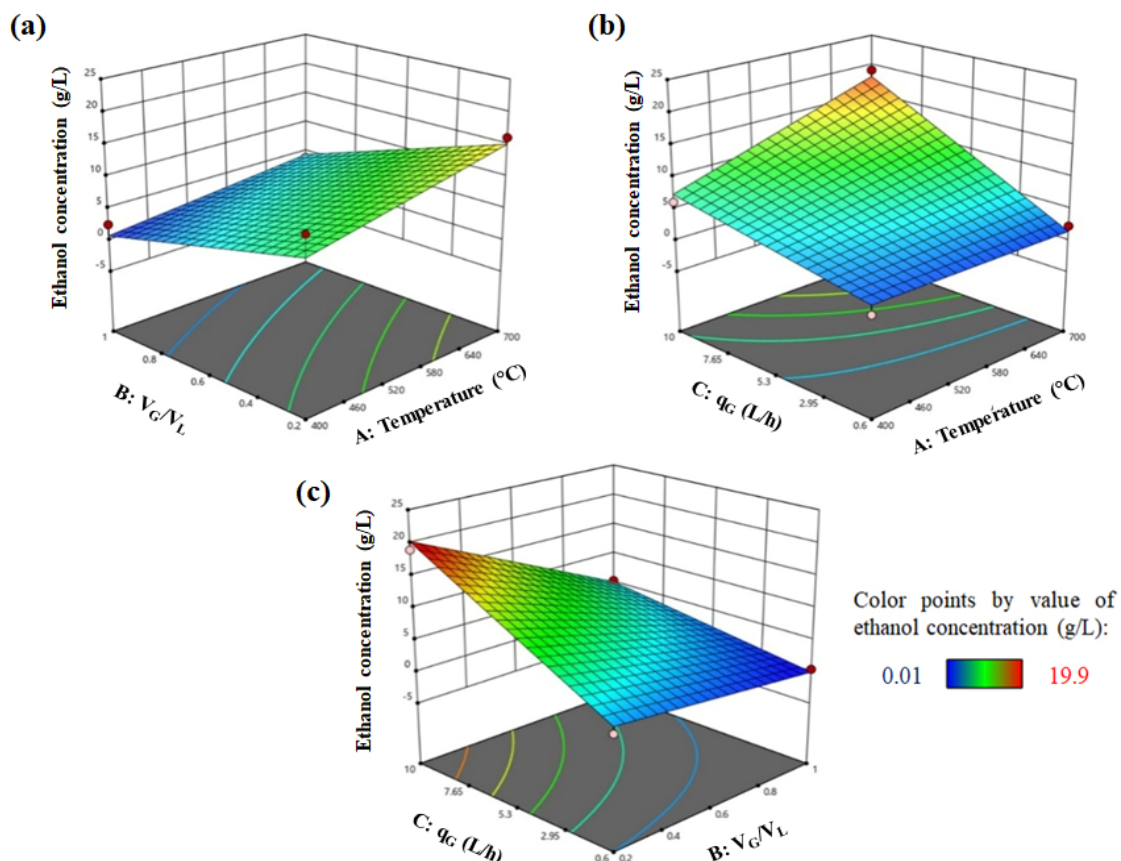


Figure 11. Response surface plots for the optimization of ethanol (g/L) production from syngas fermentation ((a–c): interaction between AB, AC and BC respectively).

From Figure 11, it is evident that the increase of variable A and C had a positive impact on the production of ethanol. This is because of the fact that with the increase of the pyrolysis temperature, T ($=A$) the concentration of all carbon substrates (CO and CO_2), and the electron donors (H_2 and CO) in the inlet gas increase, favoring the formation of ethanol. With the increase of the gas flow rate, q_G ($=C$), the mass transfer rate was enhanced and hence the growth rates and ethanol generation rates, governed by the liquid phase concentration of CO , CO_2 , and H_2 increased. As a consequence, the ethanol concentration increased with the increase of C. The increment of variable B ($=V_G/V_L$) had a negative impact on ethanol production. This can be explained by the fact that with the increase of V_G with

respect to liquid volume, the effective mass transfer to liquid phase was lowered, causing an overall decreasing trend in ethanol concentration. The optimum level of the independent variables, pyrolysis temperature, V_G/V_L , and q_G giving the maximum ethanol concentration ($=13.122$ g/L) after 30 h of semi-batch operation are 648 °C, 0.46 , and 6.7 L/h, respectively.

4.6.2. Syngas Fermentation in the Continuous Bioreactor

The second order regression equation, obtained to represent the relationships among the response, i.e., ethanol concentration, obtained after 300 h and the operating variables, namely, V_G/V_L (A), and q_G/q_L (B) is as follows:

$$\text{Ethanol concentration (g/L)} = 10.9596 + 11.9048 \times A + 0.0868944 \times B + 0.0101862 \times A \times B - 25.5316 \times A^2 - 0.000115026 \times B^2 \quad (42)$$

From the comparison between the predicted and actual values of the response variables, represented in Figure 12, and from the analysis of variance (ANOVA) presented in Table 11, it appears that the model can represent the trend of dependence of ethanol concentration, obtained under 300 h of operation on the selected operating variables, A and B, very well.

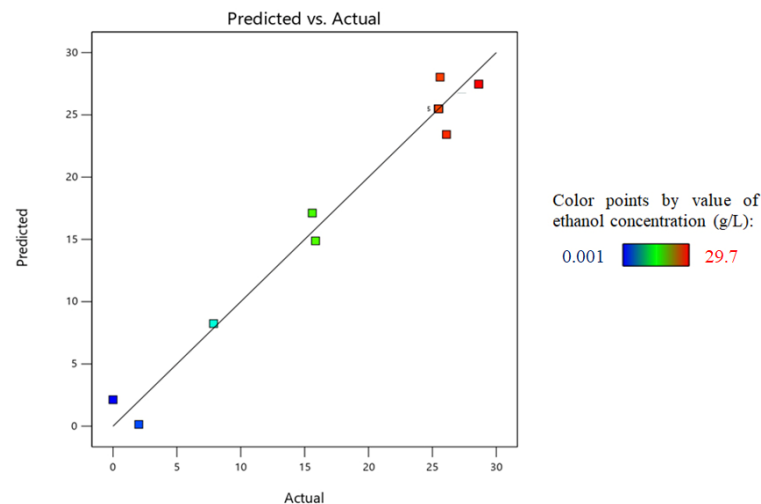


Figure 12. Comparison between the RSM-predicted and experimental values of ethanol concentration at 300 h of continuous operation.

Table 11. ANOVA table for the continuous bioreactor.

Source	Sum of Squares	df	Mean Square	F-Value	p-Value	
Model	1142.09	5	228.42	63.15	<0.0001	significant
A- V_G/V_L	329.07	1	329.07	90.97	<0.0001	
B- q_G/q_L	453.60	1	453.60	125.40	<0.0001	
AB	3.67	1	3.67	1.01	0.3475	
A^2	116.09	1	116.09	32.09	0.0008	
B^2	280.71	1	280.71	77.61	<0.0001	
Residual	25.32	7	3.62			
Lack of Fit	25.32	3	8.44			
Pure Error	0.0000	4	0.0000			
Cor Total	1167.41	12				

(Std. Dev. 1.90; Mean 19.06; C.V. (%) 9.98; R^2 0.9783; Adjusted R^2 0.9628).

From the ANOVA table, it appears that both factors, A ($=V_G/V_L$) and B (q_G/q_L), significantly affected the ethanol concentration obtained after 300 h of operation of the continuous reactor. While V_G/V_L linearly affected the response variable, the change of q_G/q_L shows a combined effect of second order and linear relationship. As the variation

of q_G/q_L simultaneously affects the gas residence time for the reaction and extent of mass transfer, the influence of this factor is large. A response surface 3D plot showing the influence of both V_G/V_L and q_G/q_L is represented in Figure 13.

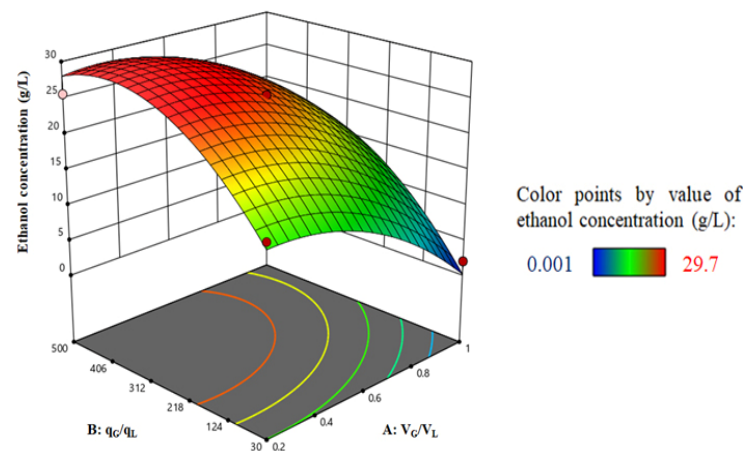


Figure 13. Response surface plots for the optimization of ethanol (g/L) production from syngas fermentation.

From Figure 13, it is evident that the increase of variable B had a positive impact on the production of ethanol from syngas fermentation. However, an increment of variable A had a negative impact on ethanol production. The optimum level of the independent variables, V_G/V_L and q_G/q_L , giving the maximum ethanol concentration (≈ 29.450 g/L) after 300 h of continuous operation are 0.28 and 335.148, respectively.

4.7. Comparison of Semi-Batch and Continuous Operation of a Pyro-Syngas Fermenter

As the semi-batch operation is always in an unsteady state, it is not suitable for large-scale fermentation. On the contrary, continuous operation is always preferred for large-scale operation. Over 30 h, 171 mL of liquid broth containing 13.12 g/L ethanol can be produced under the optimum conditions of a semi-batch fermenter. For the continuous reactor, 0.02 L/h liquid broth with an ethanol concentration of 29.45 g/L can be produced for 300 h. The average optimum production rate of ethanol is 0.074.7 g/h, calculated by dividing the product of reactor volume (≈ 0.171 L) and ethanol concentration (≈ 13.12 g/L) by operating time (≈ 30 h) obtained in semi-batch operation. In the case of continuous operation of the bioreactor, 0.589 g/h, calculated by multiplying the liquid outlet rate with ethanol concentration, can be obtained through continuous operation of the same reactor using same volumetric flow rate of gas of 6.7 L/h. However, overall, the running cost of the semi-batch bioreactor is much lower than the continuous one due to the savings in the inlet and outlet pumping rate of liquid.

4.8. Comparison with Similar Studies and Uniqueness

The operating parameters and the results of the present study are compared with similar studies in Table 12.

Table 12. Comparison of operating parameters and results of the present study with similar studies.

Feed Gas Composition	Mode of Operation	Microorganism Used	Maximum Ethanol Concentration (g/L)	Reference
CO:CO ₂ :H ₂ :N ₂ 32:8:32:28	Batch	<i>Clostridium ljungdahlii</i>	0.778	[15]
H ₂ :CO 75:25	Continuous	<i>Clostridium ljungdahlii</i>	1.304	[16]
CO:CO ₂ :H ₂ :inert 55:10:20:15	Continuous	<i>Clostridium ljungdahlii</i>	45.0	[19]

Table 12. Cont.

Feed Gas Composition	Mode of Operation	Microorganism Used	Maximum Ethanol Concentration (g/L)	Reference
100% CO	Batch	<i>Clostridium carboxidivorans</i>	0.4	[20]
100% CO	Continuous	<i>Clostridium carboxidivorans</i>	5.6	[20]
CO:CO ₂ :H ₂ :CH ₄ : N ₂ 17.0:9.1:13.3:7.1:27.0; 22.8:10.5:17.1:8.7:21.7; 23.1:10.6:17.2:8.8:21.5	Semi-batch	Clostridial consortium, <i>UACJChE1</i>	13.1	Present study
CO:CO ₂ :H ₂ :CH ₄ : N ₂ 23.1:10.6:17.2:8.8:21.5	Continuous	Clostridial consortium, <i>UACJChE1</i>	29.4	Present study

Most of the modelling studies on syngas fermentation are based on literature data of kinetic parameters, derived from experiments using simulated gas mixture. From Table 12, it is clear that the feed gas mixtures in those studies are mainly constituted of CO, H₂, and CO₂. The concentrations of CO and H₂ in the gas used in those studies usually range from 32–55% and 20–32%, respectively. In the model developed by Ruggiero et al., pure CO was used [20]. No comparison of the model predictions was made with the experimental results of a truly integrated process of gasification and fermentation. The concentrations of CO and H₂ used in the existing models are much higher than those of typical pyro-syngas. The unique feature of the present models for both semi-batch and continuous operation lies in the fact that the real pyro-gas composition was used as the input instead of any arbitrarily chosen composition. It is also clear from the table that although the concentrations of CO and H₂ of pyro-syngas, used in the present study, are much lower than those used in other similar studies, the achieved ethanol concentration is comparable with the reported ones. Although most of the studies reported the use of pure clostridial strains, the *UACJChE1*, used in the present study is the first clostridial consortium, isolated from Indian soil, which has proved to be capable of pyro-syngas fermentation.

4.9. Challenges, Model Critique, and Future Scope

The experiments were conducted in a wide range of values of different relevant parameters. For semi-batch and continuous fermenters, 17 and 13 experimental data sets were used, respectively. The agreement of the mathematical models is high for both the semi-batch and continuous modes of operation. While the values of correlation coefficient R^2 and normalized root mean square error (NRMSE) are 0.88 and 10.78, respectively, for semi batch operation, those for continuous operation are 0.97 and 8.49, respectively. The values of R^2 for the RSM model are 0.9540 and 0.9783 for semi-batch and continuous modes of operation, respectively. The adjusted values of R^2 of the RSM model are 0.9263 and 0.9628 for semi-batch and continuous bioreactors, respectively. Thus, the predictability of the model is comparable with the previously reported studies. However, widening the range will always provide more insight into the performance of pyro-syngas fermentation reactors. For any pyrolysis temperature, the pyro-syngas composition varies for different biomasses due to the difference in the lignocellulosic composition [33]. Thus, it is expected that the optimum temperature to maximize ethanol production for semi-batch and continuous operation will vary for other feedstocks. The ethanol concentration obtained at a fixed set of parameters will also vary if the biomass is changed. To explore the possibility of using diverse lignocellulosic biomasses, experiments should be conducted with different lignocellulosic feedstocks and their mixtures. However, process models using software like ASPEN Plus V10 etc. can be used to predict the performance of pyro-syngas fermentation of other feedstocks on lab and industrial scales without conducting any experiments [33]. In the ASPEN model, if the pyrolysis temperature, the composition of feedstocks with respect to the contents of lignin, cellulose, and hemicellulose, and their respective reactions

during pyrolysis are used as the inputs, the pyro-gas composition can be predicted. The performance of the fermentation of the pyro-gas can be predicted if the present model can be coupled with process modelling software. Similar studies have already been carried out by the present group to predict the performance of integrated gasification and fermentation processes for mixed lignocellulosic feedstocks [34]. In addition to the predictions of process models, economic and life cycle analyses are also important to assess the viability of pyro-syngas fermentation on large and commercial scales. Similar studies have already been carried out by the present group to predict the performance of integrated gasification and fermentation processes for mixed lignocellulosic feedstocks [35].

In the present study, pyrolytic conversion of rice straw in the temperature range of 400–700 °C was utilized for the generation of pyro-oil, pyro-gas, and pyro-char. As well as using pyro-syngas for fermentation, pyro-oil can be upgraded to liquid fuel through de-oxygenation and so on, while pyro-char can be used as an adsorbent for wastewater treatment and soil amendment. Different chemicals can also be derived from the pyro-oil portion [4]. As raw materials like rice straw etc. are agro-wastes, overall CO₂ avoidance is expected to be high. Compared to syngas fermentation using gasification as the upstream process, integration with pyrolysis seems to be more environmentally friendly, particularly for the scope of application of pyro-char for soil amendment resulting in carbon capture.

Although not very unexpected, the capability of the present consortium to utilize H₂ and CO₂ besides CO may open up more research avenues. The scope of the study can be enhanced by testing the model using the kinetic growth parameters of other syngas fermenting microbial strains and consortia for further generalization.

5. Conclusions

Deterministic mathematical models along with experimental data on the bioconversion of pyro-syngas to ethanol and acetic acid in a gas-sparged stirred tank reactor, operated in semi-batch and continuous modes, have been reported for the first time. The locally isolated clostridial consortium *UACJUChe1* was proved to be capable of utilizing CO, CO₂, and H₂ present in the pyro-syngas. The mathematical models have been validated through the comparison of the predictions with the experimental results. The optimization of the performance of the semi-batch and continuous modes of operation was achieved using response surface methodology. Since pyrolysis is used as the precursor process for syngas fermentation, other valuable products like pyro-oil and pyro-char are also generated, and the criterion of zero-waste generation for the circular economy concept is fulfilled. It is expected that the mathematical model developed in the present study can be used for the scale-up purposes needed for commercialization. The outcome of this research study can also be useful for the utilization of other lignocellulosic agro-wastes of Indian and other origins. Further data on the pyro-syngas fermentation should also be generated to check the validity of the model for other feedstocks.

Author Contributions: Methodology, D.M., R.C., R.K.C. and M.Y.M.; Software, D.M. and R.C.; Validation, D.M. and R.C.; Formal analysis, R.K.C. and M.Y.M.; Investigation, D.M., R.C. and R.K.C.; Resources, R.K.C. and M.Y.M.; Writing—original draft, R.C.; Writing—review and editing, R.K.C. and M.Y.M.; Supervision, R.C. All authors have read and agreed to the published version of the manuscript.

Funding: This research received no external funding.

Data Availability Statement: The original contributions presented in the study are included in the article, further inquiries can be directed to the corresponding author and R. Chowdhury (Research supervisor) or Dinabandhu Manna (First author).

Acknowledgments: The publication is due to research collaboration between Ranjana Chowdhury of JU, Kolkata and IBEaM, UiT. The authors are indebted to the learned reviewers for their valuable suggestions for the improvement of the manuscript.

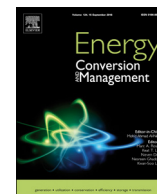
Conflicts of Interest: The authors declare no conflict of interest.

References

1. Chowdhury, R.; Ghosh, S.; Debnath, B.; Manna, D. Indian agro-wastes for 2G biorefineries: Strategic decision on conversion processes. In *Sustainable Energy Technology and Policies: A Transformational Journey*; Springer: Singapore, 2018; Volume 1, pp. 353–373.
2. Kaur, M.; Malik, D.P.; Malhi, G.S.; Sardana, V.; Bolan, N.S.; Lal, R.; Siddique, K.H. Rice residue management in the Indo-Gangetic Plains for climate and food security. A review. *Agron. Sustain. Dev.* **2022**, *42*, 92. [CrossRef]
3. Hassan, M.K.; Chowdhury, R.; Ghosh, S.; Manna, D.; Pappinen, A.; Kuittinen, S. Energy and environmental impact assessment of Indian rice straw for the production of second-generation bioethanol. *Sustain. Energy Technol. Assess.* **2021**, *47*, 101546. [CrossRef]
4. Chowdhury, R.; Ghosh, S.; Manna, D.; Das, S.; Dutta, S.; Kleinstüber, S.; Strauber, H.; Hassan, M.K.; Kuittinen, S.; Pappinen, A. Hybridization of sugar-carboxylate-syngas platforms for the production of bio-alcohols from lignocellulosic biomass (LCB)—A state-of-the-art review and recommendations. *Energy Convers. Manag.* **2019**, *200*, 112111. [CrossRef]
5. Pacheco, M.; Moura, P.; Silva, C. A Systematic Review of Syngas Bioconversion to Value-Added Products from 2012 to 2022. *Energies* **2023**, *16*, 3241. [CrossRef]
6. Faraji, M.; Saidi, M. Experimental and simulation study of peanut shell-derived activated carbon and syngas production via integrated pyrolysis-gasification technique. *Process Saf. Environ. Prot.* **2023**, *171*, 874–887. [CrossRef]
7. Li, N.; Pan, Y.; Yan, Z.; Liu, Q.; Yan, Y.; Liu, Z. Cornstalk pyrolysis for syngas in a two-stage electromagnetic induction reactor. *Fuel* **2023**, *336*, 127124. [CrossRef]
8. Chen, D.; Zhuang, X.; Gan, Z.; Cen, K.; Ba, Y.; Jia, D. Co-pyrolysis of light bio-oil leached bamboo and heavy bio-oil: Effects of mass ratio, pyrolysis temperature, and residence time on the biochar. *Chem. Eng. J.* **2022**, *437*, 135253. [CrossRef]
9. Li, X.; Liu, P.; Huang, S.; Wu, S.; Li, Y.; Wu, Y.; Lei, T. Study on the mechanism of syngas production from catalytic pyrolysis of biomass tar by Ni–Fe catalyst in CO₂ atmosphere. *Fuel* **2023**, *335*, 126705. [CrossRef]
10. Esquivel-Elizondo, S.; Delgado, A.G.; Rittmann, B.E.; Krajmalnik-Brown, R. The effects of CO₂ and H₂ on CO metabolism by pure and mixed microbial cultures. *Biotechnol. Biofuels* **2017**, *10*, 220. [CrossRef]
11. Kennes, D.; Abubakar, H.N.; Diaz, M.; Veiga, M.C.; Kennes, C. Bioethanol production from biomass: Carbohydrate vs syngas fermentation. *J. Chem. Technol. Biotechnol.* **2016**, *91*, 304–317. [CrossRef]
12. Diender, M. Exploration of Microbial Systems as Biocatalysts for Conversion of Synthesis Gas to Bio-Based Chemicals. Ph.D. Dissertation, Wageningen University and Research, Wageningen, The Netherlands, 2019. Available online: <https://research.wur.nl/en/publications/exploration-of-microbial-systems-as-biocatalysts-for-conversion-o> (accessed on 12 October 2023).
13. Siebler, F.; Lapin, A.; Takors, R. Synergistically applying 1-D modeling and CFD for designing industrial scale bubble column syngas bioreactors. *Eng. Life Sci.* **2020**, *20*, 239–251. [CrossRef] [PubMed]
14. Chen, J.; Gomez, J.A.; Höffner, K.; Barton, P.I.; Henson, M.A. Metabolic modeling of synthesis gas fermentation in bubble column reactors. *Biotechnol. Biofuels* **2015**, *8*, 89. [CrossRef] [PubMed]
15. Vandecasteele, J. Experimental and Modelling Study of Pure-Culture Syngas Fermentation for Biofuels Production. Master’s Thesis, Universiteit Gent, Gent, Belgium, 2016. Volume 356. Available online: <https://lib.ugent.be/catalog/rug01:002275054> (accessed on 10 October 2023).
16. Almeida Benalcázar, E.; Noorman, H.; MacielFilho, R.; Posada, J.A. Modeling ethanol production through gas fermentation: A biotermodynamics and mass transfer-based hybrid model for microbial growth in a large-scale bubble column bioreactor. *Biotechnol. Biofuels* **2020**, *13*, 59. [CrossRef] [PubMed]
17. Mohammadi, M.; Mohamed, A.R.; Najafpour, G.D.; Younesi, H.; Uzir, M.H. Kinetic studies on fermentative production of biofuel from synthesis gas using *Clostridium ljungdahlii*. *Sci. World J.* **2014**, *2014*, 910590. [CrossRef] [PubMed]
18. Puiman, L.; Almeida Benalcázar, E.; Picioreanu, C.; Noorman, H.J.; Haringa, C. Downscaling Industrial-Scale Syngas Fermentation to Simulate Frequent and Irregular Dissolved Gas Concentration Shocks. *Bioengineering* **2023**, *10*, 518. [CrossRef] [PubMed]
19. De Medeiros, E.M.; Posada, J.A.; Noorman, H.; Filho, R.M. Dynamic modeling of syngas fermentation in a continuous stirred-tank reactor: Multi-response parameter estimation and process optimization. *Biotechnol. Bioeng.* **2019**, *116*, 2473–2487. [CrossRef] [PubMed]
20. Ruggiero, G.; Lanzillo, F.; Raganati, F.; Russo, M.E.; Salatino, P.; Marzocchella, A. Bioreactor modelling for syngas fermentation: Kinetic characterization. *Food Bioprod. Process.* **2022**, *134*, 1–18. [CrossRef]
21. Sluiter, A.; Hames, B.; Ruiz, R.; Scarlata, C.; Sluiter, J.; Templeton, D.; Crocker, D.L.A.P. Determination of structural carbohydrates and lignin in biomass. *Lab. Anal. Proced.* **2008**, *1617*, 1–16.
22. Chowdhury, R.; Sarkar, A. Reaction kinetics and product distribution of slow pyrolysis of Indian textile wastes. *Int. J. Chem. React. Eng.* **2012**, *10*, A67. [CrossRef]
23. Sarkar, A.; Chowdhury, R. Co-pyrolysis of paper waste and mustard press cake in a semi-batch pyrolyzer—Optimization and bio-oil characterization. *Int. J. Green Energy* **2016**, *13*, 373–382. [CrossRef]
24. Ghosh, S.; Pathak, S.; Manna, D.; Chowdhury, R. Acidogenic mixed consortium isolated from soil of agricultural field: Acid production behaviour and growth kinetics under the influence of pretreatment hydrolysate of rice straw (RS). *Indian Chem. Eng.* **2021**, *63*, 206–218. [CrossRef]
25. Gill, N.K.; Appleton, M.; Baganz, F.; Lye, G.J. Quantification of power consumption and oxygen transfer characteristics of a stirred miniature bioreactor for predictive fermentation scale-up. *Biotechnol. Bioeng.* **2008**, *100*, 1144–1155. [CrossRef] [PubMed]

26. Wang, T.; Wang, Q.; Soklun, H.; Qu, G.; Xia, T.; Guo, X.; Lia, H.; Zhu, L. A green strategy for simultaneous Cu (II)-EDTA decomplexation and Cu precipitation from water by bicarbonate-activated hydrogen peroxide/chemical precipitation. *Chem. Eng. J.* **2019**, *370*, 1298–1309. [[CrossRef](#)]
27. Abubackar, H.N.; Veiga, M.C.; Kennes, C. Biological conversion of carbon monoxide: Rich syngas or waste gases to bioethanol. *Biofuels Bioprod. Biorefining* **2011**, *5*, 93–114. [[CrossRef](#)]
28. Green, D.W.; Perry, R.H. *Perry's Chemical Engineers' Handbook*; McGraw-Hill Education: New York, NY, USA, 2008.
29. Phillips, J.R.; Clausen, E.C.; Gaddy, J.L. Synthesis gas as substrate for the biological production of fuels and chemicals. *Appl. Biochem. Biotechnol.* **1994**, *45*, 145–157. [[CrossRef](#)]
30. Mohammadi, M.; Mohamed, A.R.; Najafpour, G.; Younesi, H.; Uzir, M.H. *Clostridium ljungdahlii* for production of biofuel from synthesis gas. *Energy Sources Part A Recovery Util. Environ. Eff.* **2016**, *38*, 427–434.
31. Fox, J.D.; Kerby, R.L.; Roberts, G.P.; Ludden, P.W. Characterization of the CO-induced, CO-tolerant hydrogenase from *Rhodospirillum rubrum* and the gene encoding the large subunit of the enzyme. *J. Bacteriol.* **1996**, *178*, 1515–1524. [[CrossRef](#)] [[PubMed](#)]
32. Rajagopalan, S.; Datar, R.P.; Lewis, R.S. Formation of ethanol from carbon monoxide via a new microbial catalyst. *Biomass Bioenergy* **2002**, *23*, 487–493. [[CrossRef](#)]
33. Ranzi, E.; Cuoci, A.; Faravelli, T.; Frassoldati, A.; Migliavacca, G.; Pierucci, S.; Sommariva, S. Chemical kinetics of biomass pyrolysis. *Energy Fuels* **2008**, *22*, 4292–4300. [[CrossRef](#)]
34. Pati, S.; De, S.; Chowdhury, R. Exploring the hybrid route of bio-ethanol production via biomass co-gasification and syngas fermentation from wheat straw and sugarcane bagasse: Model development and multi-objective optimization. *J. Clean. Prod.* **2023**, *395*, 136441. [[CrossRef](#)]
35. Pati, S.; De, S.; Chowdhury, R. Integrated techno-economic, investment risk and life cycle analysis of Indian lignocellulosic biomass valorisation via co-gasification and syngas fermentation. *J. Clean. Prod.* **2023**, *423*, 138744. [[CrossRef](#)]

Disclaimer/Publisher's Note: The statements, opinions and data contained in all publications are solely those of the individual author(s) and contributor(s) and not of MDPI and/or the editor(s). MDPI and/or the editor(s) disclaim responsibility for any injury to people or property resulting from any ideas, methods, instructions or products referred to in the content.



Hybridization of sugar-carboxylate-syngas platforms for the production of bio-alcohols from lignocellulosic biomass (LCB) – A state-of-the-art review and recommendations

Ranjana Chowdhury^{a,*}, Shiladitya Ghosh^a, Dinabandhu Manna^a, Sumona Das^a, Sambit Dutta^a, Sabine Kleinstaub^b, Heike Sträuber^b, Md. Kamrul Hassan^c, Suvi Kuittinen^c, Ari Pappinen^c

^a Chemical Engineering Department, Jadavpur University, Kolkata 700032, India

^b Department of Environmental Microbiology, UFZ – Helmholtz Centre for Environmental Research, Permoserstr. 15, 04318 Leipzig, Germany

^c School of Forest Sciences, University of Eastern Finland, P.O. Box 111, 80101, Finland

ARTICLE INFO

Keywords:

Bioalcohol
Lignocellulosic Biomass
Sugar-carboxylate-syngas platforms
Hybridization
Challenges
Recommendations

ABSTRACT

Lignocellulosic biomass (LCB), the most abundant renewable feedstock for bioenergy generation, is commonly converted to second generation bioalcohols, the main drop-in fuels for petroleum gasoline, through three technologies based on sugar, carboxylic acid and syngas platforms. The hybridization of either any two or three platforms altogether is a novel concept aimed at improvement of yield and quality (high heating value) of bioalcohols. This article reviews the present status of the integration techniques of hybrid platforms with an overall assessment of their advancement with respect to their individual counterpart as well as the challenges involved. It has been indicated that to extract the maximum benefit of hybridization, research studies should be spurred in the fields of kinetic analysis of all thermochemical and biochemical processes, microbial interaction, optimization of process parameters (pH, temperature), performance analysis of engine for the utilization of mixed product bioalcohols, sustainability analysis through the development of mathematical models for lab-scale operations and process simulation models for large scale units along with life cycle assessment. Moreover, pyrolysis of LCB has been identified as a unique central process for the supply of all intermediate compounds, namely, sugar, carboxylic acid and syngas during the hybrid networking of three platform technologies. In this context, the scheme of CONVER-B, a joint research project under the INNO-INDIGO partnership program, aiming at sustainable integration of the platforms to produce bio-alcohols from LCBs leaving zero effluent simultaneously with carbon sequestration potential has been introduced and discussed.

1. Introduction

Lignocellulosic biomass (LCB) derived biofuels and bioproducts are the key driver in the path of transition towards the bio-based economy all over the world, establishing absolute alliance among energy, society and environment [1,2]. It is well established that bioenergy, one of the preeminent components of bio-economy, will be mainly dependent on LCB as the chief renewable resource (feedstocks), mostly due to their worldwide abundance [1,3]. Being the most abundant feedstock appearing as residues of agriculture, forestry and as effluents from food, textile, pulping and other industrial processing, LCB could be used in biorefineries to generate myriads of renewable bioproducts; biofuels being the supreme product [4–7]. One of the advantages of using LCB as

feedstock for bioenergy generation is that it totally eliminates the up-setting social issue of ‘food vs. fuel’ competition [4,8]. Conventionally, lignocellulosic wastes are converted to biofuels (gaseous: biogas/bio-methane; biohydrogen; bio-syngas and liquid: bio-alcohols and bio-oil) either through biochemical or thermochemical routes [9–14]. As reported in the latest survey by the International Energy Agency (IEA), conventional biofuel production reached 143 billion litres (4% increment on a year-on-year basis), in the year 2017, having an equivalent energy value of 83 Mtoe [15]. Analyzing the ongoing trend of world biofuel production, IEA forecasted a 15% growth estimating to be 165 billion litres (total energy value 97 Mtoe) by 2023, 119 billion litres (approximately two-third) of which will come from bioethanol alone [15]. This fact is already being implemented globally and is

* Corresponding author.

E-mail addresses: ranjana.juchem@gmail.com (R. Chowdhury), sabine.kleinstaub@ufz.de (S. Kleinstaub), heike.strauber@ufz.de (H. Sträuber), kamrul.hassan@uef.fi (Md. Kamrul Hassan), suvi.kuittinen@uef.fi (S. Kuittinen), ari.pappinen@uef.fi (A. Pappinen).

<https://doi.org/10.1016/j.enconman.2019.112111>

Received 10 June 2019; Received in revised form 27 August 2019; Accepted 28 August 2019

Available online 29 September 2019

0196-8904/© 2019 Elsevier Ltd. All rights reserved.

reflected in the renewable energy action plans of different countries. The Indian government has planned to achieve a target of 10% blending of fossil transport fuels with bioethanol and biodiesel by 2017 and raised the target to 20% beyond 2017 [16]. The European Union (EU) has set a new binding target, in form of renewable energy directive II (RED II), to acquire at least 14% of their transport fuels from renewable resources by 2030 [17]. In Finland, the target is set about 20%, by 2020 [18]. Bio-alcohols, namely; ethanol, butanol, hexanol etc. are already proven suitable for the use in spark-ignition engines as low-emission transport fuels and hence, are the biofuels of current interest [19–22]. A recent study has shown that corn-based biobutanol can save 39–56% automobile fossil fuels and reduce CO₂ emissions by 32–48% in comparison to gasoline [23]. This transition can only be sustained by employing strategic planning and utilization of LCB feedstocks in technologically advanced frameworks ensuring maximum conversion to biofuels, minimization of waste generation and reutilization of all residues.

There are three pathways, namely sugar platform (SP), carboxylate platform (CP) and syngas platform (SyP), mainly used for the conversion of LCB feedstocks to bio-alcohols [24–26]. The names of the platforms are derived from those of the intermediate precursors through which organic or agricultural wastes are ultimately converted to bioalcohols. The sugar platform directly converts 6-carbon and 5-carbon sugar/carbohydrate compounds obtained from LCBs through pretreatment and enzymatic hydrolysis, to different bio-alcohols as the major end product [24]. Conversely, in syngas and carboxylate platforms, as described by many researchers, alcohol generation from LCBs is mediated through formation of energy-rich precursor molecules and their mixtures, namely bio-syngas and mixed carboxylic acids, respectively [25,26]. Due to the astounding diversity of composition of lignocellulosic wastes, having different distribution of cellulose, hemicellulose and lignin, it appears that none of the platforms can provide unique solution individually for the generation of bio-alcohols from LCBs, in general. Recently, few research articles demonstrated that the combination of any of the two platforms among sugar, carboxylate and syngas ones can improve the quality and productivity of bio-alcohols from LCB [27–30]. Although many informative review articles are available on individual platforms, comprehensive review on the performance and prospects of combination/hybridization of different platforms for the generation of alcohols from LCBs is rare [25,31–34]. In this article, the present status of this briskly evolving ‘hybrid technology’ in the field of bio-alcohol production from LCB is thoroughly revisited from all crucial perspectives. Ultimately, a novel “zero effluent” concept, namely; ‘CONVER-B’, of cascading of the three platforms particularly focusing on bio-alcohol production from LCB with carbon storage capability is recommended with the projection of higher energy efficiency compared to that of stand-alone platforms.

2. Analysis of three platforms

2.1. Working principles and microorganisms

The conventional working principles of the three platforms, namely; SP, CP and SyP, are technically summed up and depicted respectively in Fig. 1A, B and C, for simple understanding. The platforms fundamentally differ from each other regarding various operational aspects. According to the representation of Fig. 1A, B and C, all three platforms convert lignocellulosic biomass to bioalcohols as the chief end-product.

It is clear from Fig. 1A that in the conventional sugar platform, lignocellulosic biomass is first pretreated through hydrothermal processing using dilute mineral acids (alkali, mineral salts, organic solvents and some other catalysts are also used in different cases, acid pretreatment is considered as a representative process for all) whereby the hemicellulose portion of LCB is primarily converted to pentose sugars, namely, xylose and/or arabinose and a small part of cellulose is converted to glucose [34–37]. The cellulose present in the solid part of

pretreated mass is subsequently hydrolysed to glucose using enzymes [35,36,38]. After hydrolysis, the hydrolysed mass is filtered. The filtrate containing simple carbohydrates like pentoses and hexoses, is fermented to generate alcohols, namely, ethanol and butanol [36] and the solid filter cake containing lignin is considered either as waste stream or directly combusted to generate electricity and steam in combined heat and power (CHP) unit [39,40]. The liquid stream is passed through a centrifuge and the cell concentrate is recycled. Pure alcohol is recovered in distillation column [39,40]. The bottom liquid effluent from the distillation column is usually passed through waste water treatment plant (WWT) and the treated water is recycled. The solid waste from the WWT is sometimes utilized in an anaerobic digester (AD) to generate biogas [39,40]. All these possible units have been presented in Fig. 1A. The high temperature pretreatment and the alcohol recovery (distillation) steps require energy.

As depicted in Fig. 1B, in syngas platform the pre-dried LCBs are first converted to syngas in a gasifier using steam and air mixture and the gas-solid mixture is subsequently separated in series of two cyclones [41–43]. While the char part is recycled to the gasifier, the ash, obtained in the solid streams of the second cyclone appears as waste. Exit gas stream from the second cyclone is sometimes passed through reformer for enrichment of syngas [41]. The syngas is subsequently fermented to ethanol [41,44]. The combined outlet stream of unconverted syngas and alcohol-rich liquid product from the fermenter is usually passed through a flash drum and the two phases are separated [37]. The gas stream is bifurcated in to two lines, one recycled to the fermenter and the rest directed to a CHP [41]. Electricity and steam are generated in the CHP and steam is utilized in the gasifier, as much as possible. All these units have been included in the general schematic representation for SyP in Fig. 1B. The waste heat of flue gas from the CHP is exchanged to dry the LCB fed to the gasifier [41]. In case of carboxylate platform for alcohol generation, usually the carboxylic acids produced by acidogenic mixed microbiomes of anaerobic digestion (AD) processes are converted to alcohols either through catalytic thermochemical processes or by the combination with other bioprocesses responsible for reduction of acids to alcohols [25,45,46]. In this strategy, acetoclastic methanogenesis during anaerobic digestion is deliberately inhibited so that volatile fatty acids (VFAs) are mainly formed and hence it can be termed as an incomplete AD (IAD) process [47]. It is understandable that with selective suppression of the methanogens, any AD microbiome can be turned to an acidogenic microbiome that can be used in a CP. Energy requirement of the IAD process is mainly for the mild pretreatment of feedstock which can be fully avoided for low-lignin containing simple feedstocks [4]. On the other hand, the subsequent bioprocess generating alcohol requires energy for separation of alcohols through distillation. The basic principle of carboxylate platform extended up to bio-alcohol generation has been depicted in Fig. 1C. For both SyP and CP the methods of alcohol recovery and water treatment processes are similar to those in the SP. In another option of carboxylate platform, medium chain fatty acids (MCFAs) can be microbially derived through reversed β -oxidation of short chain fatty acids (SCFAs) produced during IAD [48]. The MCFAs can be further converted to higher alcohols with high carbon numbers and larger calorific values in subsequent fermentation processes [48]. The ‘MIXALCO’ processes converting carboxylic acids to corresponding alcohols through thermochemical routes also belong to carboxylate platform [49,50]. In the subsequent sections, discussions have been provided on basics of individual platforms in a comparative way.

In all three platforms, production of bioalcohol from simple sugar, VFAs or bio-syngas is mediated by specifically dedicated microorganisms exhibiting different metabolic ability and performance. Different strains of the solventogenic yeast *Saccharomyces cerevisiae* are most popularly used in the sugar platform to produce bioethanol utilizing simple hexose (C6) sugars [51,52]. However, wild strains of *S. cerevisiae* cannot ferment pentose (C5) sugars, such as xylose, arabinose etc. generated through the de-polymerization of hemicellulose during the

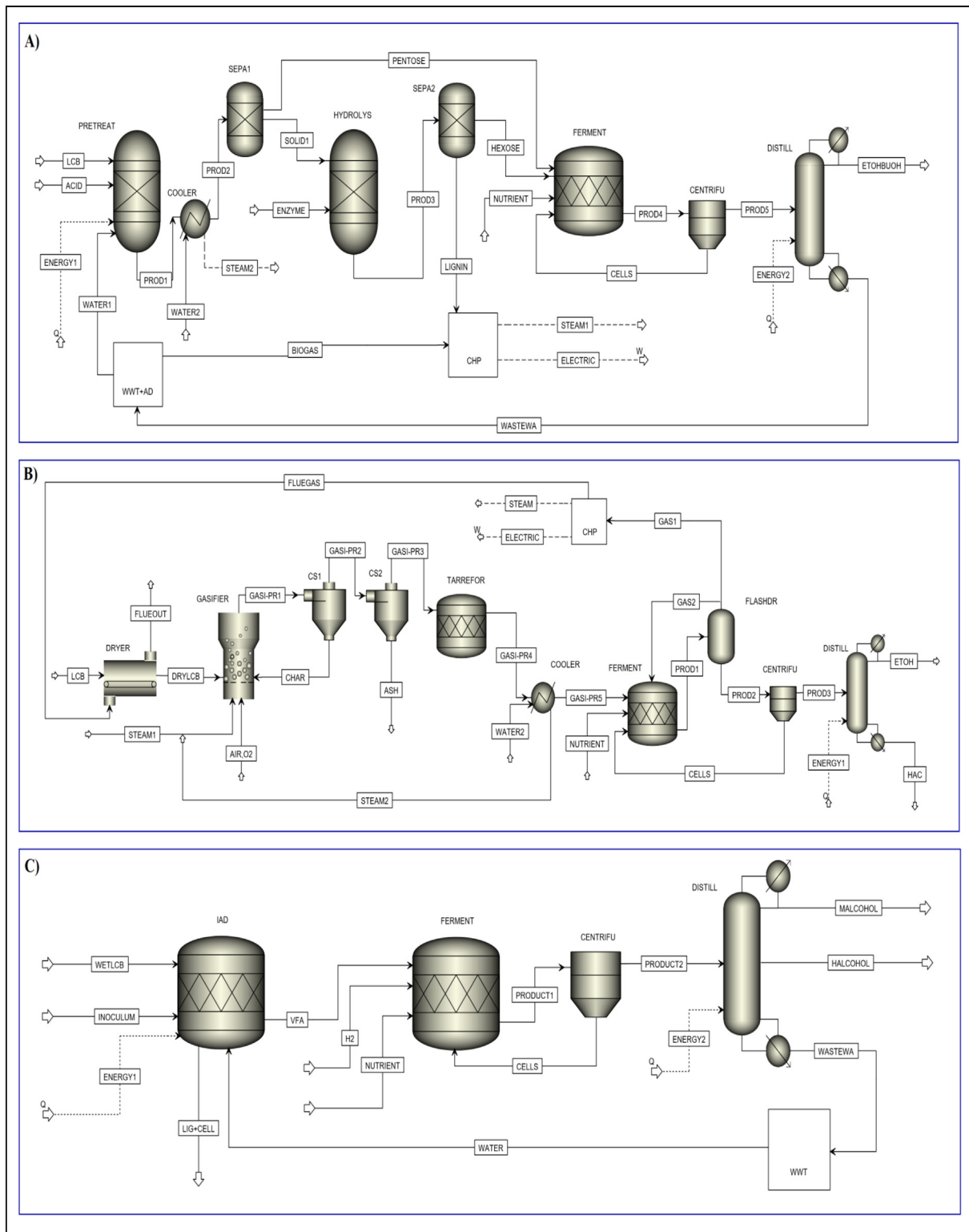


Fig. 1. Major processes, material streams and unit operations of the three individual platforms; A) Sugar Platform (SP); B) Syngas Platform (SyP); C) Carboxylate Platform (CP); PRETREAT: Pretreatment; COOLER: Cooling unit; SEPA: Separation/Filtration unit; HYDROLYS: Enzymatic hydrolysis; FERMENT: Fermenter; CENTRIFU: Centrifugation unit; DISTILL: Distillation tower; CHP: Combined Heat and Power; WWT + AD: Waste water treatment plant with anaerobic digestion unit; LCB: Lignocellulosic Biomass; PROD1 (SP): Pretreated LCB; PROD2 (SP): Cooled pretreated LCB; SOLID1 (SP): Solid fraction of cooled pretreated LCB; PROD3 (SP): Enzymatically hydrolyzed LCB; NUTRIENT: Nutrient medium for fermentation; PROD4 (SP): Fermentation products; CELLS: Microbial cells; PROD5 (SP): Cell free fermentation products; ETOHBUOH: Ethanol, butanol; WASTEWA: Waste water; CS: Cyclone separator; TARREFOR: Tar reformer; FLASHDR: Flash drum for liquid-gas separation; DRYLCB: Dry lignocellulosic biomass; O₂: Oxygen; GASI-PR: Gas-solid mixture; PROD1, PROD 2 and PROD 3 (SyP): Fermentation products; ETOH: Ethanol; HAC: Acetic acid; IAD: Incomplete anaerobic digestion; WETLCB: Wet lignocellulosic biomass; LIG + CELL: Lignin and cellulose; VFA: Volatile fatty acid; H₂: Hydrogen; PRODUCT1 and PRODUCT 2 (CP): Fermentation products; MALCOHOL: Medium alcohol; HALCOHOL: Higher alcohol; Energy 1 and 2: Input energy streams.

pretreatment of LCBs [53]. To tackle this problem, pentose-fermenting bacterial strains, namely; *Zymomonas mobilis* and genetically engineered strains of *Escherichia coli* etc. and another yeast, *Pichia* (or *Scheffersomyces*) *stipitis*, are also gaining interest recently [54–57]. For the production of butanol in the sugar platform, *Clostridium acetobutylicum* is extensively used to convert the carbohydrate monomers (C5 and C6) generated from lignocellulosic biomass [58–61]. Although *C. acetobutylicum* is the most typically used butanol producing strain in the sugar platform, lately, *C. beijerinckii*, *C. pasteurianum* and *C. saccharoperbutylacetonicum* are also being used by many researchers [62–64]. Research studies using combination of yeasts (*S. cerevisiae* and/or *P. stipitis*) and bacteria (*clostridial strains*, *E. coli* or *Z. mobilis*) as co-cultures for the simultaneous consumption and conversion of both hexoses and pentoses to alcohols have recently been reported in many studies on SP [65–69]. In the carboxylate platform, a mixture of cellulolytic and acidogenic consortia of IAD processes act on the holocellulose (cellulose and hemicellulose) fraction directly to produce SCFAs, which can in turn be converted to alcohols through biological processes using homoacetogenic microorganisms like *Clostridium ljungdahlii* having reducing capabilities [25]. On the other hand, SCFAs can be further converted to MCFAs under the action of reactor microbiomes and higher alcohols can be produced through the microbial reduction of the latter acids. For the production of MCFAs the presence of chain elongating bacteria, e.g., *Clostridium kluyveri* has to be ensured [25]. In the conventional syngas platform, syngas ($H_2 + CO$) is converted by the acetogenic bacterium, *Clostridium ljungdahlii* to ethanol and acetic acid [44,70]. Some other pure strains acetogenic/carboxidotrophic bacteria namely; *Clostridium carboxidivorans*, *Clostridium ragsdalei*, *Clostridium autoethanogenum* etc. are also being used recently for conversion of syngas to bioalcohols [71–74]. Among these bacteria, *C. carboxidivorans* can also produce higher alcohols than ethanol, namely; butanol and hexanol from syngas [71,75]. Besides these pure strains, some recent studies reported use of mixed culture for syngas fermentation producing mixed alcohols like, ethanol, propanol and butanol [76,77].

2.2. Feedstocks and requirement for pretreatment

The lignin content of the LCB feedstocks is a vital factor for all platforms because of its direct contribution to the recalcitrance [78]. In a recent publication, the Indian lignocellulosic feedstocks have been categorized according to their lignin content; high lignin (1–10%), medium lignin (10–20%) and low lignin (> 20%) to provide a basis for the selection of most viable conversion routes [4]. The primary aim of the SP and CP is to overcome the lignin barrier to gain access to the cellulose and hemicellulose fractions of the LCBs (Fig. 1A and C). Selection of proper LCB feedstocks based on the lignin content for the particular platform is a prerequisite, which can facilitate better conversion and complete utilization of the LCB feedstocks.

As per the requirement of the bioprocesses involved in the SP and CP, the use of LCBs containing low, and low-to-medium lignin content are suitable for the sugar and carboxylate platforms respectively. As the microorganisms involved in SP can only accept hexose (glucose) and pentoses (xylose, arabinose), mainly low lignin LCBs [56–67], requiring mild delignification and easy pretreatment steps for the conversion of cellulose and hemicellulose to respective monomeric simple sugar are suitable. On the other hand the bioavailability of cellulose and hemicellulose for the action of cellulolytic bacteria in the reactor microbiome is the major decisive factor for the efficient conversion of LCBs in CP [9]. To avoid energy intensive delignification process prior to the entry in CP, medium and preferably low lignin LCBs are acceptable in carboxylate or volatile fatty acid platform using an IAD microbiome [79]. This is limited in dry biomass and at high lignin content. The SyP is not influenced by the lignin content since the gasification prior to fermentation is a thermochemical process that can accept any carbon source as its reactant/feedstock [79]. Although dry LCBs are not

preferred in SP and CP, the feedstock for SyP should be preferably dry. Therefore, any dry lignocellulosic biomass can be handled by this platform irrespective of the lignin content. The SP essentially requires extensive pretreatment and enzymatic hydrolysis steps of LCB feedstocks [57,60–64]. Besides the conventional high temperature acid/alkali pretreatment, use of ultrasonication, microwave treatment, extraction with ionic liquid, organosolv pretreatment, eutectic solvent etc. have also been demonstrated to be effective [79,80]. Literature review reveals that mild pretreatment of agricultural waste like rice straw and wheat straw yields better yield of product in CP used for biogas generation [81,82]. However, many CP are run without pretreatment of biomass [83]. Currently, biochemical pretreatment of LCBs employing lignocellulolytic microorganisms are also attracting interest due to their functional effectiveness and better techno-economic-environmental attributes than the conventional pretreatments [84]. In SyP, absolutely no pretreatment step is required.

2.3. Array and yields of product, by-products and residues

From SP, usually ethanol and butanol are obtained by using pure culture of dedicated solventogenic microorganisms, namely yeast and Clostridia, respectively, as already mentioned in Section 2.2 [54–64]. In case of butanol production through this platform, acetone and ethanol are also produced as solvent by-products. A study by Wu et al., 2008, revealed that a bio-butanol plant with a capacity of 2589.12 Mg/d (1 Mg/d = 1 t(metric)/d) corn grain produces about 466 Mg/d butanol with additionally 261.6 Mg/d and 11.28 Mg/d of acetone and ethanol, respectively, as by-products [23]. This study also envisaged that 0.22L biobutanol can be obtained from 1 kg of corn. The yield of ethanol using solventogenic yeast is about 0.41 L/kg when dry-milled corn grain is used as feedstock [85]. A study on syngas platform showed that using the gaseous product generated from a gasification unit consuming 1200 Mg/d switchgrass, a subsequent bioethanol plant produces 298.77 Mg/d ethanol [86]. Holtzaple and Granda, 2009, reported a comparative theoretical analysis of the potential of SP, CP and SyP, for ethanol production from standard LCB [49]. However, in this study the Sp and CP have been defined a bit differently from the conventional ones. Contribution of lignin as the substrate in these two platforms is included with the help of an additional gasification step generating H_2 as reducing agent for CO_2 (sugar platform) and acetic acids (carboxylate platform) producing enhancing overall ethanol yield [49]. On the basis of a mole of standard biomass, composed of 31.7% lignin ($CH_{1.12}O_{0.377}$) and 68.3% holocellulosic (cellulose + hemicellulose) polysaccharides ($C_6H_{10}O_5$) on ash free basis, 3 mol of ethanol is produced through SP and CP, whereas, the SyP produces 2.5 mol ethanol [49]. It has been estimated that both sugar and carboxylate platforms have the equal ethanol production potential of 175 gallon/ton, whereas, the ethanol production potential of syngas platform is about 145 gallon/ton standard biomass [49]. The ethanol production potential of the syngas platform is less because of the partial oxidation of carbon present in the biomass feedstock during the generation of syngas in the gasification process. The yield of volatile fatty acids (acetic + propionic + butyric acids in the ratio 6:1:3 to 5:1:5) in the CP ranges from 0.118 to 0.61 g/g volatile solids [45].

During the production of biobutanol from conventional feedstocks, residues amounting to 31.1% of the total solids are formed, which are called DDGS (dried distillers grains with solubles) and comprise the solid wastes from upstream (cooking) and downstream (separation) processes [23,87]. Previous literature indicates that DDGS corresponds to 40% energy content of corn fed to the system [23]. Moreover, fatty acids generated in the fermenter are not recovered or utilized. The SyP generates 74 Mg/d ash and/or char and 49 Mg/d cell cake in a 1200 Mg/d switchgrass-based plant [86]. Since the first step in the alcohol production through carboxylate platform is IAD process (Fig. 1C), the feedstocks are generally silages, spent grains and other wet biomass solid. Digestate, generated in the IAD, is usually used as fertilizer after

Table 1
Performance of individual platforms from the perspectives of material and energy balances and economic analysis.

Platform	Feedstock	Plant capacity*	Alcohol	Pretreatment/precursor process	Process of recovery	Material balance	Energy balance	Economy	Refs.
						Alcohol yield	Whether in-house energy generated from lignin		
SP	Corn stover	2200 dry ton/day	Ethanol	Dilute acid pretreatment and enzymatic hydrolysis	Distillation followed by molecular sieve adsorption	79 gallon/ton of dry feed	Yes	Not mentioned	\$ 2.14/gallon [39]
SP	Mexican lignocellulosics	2000 t/day	Ethanol	Pretreatment and enzymatic hydrolysis	Distillation followed by molecular sieve adsorption	48.6–74.1 gallon/ton	Yes	20.7–48.9	\$ 2.05/gallon [40]
SP	Bamboo	2000 Mt/d)	Ethanol	Hot water pretreatment and enzymatic hydrolysis	Distillation followed by molecular sieve adsorption	147–198 ML/year	Yes	Not mentioned	\$ 0.589/L [93]
SP	Corn stover	729,692 ton/year	Butanol	Dilute acid pretreatment	Vacuum distillation	155 L/ton	Yes	44	\$ 1.5–1.8/L [94]
SP	Corn stover	126 kt/year	Butanol	Dilute acid pretreatment	Pervaporation and nanofiltration	0.21 kg/kg	No	Not mentioned	€ 1.09/kg [95]
SyP	Switchgrass	(2206 MT/day	Ethanol	NA	Distillation	282 L/ton	NA	Not mentioned	\$ 1.32/L [96]
SyP	Sugarcane bagasse	100 ton/h	Ethanol	NA	Distillation	0.225 ton ethanol/ton feed	From gas (25.5 MW)	43%	\$ 0.69/L [41]
CP	Korean food waste	(500 tons/day	Mixed alcohol		Not clearly mentioned	0.25–0.46 g/g	NA	Not mentioned	\$ 0.48/L ethanol equivalent [45]

* Plant capacities have been presented as reported in the respective references.

** Production costs have been presented as reported in the respective references.

neutralization and does not generate much revenue [88]. As reported in the literature, the solid part of the digestate generated from co-digestion of lignocellulosic biomass (groats: 9%; olive oil cake: 29%; triticale: 57% w/w) and chicken manure (5% (w/w)) contains about 35% carbohydrates and 21% Klason lignin at the end of the process and can be a potential feedstock for further energy conversion [89]. The carbohydrate part in the residue is rich in cellulose as the digestion rate of hemicellulose is much higher than the former [89]. Thus it can be delignified and hydrolysed enzymatically to release simple sugars and fed to an alcohol fermentation system for production of ethanol (or butanol, not reported yet) [90,91]. Since digestate is rich in lignin, it can also be used in the syngas platform for conversion to syngas and eventual fermentation to ethanol [92]. This can be particularly useful if lignin-rich feedstock has to be handled in carboxylate platform.

2.4. Energy analysis

Using the Mueller and Cuttica model, it was estimated that the energy consumption is about 0.63kWh/L butanol production from corn grain, when cooking and gas stripping/distillation were used as pre-treatment and downstream processing steps, respectively [23,87]. Cooking constituted the major share (69.9%) of energy consumption while the other energy consuming steps being fermentation and product recovery altogether accounted for 30.1% of the total energy consumption. In case of SP for alcohol production, while waste lignin stream is sometimes directly combusted for the generation of electricity, the distillation bottoms are also utilized to generate biogas, which is subsequently utilized in energy generation [39,40]. Sometimes a part of energy can be exported after being utilized for alcohol production. In other cases a part of energy has to be imported for alcohol production even after utilization of electricity produced in the plant. The energy efficiency (η) of ethanol plant has been defined according to the situations (with export/import) as follows [40]:

In case of energy export:

$$\eta = \frac{Y_{\text{bioethanol}} \times CV_{\text{bioethanol}} + Y_{\text{electricity}}}{100 \times CV_{\text{lignocellulose}}}$$

In case of energy import:

$$\eta = \frac{Y_{\text{bioethanol}} \times CV_{\text{bioethanol}} - E_{\text{import}}}{100 \times CV_{\text{lignocellulose}}}$$

where, Y = yield

In case of SyP for ethanol production, the overall energy efficiency on the higher heating value (HHV) basis is 41.95%, syngas generation and fermentation step having energy efficiencies of 66% and 63.5%, respectively [86]. The significance of different energy efficiencies (η) in this platform has been defined as follows:

$$\eta_{\text{gasification}} = \frac{\text{Output flowrate of syngas (Nm}^3/\text{h)} * HHV_{\text{syngas}} (\text{MJ/Nm}^3)}{\text{Input flowrate of biomass (kg/h)} * HHV_{\text{syngas}} (\text{MJ/kg})}$$

$$\eta_{\text{fermentation}} = \frac{\text{Output flowrate of ethanol (m}^3/\text{h)} * HHV_{\text{syngas}} (\text{MJ/m}^3)}{\text{Input flowrate of syngas (Nm}^3/\text{h)} * HHV_{\text{syngas}} (\text{MJ/Nm}^3)}$$

$$\eta_{\text{overall}} = \frac{\text{Output flowrate of ethanol (m}^3/\text{h)} * HHV_{\text{syngas}} (\text{MJ/m}^3)}{\text{Input flowrate of biomass (kg/h)} * HHV_{\text{syngas}} (\text{MJ/kg})}$$

In the efficiency calculation, the energy consumed during any process has not been considered. The most energy intensive step is the downstream processing, i.e., distillation of ethanol, consuming 31.27MWh when a plant having a capacity of 1200 Mg/d is run using switchgrass as the feedstock [86]. As mixed bacterial consortia are used in the CP, sterilization and pretreatment of the feedstock can be avoided and hence energy is saved. On the other hand, the separation step could be energy intensive since the platform produces mixed carboxylic acids [25,45]. However, systematic report on energy analysis of alcohol

Table 2
Advantages and disadvantages of different platforms for bio-alcohol production.

Platform	Advantages	Disadvantages
Sugar platform (SP)	<ul style="list-style-type: none"> ● Specificity of end products (the bio-alcohols). ● Maturity of technology. ● High yield of alcohol (ethanol production by yeast). ● Simultaneous generation of H₂ (another biofuel) when butanol is produced (ABE fermentation pathway). ● Maximum conversion of the sugars to bio-alcohols. 	<ul style="list-style-type: none"> ● Necessity of energy intensive pretreatment, in case of LCBs. ● Necessity of expensive enzymes for hydrolysis. ● Generation of lignin-rich waste streams. ● Prominent end-product inhibition exerted by the bio-alcohols on the solventogenic microorganisms.
Syngas platform (SyP)	<ul style="list-style-type: none"> ● Capability to directly convert recalcitrant lignin. ● No requirement of pretreatment. ● No requirement of external addition of enzymes. ● Specificity of end products (ethanol and acetic acid). ● Scope of waste heat recovery to self-sustain the gasification process. 	<ul style="list-style-type: none"> ● Necessity of catalyst in the gasification process to maintain the quality of syngas. ● Mass transfer limitation in syngas fermentation. ● Chance of intoxication of the microorganism/s by traces of condensable volatiles (tar) present in the syngas. ● Generation of ash during gasification and necessity of ash handling ● The technology is at a nascent state.
Carboxylate platform (CP)	<ul style="list-style-type: none"> ● Requirement of very moderate or no pretreatment. ● No requirement of external addition of enzyme or chemical catalyst. ● No requirement of sterilization of feedstock. ● High yield of VFAs and MCFAs as precursors for alcohol production. ● Biogas production from the digestate and residue of downstream processing is possible. 	<ul style="list-style-type: none"> ● The interaction between the microorganisms involved in carboxylate platform is yet to be explored. ● Mixed products (fatty acids of varying chain length). ● Stringent requirement of pH control and suppression of methanogenesis during IAD for generation of SCFAs and MCFAs as end products. ● Requirement of hydrogen or other electron donors for the conversion of carboxylic acids to alcohols.

production through CP is not much available.

Table 1 represents the comparative performance of different individual platforms with respect to material and energy balances as well as cost.

3. Integration of platforms for bio-alcohol production – state of the art

The principal processes, feedstocks, microbes, patterns of generation of products, by-products and residues, energy efficiencies and conversion data of individual SP, CP and SyP have been indicated in Table 1. The advantages and disadvantages of the individual platforms meant for production of bio-alcohols, as discussed in section 2 are compiled in Table 2. Although each platform involves combination of different processes having inherent merits and demerits, only the major ones affecting the sustainability of three production platforms are mentioned in a collective manner.

The disadvantages encountered in an individual platform, as listed in Table 2, can be tackled through the strategic inter-integration of the platforms with each other. Through the integration of different platforms, the by-product or effluent streams of one platform can be (re) used as the feed for another platform. The availability of literature on the integration of platforms for bio-alcohol production is scarce. So far, four types of twinning of platforms have been reported according to their operating sequence, namely; 1) carboxylate platform followed by sugar platform (CP-SP); 2) syngas platform followed by carboxylate platform (SyP-CP); 3) carboxylate platform followed by syngas platform (CP-SyP) and 4) sugar, carboxylate and syngas platforms operated in sequence (SP-CP-SyP). Although from the classical definition of carboxylate platform, carboxylic acids or volatile fatty acids generated through incomplete AD are precursors, in this review, the studies based on the volatile fatty acid intermediates produced from other bioprocesses using mixed or pure strains are also considered. The reactions occurring in all individual and hybrid platforms, under review, are presented in Table 3.

Different pros and cons of the reported research outcomes on integration of platforms are being revisited. Their operating strategies are presented in Figs. 2–7 and the salient features of their performances are being discussed in the following sections.

3.1. CP-SP hybrids

Two types of CP-SP hybrids have been reported in the literature. In

strategy-I, represented in Fig. 2, digestate from the acidogenic stage of the IAD process, using mildly pretreated lignocellulosic biomass, is enzymatically hydrolyzed prior to conversion through the sugar fermentation process [83,84]. According to strategy-II of CP-SP hybridization, represented in Fig. 3, supernatant from the carboxylate platform is directly fed to sugar platform. In some reported articles, instead of coupling carboxylate platform producing solely carboxylic acid through IAD, partial AD process generating biogas up to a period less than the saturation level has been considered as the representative one [92,97]. Partial AD is followed so that some of the hydrolysable sugar polymers (cellulose, hemicellulose) remain unconverted in the digestate. Hence, it can directly be introduced to enzymatic hydrolysis process and the severity of overall pretreatment step is reduced [97]. It is expected that the liquid effluent of the partial AD would contain some carboxylic acid and sugar monomers. In another report, instead of IAD, a stable mixed culture of cellulolytic, xylanolytic and acidogenic bacteria including butyrate producing ones has been used to generate carboxylic acid from lignocellulosic feedstocks [27]. The carboxylic acid fed to the sugar platform is expected to be converted to alcohol in solventogenic phase of clostridial bacteria used in the sugar platform for butanol production [27].

3.1.1. CP-SP hybrid (Strategy-I)

In a recent research study, a partial AD process has been used as a pretreatment step for the sugar platform [97]. Diverse lignocellulosic waste, namely, rice straw, sycamore and pinewood were used as feedstocks. It was claimed that for rice straw, sycamore and pinewood, the ethanol yield was increased from 32%, 19% and 10.7% of the theoretical value to 69.5%, 40% and 22.1% respectively due to this pretreatment process instead of conventional ones [97]. The maximum increase of yield in case of rice straw was explained by its lowest lignin content facilitating the hydrolytic activity of the AD microbiome. On the other hand, the presence of guaiacyl type lignin in pinewood was pointed out to be responsible for minimum increase of yield in case of pinewood [97]. The investigators also showed that most of the hemicellulose was utilized to form methane during the AD process of rice straw. The increase of cellulosic content of pretreated biomass, particularly for rice straw was also identified through the determination of crystallinity index [97]. Taking both biogas and ethanol into account, the total energy yield from rice straw and pinewood was determined to be 8.2 MJ/kg and 4.1 MJ/kg. Although partial AD process is supposed to generate (not discussed) liquid effluent rich in VFA and enzymatic hydrolysis step of solid digestate of partial AD process would have

Table 3
Reactions involved in individual and hybrid platforms.

Conversion	Reactions	Platform
Glucose to ethanol	$Glucose \rightarrow 2Ethanol + 2CO_2$	SP, CP-SP(I), SP-CP- SyP
Xylose to ethanol	$3Xylose \rightarrow 2Ethanol + 5CO_2$	SP, CP-SP(I), SP-CP- SyP
Glucose to butanol	$Glucose \rightarrow Butanol + 2CO_2 + H_2O$	SP, CP-SP(II), SP-CP- SyP
Xylose to butanol	$6Xylose \rightarrow 5Butanol + 10CO_2 + 5H_2O$	SP, CP-SP(II), SP-CP- SyP
Glucose to acetone	$Glucose + H_2O \rightarrow Acetone + 3CO_2 + 4H_2$	SP, CP-SP(II)
Xylose to acetone	$Xylose \rightarrow Acetone + 2CO_2 + 2H_2$	SP, CP-SP(II)
Syngas to acetic acid	$4H_2 + 2CO_2 \rightarrow acetate^- + H^+ + 2H_2O$ $4CO + 2H_2O \rightarrow CH_3COOH + 2CO_2$	SyP, SyP-CP, SyP-CP- SyP
Syngas to ethanol	$acetate^- + H^+ + 2H_2 \rightarrow ethanol + H_2O$ $CH_3COOH + 2CO + H_2O \rightarrow ethanol + 2CO_2 + H_2O$	SyP, SyP-CP, SyP-CP- SyP
Glucose to acetic acid	$Glucose \rightarrow 3Acetic\ Acid$	CP, CP-SP (II), SyP-CP(1-stage)
Xylose to acetic acid	$2Xylose \rightarrow 5Acetic\ Acid$	CP, CP-SP (II), SyP-CP(1-stage)
Glucose to butyric acid	$Glucose \rightarrow Butyric\ Acid + 2CO_2 + H_2$	CP, SyP-CP(1-stage), SyP-CP- SyP, Sp-CP- SyP
Xylose to butyric acid	$6Xylose \rightarrow 5Butyric\ Acid + 10CO_2 + 5H_2O$	CP, SyP-CP(1-stage), SyP-CP- SyP, Sp-CP- SyP
Acetic acid to butyric acid	$ethanol + Acetic\ Acid \rightarrow butyrate^- + H_2O$	SyP-CP(1-stage), SyP-CP- SyP, SP-CP- SyP
Butyric acid to caproic acid	$ethanol + Butyric\ Acid \rightarrow caproic\ acid + H_2O$	SyP-CP(1-stage), SyP-CP- SyP, SP-CP- SyP
Acetic acid to ethanol	$acetate^- + H^+ + 2H_2 \rightarrow ethanol + H_2O$	SP, CP-SP(I,II)
Butyric acid to butanol	$butyric\ acid + 2H_2 \rightarrow n-butanol + H_2O$	SP, CP-SP(I,II), SyP-CP(1-stage and 2-stage), SP-CP- SyP
Caproic acid to hexanol	$caproic\ acid + H^+ + 2H_2 \rightarrow n-Hexanol + H_2O$	SyP-CP(1-stage), SyP-CP- SyP, SP-CP- SyP

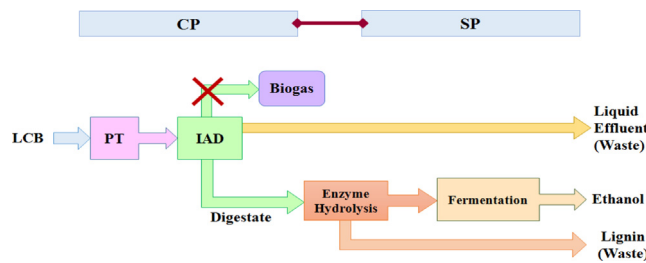


Fig. 2. Scheme of CP-SP hybrid (Strategy-I).

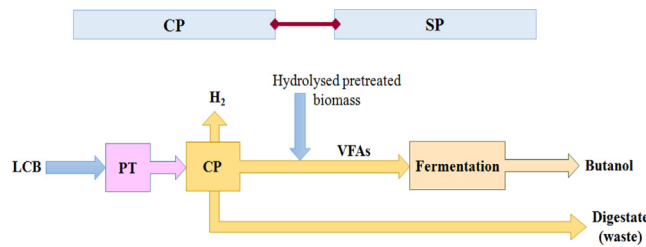


Fig. 3. Scheme of CP-SP hybrid (Strategy-II).

produced lignin rich solid residue, no attempt was made to utilize these wastes. There is a scope for the addition of ABE fermentation, a representative of SP, if the liquid effluent is rich in butyric acid. Otherwise, the carboxylic acids in the liquid effluent can be fed to a SyP to generate higher alcohols. Similarly, lignin rich waste can be introduced to a SyP so that alcohol can be generated by using the syngas produced through gasification of the solid residue.

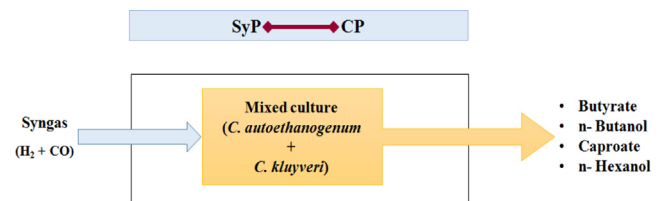


Fig. 5. Scheme of single stage SyP-CP hybrid.

Anaerobic digestion process using rumen fluid of cattle was also claimed to be effective in the enhancement of ethanol production from rice straw [98]. The group used solid digestate from the rumen fluid digestion process and the results were very similar to those using the inoculum obtained from partial AD process in biogas plant [97]. It is notable that the acidogenesis conducted by rumen microbiome produced significant amount of VFAs (Acetic acid: 159 g, Propionic acid: 83, Butyric acid: 24) when 2.5% loading of rice straw was used [98]. Inhibition of methanogens from this microbiome may turn it into a major acidogenic microbiome producing VFAs/SCFAs that can be ultimately converted in their corresponding bio-alcohols.

3.1.2. CP-SP hybrid (Strategy-II)

In a very recent attempt, rice straw was converted to biobutanol through a two-stage fermentation process [27]. The first stage represented the CP in which pretreated (alkali treated) rice straw was predominantly converted to VFAs, mainly, butyric acid and hydrogen under the action of a mixed culture, named as DCB17, dominated by cellulolytic, xylanolytic and butyric acid producing bacteria [99]. In the second stage, the butyric acid rich supernatant of the first stage (SFS)

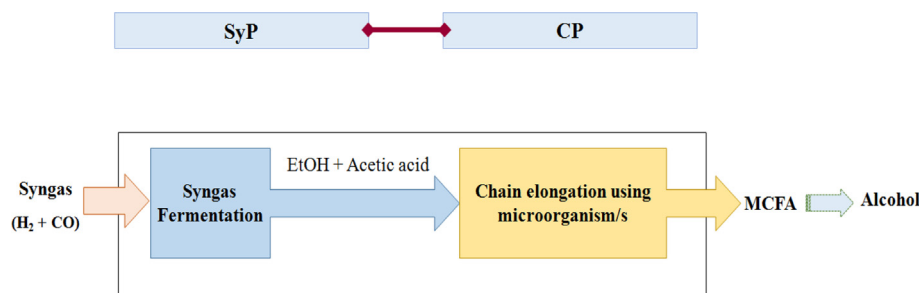


Fig. 4. Scheme of two stage SyP-CP hybrid.

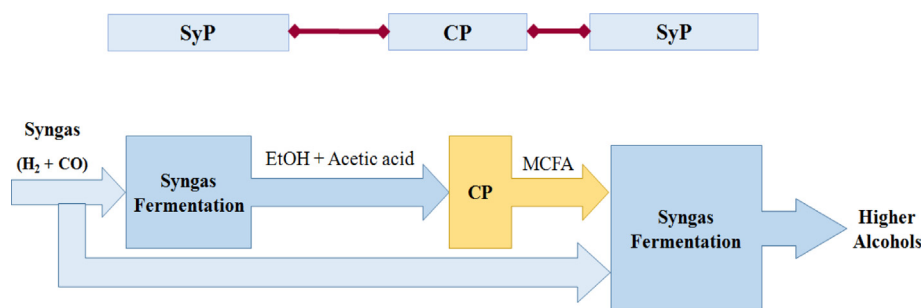


Fig. 6. Scheme of multi-stage hybridization of SyP-CP-SyP.

was co-fermented with enzymatically hydrolyzed pretreated rice straw (HPRS) using *C. beijerinckii* NCIMB 8052 to butanol [27]. The ratio of SFS:HPRS used was 2:8 on mass basis. Bio-butanol was produced along with hydrogen, acetone and ethanol as co-products. In comparison to butanol production of 80.3 g and 146 g per kg rice straw, respectively, by *C. acetobutylicum* NRRL B-591 and a mixed culture dominated by clostridia from pretreated and enzymatically hydrolyzed rice straw reported in two other studies [100,101], 230 g butanol/kg rice straw was obtained in this integrated CP-SP process [27]. The specific energy yield (9633.7 kJ/kg) of the two-stage process was much higher than that obtained using clostridial microflora (8043.5 kJ/kg) considering both butanol and hydrogen as the energy carriers in the products [27,100]. Studies showed that the enhancement of bio-butanol yield is highly influenced by the continuous supply of butyric acid, which down-regulates the enzymatic activities of acetate kinase, acetate phosphotransacetylase, phosphate butyryl transferase during solventogenesis in ABE fermentation [102–104].

Thus, the synergistic integration of carboxylate and sugar platforms not only enhances the butanol production, it also eliminates the necessity of the application of costly enzyme cocktails that is used in the conventional sugar platform. However, even after this integration, a considerable portion of biomass fraction is lost as digestate of the acidogenic stage (CP) and concentrated lignin portion during conventional enzymatic hydrolysis in the sugar platform. Thus, further attention is needed to facilitate utilization of these energy-rich effluents. A syngas platform using a thermochemical step, namely, gasification or pyrolysis could have been beneficial for recalcitrant lignin rich part. Similarly, the digestate of the acidogenic stage could have been utilized for biogas generation through AD process, the digestate of AD to be used as fertilizers. However, no investigation has been reported in this respect.

3.2. SyP-CP hybrids

The SyP-CP hybrids can be categorized as two stage and single stage ones. In the two-stage category, represented in Fig. 4, the product stream of syngas platform is fed to the carboxylate platform for further conversion of short chain fatty acids through chain elongation to MCFAs which can in turn be used as precursors for production of higher

bio-alcohols. Steinbusch et al., 2008, reported the conversion of different volatile fatty acids to corresponding alcohols by a mixed culture at high hydrogen pressure and low pH [105]. In the single stage hybrids, represented in Fig. 5, both the syngas fermentation and the biochemical processes involved in CP occur simultaneously in a single reactor for the production of MCFA. Medium chain fatty acids are ultimately converted to bio-alcohols by syngas fermenting microbes, namely, *C. ljungdahlii* or *C. autoethanogenum* present in the microbiome of the integrated system.

3.2.1. Two-Stage SyP-CP hybrids

Vasudevan et al., 2014, reported the sequential combination of SyP and CP, whereby, the effluent of the syngas fermentation process containing acetic acid and ethanol was fed to an anaerobic bioprocess driven by open reactor microbiome [28]. The mixed acidogenic consortia led to chain elongation of carboxylic acids (from acetic acid to n-caproic acid via n-butyric acid) in the presence of ethanol prevailing in the SyP effluent. The well established reversed β -oxidation pathway was proposed to be responsible for the chain elongation in this two stage hybrid of SyP and CP [28]. Although their aim was to produce n-caproic acid as the major end product, the fermentation effluent was more enriched in n-butyric acid. While the maximum value of n-caproic acid production rate reached only $1.7 \text{ g L}^{-1} \text{ d}^{-1}$, n-butyrate production rate as high as $20 \text{ g L}^{-1} \text{ d}^{-1}$ was achieved [28]. The self-inhibitory nature of n-caproic acid even at low concentration on the chain elongating microbes and hyper-sensitivity of the microbiome to pH were identified as the inherent causes for the high n-butyrate titer [28]. The maintenance of favorable pH and the avoidance of methanogenesis were suggested to be the necessities for chain elongating reactions to proceed. In another attempt, instead of mixed consortia, a pure strain of *Clostridium kluyveri* was used successfully for the integration of SyP with CP [29]. Continuous extraction of medium chain fatty acids, namely n-caproic acid, from the reactor was used to maintain its concentration below inhibitory level. *C. kluyveri* also produced n-caprylic acid in this system. The chain-elongation performance of *C. kluyveri* was observed to be better at a low ethanol to acetate ratio (3:1) and neutral pH [29]. Although these studies were not focused on alcohol production as the end-product, it was envisaged that by maintaining high partial pressure of hydrogen ultimate conversion to higher alcohols would have been

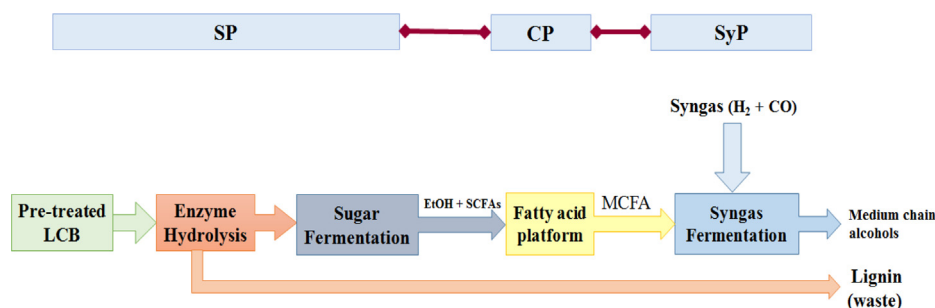


Fig. 7. Scheme of multi-stage hybridization of SP-CP-SyP.

possible, using mixed culture and low system pH [106,107]. In another study conducted by Kucek et al., 2016, the enhancement of specific production of n-caprylic acid was investigated [108]. A basal medium containing substrate ratio of 15 (COD basis) obtained by mixing high ethanol to low acetate was fed to an UAB with continuous product extraction and inoculated with a reactor microbiome grown on effluent of ethanol rich beer fermentation. From the 186 days operation of the UAB highest n-caprylic acid productivity of 19.4 g COD/L/d was achieved [108]. The microbe *Rhodocyclaceae* K82 sp. was identified as the major chain elongating bacterium in the microbiome with a relative abundance of 70.8%.

It is expected that the excess hydrogen produced in the thermochemical step (gasification/pyrolysis) of syngas platform can be used to produce higher alcohols from MCFAs by the activity of potential microbiomes. The hybrid processes, similar to MixAlco type hybridization in which the MCFA are thermochemically converted to ketones and ultimately to corresponding alcohols, can also be used [49,50,109].

3.2.2. Single-Stage SyP-CP hybrids

Diender et al., 2016, studied the performance of production of MCFA and higher alcohols (butanol, and hexanol) by co-culturing *C. kluyveri* and *C. autoethanogenum* using synthetic medium and syngas [106]. They reported that although the feeding of acetate (and ethanol) was not a pre-condition for growth of the co-culture, it drastically enhanced the higher alcohol production.

They reported that the production rates of butanol and hexanol were 3.5 ± 0.69 and 2.0 ± 0.46 mmol/L/d, respectively, and those of butyrate and caproate were 8.5 ± 1.1 and 2.5 ± 0.63 mmol/L/d, respectively [106]. pH sensitivity and toxicity of produced caproate were suggested to be major constraints for chain elongation. Like many other mixed culture driven bioprocesses as demonstrated by Ghosh et al., 2016, in this system a clear commensal interaction can be noticed between *C. kluyveri* and *C. autoethanogenum*, where the latter organism protects the former from being intoxicated by the CO [110]. Ganigué et al., 2016, studied the production of mixed fatty acids and higher alcohols using a syngas-enriched mixed culture [107]. They observed that although low pH triggered the production of alcohols, it was detrimental towards the growth of chain elongating bacteria, i.e. *C. kluyveri*. Richter et al., 2016, aimed at analyzing the production patterns of higher alcohols like butanol, hexanol and even octanol by co-culturing syngas fermenting and chain elongating bacteria, namely *C. ljungdahliae* and *C. kluyveri*, in a single reactor [30]. The optimal pH range was observed to be very narrow (pH at 6.0, but not ideal) due to inherent discrepancies between the pH optima of the two organisms [30]. Therefore, it was suggested to use organisms with very close optimum values of pH for overcoming this problem. The study found that a competitive relationship exist between the organisms for the substrate, namely SCFAs, as one organism (*C. ljungdahliae*) uses it for reduction to alcohols and the other one (*C. kluyveri*) for chain elongation [30].

3.3. Multistage cascading of different platforms

3.3.1. SyP-CP-SyP cascading

From literature review it is clear that a multistage process, namely, SyP-CP-SyP type hybrids, whereby, the carboxylate platform is integrated with the syngas platform performing ethanol and higher alcohol production and reduction of MCFAs has a high prospect [30,111,112].

In SyP-CP-SyP cascading, represented in Fig. 6, the products (ethanol and acetic acid) of the first syngas platform are fed to the carboxylate platform for their conversion to medium-chain carboxylates (MCFAs) using a chain elongating microorganism and ultimately the product MCFAs of Carboxylate platform are fed to the second syngas fermenter for the reduction of fatty acids to corresponding bio-alcohol. The problem occurring in single stage integration of SyP-CP (Fig. 5) due to pH discrepancy should disappear if separate reactors are

used. More facts are to be revealed before taking the strategic decision on optimal combination.

3.3.2. SP-CP-SyP cascading

A contemporary study reported the integration of three platforms whereby the carboxylate platform was preceded and succeeded by sugar and syngas platforms, respectively [113]. The SP-CP-SyP hybrid process is depicted in Fig. 7.

The reactor effluent of the yeast driven sugar platform using corn kernel as the feedstock was fed to a carboxylate platform where mixed fatty acids with varying chain length (C2-C6) were generated and continuously extracted from the reactor. The carboxylate platform effluent was fed to the syngas fermenter where a mixture of corresponding alcohols was produced exploiting the reductive power supplied by the syngas by *C. ljungdahliae* [113]. This process ensured the sequential utilization of the liquid effluent of sugar and carboxylate platforms as well as decreased the expenses incurred for the synthetic fermentation medium for the syngas platform. Higher alcohols, namely butanol and hexanol, were obtained in the ultimate product stream from the last stage of the integrated process [113].

A few research studies have also been reported on SP-CP combinations for the generation of MCFA from LCB [114,115]. Kucek et al., 2016, collected the liquid effluent 'wine lees' from a winery and used it as the source of nutrients and substrate in an upflow anaerobic bioreactor (UAB) for production of MCFAs, namely, n-caproic and n-caprylic acids. The wine lees is rich in residual ethanol with a concentration of 180.5 gCOD/L (40% ethanol, COD basis) which served as the major electron donor for the chain elongation process [114]. The UAB was inoculated with a chain-elongating reactor microbiome adapted to ethanol rich beer fermentation effluent. The UAB was operated at acidic pH of 5.2 with continuous extraction of products by pertraction. Maximum MCFA productivity of 3.9 g COD/L/d was obtained corresponding to 67% MCFA yield at an organic loading rate of 5.8 g COD/L/d of diluted wine lees [114]. The microbiome analysis revealed that the MCFA production in this study was conducted by the microbial members of *Bacteroides* sp., *Oscillospira* sp. and *Clostridium* sp. The typical chain elongating bacterium *C. kluyveri* was not present in the microbiome [114]. Scarborough et al., 2018, in a very recently performed study attempted to incorporate the unfermented carbohydrate (mainly xylose) rich part originating from the distillation stage of a preceding ethanol fermentation process as substrate for MCFA production [115]. The ethanol fermentation was conducted by a mutant strain of *Saccharomyces cerevisiae* Y128 using pretreated and enzymatically hydrolysed switchgrass. Analysis of the fermentation samples showed that the glucose fraction was almost fully consumed, but there was significant xylose (47% utilized) remained as unconverted carbohydrate in the fermenter [115]. Post-fermentation the effluent of the fermenter was processed in a glass distillation unit for alcohol recovery and the bottom product was recovered as the xylose and organic rich stillage. This stillage was fed to a bioreactor inoculated with sludge of an acid-phase WWTP. The microbes present in the sludge conducted mixed culture fermentation of the stillage and produced MCFAs, mainly caproic and caprylic acids as the end products with productivity values of 2.6 ± 0.3 g/L/day and 0.27 ± 0.04 g/L/day [115]. Community analysis of the microbiome of the MCFA reactor identified *Lactobacillus*, *Pseudoramibacter* and *Roseburia* as the most abundant microbial species and hence the major of producer MCFA. Based on these results it was proposed by the investigators that *Lactobacillus* produced lactate and acetate by hetero-fermentative conversion of xylose of stillage. Afterwards, the lactate is used as the initial precursor for chain elongation to the MCFAs by *Pseudoramibacter* and *Roseburia* [115]. The liquid effluent generated after MCFA recovery was processed in an AD unit to biogas. The biogas, the leftover bio-solids of the AD process and lignin residues generated at any point of the process was converted to heat and electricity using a CHP unit. The economic analysis of this system (generating ethanol, electricity and MCFAs) indicated that due to the

Table 4
Comparative performances of different hybrid strategies.

Strategy	Overall Processes involved	Input stream	Process		Advantage	Enzymatic hydrolysis	Advantage	Alcohol production performance	Ref.
			Pretreatment	Process					
CP-SP -I	CP: Acidogenesis of LCB in IAD of IAD SP: Fermentation of digestate and enzymatically hydrolysed LCB	CP: LCB SP: Digestate from CP	CP: Not required	SP: CP	Complete conversion of hemicellulose in CP. Energy saving due to avoidance of energy intensive acid pretreatment. Same as strategy I	CP: Not required SP: Required	Increase in glucose yield due to increase in the concentration of crystalline cellulose.	Much higher than conventional SP.	[97,98]
CP-SP II)	CP: Acidogenesis of LCB in IAD SP: Fermentation of VFA-rich effluent of IAD and enzymatically hydrolysed LCB	CP: LCB SP: LCB + Liquid effluent from CP	CP: Low temperature (50 °C) alkali pre-treatment SP: Acid pretreatment + enzymatic hydrolysis			CP: Not required SP: Required only for direct LCB stream.	Enzyme cost reduced due to usage of liquid effluent from CP	Much higher than conventional SP due to direct input of liquid effluent from CP.	[27,99]
Single stage SyP-CP	Simultaneous conversion of syngas to ethanol and acetic acid and production of higher alcohols through reduction of MCFAs produced through chain-elongation	Simulated syngas + synthetic medium	Not required		NA	NA	Chain elongation of SCFAs to MCFAs and reduction to alcohols in a single reactor	Medium chain alcohols (butanol, hexanol) are produced.	[106]
SyP-CP-SyP cascade	SyP: Conversion of syngas to ethanol and acetic acid CP: production of MCFAs through chain-elongation production of higher alcohols through reduction of MCFAs produced through chain-elongation	SyP (First): Syngas CP: Acetic acid and ethanol from first SyP (Second): MCFAs from CP	Not required.		NA	NA	Chain elongation of short chain fatty acids and reduction to alcohols with continuous removal of inhibitory products (caproic acid etc.) and lower necessity of pH control with respect to single stage system	Medium chain alcohols (hexanol, octanol) are produced.	[30,111]
SP-CP-SyP cascade	SP: Conventional fermentation of LCBs CP: Chain elongation of VFAs in SP effluent in to MCFAs SyP: Reduction of MCFAs to higher alcohols	SP: LCB CP: ethanol and stillage SyP: MCFAs from CP	SP: Conventional		NA	Conventional	Full utilization of effluents of SP with conversion to higher alcohols	Medium chain alcohols (butanol, hexanol) are produced.	[113]

Table 5
Special characteristics of pyrolysis process regarding hybridization.

Characteristics	Refs.
<ul style="list-style-type: none"> Pyro-gas can be used in the syngas platform for bio-alcohol generation. 	[118]
<ul style="list-style-type: none"> Levogluconan can be converted to glucose and fermented to bio-alcohols. 	[127,131–135]
<ul style="list-style-type: none"> Cellobiosan can be converted to reducing sugars. 	[136,137]
<ul style="list-style-type: none"> Acetic acid can be converted to acetyl-CoA, the central precursor for the production of fatty acids and in turn alcohols by many organisms. 	[138]
Pyro-char can be used	[139–141]
<ul style="list-style-type: none"> as an enhancer of acidogenic step in AD (and IAD processes). 	[142,143,144]
<ul style="list-style-type: none"> as a biosorbent in alcohol recovery from bioprocesses 	
<ul style="list-style-type: none"> for soil amendment and hence carbon sequestration 	

utilization of the stillage for the MCFA production the minimum ethanol selling price was 1.76 USD/gallon, which was 18% reduced price of ethanol (2.15 USD/gallon) obtained from another similar study (generating ethanol and electricity) which does not recover and use the stillage [115]. It is expected that integration of these type of SP-CP hybrids can also be extended to a SP-CP-SyP cascade just by the addition of a syngas fermentation process either in single or in combination with the CP stage.

4. Limitations of the present integration strategies for hybrid platforms

Figs. 2–7 represent different strategies of integrating sugar, carboxylate and syngas platforms. The foregoing discussions clearly demonstrated the up-to-the-minute status of the hybridization of the platforms for bioalcohol production from lignocellulosic biomass. The performance of different hybrid platforms from the perspective of processes involved, the advantages and the products have been compared, at a glance, in Table 4.

From the review of the current scenario it is revealed that the solid digestate of the carboxylate platform, proceeding via incomplete AD, can be used in the sugar platform after enzymatic hydrolysis and without an energy-intensive pretreatment process. Carboxylate platform can also serve as a complementary process for the syngas platform and vice-versa for the production of higher alcohols. The hybridization of the three platforms has been claimed to be one of the best combinations regarding production of bio-alcohols [113]. However, an in-depth scrutiny further reveals some facts that should also be incorporated in future research endeavors attempting hybridization of SP, CP and SyP. From the analysis of Figs. 2–7, it is evident that in the CP-SP combinations, studied so far, only few attempts have been made to utilize the liquid effluent and solid digestate of the carboxylate platform. The anaerobically pre-treated digestate can be used as a source of simple sugar and the liquid product of this process can act as precursors for butanol in a subsequent sugar platform, other than ethanol production. In case of SyP-CP and SyP-CP-SyP combinations, most of the previous studies have been focused on simulated systems where the starting points of SyP-CP are syngas and bioreactor-ready medium containing externally added carboxylic acid [30,113]. In fact, when complex lignocellulosic compounds are to be handled in reality, even in these attractive combinations there will be generation of digestate in the carboxylate platform and ash in the syngas platform, if gasification is used as the thermochemical process. Although the synergistic integrations of AD and pyrolysis (PY) in the form of AD-PY, PY-AD and AD-PY-AD have been successfully studied for the generation of biogas, no attempt has been made to incorporate these for bio-alcohol generation [89,116,117]. However, pyrolysis processes can be incorporated in the syngas platform in place of gasification [118]. Besides the utilization of pyro-gas in the syngas platform, other products of pyrolysis, namely, pyro-liquid and pyro-char can also be incorporated in the sugar and carboxylate platforms respectively leading to a hybrid system with zero effluent. The interesting characteristics of pyrolysis along with the general definition of the process are provided in the

following section.

5. Special characteristics of pyrolysis and its prospective role in hybrid platforms

Pyrolysis is a thermochemical process popularly used to effectively convert lignocellulosic biomass to pyro-oil, pyro-gas and pyro-char in the temperature range of 300–900 °C [13,119–122]. While cellulose and hemicellulose are converted to anhydrous-sugars, namely, levoglucosan, cellobiosan etc. and acetic acid, respectively, lignin is converted to phenols and other aromatic compounds and char is produced constituting unconverted solid fractions [123–127]. Some recent studies show high yields of pyro-gas (27.8–34.8% (w/w), pyro-oil (31–53.5% (w/w)) and pyro-char (18.7–34.2% (w/w)) during pyrolysis of lignocellulosic agro-waste (rice straw and sugarcane bagasse) and forest wastes (pine wood) [128–130]. The sugars and acids appear in the aqueous phase of pyro-oil. The pyro-gas is mainly constituted of CO, CO₂ and H₂, closely resembling the syngas [118]. Some special characteristics of the pyrolysis process have been tabulated (Table 5) and assessed to judge its suitability to be employed as a candidate process of a hybrid platform for bio-alcohol production.

From Table 5, it can be inferred that PY can be incorporated in the integration efforts, which will fulfill the zero-effluent criterion of a circular economy [145,146]. By incorporation of PY, besides the syngas, anhydrous sugars and acetic acid in the aqueous pyro-liquid (APL) can be fermented to alcohol using potential microorganism, while biochar and the non-aqueous phase of bio-oil can be obtained as valuable by-products in conventional ways [127–142]. Although it has been identified by many researchers that pyrolysis can serve as a potential process for the generation of intermediates, namely, sugar, syngas and carboxylic acid for SP, SyP and CP respectively, information on its incorporation in hybridization is not available. In one patent (US20120073199A) a low temperature long residence time pyrolysis process was claimed to convert high-lignin LCB to pyro-liquid, which can be fermented to bio-ethanol using yeast [147]. The Table 6 provides some reported facts on conversion of APL, obtained from fast pyrolysis of biomass to bioethanol.

It is clearly indicated that the anhydro-sugar, namely levoglucosan present in APL is converted, either directly or indirectly via hydrolysis to glucose and ultimately to ethanol. It is thus expected that the enrichment of levoglucosan in APL is directly related to increase in alcohol yield. A recent research article on pyrolysis of oak wood suggests that low concentration oxygen in the sweeping gas leads to higher yield of hydrolysable sugar [149]. It was recommended that the AD of pyro-liquid for the generation of biogas could be another option for producing biomethane as the biofuel [147]. Some studies also suggest that biochar obtained through pyrolysis enhances the yield of ethanol during fermentation of syngas [150]. The addition of biochar is beneficial during the chain elongation reaction using ethanol and acetic acid. Biochar has been reported to enhance the yield of caproic acid up to 21.1 g/L in comparison to 14.4 g/L obtained for control in absence of biochar [151]. Although there is also a scope for the co-fermentation of carboxylic acid (mainly acetic acid) present in the aqueous part of pyro-

Table 6
Production of ethanol from levoglucosan (LG) of LCB-derived pyro-oil.

LCB feedstock And Pyrolysis Temperature	LG content of pyro-oil %(w/w) and APL (g/L) used for Pretreatment/direct fermentation	LG to Glucose %(w/w)	Microorganism	Ethanol yield	Ref.
Red oak 500 °C	2.8 36 ± 1 g/L	NA*	<i>E. coli</i> KO11 + <i>lgk</i>	0.235 g/g LG 0.65 ± 0.08 g/L	[126,131]
Scots pine 450–500 °C	7.8 87 g/L	216	<i>S. cerevisiae</i> T2	0.46 g/g glucose	[132,148]
Waste cotton cellulose 400 °C	43 104.3 g/L***	166**	<i>S. cerevisiae</i> 2,399 <i>Z. mobilis</i> 10,232 <i>Pichia</i> sp. YZ-1	0.45 g/g glucose 16.1 g/L 0.44 g/g glucose 1.8 g/L 0.42 g/g glucose 15.1 g/L	[133]

* Directly fermented as per description in reference.

** Calculated from corresponding values in reference.

*** Calculated from corresponding value (10.43% (w/w)) in reference.

liquid with pyro-gas, containing mainly CO, H₂ and CO₂, to higher alcohols in presence of chain elongating and syngas-fermenting bacteria either in cascades or in single stage, the invention did not consider this avenue.

6. Recommendations

Although, hybridization of platforms for bio-alcohol production from LCB seems to be a very captivating research field in recent times, it involves challenges of biochemical reaction kinetics, complex mixed microbial systems, reactor design with efficient process control strategies, thermochemical reactions, mass transfer limitations, recycling of enzymes and catalysts, product recovery, utilization of bio-alcohols in engines either solely or as drop-in fuels, economic viability, energy and environmental sustainability, and hence entails an interdisciplinary approach.

Analyzing the combination of different platforms for bio-alcohol production from a holistic approach, the incorporation of the following research objectives can be useful in upgrading the present status:

- Coupling of platforms for the utilization of wastes from all individual platforms in as many ways as possible.
- Ensuring implementation of zero-waste concepts by incorporating processes like pyrolysis generating products (char) for carbon sequestration.
- Enhancing overall energy efficiency by incorporating AD processes generating biogas from the effluents of all platforms.
- Improvement of each individual platform (sugar, carboxylate and syngas) from the perspective of microbial and thermochemical reaction kinetics, better reactor design, mass transfer enhancement (syngas platform), process/bioprocess control, knowledge on microbial interactions, re-use of hydrolytic enzymes (sugar platform), catalyst design (gasification/pyrolysis) for improved gas yield, efficient downstream processing for bio-alcohol recovery.
- Development of microscopic and macroscopic mathematical models, whatever necessary, from basic material and energy balances to predict hybrid system performance and facilitation of scaling up.
- Development of process simulation models for the prediction of performance of large scale units.
- Testing of compatibility of bio-alcohols with gasoline engines.
- Process performance based life cycle assessment (LCA).

Keeping all these issues in consideration, a research strategy exploring the possibility of coupling platforms at any stage to generate bio-alcohols from lignocellulosic biomass with zero effluent is recommended from the perspective of economic, environmental and energy sustainability.

6.1. CONVER-B: an advanced model of hybridization of SP-CP-SyP platforms

The collaborative project CONVER-B (the acronym for the INNO-INDIGO research project, “Development of efficient biomass conversion routes for biofuel production and utilisation”) among the present research groups from India, Finland and Germany focuses on the hyphenation of the three platforms using this strategy as the blueprint [152]. It is intended to produce bio-alcohols, particularly higher ones (butanol, hexanol etc.) simultaneously, with biogas, hydrogen, non-aqueous pyro-oil and pyro-char as by-products with zero-waste generation from various agro-wastes as well as distillery waste, silage etc. Economic viability as well as energy and environmental sustainability will also be examined along with the proof-of-concept study of usability of the biofuels in existing gasoline engines. The conceptual framework of the research scheme ‘CONVER-B’ is represented in Fig. 8.

The scheme of project has been designed in such a manner that most of the challenges of different hybrid platforms, as discussed in section 4, can be addresses. Table 7 highlights the strategies of CONVER-B to address different shortcomings of existing hybrid cascades.

It is expected that the research outcomes of the project can be utilized to develop sustainable alcohol production units on hyphenated platforms running on various LCB feedstocks having diverse composition regarding cellulose, hemicellulose and lignin as well as elemental analysis (C,H,N,O,S). It is clear that although the presence of nitrogen and sulfur is beneficial for fermentative processes, thermochemical processing, particularly, gasification of LCBs rich in S and N is expected to generate SO_x and NO_x. While high moisture content is a must for biochemical processing, thermochemical processes become energetically inefficient when wet biomass is to be handled. The project is aimed to follow a zero-effluent criterion as each waste biomass can be converted by the best-suited approach within the overall combined process. Implementation of the research outcomes will be particularly useful for making the energy balance of rural regions of India positive, i.e., surpassing the consumption of energy by its supply from locally available agro-wastes and hence for the overall up-gradation of societal standard of those regions [4]. In Germany, the agricultural biogas sector is well developed [153,154]. However, the conversion of energy crops to biogas, which is burned in combined heat and power (CHP) plants, is economically not viable without subsidies. The implementation of advanced biorefinery concepts as envisaged in the CONVER-B approach by re-fitting the existing biogas infrastructure will open up new perspectives for the biogas sector after feed-in tariffs for biogas-generated electricity run out, and more sustainable value added chains can be established in the agricultural sector. As Finland is rich in forest residues, the implementation of outcomes of CONVER-B will be highly beneficial from the perspective of establishment of biorefineries in future [155].

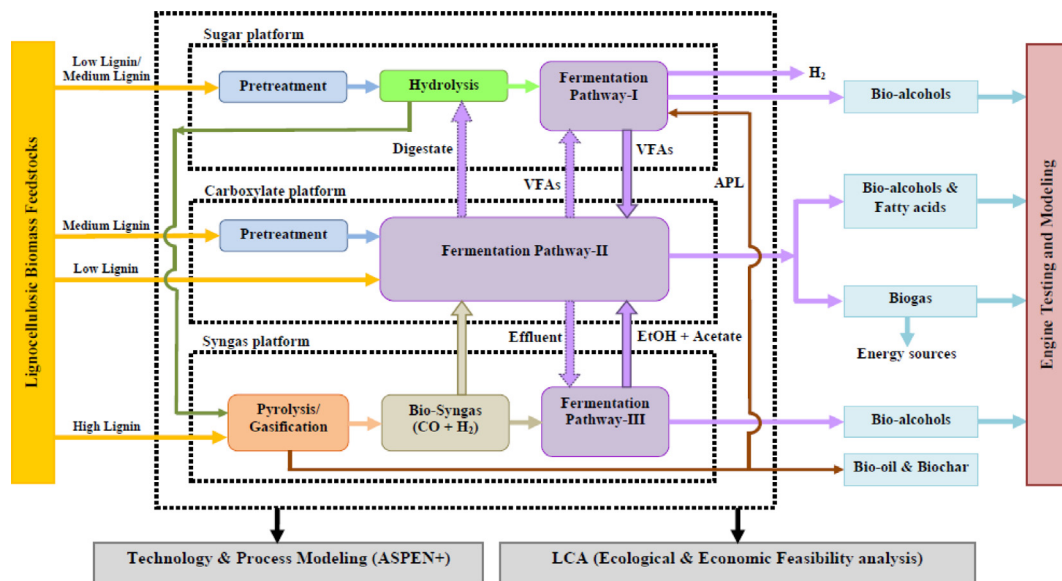


Fig. 8. Framework of the CONVER-B research scheme of hybrid platforms producing bio-alcohol from LCBs.

The results from twinned platforms clearly indicate that a mixture of alcohols would be produced particularly when the carboxylate platform relying on microbiomes is used [30,156]. Therefore, the assessment of performance of existing engines with mixtures of alcohols or their blends with gasoline by experiments and through modeling is crucial [157–160]. Although recent studies showed that the correlation between process parameters such as pH, temperature etc. with the dynamics of active microorganisms in the mixed consortia or the reactor microbiome governs the process efficiency of the carboxylate platform, data in this direction is scarce [161–164]. Since in many cases single stage arrangements for the integration of different biochemical steps are used, studies on interactions between microorganisms of different platforms are essential. Attempts of mathematical and process modeling of multi-platform systems for the prediction of performance of large scale installations or life cycle assessment have not yet been made despite their essentiality for future development of sustainable bio-alcohol units based on lignocellulosic waste. Therefore, future research should address these shortcomings.

7. Conclusions

C-5 and C-6 carbohydrates, carboxylic acids and syngas are important precursor compounds which are ultimately converted to bio-alcohols in three popular pathways, namely, sugar, carboxylate and syngas platforms. As all the platforms involve some technical loopholes, the research studies on the hybridization of any two or all three of the platforms are gaining interest. The present article focuses on the analysis of pros and cons of each platform along with the review of the

present state-of-art of the hybrid platforms for the first time. It is revealed that higher alcohols can be generated by the combination of syngas and carboxylate platforms through the utilization of reducing and chain elongating properties of microorganisms present in the former and latter ones respectively. It has been identified that the correlation between process parameters such as pH, temperature etc. with the dynamics of active microorganisms in the mixed consortia or the reactor microbiome governs the process efficiency of the carboxylate platform, and hence in the hybrid platform. Pyrolysis has been earmarked as a potential process to be used in syngas, sugar and carboxylate platforms simultaneously. From the thorough analysis of the present status of hybrid platforms important objectives for future research studies in this area have been presented. Ultimately the blueprint of research project, CONVER-B, an INDO-EU project taking care of all aspects of hybridization of SP, CP and SyP pathways for the generation of bio-alcohols from lignocellulosic wastes ensuring zero effluent has been highlighted.

Declaration of Competing Interest

The authors declare that they have no known competing financial interests or personal relationships that could have appeared to influence the work reported in this paper.

Acknowledgement

The corresponding author sincerely acknowledges DST, India for funding the INNO-INDIGO Research project CONVER-B (Sanction Ref.

Table 7
Challenges of hybrid platforms and addressing strategies in CONVER-B scheme.

Platform	Challenges	Addressing Strategy in CONVER-B
CP-SP-I	Unutilized VFA-rich liquid stream from IAD Unutilized Lignin-rich solid from enzyme hydrolysis step	Chain elongation of VFA to MCFA by combining with SyP Pyrolysis/gasification of lignin stream and utilization of syngas and aqueous part of pyro liquid in SyP and SP respectively.
CP-SP-II	Unutilized digestate of IAD process Unutilized Lignin-rich solid from enzyme hydrolysis step	Digestate of IAD is converted to biogas in an anaerobic digester Lignin rich stream is fed to syngas platform
Single stage SyP-CP	Studies are based on simulated syngas and VFA medium Microbial interaction (commensalism, mutualism etc.) among the microorganisms are not studied	Real syngas generated from pyrolysis / gasification of LCB is studied The VFA rich effluent obtained through acidogenesis in IAD of LCB is used.
2-stage SyP-CP, SyP-CP-SyP, SP-CP-SyP	Studies are based on simulated syngas and VFA medium	Microbial interaction between the microorganisms of SyP and CP is studied Real syngas generated from pyrolysis / gasification of LCB is studied The VFA rich effluent obtained through acidogenesis in IAD of LCB is used.

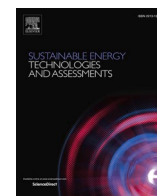
DST/IMRCD/INNO-INDIGO/CONVER-B/2017(G) DATED January 29, 2018). The authors are highly indebted to the learned reviewers for providing encouraging comments and constructive suggestions for the upgradation of the scientific quality of the present article.

References

- [1] Scarlat N, Dallemand JF, Monforti-Ferrario F, Nita V. The role of biomass and bioenergy in a future bioeconomy: policies and facts. *Environ Dev* 2015;15:3–34.
- [2] Budzinski M, Bezama A, Thrän D. Monitoring the progress towards bioeconomy using multi-regional input-output analysis: the example of wood use in Germany. *J Cleaner Prod* 2017;161:1–11.
- [3] Ullah K, Sharma VK, Dhingra S, Braccio G, Ahmad M, Sofia S. Assessing the lignocellulosic biomass resources potential in developing countries: a critical review. *Renew Sustain Energy Rev* 2015;51:682–98.
- [4] Chowdhury R, Ghosh S, Debnath B, Manna D. Indian Agro-wastes for 2G Biorefineries: Strategic Decision on Conversion Processes. *Sustainable Energy Technology and Policies*. Singapore: Springer; 2018. p. 353–73.
- [5] Giurca A, Späth P. A forest-based bioeconomy for Germany? Strengths, weaknesses and policy options for lignocellulosic biorefineries. *J Cleaner Prod* 2017;153:51–62.
- [6] Hassan MK, Villa A, Kuittinen S, Jänis J, Pappinen A. An assessment of side-stream generation from Finnish forest industry. *J Mater Cycles Waste Manage* 2018:1–16.
- [7] Satlewal A, Agrawal R, Bhagia S, Das P, Ragauskas AJ. Rice straw as a feedstock for biofuels: availability, recalcitrance, and chemical properties. *Biofuels, Bioprod Biorefin* 2018;12(1):83–107.
- [8] Graham-Rowe D. Beyond food versus fuel. *Nature* 2011;474(7352):S6.
- [9] Ziganshin AM, Liebetrau J, Pröter J, Kleinstuber S. Microbial community structure and dynamics during anaerobic digestion of various agricultural waste materials. *Appl Microbiol Biotechnol* 2013;97(11):5161–74.
- [10] Kirtay E. Recent advances in production of hydrogen from biomass. *Energy Convers Manage* 2011;52(4):1778–89.
- [11] Jia S, Ning S, Ying H, Sun Y, Xu W, Yin H. High quality syngas production from catalytic gasification of woodchip char. *Energy Convers Manage* 2017;151:457–64.
- [12] Balat M. Production of bioethanol from lignocellulosic materials via the biochemical pathway: a review. *Energy Convers Manage* 2011;52(2):858–75.
- [13] Sarkar A, Chowdhury R. Co-pyrolysis of paper waste and mustard press cake in a semi-batch pyrolyzer – optimization and bio-oil characterization. *Int J Green Energy* 2016;13(4):373–82.
- [14] Alio MA, Tugui OC, Vial C, Pons A. Microwave-assisted Organosolv pretreatment of a sawmill mixed feedstock for bioethanol production in a wood biorefinery. *Bioresour Technol* 2019;276:170–6.
- [15] <https://www.iea.org/tcep/transport/biofuels/>.
- [16] Saravanan AP, Mathimani T, Deviram G, Rajendran K, Pugazhendhi A. Biofuel policy in India: a review of policy barriers in sustainable marketing of biofuel. *J Cleaner Prod* 2018;193:734–47.
- [17] Proposal for a Directive of the European Parliament and of the Council on the promotion of the use of energy from renewable sources – Analysis of the final compromise text with a view to agreement, accessed November 2018. https://www.consilium.europa.eu/register/en/content/out?&type=ENTRY&i=LD&DOC_ID=ST-10308-2018-INIIT.
- [18] <http://task36.ieabioenergy.com/wp-content/uploads/2016/06/Energy-recovery-from-the-renewable-content-of-waste-2.pdf>.
- [19] Chen Z, Wang L, Zeng K. A comparative study on the combustion and emissions of dual-fuel engine fueled with natural gas/methanol, natural gas/ethanol, and natural gas/n-butanol. *Energy Convers Manage* 2019;192:11–9.
- [20] Ramesh A, Ashok B, Nanthagopal K, Pathy MR, Tambare A, Mali P, et al. Influence of hexanol as additive with Calophyllum Inophyllum biodiesel for CI engine applications. *Fuel* 2019;249:472–85.
- [21] Ashok B, Nanthagopal K, Darla S, Chyuan OH, Ramesh A, Jacob A, et al. Comparative assessment of hexanol and decanol as oxygenated additives with calophyllum inophyllum biodiesel. *Energy* 2019;173:494–510.
- [22] Nour M, Attia AM, Nada SA. Combustion, performance and emission analysis of diesel engine fuelled by higher alcohols (butanol, octanol and heptanol)/diesel blends. *Energy Convers Manage* 2019;185:313–29.
- [23] Wu M, Wang M, Liu J, Huo H. Assessment of potential life-cycle energy and greenhouse gas emission effects from using corn-based butanol as a transportation fuel. *Biotechnol Prog* 2008;24(6):1204–14.
- [24] Wyman CE, Dale BE. Producing biofuels via the sugar platform. *Chem Eng Prog* 2015;111:45–51.
- [25] Agler MT, Wrenn BA, Zinder SH, Angenent LT. Waste to bioproduct conversion with undefined mixed cultures: the carboxylate platform. *Trends Biotechnol* 2011;29(2):70–8.
- [26] Köpke M, Held C, Hujer S, Liesegang H, Wierze A, Wollherr A, et al. Clostridium ljungdahlii represents a microbial production platform based on syngas. *Proc Natl Acad Sci* 2010;107(29):13087–92.
- [27] Li J, Chi X, Zhang Y, Wang X. Enhanced coproduction of hydrogen and butanol from rice straw by a novel two-stage fermentation process. *Int Biodeterior Biodegrad* 2018;127:62–8.
- [28] Vasudevan D, Richter H, Angenent LT. Upgrading dilute ethanol from syngas fermentation to n-caproate with reactor microbiomes. *Bioresour Technol* 2014;151:378–82.
- [29] Gildemyn S, Molitor B, Usack JG, Nguyen M, Rabaey K, Angenent LT. Upgrading syngas fermentation effluent using Clostridium kluyveri in a continuous fermentation. *Biotechnol Biofuels* 2017;10(1):83.
- [30] Richter H, Molitor B, Diender M, Sousa DZ, Angenent LT. A narrow pH range supports butanol, hexanol, and octanol production from syngas in a continuous co-culture of Clostridium ljungdahlii and Clostridium kluyveri with in-line product extraction. *Front Microbiol* 2016;7:1773.
- [31] Khoo HH. Review of bio-conversion pathways of lignocellulose-to-ethanol: sustainability assessment based on land footprint projections. *Renew Sustain Energy Rev* 2015;46:100–19.
- [32] Prasad RK, Chatterjee S, Mazumder PB, Gupta SK, Sharma S, Vairale MG, Gupta DK. Bioethanol production from waste lignocelluloses: A review on microbial degradation potential. *Chemosphere* 2019.
- [33] Wainaina S, Horváth IS, Taherzadeh MJ. Biochemicals from food waste and recalcitrant biomass via syngas fermentation: a review. *Bioresour Technol* 2018;248:113–21.
- [34] Munasinghe PC, Khanal SK. Biomass-derived syngas fermentation into biofuels: opportunities and challenges. *Bioresour Technol* 2010;101(13):5013–22.
- [35] Yu H, Xiao W, Han L, Huang G. Characterization of mechanical pulverization/phosphoric acid pretreatment of corn stover for enzymatic hydrolysis. *Bioresour Technol* 2019;282:69–74.
- [36] Yang M, Zhang J, Kuittinen S, Vepsäläinen J, Soininen P, Keinänen M, et al. Enhanced sugar production from pretreated barley straw by additive xylanase and surfactants in enzymatic hydrolysis for acetone–butanol–ethanol fermentation. *Bioresour Technol* 2015;189:131–7.
- [37] Pu Y, Hu F, Huang F, Davison BH, Ragauskas AJ. Assessing the molecular structure basis for biomass recalcitrance during dilute acid and hydrothermal pretreatments. *Biotechnol Biofuels* 2013;6(1):15.
- [38] Sun S, Sun S, Cao X, Sun R. The role of pretreatment in improving the enzymatic hydrolysis of lignocellulosic materials. *Bioresour Technol* 2016;199:49–58.
- [39] Humbird, D., Davis, R., Tao, L., Kinchin, C., Hsu, D., Aden, A., ... & Sexton, D. (2011). Process design and economics for biochemical conversion of lignocellulosic biomass to ethanol: dilute-acid pretreatment and enzymatic hydrolysis of corn stover (No. NREL/TP-5100-47764). National Renewable Energy Lab. (NREL), Golden, CO (United States).
- [40] Sadhukhan J, Martinez-Hernandez E, Amezcua-Allieri MA, Aburto J. Economic and environmental impact evaluation of various biomass feedstock for bioethanol production and correlations to lignocellulosic composition. *Bioresour Technol Rep* 2019;7:100230.
- [41] Michailos S, Parker D, Webb C. Design, sustainability analysis and multiobjective optimisation of ethanol production via syngas fermentation. *Waste Biomass Valorization* 2019;10(4):865–76.
- [42] Chew JJ, Soh M, Sunarso J, Yong ST, Doshi V, Bhattacharya S. Gasification of torrefied oil palm biomass in a fixed-bed reactor: Effects of gasifying agents on product characteristics. *J Energy Inst* 2019.
- [43] Lee U, Dong J, Chung JN. Experimental investigation of sewage sludge solid waste conversion to syngas using high temperature steam gasification. *Energy Convers Manage* 2018;158:430–6.
- [44] Jack J, Lo J, Maness PC, Ren ZJ. Directing Clostridium ljungdahlii fermentation products via hydrogen to carbon monoxide ratio in syngas. *Biomass Bioenergy* 2019;124:95–101.
- [45] Kim NJ, Lim SJ, Chang HN. Volatile fatty acid platform: concept and application. *Emerging Areas Bioeng* 2018;1:173–90.
- [46] Xiong B, Richard TL, Kumar M. Integrated acidogenic digestion and carboxylic acid separation by nanofiltration membranes for the lignocellulosic carboxylate platform. *J Membr Sci* 2015;489:275–83.
- [47] Bonk F, Popp D, Weinrich S, Sträuber H, Kleinstuber S, Harms H, et al. Ammonia inhibition of anaerobic volatile fatty acid degrading microbial communities. *Front Microbiol* 2018;9:2921.
- [48] Kallscheuer N, Polen T, Bott M, Marienhagen J. Reversal of β -oxidative pathways for the microbial production of chemicals and polymer building blocks. *Metab Eng* 2017;42:33–42.
- [49] Holtzapfel MT, Granda CB. Carboxylate platform: the MixAlco process part 1: comparison of three biomass conversion platforms. *Appl Biochem Biotechnol* 2009;156(1–3):95–106.
- [50] Granda CB, Holtzapfel MT, Luce G, Searcy K, Mamrosh DL. Carboxylate platform: the MixAlco process part 2: process economics. *Appl Biochem Biotechnol* 2009;156(1–3):107–24.
- [51] Azhar SHM, Abdulla R, Jambo SA, Marbawi H, Gansau JA, Faik AAM, et al. Yeasts in sustainable bioethanol production: a review. *Biochem Biophys Rep* 2017;10:52–61.
- [52] Kumar R, Ghosh AK, Pal P. Fermentative energy conversion: renewable carbon source to biofuels (ethanol) using Saccharomyces cerevisiae and downstream purification through solar driven membrane distillation and nanofiltration. *Energy Convers Manage* 2017;150:545–57.
- [53] Endalur Gopinathan V, Nair NU. Pentose metabolism in Saccharomyces cerevisiae: the need to engineer global regulatory systems. *Biotechnol J* 2019;14(1):1800364.
- [54] Nguyen DTT, Praveen P, Loh KC. Zymomonas mobilis immobilization in polymeric membranes for improved resistance to lignocellulose-derived inhibitors in bioethanol fermentation. *Biochem Eng J* 2018;140:29–37.
- [55] Díaz VH, Willis MJ. Ethanol production using Zymomonas mobilis: Development of a kinetic model describing glucose and xylose co-fermentation. *Biomass Bioenergy* 2019;123:41–50.
- [56] Parra-Ramírez D, Martínez A, Cardona CA. Technical and economic potential evaluation of the strain Escherichia coli MS04 in the ethanol production from glucose and xylose. *Biochem Eng J* 2018;140:123–9.

- [57] Lin TH, Huang CF, Guo GL, Hwang WS, Huang SL. Pilot-scale ethanol production from rice straw hydrolysates using xylose-fermenting *Pichia stipitis*. *Bioresour Technol* 2012;116:314–9.
- [58] Yang M, Kuittinen S, Vepsäläinen J, Zhang J, Pappinen A. Enhanced acetone-butanol-ethanol production from lignocellulosic hydrolysates by using starchy slurry as supplement. *Bioresour Technol* 2017;243:126–34.
- [59] Yang M, Xu M, Nan Y, Kuittinen S, Hassan MK, Vepsäläinen J, et al. Influence of size reduction treatments on sugar recovery from Norway spruce for butanol production. *Bioresour Technol* 2018;257:113–20.
- [60] Yang M, Kuittinen S, Zhang J, Vepsäläinen J, Keinänen M, Pappinen A. Co-fermentation of hemicellulose and starch from barley straw and grain for efficient pentoses utilization in acetone-butanol-ethanol production. *Bioresour Technol* 2015;179:128–35.
- [61] Ibrahim MF, Abd-Aziz S, Yusoff MEM, Phang LY, Hassan MA. Simultaneous enzymatic saccharification and ABE fermentation using pretreated oil palm empty fruit bunch as substrate to produce butanol and hydrogen as biofuel. *Renewable Energy* 2015;77:447–55.
- [62] Zhang J, Jia B. Enhanced butanol production using *Clostridium beijerinckii* SE-2 from the waste of corn processing. *Biomass Bioenergy* 2018;115:260–6.
- [63] Lipovsky J, Patakova P, Paulova L, Pokorny T, Rychtera M, Melzoch K. Butanol production by *Clostridium pasteurianum* NRRL B-598 in continuous culture compared to batch and fed-batch systems. *Fuel Process Technol* 2016;144:139–44.
- [64] Yao D, Dong S, Wang P, Chen T, Wang J, Yue ZB, et al. Robustness of *Clostridium saccharoperbutylacetonicum* for acetone-butanol-ethanol production: Effects of lignocellulosic sugars and inhibitors. *Fuel* 2017;208:549–57.
- [65] Wang L, York SW, Ingram LO, Shanmugam KT. Simultaneous fermentation of biomass-derived sugars to ethanol by a co-culture of an engineered *Escherichia coli* and *Saccharomyces cerevisiae*. *Bioresour Technol* 2019;273:269–76.
- [66] Nguyen DTT, Praveen P, Loh KC. Co-culture of *Zymomonas mobilis* and *Scheffersomyces stipitis* immobilized in polymeric membranes for fermentation of glucose and xylose to ethanol. *Biochem Eng J* 2019;145:145–52.
- [67] Ntaikou I, Menis N, Alexandropoulou M, Antonopoulou G, Lyberatos G. Valorization of kitchen biowaste for ethanol production via simultaneous saccharification and fermentation using co-cultures of the yeasts *Saccharomyces cerevisiae* and *Pichia stipitis*. *Bioresour Technol* 2018;263:75–83.
- [68] Wu J, Dong L, Zhou C, Liu B, Feng L, Wu C, Cao G. Developing a coculture for enhanced butanol production by *Clostridium beijerinckii* and *Saccharomyces cerevisiae*. *Bioresour Technol Rep* 2019.
- [69] Qi G, Xiong L, Luo M, Huang Q, Huang C, Li H, et al. Solvents production from cassava by co-culture of *Clostridium acetobutylicum* and *Saccharomyces cerevisiae*. *J Environ Chem Eng* 2018;6(1):128–33.
- [70] Sathish A, Sharma A, Gable P, Skiadis I, Brown R, Wen Z. A novel bulk-gas-to-atomized-liquid reactor for enhanced mass transfer efficiency and its application to syngas fermentation. *Chem Eng J* 2019.
- [71] Sun X, Atiyeh HK, Kumar A, Zhang H, Tanner RS. Biochar enhanced ethanol and butanol production by *Clostridium carboxidivorans* from syngas. *Bioresour Technol* 2018;265:128–38.
- [72] Shen Y, Brown RC, Wen Z. Syngas fermentation by *Clostridium carboxidivorans* P7 in a horizontal rotating packed bed biofilm reactor with enhanced ethanol production. *Appl Energy* 2017;187:585–94.
- [73] Sun X, Atiyeh HK, Zhang H, Tanner RS, Huhnke RL. Enhanced ethanol production from syngas by *Clostridium ragsdalei* in continuous stirred tank reactor using medium with poultry litter biochar. *Appl Energy* 2019;236:1269–79.
- [74] Xu H, Liang C, Yuan Z, Xu J, Hua Q, Guo Y. A study of CO/syngas bioconversion by *Clostridium autoethanogenum* with a flexible gas-cultivation system. *Enzyme Microb Technol* 2017;101:24–9.
- [75] Phillips JR, Atiyeh HK, Tanner RS, Torres JR, Saxena J, Wilkins MR, et al. Butanol and hexanol production in *Clostridium carboxidivorans* syngas fermentation: medium development and culture techniques. *Bioresour Technol* 2015;190:114–21.
- [76] Liu K, Atiyeh HK, Stevenson BS, Tanner RS, Wilkins MR, Huhnke RL. Mixed culture syngas fermentation and conversion of carboxylic acids into alcohols. *Bioresour Technol* 2014;152:337–46.
- [77] Liu C, Luo G, Wang W, He Y, Zhang R, Liu G. The effects of pH and temperature on the acetate production and microbial community compositions by syngas fermentation. *Fuel* 2018;224:537–44.
- [78] Li X, Li M, Pu Y, Ragauskas AJ, Klett AS, Thies M, et al. Inhibitory effects of lignin on enzymatic hydrolysis: the role of lignin chemistry and molecular weight. *Renewable Energy* 2018;123:664–74.
- [79] Chen H, Liu J, Chang X, Chen D, Xue Y, Liu P, et al. A review on the pretreatment of lignocellulose for high-value chemicals. *Fuel Process Technol* 2017;160:196–206.
- [80] Satlewal A, Agrawal R, Bhagia S, Sangoro J, Ragauskas AJ. Natural deep eutectic solvents for lignocellulosic biomass pretreatment: recent developments, challenges and novel opportunities. *Biotechnol Adv* 2018.
- [81] Yu Q, Liu R, Li K, Ma R. A review of crop straw pretreatment methods for biogas production by anaerobic digestion in China. *Renew Sustain Energy Rev* 2019;107:51–8.
- [82] Sträuber H, Bühlig F, Kleinstaub S, Nikolaus M, Porsch K. Improved anaerobic fermentation of wheat straw by alkaline pre-treatment and addition of alkali-tolerant microorganisms. *Bioengineering* 2015;2(2):66–93.
- [83] Li H, Si D, Liu C, Feng K, Liu C. Performance of direct anaerobic digestion of dewatered sludge in long-term operation. *Bioresour Technol* 2018;250:355–64.
- [84] Ghosh S, Chowdhury R, Bhattacharya P. Sustainability of cereal straws for the fermentative production of second generation biofuels: a review of the efficiency and economics of biochemical pretreatment processes. *Appl Energy* 2017;198:284–98.
- [85] Tiffany, D., & Eidman, V. R. (2003). Factors associated with success of fuel ethanol producers.
- [86] Pardo-Planas O, Atiyeh HK, Phillips JR, Aichele CP, Mohammad S. Process simulation of ethanol production from biomass gasification and syngas fermentation. *Bioresour Technol* 2017;245:925–32.
- [87] Wu, M., Wang, M., Liu, J., Huo, H. (2007). Life-cycle assessment of corn-based butanol as a potential transportation fuel (No. ANL/ESD/07-10). Argonne National Lab. (ANL), Argonne, IL (United States).
- [88] Cotabarren IM, Moreno J, Martínez AL, Cabrera FA, Piña J. Valorization of anaerobic digestion liquid residue through the production of organic fertilizer by fluidized bed granulation. *Chem Eng Res Des* 2019.
- [89] Monlau F, Sambusiti C, Antoniou N, Barakat A, Zabanitout A. A new concept for enhancing energy recovery from agricultural residues by coupling anaerobic digestion and pyrolysis process. *Appl Energy* 2015;148:32–8.
- [90] Teater C, Yue Z, MacLellan J, Liu Y, Liao W. Assessing solid digestate from anaerobic digestion as feedstock for ethanol production. *Bioresour Technol* 2011;102(2):1856–62.
- [91] Wang D, Xi J, Ai P, Yu L, Zhai H, Yan S, et al. Enhancing ethanol production from thermophilic and mesophilic solid digestate using ozone combined with aqueous ammonia pretreatment. *Bioresour Technol* 2016;207:52–8.
- [92] Chen G, Guo X, Cheng Z, Yan B, Dan Z, Ma W. Air gasification of biogas-derived digestate in a downdraft fixed bed gasifier. *Waste Manage* 2017;69:162–9.
- [93] Littlewood J, Wang L, Turnbull C, Murphy RJ. Techno-economic potential of bioethanol from bamboo in China. *Biotechnol Biofuels* 2013;6(1):173.
- [94] Baral NR, Shah A. Techno-economic analysis of cellulosic butanol production from corn stover through acetone-butanol-ethanol fermentation. *Energy Fuels* 2016;30(7):5779–90.
- [95] Malmierca S, Díez-Antolínez R, Paniagua AI, Martín M. Technoeconomic study of biobutanol AB production. 2. Process design. *Ind Eng Chem Res* 2017;56(6):1525–33.
- [96] Phillips J, Huhnke R, Atiyeh H. Syngas fermentation: a microbial conversion process of gaseous substrates to various products. *Fermentation* 2017;3(2):28.
- [97] Bahmani MA, Shafiei M, Karimi K. Anaerobic digestion as a pretreatment to enhance ethanol yield from lignocelluloses. *Process Biochem* 2016;51(9):1256–63.
- [98] Zhang H, Zhang P, Ye J, Wu Y, Liu J, Fang W, et al. Comparison of various pretreatments for ethanol production enhancement from solid residue after rumen fluid digestion of rice straw. *Bioresour Technol* 2018;247:147–56.
- [99] Ai B, Chi X, Meng J, Sheng Z, Zheng L, Zheng X, et al. Consolidated bioprocessing for butyric acid production from rice straw with undefined mixed culture. *Front Microbiol* 2016;7:1648.
- [100] Cheng CL, Che PY, Chen BY, Lee WJ, Lin CY, Chang JS. Biobutanol production from agricultural waste by an acclimated mixed bacterial microflora. *Appl Energy* 2012;100:3–9.
- [101] Amiri H, Karimi K, Zilouei H. Organosolv pretreatment of rice straw for efficient acetone, butanol, and ethanol production. *Bioresour Technol* 2014;152:450–6.
- [102] Lee SY, Park JH, Jang SH, Nielsen LK, Kim J, Jung KS. Fermentative butanol production by *Clostridia*. *Biotechnol Bioeng* 2008;101(2):209–28.
- [103] Hartmanis MG, Klason T, Gatenbeck S. Uptake and activation of acetate and butyrate in *Clostridium acetobutylicum*. *Appl Microbiol Biotechnol* 1984;20(1):66–71.
- [104] Regestein L, Doerr EW, Staaden A, Rehmann L. Impact of butyric acid on butanol formation by *Clostridium pasteurianum*. *Bioresour Technol* 2015;196:153–9.
- [105] Steinbusch KJ, Hamelers HV, Buisman CJ. Alcohol production through volatile fatty acids reduction with hydrogen as electron donor by mixed cultures. *Water Res* 2008;42(15):4059–66.
- [106] Diender M, Stams AJ, Sousa DZ. Production of medium-chain fatty acids and higher alcohols by a synthetic co-culture grown on carbon monoxide or syngas. *Biotechnol Biofuels* 2016;9(1):82.
- [107] Ganiqué R, Sánchez-Paredes P, Bañeras L, Colprim J. Low fermentation pH is a trigger to alcohol production, but a killer to chain elongation. *Front Microbiol* 2016;7:702.
- [108] Kucek LA, Spirito CM, Angenent LT. High n-caprylate productivities and specificities from dilute ethanol and acetate: chain elongation with microbiomes to upgrade products from syngas fermentation. *Energy Environ Sci* 2016;9(11):3482–94.
- [109] Holtzapfel MT, Davison RR, Ross MK, Aldrett-Lee S, Nagwani M, Lee CM, et al. Biomass conversion to mixed alcohol fuels using the MixAlco process. *Appl Biochem Biotechnol* 1999;79(1–3):609–31.
- [110] Ghosh S, Chowdhury R, Bhattacharya P. Mixed consortia in bioprocesses: role of microbial interactions. *Appl Microbiol Biotechnol* 2016;100(10):4283–95.
- [111] Datta R, Reeves A. (2015). Syntrophic Co-culture of Anaerobic Microorganism for Production of n-Butanol from Syngas. U.S. Patent Application No. 14/812,182.
- [112] Liew F, Martin ME, Tappel RC, Heijstra BD, Mihalcea C, Köpke M. Gas fermentation—a flexible platform for commercial scale production of low-carbon-fuels and chemicals from waste and renewable feedstocks. *Front Microbiol* 2016;7:694.
- [113] Richter H, Loftus SE, Angenent LT. Integrating syngas fermentation with the carboxylate platform and yeast fermentation to reduce medium cost and improve biofuel productivity. *Environ Technol* 2013;34(13–14):1983–94.
- [114] Kucek LA, Xu J, Nguyen M, Angenent LT. Waste conversion into n-caprylate and n-caproate: resource recovery from wine lees using anaerobic reactor microbiomes and in-line extraction. *Front Microbiol* 2016;7:1892.
- [115] Scarborough MJ, Lynch G, Dickson M, McGee M, Donohue TJ, Noguera DR. Increasing the economic value of lignocellulosic stillage through medium-chain fatty acid production. *Biotechnol Biofuels* 2018;11(1):200.
- [116] Feng Q, Lin Y. Integrated processes of anaerobic digestion and pyrolysis for higher

- bioenergy recovery from lignocellulosic biomass: a brief review. *Renew Sustain Energy Rev* 2017;77:1272–87.
- [117] Monlau F, Francavilla M, Sambusiti C, Antoniou N, Solhy A, Libutti A, et al. Toward a functional integration of anaerobic digestion and pyrolysis for a sustainable resource management. Comparison between solid-digestate and its derived pyrochar as soil amendment. *Appl Energy* 2016;169:652–62.
- [118] Lü F, Hua Z, Shao L, He P. Loop bioenergy production and carbon sequestration of polymeric waste by integrating biochemical and thermochemical conversion processes: a conceptual framework and recent advances. *Renewable Energy* 2018;124:202–11.
- [119] Sarkar A, Mondal B, Chowdhury R. Mathematical modeling of a semibatch pyrolyser for sesame oil cake. *Ind Eng Chem Res* 2014;53(51):19671–80.
- [120] Chowdhury R, Sarkar A. Reaction kinetics and product distribution of slow pyrolysis of Indian textile wastes. *Int J Chem Reactor Eng* 2012;10(1).
- [121] Ray R, Bhattacharya P, Chowdhury R. Simulation and modeling of vegetable market wastes pyrolysis under progressive deactivation condition. *The Canadian Journal of Chemical Engineering* 2004;82(3):566–79.
- [122] Ghosh S, Das S, Chowdhury R. Effect of pre-pyrolysis biotreatment of banana pseudo-stem (BPS) using synergistic microbial consortium: Role in deoxygenation and enhancement of yield of pyro-oil. *Energy Convers Manage* 2019;195:114–24.
- [123] Brown RC. Hybrid thermochemical/biological processing. *Appl Biochem Biotechnol* 2007;137(1–12):947–56.
- [124] Mohan D, Pittman CU, Steele PH. Pyrolysis of wood/biomass for bio-oil: a critical review. *Energy Fuels* 2006;20(3):848–89.
- [125] Rover MR, Johnston PA, Jin T, Smith RG, Brown RC, Jarboe L. Production of clean pyrolytic sugars for fermentation. *ChemSusChem* 2014;7(6):1662–8.
- [126] Pollard AS, Rover MR, Brown RC. Characterization of bio-oil recovered as stage fractions with unique chemical and physical properties. *J Anal Appl Pyrol* 2012;93:129–38.
- [127] Westerhof RJ, Brilman DWF, Garcia-Perez M, Wang Z, Oudenhoven SR, van Swaaij WP, et al. Fractional condensation of biomass pyrolysis vapors. *Energy Fuels* 2011;25(4):1817–29.
- [128] Biswas B, Singh R, Kumar J, Singh R, Gupta P, Krishna BB, et al. Pyrolysis behavior of rice straw under carbon dioxide for production of bio-oil. *Renewable Energy* 2018;129:686–94.
- [129] Kouhi M, Shams K. Bulk features of catalytic co-pyrolysis of sugarcane bagasse and a hydrogen-rich waste: The case of waste heavy paraffin. *Renewable Energy* 2019;140:970–82.
- [130] Pham XH, Piriou B, Salvador S, Valette J, Van de Steene L. Oxidative pyrolysis of pine wood, wheat straw and miscanthus pellets in a fixed bed. *Fuel Process Technol* 2018;178:226–35.
- [131] Chi Z, Rover M, Jun E, Deaton M, Johnston P, Brown RC, et al. Overliming detoxification of pyrolytic sugar syrup for direct fermentation of levoglucosan to ethanol. *Bioresour Technol* 2013;150:220–7.
- [132] Bennett NM, Helle SS, Duff SJ. Extraction and hydrolysis of levoglucosan from pyrolysis oil. *Bioresour Technol* 2009;100(23):6059–63.
- [133] Yu Z, Zhang H. Pretreatments of cellulose pyrolysate for ethanol production by *Saccharomyces cerevisiae*, *Pichia* sp. YZ-1 and *Zymomonas mobilis*. *Biomass Bioenergy* 2003;24(3):257–62.
- [134] Layton DS, Ajjarapu A, Choi DW, Jarboe LR. Engineering ethanologenic *Escherichia coli* for levoglucosan utilization. *Bioresour Technol* 2011;102(17):8318–22.
- [135] Dai J, Yu Z, He Y, Zhang L, Bai Z, Dong Z, et al. Cloning of a novel levoglucosan kinase gene from *Lipomyces starkeyi* and its expression in *Escherichia coli*. *World J Microbiol Biotechnol* 2009;25(9):1589.
- [136] Linger JG, Hobdey SE, Franden MA, Fulk EM, Beckham GT. Conversion of levoglucosan and cellobiosan by *Pseudomonas putida* KT2440. *Metab Eng Commun* 2016;3:24–9.
- [137] Helle S, Bennett NM, Lau K, Matsui JH, Duff SJ. A kinetic model for production of glucose by hydrolysis of levoglucosan and cellobiosan from pyrolysis oil. *Carbohydr Res* 2007;342(16):2365–70.
- [138] Ratledge C. Fatty acid biosynthesis in microorganisms being used for single cell oil production. *Biochimie* 2004;86(11):807–15.
- [139] Sun C, Liu F, Song Z, Wang J, Li Y, Pan Y, et al. Feasibility of dry anaerobic digestion of beer lees for methane production and biochar enhanced performance at mesophilic and thermophilic temperature. *Bioresour Technol* 2019;276:65–73.
- [140] Luz FC, Cordiner S, Manni A, Mulone V, Rocco V, Braglia R, et al. *Ampelodesmos mauritanicus* pyrolysis biochar in anaerobic digestion process: Evaluation of the biogas yield. *Energy* 2018;161:663–9.
- [141] Pan J, Ma J, Liu X, Zhai L, Ouyang X, Liu H. Effects of different types of biochar on the anaerobic digestion of chicken manure. *Bioresour Technol* 2019;275:258–65.
- [142] Cao Y, Wang K, Wang X, Gu Z, Amblico T, Gibbons W, et al. Preparation of active carbons from corn stalk for butanol vapor adsorption. *J Energy Chem* 2017;26(1):35–41.
- [143] Galinato SP, Yoder JK, Granatstein D. The economic value of biochar in crop production and carbon sequestration. *Energy Policy* 2011;39(10):6344–50.
- [144] Smith P. Soil carbon sequestration and biochar as negative emission technologies. *Glob Change Biol* 2016;22(3):1315–24.
- [145] Zabaniotou A, Rovas D, Libutti A, Monteleone M. Boosting circular economy and closing the loop in agriculture: case study of a small-scale pyrolysis–biochar based system integrated in an olive farm in symbiosis with an olive mill. *Environ Dev* 2015;14:22–36.
- [146] Naqvi SR, Prabhakara HM, Bramer EA, Dierkes W, Akkerman R, Brem G. A critical review on recycling of end-of-life carbon fibre/glass fibre reinforced composites waste using pyrolysis towards a circular economy. *Resour Conserv Recycl* 2018;136:118–29.
- [147] Lewis FM. (2012). Pyrobiomethane process. U.S. Patent Application No. 13/136, 180.
- [148] <https://www.vtt.fi/inf/pdf/publications/1997/P306.pdf>.
- [149] Kim KH, Bai X, Rover M, Brown RC. The effect of low-concentration oxygen in sweep gas during pyrolysis of red oak using a fluidized bed reactor. *Fuel* 2014;124:49–56.
- [150] Sun X, Atiyeh HK, Kumar A, Zhang H. Enhanced ethanol production by *Clostridium ragdalei* from syngas by incorporating biochar in the fermentation medium. *Bioresour Technol* 2018;247:291–301.
- [151] Liu Y, He P, Shao L, Zhang H, Lü F. Significant enhancement by biochar of caproate production via chain elongation. *Water Res* 2017;119:150–9.
- [152] https://www.aka.fi/globalassets/32akatemiaohjelmatus/uuusi-energia/hankekuvaus/uuudet-2017/pappinen_conver-b.pdf.
- [153] Markard J, Wirth S, Truffer B. Institutional dynamics and technology legitimacy—A framework and a case study on biogas technology. *Res Policy* 2016;45(1):330–44.
- [154] Weiland P. Biomass digestion in agriculture: a successful pathway for the energy production and waste treatment in Germany. *Eng Life Sci* 2006;6(3):302–9.
- [155] Vanhala P, Repo A, Liski J. Forest bioenergy at the cost of carbon sequestration? *Curr Opin Environ Sustainability* 2013;5(1):41–6.
- [156] Spirito CM, Richter H, Rabaey K, Stams AJ, Angenent LT. Chain elongation in anaerobic reactor microbiomes to recover resources from waste. *Curr Opin Biotechnol* 2014;27:115–22.
- [157] Masum BM, Masjuki HH, Kalam MA, Palash SM, Habibullah M. Effect of alcohol–gasoline blends optimization on fuel properties, performance and emissions of a SI engine. *J Cleaner Prod* 2015;86:230–7.
- [158] Masum BM, Masjuki HH, Kalam MA, Palash SM, Wakil MA, Imtihan S. Tailoring the key fuel properties using different alcohols (C2–C6) and their evaluation in gasoline engine. *Energy Convers Manage* 2014;88:382–90.
- [159] Mourad M, Mahmoud K. Investigation into SI Engine Performance Characteristics and Emissions fueled with Ethanol/Butanol-Gasoline Blends. *Renewable Energy* 2019.
- [160] Fagundez JLS, Golke D, Martins MES, Salau NPG. An investigation on performance and combustion characteristics of pure n-butanol and a blend of n-butanol/ethanol as fuels in a spark ignition engine. *Energy* 2019;176:521–30.
- [161] De Groof V, Coma M, Arnot T, Leak DJ, Lanham AB. Medium chain carboxylic acids from complex organic feedstocks by mixed culture fermentation. *Molecules* 2019;24(3):398.
- [162] Lambrecht J, Cichocki N, Schattenberg F, Kleinstaub S, Harms H, Müller S, et al. Key sub-community dynamics of medium-chain carboxylate production. *Microb Cell Fact* 2019;18(1):92.
- [163] Sträuber H, Bühligen F, Kleinstaub S, Dittrich-Zechendorf M. Carboxylic acid production from ensiled crops in anaerobic solid-state fermentation—trace elements as pH controlling agents support microbial chain elongation with lactic acid. *Eng Life Sci* 2018;18(7):447–58.
- [164] Wu Q, Bao X, Guo W, Wang B, Li Y, Luo H, et al. Medium chain carboxylic acids production from waste biomass: current advances and perspectives. *Biotechnol Adv* 2019.



Original article

Energy and environmental impact assessment of Indian rice straw for the production of second-generation bioethanol

Md. Kamrul Hassan^{a,*}, Ranjana Chowdhury^b, Shiladitya Ghosh^b, Dinabandhu Manna^b, Ari Pappinen^a, Suvi Kuittinen^a^a School of Forest Sciences, University of Eastern Finland, P.O. Box 111, FI80101 Joensuu, Finland^b Chemical Engineering Department, Jadavpur University, Kolkata 700 032, West Bengal, India

ARTICLE INFO

Keywords:

Rice straw

Pretreatment technologies

Impact assessment

Second-generation bioethanol

Greenhouse gas emissions

ABSTRACT

This study assessed the energy and environmental impacts in terms of second-generation (2G) bioethanol production, renewable electricity generation and greenhouse gas (GHG) emissions reduction potential of surplus rice straw (SRS) in India. National rice production database, and standard procedures for life cycle assessment of rice straw to 2G bioethanol production using two different pretreatment technologies namely, dilute acid (DA) and steam explosion (SE) pretreatments were explored for the analysis. Two scenarios (benchmark and resource-efficient) were constructed to evaluate the availability of SRS and to determine the potential from 2020 to 21 to 2030–31. Under benchmark for the year 2030–31, the potential from SRS using DA and SE pretreatment methods for the production of 2G bioethanol and the surplus renewable electricity generation were estimated to be 10,547 and 11,165 million L; and 5295 and 6928 GWh, respectively, and the corresponding GHG emissions reduction potential were assessed to be 11,954 and 14,375 kt CO₂eq., respectively while generated renewable electricity replaces crude oil-driven grid electricity, and 11,498 and 14,498 kt CO₂eq., respectively while generated renewable electricity replaces coal-driven grid electricity. The study revealed that both the availability of SRS and the choice of pretreatment method play decisive roles in the determination of its potential.

Introduction

Globally, biofuels have gained interest in recent years for their enormous potential to mitigate the burgeoning gap between energy demand and supply, avoid carbon dioxide (CO₂) emissions associated with the prolific use of petro-fuels, and improve energy security and sustainability [1]. Liquid biofuels are particularly suitable for the transport sector both from the perspective of environmental and economic benefits and to enhance national energy security and international stability by reducing risks associated with overdependence on fossil fuel imports. The use of liquid biofuels to replace gasoline, diesel and jet fuel has been strongly emphasized in the Kyoto Protocols and Paris Agreement. The diversification of types and sources of biofuels has become a critical energy issue in many developed and developing countries, due to environmental and energy policies that promote sustainable development [2].

Bioethanol is one of the most common liquid biofuels and is used as an alternative to transport fuel in the USA, Brazil, and many other

countries. Presently, most of the commercial bioethanol is produced primarily from edible food crops, such as grains, sugarcane, and vegetable waste [3]. The production of this first-generation (1G) bioethanol has been increasingly questioned, over the critical concerns about food versus fuel competition. The increasing criticism around the sustainability of 1G bioethanol production systems has focused the attention on the development of processes for second-generation (2G) bioethanol from diverse lignocellulosic biomass (LCB) resources [4,5]. LCBs can be obtained as crop residues, non-edible agricultural crops, dedicated energy crops, forest residues, woody biomass, and municipal waste materials. They are almost evenly distributed globally and appear to be key resources to ensure a continuous supply of renewable feedstock for 2G bioethanol production [6]. In comparison to other fuels, the production of 2G bioethanol from LCBs has a lower greenhouse gas (GHG) emissions during the life cycle [7]. Biofuel production from biomass mainly involves four types of conversion technologies: thermal (use of heat with or without the presence of oxygen to convert biomass into forms of energy by direct combustion, pyrolysis, torrefaction process, etc.);

* Corresponding author.

E-mail address: kamrul.hassan@uef.fi (Md.K. Hassan).<https://doi.org/10.1016/j.seta.2021.101546>

Received 12 March 2021; Received in revised form 18 August 2021; Accepted 19 August 2021

Available online 31 August 2021

2213-1388/© 2021 The Authors. Published by Elsevier Ltd. This is an open access article under the CC BY license (<http://creativecommons.org/licenses/by/4.0/>).

thermochemical (application of heat and chemical processes to convert biomass into forms of energy by gasification, liquefaction, carboxylation, syngas process, etc.); chemical (use of chemical agents to convert biomass into forms of energy by transesterification, catalytic conversion, etc.); and biochemical (use of enzymes, bacteria or other microorganisms to convert biomass into forms of energy by anaerobic digestion, methanogenesis, anaerobic fermentation, etc.) [8–13]. However, biomass conversion to cellulosic ethanol production mainly involves two platforms i.e. sugar platform (through biochemical conversion routes) and syngas platform (through thermochemical conversion routes) [14].

Growing energy demands, coupled with a limited supply of petroleum fuels, the geo-politics of oil and environmental concerns have compelled India to seek different options for renewable and sustainable energy. Because of the dominance of the agricultural sector in India, biofuel generation from agro-wastes is one of the country's main areas for upcoming renewable energy programs [15]. For developing countries like India, the promotion of biofuels is associated with multiple goals, including the enhancement of energy security, increasing local investment, new job creation, rural development and the reclamation of degraded and waste lands [16]. The government of India introduced its Ethanol-Blended Petrol Programme (EBPP) in 2003 and its "National Policy on Biofuels" in 2018. Both policies are directed toward the development of 1G bioethanol from glucose-rich feedstocks (e.g., sugar cane, sugar beet, sweet sorghum) and from starch-rich corn, cassava, etc.; 2G bioethanol from LCBs (e.g., straw, bagasse, other crop residues, wood waste and forest residues); 3-G bioethanol from algae and biodiesel from vegetable oils (both edible and non-edible) and animal fat [17]. An indicative blending target was set: 5 % ethanol to petroleum fuels by 2012. This was subsequently raised to 10 % by 2017 and to 20 % after 2017 [18]. Currently, sugarcane molasses is one of the main sources of feedstock for producing bioethanol in India. However, because of slow growth in area and yield of sugarcane together with other competing usages of sugarcane molasses such as in pharmaceuticals and food industry – it seems not to be possible to produce bioethanol sustainably to meet the EBPP national blending targets [19]. A sensitive analysis on sugarcane molasses-based bioethanol production system in the country showed that the current production system is neither economically viable nor sustainable with available technology [19]. Therefore, it is imperative to focus on production of 2G-bioethanol from diverse feedstock like agricultural crop residues and other LCBs. Many developing countries have already made plans to reduce emissions by using bioethanol as an alternative transportation fuel to gasoline. India poses a daunting challenge to achieve its nationally determined contributions targets. The country must promote the production and use of alternative liquid biofuels to achieve its EBPP targets, and to reduce its dependence on imports to meet its energy requirements.

Rice is a short-lived, water-loving crop that grows in a wide range of semi-aquatic (irrigated or rainfed) environments (i.e., lowland to upland). It takes around 3–6 months to grow from seeds to mature plants, depending on the variety and environmental conditions. Rice straw (RS) is obtained as a post-harvesting residue during rice processing, which is recognized as one of the most abundant LCBs in the world. The structural composition of RS mainly constitutes cellulose (35–40 %), hemicellulose (17–25 %), lignin (10–20 %), silica (8–15 %) and a significant amount of extractives (12 %) [20,21]. The cellulose and hemicellulose fractions of RS can be converted through pretreatment and enzymatic hydrolysis processes, respectively, to pentose (xylose, arabinose) and hexose (glucose) sugars, and thereafter, these can be further fermented into ethanol [22]. In addition, the residual lignin and extractives can be utilized for the generation of heat and electricity and can be coupled with bioethanol production processes in a RS-based biorefinery plant [23–25]. A life cycle assessment (LCA) study indicates that the conversion of RS to 2G bioethanol and biogas through the biochemical pathway produces the highest environmental sustainability in terms of reduction of GHG emissions and resource depletion potentials in comparison to

other conversion routes, namely, direct combustion for electricity, production of biofertilizer and thermochemical conversion to dimethyl ether while environmental performance is taken into account [26]. As such, the conversion of RS to 2G bioethanol production seems very attractive. RS has gained considerable interest, amongst many rice producing countries, for the production of renewable energy (e.g., in the form of bioethanol, heat and electricity) and GHG emissions reduction. However, there is a lack of understanding related to the amount of RS that is accessible as feedstock in the long-term, as well as its potential for renewable energy and its environmental impacts at local to national level. These gaps in understanding are recognized as the major hindrances to the development and scaling up of RS-based bioethanol production in India.

Rice is the staple crop of India, where it is consumed daily by hundreds of millions of people. The country is not only a leading consumer of rice; it is also the second largest rice producing country, after China. About 44 million ha of land is used for the cultivation of rice in India. This produces about 157 million tons (MT) of rice grain, leaving about 157–236 MT of RS annually [25]. In India, the most common practice for the management of RS is to leave a large proportion as surplus rice straw (SRS), either at the farmyard and/or at the cultivated land site. Often these are frequently burnt to make the land ready for the next crop cycle. Considering the colossal availability, sustainable supply, and viability of the feedstock, and in need of 2G-bioethanol production in India - rice straw appears a promising and potential candidate for producing 2G bioethanol [27]. The utilization of SRS for 2G bioethanol production through biorefinery is encouraged since the process could enhance energy security, contribute to achieve EBPP targets and meet increasing transport fuel demands, reduce environmental pollution, and improve the rural economy. Although in India, several studies have focused on the prospect of utilizing crop residues for 2G bioethanol production, most of these studies have mainly concentrated on the technological aspects (i.e., energy conversion pathways) [28]. Only a few studies [29,30] have put attention on evaluating the environmental impacts. A detailed quantification of the potential of SRS regarding energy (i.e., in terms of 2G bioethanol and renewable electricity) production and environmental impacts (i.e., in term of CO₂eq. emissions reduction) at the state or national level is still absent. Thus, the present study concentrates on a national-level overview of the availability of SRS (as feedstock) in India under two supply scenarios (i.e., benchmark and resource-efficient) along with the quantification of its potential for 2G bioethanol production, renewable electricity generation and reduction of GHG emissions, from the perspective of a biofuels transition in India. This research is the first ever to undertake a comprehensive impact assessment of SRS for energy and environmental benefits in India. The study adopted novel methodological approaches to present its findings. A state-level assessment was undertaken, to consider the twelve major rice producing states of India. The study explored a rice production database, and standard procedures for the LCA of rice straw conversion process to bioethanol production using two pretreatment technologies i.e., dilute acid (DA) and steam explosion (SE) pretreatments, and for GHG emissions calculations. This paper also focuses on the availability of SRS and their utilization potential up to the year 2030–31, as well as on the trade-offs involved in the commercialization of a rice straw-based 2G bioethanol biorefinery plant through an intensive literature review. It is expected that this study will act as an aid to policy makers, energy entrepreneurs, investors, scientific communities, governmental organizations, non-governmental organizations, international organizations, and other relevant stakeholders in the development of a RS-based 2G bioethanol biorefinery plant in India.

Methodology

Collection and analysis of rice production data

The data for the study were collected via field visits and database

enquiries. Preliminary rice production data were gathered from the archive of literatures available online and by exploring several national agricultural databases (www.agricoop.nic.in & <http://eands.dacnet.nic.in>) available from the Indian government's Department of Agriculture, Cooperation & Farmers Welfare (DAC & FW) and Ministry of Agriculture & Farmers Welfare [31]. Physical field observation was also carried out in some of the states. The National rice production statistics for the year 1950–51 to 2018–19 were reviewed, and the latest eight years (2011–12 to 2018–19) rice production statistics in twelve major rice producing Indian states were explored and used for future data projections. Standard methods were followed to predict rice straw production in future years [32,33].

Terminologies used in defining crop residues and their potential

Crop residues are non-edible organic materials that can be categorized into two groups: 1) crop residues and 2) agricultural industrial residues. Crop residues are plant materials that are either generated during harvesting or co-produced during processing. Agricultural industrial residues are generated as by-products after the post-harvest processing of crops i.e., cleaning, delisting, sieving, crushing, and milling. The major Indian crop residues are available as straw, husk, bagasse, leaves, pods, press cakes, shells, stalk, peels, pseudo-stems, piths, etc. The total energy potential of the major Indian agro-residues has been reported, based on their annual availability and the higher heating values of the different residues [34]. The potential of crop residues for biofuel generation can be classified into three groups: theoretical potential, available potential, and economic potential [35]. Theoretical potential is assessed by including all the produced crop residues. Available potential is a subset of theoretical, which considers only those crop residues that are available. Economic potential is a subset of available potential and refers to the part of said *available potential* that meets the criteria of economic profitability within a given framework. This study has applied *available potential* in the estimation of SRS as feedstock for 2G bioethanol production and renewable electricity generation.

Determination of gross rice straw and surplus rice straw

Rice straw is the non-edible parts of the rice crop plant and constitutes the largest portion by weight. It is traditionally collected during rice harvesting as a byproduct. The quantity of RS is dependent on the variety, cultivation methods, environmental conditions, harvesting methods and height of the stem cutting. Typically, the generation of gross rice straw (GRS) is directly proportional to the amount of rice production and the straw to grain ratio (SGR). The SGR of a rice crop differs according to variety, environmental conditions, cultivation practices and technological inputs. The SGR value ranges between 1 and 1.5 [4]. However, a typical representative SGR value of 1.5 has been reported by several researchers for Indian rice [36,37]. This signifies that, in India, 1.5 kg of straw is generated per 1 kg of rice grain produced. We thus have considered and used the SGR value of 1.5 throughout, in our calculations.

The GRS for any state n , can be determined as follows:

$$GRS(n) = ARP(n) \times SGR \quad (1)$$

where, $GRS(n)$ = gross production of rice straw in state n in ton, $ARP(n)$ = annual rice production in state n in ton, SGR = straw to grain ratio. n = number used for the indexing of a state.

Equation (1) gives only the estimated GRS, which is generated at the farm level. However, RS generated from farms is used for a wide range of rural applications, such as ruminant feeding, roof thatching, fuel for cooking, mulching, poultry litter, mushroom cultivation, and manuring. Therefore, SRS is calculated after subtracting the portion of GRS utilized for non-biofuel applications. The availability of SRS depends on

different factors, such as farm size, rice cultivation area, productivity, the quantities of RS used for various farm applications and agro-ecological area.

The coefficient value of SRS to GRS for major rice producing states in India is reported to be between 0.23 and 0.28 [37,38], with an exception in some states such as Punjab and Haryana, where large quantities of SRS are available [15,39]. This means that 230–280 g of rice straw remains as surplus for every kilogram of gross production of rice straw. The following equation was used to estimate SRS availability:

$$SRS(n) = GRS(n) \times CvGS \quad (2)$$

where, $SRS(n)$ = surplus rice straw production in state n in ton, $CvGS$ = coefficient value of gross rice straw to surplus rice straw production.

Nevertheless, the coefficient value of 0.23 is often used for estimation of 2G bioethanol potential from SRS [25,40]. In this study, two scenarios were constructed using $CvGS$ values of 0.23 (S_1), and 0.28 (S_2). Based on the availability of SRS, the scenarios are described as S_1 : benchmark, and S_2 : resource efficient.

In the above calculations, for instances, the determination of GRS, SGR, SPS and the construction of SRS supply scenarios, we followed standard methodologies described in few earlier studies [37–42].

Biofuel conversion technologies and system boundary under consideration of this study

In the present case study, a sugar platform-based conversion of SRS to bioethanol and renewable electricity has been considered. Typically, sugar platform-based LCB conversion to bioethanol production involves four steps: 1) pretreatment that breaks down the structure of the lignocellulosic matrix, 2) enzymatic hydrolysis that depolymerizes cellulose to glucose by means of cellulolytic enzymes, 3) fermentation that metabolizes the glucose to ethanol by means of yeast strains and 4) distillation-rectification-dehydration that separates and purifies the ethanol to meet the specific fuel form [14]. The process description of bioethanol production from RS, considered in this study, is shown in Fig. 1.

Pretreatment is the first and most intensive step that exposes the cellulose present in the biomass more accessible to enzymes by breaking the lignin encasing, for rapid conversion of carbohydrate polymers into fermentable sugars with high yields [43]. Suitable pretreatment methods, such as DA, SE, alkali, organosolv, ionic liquids, deep eutectic solvents, liquid hot water and ammonia are commonly used for the production of RS and other LCBs into cellulosic ethanol [4,28]. However, this study selectively explored the LCA data available for two pretreatment methods, i.e., DA and SE, which are used for rice straw-based cellulosic ethanol production in a pilot biorefinery plant located at the Indian Oil Corporation Limited (IOCL) in Faridabad, India [29]. In the LCA, the entire value chains (the cradle to grave) of rice straw to bioethanol production pathways (i.e., the energy and emissions related to all inputs including RS harvesting, collection, baling, and transportation; chemicals use, water use, steam generation, and feedstock conversion processes) were taken into account. The features of the biorefinery technology, methodological approaches and assumptions, system boundary and functional unit, process parameters and LCA data used by Soam et al. [29] were adopted and reproduced for the present study (Fig. 1 and Table 2.). Moreover, DA and SE pretreatment technologies were considered for an assessment tool for this study since the technologies were known to be used very popularly in the conversion of rice straw to 2G bioethanol production at pilot/demo plants [44,45].

Estimation of bioethanol, renewable electricity and GHG emissions reduction potential

The study followed an indirect approach to estimate the potential of SRS for the production of bioethanol, renewable electricity generation,

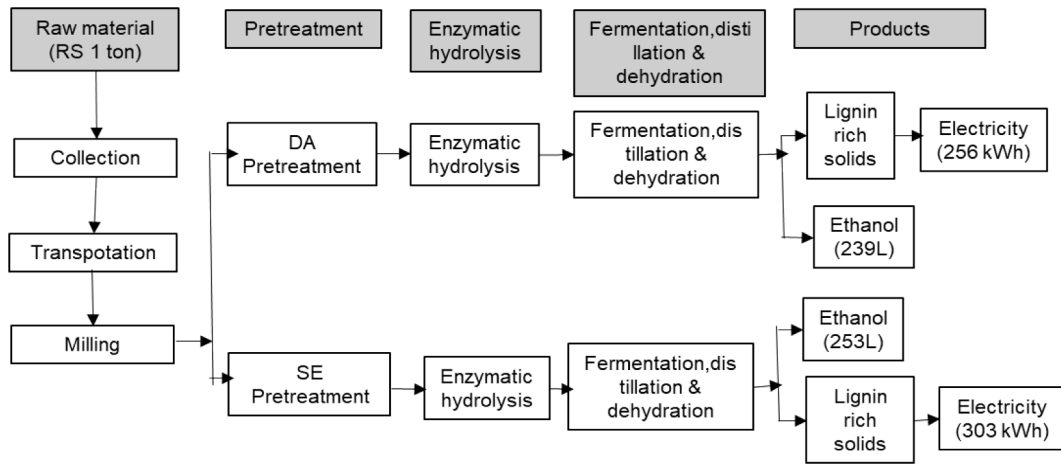


Fig. 1. Process description of bioethanol production from rice straw (RS) through biochemical conversion pathway using dilute acid (DA) and steam explosion (SE) pretreatment methods (reproduced from the information described by Soam et al. [29]).

and GHG (i.e., CO₂eq.) emissions reduction. Indeed, the recovery rate of bioethanol from RS varies with variety of rice plant, quality of RS and adopted conversion technologies [22,26], however, in our study, we examined and analyzed the process parameters and LCA data for the conversion of typical Indian RS to cellulosic ethanol production through DA and SE pretreatments, enzymatic hydrolysis and fermentation, as well as the relevant information utilized by Soam et al. [29]. In addition, the databases of the Ministry of New and Renewable Energy (<https://mnre.gov.in/>) were explored, to gather and analyze the information on policy, frameworks, and programs regarding current biofuels development in India. The following series of equations were applied for the estimations of 2G bioethanol production from SRS through biochemical conversion pathway using DA and SE pretreatment technologies:

$$BET(n) = SRS(n) \times BET(ptrs) \quad (3)$$

where, $BET(n)$ = amount of bioethanol production in state n (in L (litre)/kg), $SRS(n)$ = surplus rice straw production in state n , and $BET(ptrs)$ = bioethanol production in L/kg from one ton of typical Indian RS through the biochemical conversion pathway, using DA and SE as pretreatments.

It is assumed that during the biochemical conversion process of rice straw to bioethanol - renewable electricity is generated as a co-energy-product from burning of lignin-rich solids (i.e., from an integrated bio-refinery system). We estimated the renewable electricity generation by applying the following equation:

$$REC(n) = SRS(n) \times REC(ptrs) \quad (4)$$

where, $REC(n)$ = amount of renewable electricity generation in state n in GWh (gigawatt hour), and $REC(ptrs)$ = renewable electricity generation (in kWh/GWh) from one ton of RS through the biochemical conversion pathway, using the DA and SE pretreatments.

The generated renewable electricity is often needed to be adjusted with the energy inputs for the physio-chemical and the biochemical processes of rice straw to bioethanol production, as described in Fig. 1. Hence, the following equation is applied for the estimations of generated surplus renewable electricity:

$$SREC(n) = SRS(n) \times (REC(ptrs) - GEI(ptrs)) \quad (5)$$

where, $SREC(n)$ = amount of surplus renewable electricity generation in state n in GWh, and $GEI(ptrs)$ = grid electricity (in kWh/GWh) input for processing of a unit ton of RS through the biochemical conversion pathway, using DA and SE pretreatments, for bioethanol production.

However, to assess the effectiveness in reduction of GHG (i.e., CO₂eq.) emissions from RS-based 2G bioethanol when it is used as an

alternative fuel replacing gasoline; the following equations were applied for the calculations:

$$A = (X - Y)/X \quad (6)$$

where, A = actual CO₂eq. reduction rate, X = amount of CO₂eq. emissions reduction (kg CO₂eq./kg) when bioethanol is used instead of gasoline, i.e., CO₂ that can be reduced in accordance with the principle of carbon neutrality (CO₂eq. emissions generated during the conversion process of RS to bioethanol production were not included). Y = the amount of CO₂eq. emissions (kg CO₂eq./kg) produced during the conversion process of RS to bioethanol production (the emissions from entire energy inputs during the conversion processes were included). Taking into account the estimations of CO₂eq. reduction rate (i.e., equation (6)), the value of X and Y were calculated using the following equations:

$$X = Cvg \times \left(\frac{Cvbet}{Cvg} \right) \times EMCvg \quad (7)$$

where, Cvg = calorific value of gasoline (GJ/kg), $Cvbet$ = calorific value of bioethanol (GJ/kg), $EMCvg$ = CO₂eq. emissions (kg CO₂eq./GJ) per unit calorific value of gasoline.

$$Y = ENbp \times EMenbp \quad (8)$$

where $ENbp$ = the amount of energy input (GJ/kg) during the entire processes of RS to bioethanol production, $EMenbp$ = net CO₂eq. emissions per unit calorific value of energy input (kg CO₂eq./GJ) during the processes of RS to bioethanol production. While calculating the $EMenbp$, the credit emissions (i.e., emissions through the replacement of electricity that is produced either from crude oil or coal by the renewable electricity produced under the present study) were taken into considerations. The amounts of credit energy (i.e., that is produced through the biochemical conversion pathway using the DA and SE pretreatments), the calorific ration of ethanol and input fuel (i.e., either crude oil or coal), and CO₂eq. emissions per unit calorific value of input fuel were used to determine the credit emissions (for the values see Table 1 and Table 2).

Indeed, this study applied the carbon neutrality principle, hence the CO₂ emissions produced from using of bioethanol were not considered into the calculations. Thus, the amount of CO₂eq. emissions that could be produced from the use of gasoline that would had been considered as the amount of CO₂eq. emissions reduction. Yet, the net CO₂eq. emissions reduction rate $EMR(r)$ can be determined by multiplying the values of X and A , hence, the quantities assessment of CO₂eq. emissions reduction potential when bioethanol from SRS is used as an alternative to gasoline

Table 1

Values of different fuels properties that used in the calculations of this study [46].

Type of fuel	Fuel properties		
	Density (kg/m ³)	LHV (MJ/kg)	CO ₂ EF (kg/GJ)
Ethanol	789	26.7	–
Gasoline	737	32.7	70.8
Crude oil	856	43.05	73.5
Coal	798	25.75	95.7

N.B. LHV = Lower heating value; CO₂EF = CO₂ emission factor.

Table 2

Values of key LCA data and assumptions for rice straw to bioethanol conversion process using DA and SE pretreatment technologies that used in the calculations of this study [24,29,47].

LCA parameters and assumptions	Unit	DA method	SE method
Rice straw (input)	ton	1	1
Fossil energy (input)	MJ	2660	2471
Grid electricity use	kWh	136	146
Net energy use	MJ	1736	1378
Bioethanol (output)	L	239	253
Generated renewable energy (output)	MJ	924	1093
Generated renewable electricity	kWh	256	303

(while taking into account the entire LCA, including CO₂ emissions during the bioethanol production processes) were evaluated using the equation (9).

$$EMRP(n) = EMR(r) \times BET(n) \quad (9)$$

where, the net CO₂eq. emissions reduction rate (kg CO₂eq./kg) $EMR(r) = X \times A$ (i.e., the values of X and A from equations (6) and (7), respectively), and $EMRP(n) = \text{CO}_2\text{eq. emissions reduction potential in state } n \text{ in kg CO}_2\text{eq.}$, when bioethanol from SRS is used as an alternative fuel to gasoline.

In this study, the calculations of CO₂ emissions reduction potential from the use of SRS-based bioethanol to gasoline were performed in compliance with the GHG emissions calculation guidelines set by the Intergovernmental Panel on Climate Change (IPCC) [48]. For additional information on the methods of GHG emissions reduction calculations, please see the supporting publications [49,50]. In our calculations, standard values for basic fuel properties (i.e., calorific value at lower heating value, density, CO₂ emission factor) of different fuels (i.e., ethanol, gasoline, crude oil, coal), and key LCA data and assumptions for RS to bioethanol production were applied. For the values, see Table 1 and Table 2. Moreover, exploration of available literature was conducted to gather data on status of commercial 2G bioethanol production from RS and other LCBs. During the implementation of the present scheme (Fig. 1) of RS to ethanol production, it is recommended to construct the plant near/adjacent to the site of generation of RS. This will ensure easy collection and aid to the net environmental impact of the process in a positive way, due to avoidance of the transportation using fossil fuels and consequent emission of GHG.

Results and discussion

Statistics of rice production in India

In India, rice is grown as a “Kharif” crop (planting/sowing occurs in April–June; harvesting in September–October), an “Autumn” crop (planting/sowing in June–July; harvesting in November–December) and as a “Rabi” crop (planting/sowing in November–February; harvesting in March–June). Growing rice has long been and an important part of the national economy of the country as it is the staple diet of Indians. Between the fiscal years 1950–51 and 2018–19, the rice cultivation area in

India increased from 30.81 million ha (Mha) to 43.79 Mha. At the same time, rice production increased from 20.58 to 116.42 MT. Over the period, the area of rice cultivated, and the production of rice increased annually by 0.62 % and 6.85 %, respectively. The irrigated rice cultivation area significantly increased from 31.7 % in 1950–51 to about 60 % in 2018–2019. The rice yield level increased from 0.67 ton/ha in 1950–51 to 2.6 ton/ha in 2018–19, which amounts to a massive (288%) increase. Rice is grown in nearly all states of India, with West Bengal, Uttar Pradesh, Punjab, Andhra Pradesh, Odisha, Telangana, Chhattisgarh, and Tamil Nadu being the leading states in terms of annual production. Nationally, West Bengal, Uttar Pradesh and Punjab together accounted for about one-third of the country’s rice cultivation area and 38 % of all national rice production in 2018–19. The national rice yield rate is about 2576 kg/ha; however, the rates vary widely among the Indian states. The highest yields occur in Punjab (4132 kg/ha), followed by Tamil Nadu (3748 kg/ha), Andhra Pradesh (3733 kg/ha), and Telangana (3436 kg/ha).

From a comparative analysis of rice production data over the past eight fiscal years (2011–12 to 2018–19), it was revealed that, India experienced a fluctuation in the annual rice growth rate at the national level. This varied between –0.7 % in 2012–13 and 5.5 % in 2016–17. At the state level, there was no uniformity in the annual rice production growth rate among the states. Similar negative growth rates were also reported in parts of India by Goyal and Singh [51]. The production trend indicates that, rice production in India will increase until 2030–31 as a result from the implementation of governmental policies, frameworks, and programmes. India has a strong institutional capacity to expand rice production. Yet high labor costs, the use of low yield varieties, poor adoption of farming technologies, the low economic status of farmers, the shifting of rice cultivation land to other land-uses, and climate change impacts (i.e., erratic rainfall, flash floods, drought) are considered major constraints to boosting rice production in the country. Similar types of observations were made by Gupta and Mishra [52].

Estimation of rice straw and surplus rice straw availability

The states of West Bengal, Uttar Pradesh, Punjab, Andhra Pradesh, Odisha, Telangana, Chhattisgarh, Tamil Nadu, Bihar, Assam, and Haryana are hot spots for RS availability. Seasonal variation has an influence on the availability of RS in many states in India. For instance, RS is available year-round in West Bengal, Assam, Bihar, Jharkhand, Karnataka, Kerala, and Odisha, whereas in states like Telangana, Uttar Pradesh, and Uttarakhand—RS is only available in the “Kharif” and “Rabi” seasons. In some states, such as Punjab, Chhattisgarh, Haryana, Madhya Pradesh, and Gujarat - it is available only in the “Kharif” season. Therefore, a robust storage mechanism is required for its year-round use if its valorization from the perspective of biofuel generation is targeted. Analysis of the last eight fiscal years of rice production data suggests an overall increasing trend of RS production in Indian states, with 167.89, 179.88 and 191.86 MT estimated for 2020–21, 2025–26 and 2030–31, respectively. However, estimated SRS in Indian states for 2020–21, 2025–26 and 2030–31 under the S₁ scenario were 38.61, 41.37 and 44.13 MT, respectively and under the S₂ scenarios were 47.01, 50.37 and 53.72 MT, respectively. Estimated SRS availability in major rice producing states of India under S₁ and S₂ scenarios, are shown in Fig. 2. The analysis revealed that SRS availability under S₂ was 21.74 % higher than under S₁.

The RS produced after rice grain harvesting has traditionally been used for a wide range of farm activities, i.e., ruminant feeding, poultry litter, thatching, mulching, manuring, mushroom production, and cooking fuels, as well as different commercial activities, such as paper making, alcohol production, energy, and power generation. The quantity of SRS depends on local demands, as well as on the income attained by the farmers from collection, processing transportation and sales. Furthermore, the pattern of RS utilization varies widely amongst regions in India. For instance, a large proportion of RS in West Bengal and Assam

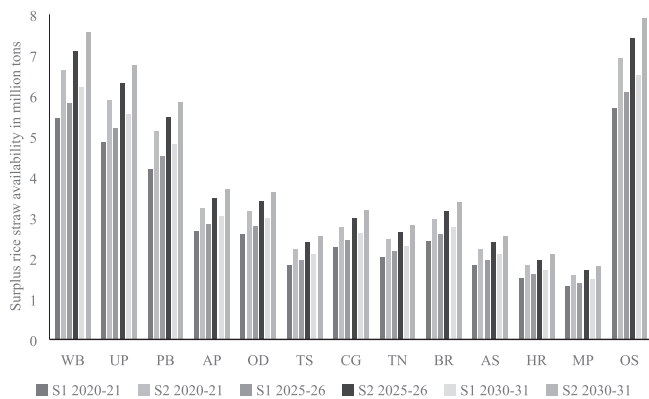


Fig. 2. Estimated surplus rice straw (SRS) availability for 2G bioethanol production in the major rice producing states of India in the year 2020–21, 2025–26 and 2030–31 under S_1 (S_1) and S_2 (S_2) scenarios (N.B. (WB = West Bengal, UP = Uttar Pradesh, PB = Punjab, AP = Andhra Pradesh, OD = Odisha, TS = Telangana, CG = Chhattisgarh, TN = Tamil Nadu, BR = Bihar, AS = Assam, HR = Haryana, MP = Madhya Pradesh, OS = Other States).

is used for farm activities, mainly for cattle feeding and thatching of cattle sheds. In states like Bihar, Gujarat, Maharashtra where forest resources are not enough - rural people use RS for domestic cooking. In Punjab, Haryana, and Uttar Pradesh, however, RS is used neither for cattle feeding nor domestic cooking; it is left as uncollected residue in the field and burnt *in situ*. Nevertheless, numerous researchers have estimated SRS at the state and national levels in India. At the state level, SRS availability is reported to vary from a minimum of 21 % in Arunachal Pradesh to a maximum of 48 % in Haryana and Punjab. At the national level, the value of SRS varies from a minimum of 23 % [40] to a maximum of 33 % [53]. However, the Ministry of New & Renewable Energy reported that an average of ~ 28 % of crop residues remains as surplus at the national level. Hence, the SRS fractions used in our study for the development and projection of scenarios are rational, timely and consistent with the previous studies.

Concurrently, several studies have reported that a large proportion of RS is not utilized and is left in the fields after rice grain harvesting and burnt *in situ* [53,54]. According to the IPCC, on an average 25 % of total crop residues in India are burnt on the farm, however, the share of RS to the total crop residues burnt is about 34 % [53]. Jain et al. [55] have reported that the fraction of crop residue subjected to burning *in situ* ranges from 8 to 80 % for rice crop across all states. The highest (80 %) *in situ* RS burning rates occur in Punjab, Haryana, and Himachal Pradesh, followed by Karnataka (50 %) and Uttar Pradesh (25 %). During 2014–15, about 8.75 and 1.29 MT of RS were burnt in Punjab and Haryana, respectively [54]. The RS is burnt *in situ* because farmers opt for a quick and inexpensive way to manage large quantities of residue and make the fields ready for the next crop. High labor costs and the mechanization of harvesting techniques were also observed reasons for *in situ* RS burning [56]. The burning of RS has several strong adverse impacts. For example, it is a source of atmospheric pollutants; it depletes air quality; it liberates soot particles into the air; it is a cause of health hazards to humans, animals and birds; and it leads to deterioration in soil health and fertility at regional and national levels [53]. This unsustainable practice also creates adverse environmental impacts that go far beyond India. To avoid these adverse effects and to take advantage of the huge volume of RS waste, some studies have suggested that it can instead be utilized in the bio-energy sector (e.g., production of biogas, biochar, bioethanol, biobutanol); industrial sector (e.g., manufacture of paper, composites, building materials); and agriculture sector (e.g., production of compost, soil fertilizer, animal feed) [39,53]. In the context of India, it has been emphasized that the utilization of SRS for bioethanol production, as a means to prevent the adverse impacts from RS burning - as well as to enhance energy security; to provide

alternatives to fossil fuels; to improve the rural economy; and to contribute to the achievement of national determined contribution (NDC) goals, national biofuel targets and EBPP targets [17,19]. Taking into account the huge quantities of unused RS and the adverse impacts of burning, our study has investigated the utilization of SRS for bioethanol production and for possible GHG emissions reduction benefits - which could thus offer an alternative means for the sustainable use of this waste resource.

Nevertheless, the two scenarios developed in this study, to predict SRS availability up to 2030–31, were based on a hierarchical order of RS uses. These scenarios simply highlight the availability of SRS for ethanol production, regardless of different plausible and consistent assumptions. Indeed, various assumptions may attribute to the estimation of SRS under each scenario. For instance, the challenges and uncertainties related to land-use change, rice cropping patterns, farmers' willingness, or unwillingness to cultivate rice, the extent of use of RS for on-farm and non-farm activities, the success of agriculture and food policy implementation, and climate change impacts may have significant influence on crop production and crop residue availability. Similar types of challenges and uncertainties, related to rice crop production and rice residue availability in India, have been reported in several studies [51,52]. Additionally, the fractions applied for the estimation of SRS under S_1 and S_2 were based on the consequences of high (77 %), and medium (72 %) fractions of RS use for various on-farm and non-farm activities, which have been endorsed by several studies. Recent studies [53,54] have emphasized that in states, such as Punjab and Haryana - a lower amount (20 %) of RS is used for different farm purposes, with the majority (80 %) left unutilized as waste. However, these are state specific or case specific and similar situations may not exist in other states. Hence, the estimations made regarding the availability of SRS, which is considered a readily available feedstock for bioethanol production and having consequent GHG emissions reduction potential under the different scenarios—may apply to average Indian conditions. Moreover, the availability of SRS was projected to be greatest during 2030–31, due to high production of rice resulting from the expected continuation of strategic policy framework implementation and technological development of the rice crop. As already mentioned earlier that this will also lead to generation of increased volume of RS and simultaneously SRS, due to the directly proportional correlation of rice to RS. Therefore, a clear and unmistakable hint of enhancement of feedstock potential of RS/SRS can be noticed regarding the future progress of RS based bioethanol and biorefineries in India, which has been demonstrated in the following section. In our analysis, the literature reports on strategic policy framework in rice crop production in India have been used as a guideline [52,57].

Estimation of bioethanol production potential from surplus rice straw

Our study estimated that, in 2020–21, in Indian states, bioethanol production from SRS using DA and SE pretreatments could reach 9229 and 9770 ML, respectively, under S_1 ; and 11,235 and 11,893 ML, respectively, under S_2 . The analysis has revealed that bioethanol production in all scenarios was greater (by 5.86 %) in cases when the SE pretreatment was used (compared to the DA treatment). By 2025–26, national bioethanol potential from SRS using DA and SE pretreatments—is forecasted to be 9888 and 10,467 ML, respectively, under S_1 ; and 12,037 and 12,743 ML, respectively, under S_2 ; and by 2030–31, would be 10,547 and 11,165 ML, respectively, under S_1 ; and 12,840 and 13,592 ML, respectively, under S_2 . Table 3a and Table 3b show the estimated 2G bioethanol production and surplus renewable electricity generation from SRS with DA and SE pretreatment methods in the major rice producing states of India in year 2020–21, 2025–26, and 2030–31 under S_1 and S_2 scenario.

Numerous authors have examined the bioethanol yield from RS, using DA and SE pretreatments. For example, Karimi et al. [58] investigated ethanol production from DA-pretreated RS by SSF (simultaneous

Table 3a

Estimated 2G bioethanol production and surplus renewable electricity generation from surplus rice straw (SRS) with dilute acid (DA) and steam explosion (SE) pretreatment methods in the major rice producing states of India in year 2020–21, 2025–26, and 2030–31 under S₁ scenario (Bioethanol production in ML and surplus renewable electricity generation in GWh).

State	2020–21				2025–26				2030–31			
	DA		SE		DA		SE		DA		SE	
	BioE	SREC	BioE	SREC	BioE	SREC	BioE	SREC	BioE	SREC	BioE	SREC
WB	1299	652	1375	853	1392	699	1473	914	1485	745	1571	975
UP	1158	581	1226	761	1241	623	1313	815	1323	664	1401	869
PB	1004	504	1063	660	1076	540	1139	707	1147	576	1215	754
AP	636	319	673	418	681	342	721	447	726	365	769	477
OD	622	312	659	409	667	335	706	438	711	357	753	467
TS	437	219	462	287	468	235	495	307	499	251	529	328
CG	545	274	577	358	584	293	618	384	623	313	659	409
TN	482	242	511	317	517	259	547	339	551	277	584	362
BR	580	291	614	381	621	312	657	408	662	333	701	435
AS	437	220	463	287	468	235	496	308	500	251	529	328
HR	359	180	380	236	385	193	407	253	410	206	434	270
MP	311	156	329	204	333	167	353	219	356	179	376	234
OS	1359	682	1438	893	1456	731	1541	956	1553	780	1644	1020
AI	9229	4634	9770	6063	9888	4965	10,467	6495	10,547	5295	11,165	6928

N.B. BioE = Bioethanol; SREC = Surplus Renewable Electricity; AI = All India.

Table 3b

Estimated 2G bioethanol production and surplus renewable electricity generation from surplus rice straw (SRS) with dilute acid (DA) and steam explosion (SE) pretreatment methods in the major rice producing states of India in year 2020–21, 2025–26, and 2030–31 under S₂ scenario (Bioethanol production in ML and surplus renewable electricity generation in GWh).

State	2020–21				2025–26				2030–31			
	DA		SE		DA		SE		DA		SE	
	BioE	SREC	BioE	SREC	BioE	SREC	BioE	SREC	BioE	SREC	BioE	SREC
WB	1581	794	1674	1039	1694	851	1794	1113	1807	907	1913	1187
UP	1410	708	1492	926	1510	758	1599	992	1611	809	1705	1058
PB	1222	614	1294	803	1310	658	1386	860	1397	701	1479	918
AP	774	389	819	508	829	416	878	545	884	444	936	581
OD	758	380	802	498	812	408	859	533	866	435	916	569
TS	532	267	563	349	570	286	603	374	608	305	643	399
CG	664	333	702	436	711	357	753	467	758	381	803	498
TN	587	295	622	386	629	316	666	413	671	337	710	441
BR	706	354	747	464	756	380	800	497	806	405	854	530
AS	532	267	563	350	570	286	604	375	608	305	644	400
HR	437	220	463	287	468	235	496	308	500	251	529	328
MP	379	190	401	249	406	204	430	267	433	217	458	284
OS	1654	830	1751	1087	1772	890	1876	1164	1890	949	2001	1242
AI	11,235	5641	11,893	7380	12,037	6044	12,743	7907	12,840	6447	13,592	8434

N.B. BioE = Bioethanol; SREC = Surplus Renewable Electricity; AI = All India.

saccharification and fermentation). They found that 1 kg of RS contains 390 g cellulose, from which the cellulose-driven ethanol production was 208 mL, and the xylose-driven ethanol was 83 mL, with a total ethanol yield of 291 mL or 291 L from 1 ton of RS. In addition to ethanol, the study enumerated the yields of other byproducts from 1 kg of RS as: glycerol (18.7 mg/g), lactic acid (59.4 mg/g), acetic acid (3.4 mg/g) and pyruvic acid (1.2 mg/g). Lee et al. [44] observed the ethanol yield from RS using DA pretreatment to be at 0.2 g/g, or 253 L ethanol from 1 ton of RS. Higher ethanol yields have also been reported by Zhu et al. [59] where RS was pretreated in a two-step process using DA and sulfomethylation reagent and produced approximately 430 mL ethanol and 162 g of lignin residue from 1 kg of RS, or 430 L of ethanol and 162 kg of lignin from 1 ton of RS. Ethanol yield was reported to be 230 L/dry ton RS from an integrated bioprocess demonstration facility located in the Biochemical Engineering Research Center at IIT Delhi with a capacity of 50 L bioethanol per day [60]. Although the DA pretreatment process seemed to be efficient, economic, and environmental sustainability were not evaluated. Relatively higher ethanol yields from RS, using SE pretreatment, have been reported by several authors. For example, Kami Delivand et al. [61] found that ethanol yield is about 260 L/ dry ton RS using lime and DA and SE pretreatments. Meanwhile, Nakamura et al.,

[62] reported an ethanol yield rate from RS (using the SE pretreatment method) of about 0.32 g/g or 405 L bioethanol/dry ton of RS, with a recovery rate of 86 % (w/w). A slightly higher theoretical recovery rate of 420 L bioethanol/dry ton of RS was reported by Zhu et al. [59]. Banoth et al. [63] investigated the optimization of bioethanol production using an improved SE pretreatment method and observed an ethanol yield from RS hydrolysate of 0.44 g/g, with a fermentation efficiency of 87.03 %. However, Sharma et al. [45] studied the SE pretreatment method and the mass balance for higher sugar recovery from RS. They found that water- and sulfuric acid-assisted SE pretreatments perform well, producing a total saccharification yield of 81.8 and 77.1 %, respectively, and thereby an enhanced ethanol yield. However, the trade-offs between the advantages and disadvantages of the processes, and their applicability for large-scale plants - are still unknown.

As described earlier, cellulose, hemicellulose and lignin are the major molecular fractions of RS, although variations of these compositions affect the yield of bioethanol production [22]. Cellulose is a polysaccharide that is composed of d-glucose and can be degraded chemically or enzymatically into a homopolymer of repeating sugar units of glucose linked by β -1, 4 glycosidic bonds [64]. Hemicellulose is also a polysaccharide but is a relatively short and highly branched

polymer. Unlike cellulose, it is derived from a heterogeneous group of sugars, mostly composed of d-xylose, d-mannose, d-galactose, l-arabinose, and 4-O-methyl-d-glucuronic acid. Glucose (sugar containing six carbons) is produced from cellulose via pretreatment and hydrolysis, whereas xylose (sugar containing five carbons), arabinose (sugar containing five carbons) and mannose (sugar containing six carbons) are the main products of pretreatment stage only. These are produced from hemicellulose via pretreatment [65]. Subsequently, the sugars can be converted into biofuels (i.e., bioethanol, biobutanol) via fermentation. Lignin is a cross-linked phenolic polymer (i.e., monolignols that are aromatic alcohols) and is not composed of carbohydrate (sugar) monomers. It is hydrophobic in nature and composed of phenylpropanyl (C9) randomly branched units, mostly a 3-dimensional aromatic polymer of p-hydroxyphenylpropanoid units connected through carbon-carbon and carbon-oxygen-carbon bonds. However, in the sugar platform-based conversion process, bioethanol (as the main product) is produced through pretreatment, hydrolysis, fermentation, and distillation. Lignin is retained as a residue, which can be used as a source of heat and electricity generation through combustion [66].

In the sugar platform, pretreatment is an essential step that reduces RS recalcitrance by altering the interactions of cellulose, hemicellulose, and lignin. It increases cellulose accessibility, removes lignin-carbohydrates complexes, reduces cellulose crystallinity, and helps enhance the susceptibility of the RS substrates to enzymatic actions. It thereby increases bioethanol yields [67]. Several pretreatment methods (i.e., dilute acid, alkali, steam explosion, organosolv, AFEX (ammonia fiber explosion), ionic liquid, fenton and deep eutectic solvents) are proven to be suitable for the conversion of RS biomass to bioethanol production. However, the DA and SE pretreatment technologies are the most popular, due to their low cost, their low (for DA) or zero (for SE) chemical requirements, and their high recovery of monomeric sugar, for instance [44,45]. A number of studies [68–70] have also evaluated the performance of pretreatment technologies for bioethanol production from RS and other LCBs. However, most of these studies are either at laboratory scale or contain insufficient data to evaluate the LCA at pilot scale and/or at a demonstration biorefinery plant. In the context of India, Soam et al. [29] undertook a LCA of cellulosic ethanol from baseline data obtained from the IOCL-owned pilot-scale biorefinery plant at Faridabad. The LCA data provided crucial statistics on the RS to bioethanol production process in a good-sized biorefinery plant. Hence, the LCA default values were explored and used in our estimations.

Estimation of renewable electricity and surplus electricity generation potential from surplus rice straw

Renewable electricity can be generated from RS using a wide range of technologies that include chemical, biological, electrolytic, photolytic, thermochemical, and biochemical processes. This study has highlighted the estimation of renewable electricity potential produced through biochemical conversion of RS to ethanol production. During the cellulosic ethanol production process, RS-driven hydrolysate mixtures are processed through fermentation and distillation to recover anhydrous ethanol where the lignin rich solids are separated as process by-products. These solids are mainly composed of lignin, which is subsequently transformed into electricity at the energy plant. Electricity is thus generated from the utilization of the waste lignin fraction. Our study showed that, in 2020–21, the national potential for renewable electricity generation from SRS using DA and SE pretreatments could amount to 9885 and 11,700 GWh, respectively, under S_1 ; and to 12,034 and 14,244 GWh, respectively, under S_2 . By 2025–26, the nation potential is projected to be 10,591 and 12,536 GWh, respectively, under S_1 ; and 12,894 and 15,261 GWh, respectively, under S_2 , and by 2030–31, to be 11,297 and 13,371 GWh, respectively, under S_1 ; and 13,753 and 16,278 GWh, respectively, under S_2 . However, while taking into account the amount of grid electricity input for the RS conversion to bioethanol processes - in the base year 2020–21, the national potential of surplus

renewable electricity generation from SRS using DA and SE pretreatments could amount to 4634 and 6063 GWh, respectively, under S_1 ; and to 5641 and 7380 GWh, respectively, under S_2 . Table 3a and Table 3b represent the co-generated amount of surplus renewable electricity generation from SRS with DA and SE pretreatment methods in the major rice producing states of India in year 2020–21, 2025–26, and 2030–31 under S_1 and S_2 scenario, respectively. Our analysis has revealed that renewable electricity (18.4 %) and surplus renewable electricity generation (30.8 %) were optimum, in all scenarios, with the SE pretreatment method.

Nevertheless, studies evaluating surplus renewable electricity generation employing bioethanol recovery technologies (i.e., biochemical conversion method) from RS are scarce. Kazi et al. [47] found that surplus electricity production from DA pretreatment of LCB to ethanol production is about 1.07 kWh/L ethanol. Meanwhile, Kumar and Murthy [24] found surplus electricity production through DA and SE pretreatments to be about 0.77 and 1.78 kWh/L ethanol, respectively, with an efficiency of 30 % of lignin energy to electricity conversion. However, Soam et al. [29] reported that surplus electricity production through DA and SE pretreatment of RS from a RS-based ethanol pilot biorefinery plant was 1.07 and 1.20 kWh/L ethanol, respectively. This has been explored in our estimation. However, in the process to evaluate the net renewable electricity credit, several important assumptions should be considered besides the practical factors. These include renewable electricity production efficiency from solids, as well as tradeoffs in feedstock costs, enzymes, pretreatments, downstream processing technologies and other investment costs associated with the biomass to bioethanol conversion process. In many cases, the electricity produced from lignocellulosic ethanol plants may lead to a lower electricity credit than the baseline (i.e., when LCBs is used for electricity production through thermal conversion) case. Indeed, the electricity produced from lignocellulosic ethanol plants leads to lower net electricity consumption during the production process due to the counterbalance created through the ‘consumption-generation’ of electricity. At the same time, significant electricity benefits are observed when compared to the electricity consumption and co-generation of electricity by the plant [23].

Estimation of GHG emissions reduction potential

Bioethanol is one alternative to petroleum's use as a ‘drop-in’ transportation fuel in existing gasoline vehicles. For use in a vehicle, ethanol is blended with gasoline to a specific level (i.e., E5 - a mixture of 5 % ethanol by volume; E10 a mixture of 10 % ethanol by volume; E20 - a mixture of 20 % ethanol by volume). This can offer emissions benefits regarding vehicular emissions, depending on the vehicle type, engine calibration and blend level. Our study highlighted the GHG emissions reduction potential from SRS-derived bioethanol, when used as an alternative fuel to gasoline. In the base year (2020–21), the emissions reduction potential in Indian states from the use of SRS-derived bioethanol, using DA and SE pretreatments, would amount to about 10,460 and 12,579 kt CO₂eq., respectively under S_1 ; and 12,734 and 15,313 kt CO₂eq., respectively, under S_2 when the generated renewable electricity replaces crude oil-driven grid electricity. In contrast, when the generated renewable electricity replaces coal-driven grid electricity, the values are 10,061 and 12,687 kt CO₂eq., respectively, under S_1 ; and 12,249 and 15,445 kt CO₂eq., respectively, under S_2 . The projected CO₂ emissions reduction potential from SRS, through DA and SE pretreatments, in India's major rice producing states for the year 2020–21, 2025–26 and 2030–31 under S_1 and S_2 scenario are shown in Table 4a and Table 4b, respectively. In comparison to gasoline, the emissions reduction potential from SRS-derived bioethanol using DA and SE pretreatments was 76 and 86.3 % when the generated renewable electricity replaced crude oil-driven grid electricity; and 73.1 and 87.1 % when the generated renewable electricity replaced coal-driven grid electricity. Our analysis reveals that the emissions avoidance potential is greater

Table 4a

Estimated carbon dioxide (CO₂) emissions reduction potential from surplus rice straw availability (SRS) with dilute acid (DA) and steam explosion (SE) methods in the major rice producing states in India in 2020–21, 2025–26, and 2030–31 under S₁ scenario (Emissions in kt CO₂ eq.).

State	2020–21				2025–26				2030–31			
	E ¹ (DA)	E ¹ (SE)	E ² (DA)	E ² (SE)	E ¹ (DA)	E ¹ (SE)	E ² (DA)	E ² (SE)	E ¹ (DA)	E ¹ (SE)	E ² (DA)	E ² (SE)
WB	1472	1771	1416	1786	1577	1897	1517	1913	1683	2023	1618	2041
UP	1312	1578	1262	1592	1406	1691	1352	1705	1500	1804	1443	1819
PB	1138	1368	1095	1380	1219	1466	1173	1479	1300	1564	1251	1577
AP	720	866	693	874	772	928	742	936	823	990	792	999
OD	705	848	678	855	756	909	727	917	806	969	775	978
TS	495	595	476	601	531	638	510	643	566	681	544	686
CG	618	743	594	749	662	796	637	803	706	849	679	856
TN	547	657	526	663	586	704	563	710	625	751	601	758
BR	657	790	632	797	704	846	677	854	751	903	722	911
AS	496	596	477	601	531	639	511	644	566	681	545	687
HR	407	490	392	494	436	524	420	529	465	559	447	564
MP	353	424	339	428	378	454	363	458	403	485	388	489
OS	1540	1852	1481	1868	1650	1984	1587	2001	1760	2116	1693	2134
AI	10,460	12,579	10,061	12,687	11,207	13,477	10,780	13,593	11,954	14,375	11,498	14,498

N.B. E¹ = Emissions reduction potential from SRS by using ethanol instead of gasoline when the generated renewable electricity replaces crude oil-driven grid electricity; E² = Emissions reduction potential from SRS by using ethanol instead of gasoline when the generated renewable electricity replaces coal-driven grid electricity.

Table 4b

Estimated carbon dioxide (CO₂) emissions reduction potential from surplus rice straw availability (SRS) with dilute acid (DA) and steam explosion (SE) methods in the major rice producing states in India in 2020–21, 2025–26, and 2030–31 under S₂ scenario (Emissions in kt CO₂ eq.).

State	2020–21				2025–26				2030–31			
	E ¹ (DA)	E ¹ (SE)	E ² (DA)	E ² (SE)	E ¹ (DA)	E ¹ (SE)	E ² (DA)	E ² (SE)	E ¹ (DA)	E ¹ (SE)	E ² (DA)	E ² (SE)
WB	1792	2155	1724	2174	1920	2309	1847	2329	2048	2463	1970	2484
UP	1598	1921	1537	1938	1712	2058	1646	2076	1826	2196	1756	2214
PB	1385	1666	1333	1680	1484	1785	1428	1800	1583	1904	1523	1920
AP	877	1055	844	1064	940	1130	904	1140	1002	1205	964	1216
OD	859	1033	826	1041	920	1106	885	1116	981	1180	944	1190
TS	603	725	580	731	646	777	621	783	689	828	663	836
CG	752	904	723	912	806	969	775	977	859	1034	827	1042
TN	666	800	640	807	713	858	686	865	761	915	732	923
BR	800	962	769	970	857	1030	824	1039	914	1099	879	1108
AS	603	726	580	732	646	777	622	784	689	829	663	836
HR	496	596	477	601	531	639	511	644	566	681	545	687
MP	429	516	413	521	460	553	442	558	491	590	472	595
OS	1875	2254	1803	2274	2009	2415	1932	2436	2142	2576	2061	2598
AI	12,734	15,313	12,249	15,445	13,643	16,407	13,123	16,547	14,552	17,500	13,998	17,650

N.B. E¹ = Emissions reduction potential from SRS by using ethanol instead of gasoline when the generated renewable electricity replaces crude oil-driven grid electricity; E² = Emissions reduction potential from SRS by using ethanol instead of gasoline when the generated renewable electricity replaces coal-driven grid electricity.

with SE pretreatment than with DA pretreatment by 20.3 and 26.1 %, respectively when the generated renewable electricity replaces crude oil-driven grid electricity and coal-driven grid electricity. The reasons might be due to lower requirements of chemicals and net energy input, and higher amount of energy production (in the form of bioethanol as the major product) during RS conversion process of RS in SE pretreatment - compared to DA pretreatment. Furthermore, the projection data has revealed that, by 2030–31, the emissions reduction potential from the alternative use of SRS-derived bioethanol to gasoline can reach 14,375 and 17,500 kt CO₂eq. under S₁, and S₂, respectively, when the SRS is processed using SE pretreatment and the generated renewable electricity from the biorefinery plant replaces crude oil-driven electricity; while the values would reach at 14,498 and 17,650 kt CO₂eq. under S₁, and S₂, respectively, when the generated renewable electricity replaces coal-driven electricity - indicated that the SE pretreatment maximizes the emissions reduction potential while the generated electricity replaces coal-driven grid electricity.

Indeed, detailed studies on LCA to analyze the energy potential and environmental impacts of lignocellulosic-based power and 2G bioethanol production technologies are scarce, only a few [27,29] have focused on the LCA of 2G bioethanol obtained from RS. The environmental aspects mainly deal with GHG emissions during the entire

process of bioethanol production and its use as an alternative fuel to gasoline in the transport sector. Nevertheless, various factors such as the method use in cellulosic ethanol production (especially the pretreatment process), the hydrolysis and fermentation processes, and varying system boundaries exhibit impact on the ethanol production [24]. As such, the variability in factors produces a range of results in different ethanol LCA studies. For example, a study from Thailand showed that the net GHG emissions reduction potential from RS-based bioethanol option (24 ML capacity) and electricity option (10 MWh capacity) would be 504 and 447 kg CO₂eq./dry ton of RS, respectively [61]. This indicated that RS-based bioethanol option offers comparatively greater GHG emissions reduction potential than the electricity option. The underlying reason might be, during the biochemical conversion process of RS - the unused lignin-rich solids are burnt to produce electricity that compensates for energy consumption and, thereby, lowers net GHG emissions from the biorefinery plant itself. A contemporary study from Japan revealed that the alternative use of RS-based bioethanol (versus gasoline) can provide a net emissions reduction of 1.69 kg CO₂eq./L bioethanol or 1690 kg CO₂eq./m³ bioethanol, when RS is processed through an intensive RT-CaCCO process [71]. The study indicated that the biochemical conversion pathway of RS to bioethanol production provides higher environmental benefits. Meanwhile, Silalertruksa and Gheewala [26] made a

comprehensive LCA study of RS-based bioethanol in a cogeneration plant in Thailand and they found that the net GHG emissions reduction potential using DA pretreatment was about 283 kg CO₂eq./dry ton of RS. This accounts for 60 % GHG emissions reduction, compared to conventional gasoline. They concluded that the biochemical conversion of RS to the bioethanol pathway provides the highest environmental benefits, in terms of emissions reduction and resource depletion.

Soam et al. [29] examined the LCA data from a pilot study at a RS-based bioethanol plant in India and reported that the use of RS-driven bioethanol (E100) instead of gasoline has enormous environmental benefits, regarding emissions reduction and environmental sustainability. They found that bioethanol production from RS with DA and SE pretreatments provides a net emission reduction of 77 % and 89 %, respectively, compared to gasoline. This is consistent with the findings in our study. This GHG performance of RS-based 2G bioethanol production complies with the binding criteria for saving a minimum of 60 % and 71 % GHG emissions (compared to gasoline), as set by the US EPA (US EPA 2018) and the EU-RES Directives, respectively. In the context of India, guidelines, methods, procedures, and protocols for the standard quality and GHG performance criteria of ethanol and other biofuels are currently being defined. However, the Bureau of Indian Standards (BIS) has evolved a standard (IS-15607) for biodiesel (B 100). Likewise, it has adopted the American Standard ASTM D-6751 and European Standard EN-14214, which describe the requirements and test methods for biodiesel blends.

Trade-offs on commercialization of straw-based 2G bioethanol production and relevance to India

The 2G-bioethanol production from LCBs through biochemical conversion route is known to reach the maturity stage. The technology is gaining considerable interest for commercial applications [72]. Available data showed that until the end of 2015, some 69 existing and 21 proposed cellulosic ethanol plants with an annual capacity of 1390 and 1747 million L, respectively were confined across the world, which are mainly concentrated in EU countries, USA, Canada, Brazil, and China [73]. The existing cellulosic ethanol plants are known to operate for producing 2G bioethanol from LCBs either at demo level or at full-scale commercial level. Indeed, the projects and plants in those countries vary significantly in their technological approaches and feedstocks used to deploy 2G-bioethanol production facilities. Straws are largely used as the main feedstock in many of the existing plants. The Beta Renewables in Crescentino Biorefinery, Italy is the world's first commercial-scale 2G-bioethanol plant that processes about 200 000 tons of dry residue biomass (mainly wheat straw, RS, and giant reed) to produce 40,000 tons of 2G-bioethanol and 13 MWh of renewable electricity annually. The Clariant-sunliquid in Munich, Germany; the Inbicon in Kalundborg, Denmark; and the Abengoa in Salamanca, Spain have developed straw-based demo level 2G bioethanol plant with an annual capacity of 1.2, 5.4 and 5 million L, respectively. Apart, the Clariant-sunliquid has recently established a demo straw-based 2G bioethanol plant in southern Romania with a capacity of 50,000 tons per year. Nonetheless, the USA poses the top in terms of the number of 2G-bioethanol plants and installation capacity. The country has 28 existing 2G-bioethanol plants with an annual capacity of 480 million L. The notable straw-based 2G bioethanol plants are the INEOS New Planet BioEnergy at Vero Beach, Florida (capacity 30 million L and 6 MWh renewable electricity per year), the Poet-DSM Advanced Biofuels LLC at Emmetsburg, Iowa, the Abengoa Bioenergy Biomass of Kansas LLC located at Hugoton, the DuPont Cellulosic Ethanol LLC plant at Nevada, Iowa and the ZeaChem Boardman Biorefinery LLC at Broadman, Oregon. Notwithstanding, the Iogen Corporation located at Ottawa (capacity 2 million L per year), and the Shell located at Sombra in Ontario are the notable Canadian's commercial scale straw-based 2G bioethanol facilities. Yet, China is the second most country in production of 2G bioethanol from its 12 existing plants with an annual capacity of 340 million L. The Novozymes,

Longlive Biotechnology, Shandong Zesheng Biotech, Henan Tianguan Group, COFCO Zhaodong, Jilin Fuel Alcohol, and Beta Renewables-Fuyang Bioproject are notable 2G bioethanol facilities where RS is used as the main feedstock. In January 2020, the Anhui Guozhen and the Chemtex Chemical Engineering announced to establish a commercial biorefinery in Fuyang, China with an annual capacity of 50,000 tons 2G bioethanol from RS and other crop residues using Clariant's sunliquid®cellulosic ethanol technology. However, in India the production of 2G bioethanol from straw and other LCBs is still at its nascent stage. Until now, only a demo plant has been established at Kashipur in Uttarakhand where daily about 10 tons of various LCBs (mainly RS, wheat straw, cotton stalk, corn stover and bagasse) are used to produce 2G bioethanol, yet the techno-economic viability of the plant is unknown.

Although many countries are producing 2G-bioethanol from straw and other cellulosic biomasses at different developmental stages, there are concerns remain about the economic viability of its large-scale commercial production mainly due to high conversion processing cost [74]. Studies showed that the high capital investment cost, high production and operational costs, lack of market competitiveness, and low-profit margin were the significant challenges to ensure the economic viability of a commercial 2G bioethanol plant [75], and in context of biofuels perspectives in India - these are highly relevance to produce 2G bioethanol from mainly RS and other crop residues [27,30]. To reduce the production cost, several considerations are needed to be addressed - these include collection, transportation, and procurement costs of RS, conversion processing (i.e., cost for pretreatment, enzymatic hydrolysis, and microbial fermentation) costs and other operational costs. A study from Thailand revealed that without governmental biofuels subsidies - the straw collection cost at a price of \$25/ton from a transport distance beyond 90 km, the utilization of straw for 2G-bioethanol production is no longer economically feasible [26]. Another study from Japan revealed that, despite the higher environmental benefit potential of RS-based bioethanol production, the economic viability of the system is doubtful unless the innovative technologies along with the renewable energy policy and stakeholders participation are taken into consideration [71]. Therefore, low costs for straw collection and supply chain logistics, low operational costs, and governmental subsidies are essential to promote the economic sustainability of a 2G bioethanol biorefinery plant. In addition, in-depth studies of novel and efficient conversion technologies (i.e. efficient pretreatment, enzymatic hydrolysis, fermentation, and separation methods), central and state-level policy (i.e. national policy on biofuels - 2018, national policy for management of crop residues etc.) and scheme supports (i.e. ban of burning of paddy straw, mandatory biofuels blend etc.), introduction of supporting services (biofuels' market subsidies, financial supports, tax, duty, levy incentives, lending facilities, carbon financing opportunities, investment facilities, biofuels marketing facilities etc.), development of infrastructure for biofuels, development of biofuels and biochemicals standards/certification schemes, institutional and governance arrangements, ensuring the roles of various stakeholders like private sector, non-governmental organizations, public agencies, and development of international cooperation (i.e. international expert, foreign funds) are vitally important, to aid in the commercialization of a RS-based bioethanol production in India. In the meantime, our study has drawn an empirical picture of the potential of SRS-based 2G bioethanol production and GHG emissions reduction in India's major rice producing states. This potential could be attractive for policy makers, investors, bioenergy research community, and other stakeholders—and may accelerate the development of commercial 2G bioethanol production from this abundant bio-resource in India and other rice producing countries in the near future.

Conclusions

The present study has estimated SRS and assessed the energy and

environmental impacts in terms of 2G bioethanol production, renewable electricity generation and GHG emissions reduction potential considering the major rice producing states of India. Nationally, an estimated amount of 168 MT gross RS is produced of which about 39 to 47 MT (23–28 %) of rice straw is available as surplus. West Bengal, Uttar Pradesh, Punjab, Andhra Pradesh, Odisha, Telangana, Chhattisgarh, Assam, and Tamil Nadu are the leading rice producing states in India. Large quantities of SRS are known to be available as unused virgin waste in states like Punjab, Andhra Pradesh, and Haryana. The SRS could be utilized as a great feedstock for bioethanol production. This resource not only offers bioethanol production, renewable electricity generation and GHG emissions reduction; it also prevents resource depletion, and improves environmental, economic, and social sustainability. The bioethanol production, surplus renewable electricity generation and GHG emissions reduction potential would be substantial, if RS is pre-processed using the SE pretreatment method (compared to the DA method). GHG emissions benefits could likewise be maximized if the generated renewable electricity replaces coal-driven grid electricity. Bioethanol is a 'drop-in' renewable fuel it can be used in the transport sector as an alternative to gasoline. However, the commercial production of 2G bioethanol from RS has not yet been developed in India, due to several factors including improper resources management, lack of adequate governmental policies supports, lack of efficient conversion technologies that must be overcome to make commercially RS-based bioethanol economically viable. Intensive R&D activities, governmental and public support, cooperation from relevant experts and private entrepreneurs are, therefore, of critical importance. Data on other externalities must also be quantified, prior to the establishment of a commercial RS-based bioethanol plant. These include trade-offs regarding the willingness or unwillingness of farmers to cultivate rice, straw generation, handling and consumption patterns, production of food versus energy issues, analysis of economic viability and social aspects. Therefore, further site-specific technoeconomic research is recommended.

Declaration of Competing Interest

The authors declare that they have no known competing financial interests or personal relationships that could have appeared to influence the work reported in this paper.

Acknowledgements

Financial support for the research study was received from CONVER-B, a joint (EU-India) R&D project under the INNO INDIGO partnership program, funded by the Academy of Finland (AKA Grant no. 311972). The Indian authors sincerely acknowledge the Department of Science & Technology (DST), Govt. of India for extending the financial support necessary for this collaborative research (Sanction Ref. DST/IMRCD/INNO-INDIGO/CONVER-B/2017). Authors sincerely express their gratitude to the anonymous reviewers for providing encouraging comments that were very useful in the betterment of the scientific merit of the present article.

References

- [1] Mustapha WF, Kirkerud JG, Bolkesjø TF, Trømborg E. Large-scale forest-based biofuels production : Impacts on the Nordic energy sector Balmorel. *Energy Convers Manage* 2019;187:93–102. <https://doi.org/10.1016/j.enconman.2019.03.016>.
- [2] Kashanian M, Pishvae MS, Sahebi H. Sustainable biomass portfolio sourcing plan using multi-stage stochastic programming. *Energy* 2020;204:117923. <https://doi.org/10.1016/j.energy.2020.117923>.
- [3] Melikoglu M, Turkmen B. Food waste to energy : Forecasting Turkey ' s bioethanol generation potential from wasted crops and cereals till 2030. *Sustainable Energy Technol Assess* 2019;36:100553. <https://doi.org/10.1016/j.seta.2019.100553>.
- [4] Ghosh S, Chowdhury R, Bhattacharya P. Sustainability of cereal straws for the fermentative production of second generation biofuels : A review of the efficiency and economics of biochemical pretreatment processes. *Appl Energy* 2017;198:284–98. <https://doi.org/10.1016/j.apenergy.2016.12.091>.
- [5] Yang M, Xu M, Nan Y, Kuittinen S, Kamrul Hassan Md, Vepsäläinen J, et al. Influence of size reduction treatments on sugar recovery from Norway spruce for butanol production. *Bioresour Technol* 2018;257:113–20. <https://doi.org/10.1016/j.biortech.2018.02.072>.
- [6] Brethauer S, Studer MH. Biochemical conversion processes of lignocellulosic biomass to fuels and chemicals - A review. *Chimia* 2015;69(10):572–81. <https://doi.org/10.2533/chimia.2015.572>.
- [7] Spatari S, Bagley DM, MacLean HL. Life cycle evaluation of emerging lignocellulosic ethanol conversion technologies. *Bioresour Technol* 2010;101(2):654–67. <https://doi.org/10.1016/j.biortech.2009.08.067>.
- [8] Hoque E, Rashid F, Aziz M. Gasification and Power Generation Characteristics of Rice Husk , Sawdust , and Coconut Shell Using a Fixed-Bed Downdraft Gasifier 2021:1–19.
- [9] Abdelhady S, Borello D, Shaban A. Techno-economic assessment of biomass power plant fed with rice straw : Sensitivity and parametric analysis of the performance and the LCOE Techno-economic assessment of biomass power plant fed with rice straw : Sensitivity and parametric analysis of the performance and the LCOE. *Renewable Energy* 2017;115:1026–34. <https://doi.org/10.1016/j.renene.2017.09.040>.
- [10] Darmawan A, Biddinika MK, Huda M, Tokimatsu K. Toward Sustainable Agricultural : Integrated System of Rice Processing and Electricity Generation 2018;70:1669–74. <https://doi.org/10.3303/CET1870279>.
- [11] Kung C, Zhang N. Renewable energy from pyrolysis using crops and agricultural residuals : An economic and environmental evaluation 2015;90:1532–44. <https://doi.org/10.1016/j.energy.2015.06.114>.
- [12] Ghosh S, Dutta S, Chowdhury R. Ameliorated hydrogen production through integrated dark-photo fermentation in a flat plate photobioreactor: Mathematical modelling and optimization of energy efficiency. *Energy Convers Manage* 2020;226:113549. <https://doi.org/10.1016/j.enconman.2020.113549>.
- [13] Ghosh S, Das S, Chowdhury R. Effect of pre-pyrolysis biotreatment of banana pseudo-stem (BPS) using synergistic microbial consortium : Role in deoxygenation and enhancement of yield of pyro-oil. *Energy Convers Manage* 2019;195:114–24. <https://doi.org/10.1016/j.enconman.2019.04.094>.
- [14] Chowdhury R, Ghosh S, Manna D, Das S, Dutta S, Kleinstuber S, et al. Hybridization of sugar-carboxylate-syngas platforms for the production of bio-alcohols from lignocellulosic biomass (LCB) – A state-of-the-art review and recommendations. *Energy Convers Manage* 2019;200:112111. <https://doi.org/10.1016/j.enconman.2019.112111>.
- [15] Hiloidhari M, Das D, Baruah DC. Bioenergy potential from crop residue biomass in India. *Renew Sustain Energy Rev* 2014;32:504–12. <https://doi.org/10.1016/j.rser.2014.01.025>.
- [16] Ravindranath NH, Sita Lakshmi C, Manuvie R, Balachandra P. Biofuel production and implications for land use, food production and environment in India. *Energy Policy* 2011;39(10):5737–45. <https://doi.org/10.1016/j.enpol.2010.07.044>.
- [17] Das S. The National Policy of biofuels of India – A perspective. *Energy Policy* 2020;143:111595. <https://doi.org/10.1016/j.enpol.2020.111595>.
- [18] Saravanan AP, Mathimani T, Deviram G, Rajendran K, Pugazhendhi A. Biofuel policy in India: A review of policy barriers in sustainable marketing of biofuel. *J Cleaner Prod* 2018;193:734–47. <https://doi.org/10.1016/j.jclepro.2018.05.033>.
- [19] Parappurathu S. India ' s biofuels production programme : Need for prioritizing the alternative options. *Indian J Agric Sci* 2011;81:391–7.
- [20] Raj T, Kapoor M, Gaur R, Christopher J, Lamba B, Tuli DK, et al. Physical and chemical characterization of various indian agriculture residues for biofuels production. *Energy Fuels* 2015;29(5):3111–8. <https://doi.org/10.1021/ef5027373>.
- [21] Krishania M, Kumar V, Sangwan RS. Integrated approach for extraction of xylose, cellulose, lignin and silica from rice straw. *Bioresour Technology Reports* 2018;1:89–93. <https://doi.org/10.1016/j.biteb.2018.01.001>.
- [22] Takano M, Hoshino K. Bioethanol production from rice straw by simultaneous saccharification and fermentation with statistical optimized cellulase cocktail and fermenting fungus. *Bioresources and Bioprocessing* 2018;5(1). <https://doi.org/10.1186/s40643-018-0203-y>.
- [23] Kazi FK, Fortman JA, Anex RP, Hsu DD, Aden A, Dutta A, et al. Techno-economic comparison of process technologies for biochemical ethanol production from corn stover. *Fuel* 2010;89:S20–8. <https://doi.org/10.1016/j.fuel.2010.01.001>.
- [24] Kumar D, Murthy GS. Life cycle assessment of energy and GHG emissions during ethanol production from grass straws using various pretreatment processes. *Int J Life Cycle Assess* 2012;17(4):388–401. <https://doi.org/10.1007/s11367-011-0376-5>.
- [25] Abraham A, Mathew AK, Sindhu R, Pandey A, Binod P. Potential of rice straw for bio-refining: An overview. *Bioresour Technol* 2016;215:29–36. <https://doi.org/10.1016/j.biortech.2016.04.011>.
- [26] Silalertruksa T, Gheewala SH. A comparative LCA of rice straw utilization for fuels and fertilizer in Thailand. *Bioresour Technol* 2013;150:412–9. <https://doi.org/10.1016/j.biortech.2013.09.015>.
- [27] Singh R, Srivastava M, Shukla A. Environmental sustainability of bioethanol production from rice straw in India: A review. *Renew Sustain Energy Rev* 2016;54:202–16. <https://doi.org/10.1016/j.rser.2015.10.005>.
- [28] Jahnavi G, Prashanthi GS, Sravanthi K, Rao LV. Status of availability of lignocellulosic feed stocks in India: Biotechnological strategies involved in the production of Bioethanol. *Renew Sustain Energy Rev* 2017;73:798–820. <https://doi.org/10.1016/j.rser.2017.02.018>.
- [29] Soam S, Kapoor M, Kumar R, Borjesson P, Gupta RP, Tuli DK. Global warming potential and energy analysis of second generation ethanol production from rice



- straw in India. *Appl Energy* 2016;184:353–64. <https://doi.org/10.1016/j.apenergy.2016.10.034>.
- [30] Singh A, Basak P. Economic and environmental evaluation of rice straw processing technologies for energy generation: A case study of Punjab, India. *J Cleaner Product* 2019;212:343–52. <https://doi.org/10.1016/j.jclepro.2018.12.033>.
- [31] Govt. of India M of A & FW. Agricultural Statistics at a glance 2019. Minist Agric Farmers Welf Dep - Dep Agric Coop Farmers Welf Dir Econ Stat. <<https://eands.dacnet.nic.in/PDF/At%20a%20Glance%202019%20Eng.pdf>> [retrieved at 20.08.20].
- [32] Tunio A, Magsi H, Solangi MA, Agri IJ, Agri R. Analyses of growth trends and production forecast of cash crops in Pakistan. *Int J Agri Agri Res* 2016;9: 2223–7054.
- [33] Hassan MK, Pelkonen P, Pappinen A. Assessment of Bioenergy Potential from Major Crop Residues and Wood Fuels in Bangladesh. *J Basic Appl Sci Res* 2011;1: 1039–51.
- [34] Chowdhury R, Ghosh S, Debnath B, Manna D. Indian agro-wastes for 2G biorefineries: Strategic decision on conversion processes. *Green Energy and Technology* 2018:353–73. https://doi.org/10.1007/978-981-10-7188-1_16.
- [35] Hassan MK. Supply and demand of biomass based energy: rural people's perspectives in Bangladesh. vol. 2015. 2015. <https://doi.org/10.14214/df.210>.
- [36] Cardoen D, Joshi P, Diels L, Sarma PM, Pant D. Agriculture biomass in India: Part 2. Post-harvest losses, cost and environmental impacts. *Resour Conserv Recycl* 2015; 101:143–53. <https://doi.org/10.1016/j.resconrec.2015.06.002>.
- [37] Hiloidhari M, Baruah DC. Rice straw residue biomass potential for decentralized electricity generation: A GIS based study in Lakhimpur district of Assam. *India. Energy for Sustainable Development* 2011;15(3):214–22. <https://doi.org/10.1016/j.esd.2011.05.004>.
- [38] Yadav GS, Lal R, Meena RS, Datta M, Babu S, Das A, et al. Energy budgeting for designing sustainable and environmentally clean/safer cropping systems for rainfed rice fallow lands in India. *J Cleaner Prod* 2017;158:29–37. <https://doi.org/10.1016/j.jclepro.2017.04.170>.
- [39] Kaur A. Crop Residue in Punjab Agriculture-Status and Constraints. *Journal of Krishi Vigyan* 2017;5:22. <https://doi.org/10.5958/2349-4433.2017.00005.8>.
- [40] Gadde B, Menke C, Wassmann R. Rice straw as a renewable energy source in India, Thailand, and the Philippines: Overall potential and limitations for energy contribution and greenhouse gas mitigation. *Biomass Bioenergy* 2009;33(11): 1532–46. <https://doi.org/10.1016/j.biombioe.2009.07.018>.
- [41] Anshar M, Ani FN, Kader AS. Potential surplus of rice straw as a source of energy for rural communities in Indonesia. *Applied Mech Mater* 2014;695:806–10. <https://doi.org/10.4028/www.scientific.net/amm.695.806>.
- [42] Piotrowski S, Carus M, Essel R. Sustainable biomass supply and demand: A scenario analysis. *Open Agriculture* 2016;1:18–28. <https://doi.org/10.1515/opag-2016-0003>.
- [43] Mosier N, Wyman C, Dale B, Elander R, Lee YY, Holtzapple M, et al. Features of promising technologies for pretreatment of lignocellulosic biomass. *Bioresour Technol* 2005;96:673–86. <https://doi.org/10.1016/j.biortech.2004.06.025>.
- [44] Lee C, Zheng Y, VanderGheynst JS. Effects of pretreatment conditions and post-pretreatment washing on ethanol production from dilute acid pretreated rice straw. *Biosyst Eng* 2015;137:36–42. <https://doi.org/10.1016/j.biosystemseng.2015.07.001>.
- [45] Sharma S, Kumar R, Gaur R, Agrawal R, Gupta RP, Tuli DK, et al. Pilot scale study on steam explosion and mass balance for higher sugar recovery from rice straw. *Bioresour Technol* 2015;175:350–7. <https://doi.org/10.1016/j.biortech.2014.10.112>.
- [46] Staffel I. The Energy and Fuel Data Sheet 2011. University of Birmingham, UK. <https://www.academia.edu/1073990/The_Energy_and_Fuel_Data_Sheet> [retrieved at 18.09.20].
- [47] Kazi FK, Fortman J, Anex R. Techno-economic analysis of biochemical scenarios for production of cellulosic ethanol. NREL 2010.
- [48] IPCC. 2006 IPCC Guidelines for National Greenhouse Inventories – A primer, Prepared by the National Greenhouse Gas Inventories Programme, Eggleston H.S., Miwa K., Srivastava N. and Tanabe K. Iges 2006:20.
- [49] Koga N, Tajima R. Assessing energy efficiencies and greenhouse gas emissions under bioethanol-oriented paddy rice production in northern Japan. *J Environ Manage* 2011;92(3):967–73. <https://doi.org/10.1016/j.jenvman.2010.11.008>.
- [50] Yamashita M, Aimoto H. Can bio-ethanol be regarded as carbon neutral? Assessment of the effect of reducing oil use. *Resour Environ* 2012;2(5):240–7. <https://doi.org/10.5923/j.re.20120205.07>.
- [51] Goyal SK, Singh JP. Demand versus supply of foodgrains in india: implications to food security. 13th Int Farm Manag Congr 2002:1–21.
- [52] Gupta R, Mishra A. Climate change induced impact and uncertainty of rice yield of agro-ecological zones of India. *Agric Syst* 2019;173:1–11. <https://doi.org/10.1016/j.agry.2019.01.009>.
- [53] Bhuvaneshwari S, Hettiarachchi H, Meegoda J. Crop residue burning in India: Policy challenges and potential solutions. *Int J Environ Res Public Health* 2019;16 (5):832. <https://doi.org/10.3390/ijerph16050832>.
- [54] Lohan SK, Jat HS, Yadav AK, Sidhu HS, Jat ML, Choudhary M, et al. Burning issues of paddy residue management in north-west states of India. *Renew Sustain Energy Rev* 2018;81:693–706. <https://doi.org/10.1016/j.rser.2017.08.057>.
- [55] Jain N, Bhatia A, Pathak H. Emission of air pollutants from crop residue burning in India. *Aerosol Air Qual Res* 2014;14(1):422–30. <https://doi.org/10.4209/aaqr.2013.01.0031>.
- [56] Erenstein O. Cropping systems and crop residue management in the Trans-Gangetic Plains: Issues and challenges for conservation agriculture from village surveys. *Agric Syst* 2011;104(1):54–62. <https://doi.org/10.1016/j.agry.2010.09.005>.
- [57] Central Rice Research Institute. Vision 2030. Indian Council of Agricultural Research, Cuttack 753 006, India; 2011. <http://www.crrri.nic.in/crrri_vision2030_2011.pdf> [retrieved at 18.11.19].
- [58] Karimi K, Kheradmandinia S, Taherzadeh MJ. Conversion of rice straw to sugars by dilute-acid hydrolysis. *Biomass Bioenergy* 2006;30(3):247–53. <https://doi.org/10.1016/j.biombioe.2005.11.015>.
- [59] Zhu S, Huang W, Huang W, Wang K, Chen Q, Wu Y. Pretreatment of rice straw for ethanol production by a two-step process using dilute sulfuric acid and sulfomethylation reagent. *Appl Energy* 2015;154:190–6. <https://doi.org/10.1016/j.apenergy.2015.05.008>.
- [60] Sukumaran RK, Surender VJ, Sindhu R, Binod P, Janu KU, Sajna KV, et al. Lignocellulosic ethanol in India: Prospects, challenges and feedstock availability. *Bioresour Technol* 2010;101(13):4826–33. <https://doi.org/10.1016/j.biortech.2009.11.049>.
- [61] Kami Delivand M, Barz M, Gheewala SH, Sajjakulnukit B. Environmental and socio-economic feasibility assessment of rice straw conversion to power and ethanol in Thailand. *J Cleaner Prod* 2012;37:29–41. <https://doi.org/10.1016/j.jclepro.2012.06.005>.
- [62] Nakamura Y, Sawada T, Inoue E. Enhanced ethanol production from enzymatically treated steam-exploded rice straw using extractive fermentation. *J Chem Technol Biotechnol* 2001;76(8):879–84. [https://doi.org/10.1002/\(ISSN\)1097-466010.1002/jctb.v76:810.1002/jctb.465](https://doi.org/10.1002/(ISSN)1097-466010.1002/jctb.v76:810.1002/jctb.465).
- [63] Banoth C, Sunkar B, Tondamanati PR, Bhukya B. Improved physicochemical pretreatment and enzymatic hydrolysis of rice straw for bioethanol production by yeast fermentation. 3. *Biotech* 2017;7:1–11. <https://doi.org/10.1007/s13205-017-0980-6>.
- [64] Pérez J, Muñoz-Dorado J, de la Rubia T, Martínez J. Biodegradation and biological treatments of cellulose, hemicellulose and lignin: An overview. *Int Microbiol* 2002; 5(2):53–63. <https://doi.org/10.1007/s10123-002-0062-3>.
- [65] Hendriks ATWM, Zeeman G. Pretreatments to enhance the digestibility of lignocellulosic biomass. *Bioresour Technol* 2009;100(1):10–8. <https://doi.org/10.1016/j.biortech.2008.05.027>.
- [66] Tye YY, Lee KT, Wan Abdullah WN, Leh CP. The world availability of non-wood lignocellulosic biomass for the production of cellulosic ethanol and potential pretreatments for the enhancement of enzymatic saccharification. *Renew Sustain Energy Rev* 2016;60:155–72. <https://doi.org/10.1016/j.rser.2016.01.072>.
- [67] Kim SB, Lee SJ, Jang EJ, Han SO, Park C, Kim SW. Sugar recovery from rice straw by dilute acid pretreatment. *J Ind Eng Chem* 2012;18(1):183–7. <https://doi.org/10.1016/j.jiec.2011.11.016>.
- [68] Chen WH, Tsai CC, Lin CF, Tsai PY, Hwang WS. Pilot-scale study on the acid-catalyzed steam explosion of rice straw using a continuous pretreatment system. *Bioresour Technol* 2013;128:297–304. <https://doi.org/10.1016/j.biortech.2012.10.111>.
- [69] Saga K, Imou K, Yokoyama S, Minowa T. Net energy analysis of bioethanol production system from high-yield rice plant in Japan. *Appl Energy* 2010;87(7): 2164–8. <https://doi.org/10.1016/j.apenergy.2009.12.014>.
- [70] Prasad A, Sotenko M, Blenkinsopp T, Coles SR. Life cycle assessment of lignocellulosic biomass pretreatment methods in biofuel production. *Int J Life Cycle Assess* 2016;21(1):44–50. <https://doi.org/10.1007/s11367-015-0985-5>.
- [71] Roy P, Tokuyasu K, Orikasa T, Nakamura N, Shiina T. A techno-economic and environmental evaluation of the life cycle of bioethanol produced from rice straw by RT-CaCCO process. *Biomass Bioenergy* 2012;37:188–95. <https://doi.org/10.1016/j.biombioe.2011.12.013>.
- [72] Balan V. Review of US and EU initiatives toward development , demonstration , and commercialization of lignocellulosic biofuels 2013. <https://doi.org/10.1002/bbb>.
- [73] United Nations. Second Generation Biofuel Markes: Sate of Play, Trade and Developing Countries Perspectives. 2016. <https://unctad.org/en/PublicationsLibrary/ditcted2015d8_en.pdf> [retrieved at 22.09.20].
- [74] Passoth V, Sandgren M. Biofuel production from straw hydrolysates: current achievements and perspectives. *Appl Microbiol Biotechnol* 2019;103(13):5105–16. <https://doi.org/10.1007/s00253-019-09863-3>.
- [75] Ren J, Yu P, Xu X. Straw utilization in China-status and recommendations. *Sustainability (Switzerland)* 2019;11:1–17. <https://doi.org/10.3390/su11061762>.


Energy and environmental performance of a near-zero-effluent rice straw to butanol production plant

Sambit Dutta, Shiladitya Ghosh, Dinabandhu Manna & Ranjana Chowdhury


To cite this article: Sambit Dutta, Shiladitya Ghosh, Dinabandhu Manna & Ranjana Chowdhury (2021) Energy and environmental performance of a near-zero-effluent rice straw to butanol production plant, *Indian Chemical Engineer*, 63:2, 139-151, DOI: [10.1080/00194506.2020.1831406](https://doi.org/10.1080/00194506.2020.1831406)


To link to this article: <https://doi.org/10.1080/00194506.2020.1831406>

 View supplementary material 

 Published online: 13 Oct 2020.

 Submit your article to this journal 

 Article views: 153

 View related articles 

 View Crossmark data 



Energy and environmental performance of a near-zero-effluent rice straw to butanol production plant

Sambit Dutta, Shiladitya Ghosh, Dinabandhu Manna and Ranjana Chowdhury

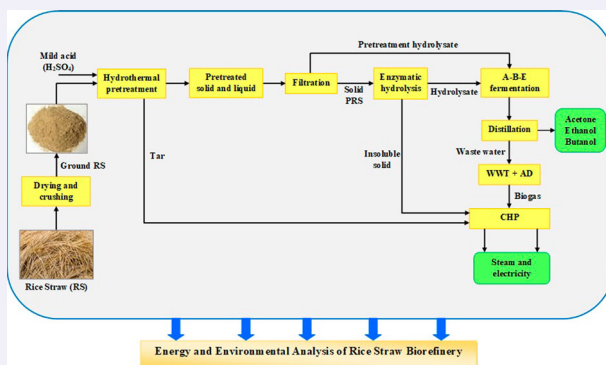
Chemical Engineering Department, Jadavpur University, Kolkata, India

ABSTRACT

Present article focuses on the energy and environmental performance of a rice straw (RS) biorefinery producing bio-butanol as the main product, ethanol and acetone as the by-products and combined heat and power. The analysis highlights the strategic usage of RS-derived glucose and xylose as primary substrates for biobutanol production. The principle of utilization of total carbon and the fulfillment of the criterion of zero-waste management has been followed along with the generation of in-house energy to offset the energy expenditure and reduce CO₂ emission. The overall yields of butanol, ethanol and acetone are 28.53kg, 0.84kg and 6.61kg respectively from 100kg RS. By performing energy analysis in this system for 100kg RS, energy content of lignin, extractives and biogas introduced to CHP have been estimated to be 674.78MJ. Net energy input to the steam turbine of the CHP is 539.83MJ and the outputs of electricity and heat energy are 130MJ and 194MJ, respectively. While the energy efficiency of CHP is 87%, the overall efficiency of the biorefinery through generation of alcohol/solvents and recovery of waste energy in the CHP is 68.2%. Due to the substitution of gasoline by butanol and through electricity generation, reduction of CO₂ emission by 36.14kg is possible.

KEYWORDS

Lignocellulosic biomass; biobutanol; rice straw; biorefinery; energy and environmental analysis



1. Introduction

Surge in the consumption of non-renewable energy sources for functioning of various engines has led to an overexploitation of fossil fuels [1]. It led to increasing demands for energy sources for industry and motorised vehicles as we move forward in the twenty-first century. Presently, fossil

CONTACT Ranjana Chowdhury ✉ ranjana.juchem@gmail.com 📠 Chemical Engineering Department, Jadavpur University, Kolkata 700032, India

Supplemental data for this article can be accessed <https://doi.org/10.1080/00194506.2020.1831406>

© 2020 Indian Institute of Chemical Engineers

fuels contribute to 80% of global primary energy source consumed by the world, of which 58% is consumed by the transport sector [2]. Although fossil fuels are used as the efficient energy source around the globe, they are the chief root causes for the release of greenhouse gases during the combustion of their hydrocarbon compounds. To reduce the carbon dioxide (CO₂) emission which poses a threat to the environment, we must explore alternative sources of energy mainly for motorised vehicles. Due to their renewability, energy efficiency and producing acceptable quality exhaust gas, biofuels can replace fossil fuels. Although the production of bioethanol from lignocellulosic biomass is being focused by scientists for years, the disadvantages of ethanol as drop-in fuel is also being highlighted by many researchers. Highly hygroscopic nature, low calorific value and high volatility of ethanol have been identified as some of the detrimental properties for blending with gasoline [3–6]. However, biobutanol, another second-generation (2G) alcohol, having a higher heating value, low volatility and low moisture absorptivity is much attractive as a drop-in fuel [4]. It is mainly derived from the fermentation of simple sugars present in organic feedstocks or processed lignocellulose [7]. The most common method of producing biobutanol is the fermentation of simple sugars in biomass feedstock such as food crops, agricultural waste, municipal waste, industrial waste, waste cooking oils and animal fats [7]. The dilute mineral acid pre-treatment and that followed by enzymatic hydrolysis releasing, mainly xylose and glucose, respectively, are the pre-processes for butanol fermentation [8]. *Clostridium acetobutylicum* and *Clostridium beijerinckii* are the main microorganisms those use glucose and xylose to produce biobutanol [9]. Unlike *S. cerevisiae* used for bioethanol production, both pentose and hexose sugars are proficiently metabolised by *Clostridium* sp [9]. Although biobutanol yield is lower by 20% than bioethanol, its energy content is 32% higher than the latter. Utilising glucose and xylose either directly or from hydrolysates of lignocellulosic feedstocks, biobutanol yields through batch and continuous fermentation processes are 0.17–0.49 g/g [10,11] and 0.40–0.52 g/g [12,13], respectively. Rice straw (RS) is a relatively cheap and the most abundant agricultural waste in India [14]. The contents of cellulose and hemicellulose of rice straw are also favourable for extraction of fermentable sugar for 2G bio alcohol production. In spite of this, field firing of such agricultural wastes very often creates pollution. To mitigate these issues, RS can be utilised for biobutanol production. For the planning of RS-based large-scale butanol plants and its integration in 2G-biorefineries, an energy and environmental impact assessment is necessary. Although reports are available on the assessment of feasibility of using lignocellulosic waste-to-ethanol processes in biorefineries through energy and environmental analysis, such studies for bio-butanol are rare [15]. In a pioneering study, the effects of composition of different lignocellulosic wastes on bioethanol yield and economic and environmental performances in an integrated biorefinery co-producing combined heat and power (CHP) have been made through a comprehensive process, economic and life cycle assessment modelling [15].

The main focus of this article is to perform an energy and environmental analysis of a 100 kg RS-to-biobutanol-based 2G-biorefinery, producing butanol as the main product, ethanol and acetone as the by-products and combined heat and power utilising all waste streams of the process as energy outputs. Basic principle followed in the case of ethanol production has been followed in this analysis [15]. The other relevant data, including enzymatic hydrolysis, fermentative production of butanol, distillation, generation of heat and power, etc., have been obtained from the literature.

2. Materials and methods

2.1. Rice straw

Rice straw, obtained from a local farm house, was used as waste lignocellulosic biomass feedstock for the production of fermentable sugars in the present RS-to-biobutanol-based 2G-biorefinery.

2.2. Analytical methods

Composition of structural carbohydrates and lignin in Indian rice straw was determined using NREL protocol [16]. The results of the analysis were supplied by the University of Eastern Finland that had generated the data following the protocols described in the Technical Report of National Renewable Energy Laboratory (NREL/TP-510-42618; Revised August 2012) on 'Determination of Structural Carbohydrates and Lignin in Biomass: Laboratory Analytical Procedure (LAP) Issue Date: April 2008 Revision Date: August 2012 (Version 08-03-2012)' [16–18]. The composition has been reported on dry basis. The moisture content and percentage of acid insoluble ash in the rice straw were also obtained from the method.

2.3. Method for energy and environmental performance assessment

Energy and environmental performance assessment of rice straw to biobutanol biorefinery has been estimated based on the generic scheme represented in Figure 1. The sequences of processes and unit operations are (1) drying, (2) crushing, (3) dilute mineral acid pre-treatment, (4) separation and detoxification of solid pre-treated RS and liquid hydrolysate of pre-treatment, (5) enzymatic hydrolysis of pre-treated solid, (6) separation of lignin and enzymatic hydrolysate, (7) simultaneous fermentation of hydrolysates of pre-treatment and enzymatic hydrolysis, (8) recovery of butanol through distillation, (9) energy recovery from lignin stream using co-generation of heat and power, (10) anaerobic digestion of waste stream from distillation unit for generation of biogas and utilisation in CHP unit, as shown in Figure 1. Figure 1 has been constructed using the Aspen plus® V11 software.

3. Theoretical analysis

Assumptions

1. The behaviour of constituent carbohydrate polymers (glucan, xylan, arabinan, etc.) and lignin towards different pre-treatment processes (acid and enzymatic hydrolysis) remain the same irrespective of the lignocellulosic biomass if the processes are conducted under identical conditions. The consideration has been made by Sadhukhan et al., during their analysis [15].
2. The behaviour of microorganisms regarding product and biomass yields during the growth on hexose (glucose) and pentose (xylose, arabinose etc.) sugars remains the same irrespective of the source of sugars (conventional sugar cane, beetroot or non-conventional lignocellulosic wastes).
3. The microorganism (*C. acetobutylicum*) can only convert glucose and xylose and cannot convert arabinose.
4. Water used in the overall process does not affect the mass balance of components containing carbon and hence water balance is avoided.
5. The CHP plant is based on steam turbine in which electrical energy to heat energy output ratio (α) is 1.49 and the electricity generation efficiency is 35% [19,20].

In this work, biochemical conversions used by NREL [21] have been taken as the basis for energy and environmental analysis. The mild acid pre-treatment data of RS, based on NREL protocol, with a solid loading of 30% (w/w) and 1.1% (w/w) sulphuric acid loading at a temperature of 158°C and a pressure of 5.57 bar for 5 mins, were considered [21]. Accordingly, conversions of glucan (cellulose) to glucose, xylan to xylose and arabinan to arabinose through pre-treatment have been considered to be 9.9% (w/w) and 90% (w/w) for the other two carbohydrate polymers, respectively. During acid hydrolysis, 5% (w/w) of each of xylan and arabinan is converted to furfural and 0.3% of glucan is converted to 5-HMF. Detoxification and neutralisation

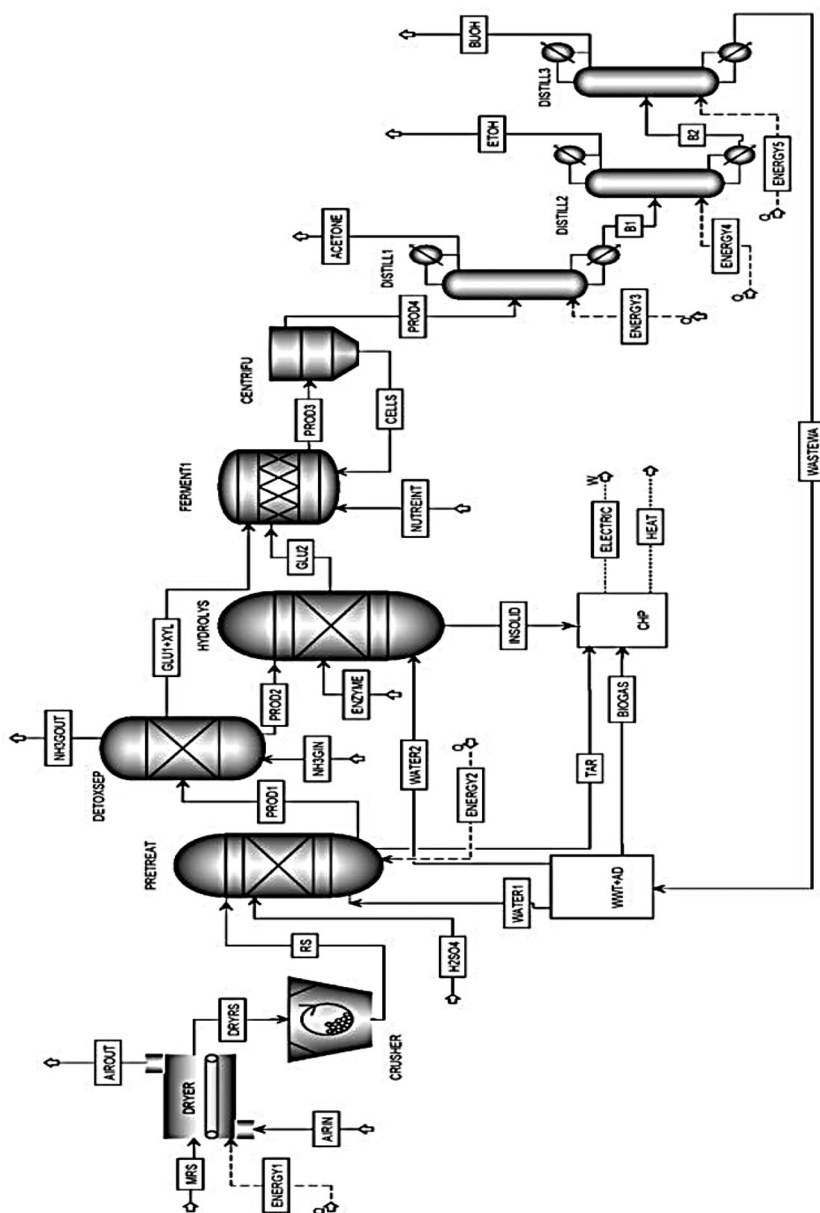
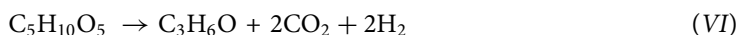
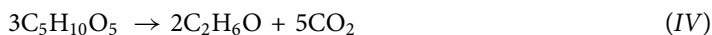
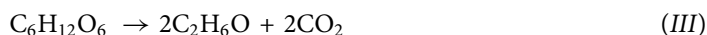
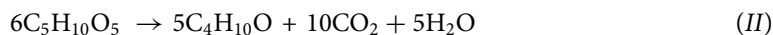
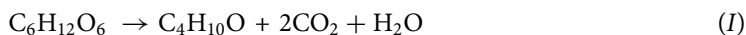


Figure 1. Major processes, material streams and unit operations of RS-to-biobutanol; PRE-TREAT: Pre-treatment; DETOXSEP: Detoxification and separation; HYDROLYS: Enzymatic hydrolysis; FERMENT1: Fermentation; CENTRIFU: Centrifugation unit; DISTILL: Distillation tower; CHP: Combined heat and power; WWT + AD: Waste water treatment plant with anaerobic digestion; MRS: Moist rice straw; RS: Rice straw; PROD1: Pre-treated RS; PROD2: Detoxified pre-treated RS; INSOLID: Insoluble solids; GLU1 and GLU2: Glucose; XYL: Xylose; PROD3: Fermentation products; PROD4: Cells free fermentation products; H2SO4: Sulphuric acid; NH3G: Ammonia gas CELLS: Microbial cells; ACETONE: Acetone; ETOH: Ethanol; BUOH: Biobutanol; B1,2: Bottoms; WASTEWA: Wastewater; ENERGY1,2,3,4,5: Energy Input Streams.

of pre-treatment products by ammonia gas result in losses of xylose and glucose of 1% and 0%, respectively [15]. Enzymatic hydrolysis of mild acid pre-treated RS with a solid loading of 20% (w/w) and cellulase loading of 20 mg protein/g cellulose at a temperature of 48°C for 84 h was considered following NREL protocol [21]. In enzymatic hydrolysis unit, conversion of cellulose

to glucose is 90% as per NREL. Biobutanol yields from glucose and xylose using *C. acetobutylicum* are 0.196 and 0.213 g/g, respectively [22]. While yields of ethanol and acetone from glucose are 0.024 and 0.045 g/g, respectively those from xylose are 0.0236 and 0.0566 g/g, respectively with respect to sugar utilised by microorganism [22].

The theoretical yields (Y_{i-Xy}^{TH} or Y_{i-Glc}^{TH}) of butanol, acetone and ethanol with respect to xylose and glucose in the fermentation unit have been calculated using the following reactions [23]:



The actual values of yields (Y_{i-Xy}^{ACT} or Y_{i-Glc}^{ACT}) have been obtained from a reported research study on butanol production [24]. Fractional theoretical conversions have been defined as follows:

$$f_{i-xy} = \frac{Y_{i-Xy}^{ACT}}{Y_{i-Xy}^{TH}} \quad (A)$$

$$f_{i-Glc} = \frac{Y_{i-Glc}^{ACT}}{Y_{i-Glc}^{TH}} \quad (B)$$

where i = butanol (bu) or ethanol (eth) or acetone (ace); $-Xy$ = with respect to xylose; $-Glc$ = with respect to glucose.

According to the consideration of the present model, the liquid effluent from the fermenter enters the centrifuge, the sedimented cells are recycled to the fermenter and the liquid, containing acetone, butanol and ethanol, enters the distillation unit. In accordance with NREL, losses in the fermentation unit of 3%, and hence an output of 97% of the produced butanol, ethanol and acetone have been considered [21]. Solvent recovery of 99.5% has been considered according to Wu et al. [25] assuming the same operational conditions of the distillation unit to be considered as per characteristics of butanol, ethanol and acetone. Tar constituted of all furfural and 5-HMF generated in acidic pre-treatment process and all lignin remaining as a solid residue of enzymatic hydrolysis process is fed to CHP unit for energy generation. The bottoms of distillation unit along with all unconverted feedstock components except tar and lignin are fed to an anaerobic digestion unit via a waste water treatment plant. Biogas generated is also fed to the CHP unit for energy generation.

3.1. Energy efficiency analysis

Basis of calculation: 100 kg dry Rice straw (25 wt% moisture)

Mass of butanol (W_{butanol}), ethanol (W_{ethanol}) and acetone (W_{acetone}) have been calculated using Equations (1)–(3), respectively:

$$W_{\text{butanol}} = R_{\text{dbu}} \times (1 - L_p^{\text{Ferm}}) [(W_{\text{xylan}} (X_{\text{Xyn-Xy}}^{\text{APT}} (1 - L_{\text{Xy}}^{\text{DTX}}) Y_{\text{bu-Xy}}^{\text{TH}} \times f_{\text{bu-Xy}}) + (W_{\text{glucan}} (X_{\text{Gln-Glc}}^{\text{APT}} + (1 - X_{\text{Gln-Glc}}^{\text{APT}}) X_{\text{Gln-Glc}}^{\text{EH}}) Y_{\text{bu-Glc}}^{\text{TH}} \times f_{\text{bu-Glc}})]; \quad (1)$$

$$W_{\text{ethanol}} = R_{\text{deth}} \times (1 - L_p^{\text{Ferm}}) [(W_{\text{xylan}} (X_{\text{Xyn-Xy}}^{\text{APT}} (1 - L_{\text{Xy}}^{\text{DTX}}) Y_{\text{eth-Xy}}^{\text{TH}} \times f_{\text{eth-Xy}}) + (W_{\text{glucan}} (X_{\text{Gln-Glc}}^{\text{APT}} + (1 - X_{\text{Gln-Glc}}^{\text{APT}}) X_{\text{Gln-Glc}}^{\text{EH}}) Y_{\text{eth-Glc}}^{\text{TH}} \times f_{\text{eth-Glc}})]; \quad (2)$$

$$W_{\text{acetone}} = R_{\text{dbu}} \times (1 - L_p^{\text{Ferm}}) [(W_{\text{xylan}} (X_{\text{Xyn-Xy}}^{\text{APT}} (1 - L_{\text{Xy}}^{\text{DTX}}) Y_{\text{ace-Xy}}^{\text{TH}} \times f_{\text{ace-Xy}}) + (W_{\text{glucan}} (X_{\text{Gln-Glc}}^{\text{APT}} + (1 - X_{\text{Gln-Glc}}^{\text{APT}}) X_{\text{Gln-Glc}}^{\text{EH}}) Y_{\text{ace-Glc}}^{\text{TH}} \times f_{\text{ace-Glc}})]; \quad (3)$$

$$W_{\text{arabinose}} = W_{\text{arabinan}} * X_{\text{Arn-Ara}}^{\text{APT}} \quad (4)$$

From the mass balance, the total organic mass fed to anaerobic digestion (F_{AD}) is calculated by equation (5), where W_i is the percentage mass composition of component i in native RS.

$$\begin{aligned} F_{\text{AD}} = & 100 - W_{\text{moisture}} - W_{\text{ash}} - W_{\text{Klassonlignin}} - W_{\text{uac}} - W_{\text{butanol}} - W_{\text{ethanol}} \\ & - W_{\text{acetone}} - ((1 - X_{\text{xyn-fur}}^{\text{APT}} + X_{\text{Xyn-Xy}}^{\text{APT}}) \times W_{\text{xylan}}) - ((1 - X_{\text{xyn-fur}}^{\text{APT}} + X_{\text{Arn-Ara}}^{\text{APT}}) \times W_{\text{arabinan}}) \\ & - ((1 - X_{\text{Gln-hmf}}^{\text{APT}} + X_{\text{Gln-Glc}}^{\text{APT}}) \times (1 - X_{\text{Gln-Glc}}^{\text{EH}}) \times W_{\text{glucan}}) - Y_{\text{tar}} \end{aligned} \quad (5)$$

Yield of tar (W_{tar}) via 5-hydroxymethylfurfural (HMF) and furfural produced in pre-treatment stage from disintegration of xylan, and glucan corresponds to Equation (6):

$$Y_{\text{tar}} = (X_{\text{xyn-fur}}^{\text{APT}} \times W_{\text{xylan}}) + (X_{\text{xyn-fur}}^{\text{APT}} \times W_{\text{arabinan}}) + (X_{\text{Gln-hmf}}^{\text{APT}} \times W_{\text{glucan}}) \quad (6)$$

Biogas yield from the anaerobic digestion unit is estimated to be 30% [26] and thus calculated in Equation (7):

$$Y_{\text{biogas}} = Y_{\text{AD}}^{\text{bg}} \times F_{\text{AD}} \quad (7)$$

Lignin, unspent fraction of cellulose and hemicellulose, biogas and tar are fed to the CHP unit. Thus, total energy content of the waste stream per 100 kg of RS fed is calculated using Equation (8):

$$\begin{aligned} E_{\text{CHP}_{\text{in}}} = & CV_{\text{biogas}} \times Y_{\text{biogas}} + CV_{\text{lignin}} \times (W_{\text{Klassonlignin}} + W_{\text{uac}}) + CV_{\text{cellulose}} \times W_{\text{clef}} \\ & + CV_{\text{hemicellulose}} \times W_{\text{hclef}} + CV_{\text{tar}} \times Y_{\text{tar}} \end{aligned} \quad (8)$$

Energy content of steam generated for the utilisation in the steam turbine of CHP and in-house consumption for the production of butanol and the by-products (ethanol and acetone) is calculated from Equation (9) in MJ per 100 kg of RS fed by assuming an energy efficiency of the boiler to be 80% [15,27].

$$E_{\text{steam}} = 0.8 \times E_{\text{CHP}_{\text{in}}} \quad (9)$$

Net energy consumed for the total solvent i.e. acetone, butanol and ethanol (A-B-E) is estimated to be 4.68 MJ per kg of solvent production. Therefore, the in-house energy (E_{IH}) consumption is as follows:

$$E_{\text{IH}} = (4.68 \times (W_{\text{biobutanol}} + W_{\text{ethanol}} + W_{\text{acetone}})) \quad (10)$$

Energy input to steam turbine of CHP

$$E_{ST} = E_{\text{steam}} - E_{IH} \quad (11)$$

According to assumption 5, the electrical efficiency of CHP is 35%. Therefore, the net energy output can be assessed in MJ per 100 kg of RS fed by Equation (12):

$$E_E = 0.35 \times E_{ST} \quad (12)$$

Again, according to assumption 5, the ratio of output of heat to electrical energy output (α) of the CHP is 1.49. Therefore,

$$\alpha = \frac{E_{HE}}{E_{EE}} = 1.49 \quad (13)$$

Hence, the thermal energy output is

$$E_H = 1.49 \times E_E \quad (14)$$

The efficiency (η_{CHP}) of the CHP is

$$\eta_{CHP} = \frac{E_E + E_H}{E_{ST}} \quad (15)$$

The overall energy efficiency of the bio-refinery is

$$\eta = \frac{(W_{\text{but}} \times CV_{\text{but}}) + (W_{\text{eth}} \times CV_{\text{eth}}) + (W_{\text{ace}} \times CV_{\text{ace}}) + E_E + E_H}{100 \times CV_{RS}} \quad (16)$$

Using the equations 1–16, material and energy balance calculations were carried out using the MATLAB (version R2018a) software and the data provided in Table 1. Details of the sample calculations are provided in the supplementary material for clarification Table S1.

3.2. Environmental impact analysis

By comparing the heating value of biobutanol (23.652MJ/L) with that of gasoline (35.724MJ/L), the capability of substitution of gasoline by biobutanol, expressed in % (v/v), can be determined as follows:

$$\% \text{ substitution } \left(\frac{v}{v} \right) = \frac{\text{Heating value of biobutanol} \left(23.652 \frac{\text{MJ}}{\text{L}} \right)}{\text{Heating value of gasoline} \left(35.724 \frac{\text{MJ}}{\text{L}} \right)} * 100 \quad (17)$$

The value of CO₂ factor (F_{CO_2}) i.e. kg CO₂ emitted/MJ of energy generated in an Indian coal-based power plant, has been taken from the literature [31]. The electricity generated in the butanol plant avoids the usage of the same quantity of grid energy supposed to be generated in coal-based power plant, particularly in India. Therefore, reduction in CO₂ emission (R_{CO_2}) as a result of electricity generated from this biorefinery can be estimated using the following equation:

$$R_{CO_2} = E_E(\text{MJ}) \times F_{CO_2} \quad (18)$$

$F_{CO_2} = 0.278 \text{ kg CO}_2/\text{MJ electricity produced}$ (or, 1 kg CO₂/kWh electricity produced)

Table 1. Yield factors and parameters for energy efficiency analysis.

Composition of Rice Straw Mass Fraction (%) [This study]								
W _{glucan}	W _{xylan}	W _{arabinan}	W _{klasson lignin}	W _{acid soluble lignin}	W _{moisture}	W _{wash}		
38.2	17.5	3.2	14.3	2.5	0	24.3		
Heating Values (MJ/kg) [15,28,29,30]								
CV _{RS}	CV _{lignin}	CV _{acetone}	CV _{butanol}	CV _{ethanol}	CV _{biogas}	CV _{tar}	CV _{cellulose}	CV _{hemicellulose}
22.33	23.5	29.6	34.4	26.7	23	36	27.5	26.5
Conversion during Pre-treatment [21]								
$X_{Xyn-Ara}^{APT}$				$X_{Gln-Glc}^{APT}$		$X_{Arn-Ara}^{APT}$		
0.9				0.099		0.9		
Formation of Tar during Pre-treatment [15]								
$X_{xyn-fur}^{APT}$				$X_{ara-fur}^{APT}$		$X_{Gln-hmf}^{APT}$		
0.05				0.05		0.003		
Loss during detoxification [15]								
L_{xy}^{DTX}					L_{Ara}^{DTX}			
0.01					0.01			
Conversion of glucan to glucose by enzymatic hydrolysis [21]								
				$X_{Gln-Glc}^{EH}$				
				0.9				
Fermentation								
Conversion of xylose to butanol [23,24]								
γ_{bu-Xy}^{TH}				f_{bu-Xy}		γ_{bu-Xy}^{ACT}		
0.66				0.88		0.59		
Conversion of glucose to butanol [23,24]								
γ_{bu-Glc}^{TH}				f_{bu-Glc}		γ_{bu-Glc}^{ACT}		
0.66				0.88		0.58		
Conversion of xylose to acetone [23,24]								
γ_{ace-Xy}^{TH}				f_{ace-Xy}		γ_{ace-Xy}^{ACT}		
0.5				0.27		0.1361		
$\gamma_{ace-Glc}^{TH}$				$f_{ace-Glc}$		$\gamma_{ace-Glc}^{ACT}$		
0.6				0.227		0.1361		
Conversion of xylose to ethanol [23,24]								
γ_{eth-Xy}^{TH}				f_{eth-Xy}		γ_{eth-Xy}^{ACT}		
0.26				0.064		0.0173		
Conversion of xylose to ethanol [23,24]								
$\gamma_{eth-Glc}^{TH}$				$f_{eth-Glc}$		$\gamma_{eth-Glc}^{ACT}$		
0.66				0.026		0.0173		
Mass fraction of product loss in fermentation [15]								
				$L_p^{Ferm} = 0.03$				
Biogas yield from anaerobic digestion unit [26]								
				$Y_{bg/AD} = 0.3$				
Product recovery by distillation [25]								
	Butanol			Acetone		Ethanol		
	0.995			0.995		0.995		
Mass fed to CHP unit (in kg)								
Cellulose	Hemicellulose		Ash	Unconverted acid soluble lignin		Klasson Lignin		
3.43	1.035		24.3	2.375		14.3		

4. Results and discussion

The structural carbohydrates and lignin composition of native RS on dry basis are glucan (38.2% w/w), xylan (17.5% w/w), arabinan (3.2% w/w), Klasson lignin (14.3% w/w) and acid soluble lignin (2.5% w/w). The same RS having this composition has been recently used in another study and reported by our group [32]. The moisture content and percentage of acid insoluble ash (dry basis) in the native rice straw have been determined to be 25% (w/w) and 24.3% (w/w), respectively.

4.1. Biobutanol yield and energy analysis

In Figure 2, the complete material and energy balances of the present bio-refinery producing butanol as the main product and acetone and ethanol as the by-products along with integrated CHP

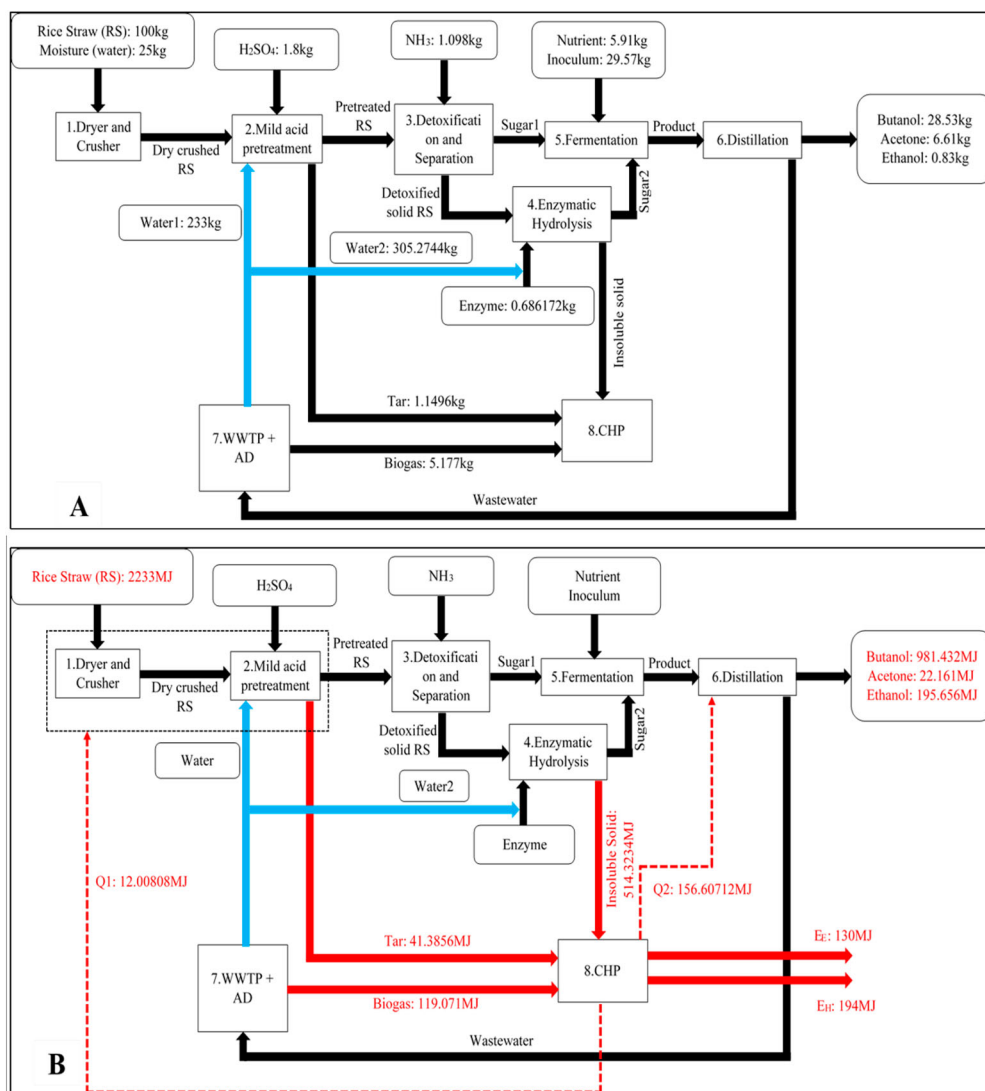


Figure 2. Complete (A) Material flow and (B) Energy flow, diagrams of the RS to butanol biorefinery.

have been represented. The complete material flows (black lines) among all process units have been indicated in Figure 2(A). Figure 2(B) is distinctly showing the energy flows (red lines) among all process units of the biorefinery. Specific numerical values for each material component and energy component, as considered for the detailed material and energy balance of the biorefinery, are provided in Table S1, supplementary section. All the data have been obtained through the energy analysis, described in section 3.1.

The flow sheet (Figure 2(A,B)) illustrates the complete block-wise performance of the refinery. It is evident that there is a loss of xylose due to detoxification. When mixed sugar stream containing xylose and glucose is fed to the fermenter, butanol yield of 0.2853 g butanol/g rice straw is achieved. Similarly, ethanol yield is 0.0084 g ethanol/g rice straw, respectively, while that of acetone is 0.0661 g acetone/g rice straw is achieved. The tar is constituted of all furfural and 5-HMF generated in the acidic pre-treatment process. As per the calculation, elaborated in the supplementary section, the composition of tar is 90.03% furfural and 9.975% HMF.

From the heating value of biogas, lignin, unspent cellulose and hemicellulose and tar, the net energy available from the wastes has been calculated to be 674.78MJ per 100 kg RS fed. Steam generated utilising the waste energy amounts to 539.83MJ. Out of this, 168.6MJ is consumed in-house for conducting different processes to produce butanol and the by-products (acetone and ethanol) from RS. The rest energy (371.23MJ) is fed to the steam turbine of the CHP. The electrical and thermal energy outputs of the CHP amount to 130MJ and 194MJ, respectively. A Table S has been provided in the supplementary section incorporating all material and energy flow streams. Energy efficiency of the biorefinery has been calculated to be 68.2%, while that of the CHP unit is 87%. Results of overall energy analysis are provided in Figure 3. Therefore, it is clear that the energy efficiency of a biorefinery producing butanol is much higher than that obtainable in the case of ethanol-based ones lying in the range of 20.7%–48.9%, as reported in the literature [15]. This is because of higher calorific value of butanol, compared to ethanol. Moreover, high contents of cellulose and lignin in rice straw are also responsible for the high output of energy due to (1) easy conversion of cellulose to glucose to be converted to butanol; (2) high power generation in CHP from residual lignin. The findings are in agreement with those of biorefineries based on the production of ethanol and combined heat and power from straw-type agricultural residues, as reported in the literature.

Details of all calculations are provided in the supplementary material.

4.2. Environmental analysis of biobutanol production

The electricity generation from this biorefinery can offset conventional energy generation by consuming fossil fuels. Biobutanol can replace gasoline, which can result in the preservation of fossil fuel thus leading to environmental savings. As described in section 3.2, 1L of biobutanol has the capability to replace 0.662L (or 66.2 vol%) of gasoline. As determined in section 3.2, electricity generated in the biorefinery can reduce CO₂ emission to the extent of 36.14 kg by avoiding the use of grid energy generated in a coal-based power plant. High value of CO₂ avoidance clearly indicates a positive environmental impact. This is possible because of the utilisation of energy generated in the in-house CHP, principally based on the lignin residues, causing reduction in the consumption of grid power generated in coal-based power plants in India.

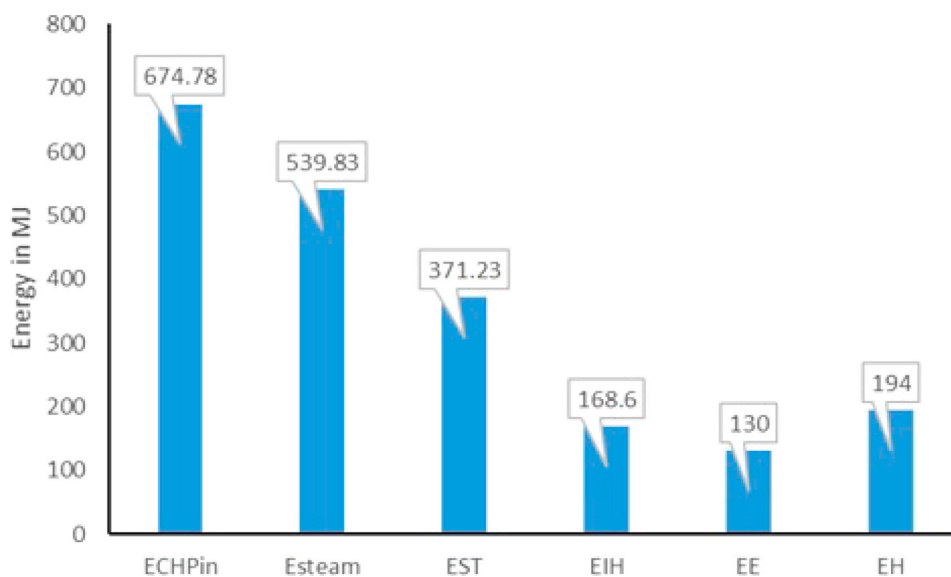


Figure 3. Generation and consumption of energy in the biorefinery; ECHPin: Total energy content of the waste; Esteam: Energy content of steam generated for the utilisation in the steam turbine of CHP; EST: Energy input to steam turbine of CHP; EIH: In-house energy requirement; EE: Total electrical energy generated; EH: Thermal energy output.

As no previous data are available in the literature on energy and environmental analysis of biorefineries producing bio-butanol and CHP using rice straw, comparison with literature data is not possible. From the energy and environmental analyses, it is established that rice straw, an abundantly available Indian agricultural residue, containing considerable amount of cellulose and lignin is a suitable feedstock for biorefineries.

5. Conclusion

RS-based biorefinery, producing biobutanol and heat and power, has been evaluated on the basis of energy and environmental point of view. Theoretically obtained values of xylose (15.75 kg) and glucose (3.78 kg), generated through mild acid catalysed hydrothermal pre-treatment of RS, have been used in the analysis. Glucose concentration (30.87 kg) in the liquid hydrolysate of the enzymatic hydrolysis unit was calculated from the real content of glucan (38.2% w/w) in RS used, considering the percentage of glucan conversion during hydrolysis for LCB reported by NREL. The values of yield of butanol in the fermentation unit and recovery in the distillation unit have been used from the reported literature. The above analysis defines the strategic use of glucose and xylose from lignocellulosic RS as chief substrates for production of biobutanol along with total carbon utilisation and utilisation of all waste streams of pre-treatment, hydrolysis, fermentation and distillation stage to achieve the criteria of zero waste management. This process also sheds light on in-house energy generation to offset energy expenditure and to export energy in order to reduce CO₂ emission. The inference of the study is that the results can aid to direct future research efforts to make the process sustainable and economically viable.

Acknowledgements

The cooperation rendered by the University of Eastern Finland regarding the compositional analysis of RS and supplying the results is being acknowledged gratefully.

Disclosure statement

No potential conflict of interest was reported by the author(s).

Funding

The corresponding author sincerely acknowledges Department of Science and Technology, India for sanctioning the financial support necessary for this research study under INNO-INDIGO Research project CONVER-B (Sanction Ref. DST/IMRCD/INNO-INDIGO/CONVER-B/2017(G) DATED January 29, 2018 and DST/IMRCD/INNO-INDIGO/CONVER-B/2017(C) DATED April 11, 2018).

References

- [1] Agarwal A.K., "Biofuels (Alcohols and Biodiesel) Applications as Fuels for Internal Combustion Engines", *Prog. Energy Combust. Sci.*, 33(3), pp. 233–271 (2007).
- [2] Bharathiraja B., Jayamuthunagai J., Sudharsanaa T., Bharghavi A., Praveenkumar R., Chakravarthy M. and Yuvaraj D., "Biobutanol—An Impending Biofuel for Future: A Review on Upstream and Downstream Processing Techniques", *Renew. Sustain. Energy Rev.*, 68, pp. 788–807 (2017).
- [3] Pfromm P.H., Amanor-Boadu V., Nelson R., Vadlani P. and Madl R., "Bio-Butanol vs. Bio-Ethanol: a Technical and Economic Assessment for Corn and Switchgrass Fermented by Yeast or *Clostridium Acetobutylicum*", *Biomass Bioenergy*, 34(4), pp. 515–524 (2010).
- [4] Qureshi N., Saha B.C., Cotta M.A. and Singh V., "An Economic Evaluation of Biological Conversion of Wheat Straw to Butanol: A Biofuel", *Energy Convers. Manage.*, 65, pp. 456–462 (2013).
- [5] Green E.M., "Fermentative Production of Butanol—the Industrial Perspective", *Curr. Opin. Biotechnol.*, 22(3), pp. 337–343 (2011).

- [6] Kumar M., Goyal Y., Sarkar A. and Gayen K., “Comparative Economic Assessment of ABE Fermentation Based on Cellulosic and non-Cellulosic Feedstocks”, *Appl. Energy*, 93, pp. 193–204 (2012).
- [7] Kolesinska B., Fraczyk J., Binczarski M., Modelska M., Berłowska J., Dziugan P., Antolak H., Kaminski Z.J., Witonska I.A. and Kregiel D., “Butanol Synthesis Routes for Biofuel Production: Trends and Perspectives”, *Materials. (Basel)*, 12(3), pp. 350 (2019).
- [8] Wu Y., Bai Y., Zhang D., Cheng C., Chen L., Bai F. and Xue C., “Pleiotropic Regulation of a Glucose-Specific PTS in *Clostridium Acetobutylicum* for High-Efficient Butanol Production From Corn Stover Without Detoxification”, *Biotechnol. Biofuels*, 12(1), pp. 264 (2019).
- [9] Xin F., Yan W., Zhou J., Wu H., Dong W., Ma J., Zhang W. and Jiang M., “Exploitation of Novel Wild Type Solventogenic Strains for Butanol Production”, *Biotechnol. Biofuels*, 11(1), pp. 252 (2018).
- [10] Khedkar M.A., Nimbalkar P.R., Chavan P.V., Chendake Y.J. and Bankar S.B., “Cauliflower Waste Utilization for Sustainable Biobutanol Production: Revelation of Drying Kinetics and Bioprocess Development”, *Bioprocess Biosyst. Eng.*, 40(10), pp. 1493–1506 (2017).
- [11] Ezeji T.C., Qureshi N. and Blaschek H.P., “Continuous Butanol Fermentation and Feed Starch Retrogradation: Butanol Fermentation Sustainability Using *Clostridium Beijerinckii* BA101”, *J. Biotechnol.*, 115(2), pp. 179–187 (2005).
- [12] Yang Y., Hoogewind A., Moon Y.H. and Day D., “Production of Butanol and Isopropanol with an Immobilized *Clostridium*”, *Bioprocess Biosyst. Eng.*, 39(3), pp. 421–428 (2016).
- [13] Gallazzi A., Branska B., Marinelli F. and Patakova P., “Continuous Production of n-Butanol by *Clostridium Pasteurianum* DSM 525 Using Suspended and Surface-Immobilized Cells”, *J. Biotechnol.*, 216, pp. 29–35 (2015).
- [14] Chowdhury, R., Ghosh, S., Debnath, B., and Manna, D., “Indian Agro-Wastes for 2G Biorefineries: Strategic Decision on Conversion Processes”. In *Sustainable Energy Technology and Policies*, De, S., Bandyopadhyay, S., Assadi, M., and Mukherjee, D., eds., (pp. 353–373). Springer, Singapore (2018).
- [15] Sadhukhan J., Martinez-Hernandez E., Amezcua-Allieri M.A. and Aburto J., “Economic and Environmental Impact Evaluation of Various Biomass Feedstock for Bioethanol Production and Correlations to Lignocellulosic Composition”, *Bioresour. Technol. Rep.*, 7, pp. 100230 (2019).
- [16] Sluiter A., Hames B., Ruiz R., Scarlata C., Sluiter J., Templeton D. and Crocker D., “Determination of Structural Carbohydrates and Lignin in Biomass”, *Lab. Anal. Proced.*, 1617, pp. 1–16 (2008).
- [17] Nan Y., Yang M., Xin D., Li K., Kuittinen S., Pappinen A. and Zhang J., “Acetone-butanol-ethanol Solvents Improved Enzymatic Hydrolysis of Pretreated Energy Grass”, *Fuel*, 245, pp. 406–412 (2019).
- [18] Yang M., Xu M., Nan Y., Kuittinen S., Hassan M.K., Vepsäläinen J., Xin D., Zhang J. and Pappinen A., “Influence of Size Reduction Treatments on Sugar Recovery From Norway Spruce for Butanol Production”, *Bioresour. Technol.*, 257, pp. 113–120 (2018).
- [19] Salomón M., Savola T., Martin A., Fogelholm C.J. and Fransson T., “Small-scale Biomass CHP Plants in Sweden and Finland”, *Renew. Sustain. Energy Rev.*, 15(9), pp. 4451–4465 (2011).
- [20] Yin S., Xia J. and Jiang Y., “Characteristics Analysis of the Heat-to-Power Ratio From the Supply and Demand Sides of Cities in Northern China”, *Energies*, 13(1), pp. 242 (2020).
- [21] Humbird D., Davis R., Tao L., Kinchin C., Hsu D., Aden A., Schoen P., Lukas J., Olthof B., Worley M. and Sexton D., *Process design and economics for biochemical conversion of lignocellulosic biomass to ethanol: dilute-acid pretreatment and enzymatic hydrolysis of corn stover* (No. NREL/TP-5100-47764). National Renewable Energy Lab.(NREL), Golden, CO (United States) (2011).
- [22] Chen Y., Zhou T., Liu D., Li A., Xu S., Liu Q., Li B. and Ying H., “Production of Butanol From Glucose and Xylose with Immobilized Cells of *Clostridium Acetobutylicum*”, *Biotechnol. Bioprocess Eng.*, 18(2), pp. 234–241 (2013).
- [23] Chowdhury R., Ghosh S., Manna D., Das S., Dutta S., Kleinstuber S., Sträuber H., Hassan M.K., Kuittinen S. and Pappinen A., “Hybridization of Sugar-Carboxylate-Syngas Platforms for the Production of bio-Alcohols From Lignocellulosic Biomass (LCB)—A State-of-the-art Review and Recommendations”, *Energy Convers. Manage.*, 200, pp. 112111 (2019).
- [24] Baral N.R. and Shah A., “Techno-economic Analysis of Cellulosic Butanol Production From Corn Stover Through Acetone–Butanol–Ethanol Fermentation”, *Energy Fuels*, 30(7), pp. 5779–5790 (2016).
- [25] Wu M., Wang M., Liu J. and Huo H., *Life-cycle assessment of corn-based butanol as a potential transportation fuel* (No. ANL/ESD/07-10). Argonne National Lab.(ANL), Argonne, IL (United States) (2007).
- [26] Sadhukhan J., “Distributed and Micro-Generation From Biogas and Agricultural Application of Sewage Sludge: Comparative Environmental Performance Analysis Using Life Cycle Approaches”, *Appl. Energy*, 122, pp. 196–206 (2014).
- [27] Qu M., Abdelaziz O. and Yin H., “New Configurations of a Heat Recovery Absorption Heat Pump Integrated with a Natural gas Boiler for Boiler Efficiency Improvement”, *Energy Convers. Manage.*, 87, pp. 175–184 (2014).
- [28] Kim D., Park K.Y. and Yoshikawa K., “Conversion of Municipal Solid Wastes Into Biochar Through Hydrothermal Carbonization”, *Engineering Applications of Biochar*, 31, pp. 31–46 (2017).

- [29] Engineering ToolBox, *Fuels - Higher and Lower Calorific Values*. [online] Available at: https://www.engineeringtoolbox.com/fuels-higher-calorific-values-d_169.html [Accessed 18/04/2020]. (2003).
- [30] Dhakate S.R., Pathak A.K., Jain P., Singh M., Singh B.P., Subhedar K.M., Sharda S.S. and Seth R.K., "Rice Straw Biomass to High Energy Yield Biocoal by Torrefaction: Indian Perspective", *Curr. Sci.*, 116(5), pp. 00113891 (2019).
- [31] Chakraborty N., Mukherjee I., Santra A.K., Chowdhury S., Chakraborty S., Bhattacharya S., Mitra A.P. and Sharma C., "Measurement of CO₂, CO, SO₂, and NO Emissions From Coal-Based Thermal Power Plants in India", *Atmos. Environ.*, 42(6), pp. 1073–1082 (2008).
- [32] Ghosh S., Pathak S., Manna D. and Chowdhury R., "Acidogenic Mixed Consortium Isolated From Soil of Agricultural Field: Acid Production Behaviour and Growth Kinetics Under the Influence of Pretreatment Hydrolysate of Rice Straw (RS)", *Indian Chem. Eng.*, pp. 1–13 (2020). doi:10.1080/00194506.2020.1815597.

Indian Agro-wastes for 2G Biorefineries: Strategic Decision on Conversion Processes

Ranjana Chowdhury, Shiladitya Ghosh, Biswajit Debnath
and Dinabandhu Manna

Abstract Biorefineries are globally contemplated as the viable platforms for the highly anticipated substitution of fossil-based economy by the bio-based economy. A biorefinery offers the advantage of converting a remarkable variety of biomass feedstocks to different types of biofuels and biochemicals. A great extent of rigorous effort is currently being made for the upgrading of existing biorefinery frameworks to fully attain the sustainability standards required to warrant their full-scale implementation. As a consequence of the mandatory inclusion of the sustainability goals into the biorefinery concept and the escalating concern on the ‘food-fuel conflict’, the second generation (2G) of biorefineries are garnering quick popularity over their first-generation counterparts. In India, there exist huge prospects of development of 2G biorefineries exploiting the abundant resources of the lignocellulosic agro-wastes. Indian agro-wastes display an extraordinary variety of lignocellulosic biomass and round-the-year availability in copious amounts. Unfortunately, due to lack of awareness and poor valorization, these valuable agro-wastes are often destroyed in mass scale for waste management instead of being utilized in a productive way. The major focus of the present chapter is to present a categorical classification of Indian agro-wastes based on their appearance in the supply chain. The adaptability of Indian agro-wastes towards 2G biorefinery has been assessed using their availability, thermochemical properties and composition of a few specific feedstocks, namely, rice straw, rice husk, wheat straw, oil seed press cakes, sugarcane bagasse, coconut shell, banana peels and stems. The analytic hierarchy process (AHP) has been used to decide on the strategy of application of stand-alone biochemical or thermochemical processes and their hybrids for the conversion of different candidate feedstocks in the 2G biorefineries with respect to sustainability parameters.

Keywords Agro-wastes • Abundance in India • Energy potential
2G biorefineries analytic hierarchy process (AHP) • Guideline on strategic decision on conversion route

R. Chowdhury (✉) · S. Ghosh · B. Debnath · D. Manna
Chemical Engineering Department, Jadavpur University, Kolkata 700032, India
e-mail: ranjana.juchem@gmail.com

1 Introduction

Notable attempts for the switch over from ‘fossil-dominated’ to ‘bio-based’ economy have already been initiated worldwide [1, 2]. Rapid decline in fossil fuel reserves and consequent tremendous future energy insecurity, rapid environmental deterioration due to GHG emission, progressive global warming and threatening issues of stagnation of socio-economic growth are the prime drivers of this paradigm shift [1–3]. The utilization of renewable resources (biofuels, biochemicals, biomaterials) in place of exhaustible non-renewables (petro-fuels and petrochemicals) bears the vital significance in this particular context and should be made compulsory worldwide through governmental enforcements. As envisioned by the international energy agency (IEA), this will require the ultimate diversification of primary energy sources by the countries around the world as an immediate measure [4]. Biomass, more specifically the solid lignocellulosic ones, originated from different natural resources can become the dependable alternatives of petro-based fuels as the primary energy source upon proper planning and implementation [5–7]. Significant technological progress made in the past few decades in the conversion of solid biomass to different liquid and gaseous biofuels has incremented the efficacy of end use of the biomass to several folds [8–13]. However, the current status of biofuels regarding competition with the conventional fossil fuels is far behind the baseline required to replace their usage as primary energy source. The major barriers are absence of proper categorization and poor valorization of biomass, unplanned use in non-compatible conversion processes resulting in incomplete recovery of energy and waste of valuable by-products due to lack of planning. It is apparent that the biofuels can never attain a competitive space with the crude-oil fuels if the high cost of production is not scaled down to significant extents [14, 15]. To achieve this particular goal, IEA has brought the focus of bioenergy planners on the concept of ‘bio-refining of biomass’ to facilitate the simultaneous production of (bio)chemicals, heat, power, food, feed and (bio)materials along with (bio)fuels from different variety of biomass in a single facility combining multi-step processes, popularly known as a ‘biorefinery’ [4]. The biorefinery concept has quickly garnered widespread acceptance all over the world and now exhibits a myriad of conceptual, technological and regional variants.

The developing countries with dynamically emerging industrial and economic growth, like the BRICS (Brazil, Russia, India, China and South Africa), display massive requirements of energy in form of oil and other fossil-based fuels to sustain the pace of rapid development [15, 16]. Demand of energy and security of energy availability differ significantly among these countries. Regarding energy security, India portrays a precarious nature, reflected from a history of continually increasing dependence (roughly 30% of energy demand) on imported sources of primary energy vectors [17]. According to the latest report by MPNG, India imports 14, 70 and 30% of its primary energy demand, respectively, in terms of coal, oil and natural gas, totalling in almost worth 150 billion USD [17]. It is being envisaged that cost of this energy import will reach a soaring 3.6 trillion USD by 2030 if

alternative measures are not administered urgently [17]. In this context, the conversion of varieties of Indian lignocellulosic biomass, often mistreated as just waste materials, to energy efficient biofuels has become a supreme concern of Indian bioenergy researchers as well as energy policy makers [18, 19]. India is largely known as an agriculture-based country with huge land coverage of productive agricultural fields spread throughout the country's vast rural expanse. Naturally, enormous quantities of agro-residues are annually generated in India as by-products of the crop cultivation and crop-processing sectors [19, 20]. Besides year-round availability, most of these agro-residues possess suitable biochemical composition and excellent energy content to be utilized as potential candidate feedstocks for the development of agro-waste-based biorefineries [21, 22]. Strategic planning and successful implementation of such biorefineries hold great promise in lessening of the country's forthcoming energy insecurity and existing wide gap between the energy demand and supply.

2 Classification of Biorefineries

As already mentioned in the preceding section, biorefineries currently display myriads of variants based on different basis of classification. Biorefineries have been majorly classified based on the sources of feedstock, generation technology and biomass conversion routes used and/or product/s targeted [23, 24]. Cherubini et al. classified the biorefineries based on four selected features namely platforms, products, feedstocks and processes in a recently published article [25]. In the article, they clearly stated that 'classification approach is flexible' for biorefineries, as new subgroups are continually appearing from the rapid progress of the emerging field. Taking advantage of this flexibility of classification, a simplistic approach of classifying the biorefineries has been adopted keeping direct accordance with the well-known generations of biofuels based on feedstock sourcing [23, 26, 27]. On the basis of origin and type of feedstock to be handled, we have simply classified the biorefineries into three major 'generations' as the following: (1) first-generation (1G) biorefinery, (2) second-generation (2G) biorefinery and (3) third-generation (3G) biorefinery. The classification of biorefineries is schematically represented in Fig. 1.

The 1G biorefineries use different simple sugar, cereal starch, vegetable oils and animal fats as feedstocks for production of biofuels and biochemicals [23]. The 2G biorefineries, also referred as the advanced biorefineries, will particularly use several lignocellulosic feedstocks including agro-wastes, energy crops, woody forestry residues and lignocellulosic fraction of industrial and municipal solid wastes (MSW) as feedstocks [23]. 3G biorefineries will rely on different freshwater and marine algal biomass as the feedstocks for biofuel and biomaterial production. It is distinctively ascertained that the feedstocks used in the 1G biorefineries are having food/feed value and are fit for human consumption, whereas all feedstocks of the

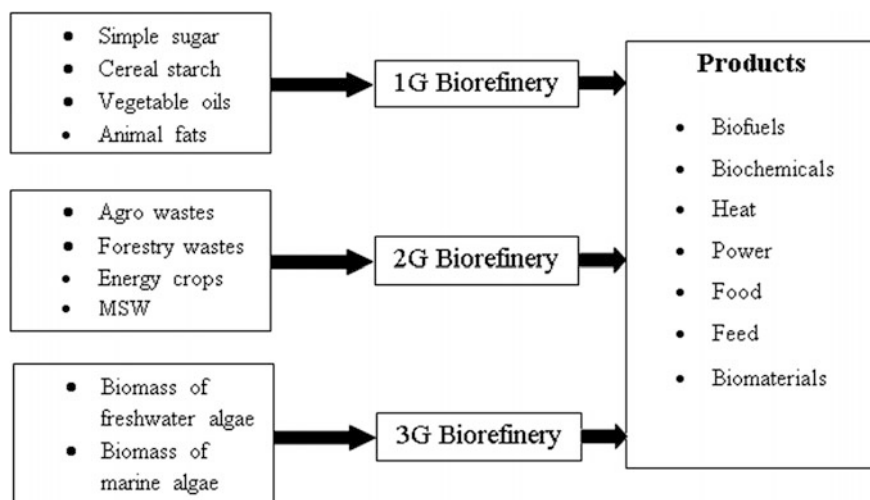


Fig. 1 Three classes of biorefineries based on feedstock sourcing

2G biorefineries are completely non-food in nature [28, 29]. This distinction in feedstock resourcing renders superiority of the 2G biorefineries over the 1G ones from the perspective of ‘food versus fuel’ issues, which makes the 1G technology highly unsustainable [28, 29]. In our discussion, we will specifically focus on the 2G biorefineries meant for the conversion of various Indian lignocellulosic agro-wastes to biofuels and multiple added-value products. The usage of dedicated energy crops has been intentionally excluded due to another controversial issue of ‘land versus fuel’ [28], which should be avoided in an exclusively agriculture-oriented country like India. Most compatible combinations of ‘feed-stocks and conversion routes’ will be assessed and recommended for future implementation based on the maximized level of attainable sustainability standard in the Indian context.

3 Categorization of Indian Agro-wastes

Before planning the utilization of different Indian agro-wastes as feedstock for biofuel production either through individual conversion routes or in a 2G biorefinery facility, proper categorization is a requisite. This will greatly help in assessing the probable economic value of the particular feedstocks and eventual valorization through policy making from the perspective of their usage in biofuel and biochemical production. This is rather a difficult job because of the existence of extremely diverse types of Indian agro-biomass [18–20]. To categorize the Indian agro-wastes, primarily they have been divided into two distinct classes, depending

on their appearance on the supply chain (from the cultivation field to the agro-processing sectors). First class is the agro-wastes directly produced during or after the harvesting of the crop/agricultural plants, termed as ‘post-harvesting residues’. Post-harvesting leftovers may also be regarded as the ‘field residues’ as most of the times these are left in the field at/or close to the site of cultivation. Second class of agro-biomass is represented by the remainings generated as by-products of different processing units handling the crops to harness the edible parts, termed as ‘post-processing residues’. Varieties of different major Indian agricultural crops and the residual agro-wastes derived from them [18, 19, 30], both post-harvesting and post-processing, have been tabulated in Table 1.

Depending on the variation in climatic conditions and soil properties, different types of agricultural crops are cultivated in different parts of India. Rice, being the staple food of majority of Indians, is the most prominently cultivated crop in India. Rice is cultivated in mass scale in 21 states among the total 28 major states of the country [30]. Naturally, quantity-wise a huge fraction of the Indian agro-wastes is dominated by the residues produced from rice. Besides rice, the other crop varieties cultivated in large scale are reported in Table 1 along with the agro-wastes subsequently produced from them. The lignocellulosic agro-wastes generated from all these crops can serve as potential feedstocks for generation of bioenergy through different conversion routes.

Table 1 Major types of Indian crops and the post-harvesting and post-processing residues derived from them

Indian crops	Post-harvesting residue	Post-processing residue
Rice	Straw/stalk, leaves, stubble,	Husk/hull
Wheat	Straw/stalk, leaves, stubble	Pod/panicle
Sugarcane	Top, leaves	Bagasse
Maize	Stalks	Cobs
Banana	Leaves, pseudo-stem, fruit branch	Pith, fruit peels
Mustard	Stalks	Husk, press cakes
Sesame	Stalks	Press cakes
Castor	Stalks	Husk, press cakes
Soybean	Stalks	N.A.
Coconut	Fruit brunch, fronds	Husk/coir, pith, shell
Areca nut	Fruit brunch, fronds	Husk
Groundnut	Stalks	Shell
Bajra	Stalks	Husk, cobs
Jowar	Stalks	Husk, cobs
Ragi	Stalks	N.A.
Pulses*	Stalks	Husk

Sourced from [18, 19, 30], *Arhar, gram, masoor, moong, urad

4 Availability and Conventional Use of Indian Agro-wastes

Table 1 provides an overview of the extremely diversified agro-waste varieties produced in India. Most of the tabulated agro-wastes are available round the year due to the continuous production of the crops in rotational manner for the production of food and feed to satiate the hunger of the huge population of India. As a natural consequence, the non-edible lignocellulosic agro-residues originating from the cultivation and processing of the Indian food crops are absolutely huge for the prime crop varieties [18, 19, 30]. Regarding the quantity, agro-wastes produced from rice, wheat, sugarcane, maize, banana, oilseed crops (mustard, sesame, castor), nuts (coconut, areca nut, ground nut), millets (jowar, bajra, ragi) and pulses are substantially huge in India [19]. Annually available amount of these agro-wastes have been tabulated and presented in Table 2.

From the data presented in Table 2, it is evident that among the Indian agro-wastes generated through the cultivation and processing of crops, residues of rice hold the majorly significant fraction of produced agro-wastes. Other than rice, wheat, sugarcane, banana, maize, coconut, groundnut, jowar, bajra are the other Indian crop varieties, which produce significantly high amount of lignocellulosic wastes. Agro-wastes produced from the oilseeds are also considerably high, particularly for mustard (Table 2). However, the availability of data on the quantity of the 'press cakes' produced as post-processing residues from the oilseeds is scarce, which can be significantly added to the agro-wastes of Indian oilseeds. Also, quantitative data on the amount of stubble of rice and wheat are not available, which are important lignocellulosic agro-wastes of these two cereal crops.

Clearly, there is an absolute abundance of agro-wastes in India, which also poses difficulties in proper management and handling of the massive volume of solid biomass continuously being produced. In India, there are mainly two conventional ways/methods, through which the agro-wastes are managed. The first method has a long history of traditional usage in India, which is the use of dry agro-residues as solid fuel in earthen/clay ovens or house stoves in the rural areas for cooking and producing heat [31]. Huge amount of GHGs (particularly CO_2 , NO_x , SO_x) and respirable particulates are produced during the burning of the lignocellulosic agro-residues in this method of usage [31]. This is neither an eco-friendly nor a healthy way of utilization of the agro-wastes. It notably adds up to the atmospheric GHG load in one hand, and on the other, it adversely affects the respiratory system of the persons directly exposed to the smoke caused during the burning [31]. The straws or stalks, residual leaves, nut shells and fronds of the crop plants are primarily used through this method. The second way of agro-waste management practiced in India is leaving the wet parts of the agro-wastes openly in the site of cultivation for the amendment of soil by the fertilizer produced through the microbial decay of the biomass. This process, although apparently looks harmless, causes emission of another potent GHG, viz. CH_4 to the environment in mass scales. The CH_4 is produced during the microbial degradation of the agro-biomass

Table 2 Annual availability of agro-wastes of major agricultural crop varieties of India

Indian crops (corresponding agro-wastes)	Annual availability (Kt/year)	Reference
Rice waste	161893.00	[20]
Rice straw	141120.00	
Rice husk	20773.00	
Wheat (straw)	122991.00	[20]
Sugarcane wastes	114761.00	[20]
Sugarcane bagasse	73775.00	
Sugarcane tops and leaves	40986.00	
Maize waste	33720.00	[20]
Maize straw	28396.00	
Maize cobs	5324.00	
Banana waste	67776.00	[20]
Banana fruit peels	393.00	
Banana pseudo-stem	67383.00	
Mustard waste	16877.00	[20]
Mustard press cake	2681.00	
Mustard seedpod	1355.00	
Mustard stalks	12841.00	
Sesame (stalks)	1207.70	[19]
Soybean husk	671.00	[20]
Coconut waste	9060.00	[20]
Coconut fronds	7769.00	
Coconut shell	726.00	
Coconut coir pith	565.00	
Areca nut (fronds, husk)	1000.80	[19]
Groundnut (shells)	1385.00	[20]
Bajra(stalks, cobs, husk)	15831.80	[19]
Jowar (cobs, stalks, husk)	24207.80	[19]
Ragi (straw)	2630.20	[19]
Cotton waste	38281.00	[20]
Cotton stalks	35397.00	
Cotton hull	2884.00	
Pulses* (stalks, husk)	13462.90	[19]

*Arhar, gram, masoor, moong, urad

by the native decaying microorganisms present in the soil. So, from an environmental perspective, this method is also not eco-friendly. This method is particularly used for the agro-biomass of the pulses for recycling back the nitrogen into the soil in a traditional belief. Another commonly practiced method for managing the enormous volume of straw and stubble is the open-field burning for mass destruction of the dry agro-wastes [32, 33]. It is easily understandable that this is an environmentally detrimental process due to the massive GHG (CO₂, CO, NO_x, SO_x etc.) emission, during the open-air combustion of the carbonaceous straws/stubbles [33]. Lack of awareness and infrastructural inabilities are the two major reasons for the persistence of these malpractices in India. True valorization of the

Indian agro-wastes through proper identification of their prospects for the production of biofuels and additional value-added products is urgent to stop the mis-handling of the immensely valuable agro-wastes.

5 Characterization of Indian Agro-wastes

It is of crucial importance to clearly understand the physico-chemical characteristics of the lignocellulosic agro-wastes to facilitate optimal processing and efficient conversion into biofuels and other value-added products in a 2G biorefinery. Principal components of all of the tabulated agro-wastes, both post-harvesting and post-processing, are the three complex biopolymers, namely lignin, cellulose and hemicellulose [34]. Lignin is the rigid aromatic hetero-biopolymer which forms the outermost protective layer of all lignocellulosic biomass [35]. The polysaccharide duo, cellulose and hemicellulose form the core carbohydrate moiety of lignocelluloses and are the target components for biofuel production [35]. Contents of lignin, cellulose and hemicellulose substantially vary among various lignocellulosic biomass depending on species, season, region and climatic conditions [19, 30, 34, 35]. Owing to the natural recalcitrance and compositional complexity, lignin content plays the pivotal role regarding the choice of the conversion route, namely biochemical or thermochemical or their hybrid, for the generation of biofuels from the agro-residues. Hence, it seems beneficial to primarily select the route of conversion for the Indian agro-wastes to biofuels based on the lignin content; this strategy is discussed in detail in a later section. Lignin, cellulose and hemicellulose contents of some major agricultural wastes have been presented in Table 3.

5.1 *Lignin-Based Classification of Indian Agro-wastes*

Based on the lignin contents of the Indian agro-wastes, as reported in Table 3, a three-class categorization has been done. The three classes of agro-wastes are namely low lignin (LL), medium lignin (ML) and high lignin (HL). The characteristic range of lignin contents (%) of the three classes are 1–10 (LL), 10–20 (ML) and HL (above 20), respectively. According to this lignin-based classification, the distribution of different agro-wastes (Table 3) is as follows:

1. HL: rice husk, sugarcane tops, sugarcane leaves, coconut shell, groundnut shell, barley straw.
2. ML: rice straw, wheat straw, sugarcane bagasse, maize stems, coconut coir.
3. LL: mustard stalks, soybean husk, sesame press cake, banana pseudo-stem.

Table 3 Lignocellulose contents of different Indian agro-wastes

Agro-waste	Lignin (%)	Hemicellulose (%)	Cellulose (%)	Reference
Rice straw	17.00	22.00	42.00	[20]
Rice husk	24.60	31.60	43.80	[34]
Wheat straw	13.00	30.00	42.00	[20]
Mustard press cake	–	3.00	4–5	[46]
Mustard stalks	2.20	18.70	39.50	[47]
Soybean husk	9.88	17.15	33.49	[48]
Sesame press cake	1.00	–	–	[49]
Sugarcane bagasse	13.40	9.20	58.20	[20]
Sugarcane tops	21.70	32.00	39.70	[50]
Sugarcane leaves	22.70	28.70	40.80	[50]
Maize stems	19.90	21.10	–	[51]
Coconut shell	28.70	25.10	36.30	[52]
Coconut coir	17.80	25.90	47.70	[52]
Banana pseudo-stem	8.07	18.40	44.00	[53]
Groundnut shell	30.20	18.70	35.70	[52]
Barley straw	20.78	–	–	[54]

5.2 Elemental Analysis

The elemental composition of different Indian agro-wastes has been presented in Table 4.

5.3 Energy Potential of Indian Agro-wastes

Estimation of total energy potential of candidate agro-wastes in a year-wise basis is an important consideration to select the most promising feedstocks for 2G biorefinery. This will help in the primary decision-making process considering the abundance and higher heating value (HHV) of a particular agro-waste ensuring its uninterrupted availability. The elemental composition, particularly C–H–O analysis of any lignocellulosic biomass, affects the energy content of the feedstock. The higher heating values (HHV) of the Indian agro-wastes have been calculated using the Dulong's equation as follows [36]:

$$\text{HHV (kJ/kg)} = [(337.7 \times \text{C}) + \{1437.9 \times (\text{H} - (\text{O}/8))\}] \quad (1)$$

The values of C, H and O have been obtained from Table 4.

Table 5 represents the quantitative data on the HHV and total energy potential of some major Indian agro-wastes, calculated based on the annual availability of the wastes, as provided in Table 2.

Table 4 Elemental composition of different agro-wastes and their higher heating values

Agro-waste	C (%)	H (%)	O (%)	N (%)	S (%)	Reference
Rice straw	38.80	6.70	38.80	0.20	0.20	[55]
Rice husk	39.80	5.70	39.80	0.50	0.20	[55]
Wheat straw	41.70	5.00	41.70	0.40	0.30	[55]
Mustard press cake	40.26	6.03	46.14	6.46	1.11	[46]
Mustard seedpod	44.30	8.80	43.00	0.38	0.19	[20]
Mustard stalks	43.80	5.90	43.80	0.30	0.30	[55]
Castor shell	49.80	5.30	43.90	0.90	0.10	[56]
Soybean husk	43.10	6.40	44.50	0.80	0.09	[20]
Sesame press cake	45.19	7.55	39.27	7.26	0.72	[57]
Sesame stalks	49.16	6.59	34.06	0.85	0.31	[58]
Sugarcane bagasse	48.60	5.90	42.80	0.16	0.04	[20]
Sugarcane tops and leaves	39.80	5.60	46.80	1.70	–	[20]
Maize straw	47.09	5.54	39.79	0.81	0.12	[20]
Maize cobs	41.40	6.00	51.30	0.14	0.01	[20]
Coconut fronds	48.60	5.80	42.40	–	–	[20]
Coconut shell	52.30	6.60	39.50	0.30	0.80	[20]
Coconut coir pith	50.30	5.10	39.60	0.45	0.16	[20]
Banana pseudo-stem	43.28	6.23	49.02	0.98	0.49	[59]
Banana fruit peels	35.58	4.62	57.16	2.19	0.45	[59]
Areca nut husk	44.70	3.80	51.20	0.40	–	[60]
Groundnut shell	33.90	2.00	59.90	1.10	0.12	[20]
Cotton stalks	41.50	6.20	47.50	1.81	0.02	[20]
Cotton hull	50.40	8.40	39.80	1.40	0.10	[20]
Barley straw	45.67	6.15	38.26	0.43	0.11	[61]
Barley chaff	46.77	5.94	39.98	1.45	0.15	[61]

From the data presented in Table 5, it is evidently seen that agro-wastes derived from rice possess the highest annual energy potential and are much greater than any other agro-wastes. This is followed by wastes of wheat, banana, sugarcane, cotton and maize; the annual energy potentials of which are also significantly high for India. Other noteworthy agro-wastes with substantially high energy potential ranging between 100 and 200 PJ/year are namely mustard and coconut. Hence, it is assessed that agro-wastes of these crops can serve as abundant source of feedstocks for an Indian agro-waste-based 2G biorefinery. Total annual energy potential of the agro-wastes of 8591.67PJ is comparable to the total coal-based thermal power of 194553 MW in India [37]. The actual potential is, however, dependent on the efficiency of the conversion process to be selected for the generation of energy from the wastes.

Table 5 Total annual energy potential of selected Indian agro-wastes

Agro-waste	HHV (MJ/kg)	Energy potential in PJ/year (= Annual availability * HHV)	Reference
Rice straw	15.76	2224.05	[55]
Rice husk	14.48	300.79	[55]
Wheat straw	13.77	1693.58	[55]
Mustard press cake	13.97	37.45	[46]
Mustard seedpod	19.88	1.37	[20]
Mustard stalks	15.40	197.75	[55]
Soybean husk	15.76	10.57	[20]
Sesame stalks	19.95	24.09	[58]
Sugarcane bagasse	17.20	1268.93	[20]
Sugarcane tops and leaves	13.52	554.13	[20]
Maize straw	16.72	474.78	[61]
Maize cobs	13.39	71.29	[20]
Coconut fronds	17.06	132.54	[20]
Coconut shell	20.05	14.55	[20]
Coconut coir pith	17.20	9.72	[20]
Banana pseudo-stem	14.77	995.25	[59]
Banana fruit peels	8.38	3.29	[59]
Groundnut shell	3.55	4.91	[20]
Cotton stalks	14.39	509.36	[20]
Cotton hull	21.94	63.27	[20]
Total		8591.67	

6 Biomass Conversion Processes of 2G Biorefinery Platform

Lignocellulosic biomass can be converted to an array of various biofuels and chemicals/biochemicals via selection of different route of conversion. Both thermochemical and biochemical conversion processes are in common practice worldwide [9, 38]. As individual processes, all of the biomass conversion routes produce some energy products (heat and fuels) and some material products (chemicals, biochemicals, biomaterials). In a 2G biorefinery platform, more than one of these processes are advantageously used together to increase the extent of biomass conversion, number of marketable products and reduction of waste generation. However, selection of particular conversion processes in 2G biorefinery platforms in different countries is highly dependent on several factors. Type and availability of biomass, awareness and willingness of the biomass producers to supply biomass residues to conversion plants, progress in biomass conversion technologies and proper planning of utilization by the bioenergy leaders are some

prime driving factors. As a primary focus of this chapter, suitability of different conversion routes for the conversion of Indian agro-wastes, categorized on the basis of lignin content, has been assessed. Table 6 provides the thermochemical, biochemical conversion routes and their hybrids under consideration.

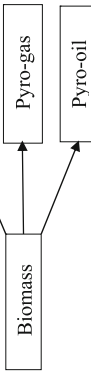
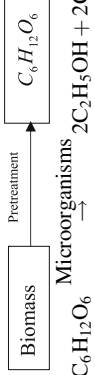
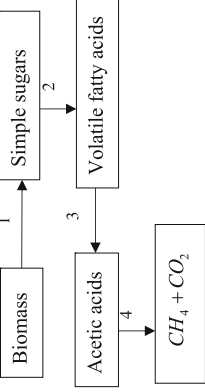
7 Strategies for the Utilization of Indian Agro-wastes in 2G Refinery

Lignin is the most recalcitrant substance present in all lignocellulosic materials, including the agro-wastes; it highly influences the rate of conversion of biomass through any route, particularly the biochemical ones [35]. Hence, it seems beneficial to primarily select the specific route, either thermochemical or biochemical, to ensure maximum biomass conversion with enhanced efficiency. It is understandable that biomass with very high percentage of lignin is not suitable as feedstocks for biochemical routes due to the requirement of extensive pre-treatments. Although it is not very easy to assess the difficulties or advantages of using any agro-waste as feedstock for any conversion route, an assessment considering major influencing factors is necessary. To facilitate the clear understanding on proper and specific selection of biomass and its most compatible conversion route, a strategic decision-making approach has been adopted here. In the approach, lignin content of the agro-wastes has been considered as the first basis of categorization to be used for the selection of the best conversion route among available options. Afterwards, a well-known strategic decision-making tool has been used to assess the feasibility of agro-waste conversion in a 2G biorefinery framework shown in Fig. 2.

Figure 2 depicts the overall scheme of the proposed 2G biorefinery framework comprising all options of biomass classes, pre-treatment units, conversion routes and product series. In Fig. 2, the three-class categorization of lignin-based biomass has been shown along with their probable point of entry in different option of conversion routes. For the three biomass classes, a total of five conversion routes (Table 6) have been proposed as options as following:

- A. Thermochemical routes (no biomass pre-treatment is considered)
 - 1. Gasification (GA)
 - 2. Gasification followed by Fischer–Tropsch synthesis (GA-FT)
 - 3. Pyrolysis (PY)
- B. Biochemical routes (acid hydrolysis (AH) of biomass is considered as an initial step)
 - 1. Anaerobic digestion (AH-AD)
 - 2. Alcohol fermentation (AH-AF)
- C. Hybrid process (thermochemical + biochemical)
 - 1. Gasification followed by alcohol fermentation (GA-ALF)

Table 6 The biomass conversion processes of the 2G biorefinery platform

Conversion process	Technology used	Reactions	Product uses
Thermochemical processes	Gasification	$\begin{aligned} \text{C} + \text{O}_2 &\rightarrow \text{CO}_2 \\ \text{CO}_2 + \text{C} &\rightarrow 2\text{CO} \\ \text{C} + \text{H}_2\text{O} &\rightarrow \text{CO} + \text{H}_2 \\ \text{CO} + \text{H}_2\text{O} &\leftrightarrow \text{CO}_2 + \text{H}_2 \\ \text{C} + 2\text{H}_2 &\rightarrow \text{CH}_4 \end{aligned}$	Fuel
	Gasification followed by: Fischer-Tropsch	$\begin{aligned} n\text{CO} + (2n+1)\text{H}_2 &\xrightarrow{\text{Catalyst}} \text{C}_n\text{H}_{2n} + 2 + n\text{H}_2\text{O} \\ n\text{CO} + 2n\text{H}_2 &\xrightarrow{\text{Catalyst}} \text{C}_n\text{H}_{2n} + n\text{H}_2\text{O} \end{aligned}$	Fuel
	Pyrolysis	 <pre> graph TD Biomass --> Pyro-char Biomass --> Pyro-gas Biomass --> Pyro-oil </pre>	Char: adsorption and soil amendment; Oil: fuel and biochemical Gas: fuel
Biochemical processes	Alcohol fermentation	 <pre> graph TD Biomass -- Pretreatment --> C6H12O6 C6H12O6 -- Microorganisms --> Ethanol[2C2H5OH + 2CO2] </pre>	Alcohol: Fuel Lignin residues: Chemical
	Biogas production	 <pre> graph TD Biomass -- 1 --> SimpleSugars[Simple sugars] SimpleSugars -- 2 --> VolatileFattyAcids[Volatile fatty acids] Biomass -- 3 --> AceticAcids[Acetic acids] AceticAcids -- 4 --> CH4_CO2[CH4 + CO2] </pre>	Biogas: Fuel; Solid waste: Fertilizer
Hybrid process	Syngas fermentation	$\begin{aligned} 6\text{CO} + 3\text{H}_2\text{O} &\rightarrow \text{CH}_3\text{CH}_2\text{OH} + 4\text{CO}_2 \\ 2\text{CO}_2 + 6\text{H}_2 &\rightarrow \text{CH}_3\text{CH}_2\text{OH} + 3\text{H}_2\text{O} \end{aligned}$	Lower alcohols: Drop-in fuel; Higher alcohols: Drop-in fuel

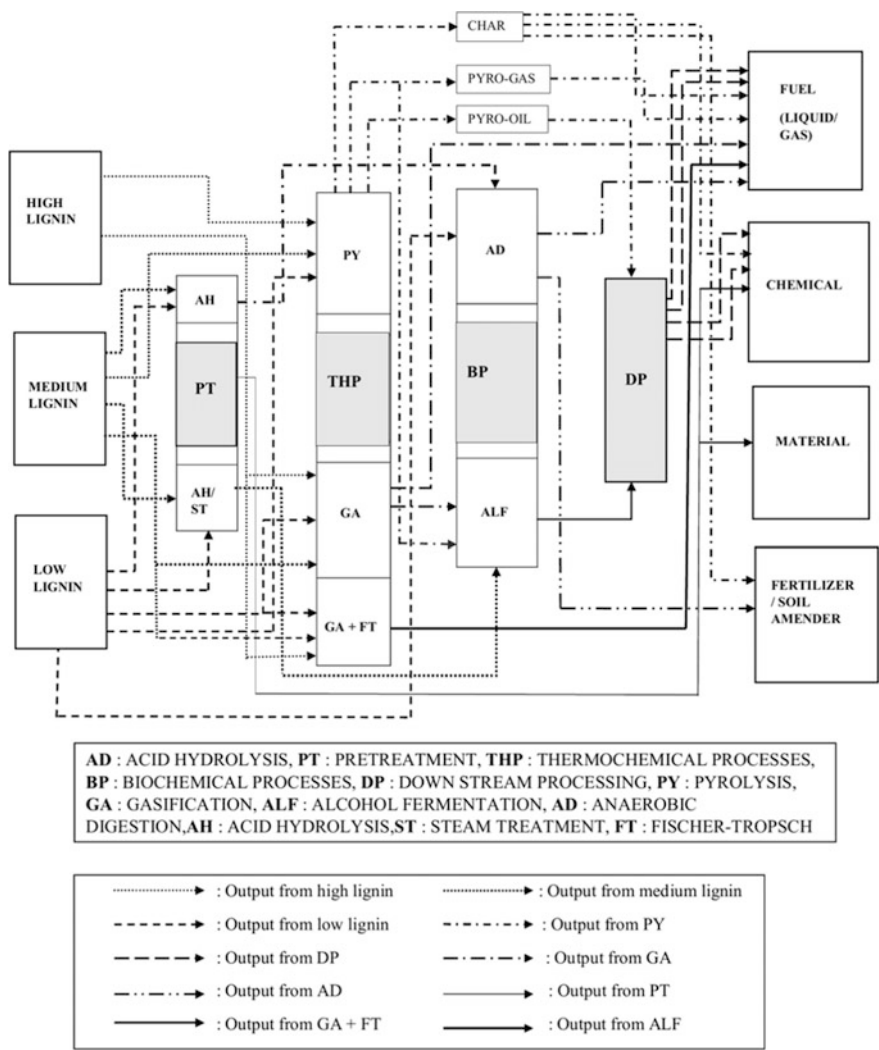


Fig. 2 Schematic of the Indian agro-waste-based 2G biorefinery framework

After defining all the available options for biomass and conversion routes, feasibility analysis has been conducted to clearly assess the suitability of conversion of particular agro-wastes from Indian context.

7.1 Analytical Hierarchical Process (AHP) Model

The analytical hierarchical process (AHP) in this study has been carried out using the super decision software following the basic steps proposed by Saaty [39–43]. The AHP used in this study is a four-tier structure consisting of one goal, one criteria cluster, one sub-criteria cluster and one alternatives cluster illustrated in Fig. 3.

The goal of this study is to find out the best compatible route for conversion of biomass of varying lignin content in the Indian context. The criteria set for the analysis is environmental aspects, economical aspects and the maturity of the technologies considered for conversion of biomass. The sub-criteria have been set to be different lignin content of biomass, i.e. high lignin content, medium lignin content and low lignin content. The alternatives chosen are pyrolysis (PY), gasification followed by alcohol fermentation (GA-ALF), gasification followed by Fischer–Tropsch process (GA-FT), anaerobic digestion with acid hydrolysis as pre-treatment (AH-AD) and alcohol fermentation with acid hydrolysis as

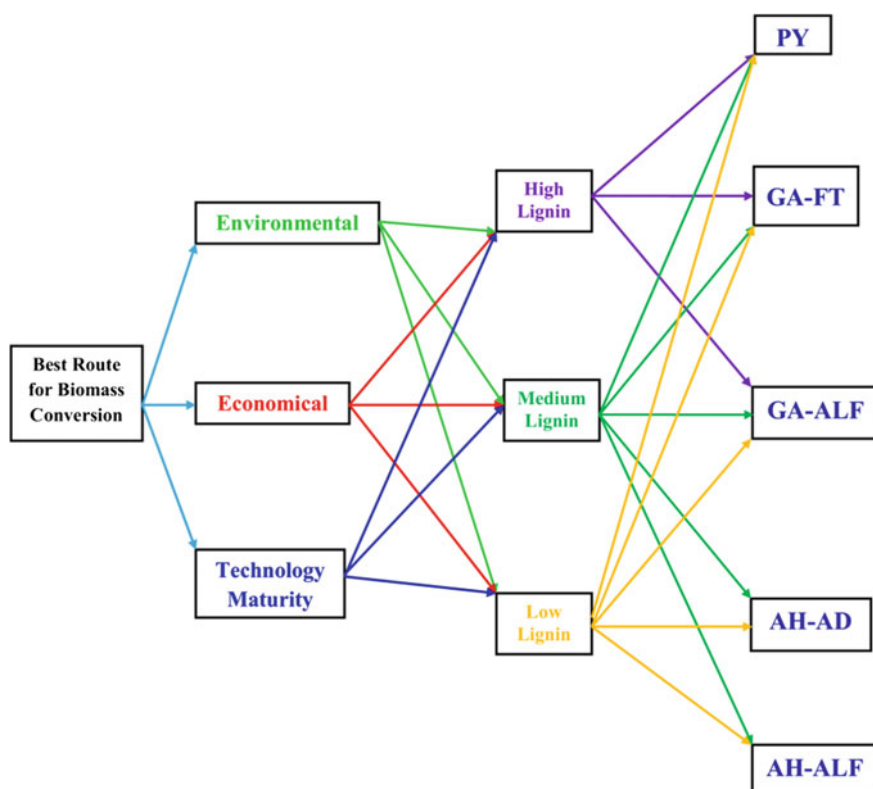
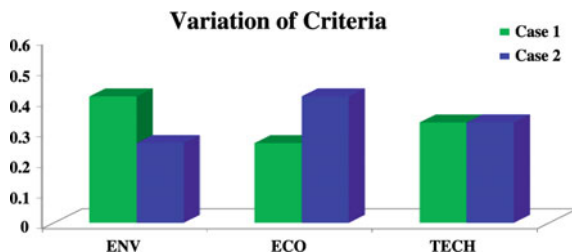


Fig. 3 Four-tier AHP model of the Indian agro-waste-based 2G biorefinery

Fig. 4 Variation of criteria in case 1 and 2



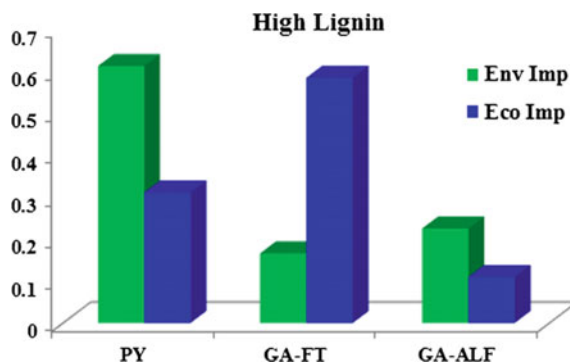
pre-treatment (AH-ALF). Since direct conversion through biochemical route is impracticable for high lignin biomass, the alternatives are set to PY, GA-ALF and GA-FT. For both medium and low lignin biomass, all the five alternatives are applicable. The ratings have been provided by means of detailed literature review, subsequent analysis and brain-storming sessions. The Saaty scale has been strictly followed for this purpose [44, 45]. In order to avoid any ambiguity and biasness towards the ratings, the AHP has been carried out twice by assigning different weightage to the environmental and economic criteria, defined as case 1 and case 2, respectively (Fig. 4). The technological maturity has been left unperturbed as that dictates a fact or current status about that technology, and introducing perturbation in that is meaningless. On a scale of 100, for case 1, weightages on economics, environmental impact and technological maturity are set in the ratio of 26:41.2:32.8. In case 2, the weightages on environment and economics have been interchanged. Thus, the eco: env: tech is set as 41.2:26:32.8.

7.2 AHP Results for Three Classes of Biomass

7.2.1 High Lignin Biomass

For high lignin content biomass, for case 1, the pyrolysis is the most preferable route followed by GA-ALF and GA-FT. This is justifiable as pyrolysis has lesser environmental footprint than gasification process. In addition to that, the pyro-char obtained as a product of pyrolysis is used in soil fixation which has positive environmental footprint. With respect to the economical preference (case 2) for high lignin biomass, GA-FT is the best suitable route followed by GA-ALF. In this case, GA-FT is the best solution because the economics of this process is well established and the demands of the final products are also high. Also, gasification is a self-sustained process compared to pyrolysis, and no additional cost is required to maintain an inert atmosphere inside the reactor. Pyrolysis comes as second option as the process is economically feasible more than the GA-ALF process as the yield is less in case of GA-ALF. The results are depicted in Fig. 5.

Fig. 5 AHP rating for suitable conversion processes for HL



7.2.2 Medium and Low Lignin

For medium and low lignin biomass, pyrolysis followed by AH-AD and AH-ALF is the most suitable options, and GA-ALF and GA-FT are the least suitable options when the analysis is biased on environmental impact. Due to the positive environmental footprints, as discussed before, pyrolysis comes up as the best preference compared to AH-AD and AH-ALF, as both the latter processes have energy requirement and water footprint. In addition to that, AH-AD have higher footprint if methane leakage occurs. GA-ALF and GA-FT are least preferable options as the overall environmental footprint is much higher. For case 2 with higher biasness to economics, AH-AD, pyrolysis and GA-FT are the best suitable routes, whereas AH-ALF and GA-ALF are the least suitable routes. AH-ALF and GA-ALF lag behind mainly due to low conversion. AH-AD dominates the top position as installation cost, operating cost and maintenance cost are less compared to pyrolysis and GA-FT. The results are depicted in Fig. 6.

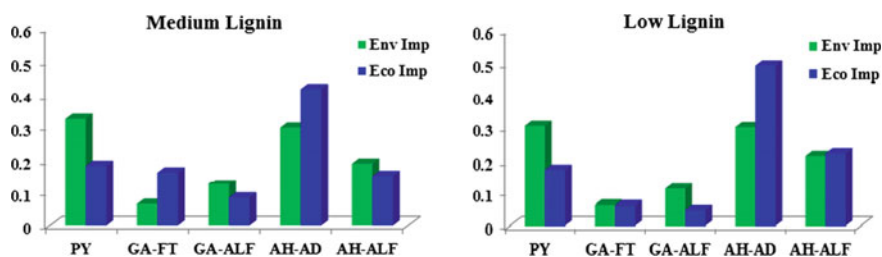


Fig. 6 AHP rating for suitable conversion processes for ML and LL

8 Recommendation on Strategic Decision on Feasible Conversion Processes

From the AHP analysis, it is clear that the choice of the conversion processes to be used in the 2G biorefineries depends on the type of agro-waste and the environmental and economic impacts of the process. Different sets of conversion processes are suitable if the biasness on environment and economics is interchanged. Therefore, for the setting up of a 2G refinery in any agricultural hub, the policy makers have to decide on the priority consideration, i.e. whether environmental impact or economic returns is to be given more stress. For the same level of environmental impact, better economy is expected if the technological maturity increases. Hence, more thrust should be given on research and development to unwind the mechanisms to address the challenges of the conversion processes. The analysis also indicates that parallel processing of high, low and medium lignin feedstocks should be done using different conversion processes in the same 2G biorefinery to exploit the maximum benefit from all agro-residues.

9 Conclusions

From the available database, an assessment on the abundance of Indian agro-residues and their overall energy potential has been made. Based on the lignin content, the residues have been classified as high lignin, medium lignin and low lignin ones. Considering an array of thermochemical, biochemical and hybrid processes, an AHP model has been developed to draw a guideline for the strategic decision on the utilization of the conversion path for different types of biomass in a single 2G refinery. The analysis clearly indicates that the suitability of routes changes with the interchange of priority on environmental impact and economic return. It is expected that the findings presented in the article will be useful for the scientists to focus on the research and development on suitable conversion processes for different types of agro-residues and for the policy makers to decide on setting up of 2G biorefineries near agricultural hubs in rural sectors.

Acknowledgements The corresponding author acknowledges INNO-INDIGO for the selection of collaborative CONVER-B project on Biobased Energy. All authors acknowledge the valuable comments made by the learned reviewers for the upgradation of the quality of the manuscript.

References

1. Viaggi D, Mantino F, Mazzocchi M, Moro D, Stefani G (2012) From agricultural to bio-based economics? Context, state of the art and challenges. *Bio-based Appl Econ* 1(1):3–11
2. Priefer C, Jörisen J, Frör O (2017) Pathways to Shape the Bioeconomy. *Resources* 6(1):10

3. Philp JC, Pavanan KC (2013) Bio-based production in a bioeconomy. *Asian Biotechnol Develop Rev* 15(2):81–88
4. De Jong E, Higson A, Walsh P, Wellisch M (2012). Bio-based chemicals value added products from biorefineries. IEA Bioenergy Task42 Biorefinery
5. Sun R (2010) Cereal straw as a resource for sustainable biomaterials and biofuels: chemistry, extractives, lignins, hemicelluloses and cellulose. Elsevier
6. Mtui GY (2009) Recent advances in pretreatment of lignocellulosic wastes and production of value added products. *African J Biotechnol* 8(8)
7. Rooni V, Raud M, Kikas T (2017) Technical solutions used in different pretreatments of lignocellulosic biomass: a review. *Agron Res* 15(3):848–858
8. Wi SG, Cho EJ, Lee DS, Lee SJ, Lee YJ, Bae HJ (2015) Lignocellulose conversion for biofuel: a new pretreatment greatly improves downstream biocatalytic hydrolysis of various lignocellulosic materials. *Biotechnol Biofuels* 8(1):228
9. Brethauer S, Studer MH (2015) Biochemical conversion processes of lignocellulosic biomass to fuels and chemicals—a review. *CHIMIA Int J Chem* 69(10):572–581
10. Nanda S, Mohammad J, Reddy SN, Kozinski JA, Dalai AK (2014) Pathways of lignocellulosic biomass conversion to renewable fuels. *Biomass Convers Biorefinery* 4(2):157–191
11. Limayem A, Ricke SC (2012) Lignocellulosic biomass for bioethanol production: current perspectives, potential issues and future prospects. *Prog Energy Combust Sci* 38(4):449–467
12. Sarkar A, Chowdhury R (2016) Co-pyrolysis of paper waste and mustard press cake in a semi-batch pyrolyzer—optimization and bio-oil characterization. *Int J Green Energy* 13(4):373–382
13. Arvidsson M, Morandin M, Harvey S (2015) Biomass gasification-based syngas production for a conventional oxo synthesis plant—greenhouse gas emission balances and economic evaluation. *J Clean Prod* 99:192–205
14. Hill J, Nelson E, Tilman D, Polasky S, Tiffany D (2006) Environmental, economic, and energetic costs and benefits of biodiesel and ethanol biofuels. *Proc Natl Acad Sci* 103(30):11206–11210
15. Gowen MM (1989) Biofuel v fossil fuel economics in developing countries: How green is the pasture? *Energy Policy* 17(5):455–470
16. Sasana H, Ghazali I (2017) The impact of fossil and renewable energy consumption on the economic growth in Brazil, Russia, India, China and South Africa. *Int J Energy Econ Policy* 7(3):194–200
17. Ahmed K (2017) Revisiting the role of financial development for energy-growth-trade nexus in BRICS economies. *Energy* 128:487–495
18. Singh J, Gu S (2010) Biomass conversion to energy in India—a critique. *Renew Sustain Energy Rev* 14(5):1367–1378
19. Kumar A, Kumar N, Baredar P, Shukla A (2015) A review on biomass energy resources, potential, conversion and policy in India. *Renew Sustain Energy Rev* 45:530–539
20. Cardoen D, Joshi P, Diels L, Sarma PM, Pant D (2015) Agriculture biomass in India: Part 1. estimation and characterization. *Resour Conserv Recycl* 102:39–48
21. Gabhane J, Tripathi A, Athar S, William SP, Vaidya AN, Wate SR (2016) Assessment of bioenergy potential of agricultural wastes: a case study cum template. *J Biofuels Bioenergy* 2(2):122–131
22. Abraham A, Mathew AK, Sindhu R, Pandey A, Binod P (2016) Potential of rice straw for bio-refining: an overview. *Biores Technol* 215:29–36
23. Demirbas A (2010) Biorefineries for biomass upgrading facilities. *Green Energy Technol*
24. De Jong E, Jungmeier G (2015) Biorefinery concepts in comparison to petrochemical refineries. *Ind Biorefineries White Biotechnol* 3–33
25. Cherubini F, Jungmeier G, Wellisch M, Willke T, Skiadas I, Van Ree R, De Jong E (2009) Toward a common classification approach for biorefinery systems. *Biofuels, Bioprod Biorefin* 3(5):534–546

26. Naik SN, Goud VV, Rout PK, Dalai AK (2010) Production of first and second generation biofuels: a comprehensive review. *Renew Sustain Energy Rev* 14(2):578–597
27. Alaswad A, Dassisti M, Prescott T, Olabi AG (2015) Technologies and developments of third generation biofuel production. *Renew Sustain Energy Rev* 51:1446–1460
28. Valentine J, Clifton-Brown J, Hastings A, Robson P, Allison G, Smith P (2012) Food vs. fuel: the use of land for lignocellulosic ‘next generation’ energy crops that minimize competition with primary food production. *GCB Bioenergy* 4(1):1–19
29. Thompson PB (2012) The agricultural ethics of biofuels: the food vs. fuel debate. *Agriculture* 2(4):339–358
30. Mohanty P, Pant KK, Naik SN, Das LM, Vasudevan P (2011) Fuel production from biomass: Indian perspective for pyrolysis oil
31. Ingale LT, Dube KJ, Sarode DB, Attarde SB, Ingle ST (2013) Monitoring and respiratory health assessment of the population exposed to cooking fuel emissions in a rural area of Jalgaon District, India. *Asia Pacific J Public Health* 25(6):463–475
32. Paliwal U, Sharma M, Burkhart JF (2016) Monthly and spatially resolved black carbon emission inventory of India: uncertainty analysis. *Atmos Chem Phys* 6(19):12457–12476
33. Trivedi A, Verma AR, Kaur S, Jha B, Vijay V, Chandra R, Prasad R (2017) Sustainable bio-energy production models for eradicating open field burning of paddy straw in Punjab, India. *Energy* 127:310–317
34. Kataki R, Chutia RS, Mishra M, Bordoloi N, Saikia R, Bhaskar T (2015) Feedstock suitability for thermochemical processes
35. Ghosh S, Chowdhury R, Bhattacharya P (2017) Sustainability of cereal straws for the fermentative production of second generation biofuels: a review of the efficiency and economics of biochemical pretreatment processes. *Appl Energy* 198:284–298
36. Sarkar S (1974) Fuels and combustion. Universities Press
37. <http://powermin.nic.in/en/content/power-sector-glance-all-india>
38. Tanager P, Field JL, Jahn CE, DeFoort MW, Leach JE (2013) Biomass for thermochemical conversion: targets and challenges. *Frontiers Plant Sci* 4
39. Debnath B, Biswas NT, Baidya R, Ghosh SK (2014) Nanotechnology in waste water treatment: a review. *Ecol Urban Areas* 2014:563
40. Saaty TL (2002) Decision making with the analytic hierarchy process. *Scientia Iranica* 9 (3):215–229
41. Saaty TL (2008) Decision making with the analytic hierarchy process. *Int J Serv Sci* 1(1):83–98
42. Saaty TL, Kearns KP (2014) Analytical planning: the organization of system, vol 7. Elsevier
43. Baidya R, Ghosh SK, Debnath B (2015) Analysis of parameters for green computing approach using the analytical hierarchy process. In: 2015 International conference on energy economics and environment (ICEEE), pp. 1–4. IEEE
44. Saaty TL (1980) The analytic hierarchy process. McGraw—Hill, New York
45. Saaty TL (1985) Decision making for leaders. *IEEE Trans Sys Man Cybern* 3:450–452
46. Sehswag S, Das M (2015) A brief overview: present status on utilization of mustard oil and cake
47. Raj T, Kapoor M, Gaur R, Christopher J, Lamba B, Tuli DK, Kumar R (2015) Physical and chemical characterization of various Indian agriculture residues for biofuels production. *Energy Fuels* 29(5):3111–3118
48. Brijwani K, Vadlani PV (2011) Solid state fermentation of soybean hulls for cellulolytic enzymes production. *Soybean-Appl Technol*
49. Balan V, Rogers CA, Chundawat SP, da Costa Sousa L, Slininger PJ, Gupta R, Dale BE (2009) Conversion of extracted oil cake fibers into bioethanol including DDGS, canola, sunflower, sesame, soy, and peanut for integrated biodiesel processing. *J American Oil Chemists’ Soc* 86(2):157–165
50. Franco HCJ, Pimenta MTB, Carvalho JLN, Magalhães PS, Rossell CEV, Braunbeck OA, Rossi Neto J (2013) Assessment of sugarcane trash for agronomic and energy purposes in Brazil. *Scientia Agricola* 70(5):305–312

51. Xiao B, Sun X, Sun R (2001) Chemical, structural, and thermal characterizations of alkali-soluble lignins and hemicelluloses, and cellulose from maize stems, rye straw, and rice straw. *Polym Degrad Stab* 74(2):307–319
52. http://shodhganga.inflibnet.ac.in/bitstream/10603/17540/7/07_chapter%202.pdf
53. Fernandes ERK, Marangoni C, Medeiros SHW, Souza O, Sellin N (2012) Slow pyrolysis of banana culture waste: leaves and pseudostem. In: 3rd International conference on industrial and hazardous waste management
54. Ross K, Mazza G (2011) Comparative analysis of pyrolysis products from a variety of herbaceous Canadian crop residues. *World J Agric Sci* 7(6):763–776
55. Raj T, Kapoor M, Gaur R, Christopher J, Lamba B, Tuli DK, Kumar R (2015) Physical and chemical characterization of various Indian agriculture residues for biofuels production. *Energy Fuels* 29(5):3111–3118
56. Mohammed TH, Lakhmiri R, Azmani A, Hassan II (2014) Bio-oil from pyrolysis of castor shell. *Int J Basic Appl Sci* 1–5
57. Sarkar A, Mondal B, Chowdhury R (2014) Mathematical modeling of a semibatch pyrolyser for sesame oil cake. *Ind Eng Chem Res* 53(51):19671–19680
58. Li J, Chen Y, Yang H, Zhu D, Chen X, Wang X, Chen H (2017) The correlation of feedstock and bio-oil compounds distribution. *Energy Fuels*
59. Abdullah N, Sulaiman F, Miskam MA, Taib RM (2014) Characterization of banana (*Musa spp.*) pseudo-stem and fruit-bunch-stem as a potential renewable energy resource. *Int J Biol Vet Agric Food Eng* 8(8):712
60. Pilon G (2007) Utilization of arecanut (*Areca catechu*) husk for gasification
61. Ramachandra TV, Kamakshi G (2005) Bioresource potential of Karnataka (No. 109). Technical report

Dr. Ranjana Chowdhury
Professor
Chemical Engineering Department
JADAVPUR UNIVERSITY
Kolkata-700 032

Ranjana Chowdhury
19/3/2024

Simabandhu Manna
19/03/2024